Formulation d'hydrogels injectables poreux et modulables : nouvelles perspectives pour la régénération du tissu musculaire squelettique et l'évaluation de la myogénèse in vitro

Louise Griveau

N°d'ordre NNT :
2021LYSE1075

THESE de DOCTORAT DE L'UNIVERSITE DE LYON
opérée au sein de
l'Université Claude Bernard Lyon 1

Ecole Doctorale N° ED 205
Ecole Doctorale Interdisciplinaire Science-Santé

Spécialité de doctorat :
Discipline : Ingénierie biologique et médicale, Biotechnologie

Soutenue publiquement le 29/04/2021, par :
Louise GRIVEAU

Design of versatile injectable porous hydrogels: new perspectives for skeletal muscle tissue regeneration and *in vitro* evaluation of myogenesis

---

Devant le jury composé de :

Pr. David, Laurent, Professeur/Université Claude Bernard Lyon1		Président
Dr. Anselme, Karine	Directrice de recherche/ CNRS	Rapporteure
Pr. Banzet, Sébastien	Professeur agrégé du Val de Grâce	Rapporteur
Pr. Frieden, Maud,	Professeure associée/Université de Genève	Rapporteure
Dr. Le Visage Catherine,	Directrice de Recherche/ INSERM	Examinatrice
Dr. Sohier, Jérôme,	Chargé de recherche/CNRS	Directeur de thèse
Dr. Debret, Romain,	Chargé de recherche/CNRS	Co-directeur de thèse
Dr. Gache, Vincent,	Chargé de recherche/INSERM	Invité

Lieu de réalisation de la thèse :

Institut de Biologie et Chimie des protéines (IBCP)

UMR-5305, CNRS, UCBL 1 Laboratoire de Biologie Tissulaire et d'ingénierie thérapeutique (LBTI)

Equipe : Fonctionnalité et Dynamique du tissu Cutané puis équipe Vecteurs colloïdaux et transport tissulaire

7 Passage du Vercors 69367 Lyon Cedex 07, France

Et

Institut NeuroMyogène (INMG)

CNRS UMR 5310 - INSERM U1217 - UCBL1-Université de Lyon

Equipe : MNCA (Muscle Nuclear & Cytoskeleton Architecture)

8 avenue Rockefeller 69008 Lyon, France

Et

Laboratoire des matériaux (Mateis) UMR-5510, CNRS, INSA

Equipe : Interactions Biologiques et biomatériaux

Site de la Buire Bâtiment B Rue Guillaume Paradin 69008 Lyon, France

Financement :

Ce travail de thèse a été financé par l'agence nationale de la recherche GELIHPARBAL ANR-17-CE19-0009

Encadrement :

Ce travail de thèse a été encadré par Dr. Jérôme Sohier et Dr. Romain Debret (UMR 5305)

Remerciements

Je tiens tout d'abord à remercier l'intégralité des personnels des 3 unités de recherche dans lesquelles s'est inscrit mon travail de thèse : CNRS UMR 5305, Laboratoire de Biologie tissulaire et d'ingénierie thérapeutique (LBTI) ; CNRS UMR 5510, Matériaux : ingénierie et science (Mateis) et CNRS UMR 5310 - INSERM U1217, Institut Neuromyogène (INMG). Je remercie l'agence nationale de la recherche (ANR) et le centre national de la recherche scientifique (CNRS) pour le financement de ces travaux de thèse.

Je tiens à remercier Dr. **Karine Anselme**, Pr. **Sébastien Banzet** et Pr. **Maud Frieden** de m'avoir fait l'honneur d'évaluer ce travail en tant que rapporteurs, ainsi que Pr. **Laurent David** et Dr. **Catherine Le Visage** d'avoir accepté de faire partie de mon jury en tant qu'examinateurs.

Je remercie également l'ensemble des membres de mes comités de suivi de thèse : Dr. **Thomas Trimaille**, Dr. **Emeline Perrier-Groult**, **Valérie Orea** et Dr. **Bénédicte Chazaud**. Merci pour votre disponibilité et vos conseils scientifiques avisés tout au long de ma thèse qui m'ont permis d'orienter au mieux mes questions scientifiques.

Je souhaite également remercier très chaleureusement mes deux directeurs de thèse, Dr. **Jérôme Sohier** et Dr. **Romain Debret**. Je vous remercie tous les deux de m'avoir donné l'immense privilège de réaliser ce projet. Merci de votre confiance et de m'avoir laissé l'autonomie nécessaire pour murir tant scientifiquement que personnellement. J'ai énormément appris à vos côtés, par votre manière d'envisager la recherche et de la mener. Vous êtes deux personnes d'une grande richesse à la fois sur le plan scientifique et humain. Jérôme, je te remercie particulièrement de m'avoir formée avec une grande rigueur scientifique. Merci aussi de m'avoir soutenue et accompagnée tout au long de cette thèse et de ne pas avoir lâché l'affaire, même dans les moments difficiles (il s'en est fallu de peu). Tu m'as beaucoup aidée à évoluer, à prendre de l'assurance et à apprendre à être fière de mon travail. Romain je te remercie d'avoir accepté de co-encadrer ce travail et pour l'aide que tu m'as apportée à différents moments de ma thèse. Merci pour la qualité de tes conseils scientifiques qui ont toujours été très justes et pour ta vision qui m'a permis de prendre du recul sur mes travaux. Merci aussi à tous les deux pour les moments passés autour de bières et de verveines, j'aurai beaucoup ri.

Je tiens aussi particulièrement à exprimer ma reconnaissance au Dr. **Vincent Gache** pour son accueil très chaleureux au sein de son équipe « architecture du noyau et du cytosquelette musculaire » à l'INMG. Merci de m'avoir offert une place dans ton équipe à un moment très important pour moi. Merci pour tes nombreux conseils scientifiques, ton soutien et ta patience malgré mon entêtement (d'ailleurs, je pense toujours que ce sont des vaisseaux). Merci aussi pour la mâche.

Je remercie les stagiaires que j'ai eu la chance d'accompagner pendant ma thèse : **Clémence Drouglazet**, **Baptiste Robbiani** et **Héloïse Le Goff**. J'espère que votre expérience a été aussi enrichissante pour vous qu'elle ne l'a été pour moi.

Je remercie **Akkiz Bekel**, **Mariana Carrancá**, **Joshua Dulong**, **Daniel Ferri-Angulo** et **Emma Ruby** pour la relecture de certaines parties de ce manuscrit et leur aide dans la reformulation de certaines idées.

Ma thèse a aussi été l'occasion de de travailler avec de nombreuses personnes au sein de collaborations riches :

-Je remercie **Marianne Lafont**, **Catherine le Visage** et **Pierre Weiss** du laboratoire Regenerative medecine and skeleton (RMeS) sans qui l'étude rhéologique des hydrogels n'aurait pas été possible. Merci aussi pour vos conseils avisés lors des réunions.

-Un grand merci à **Naima el Kholti** de la plateforme PrimaTiss pour sa participation à l'étude de biocompatibilité. Merci pour ta disponibilité, ton efficacité et tes supers coupes et marquages.

-Je remercie **Isabelle Grosjean** de la plateforme IPS de l'INMG pour sa supervision des manipulations sur les IPS et leur différentiation en cardiomyocytes.

-Je remercie **Aurélie Pagnon** de l'entreprise Novotec pour son aide dans la mise au point des protocoles de marquages des macrophages.

-Je remercie **Valérie Orea** de la plateforme Aniphy pour son accompagnement dans la rédaction des demandes d'autorisations de projets, pour sa disponibilité et ses remarques qui m'ont aidé à préciser mon propos.

-Je remercie **Thomas Laumonier** de l'Université de Genève pour l'envoi des cellules primaires humaines qui nous ont permis d'orienter différemment ce travail de thèse.

-Merci à **Dominique Sigaudo Roussel** et au personnel de l'animalerie de l'institut de biologie et de chimie des protéines (IBCP) pour leur aide dans la mise en place et la réalisation des études de biocompatibilité.

-Je remercie **Sabine Richard** de l'Institut de Génomique Fonctionnelle de Lyon (EGFL) pour m'avoir formée au vibratome et m'avoir laissée l'utiliser librement tout au long de ma thèse.

Je souhaiterais de même exprimer ma gratitude à toutes les personnes ayant collaboré de près ou de loin à ce projet de thèse. Tout particulièrement je remercie **Emilie Christin** pour son aide précieuse concernant la culture des cellules musculaires et pour m'avoir accompagnée tout au long de cette aventure tant sur le plan professionnel que personnel. Ce travail n'aurait sans doute pas pu être mené à bien sans l'aide de **Mariana Carrancá** qui m'a formée et soutenue tout au long de ce travail sur les biomatériaux dans un univers bio. J'ai particulièrement aimé nos 'manip à deux'. Merci à **Alireza Ghasemizadeh** pour son aide quotidienne, et son expertise RT-qPCR. Merci aussi pour les pizzas et les chips. Merci à **Aurore Berthier** pour la production de la protéine élastique et pour s'être rendue toujours disponible et prête à aider.

Enfin, j'aimerais remercier toutes les personnes ayant contribué à mon intégration dans les différentes équipes. Je n'aurais jamais pu réaliser ce travail sans le soutien d'un grand nombre de personnes. Particulièrement, merci à la team biomat qui m'a soutenue tout au long de l'aventure : Aurore, Daniel, Jérôme, Kardelen, Kevin, Marie, Marine, Mariana, Romain, Sarah, et Silvia. Merci à l'équipe MNCA, à savoir Carole, Emilie, Nathalie, Peggy, Shayan et Vincent. Merci à mes gars sûrs de l'équipe FDTC, Ben, Cécile et Joshua. Merci aussi aux doctorants Mateis pour avoir rendu une parenthèse particulière de ma thèse moins pénible, tout particulièrement Akkiz.

Résumé en Français

Formulation d'hydrogels injectables poreux et modulables : nouvelles perspectives pour la régénération du tissu musculaire squelettique et l'évaluation de la myogénèse *in vitro*.

Les pertes musculaires volumétriques issues d'incidents traumatiques baissent drastiquement les capacités de régénération du muscle et manquent de traitements efficaces. Les hydrogels injectables sont des candidats thérapeutiques prometteurs mais leur potentiel repose fortement sur la présence d'une porosité permettant l'infiltration de cellules et de vaisseaux en leur sein. Par conséquent, ce travail vise à (1) créer des hydrogels injectables et poreux à base de dendrimères greffés de poly(L-lysine) (DGL) et de NHS-polyéthylène-glycol (PEG) par une approche effervescente ; et (2) à évaluer leur capacité à soutenir la différenciation de progéniteurs des cellules musculaires pour la régénération du muscle strié squelettique.

Dans ce travail de thèse, le comportement de myoblastes a d'abord été étudié sur des hydrogels denses DGL/PEG et a montré être corrélé aux propriétés mécaniques et à la composition du support. Des conditions favorables pour la prolifération et la différentiation des myoblastes ont donc été identifiées puis ciblées pour la mise en place d'une porosité permettant l'infiltration cellulaire au sein de l'hydrogel. Pour cela, les hydrogels ont été préparés en dissolvant un acide carboxylique et une base carbonée aux précurseurs liquides de DGL et de PEG afin de permettre la génération contrôlée de bulles de CO_2 par effervescence. La simultanéité de l'effervescence à la réaction de réticulation de l'hydrogel DGL/PEG a permis de piéger les bulles de CO_2 à l'intérieur du réseau polymérique, menant à la création d'une porosité interconnectée. Les hydrogels poreux effervescents (EPH) injectés en sous-cutané chez la souris via un système de seringue double se sont révélés biocompatibles et capables de promouvoir une vascularisation étendue. Finalement, des myoblastes primaires humains cultivés au sein des EPH ont démontré leur capacité à fusionner ensemble pour former des myotubes avec une striation visible, capables de contracter spontanément. La présence de cellules non prolifératives, n'entrant pas en différentiation et exprimant le marqueur de cellules souches musculaire (Pax7) ont aussi été observées dans les EPH. Ces résultats consolident le potentiel des EPH à soutenir la maturation de fibres musculaires tout en intégrant la formation et le réapprovisionnement des niches de cellules souches. Par conséquent, nous décrivons dans ce travail un hydrogel poreux innovant ayant un potentiel pour la prise en charge des pertes musculaires volumétriques à travers une application rapide et directe par injection.

Mots clés : Hydrogels ; injectable et poreux ; régénération musculaire, ingénierie tissulaire, effervescence

Abstract

Design of versatile injectable porous hydrogels: new perspectives for skeletal muscle tissue regeneration and *in vitro* evaluation of myogenesis

Volumetric muscle loss (VML) decreases muscle regeneration capacity and lacks treatments. Injectable hydrogels are promising therapeutic candidates but their potential strongly relies on the presence of porosity allowing cell infiltration and vascularization. Therefore, this work aimed (1) to create injectable and porous hydrogels based on poly-(L-lysine) grafted dendrimers (DGL) and NHS-polyethylene-glycol (PEG) through an effervescent approach and (2) to evaluate their ability to sustain muscle cells progenitor differentiation for skeletal muscle regeneration.

First, myoblasts behaviour in contact with dense DGL/PEG hydrogels of various condition has been shown to be correlated with substrate stiffness and composition. Conditions of interest for myoblasts proliferation and differentiation could be targeted for the engineering of a porosity able to sustain cellular infiltration inside the hydrogel. We found that effervescent porous hydrogels (EPH) of versatile mechanical properties could be prepared by dissolving a carboxylic acid and a carbonated base to DGL and PEG solutions, to generate CO_2 bubbles by effervescence. The simultaneous reaction of effervescence with the DGL/PEG crosslinking entrapped the CO_2 bubbles inside DGL/PEG network, leading to the formation a spontaneous, homogeneous and interconnected porosity. The use of sole precursor solutions allows to inject the formulations with a dual-chamber syringe and a static mixer, leading to porous hydrogels that were proven biocompatible by subcutaneous injection in mice. As a striking result, primary human myoblasts seeded into 3D EPH showed extensive myotube formation with visible striation and ability to spontaneously contract. The presence of quiescent and non-differentiated cells inside EPH was confirmed with myogenic regulatory factor Pax7. These results consolidate EPH potential for muscle fibre maturation while preserving a pool of reserve cells, holding promise for tissue engineering applications.

In conclusion, we describe a novel porous hydrogel with potential as scalable solution for VML treatments within a swift and straightforward injectable delivery, which provides an optimal substrate for muscle cells progenitors to differentiate into contractile myotubes while maintaining a pool of muscle stem cells.

Keywords: Hydrogel ; Injectable and porous; Skeletal muscle regeneration; Tissue engineering ; effervescence

Table of contents

Abbreviation

2D	Two-dimensional
3D	Three-dimensional
Ach	Acetylcholine
BAM	Bioartificial muscle
BSA	Bovine serum albumin
Ca	Citric acid
CaC	Calcium carbonate
CBB	Coomassie Brilliant Blue
CEE	Chicken embryo extract
CTGF	Connective tissue growth factor
DAPI	4′,6-Diamidino-2-phenylindole dihydrochloride
DGL	Poly(L-lysine)- grafted dendrimers
DM	Differentiation medium
DMA	Dynamic mechanical analysis
DMD	Duchenne muscular dystrophy
DMEM	Dulbecco/Vogt modified Eagle's minimal essential medium
DMF	N,N-Dimethylformamide
DMSO	Dimethyl sulfoxide
DPBS	Dulbecco’s Phosphate Buffered Saline
E’	Storage modulus in compression
E’’	Loss modulus in compression
E*	Complex modulus in compression
EBP	Elastin binding protein
ECM	Extracellular matrix
EDL	Extensor digitorum longus muscle
ELP	‘In house’ Elastin-like polypeptide
EPH	Effervescent porous hydrogel
EtOH	Ethanol
FA	Focal adhesion
FAP	Fibro-adipogenic progenitors
FBS	Fetal Bovine serum
FDA	US Food and drug administration
FGF-2	Fibroblast growth factor 2
FITC	Fluorescein isothiocyanate
Gaa	Glacial acetic acid
G’	Storage modulus in shear stress

G''	Loss modulus in shear stress
GF	Growth factors
GM	Growth medium
GMB	Gelatine microbeads
GMSCs	Gingival mesenchymal stem cells
HA	Hyaluronic acid
hESCs	Human embryonic stem cells
HGF	Hepatocyte growth factor
HPMC	Hydroxypropyl methylcellulose
HS	Horse serum
HUVEC	Human umbilical vein endothelial cells
IFNγ	Interferon gamma
IGF-1	Insulin-like growth factor
iHMs	Immortalized human myoblasts
iPSC	Human induced pluripotent stem cells
IMDM	Iscove's Modified Dulbecco's medium
KC	Potassium carbonate
LSCM	Laser scanning confocal microscopy
MMP	Matrix metalloproteinase
MPs	Microparticles
MRF	Myogenic regulatory factors
MSCs	Mesenchymal stem cells
MyHC	Myosin heavy chain
MyoD	Myogenic determination factor
MyoG	Myogenin
NaC	Sodium carbonate
NabC	Sodium bicarbonate
NHDF	Normal human dermal fibroblasts
NHS	N-Hydroxysuccinimide
NMJ	Neuromuscular junction
OCT	Optimal cutting solution
PAA	Poly(acrylic acid)
PAAm	Poly(acrylamide)
PAMAM	Poly(amidoamine)
PCL	Poly (ε-caprolactone)
PEG	Polyethylene glycol
PEGDA	poly(etgylene glycol) diacrylate
PEG-NHS	O,O′-Bis[2-(N-Succinimidyl-succinylamino)ethyl]polyethylene glycol

PEI	Polyethylene-imine
PEO	Poly[ethlylene] oxide
PGA	Poly(glycolic acid)
pHMs	Primary human myoblasts
PLA	Polylactic acid
PLGA	Poly(lactic-co-glycolic acid)
PLLA	Polylactic acid
pMMs	Primary mice myoblasts
Poly-HEMA	Poly(2-hydroxyethyl methacrylate)
P/S	Penicillin / streptomycin
PTFE	polytetrafluoroethylene
PVA	Poly(vinyl alcohol)
RGD	Sequence Arginine-Glycine-Aspartic Acid
RT	Room temperature
Sa	Succinic acid
SDS	Sodium dodecyl sulfate
SC	Satellite cells
SR	Sarcoplasmic reticulum
TA	Tibialis anterior
TGF-β	Transforming growth factor beta
TNF-α	Tumor necrosis factor
VML	Volumetric muscle loss

LIST OF FIGURES

LIST OF TABLES

Contexte général

Le muscle strié squelettique est un tissu possédant une grande capacité de régénération. Après une lésion, il est capable de recouvrer complètement son architecture et sa fonctionnalité. Cependant, les plaies volumétriques, caractérisées par une perte d'au moins 20% de la masse du muscle, bouleversent cette capacité de régénération et entrainent des déficits fonctionnels et des possibles handicaps.

Le muscle strié squelettique est principalement constitué de fibres musculaires multinucléées résultant de la fusion de centaines de cellules spécialisées, les myoblastes. Ces fibres s'organisent en faisceaux alignés afin de fournir au muscle sa capacité de contraction. On sait maintenant depuis plusieurs décennies que la régénération du muscle est liée aux cellules satellites, les cellules souches logeant le long des fibres musculaires. Suite à une blessure, elles sont activées, migrent sur le site de la plaie pour y proliférer et se différentier en myoblastes, eux-mêmes capable de fusionner entre eux afin de reformer des fibres musculaires contractiles. Ainsi, elles participent activement à la régénération des fibres musculaires et au maintien de l'homéostasie du tissue.

Cependant, dans le cas d'une perte volumétrique, la destruction partielle des cellules satellites et de la matrice extracellulaire (ECM) sur laquelle elles évoluent empêchent le bon déroulé du processus de régénération. Un déséquilibre entre le recrutement de cellules satellites et l'entrée de fibroblastes pour combler la plaie entraine un dépôt excessif de collagène et le remplacement progressif du muscle par un tissu fibreux n'ayant pas la capacité de contracter. Des traitements cliniques ont été développé et ont pour but de limiter la fibrose et retrouver la fonctionnalité du muscle. Ils consistent à débrider la plaie et à transplanter des greffons autologues de muscles. Cependant, l'utilisation de greffons est associée à de nombreuses limites, parmi lesquelles le manque de greffons et le risque de morbidité sur le site donneur sans oublier la nécessité de réaliser une seconde intervention chirurgicale, traumatique pour le patient. Des tentatives d'amélioration de la réparation tissulaire ont été étudiée via l'injection de cellules souches ou de facteurs de croissance spécifiques dans les plaies. Cependant, ces tentatives se sont révélées infructueuses suite à la mortalité cellulaire et à une élimination trop rapide des molécules dans le sang.

Dans ce contexte, des stratégies basées sur l'ingénierie tissulaire et la médecine régénératrice ont été développées afin d'éviter les limitations associées aux greffes et à la thérapie cellulaire. Ces approches exploitent les principes de l'ingénierie et de la science de la vie vers le développement de substituts biologiques à forts potentiels capables de guider les cellules vers la régénération fonctionnelle des tissus. Dans le cas de blessures musculaires volumétriques, l'implantation dans le lit de la plaie d'une structure 3D susceptible de remplacer temporairement la matrice extracellulaire pour guider les cellules satellites vers la régénération fonctionnelle du tissu représente une thérapie prometteuse. Pour cela, la communauté scientifique s'est intéressée au développement de biomatériaux d'intérêt pouvant fournir ce

support aux cellules. Ces dernières décennies, il a été abondamment montré que le microenvironnement cellulaire est un puissant régulateur de leur comportement à travers des signaux physiques, biochimiques et architecturaux. Particulièrement, dans le cas de la régénération du muscle strié squelettique, le design de biomatériaux s'est concentré sur la chimie et les propriétés mécaniques du support pour la promotion d'interactions spécifiques avec les cellules musculaires à l'intérieur d'une architecture 3D.

Idéalement, les biomatériaux formulés pour le traitement des défauts musculaires volumétriques devraient être injectables pour se conformer à des lésions complexes tout en interagissant étroitement avec les tissus environnants. Une porosité adéquate au sein du biomatériau est par ailleurs importante pour permettre la néo-vascularisation, l'innervation et l'entrée des cellules précurseurs de fibres musculaires au sein de la matrice. Pour cela, les hydrogels ont été largement étudiés pour leur excellente biocompatibilité, leur similarité avec les matrices extracellulaires natives en termes de rétention aqueuse et d'adhésion cellulaire ainsi que leur potentielle injectabilité.

Récemment un hydrogel a été décrit au sein du laboratoire de biologie tissulaire et d'ingénierie thérapeutique, réalisé à partir de la réticulation de deux éléments standardisés : les dendrimères greffés de poly(L-lysine) (DGL) et le poly(éthylène) glycol (PEG). La nature synthétique de l'hydrogel permet un contrôle précis de sa chimie de réticulation ainsi que de ses propriétés mécaniques, hautement modulables. Contrairement à d'autres hydrogels synthétiques, l'hydrogel DGL/PEG possède une cytocompatibilité inhérente grâce aux charges positives apportées par les groupes amines des DGL ce qui lui permet d'interagir facilement avec les cellules

L'utilisation de précurseurs liquides non cytotoxiques permet d'inclure une protéine élastique biomimétique (ELP) au sein de l'hydrogel. L'ajout de cette protéine au niveau du réseau polymérique de l'hydrogel a montré une augmentation de la prolifération et de la vitesse de migration des cellules sur le support. Une très bonne tolérance *in vivo* de l'hydrogel DGL/PEG implanté en sous-cutané a été observée, confirmant sa potentielle utilisation pour la régénération tissulaire. Cet hydrogel est d'autant plus prometteur qu'il est techniquement injectable grâce au mélange de précurseurs liquides. En considérant ces caractéristiques très intéressantes, le potentiel de cet hydrogel a été étudié plus avant dans cette thèse.

Objectifs de la thèse

Bien que beaucoup d'efforts aient déjà été dédiés à la production de matrices pour la réparation du muscle strié squelettique, la plupart se fient à l'utilisation de cellules embarquées pour la régénération fonctionnelle du tissu. Cependant, l'incorporation de cellules limite le passage de ces matrices en étude clinique par les instances réglementaires. L'objectif de la thèse est donc d'évaluer l'hydrogel DGL/PEG comme support de la régénération musculaire. Pour répondre à cette problématique, nous proposons donc dans ce travail d'étudier plusieurs aspects du développement d'un hydrogel afin de proposer un support optimal pour guides les cellules musculaires vers une régénération fonctionnelle.

I- Dans un premier chapitre, **la capacité des hydrogels denses de DGL/PEG à fournir un support permettant le contrôle du comportement de myoblastes a été étudié**. Les hydrogels sont des réseaux polymériques hautement hydratés pouvant mimer la matrice extracellulaire native. Parmi les hydrogels, ceux réalisés à partir de précurseurs synthétiques peuvent être ajustés précisément afin de moduler leurs propriétés mécaniques. Dans ce travail, les propriétés mécaniques apportées par les hydrogels DGL/PEG ont été modulées afin de contrôler le comportement de cellules musculaires. En plus de la rigidité du support, l'influence des quantités de DGL et d'ELP au sein de l'hydrogel sur le destin cellulaire ont été étudiées. Nous avons donc évalué l'effet de (1) six rigidités, (2) quatre ratios molaires de DGL: PEG et (3) une concentration d'ELP au sein des hydrogels. Pour valider l'effet des propriétés mécaniques et de la présentation de motifs biochimiques sur les cellules musculaires, trois types de myoblastes différents ont été utilisés : une lignée immortalisée de myoblastes murins (C2C12), des myoblastes primaires de souris et des myoblastes immortalisés humains. Ce chapitre nous a permis de cibler des conditions optimales capables d'interagir avec les cellules musculaires, leur fournissant à la fois un support permettant leur prolifération ainsi que leur fusion.

II- Dans un deuxième chapitre, **la possibilité de créer une porosité à l'intérieur de l'hydrogel DGL/PEG tout en préservant son potentiel injectable a été évaluée**. Les exemples de biomatériaux à la fois directement injectables dans le corps et présentant une porosité permettant l'infiltration des cellules sont peu décrits dans la littérature. En particulier, très peu de cas ont été évalués pour la régénération fonctionnelle du muscle strié squelettique bien que l'injectabilité permettrait à l'hydrogel de se conformer à des plaies complexes tout en interagissant étroitement avec le tissu dans lequel il est placé. Par conséquent, le développement d'une formulation de l'hydrogel DGL/PEG à la fois injectable et poreuse pourrait offrir de nombreuses possibilités thérapeutiques pour la régénération des tissus mous

parmi lesquelles la gestion des plaies musculaires volumétriques. Dans ce travail, diverses méthodes ont été évaluées pour créer une porosité à l'intérieur de l'hydrogel DGL/PEG tout en maintenant sa possible délivrance par injection. La porosité résultante et sa modulation éventuelle ont été évaluées par l'intermédiaire de différents paramètres. L'infiltration cellulaire au sein de la structure poreuse et son potentiel pour la formation de tissu ont été étudiés. Enfin, en vue d'une application clinique potentielle, la biocompatibilité des nouvelles formulations a été validée par des injections en sous-cutané dans un modèle murin.

III- Dans un troisième chapitre, **l'interaction de cellules musculaires squelettiques avec les nouvelles formulations injectables et poreuses a été évaluée.** Particulièrement, l'accent a été mis sur le potentiel de ces nouvelles formulations comme support permettant la prolifération et la différentiation de myoblastes, en vue d'étudier le processus de myogenèse tout en ouvrant la voie pour une future utilisation en ingénierie tissulaire. Par conséquent, le comportement de lignées murines et humaines ainsi que de myoblastes primaires murins et humains au sein des nouveaux hydrogels poreux effervescents a été apprécié.

L'ensemble de ces résultats a finalement été discuté afin de déterminer le potentiel de ces nouvelles formulations en tant que modèle 3D *in vitro* pour la compréhension du processus de myogénèse. Finalement, ils ont permis d'ouvrir des perspectives vers l'établissement de protocoles d'optimisation permettant l'injection des hydrogels poreux effervescents au sein de plaies pour l'ingénierie tissulaire du muscle strié squelettique.

BIBLIOGRAPHIC INTRODUCTION

1 The skeletal muscle tissue: structure, function and regeneration process after injuries

Skeletal muscle tissue injuries are one of the most prevalent disabling injuries faced by military personnel and civilians. It is therefore an emerging focus area among orthopaedic and regenerative medicine fields. In particular, volumetric muscle loss (VML) is the result of an abrupt and frank loss of tissue that arises from traumatic or surgical events. The loss of skeletal muscle tissue characterizing VML often leads to functional impairment. It has been reported that VML is mainly the consequence of military exercise, vehicular accidents, machinery, moving objects, and also gunshots among civilians [1],[2]. It is estimated that emergencies for musculoskeletal injuries accounted for 15% of all emergency departments in the US in 2010. Among musculoskeletal injuries, amputation, open wounds and open fractures that can result in VML represented a 26.5 million dollars burden in 2010 for the US. The exact incidence of VML among civilians or soldiers has not been rigorously assessed in Europe and France. Nevertheless, a 15-years review of epidemiologic factors of open fractures among civilians estimates an incidence of 30.7 per 100.000 in the United Kingdom [3]. In addition, the number of car accidents in Europe, stated by the Annual accident report 2020 of the European Commission has been estimated to 56016 car accidents in France in 2019. Moreover, the increasing number of penetrating traumas (estimated at 5 to 13 % of traumatisms in France in 2012 [4]) is particularity worrying in the current tense societal context of terrorist acts against civilians. These incidents, which are often associated with tissue loss, highlight VML preponderance over the complications faced by civilians. Unfortunately, traditional medicine and rehabilitation (i.e. wound debridement, advanced bracing) do not address the loss of functionality due to VML injuries. Moreover, the current standard of care consisting in skeletal muscle autografts suffer from many outcomes including grafts availability, donor site morbidity and the need for a second surgical procedure. Considering that VML traumas were related to lost workdays in the US in 2011 [5] and can lead to persistent functional deficit and long term muscle-related disability [6],[7], they represent a significant issue in health care with major socioeconomic impacts. It appears therefore of high clinical relevance to develop adapted treatments and therapeutic strategies for tissue functional regeneration related to volumetric muscle injuries.

To develop such relevant and adapted therapeutic strategies, a good understanding of the skeletal muscle structure, and the processes occurring after an injury is mandatory.

1.1 The skeletal muscle tissue - Structure and functions

Movements of the body are fundamental for life in the whole animal kingdom. Conscious movements of the entire organism such as walking, mastication, and swallowing enable vital food intake while unconscious movements of the oesophagus and stomach absorb and digest food. Besides, heartbeats are essential for the repartition of nutrients and oxygen throughout the entire body. The tissue responsible for movements in the body is the muscle, which accounts for much of the energy-consuming cellular work in active animals.

To allow all these different movements, three highly specialized muscles are reported and categorized as **striated** and **smooth**.

The **smooth muscle** is mainly found in the walls of hollow organs (blood vessels, uterus, and digestive organs). It is responsible for involuntary body activities such as arteries constrictions and gastrointestinal tract movements during digestion.

On another hand, the striated muscle, contrarily to the smooth muscle, is characterized by a striated appearance under light microscopy, a consequence of the highly organized structure within the cells. Inside the striated muscle, two muscle types are reported: **the cardiac muscle** or myocardium, only represented in the heart, forming the contractile walls allowing beating, and **the skeletal muscle**.

With more than 600 individual muscles with distinct functions, the skeletal muscle tissue represents about 30 to 45 % of the total human body mass [8]. Skeletal muscle tissue is mainly composed of multinucleated cells, particularly arranged in bundles inside an organized extracellular matrix (ECM) supplied by blood capillaries. Each cell is in close contact with a network of nerves connected to the central nervous system [9]. Forces developed by the skeletal muscle are transferred to bones by tendons to trigger skeletal movements.

The skeletal muscle tissue is therefore involved in mechanical and metabolic functions inside the body. Its primary function is the conversion of chemical energy into mechanical work to generate the force that drives many functions of the human body. It results in the ability to maintain the posture and voluntary movements of the skeleton allowing precise prehension, mastication, ocular movement, or locomotion among others [10]. It is the only type of muscle that can be consciously contracted. A second function is its role in body metabolism regulation, producing heat, and acting as a storage for substrates like amino acids [9].

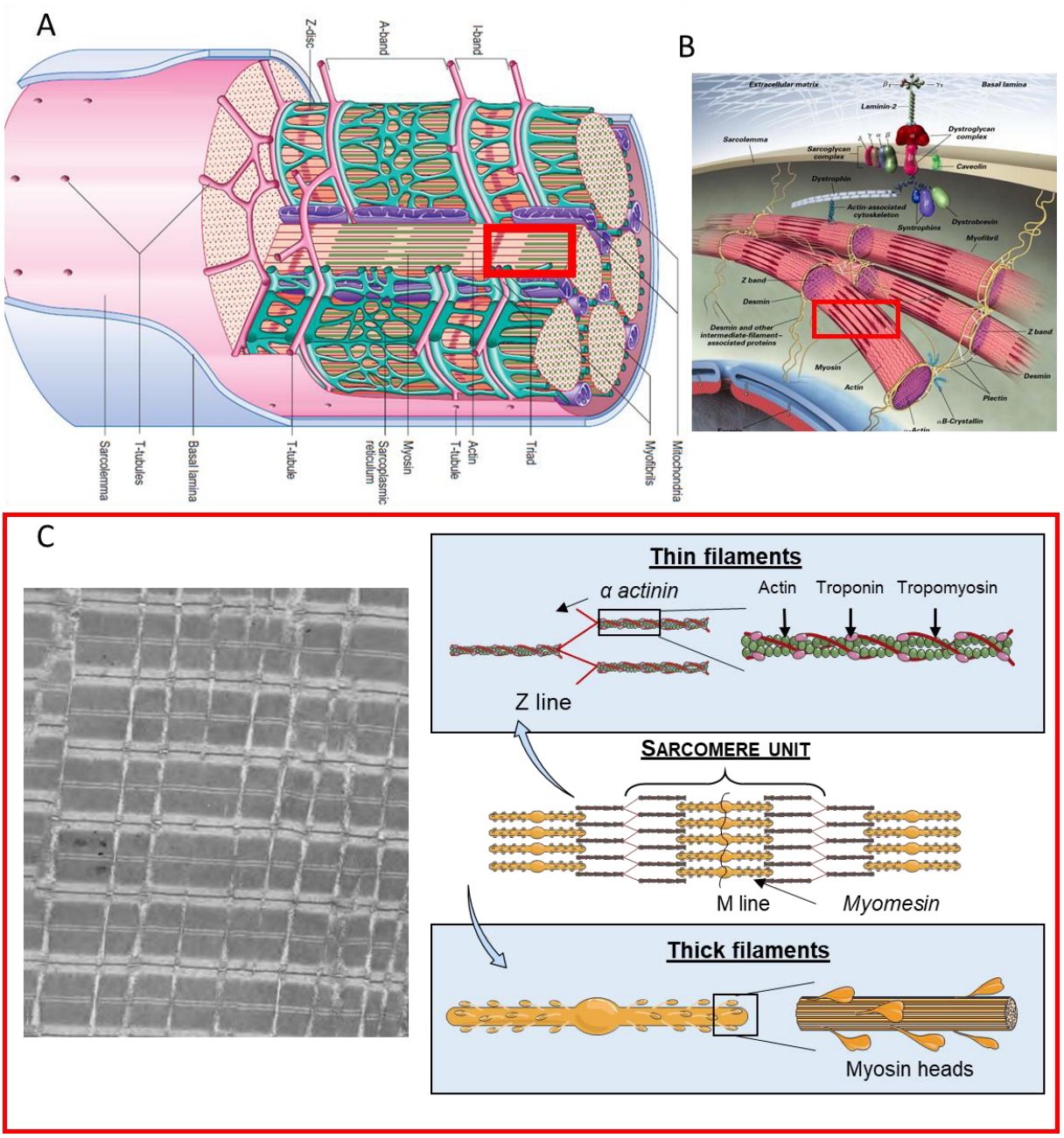

Figure 1: The contractile machinery organization within muscle cells
A) Muscle fibre organization - 3D reconstitution: myofibrils fill almost the entire cells leaving little space for organelles. B) Myofibrils bundles anchored from each other and with the cellular cytoskeleton through intermediate filaments. C) Skeletal muscle cell striated appearance is mainly due to the highly and specific organization of myofilaments (thin and thick filaments) into repeated structure called sarcomeres. A group of 200 myofilaments forms myofibrils, the contractile machinery inside the muscle fibre.
Pictures adapted from:
-The Gray's anatomy, 2016 edition;
-Dalakas et al., N Engl J Med 2000 DOI: 10.1056/NEJM200003163421104,
-Koubassova and Tsaturyan, Biochemistry 2011 DOI: 10.1134/S0006297911130086,
-Servier medical art

1.1.1 The striated muscle fibre

Skeletal muscle tissue is mostly composed of contractile cells: **muscle fibres** or myofibres (Figure 1A and B). These multinucleated cells (syncytia) are organized in bundles of long fibres running the length of the muscle. A developed muscle is made of an association of hundreds of myofibres [11]. Muscle fibres highly specific organization, distribution, and alignment are determinant to provide the tissue its mechanical properties and ability to contract [12].

The skeletal muscle striated appearance under microscopic observation is owed to a particular organization of contractile proteins: **actin and myosin**, organized in **myofilaments,** that constitute more than 80% of muscle fibre volume [13] (Figure 2C). Two strands of actin are organized to form thin filaments that contain regulatory proteins coiled around one another. Myosin molecules are arranged in a shifted network to form thick filaments. Myofilaments form highly regular structures called '**sarcomeres**' that create a repeated pattern of light and dark bands (Figure 1Cand D). By convention, a sarcomere unit is defined as the region contained between two cytoskeletal structures called Z-lines. These lines contain a high density of proteins such as titin and **α-actinin** (190 kDa) anchoring thin filaments that run across the sarcomere to reach its centre where they overlap and intercalate in between thick filaments. In the middle of two adjacent Z-line, the M-line is composed of myomesin that anchors and stabilizes thick filaments by interacting with the myosin tail domain. A group of about 200 myofilaments (thin and thick) [13] are packed together and surrounded by the sarcoplasmic reticulum (SR) to form the contractile machinery, **myofibrils** (Figure 1B). The 3D organization and mechanical stability of sarcomeres are provided by intermediate filaments which adhere to the sarcomere periphery and form transverse connections between adjacent myofibrils [14] (Figure 1B and C). Plectin, for instance, anchors Z-lines to adjacent myofibrils while **desmin** proteins maintain myofibril alignment by a connection to the muscle fibre cytoskeleton allowing to evenly distribute the contractile force [15]. These proteins maintain thousands of thin and thick filaments in parallel to one another and lead to sarcomeres coordinated movement.

A muscle fibre is composed of thousands of myofibrils, constrained by the sarcolemma that fills almost the entire cell, leaving small spaces for organelles grouped inside the cytoplasm, termed **sarcoplasm**. Mitochondria, ribosomes, golgi apparatus are present around nuclei located at the periphery of the cell and small clusters of glycogen droplets are available in the sarcoplasm, providing a straightforward source of anaerobic energy independent of blood flow in case of burst activity. One muscle fibre can contain hundreds of nuclei underneath the sarcolemma, itself surrounded by the basal lamina of the cell. At the periphery of muscle fibres is located another cell type, **satellite cells** (SC) (Figure 2). SC comprise 30-35 % [16] of all muscle fibre nuclei in postnatal mouse muscle to reach 2.5-6 % in adult mouse muscles [17]. Although we lack details in the postnatal human muscle, similar percentages of SC were reported in adult human muscle (4 ± 2 %) [18]. They are mitotically quiescent cells first discovered by Mauro in 1961 [19] located in niches between the sarcolemma and the basal

lamina. SC function is tightly regulated by numerous signals of their microenvironment and their role during injury and muscle regeneration will be further detailed.

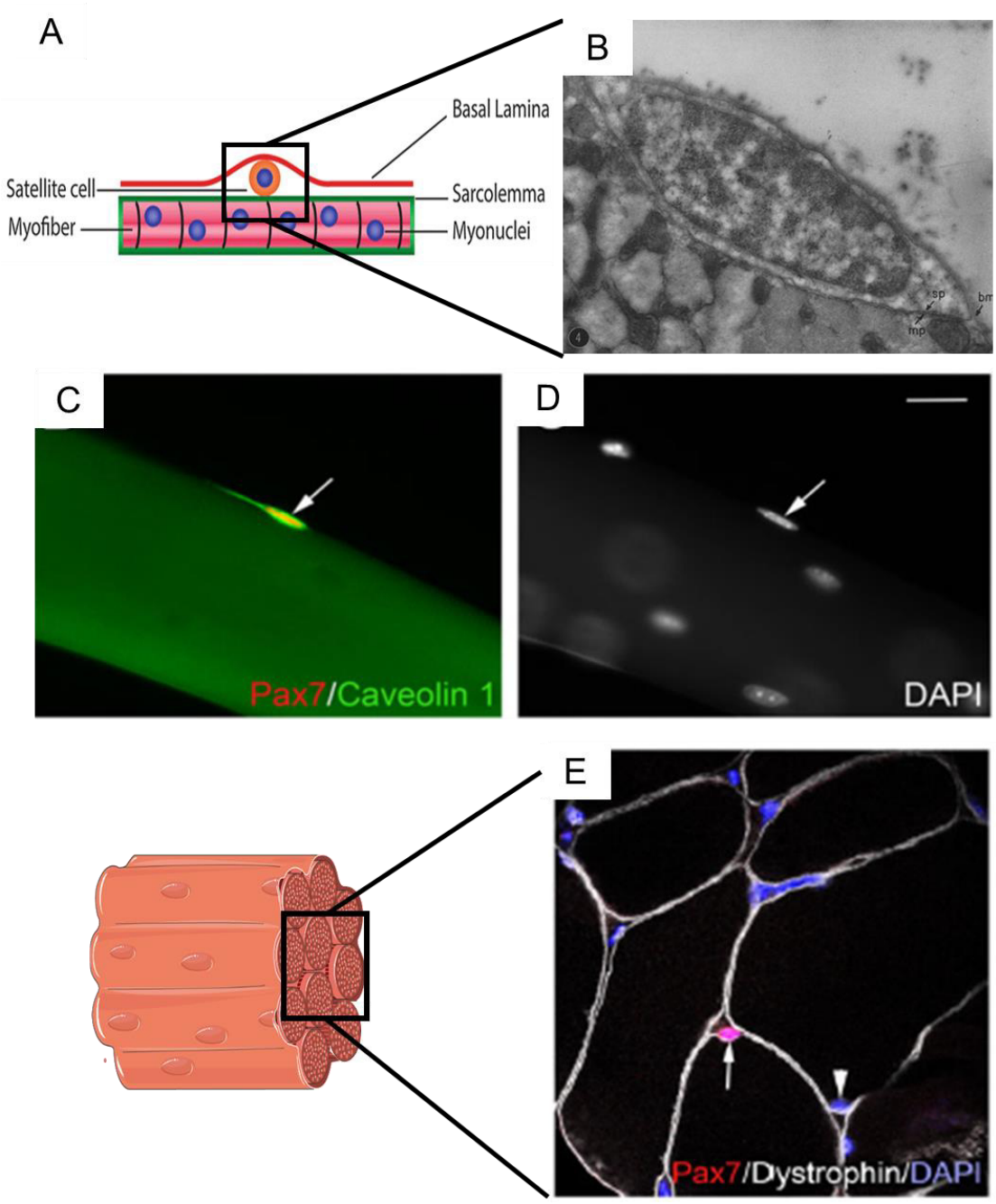

Figure 2: Skeletal muscle cell progenitors – satellite cells
A) Illustrative representation of satellite cell location at the periphery of muscle fibres: between the sarcolemma and the basal lamina of the cell. B) First picture of a satellite cells discovered by Mauro et al., (1960) in the frog (Stained with PbOH. X 22,000. Satellite cell of skeletal muscle fibres. Alexander Mauro from The Rockefeller Institute [19]*). C) Satellite cell expressing pax 7 (in red) in its niche located on muscle fibre edges with D) DAPI (blue) counterstaining showing myonuclei of muscle fibres, scale bar 20µm. E) Transverse section of muscle stained for Pax 7 (red), dystrophin (white) to delimit myofibre membranes and nuclei were counterstaining with DAPI (blue). Arrows indicates pax 7 positive cells and arrowheads DAPI nuclei*
C,D,E adult mouse extensor difitorum longus muscle, pictures adapted from Relaix and Zammit Developement, 2012. doi: 10.1242/dev.069088 [20]

1.1.2 Innervation – control of the contractile process in skeletal muscle

The coordinated contraction of all the myofibres inside the muscle leading to movement is triggered by the nervous system. To do so, skeletal muscle tissue is supplied by nerves known as 'motor neurons'. They establish close contact with each muscle fibre, forming a specialized synapse, the neuromuscular junction (NMJ). Motor neurons enable skeletal muscles to respond to functional needs through the propagation of action potentials that are brief and local reversals of cell membrane polarity. One motor neuron and the muscle fibres supplied are called 'motor unit'. The number of muscle fibres connected to one motor neuron is dependent on each muscle. For muscles that need accurate control, like ocular movements, motor units will be smaller than for posture muscles that do not require precise movements and regroup thousands of muscle fibres for one motor neuron [21].

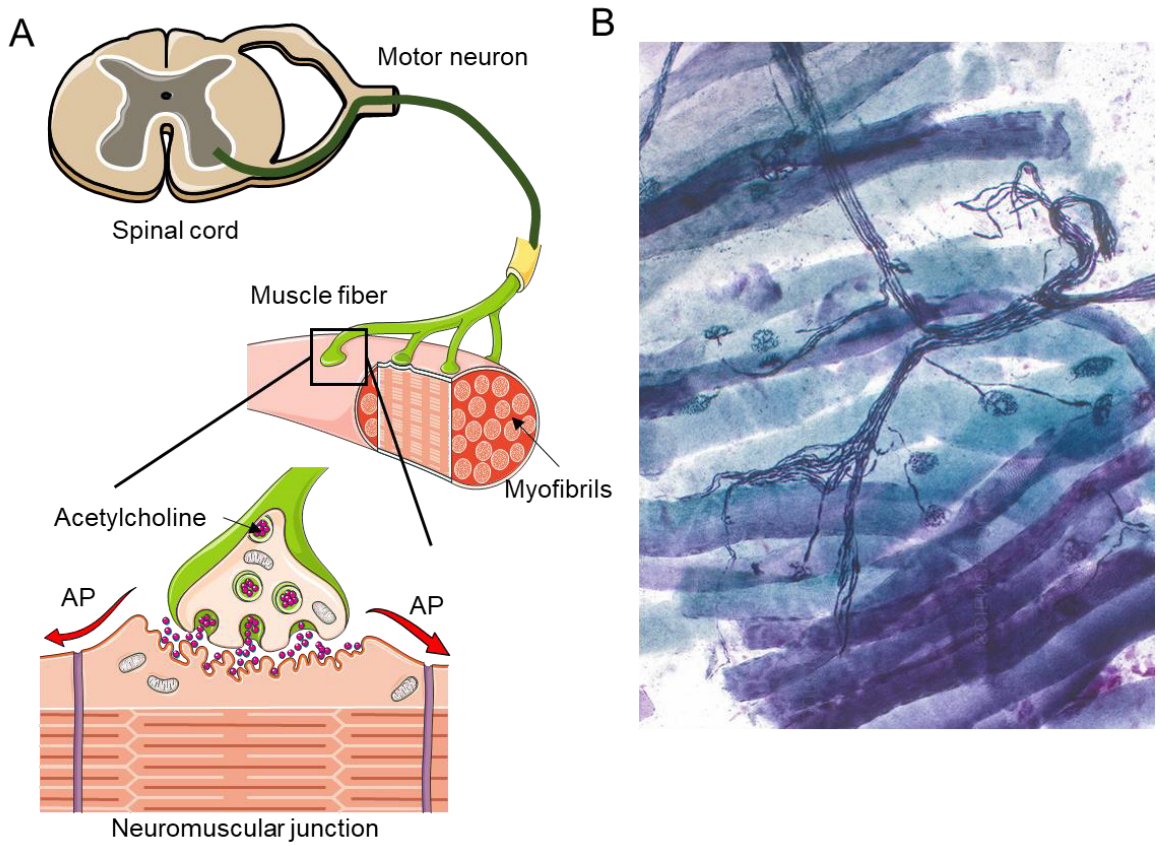

Figure 3: Skeletal muscle fibre innervation by motor neuron
A) Illustration of skeletal muscle innervation.
-Motor neuron are located in the ventral horn of the spinal cord
-Each muscle fibre in skeletal muscle is innervated with motor end plates at the neuromuscular junctions
-Neuromuscular junction with acetylcholine vesicles, acetylcholine receptors, and action potential (AP) migrating along muscle fibre sarcolemma. Adapted from Servier Medical art
B) Motor nerve ending. Picture showing motor nerve ending. Iron Hemotoylin stain, 126X. Light micrograph. Alvin Telser Science Source

When the motor neuron is excited, it propagates an action potential with its axon and its branches to reach all the innervated muscle fibres. This action potential reaches the NMJ and triggers acetylcholine (Ach) release between the nerve ending and the muscle fibre sarcolemma. It generates an instantaneous and local depolarization of the sarcolemma that initiate another action potential all along the sarcolemma to cover the entire surface and depth of the muscle fibre via its invaginations (t-tubules) (Figure 3). Via a calcium release in the cytosol, it leads to sarcomere shortening and contraction through a specific mechanism involving actin and myosin myofilaments that go beyond the scope of this work (reviewed [22]).

To allow movement of bones through skeletal muscle contraction, muscle fibres need to be included inside a functional unit. Therefore, each muscle fibre contains specific chains of molecules including the dystrophin-glycoprotein complex, evenly distributed along the sarcolemma, that connect the contractile myofilament to the extracellular matrix (ECM), which is subdivided into 3 different levels of organization [23] (Figure 4).

1.1.3 The extracellular matrix: the structure supporting muscle fibres organization

Each mature muscle fibre is enclosed within the basal lamina, which is mainly composed of type IV collagen, laminin, fibronectin, and heparin sulfate proteoglycans and is immediately surrounded by the **endomysium**. As such, the endomysium represents muscle fibre immediate external environment and the innermost layer of skeletal muscle tissue. It is crossed by small capillaries and shelter satellite cells (SC) through α7β1 integrin that bind to laminin [24]. Ten to 100 muscle fibres, surrounded by the endomysium, form parallel bundles called **fascicles** surrounded by the **perimysium**. The perimysium is mainly composed of type I collagen [25] and carry larger blood vessels and nerves. It can contain elastin as well [26] but less than 1% of dry weight [27]. All the fascicles, surrounded by the perimysium are then gathered inside the **epimysium** to form the **whole muscle**. The epimysium is the external sheet of the deep fascia and is mainly composed of type I collagen [25] (Figure 4).

All these conjunctive tissues (Endo-, peri- and epi-mysium) emerge to form the **myotendinous junctions** (where the muscle reaches tendon) and anchor the structure to the bone to form the **musculoskeletal system**. These 3 conjunctive tissues convert the muscle into a functional unit and have an effective coordinated function [28]. They represent up to 10% [29] of the skeletal muscle weight. Due to this particular attachment, muscle fibres possess the strength to withstand considerable force. The skeletal muscle ECM is therefore largely involved in force transmission to drive movements [30] and ensure a functional link between the skeletal muscle cells and the bone.

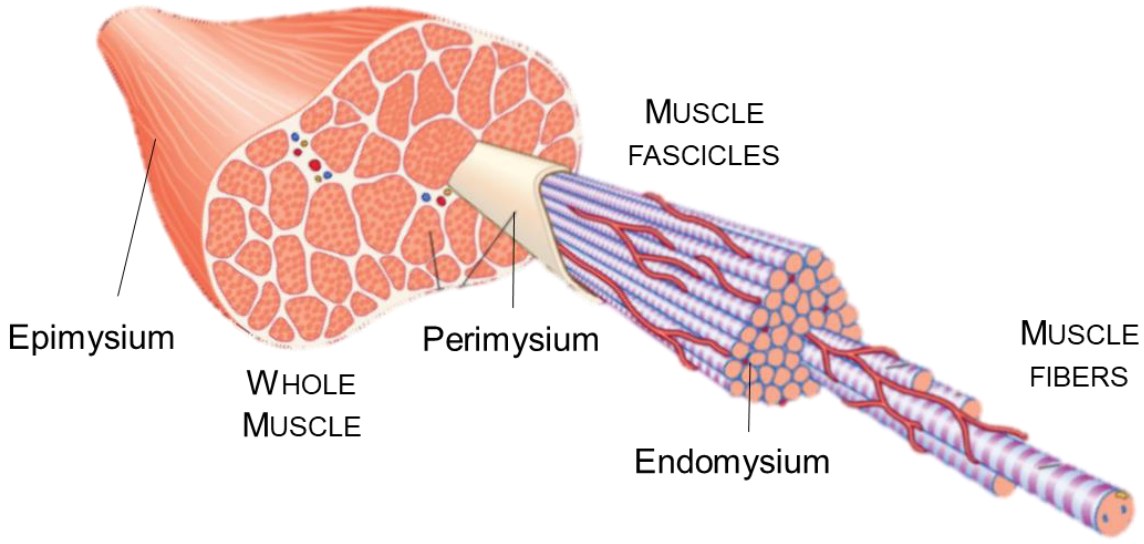

Figure 4: Skeletal muscle structure and organization.
Muscle fibres are the constitutive cells forming fascicles driving the whole muscle organization. Each muscle fibre is surrounded by the Endomysium. Ten to one hundred muscle fibres are organized in bundles to form fascicles enclosed inside the perimysium. All the fascicles are then forming the whole muscle enveloped inside the epimysium. Tissue (cm), fascicle (mm), muscle fibres (µm), myofibril (nm).Pictures adapted from the Gray's anatomy, 2016 edition

Regarding ECM composition, endo-, peri-, and epimysium are mainly composed of collagen (about 9 to 30% of the muscle dry weight [23], [31]), that is present at the gene and/or protein level (reviewed in [32]). Type I and III collagens are the most abundant [25] Type I collagen forms strong parallel fibres that provide tensile strength and rigidity to the muscle while type III provides elasticity through a loose network of fibres. In addition to collagen, elastin is also present at a concentration of 11.1 ± 2.1 µg/ml [33] to confer rubber-like elasticity to the tissue, enabling to undergo deformation without rupture. Inside the ECM network, proteoglycans interact with collagen to maintain the structure and organization of the matrix [33]. They also provide high water content properties to the ECM through negatively charged sulfates enabling water retention. As such, they are able to bind with signalling molecules that are secreted locally to ensure cells and tissue cohesion [34]. The ECM is also composed of glycoproteins such as fibronectin and laminin [31] that interact both with cells and with collagen. Therefore, these molecules represent a link between cells and their direct environment allowing them to communicate tightly through interaction with cell surface receptors [35].

Similarly to other tissues, the skeletal muscle ECM represents a complex meshwork of proteins that provides structural support with unique architecture and mechanical properties. The latter can vary from muscle localization and function in the human body. In addition to stiffness, the ECM structural properties also play a significant role in cell behaviour and fate by conferring them with an optimal environment. For instance, skeletal muscle ECM, when decellularized, exhibits a high interconnected porous structure of about 80% porosity with longitudinal orientation [31] providing directional guidance for muscle contraction. ECM turnover and equilibrium between synthesis and degradation are required for cell migration, muscle fibre formation, and matrix reorganization by the action of remodelling enzymes, the metalloproteinase (MMPs). MMPs are calcium-dependent proteolytic enzymes, present in most tissues, able to remodel the pericellular environment by selectively digesting individual components of the ECM. For instance, MMP-1, -8, -13 can cleave type I, II and III collagens while MMP-2 and -9 degrade denatured type IV, VII and X collagens. Thus, they play a critical role by remodelling the ECM on which cells can evolve, participating in cellular migration. MMPs roles have been described in a range of developmental, functional and pathological processes in skeletal muscle tissue. For example, MMPs act in cell migration and differentiation following injury, notably MMP-1, MMP-2, and MMP-9 [36].

The skeletal muscle ECM and its constant remodelling plays a crucial role to fulfil functions of tissue maintenance, in normal conditions, or during regeneration [37] and inflammatory activities.

To conclude, in physiological conditions, the skeletal muscle ability to contract is highly dependent on a complex cellular organization mediated by the nervous system inside a vascularized and dynamic ECM. Therefore, in pathological or traumatic conditions, the restoration of cells' contraction is linked to the recovery of this specific homeostasis. To do so,

many mechanisms are at play involving considerable cell crosstalk to coordinate myogenesis through ECM remodelling, neovascularization, and restoration of the innervation.

1.2 Biological processes allowing skeletal muscle healing after injuries

Damage to the skeletal muscle caused by direct trauma (e.g. car accidents, sports activities, surgical procedures, and military conflicts) or by indirect trauma (e.g. ischemia) are common. Given its implication in an unlimited number of tasks, it is easy to understand the reason why skeletal muscle integrity is so vital to maintain.

Understanding the mechanisms by which skeletal tissue recovers its homeostasis is crucial to develop relevant treatments and innovative therapeutic strategies. Many studies have utilized different injury models to understand skeletal muscle regeneration. These models include, freeze injuries, crush injuries, or cardiotoxin induced injuries [38], [39]. However, the kinetic of regeneration is highly dependent on the extent of degeneration, the injured muscle type and the animal model. Among the various models, cardiotoxin induced injuries are easy to deliver without requiring a surgical procedure while being reproducible and maintaining the ECM structure. They are based on the injection of a peptide isolated from *Naja nigricollis* venom that induces depolarization of muscle cells and destroys their membranes. These traumatic injuries result in profound histopathological changes and loss of muscle function. Muscle recovery from these injuries requires damaged myofibres to be degraded and replaced through the orderly differentiation of satellite cells (SC). It has thus converted into an interesting model to study the process of regeneration and the cell types involved inside an intact ECM structure [40], [41].

Whatever the method used, the inflammation reaction, the activation of satellite cells (SC), and muscle remodelling are various overlapping phases playing a critical role during muscle repair.

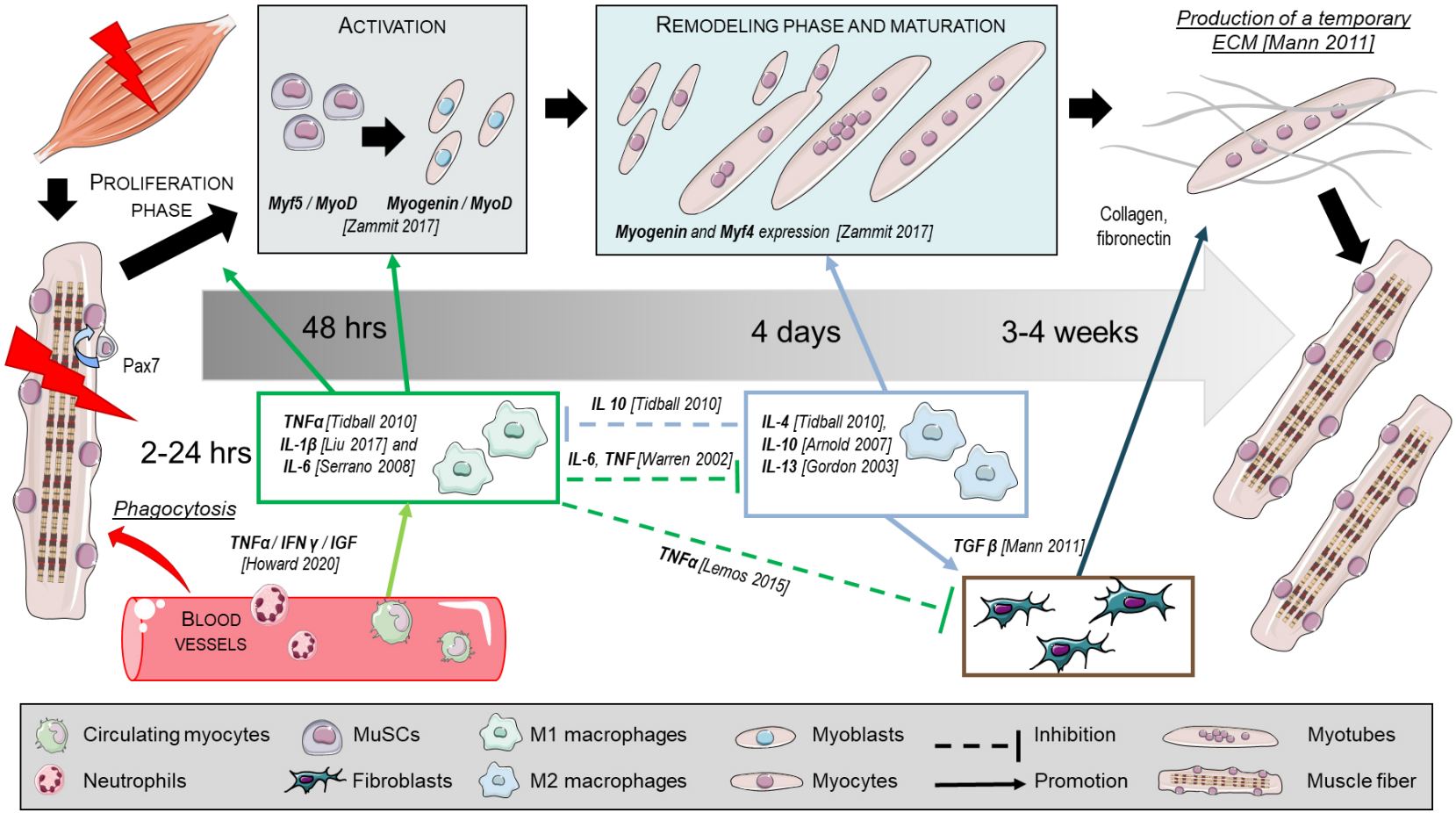

Figure 5: Overall view of various cell populations involved in skeletal muscle regeneration
***Top**: Following injury, MuSCs (particularly satellite cells located on muscle fibre edges and expressing Pax7) leave their quiescent state to migrate within the site of injury and become proliferative myoblasts. They then proliferate and differentiate into myocytes able to fuse together or with damaged fibres to form myotubes that mature to repair the tissue. To do so, various myogenic regulatory factors (MRF) are implicated at various points. Finally, the whole process is possible due to the presence of the ECM acting as a support for stem cells to migrate and myotubes to mature providing stiffness and biochemical feedback to cells. **Bottom**: Other cell populations such as macrophages, monocytes, and fibroblasts are also critical, orchestrating the regeneration process through cytokines and growth factors release. Zammit 2017* [42], *Howard 2020* [43], *Tidball 2010* [44], *Warren 2002* [45], *Liu 2017* [46], *Serrano 2008* [47],, *Arnold 2007* [48], *Gordon 2003* [49], *Mann 2011* [50], *Lemos 2015* [51].

1.2.1 Muscle fibre regeneration process

1.2.1.1 Activation of satellite cells

As the post-mitotic condition of mature muscle fibres prevents them to proliferate [52], myogenic stem cells represent the key component to a successful regeneration program in case of injury or for the maintenance of homeostasis [53]. Particularly, skeletal muscle SC act as a reserve population of cells, able to proliferate in response to injury and give rise to new muscle fibres. Their role is critical as their depletion results in a drastic muscle regeneration impairment [54].

In adult skeletal muscle, SC are localized in niches between the sarcolemma and basement membrane of mature muscle fibres [55]. They are quiescent cells that are specified by the expression of Pax7 marker, a transcription factor involved in embryonic myogenesis. SC are linked to Pax7 since its inactivation has been related to their severe depletion in animal models [56]. In addition to providing the progeny destined for differentiation, SC are able to maintain their population with a self-renewal ability [57] to ensure a constant undifferentiated population. Therefore, in response to injury, SC leave their quiescent state: a pool of satellite cells undergoes self-renewal to ensure niche replenishment, and others become activated by downregulating Pax7. Activated SC migrate from distant undamaged areas to the injury site where they undergo myogenic commitment to become spindle-shaped **myoblasts** [58],[44]. Myoblasts migrate, differentiate into **myocytes** to finally fuse to form muscle fibres *de novo* or with pre-existing damaged fibres. After muscle fibres regeneration, quiescent SC expressing Pax7 colonize again the niche between the sarcolemma and the basal lamina. The time course of SC response to injury in humans has been shown to peak at 7-8 days following injury while a residual elevation was still evidenced 30 days post injury [59]. The myogenesis process occurring during regeneration is simplified in Figure 5.

Given SC behaviour is highly dependent on their microenvironment (niche, neighbouring, and ECM), their proliferation inside wounds is helped by the scaffolds provided by the intact ECM characterizing cardiotoxin-induced injuries. Moreover, one of the major factors allowing successful regeneration is the maintenance of the basal lamina below which SC are located. Therefore, the destruction of the basal lamina or the scaffolds on which cells can evolve can drastically impair the regeneration process by preventing SC migration to the injured site.

Satellite cells are not the only cell type involved in muscle regeneration. Few studies have revealed the implication of other myogenic stem cells during skeletal muscle tissue regeneration, including bone marrow mesenchymal stem cells [60]; an undifferentiated resident population termed muscle-derived hematopoietic stem cells (MD-HSC) and a population of embryonic-like stem cells residing in adult tissues (reviewed in [61]).

1.2.1.2 From satellite cell activation towards muscle fibre maturation, the role of myogenic regulatory factors.

Following their activation, SC experience differentiation towards mature muscle fibres to recover the tissue functionality. Each skeletal muscle fibre is a syncytium that forms as a result of the fusion of hundreds of myoblasts [62]. Myogenic regulatory factors (MRFs) are muscle-specific helix-loop-helix transcription factors (including Myf5, MyoD, myogenin and Mrf4) that are involved in that regeneration process. The time specific implication of MRF in myogenesis during muscle regeneration is simplified in Figure 5.

MyoD and **Myf5** are the first MRFs involved in muscle fibre regeneration. They are mainly implicated in SC activation towards myoblasts and in muscle specification to trigger non-muscle cell (fibroblasts) conversion into muscle [63]. During their activation, SC first express Myf5 while downregulating Pax7 to promote their proliferation to become myoblasts. Then, MyoD expression triggers their withdrawal from the cell cycle and entrance to differentiation. MyoD has been demonstrated to be a key factor in the regeneration process as its depletion in mice markedly impairs muscle regeneration [64]. The transition from activated SC to muscle differentiation to form muscle fibers is linked to the expression of **Myogenin** and **Mrf4**. Before fusion, mononucleated highly proliferative myoblasts exit the cell cycle to become myocytes that are specialized cells possessing the potential to fuse with each other. Expression of myogenin has a crucial role in myocytes fusion enabling them to fuse among themselves forming new myotubes or with existing damaged fibres. As myocytes fuse, they form multinucleated immature muscle fibres with nuclei aligned in the centre of the cells, the myotubes [65]. As myotubes mature into myofibres, contractile units form, which is concomitant with the expression of sarcomeric proteins such as **myosin heavy chain (MyHC)** [66]. New myofibres grow in size through the implication of mrf4 myogenic regulatory factor (also known as myf6) [67], involved in myofilament rearrangement and myonuclei repositioning from a central to a subsarcolemmal position to form the characteristic morphology of adult skeletal muscle fibres.

1.2.2 The inflammatory process

Like for other tissues, directly after the injury, an inflammatory response occurs to orchestrate of the various phase of regeneration. This is the huge interaction between injured muscle and the immune system that regulates skeletal muscle regeneration. This phenomenon has been reviewed elsewhere [44] and is summarized in Figure 5.

1.2.2.1 The role of macrophages

Briefly, right after a skeletal-muscle injury, and regardless of the injury models used [39], an oedema formation and the activation of the complement system [68] trigger immune cell recruitment within the wound. Neutrophils (involved within 2 hours post-injury and peaking between 6&24 hours) participate in the digestion of damaged and necrotic myofibres as well as cell debris by phagocytosis [69]. Soon after neutrophil extravasation into injured muscle, circulating monocytes are recruited and convert into pro-inflammatory M1 macrophages (24 hours post-injury and peaking at day 2 before declining) joined by their epimysium and perimysium resident counterparts. M1 macrophages participate in the inflammatory phase by cell debris phagocytosis and with the release of cytokines (TNFα [43], IL-1β [46] and IL-6 [47]) that drives the apoptosis of fibroblast cells and activates resident muscle stem cells (MuSC) and more specifically, SC proliferation [70]. There is a shift from the inflammatory phase to the remodelling phase through macrophages switching from M1 (pro-inflammatory) to M2 (anti-inflammatory) phenotype [71]. M2 macrophages peak at day 4 post-injury which coincides with the moment when muscle regeneration begins to proceed rapidly and they can persist during the remodelling phase. M2 macrophages attenuate the inflammatory response and promote muscle tissue repair by initiating the early differentiation phase of myogenesis. Macrophages have thus a central regulatory role in the muscle response to injury by removing necrotic tissue and promoting muscle regeneration. Particularly, M2 macrophage depletion can drastically disturbs myoblasts fusion and myotubes maturation through the persistence of high levels of myoD in muscle 4 days post-injury [72]. Therefore, a clear correlation exists between M2 macrophages and regulatory factors for muscle regeneration including MyoD and myogenin which confirms their role in regulating the process of skeletal muscle repair and maturation [46]. The ability of both M1 and M2 macrophages to orchestrate the phase of regeneration is mainly due to their cytokines and growth factors secretion in the wound site.

1.2.2.2 Growth factors and cytokine release

The presence of macrophages and therefore growth factors (GF) and cytokines release can drastically impact the regeneration process in many tissues and organs. In particular, during skeletal muscle repair, GF and cytokines are secreted by damaged fibres or macrophages.

Among these molecules, the release of TNF-α by M1 macrophages participates in damaged muscle fibres proteolysis while promoting SC proliferation and differentiation [45]. However, TNF-α persistence is related to muscle repair impairment by inhibiting the fusion of myoblasts

[73]. In addition, the release of pro-fibrotic molecules (TGF-β) by M2 macrophages has been related to fibroblast activation, which is required for efficient muscle repair. However, the *in vitro* inhibition of SC proliferation and differentiation in contact with TGF- β confirms its role at end-stages of repair highlighting the drastic regeneration impairment it could trigger if released too soon.

These examples demonstrate GF follow a strict release kinetic which perturbation can lead to aberrant repair. Therefore, skeletal muscle regeneration is complex and follows a strict temporal scheme.

1.2.3 The role of ECM remodelling and nerve supply during repair

While there is strong evidence of SC critical role in skeletal muscle regeneration, other cell types are implicated to various stages of the repair process. Among these cells, fibroblasts, macrophages, endothelial cells, and their associated pericytes are major cell types residing in the muscle ECM. While the regulatory effects of pro- and anti-inflammatory macrophages on myogenic cell stimulation and orchestration was previously described, increasing evidence also points to an important role of **fibroblasts**. Aside muscle fibres, fibroblasts are the main cell type present in the ECM. Their depletion in mice has been related to smaller regenerated myofibres due to their suspected interaction with SC dynamics, proliferating nearby at early stages of regeneration [74]. Fibroblasts have also been shown to enhance myogenic differentiation and fusion when *in vitro* cultured in contact with myoblasts [75] confirming their determinant role in skeletal muscle regeneration. Also, the number of fibroblasts in human injured skeletal muscles is increased on day 7 after injury with a further expansion by day 30 (4-time control levels) [75]. The clear increase of fibroblast number can be related to a demand for ECM remodelling and rebuilding. During repair, fibroblasts are activated into α-smooth muscle actin (α-SMA)-expressing myofibroblasts. Myofibroblasts produce ECM components such as fibronectin or collagen that serve as a temporary scaffold to sustain muscle fibres growth and muscle regeneration through vascularization. This scaffold maintains the damaged tissue integrity and bridges the gap between ruptured myofibres [50]. Supported by the newly transient fibroblastic scaffold, muscle fibres form attachments to both native and new ECM, to let the muscle tissue to return to its homeostasis. Moreover, through this temporary scaffold, the tissue experiences the invasion of blood vessels and nerves to enhance tissue ingrowth and myotubes maturation. In addition to provide the framework structure that holds and guides the parallel alignment of myofibres, the ECM has also a role in nerve growth [76]. It has been demonstrated that the ECM interacts with Schwann cells for the regeneration of peripheral nerve and that the presence of collagen participates in nerve growth and regeneration [77]. This is of high relevance as the final maturation and growth of newly formed myotubes require the presence of nerves to be contractile. Therefore, the presence of the ECM during regeneration is critical to mechanically support activated SC and newly generated myofibres

inside a vascularized and innervated tissue. The ECM deposition is under the control of some GF particularly TGF-β, secreted by M2 macrophages at end-stages of regeneration.

Finally, after ECM secretion, it's remodelling and resorption is critical to ultimately recover tissue homeostasis. Therefore, MMPs have a relevant role in skeletal muscle repair by mediating ECM remodelling for scar tissue resorption and function restoration. For instance, MMP-2 is essential quickly after injury given its role in type IV collagen degradation helping myoblast proliferation and thus, new fibre formation [36]. Nevertheless, a too late MMP-2 release can impair regeneration due to type IV collagen degradation of the basement membrane of newly formed cells [78], further confirming the need for a well-orchestrated release of signals for efficient regeneration. In addition to MMP-2, MMP-9 has also been associated with SC activation during the first stage of regeneration [79]. On the contrary, MMP-13 activity *in vivo* was shown to peak at days 15 and 37 post-injury revealing its role in the long-term remodelling of wound connective tissues [80]. All these MMPs participate to the balance between ECM production and degradation to recover tissue architecture and guide regeneration.

Muscle repair can be considered achieved when tissue architecture, vascularization, innervation and ability to contract have been fully restored. For instance, initial forces can be recovered 3-4 weeks after cardiotoxin-induced injuries [81].

1.3 Injuries and diseases overwhelming the regeneration capacity

Despite the rapid and well-orchestrated skeletal muscle repair, the process can be compromised in several pathological conditions, during diseases like myopathies or following severe traumas and infections. Cardiotoxin-induced injuries are relevant to understand the regeneration mechanisms at play in case of the preservation of a scaffold maintaining tissue integrity. However, these types of injuries are not appropriate to study abnormal muscle repair when a destruction of the ECM is experienced.

1.3.1 Volumetric muscle loss

Contrary to cardiotoxin-induced injuries, some severe lesions can overwhelm the regeneration capacity described above. Volumetric muscle loss (VML) for instance, is characterized by a loss of more than 20% of the muscle mass and a destruction of the basal lamina [82]. Injuries with VML result in excessive tissue loss creating defects devoid of matrix, cells, and vasculature. The first major outcome in VML injuries, is the complete destruction of muscle fibres and ECM leading to SC niches deletion. The regeneration capacity, normally governed by SC proliferation, is thus drastically impaired. Therefore, VML regeneration relies on SC still located on wound edges. However, without any support, SC are devoted to stay on wound rims, unable to enter the wound to begin the regeneration program. The histological analysis of these injuries revealed a progressive fibrosis inside the wound with macrophages infiltration and minimal muscle fibre regeneration over time, leading to a marked scar tissue deposition and serious morbidity [83].

1.3.1.1 Normal repair versus fibrosis development

Fibrosis is an unusual deposition of ECM components during wound healing leading to a loss of tissue architecture and functionality. Fibrosis of skeletal muscle tissue is characteristic of severe injuries but also of muscle dystrophies which showed the same set of chronic tissue damage. Fibrosis is the consequence of an excessive amount of ECM inside the wound that can be triggered by an aberrant production of ECM proteins, alteration in ECM-degrading activities, or a combination of both. The fibrotic process usually begins 2 to 3 weeks after injury and leads to the conversion of muscle into non-functional fibrotic tissue. No fibrosis is observed in cardiotoxin-induced injuries after 1 month [39] restricting the model for the understanding of normal repair mechanisms and stem cell properties in these conditions.

As described previously, the presence of fibroblasts is required for an efficient skeletal muscle regeneration process. Fibroblasts secrete ECM proteins [84] to provide the bio-scaffold sustaining SC infiltration and proliferation along with myotubes formation. This transient scaffold is then degraded as regeneration and growth of new myofibres proceed. Although necessary to tissue repair, fibroblasts are critical intermediates to chronic fibrosis. In nature, the survival of an organism depends on the rapid closure of wounds, which are gateways to toxins or infections. Highly proliferative fibroblasts are thus activated into myofibroblasts, to

produce collagen to close the wound. Due to the destruction of the basal lamina below which SC are located, myofibroblasts proceed more rapidly than myotubes formation to close the wound. They create a fibrotic tissue, forming a mechanical barrier inside the wound [69]. During the delayed skeletal muscle regeneration, muscle fibres initiate an attempt at regeneration, which is blocked by fibrosis. Due to the impossibility for muscle fibres to bridge the gap between wound edges, a part of the muscle can remain innervated as the dense fibrotic tissue prevents new axons from reaching the cells (Figure 6) [50]. Given this aberrant repair, VML can result in a lack of functionality of the whole muscle leading to an inability to contract and a decrease in muscle strength generation [85]. The presence of fibrosis resulting from VML can evolve towards permanent disabilities depending on the muscle type and location [86]. Moreover, the fibrotic tissue, lacking the native ECM elasticity renders the muscle susceptible to re-injury [87].

This fibrosis is the result of a complex crosstalk between cells, the immune system, and the ECM. Events leading to fibrosis have been particularly characterized in the case of muscular dystrophies.

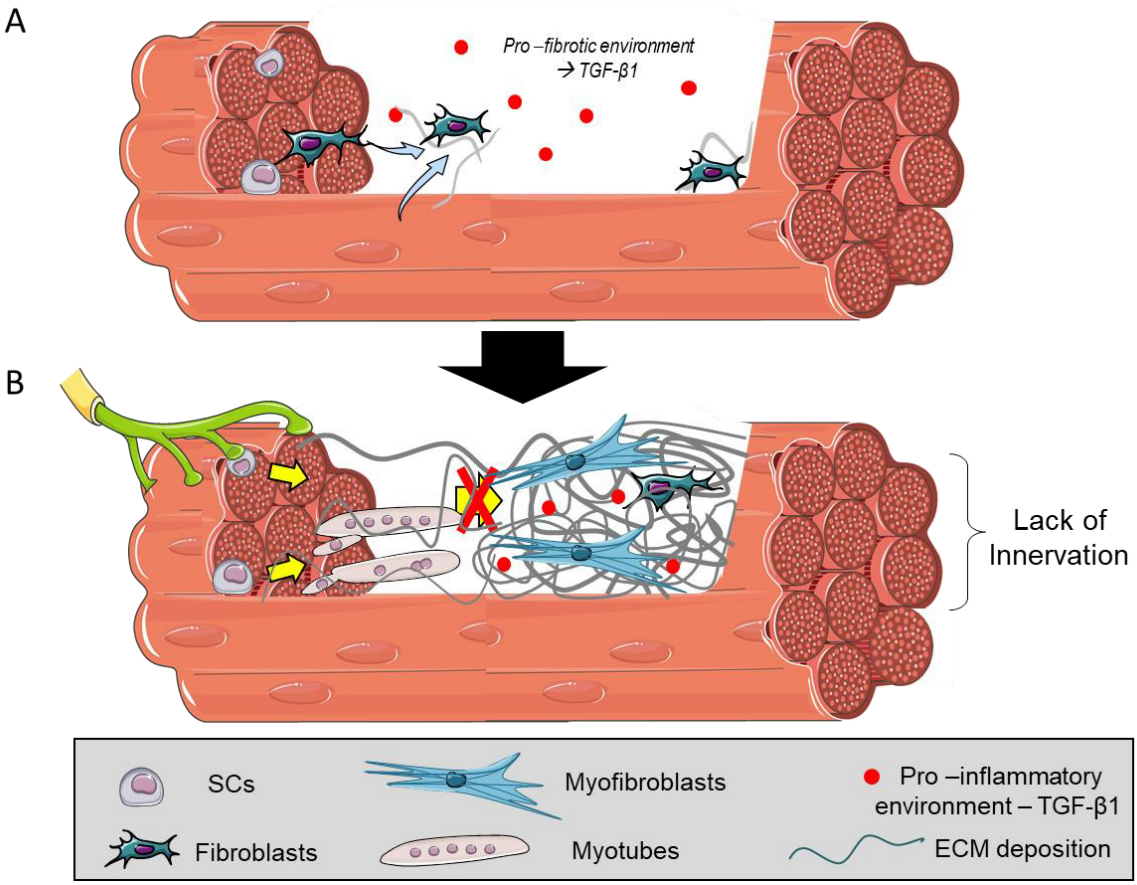

Figure 6: Injuries resulting in VML overwhelm the regeneration process
A) Fibroblasts proceed more rapidly than muscle regeneration to fill large volume defect. The destruction of the basal lamina of muscle fibre, drastically reduces satellite cell number and the lack of ECM their capacity to infiltrate the defect. B) Fibrotic tissue formation prevents the newly formed muscle fibres to bridge the gap leading to a lack of innervation and a loss of functionality.

1.3.1.2 Muscular dystrophies, a model to understand muscle fibrosis

In skeletal muscle, fibrosis is mostly associated with a group of diseases known as muscular dystrophies. Muscular dystrophies are inherited skeletal muscle diseases caused by gene mutations [88]. All dystrophies share common characteristics such as progressive weakness linked to cycles of myofibre degeneration and regeneration and a progressive replacement of the skeletal muscle tissue by fibrotic and fat tissues. These diseases are thus characterized by a gradual replacement of functional muscle with scar tissue [89]. Nine major dystrophies are reported including Duchenne muscular dystrophy (DMD) which is the most severe form. DMD is caused by a mutation in the X-linked dystrophin gene, involving proteins able to link the muscle cell to the ECM. This lack of dystrophin protein decreases muscle fibre sarcolemma stability rendering fibres to be weak and break upon contraction. A mice model of DMD has been developed (mdx mice) in order to study the disease and has been extensively used over the last 30 years [90].

Chronic inflammation

In normal muscle repair, the injury elicits an acute inflammation that leads to dead fibre phagocytosis after damage. In the case of dystrophies, the constant cycles of fibre degeneration is associated with a preservation of the inflammatory infiltrates over time, leading to chronic inflammation. As a result, an accumulation of specific growth factors (GF) and cytokines triggers the fibrosis experienced by dystrophic muscle through pro- or anti-inflammatory cytokine deregulation [91]. The altered expression and secretion of cytokines and GF disrupt cell-cell communication and their resulting behaviour. The ability of SC to repopulate the tissue is then blocked while fibrogenic cells are continuously activated. It has been described that among these factors, TGF-β is highly over-expressed in dystrophic muscles and has thus been considered a major therapeutic target [89]. It is a GF stored in the ECM, and once released, mediates fibroblast activation into α-SMA-expressing myofibroblasts and the decrease production of matrix metalloproteinases (MMPs) [84] having a dual effect on fibrosis. Myofibroblasts are indeed the primary cell source of fibrotic components, triggering an excessive ECM deposition through type I and III collagens, fibronectin and tenascin C expression [92]. These cells also develop stress fibres to generate contractile force and exert tension on their surrounding microenvironment. Recent results have shown that skeletal muscle myofibroblasts can derive from fibro-adipogenic progenitors (FAP), which are a resident population of mesenchymal stem cell-like cells. They have the potential to differentiate into myofibroblasts or in adipocytes depending on the external environment. The presence of chronic inflammation during aberrant muscle injuries or dystrophies is widely accepted to trigger this apparent FAP and fibroblasts disrupted behaviour [84], [93]. Along with TGF-β1, other cytokines such as connective tissue growth factor (CTGF) [94], and osteopontin [95] have be related to fibrotic tissue formation through various pathways. Similarly to dystrophies, the extensive loss of ECM characterizing VML appeared to stimulate complement system and

TGF-β1 signalling in a sustained fashion [96], being the origin of the excessive fibrotic deposition and preventing SC to enter differentiation.

Imbalance between M1 and M2 macrophages

The chronic inflammation experienced during aberrant repair or dystrophies can be powered by the disturbance of the balance between M1 and M2 macrophages [76]. Macrophages being either pro- and anti-inflammatory constitute a heterogeneous population in regenerating muscle as their activities can be opposed and follow various kinetics. For instance, the M1/M2 macrophage imbalance brought by the deletion of IL-10 in mdx mice has been associated with a reduced muscle strength [97].

Particularly, M2 macrophages are generally considered the most important pro-fibrotic regulator through the release of TGF-β1 and several types of tissue inhibitors of MMPs (TIMP). Their presence has been shown to increase with age in mdx mice which was related to fibrosis aggravation [98]. Severe injuries resulting in volumetric muscle loss have also been related to macrophages infiltration [83] and their accumulation and persistence in lacerated mouse muscle accompanied by persistent collagen deposition [50], [99]. These results strengthen the role of macrophages and their cytokine release in the formation of fibrotic tissue. Moreover, their huge influence on SC proliferation and differentiation can be the result of SC inability to reform muscle fibres in aberrant repair due to wrong signals.

The persistent hypoxia

Among the processes leading to fibrosis, hypoxia is also an inducer of the fibrotic program. Hypoxic conditions have been found to enhance the proliferation of human dermal fibroblasts seeded as single cells [100]. More interestingly, fibroblasts *in vitro* have shown to drastically upregulate the secretion of TGF-β1 and collagen when exposed to acute hypoxic conditions [101]. This phenomenon follows a classic healing process. When the tissue is injured, blood vessels break leading to basal ischemia and local hypoxia helping fibroblasts to enter proliferation and close the wound with procollagen synthesis. However, successful healing ultimately requires the stepwise restoration of physioxic conditions through revascularization as high oxygen percentages have been shown to induce fibroblast differentiation into myofibroblasts [102]. DMD patients are susceptible to hypoxia due to sarcolemmal localization of neuronal nitric oxide (nNOS) that plays a critical role in preventing vasoconstriction during exercise [103]. Due to nNOS dependence to the dystrophin-glycoprotein complex DMD patients experience local regions of ischemia during muscle activity that can lead to hypoxia [104].The master regulator of oxygen homeostasis known as hypoxia-inducible factor-1 (HIF-1) has been found to be a major determinant of the healing process [105] with an increased expression in DMD patients [106]. Therefore, the persistent hypoxia in DMD patients can thus notably influence the formation of fibrosis. A parallel can be drawn with VML wound where the ischemia generated by blood vessel rupture is related to a delay in wound healing with a continuous increase of TGF-β1 resulting in scar tissue formation.

The stiffness modification

Finally, the regulation of the tissue stiffness can also be a potent pro-fibrotic signal in multiple tissues [107]. Fibrotic tissues are known to be stiffer than the native skeletal muscle tissue due to ECM deposition rich in fibrillary collagens [108] in a particular organization [109]. Therefore, the mechanosensory behaviour and the signalling cascade of skeletal muscle cells and all the cells involved in muscle fibrosis (resident fibroblasts, inflammatory cells, fibroadipogenic progenitors, pericytes) are influenced [110]. Mechanical forces can also act on soluble factors such as TGF-β1 which is stored in a latent form in the ECM and can be activated as a direct result of mechanical tension [111].

Altogether these signals act synergistically to ultimately lead to the formation of a fibrotic tissue.

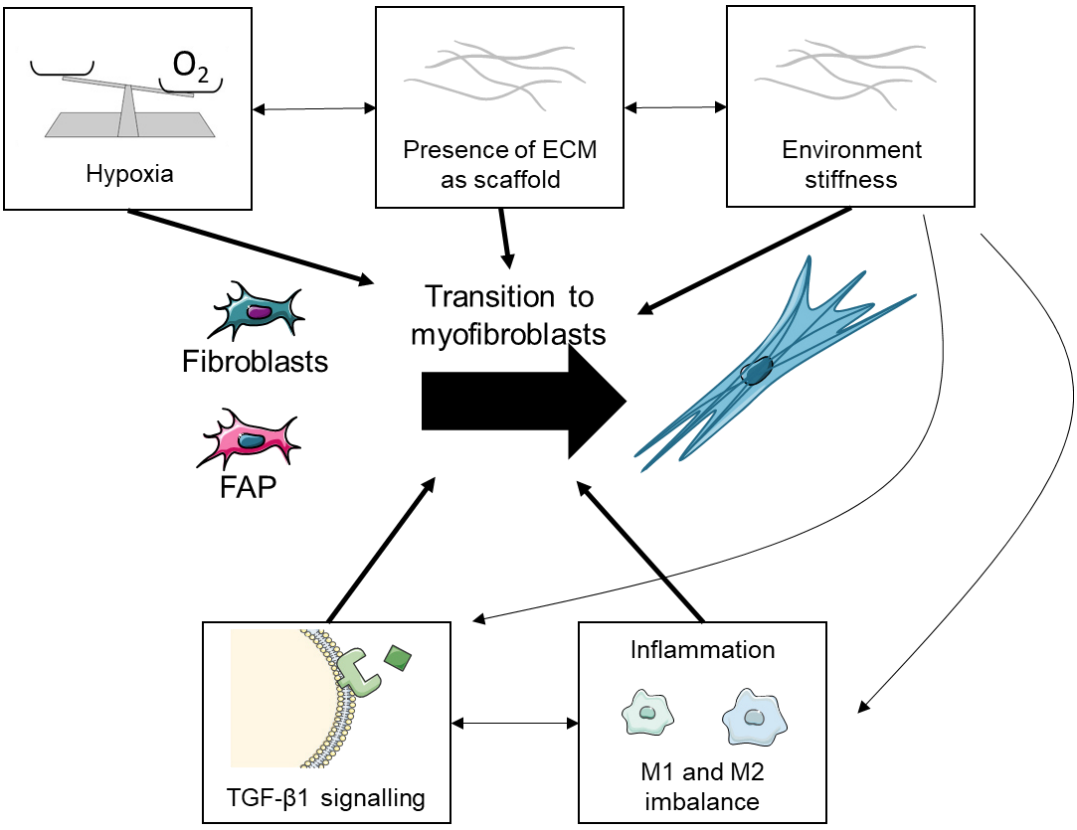

Figure 7 : Some of the key signals influencing the transition of various cell types into myofibroblasts
Various signals (hypoxia, presence of the ECM scaffold as support, environment stiffness, GF signalling and macrophages) can trigger a scar tissue formation in the skeletal muscle tissue and act synergistically.

1.3.2 Current trend and strategy for treatment

Although the treatment of fibrosis in paramount to recover limb functionality, the paradigm of severe injury management is mainly focused on bone healing without considering the importance of soft-tissue repair. For example, the recovery from VML is poor and leads to significant long-term disabilities with an increasing rate of delayed amputation of deficient limbs.

Given the nature of VML injuries, it is of interest to develop therapeutic strategies that could promote muscle fibre regeneration and thus restore muscle strength and function while minimizing fibrosis. The current management options for VML consist of a wound debridement within 12 hours followed by attempts to tissue coverage and the use of advanced bracing. These approaches are unfortunately poor and insubstantial for efficient tissue regeneration [112]. Also, protocols of closure are controversial. Some strategies recommend leaving the wound open after debridement, however increasing chances for contamination, while others recommend the use of muscle autografts/flaps to close wounds [113],[114]. Nonetheless, this option is mainly limited by alterations of anatomy in donor and recipient sites, extensive physical rehabilitation, and a limitation of suitable muscle graft/flap availability [115]. This technique also requires a second surgical procedure that increases the risk of complications and the total cost of the treatment. In addition to all these limitations, it does not carry a guarantee of the full restoration of muscle function and the ability to contract.

There is therefore a need to develop other therapeutic approaches to guide striated skeletal muscle regeneration.

1.3.2.1 The choice of relevant *in vivo* models to assess treatments

For the regeneration of VML, there is a need to evaluate innovative treatments functionality and assess their effect on cells and tissues. To do so, researchers have to target adequate animal models for the preclinical evaluation of these new therapeutic approaches. The requirements of such models are multiple: (1) remove more than 20 % of the muscle mass of a defined muscle to (2) produce a loss of functionality through fibrosis after healing without experiencing (3) spontaneous functional healing or (4) compensation with other muscles. Also, the injury has to be reproducible to generate reliable statistics between treated and untreated injuries. To this end, many groups have developed VML in various animal models with mice and rats being largely used.

The mice tibialis anterior (TA) volumetric muscle loss is a well-spread model to assess the functionality of treatments due to its limited endogenous regenerative capacity, functional impairment and the relatively easy access to the TA [116], [117]. Moreover, the establishment of studies to evaluate the functional recovery can easily be achieve through the testing of animal movement. Other hind limb muscles have been targeted for the same reasons such as the quadriceps [118], [119], with a decreased running speed maintained 6 weeks post-injury

[120]. Other models exploring a VML in the latissimus dorsi of mice have also been reported [121]. However, models based on mice muscles limit the maximal size of the defect and can prevent the validation of various treatments.

Therefore, the use of rats has been fuelled by the need to have animal models with larger defects. The rat tibialis anterior (TA) is a well-spread model to assess the functional of treatments [122],[123]. Wu and others have developed a standardized method to create the defect presenting no spontaneous healing [124]. They assessed a loss a maximal tetanic force generated by the muscle at both 2 and 4 months post-injury. However, they found a 20% loss of the TA weight was associated with a 15% and 17% increase in extensor digitorum longus muscle (EDL) mass after 2 and 4 months post-injury, respectively [124]. Many studies have described this significant compensatory hypertrophy of the rat hind limb EDL after partial or complete removal of the TA [125]. This propensity to compensate TA hinders the clear interpretation of *in vivo* functional repair and, therefore, complicates the assessment and the comparison of treatments for muscle regeneration. Other models have thus been described. For example, Merritt and colleagues have found a defect in the lateral gastrocnemius helped discriminate the amount of regenerating skeletal myofibres and blood vessels between various regeneration strategies [126].
In addition to limb muscles, some researchers have been developing a model of excision of the external and internal oblique layers of abdominal wall [127]. They tested resultant contractile and fatigue force after 26 weeks of implantation and highlighted significant differences between various treatments. However, they did not perfectly assess their model as no negative control without intervention were performed.

To conclude, animal models have been developed in a variety of muscles. Nevertheless, the high cost, the technical complications, and the inability to perform reproducible defects for reliable statistics limit the assessment of treatments made in the field. The lack of a standardized model also limits the comparisons among treatments. The choice of a relevant model still represents an issue for the validation of promising strategies.
However, based on these models, attempts have been made to develop new treatments and test their efficacy. Strategies to improve skeletal muscle regeneration have been mainly based on 2 paradigms: muscle regeneration improvement and/or fibrosis inhibition.

1.3.2.2 Injectable soluble biochemical cues

The main trend for the enhancement of muscle regeneration is the use of injectable soluble biochemical cues.

As previously described, skeletal muscle tissue regeneration is characterized by an extensive cytokine release from inflammatory cells and injured muscle cells. These factors can drastically affect regeneration efficacy when injected in the wound, with instances reported through the injection of IGF (insulin-like factor I and II) [128] or HGF [129] to promote the transition of macrophages to the M2 phenotype. Besides, the administration of exogenous IL-10 to muscle cells *in vitro* has been associated with an increase of the cell proportion expressing myogenin [48] confirming its possible use to enhance muscle regeneration. The use of chemokines like SDF-1α [130] is also of interest as chemoattractant to recruit progenitor cells in the injury site and improve overall regeneration.

Another strategy would be to modulate the biochemical microenvironment in a site-specific manner to prevent fibrosis [92]. The dominant role of TGF-β1 makes it an obvious target for anti-fibrotic treatments [131]. Its inactivation at a specific time or the administration of macrophage-released factors in the wound to stimulate myogenic cell proliferation [132] and regulate fibroblasts could be a way to control subsequent ECM production. TGF-β1 inhibition has been reported with nilotinib, a kinase inhibitor, to reduce muscle fibrosis in mdx mice [51]. It has also been described with interferon-gamma INF-γ that decreased fibrosis and improved muscle strength when injected in a mouse laceration model [133]. The use of IFN-γ, losartan [134], and suramin [135] are great therapeutic candidates involved in various stages of the TGF-β1 signalling pathway and already approved by the FDA [136].

The major advantage in the use of soluble biochemical to treat muscle injury is their easy administration through safe injection. However, GF structural integrity can be severely comprised during injection leading to the need for high concentrations to elicit a measurable effect. Besides, the short half-life of growth factors and cytokines requires multiplying the number of injections and does not prevent their fast clearance by the vascular system [137], [138].

1.3.2.3 Cell therapy

Cell therapy is another reported way to influence skeletal muscle regeneration. It consists of the injection of cells of interest to enhance or guide functional regeneration. Two strategies can be used: (I) cells obtained from a donor that requires an immune suppression treatment or (II) cells obtained from the patient, to prevent further treatments. For instance, cell therapy with exogenous M1 macrophages [99] has been successfully reported. This approach helped to reduce fibroblast proliferation and subsequent collagen accumulation through TNF-α expression while improving regeneration with a force production enhanced after treatment

[139]. On another hand, early anti-inflammatory M2 macrophage delivery has been described to improve myofibre size but along with persistent fibrosis leading to a lower force production.

These strategies though are ambivalent due to the sensitive equilibrium between pro- and anti-inflammatory cues during muscle repair. Boosting the pro-inflammatory phase through M1 macrophages or HGF and IGF administration can ultimately lead to a chronic inflammation responsible for fibrosis. On the other hand, increasing M2 macrophages or anti-inflammatory cytokines involved in cell fusion could be an interesting strategy but eventually result in a higher fibroblast stimulation, M2 macrophages being implicated in fibrosis in numerous tissues [91].

The use of stem cells

To avoid these limitations, injected stem cells are of utmost interest given their high regeneration potential. For instance, bone marrow-derived mesenchymal stromal cells (BM-MSC) injection in muscle defect, has been shown to decrease collagen deposition and increase myofibre diameter in combination with skeletal muscle surgery [140], [141]. As described above, satellite cells (SC) play a significant role in skeletal muscle regeneration and can be isolated [142] to be used for cell therapy approaches. Fluorescence-activated cell sorting (FACS) techniques were developed to isolate SC and their progeny, the myoblasts, from striated skeletal muscle biopsies. These techniques are based on cell surface markers expressed on these cells [143], and enable them to isolate pure populations of human myoblasts from muscle samples. Cell therapy using SC or their myoblast progeny has been extensively described as treatments for muscular dystrophies (reviewed in [144], [145]). However, these examples generally resulted in human trial failure mainly due to the poor survival of injected cells. Finding a way to prevent massive and rapid cellular death during and after injection is one of the primary hurdles for successful cell transfer therapy. The second huge restriction in using cells is, as mentioned above, their origin, compelling the use of immunosuppressive therapy or the burdensome necessity to amplify patient cells before treatment without guarantee of maintaining their undifferentiated state. Therefore, cell therapy remains too restrictive in case of emergency treatments although being promising.

In addition to these drawbacks, the use of cells or growth factors for direct injection in the case of VML results generally in poor integration due to the lack of ECM that guides the regenerative response [146] in addition to massive cellular death and extensive molecule washing by blood. Although these strategies can be operant in small defects, the presence of a large and consistent gap between edges characterizing VML prevents their efficacy.

Given the extensive tissue loss characterizing VML, biomaterial-based technologies that could fill the gap between wound edges hold significant promise for the restoration of functional tissue.

2 Tissue engineering: new insights in skeletal muscle functional regeneration

It has always been the dream of the humankind to be able to restore bodies and ultimately the function of tissues and organs. Recently, whole fields of reconstructive surgery have emerged to improve life quality, with tissue and organ reconstruction being the ambitious goal of regenerative medicine for these last 25 years. It is within this context that the field of **tissue-engineering** (TE) was developed. In the actual situation where organ donor shortage represents an unsolved burden for our society, TE approaches have been heralded as an alternative treatment strategy that may circumvent the limitations associated with auto and allograft procedures. Shalak and Fox at the first tissue-engineering meeting held in 1988 in California defined TE as the application of the principles and methods of engineering and life sciences towards the development of biological substitutes that restore, maintain or improve tissue function. TE principle is based on the postulate that living cells are required to regenerate tissues *de novo*. Accordingly, TE strategies generally combine the use of **cells** within an engineered environment composed of **growth factors** and **biomaterials** to drive functional tissue regeneration in general, and skeletal muscle in particular (Figure 8).

As raised above, the use of cells and growth factors (GF) is of high relevance for the regeneration of tissue but are often associated with cell mortality and GF dispersion in tissues. To overcome these drawbacks, biomaterials have been developed to fill tissue voids, carry cells and GF and enhance cell migration, growth, and differentiation towards an organized, mature, and healthy tissue. Biomaterials are defined as biological or synthetic constructs introduced in the body to interact with tissues and cells for medical purposes (therapeutic or diagnostic). To do so, various types of biomaterials have been developed and characterized including metal, ceramics, polymers, and composites [147]. While ceramics and metal have been largely described for bone repair or bone substitutes [148], polymers have been particularly explored for soft tissue applications. Polymer-based biomaterials, either from natural origin or synthetic, are formulated through physical or chemical reactions between polymer chains to form three-dimensional networks. They can be fashioned into various shapes including fibres, microparticles, 3D bio-printed scaffolds, gels, pastes, and sponges [149], [150].

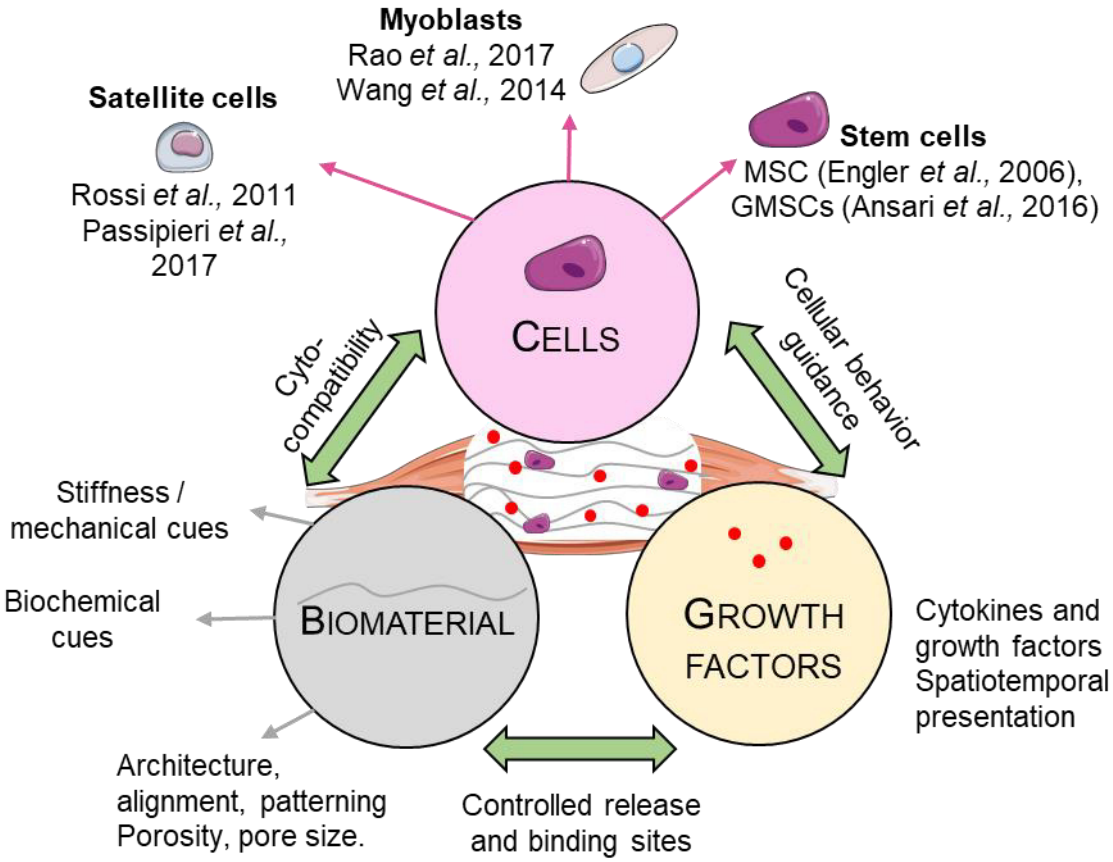

Figure 8: Skeletal muscle tissue engineering (SMTE) combined strategies
Classic strategies rely on the combination of cells and growth factors inside a biomaterials able to mimic the environment encountered in native ECM. Many cell types can be used for SMTE, including satellite cells or their progeny, myoblasts, which are responsible for the maintenance of the regenerative capacity of skeletal muscle. However, their high mortality after injection in the body have prompted researcher to explore the potential of biomaterials to act as template for cells. In addition to be a support, biomaterials crosslinking chemistry can be adapted to allow the binding to growth factors and their controlled release to help cell proliferation and/or differentiation into contractile skeletal muscle. Biomaterials architecture and stiffness modulation can also increase cytocompatibility towards cells.

2.1 Interaction between cells and biomaterials for skeletal muscle tissue engineering purposes

Skeletal muscle tissue engineering (SMTE) using polymer-based biomaterials holds significant promise for functional tissue regeneration. Indeed, it provides a tool to answer the drawbacks of the aforementioned approaches (i.e. cells and/or growth factors (GF) injection). The use of biomaterials could thus act as a cell carrier to prevent their elimination while providing a support on which they can evolve toward mature skeletal muscle tissue. Although being of high clinical relevance, the design of biomaterial for SMTE must answer complex specifications to interact with cells and tissues.

In following paragraphs, we thus focus on existing biomaterial-based approaches developed for SMTE highlighting their advantages and drawbacks. First, the cell types used in these strategies are rapidly reviewed along with the mechanisms by which they interact with their microenvironment. The latter provides signals (including mechanical, biochemical and architectural cues) that affect cellular behaviour and that can be recapitulated by biomaterials. Therefore, the design of biomaterial is quickly addressed for general TE applications, to then emphasis on how they can be adapted to drive cells fate towards skeletal muscle tissue regeneration.

2.1.1 Cells used in SMTE and their interaction with their microenvironment

Considering that skeletal muscle tissue regeneration is highly dependent on stem cells differentiation into muscle fibre, the use of cells has been highly explored. Mostly, TE protocols using cells start with a biopsy to isolate cell populations with a potential for regeneration. Cells are either amplified or differentiated *in vitro* depending on the specific protocol used, to be seeded onto or embedded into a biomaterial scaffold. The cells inside the scaffolds are then placed or injected in VML injury sites to restore structure and function. Whatever the approach used, developing a successful cell-based strategy for SMTE relies on choosing the proper source of cells. Ideally, cells should be easy to isolate, purify, and expand *in vitro* without losing their myogenic potential. Stem cells are widely used in TE strategies due to their ability to self-renew and differentiate into tissue-specific lineages. Protocols to harvest, purify, amplify, and use these cells will not be detailed here as it goes beyond the scope of this work. However, protocols have been reviewed in detail elsewhere [151].

2.1.1.1 Cell types used in SMTE

Muscle-derived stem cells (MDSC) are often considered the best cell source for SMTE because of their unique multi-lineage differentiation potential. For instance, some groups have demonstrated that human MDSC combined with fibrin biomaterials shaped as gel or micro-thread to treat VML injuries could differentiate into new muscle fibres with reduced fibrotic tissue deposition [152], [153]. Particularly, among MDSC, **satellite cells** (SC) are great candidates due to their contribution to skeletal muscle regeneration and homeostasis. They can regenerate hundreds of new muscle fibres when associated with only one muscle fibre [154]. The potential of SC in SMTE has been evaluated in several studies. For example, a hyaluronan-based biomaterial applied to a mice tibialis anterior (TA) muscle defect showed a major structure improvement and an increased number of new muscle fibres when implanted with SC compared with the biomaterial alone [155]. SC have also been involved in mice TA muscle healing when delivered inside synthetic poly(ethylene glycol) (PEG) based support [156]. Hill *et al.* also demonstrated that unlike injected cells alone, SC delivered on alginate scaffolds led to an increase in muscle fibre regeneration in an injured mice muscle model [157], further confirming the biomaterial critical role to restore the tissue.

Fewer studies have also focused on SC progeny, **myoblasts**, showing an interesting potential for regeneration [158]. Among myoblasts, the mouse immortalized cell line C2C12 manages to decrease the variability of primary cell isolation while its use makes possible comparative analysis between research groups. Due to their murine origin, C2C12 encapsulated in scaffolds are meant to be implanted in mice models [159].

Not only SC or their progeny are of interest, for instances **mesenchymal stem cells** (MSC) have been reported in SMTE approaches due to their contribution to skeletal muscle regeneration [160]. After embedding in fibrin and collagen 3D culture models, they could successfully differentiate *in vitro* into myogenic lineage, as indicated by desmin, MyHC, and alpha sarcomeric actinin expression [161]. As for SC, the use of ECM matrices to carry MSC has shown to increase their capacity for functional skeletal muscle regeneration in a defect in the lateral gastrocnemius of rats [126], in comparison to cell injected alone. As a result, MSC exhibit features that are attractive in TE applications linked to their self-renewal ability, multipotency, and secretion of growth factors (GF) and cytokines. Additionally, they can be relatively easily isolated from bone marrow, fat, and umbilical cord tissues [162]. Finally, given MSC pluripotent nature, in addition to their differentiation towards muscle cells, they may participate in peripheral nerve repair and angiogenesis, which both play critical roles in muscle regeneration.

Muscle derived pericytes and **gingival mesenchymal stem cells** (GMSC) have also been successfully embedded inside polyethylene glycol-based biomaterials or 3D scaffolds respectively to guide myogenic differentiation *in vitro* and *in vivo* [163],[164]. These instances

further consolidate the possible use of various cell origins to drive skeletal muscle regeneration.

Various cell types can thus be considered for SMTE, which all need to be collected before re-seeding, amplification and implantation. However, during their amplification, they experience drastic stiffness and biochemical environment differences compared to their native niche, which can alter their ability for regeneration. Consequently, freshly isolated SC contribute more significantly to muscle regeneration than cultured activated myoblasts [165] as their expansion in standard tissue culture plastic results in a loss of their self-renewal capability and clinical utility [166]. Other muscle cell populations including myoblasts or myotubes have been shown to be influenced by the substrate stiffness and composition *in vitro* [166]–[168]. In addition to skeletal muscle cells, Engler *et al.* have demonstrated that substrate stiffness can drive lineage specifications of naïve MSC *in vitro* toward muscle, neurons, or bone [169]. Therefore, to drive cell fate towards skeletal muscle tissue once implanted, biomaterials should be able to reproduce the native extracellular matrix signals experienced by skeletal muscle cells *in vivo*. Accordingly, culturing SC on softer substrates, better mimicking their native environment, could preserve their self-renewal capability and contribute extensively to muscle regeneration when transplanted *in vivo*.

Given the foregoing, the field of biomaterial's design has evolved over the past decades from developing materials that are strictly biocompatible, towards creating those that elicit a specific response from surrounding tissue and cells [170]. Biomaterials designed for TE applications have been shown to interact *in vitro* and *in vivo* with cells and tissues through many signalling mechanisms that can be resumed as **mechanical**, **biochemical**, and **architectural**. By presenting these cues, biomaterials can help cells enter the natural cascade of regeneration. Consequently, unravelling the interaction between multiple micro-environmental factors and cells, as well as understanding the underlying mechanisms by which cells recognize and interact with their immediate and distant environment is of utmost importance for biomaterial development.

2.1.1.2 Cells interaction with their microenvironment

The regulation of interactions between cells and their microenvironment is archived by many mechanisms. Among these mechanisms, signalling molecules including growth factors (GF), cytokines and neurotransmitters can bind to specific receptors on cell membrane to initiate responses. These responses go from gene expression changes to the induction of whole processes such as cell division. Variation in the microenvironment can thus cause perturbations in the cell signalling process and might be associated to multiple pathologies. In addition, cells can respond to their immediate microenvironment through ubiquitous cell surface receptors known as integrins (Figure 9).

Integrins are a large family of heterodimeric transmembrane proteins, formed by non-covalently associated α and β subunits. Integrins bind ECM **ligands** through an extracellular domain and connect to the cell cytoskeleton via an intracellular domain. In humans, the integrin family contains 18 α and 8 β subunits that bind to form 24 αβ subunits, which combination, determine ligand specificity [171]. For example, a great number of integrins (e.g. αvβ3, αvβ1, αvβ5) binds molecules via the arginine-glycone-aspartic acid (RGD) sequence presents on some ECM proteins (such as fibronectin and vitronectin), while α subunits containing an αA-domain (α1, α2, α10 and α11) combine with β1 to form a distinct laminin/collagen binding subfamily [172]. Integrins are particularly involved in cellular adhesion to substrates through a cascade of events starting with conformational changes of integrin ectodomains (low to high-affinity integrins) after recognizing specific amino acid sequences on ECM proteins [173]. Once they have recognized specific ligands, integrins aggregate to form cell focal adhesions points (FA) [174]. At FA, integrin clusters are linked to actin cytoskeleton converting FA into major sites of cell-ECM crosstalk. To do so, structural linker proteins such as talin, vinculin, paxillin, focal adhesion kinase (FAK) and tensin, connect integrins to the actin cytoskeleton [175]. Therefore, integrin clustering allows cell spreading and cytoskeleton rearrangement. Besides promoting cellular adhesion, integrins can transmit information to cells, working as a regulator of cell functions including cell migration and differentiation. Integrins are involved in mediating cell-ECM contact interaction being thus a major mean by which cells communicate with their environment.

Particularly, integrins can be implicated during skeletal muscle cell growth and differentiation. For instance, αvβ3 and αvβ5 integrins are expressed in muscle precursors cells and their blocking have shown to inhibit cell adhesion and migration on supports made of ECM proteins (fibronectin and vitronectin) [176]. Moreover, the αvβ3 integrin and more specifically the expression of β3 subunits, are drastically down-regulated during myoblasts terminal differentiation confirming their role during myogenesis [177]. It also appears that skeletal muscle satellite cells can sense environmental cues through β3 subunits to initiate their differentiation [178]. Indeed, the knockdown of β3 integrin expression triggers a focal adhesion disruption and an actin cytoskeleton disorganization impairing myoblasts migration and

subsequent differentiation [178]. The ECM receptors of the β1 subunit have also been shown to regulate the formation of a protein complex important for myoblasts fusion and to be involved in the assembly of the muscle fibre cytoskeleton [179]. These instances highlight the essential role of integrins and thus environmental stimuli on skeletal muscle cell behaviour.

Therefore, the local environment surrounding muscle cells plays an important role in influencing their fate through cell-ECM communication.

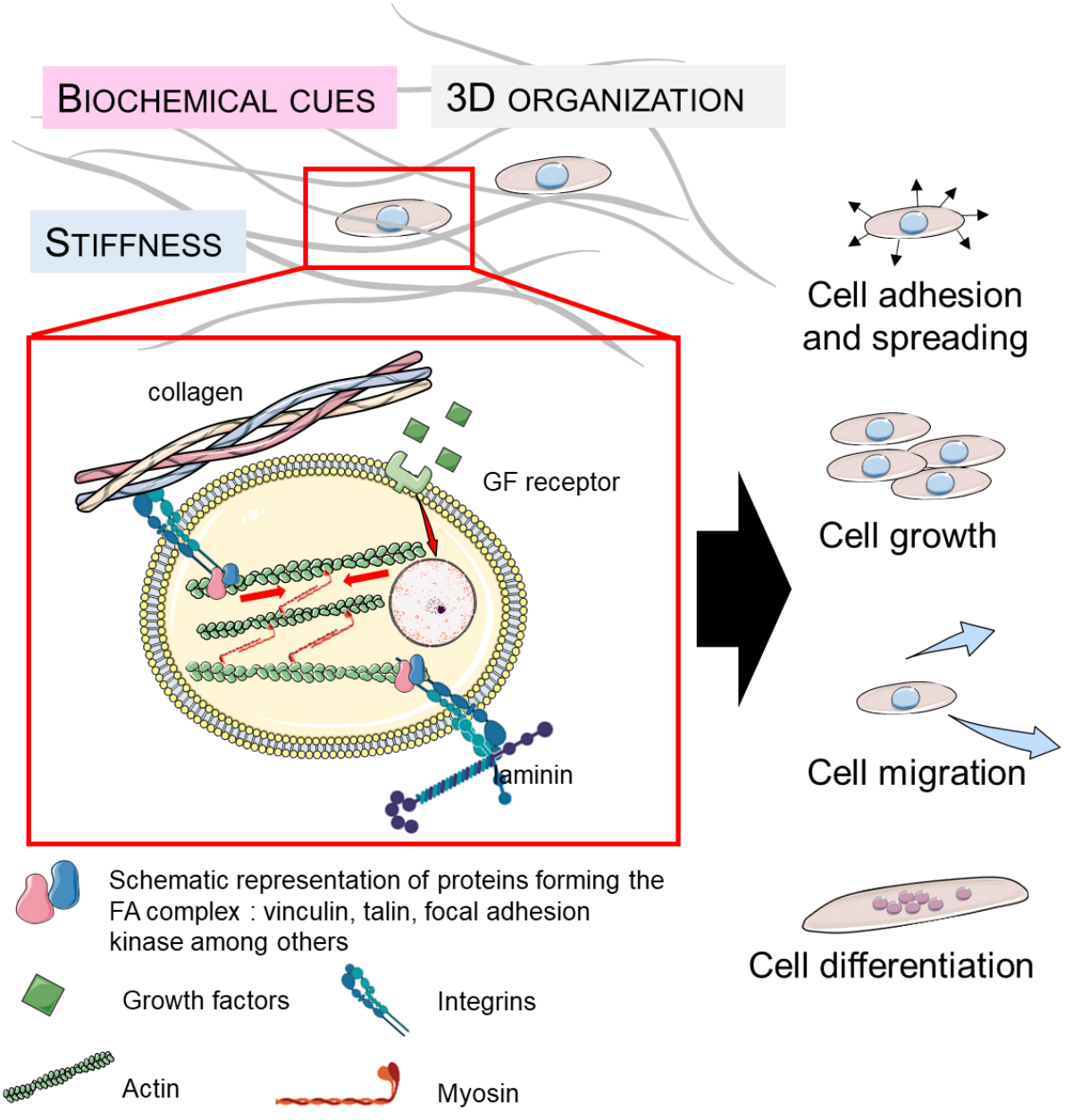

Figure 9 : Cell microenvironmental signals
Cell behaviour can be modulated by various signals, either from their immediate or distant microenvironment. These signals influence cell ability to adhere, spread, grow, migrate and enter various paths of differentiation on the substrate. Pictures adapted from Servier Medical art

2.1.2 Cell response to mechanical cues

Living cells are constantly exposed to mechanical stimuli arising from their immediate external environment. One important environmental factor is the stiffness of the ECM, which has a major effect on cells [180], [181]. The mechanical properties of tissues are highly dependent on their location and their function within the body. For instance, while the brain exhibits a very low elastic modulus of about 1-3 kPa, bone can reach 10 Gpa (reviewed [182]). This provides mechanical information to the surrounding cells and contribute to tissue function.

2.1.2.1 The process of mechanotransduction

Mechanotransduction can be defined as the mechanism by which cells recognize and respond to chemico-physical stimuli to process them into biochemical response or gene expression changes [183]. Various molecules, acting as mechanoreceptors, mediate this sensing process including integrins, stretch-activated ion channels and growth factor receptors [184]. While the precise underlying mechanisms by which mechanotransduction occurs remain so far elusive, it has been described that at cellular FA, cells transduce myosin-generated traction forces from the ECM to the cytoskeleton. Then, a highly complex mechanical signalling cascade leads to global cytoskeleton rearrangements and dynamics events that will ultimately guide their fate. What is currently known is that in response to external stimuli, focal adhesion kinases are recruited in developing FA. Moreover, the increased presence of vinculin [185], talin, and paxillin proteins has been related to the force applied on FA, confirming FA role in force transduction. Accordingly, the variation of substrate stiffness on which cells are seeded can drastically influence their adhesion, morphology and migration [186]. Based on these studies, it seems that tissue-specific progenitors can be differentiated and induced to maturation when cultured on substrates close to their physiological environment.

2.1.2.2 Biomaterials stiffness variation to match tissues requirements

Substrate stiffness has become an essential aspect in the development of tissue-engineered constructs to direct and regulate cell fate. In this context, synthetic-based biomaterials have been extensively described as they can be fashioned through various processing technologies allowing a strict control over their mechanical, structural, and chemical properties. Among synthetic materials, the use of polymers such as poly(acrylamide) (PAAm), Polyethylene glycol (PEG), poly (lactic-co-glycolic acid) (PLGA), Polylactic acid (PLA), Poly (ε-caprolactone) (PCL) [187] and Poly(glycolic acid) PGA have been described for various TE applications [188]. For instance, the stiffness of gels made of polymers such as PAAm can be easily controlled by varying the quantity of acrylamide monomer or bisacrylamide crosslinker [189]. Particularly, PEG [166] or PCL [167] gel-like constructs with tuneable mechanical properties have also been described for SMTE.

Skeletal muscle ECM exhibits a particular stiffness between 5.6 ± 0.9 and 129.1 ± 38.9 kPa depending on the muscle location and method of measurement (see Table 1). The impact of

ECM stiffness during muscle regeneration has been highlighted by the lack of type IV collagen in mice which influences the niche stiffness and causes a reduction in satellite cell self-renewal capability [190]. Therefore, some studies have tried to approach skeletal muscle tissue stiffness with biomaterials.

Table 1: Striated skeletal muscle tissue stiffness
The skeletal muscle tissue stiffness depends on the muscle type, its location in the body, the direction of measurements, and working conditions.

Muscle location	Methods / load	Parameters studied	Elastic modulus	Ref
Biceps	Magnetic resonance electrography	Lateral	**13** ± 4 kPa	[191]
		Longitudinal	**185** ± 60 kPa	
		Shear modulus	**54** ± 34 kPa	
Gastrocnemius and rectus femoris Adolescent under performance	Shear wave elastography	Gastrocnemius Lateral	**11.8** ± 4.7 kPa	[192]
		Gastrocnemius Medial	**9.5** ± 2.8 kPa	
		Rectus femoris	**11.1** ± 2.2 kPa	
Biceps Brachii Young and old adults	Shear wave elastography Young's modulus	90°C elbow flexion	**5.6** ± 0.9 kPa	[193]
		Full extension	**16.9** ± 3.2 kPa	
Upper trapezius Shear modulus Young man	Shear wave elastography	with arm at 0, 30 and 60°C of shoulder	About **10** kPa	[194]
Lateral gastrocnemius Developing child	Shear modulus by shear wave ultrasound elastography	With 20° plantar flexion	**7.1** kPa	[195]
		With 20° dorsi flexion	**36.2** kPa	
Tibialis anterior Adults	Shear modulus supersonic shear imaging	At 20% maximal voluntary contraction	**43.2** ± 12.8 kPa	[196]
		At 60% maximal voluntary contraction	**129.1** ± 38.9 kPa	
Muscle cell layer C2C12 Transverse force	Atomic force microscopy (AFM)	Undifferentiated cells	**11.5** ± 1.3 kPa for	[197]
		8 days in differentiation	**45.3** ± 4.0 kPa	

Ansari *et al.* demonstrated that *in vitro* myogenic differentiation of encapsulated GMSC was only observed inside alginate biomaterials close to the skeletal muscle stiffness (i.e. 10-16kPa) in comparison to softer (<5 kPa) or stiffer (>20kPa) substrates [164]. Similarly, Engler *et al.* have highlighted that myotubes were better striated *in vitro* on substrates with stiffness resembling that of native muscle [198] in comparison with softer or stiffer supports. More interestingly, the same trend has been observed for *in vivo* skeletal muscle injury models. Garcia and colleagues have shown that the stiffness of acid hyaluronic scaffolds was an important parameter to control VML repair by directing SC fate [199]. Given these considerations, various groups have focused their research on the design of biomaterials for VML treatment with controlled stiffness to enhance skeletal muscle regeneration [200],[201].

Although being appealing through their stiffness modulation, synthetic materials often lack cell adhesive motifs preventing optimal cellular adhesion and growth on their surface. Moreover, they can be related to inflammatory responses and long term auto-immunity (after degradation or through prolonged persistence at the injury site) [202]. Therefore, they are generally combined with biocompatible natural-based biomaterials that can present biological cues for cell recognition and attachment such as integrin-binding motives.

2.1.3 Cell response to biochemical cues

One of the most basic and vital cell functions is cellular adhesion to the substrate that can be easily promoted by modifying the surface chemistry of biomaterials with functional groups [203]. Ideally, biomaterials should present these cell-recognition moieties to support cell adhesion and control cell fate through communication with integrins. In many instances, biochemical cues act synergistically with compliant substrates stiffness [204]. Particularity, skeletal muscle cells have revealed to be sensitive to their microenvironment through biochemical moieties and bindings to specific receptors.

2.1.3.1 Naturally-derived biomaterials and matrices

Therefore, the addition of RGD adhesion ligands can be a way to modulate early cell adhesion to engineered substrates. The covalent modification of natural and synthetic polymer-based surfaces with RGD adhesive peptide favoured the recognition and interaction of myoblasts with the substrate [205],[206]. *In vitro* RGD ligand density and distribution have been shown to enhance and regulate myoblasts proliferation and differentiation on surfaces [207].

Naturally-derived polymers have also been extensively used due to their structural similarity to native ECM, which allows them to recapitulate receptor-mediated signals to promote cell adhesion. In addition, these biomaterials are easily degraded in the body and biocompatible. Therefore, using natural polymers to form scaffolds for skeletal muscle injuries has become a well-known research avenue. One of the most common materials used is collagen [208], [120] due to its abundance in skeletal muscle ECM. The use of other ECM proteins such as fibronectin, laminin, elastin or tenascin C [199] or the use of fibrin [161], [116] have also been reported for a variety of SMTE applications.

The use of laminin

Among the aforementioned ECM proteins, **laminin** is of high interest for skeletal muscle cells due to its interaction with SC through α7β1 integrins [24]. Laminin is naturally present in the basal lamina [209] and has shown to have a great influence on muscle resident cell behaviour [210] and myoblasts locomotion and differentiation [211]. Given these considerations, collagen and gelatine sponges functionalized with laminin-111 have been developed, displaying high levels of *in vitro* myoblasts stimulation [212]. Moreover, when seeded on fibrin scaffolds functionalized with laminin, myoblasts increased their synthesis of MyoD and Desmin protein in comparison to myoblasts seeded on their pure fibrin scaffolds counterparts [213]. Cimenci

and others described an acceleration of SC activation with a better myofibre regeneration following injury using laminin nanofibres *in vivo* compared with untreated injuries [214]. Therefore, many groups have used laminin to provide the SC and their progeny adequate stimuli for their differentiation *in vivo* and *in vitro*, [101], [102]. Interestingly, the use of naturally-derived materials can be combined with synthetic polymers to recapitulate both mechanical versatility along with the presence of naturally-derived receptors for cells. For instance, to remedy the lack of functionality that synthetic materials can encounter, poly(etgylene glycol) diacrylate PEGDA biomaterials have been functionalized with laminin to enable a better spread-out morphology of C2C12 compared to the rounded cells forming clusters observed on pure PEGDA supports [217].

The elastin, a step towards providing both biochemical and mechanical cues

Some ECM proteins have the dual role of providing mechanical strength and interact with cells. Collagen, for instance, provides tensile strength to a variety of tissues while binding with cells through integrins [218]. In addition to strength, the flexibility and the elasticity are essential requirements in many tissues and organs of the body and particularly in skin, lungs, or arteries, in which high deformations are required [219]. The major source of elasticity in tissues are elastic fibres. Elastic fibres consist of insoluble fibrillary structures made of around thirty ECM proteins that assemble to confer long-range deformability to connective tissues, complementing collagen tensile strength. These properties are critical for dynamic organs and tissues that undergo repeated cycles of extension and recoil [220]. In vertebrates, elastic fibres synthesis involves deposition and assembly of tropoelastin, the elastin monomer, upon microfibril structures to form mature elastic fibres. Besides their unique elastomeric properties, tropoelastin assembly, and presence in ECM influence cell growth and tissue homeostasis [219]. The mediation of the interaction of tropoelastin with cells has been mainly attributed to the elastin binding protein (EBP), which recognizes the pentapeptide GXXPG (in which the X can be substituted by any amino acid except proline) located in domain 24 of tropoelastin [221]. Weiss and colleagues proved that soluble tropoelastin also interacts with cells through a binding site encompassing the domain 36 known as RKRK motif able to bind to cells in a divalent cation–dependent manner through integrin αvβ3 [222], [223]. Moreover, Broekelmann and others identified a cell interaction site at the C-terminal of tropoelastin that binds cell glycosaminoglycans including heparan sulfate and chondroitin sulfate [224]. In addition to the C-terminal tail of tropoelastin, cells can interact also in a divalent cation-dependent manner with integrin αvβ5 between domains 17 and 18 located in the centre of tropoelastin [225].

As such, the use of elastin-based biomaterials is promising to reproduce the natural elasticity of tissues and provide more relevant biochemical cues to cells [226]. Some instances have reported the use of recombinant human tropoelastin to form 3D scaffolds by electrospinning for dermal tissue engineering purposes [227]. Others highlighted the potential of a α-elastin gel-like biomaterial for soft tissue engineering applications [228].

Elastin sources

Although elastin is an essential protein for ECM structure and properties, it remains under represented in biomaterials given its difficult purification and its calcium affinity when extracted from animal sources [229]. Moreover, elastin's insoluble nature precludes its manipulation. Researchers have thus considered soluble sources of elastin for elastin-based materials through constructs reproducing selected parts of elastin. Particularly, elastin-like polypeptides (ELP), synthesized either chemically or by recombinant techniques have been promising biocompatible candidates for TE applications [230]. ELP are biological polymer oligopeptides based on the repetition of an amino acid sequence, VPGXG, in which the X can be substituted by any amino acid except proline. This sequence is the most frequent in native elastin and confers its hydrophobic behaviour.

In particular, a group has recently shown that recombinant elastin-like polypeptides can enhance myoblasts adhesion, proliferation, and differentiation when grafted on plastic dishes [231]–[233]. Given their ability to stimulate myogenesis, ELP were enzymatically crosslinked, providing a successful step toward the development of elastin-based biomaterials for skeletal muscle tissue engineering [234]. These biomaterials have been able to recapitulate the rubber-like elasticity found in native tissues and to interact with cells combining both biochemical and mechanical cues.

The use of Matrigel

Given that naturally-derived moieties are interesting for the behaviour of cells, Matrigel®, secreted by Engelbreth-Holm-Swarm (EHS) mouse sarcoma is also appealing as a biomaterial [235]. Matrigel is a complex environment resembling basal membrane ECM that contains niche factors such as laminin, type IV collagen, and heparan sulphate proteoglycans along with growth factors that greatly improve muscle regeneration by both the maintenance of $Pax7^+$ cells and the increase of $MyoD^+$ cells [236]. The use of matrigel *in vitro* has been related to myotubes formation enhancement with greater myoD and myogenin expression [237]. Due to its beneficial impact on tissue growth, matrigel has been largely used *in vitro* for the formation of bioartificial muscles (BAMs) [238], with collagen to regenerate chemical injuries [239] and to fabricate electrically stimulated contractile tissue-engineered skeletal muscles [240]. Particularity, in Vincent Gache group at the NeuroMyoGene Institute, the use of matrigel layers surrounding mice primary cells have been developed to mimic a propitious environment enhancing the maturation of myotubes with contractile units similar to what is observed in mature myofibres. This *in vitro* model enables them to maintain contractile myofibre layers up to 10 days to study proteins involved in muscle fibre formation and maturation with a special focus on nuclei repositioning and cytoskeleton rearrangement. However, despite its excellent cytocompatibility, by providing a great ECM substitute for cells *in vitro*, matrigel's malignant source derived from murine sarcoma makes it unsuitable for clinical application with no potential for translatability.

2.1.3.2 Biomaterials as growth factors vehicles

In addition to the biochemical cues provided by the immediate microenvironment, cells are also receptive to soluble factors. Growth factors (GF) and cytokines are among some of the most commonly investigated molecules to enhance skeletal muscle functional regeneration and prevent fibrosis. In this context, some scaffolds have been engineered to carry GF by encapsulation, absorption, or binding. GF are naturally stored by ECM glycosaminoglycans (GAG) through non-covalent interactions or are bound to ECM proteins. Some biomaterials have thus recapitulated these bindings with heparin sulfate-mimetic decorated scaffolds [241] or collagen based scaffolds [161] that present GF-binding motives. The use of biomaterials to control GF release is attractive as they can serve as carriers, protecting GF from early degradation or clearing while allowing a controlled release over time. Once carried by scaffolds, GF can influence embedded cell differentiation and help them to regenerate muscle tissues. Many instances have been described in literature for SMTE, with IGF-1, HGF, or FGF being largely used due to their critical role in stimulating SC recruitment, proliferation, and differentiation during muscle repair [242], [243]. For instance, alginate matrices have shown to better promote the survival and migration of transplanted primary myoblasts when the scaffolds delivered GF (HGF, FGF2) during cell activation [157], [244]. Tomblyn and colleagues reported the high potential of a keratin scaffold as a muscle progenitor cell carrier together with controlled release of VEGF, IGF-1, and bFGF for skeletal muscle regeneration [245].

The use of GF has also been reported to enhance host cell recruitment inside acellular scaffolds after implantation. Ju and others have highlighted that muscle formation within an acellular gelatine-based scaffold was significantly accelerated in presence of IGF-1 loaded scaffolds. This tissue acceleration could be related to a better SC recruitment as they showed a higher presence of Pax7+ muscle cells in IGF-1 loaded scaffolds [246]. Grasman and colleagues further emphasized this trend by demonstrating HGF loaded fibrin micro-thread scaffolds significantly enhanced muscle tissue regeneration after 60 days [247]. These results were correlated with a higher presence of myogenin positive cells within the HGF loaded scaffolds compared with their non-loaded counterparts. Passipieri *et al.* went further, showing that keratin gels-like biomaterials loaded with GF (i.e. IGF-1, bFGF, or a combination of both) were more relevant to sustain functional recovery than scaffolds embedding skeletal muscle progenitor cells in skeletal muscle injuries in rats [248]. However, while promising results have been reported, the expensive nature of GF together with the need for extensive clinical trials to ensure their safety have slowed their progress towards clinical applications.

In conclusion, biochemical cues provided by the biomaterial are important regulators of cell behaviour. Therefore, in the last decades, development of polymer-based biomaterials has been mainly focused on the choice of relevant polymer precursors to provide adequate biochemical and mechanical cues to interact with cells and/or GF.

2.1.4 Cell response to architectural cues and topography

Besides mechanical and biochemical cues, architectural 3D organization of the ECM, in which cells are embedded, provides them with another feedback. While the exact role of the surrounding 3D organization toward cells still remains unclear, some efforts have been made by the scientific community to understand underlying processes and further mimic invivo conditions.

2.1.4.1 Influence of 3D organisational signals on cells

The 3D architecture has a profound influence on cell behaviour as evidenced by the effect of ECM fibre architecture during tumour development and disease progression [249]. Szulczewski and others demonstrated that organizational and mechanical signals provided by local environments acted synergistically on resulting cell comportment [250] highlighting how 3D organization of the ECM may affect the way the matrix deforms due to force produced by cells. This can be related to the fact that cells fully embedded within 3D matrices form fewer FA clusters compared with cells in 2D substrates. Despite the reduction of FA in 3D, proteins involved in integrin communication are found dispersed throughout the cytoplasm, modulating cell demeanour [251]. More interestingly, curvotaxis has been recently identified to be the cell's ability to respond to curvature variation, as a new physical cue affecting cell FA organization and gene expression [252]. It has been showed that cells naturally migrate toward the environment exerting less mechanical stress on their nuclei [253], extending the knowledge of the stimulus able to drive cell behaviour. Altogether, these instances highlight that dimensionality of cell-biomaterial interaction has a huge impact on cells and must be taken into consideration in biomaterial design, particularly for skeletal muscle tissue regeneration.

2.1.4.2 The use of decellularized extracellular matrices

To encompass biomechanical, biochemical, and architectural cues, a potential strategy consists in using decellularized ECM as biomaterials. They are natural scaffolds derived from tissues in which cellular contents have been removed while preserving the 3D ECM structure and composition. Decellularization of tissues can be achieved by soaking them in detergent mixture and chloroform for several days to remove cellular content and extract lipid, respectively [254]. Such scaffolds retain partly the biological activity and native ligands of the native tissue while maintaining the ECM anisotropy. Moreover, due to their degradation by immune cells, they can release native GF and ECM proteins, promoting host cell infiltration.

Decellularized scaffolds have been studied as promising candidates for VML treatment by retaining ECM native structure and grooves between muscle fibres able to naturally guide cell differentiation (reviewed in [255]). For example, the use of skeletal muscle decellularized ECM was linked to an extensive recovery in a rat lateral gastrocnemius injury model [256] by supporting muscle regeneration and reducing fibrosis compared with a collagen-based biomaterial or with autograft implantation (clinical standard) [257]. Other groups have

described the use of decellularized porcine small intestinal submucosa ECM [118] with complete functional recovery after 6 months implantation in a rodent abdominal wall model in comparison with synthetic-based biomaterial [127]. Due to promising results in animal models, decellularized ECM scaffolds have been clinically evaluated for VML treatment. Mase and colleagues provided the first instance of a biologic scaffold composed of porcine small intestinal mucosa ECM for the functional regeneration of VML from military trauma [258]. They described a gain in strength and endurance of the targeted muscle 4 months after the surgery. In addition, Sicari and colleagues implanted porcine urinary bladder ECM in five male patient muscles presenting a minimum 25% functional and structural deficit. After 6-months of implantation, three of five patients presented a 20% functional improvement of the affected limb linked with the presence of desmin^{+} skeletal muscle cells and vascularization inside the decellularized scaffold [259]. These studies showed that decellularized ECM may serve as scaffolds to promote skeletal muscle remodelling without administration of exogenous cells. This further consolidate the relevance of recapitulating all the signals experienced by cells *in vivo* to regenerate skeletal muscle tissue.

To conclude, decellularized scaffolds provide promising results in the design of inductive niches avoiding regulatory barriers associated with embedded cells, and potential cell-related immune response. However, the origin and availability of decellularized scaffolds still raise questions for a VML standardized treatment and their clinical use remains limited by outcomes and variability among patients. In addition, decellularization processes and lipid extraction need to be improved to avoid possible modification of the scaffold biochemistry interacting with cells.

2.1.4.3 The use of manufactured macroporous scaffolds

Due to the drawbacks associated with decellularized scaffolds, various approaches have been developed to design and produce scaffolds that recapitulate mechanical, biochemical and architectural signals encountered in native ECM. Since 2D substrates inherently misrepresent the in vivo behaviour of most cells, there has been a shift towards 3D tissue culture systems using biomaterials. Additionally, for tissue engineering purposes, a porosity inside biomaterials is an asset to sustain the migration of cells inside the scaffold and potentially regenerate the tissue de novo. Furthermore, porosity appears as well critical to allow vascular infiltration and nutrient and oxygen diffusion along with waste disposal to prevent necrosis in central regions of implanted biomaterials.

Macroporous scaffold requirements

Many strategies rely on the creation of porosity and pathways inside biomaterials to better mimic the *in vivo* environment while sustaining cellular infiltration. As the physical architecture varies drastically between tissues and has a profound impact on its properties, porosity modulation has become a potential approach to improve and enhance tissue formation and function. Numerous cell types have been shown to behave differently depending on the final **pore size** generated inside a biomaterial in terms of cell infiltration, proliferation, migration, and differentiation [260],[261]. For instance, pores ranging from 100 to 200 µm have been proven to be the most effective in developing myotubes for skeletal muscle regeneration [262], [263]. On the other hand, pores of 300-400 µm facilitated osteoblasts infiltration and mineralization in bone tissue engineering approaches [264], [265], while pores between 80 and 120 µm were particularly interesting for chondrocytes proliferation and ECM production [266]. In addition to pore size, pore interconnectivity, which is the pathway between pores (voids linking one pore to another), is required to enable cellular movement inside the scaffold. The size between pores should be suitably large for cellular migration in the initial stage and is thus as critical as the pore size. Consequently, optimal pore size and windows of interconnections are dependent on the tissue organization and cell types as cell size may drastically vary from 2-7 µm for erythrocytes to about 100 µm for osteoclasts [267]. Pore size and windows of interconnection should allow cellular and vascular infiltration but should not be too large to prevent a significant decrease of the specific surface area or the production of weak scaffolds unable to sustain load-bearing mechanical strain. Indeed, porous biomaterials should achieve sufficient stiffness and strength to provide adequate mechanical integrity to the tissue.

Instances of relevant macroporous scaffolds for SMTE

The formation of a porosity inside biomaterials is thus relevant for many applications and particularly for SMTE, since muscle fibres must form over long distances (12 cm for the longest muscle fibres in the human body [268]). Considering myoblasts alignment is an essential step during regeneration and remodelling, many methods have explored the inducement of an oriented porosity inside biomaterials with patterned surfaces. Jana *et al.* have shown that scaffolds closely mimicking the native organization of skeletal muscle ECM are of relevance for the design of tissue-engineered constructs (reviewed [269]). For instance, scaffolds fashioned by **casting processes** on moulds with unidirectional channels have been reported using gelatine [201] or collagen [270]. The longitudinal orientation of channels has been shown to greatly influence myotubes width upon fusion by the maintenance of their alignment. For example, micropatterned 2D supports with 200-380 µm concave microgrooves could guide the unidirectional contraction of myotubes *in vitro* [270]. However, while these techniques remain attractive to understand and guide myotubes growth or form pre-patterned cell sheets, they present huge limitations to be used *in vivo* due to the lack of complete 3D architecture (Figure 10A).

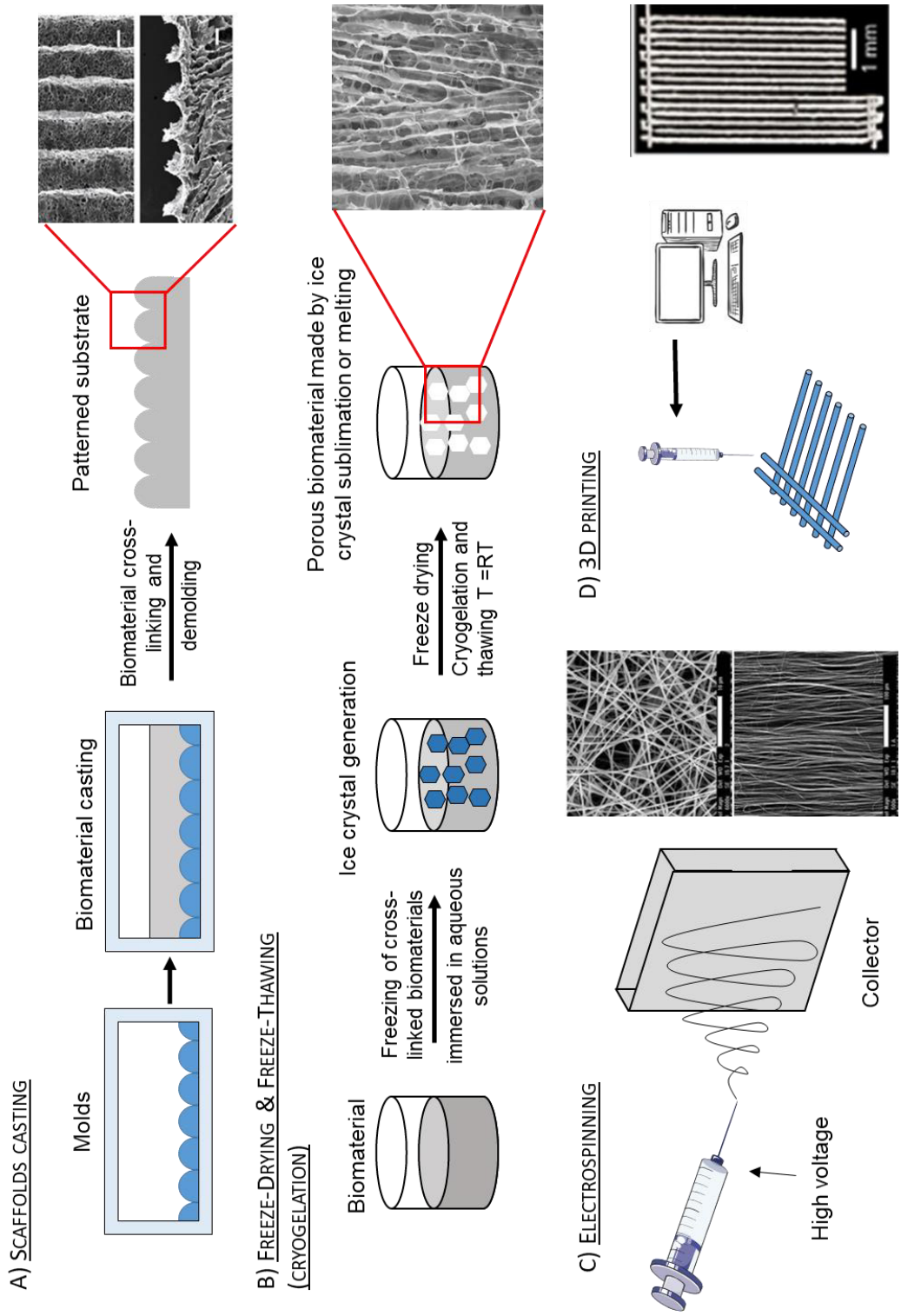

Figure 10: *Some of the methods reviewed in this work to create an oriented porosity inside biomaterials A) Scaffold casting can be simply achieved by pouring biomaterials liquid precursors in a mould with unidirectional channels. Picture adapted from Chen et al., 2015, Biomaterials* [270]*, B) Unidirectional freeze drying methods are based on the cooling and freezing of aqueous dispersion inside crosslinked biomaterials using a defined temperature gradient. The resulting unidirectional ice crystals are then sublimed to form a porous structure. Picture adapted from Kroehne et al., 2008 J. Cell. Mol. Med.* [271] *C) Electrospinning and D) 3D printing can form biomaterials of complex shapes with spaces allowing cellular infiltration inside a highly oriented structure. Pictures adapted from C) Montero et al., 2012 Acta biomater* [272] *and D) Kim et al., 2017 ACS applied Mat and Interfaces* [273].

The creation of interconnected porosity inside scaffolds can be achieved by various approaches. One of these strategies consist of controlling the formation of ice crystals inside biomaterials through the progressive cooling the aqueous components, followed by their removal by sublimation (**freeze-drying techniques**), or by thawing (**cryogelation**) to create pores (Figure 10B). Sponge-based scaffolds obtained from these techniques have been associated with a decreased scar tissue formation and an increased number of muscle fibres when implanted into a partial resection of the vastus lateralis muscle in a rabbit model in comparison with the untreated injury [274]. This paper showed that crosslinked collagen shaped like 3D sponges with pore diameter ranging from 50 to 100 µm sustained efficient autologous cell recruitment for regeneration. In addition to collagen, Elowsson and colleagues have described a casein/gelatine interconnected porous scaffold with a pore size of 10 -80 µm by cryogelation with potential to be used for SMTE [275]. Another example described freeze-dried porous sponges also made of a mix of gelatine, collagen, and laminin able to sustain an extensive autologous cell infiltration and differentiation in a VML mouse model after 2 weeks of implantation [212]. This could be explained by a highly interconnected porosity of pores from 63-84 µm in diameter and a high porosity percentage of 93%, increasing the available surface for cells. While they presented limited muscle fibres regeneration, the scaffold protected the remaining muscle mass from chronic injury further sustaining the importance of biomaterials not only as matrices for cell infiltration but as mechanical support for the injured tissue.

More interestingly, by varying the freezing kinetic and applying a uniaxial temperature gradient, the porosity inside biomaterials and sponges can be controlled and oriented with interconnections. For example, 3D scaffolds with aligned tubular structures using freeze-drying techniques have been described with chitosan [276] or collagen [271] crosslinked polymers, providing early orientation cues to obtain more mature and larger myotubes.

Electrospinning has also gained significant attention in the past few years in the field of TE applications [277], [278]. The technique is based on the application of an electric field to draw fibres from a polymer solution towards an oppositely charged collector (Figure 10C). The applied voltage or viscosity of the solution can be modulated to control the resulting porosity created by the voids existing between fibres, forming interconnected pathways on which cells can migrate. In addition, the resultant electrospun nanofibres specific orientation and structural similarity to the native morphology of ECM makes them especially interesting for biomedical applications.

For example, fibrous meshes of poly(lactic acid) (PLLA) implanted in TA of rats demonstrated successful mobilization of host muscle stem cells, recruited into the scaffolds through pores of 50-100 µm [246]. McKeon-Fischer and colleagues also showed efficient infiltration and growth of myogenic cells inside PCL and poly(acrylic acid)/poly(vinyl alcohol) electrospun scaffold implanted for 28 days in vastus lateralis muscle in a rat model confirming the use of autologous cells to restore the tissue [279]. The use of natural polymer, such as collagen has also been

reported with potential for SMTE [280]. After cell infiltration inside the porosity, the architectural cues brought by fibre alignment stimulate muscle cell progenitors into exhibiting greater cytoskeleton alignment, striated myotubes formation, and expression of myogenic proteins [281],[282]. For instance, Gilbert-Honick and colleagues demonstrated that electrospun fibrin scaffolds can provide pro-myogenic alignment cues for efficient regeneration in a VML in TA mouse model [200]. Similarly, Nakayama and colleagues showed that 3D-parallel-aligned nano fibrillar collagen scaffolds better participated in VML recovery, through vascularization and innervation, than randomly oriented nanofibrillar scaffolds [283]. Overall, these findings consolidate the importance of orientation for efficient regeneration.

3D printing has also been considered a promising strategy to pattern biomaterials with high precision. It is based on the deposition of a wide range of biomaterials in successive layers to generate predesigned porous structures (Figure 10D) [284]. Scaffolds made by 3D printing have been described to guide axon regeneration of neurons in spinal cord repair [285] and for heart tissue engineering [286]. It has also gain interest for SMTE. For instance, Seyedmahmoud and others formulated a 3D bio-printed gelatine methacryloyl-alginate scaffold with suitable application in SMTE. Likewise, 3D printed collagen and PCL patterned struts have shown to significantly increase the expression of myogenic genes in comparison to un-patterned control scaffolds [273]. Further studies on the use of 3D printing to produce scaffolds for SMTE has been reviewed elsewhere [287].

Considering what is highlighted in preceding paragraphs, the conception of biomaterials for SMTE requires many features particularly for volumetric muscle loss (VML) treatment. Many groups have described various biomaterials and various strategies to enhance the formation of skeletal muscle tissue *in vitro* or *in vivo* for skeletal muscle tissue regeneration. Some of them have been reviewed in this introduction and are resumed in Table 2.

Table 2 : Review of the various strategies described in literature for skeletal muscle tissue regeneration using biomaterials

Strategy for regeneration *Key parameters of the strategy*	Polymers used for biomaterial design	Application	Advantages and limitations /parameters of interest	Ref
Stiffness variation G': 1, 2 or 3 kPa E': 5, 15, 30 or 45 kPa -11 kPa -12 kPa	-Hyaluronic acid and PEGDA -Alginate -polyacrylamide -Fibrin	VML defect Muscle injury	(+) Mimic the native stiffness of skeletal muscle tissue. Control on cell fate by varying gel-like biomaterial stiffness. (-) Difficulty to precisely tune the mechanical behaviour of natural polymer-based biomaterials.	[199] [164] [189] [200]
Native structural cues Functionalization with -fibronectin, laminin tenascin-C, fibrinogen and RGD moieties -autologous minced muscle graft	-Hyaluronic acid and PEGDA -Laminin-111 -Laminin peptide nanofibres -Collagen	VML Penetrating trauma	(+) Enhance regeneration by providing natives cues. Match the biochemical characteristics of muscle tissue. Help cells to recognize their environment and evolve towards mature muscle fibres.	[199], [207] [214] [208] [212] [215] [217]
Biomaterials as delivery vehicle -Muscle stem cells / Primary human muscle derived and hECS / rASCs / MPCs / MP / bone marrow MSCs -Growth factors: IGF-1 / bFGF / HGF	-Matrigel/collagen - Four-arm PEG–MAL macromere -Alginate -Gelatine -type I collagen -Fibrin -Electrospun Chitosan/PVA -Fibrin micro-thread -Keratin	*In situ* growth factor and/or cell delivery Ischemia/VML-like defect/ Duchenne myopathy VML	(+) Protect cells and growth factors during administration and prevent washing. Allow to provide cells for efficient regeneration. Biomaterials carrying cells and/or GFs generally showed higher regeneration potential than their non-loaded counterparts. (-) Most of the instances lack porosity to ensure cell survival in centre regions of biomaterials.	[152], [156], [161] [163], [164] [206], [244] [245], [246] [247], [288]
Injectability Embedded cells (Primary myoblasts, Satellite cells, MPCs, C2C12 cells, GMSCs, MDSCs)	-Gel-like biomaterial derived from decellularized skeletal -Alginate -Hyaluronic acid -Fibrin -Chitosan/dextran -Keratin	Cardiovascular engineering Muscle injury VML repair	(+) Minimally invasive delivery / conform to the shape of complex wounds / easy to handle/ easy to keep sterilized/ Cellular and GFs protection during injection. (-) Main limitation due to the lack of porosity: Cells mortality in the centre of constructs: reflected probable diffusion limitations of nutrients toward the centre of the construct. Degradation not controllable, no support for the tissue.	[164] [153], [155] [289], [159] [122]

Table 2: Review of the various strategies described in literature for skeletal muscle tissue regeneration using biomaterials (continued)

Strategy for regeneration *Key parameters of the strategy*	Polymers used for biomaterial design	Application	Advantages and limitations /parameters of interest	Ref
Decellularized matrices for biochemical cues	-Skeletal Muscle ECM -Porcine small intestinal submucosa–extracellular matrix	Transection injury with tissue loss VML model Physical model of skeletal muscle	(+) Mimic the natural structural organization and composition of native ECM. Preserve biological signals. (-) Difficulty to transpose the technique to large animal model (lack of tissue and difficulty to treat them). Harsh treatment to prepare ECM not transposable to injectable purposes. Regulatory limitations.	[256] [259], [118] [127] [31] [257]
Porosity Tailorable and aligned/oriented -3D printing -Freeze drying -Cryogelation -Sphere creation + photo-patterning process	-Chitosan -Collagen / fibrin -Gelatine methacryloyl / alginate -Casein -Gelatine -Ovalbumin -poly(2-hydroxyethyl methacrylate)	*Ex vivo* engineered tissue *In vitro* cell alignment and fusion Regeneration of defect in TA Muscle defect in vastus lateralis	(+) Cellular infiltration and migration inside scaffolds to enhance regeneration. Possibility to modulate porosity to meet the requirements of tissues and drive cell fate through 3D architecture resembling native ECM. Higher surface area for cell loading. Pore size between 100-200 µm have shown optimal myotibe behaviour. (-) Lack of injectability and of conformation to the defect. Key parameters for optimization: Interconnectivity.	[262], [276] [263], [271] [275], [212], [280], [274] [246] [279]
2D/3D topographical cues Aligned pores and grooved scaffolds -Electrospinning -Micro-nano molding techniques -Water dispensing and freeze drying -3D printing	-Collagen -PEGDA macromere -Gelatine -Collagen + PCL + PVA -PCL + silk fibroin + polyaniline	-*Ex vivo* engineered tissue -*In vitro* cell alignment and fusion -Promotion of cell alignment improved with smaller channel -Regeneration of muscle defect	(+) Possibility to modulate topography as a tool to control myotubes length and width/ promote orientation and elongation and influence cell behaviour. Interesting for *in vitro* study of myogenesis. (-) Difficulty to be transposed *in vivo* or for clinical usage due to the limited thickness and 2D shapeability. Not suitable for large volume defects / No injectability due to controlled pre-shaping of 2D or 3D patterns (highly aligned).	[270] [201] [273]

MPCs: Skeletal muscle progenitor cells, GMSCs: Gingival mesenchymal stem cells, MDSCs: Muscle derived stem cells, MP: Muscle derived-Pericytes, rASCs: rat adipose-derived mesenchymal stem cells, hESCs: Human embryonic stem cells.
PVA: poly(vinyl alcohol), PCL: poly(ε-caprolactone), PEG: poly (ethylene glycol), PEGDA: poly(ethylene glycol diacrylate).

2.2 The design of an innovative biomaterial for volumetric muscle loss management

Considering the complex interaction between cells and their environment, the design of relevant biomaterials for SMTE is a challenging task. In the following section we have enlisted and summarized the specific requirements for the development of an ideal biomaterial for volumetric muscle loss (VML) management. To do so, we first identified the features characterizing such injuries to define clinical needs. Subsequently, we analysed multiple aspects of an innovative biomaterial design to propose a novel solution for the treatment of these injuries.

2.2.1 Clinical needs

As previously mentioned, injuries resulting in VML are of high prevalence worldwide and are most of the time occurring to patients presenting poly traumas involving bones, organs, and soft tissues. Patient care is mainly focused on the repair of life-threatening injuries for the maintenance of their lives prioritizing bone healing and preventing possible infections and organ failure. In this context, patients experiencing VML can suffer from persistent functional muscle deficits resulting from their initial untreated injuries or the related surgical procedures [290].

Current clinical treatments for VML consist of wound debridement and engraftments of autologous local muscle flaps/grafts to cover the wounds. These treatments are associated with certain limitations including muscle flap/graft shortage and possible morbidity at the donor site [291]. While attempts for stem cell or growth factors (GF) injection inside wounds have been reported, they have failed to enhance regeneration due to the too large tissue void associated with extensive cell mortality and molecule washing. In major limb trauma, the question remains whether to salvage or amputate the injured limb. Up to date, extensive work and attention have been dedicated to the design and commercialization of prosthetics rather than on the design of constructs able to guide functional tissue regeneration [292].

Given these considerations, there is a need to develop a wound filler material that could be applied after debridement (12 hours post-injury) to bridge wound edges and help cells creating autologous neo-muscle *in vivo*. However, as the cell microenvironment regulates their fate and is of high significance in determining their functions, cells need to be introduced in a configuration optimizing differentiation into muscle fibres. Therefore, the development of an optimal environment appears critical to recover the functionality of the skeletal muscle tissue after injury.

2.2.2 Biomaterial requirements

Although stem cells and particularly SC hold great therapeutic potential to regenerate skeletal muscle tissue, the vast number of needed cells and their phenotypic changes after *in vitro* amplification and culture limit their use. In the case of emergency interventions, the use of cells remains difficult due to the time needed to harvest, amplify, and re-implant them. Moreover, their implantation in humans is still controversial and their commercialization is hampered by regulatory bodies demanding extensive pre-clinical and clinical development. As an alternative to cell-based tissue-engineering therapies, some groups have evaluated acellular biomaterials. The strategy relies on biomaterial ability to create an environment that minimizes infection, promotes moisture balance, and regulates cell behaviour to promote tissue repair. Implantation of acellular scaffolds offers advantages over cell-based biomaterial including faster and simpler fabrication and storage while offering lower regulatory barriers and quicker paths of commercialization both in Europe and the US [293].
However to be implanted as an acellular support to answer the complexity associated with VML injuries, the biomaterials should answer many requirements. We identified the following parameters as key characteristics to be studied for the development of a relevant biomaterial (Figure 11):

-**The biocompatibility** of the biomaterials in contact with living tissue. The biomaterial designed should not damage surrounding tissues nor induce systemic adverse effects.

-**The cytocompatibility** and cytotoxicity should be considered. The biomaterials should be formulated in a way that enhances cellular proliferation and differentiation while preventing their early death.

-**The injectability** of the biomaterial would be appreciated. To be used as an acellular support, the biomaterial should provide superior adhesion to tissues to encourage some degree of host stem cell recruitment for subsequent tissue regeneration. The delivery of liquid precursors that could conform accurately with the shape of complex defects without leaving dead spaces could lead to tight interaction between the biomaterial and the surrounding tissues. This tight contact would allow close interaction with resident stem cells to enhance their recruitment. In addition to being delivered in a minimally invasive manner, injectable biomaterials would be valued for their easy handling while staying sterile in case of emergency.

-**The creation of a 3D architecture** needs to be studied to enable cellular and vascular infiltration and thus sustain host tissue ingrowth for large defects. As the architecture can drive cell behaviour, the porosity should be varied to be able to match the requirements of muscle cells (alignments, muscle fibre diameters, and length). Also, the porosity should match the biomaterial injectability delivery (be formulated in adequate time without the use of toxic solvents).

-**The stiffness** of the biomaterial should be taken into consideration. At a macroscopic level, the biomaterial should be compliant with skeletal muscle tissue to withstand fatigue in unidirectional stress and potentially transmit the remaining muscle contraction. At a cellular level, the stiffness should be varied to study its effect on cell behaviour and cell recruitment inside the structure.

-The biomaterial **surface properties** should encourage cellular adhesion, satellite cells (SC) migration, and differentiation along with myoblasts fusion to guide wound healing and tissue ingrowth.

-The biodegradability of the biomaterial should match the rate of regeneration of the muscle with gradual resorption providing a template for the tissue during the time of repair.

-The resulting biomaterials sterilization, transportation, and storage should also be evaluated since the biomaterial should be used in hospital within 24 hours after patient arrival.

-Ultimately, the biomaterial designed should be reproducible and cost-effective. For VML treatment, the cost of this material is an important consideration as it will be upscale for large-volume wounds.

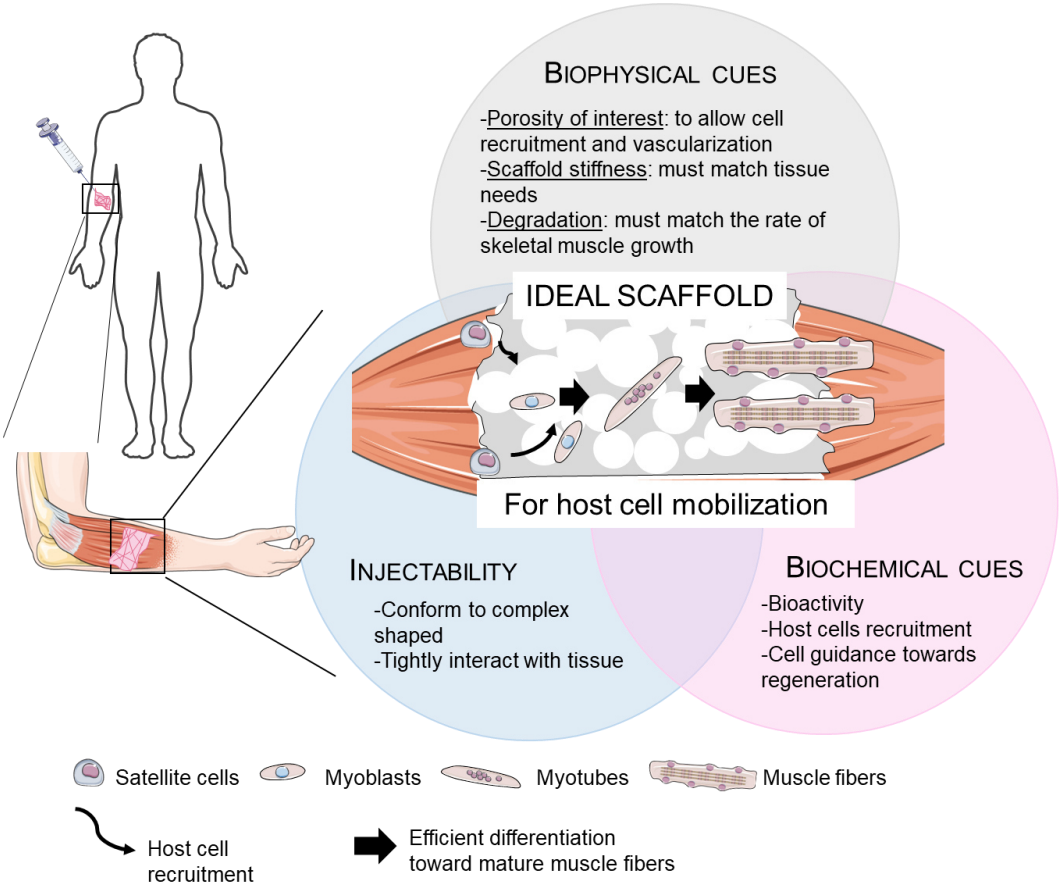

Figure 11: Product specification of an acellular scaffold able to guide skeletal muscle tissue regeneration The scaffold needs to interact tightly with the surrounding tissue to enable muscle stem cells (MuSC) recruitment while exhibiting an interconnected porosity for efficient cell entry. The scaffolds should possess mechanical, architectural and biochemical signals able to drive MuSC behaviour towards skeletal muscle tissue regeneration. Pictures adapted from Servier Medical art.

Considering the complex requirements defined above, the chosen biomaterial should thus be highly tailorable while maintaining common elements to the native ECM for cell to evolve. Accordingly, hydrogels appear to be promising, since they recapitulate many of the aforementioned requirements.

Since the first example of contact lenses in 1960 by Wichterle and Lim [294], the interest in hydrogels has grown rapidly and their use as wound dressing, drug delivery devices (reviewed [295]), or cell carrier has demonstrated their potential in the biomedical field. They are particularly attractive as 3D support for cell growth and tissue restoration or replacement since they are easily made porous using conventional approaches. Owing to their similarity to native ECM and excellent biocompatibility, hydrogels can be used as alternative acellular scaffolds to decellularized ECM. Moreover, the possibility to precisely control their mechanical and degradation properties compared with decellularized ECM is of especial interest.

2.2.3 Hydrogels: interesting candidates for tissue regeneration

Hydrogels are hydrophilic polymer networks assembled by physical or chemical crosslinking (reviewed [296]) that can absorb aqueous solutions up to a thousand-fold their dry weight while maintaining their structural integrity without dissolving. Their high water content offers a great advantage over dry sponges or meshes, since it enable them to mimic the moisture balance encountered *in vivo*.

2.2.3.1 Methods of production and hydrogel network

Hydrogels can be classified as chemical or physical depending on the crosslinking points formed between hydrophilic polymers, either covalent or non-covalent. Crosslinking methods have a direct influence on the structural integrity of resulting hydrogels.

Reversible physical hydrogels are characterized by non-covalent crosslinks including physical entangled networks such as intramolecular interactions in response to changes in external conditions (pH, temperature, ionic strength), and secondary forces interactions such as hydrogen bonds, electrostatic interactions or hydrophobic forces (reviewed [297]). These hydrogels have interesting reversibility and may benefit from an absence of chemical reaction making them attractive to avoid extensive washing before implantation to withdraw possible toxic crosslinkers. However, they generally exhibit poor mechanical properties and stability over time.

Contrary to physical hydrogels, covalently crosslinked polymer networks referred to as chemical hydrogels, result in stronger interactions at intersection points of polymers chains, providing excellent mechanical stability. Generally, carboxyl, hydroxyl, and amine groups are the most targeted groups to form covalent interactions through Michael-type addition, click chemistry, photopolymerization, or the use of crosslinking agents [298]. These covalent networks form stable structures with tuneable mechanical properties. However, cytocompatibility and biocompatibility must be considered depending on the chemical reagents

used for the reaction and the release of toxic products in the case of direct *in situ* injectability purposes.

The intrinsic characteristics of hydrogels are strongly influenced by the crosslinking method. At a molecular scale, physical and chemical hydrogels can be considered as porous polymer networks with pore space filled with water (Figure 12). The network structure is referred to as the hydrogel mesh with the distance between crosslinking points in the network called mesh size. Mesh size for typical hydrogels is in the 1-100 nm range [299] and is linked to the water retention capacity of hydrogels. Depending on the crosslinking reaction as well as polymers concentration and nature, hydrogels mesh size and subsequent mechanical properties vary. In the crosslinked state, hydrogels reach an equilibrium swelling in aqueous solutions that depends on the polymer network density and determine their overall nutrient and oxygen permeation. These hydrogel's intrinsic swelling properties, aside from being very attractive to resemble the ECM, allow them to capture and release growth factors (GF) in a controlled manner strengthening their use as smart biomaterials for TE applications [300]. Many of the aforementioned instances directed toward SMTE used swollen hydrogels as a tool to capture GF while regulating their diffusion and release through hydrogels mesh size to enhance skeletal muscle regeneration with alginate [244], keratin [248],[245], or PEG [156] based hydrogels.

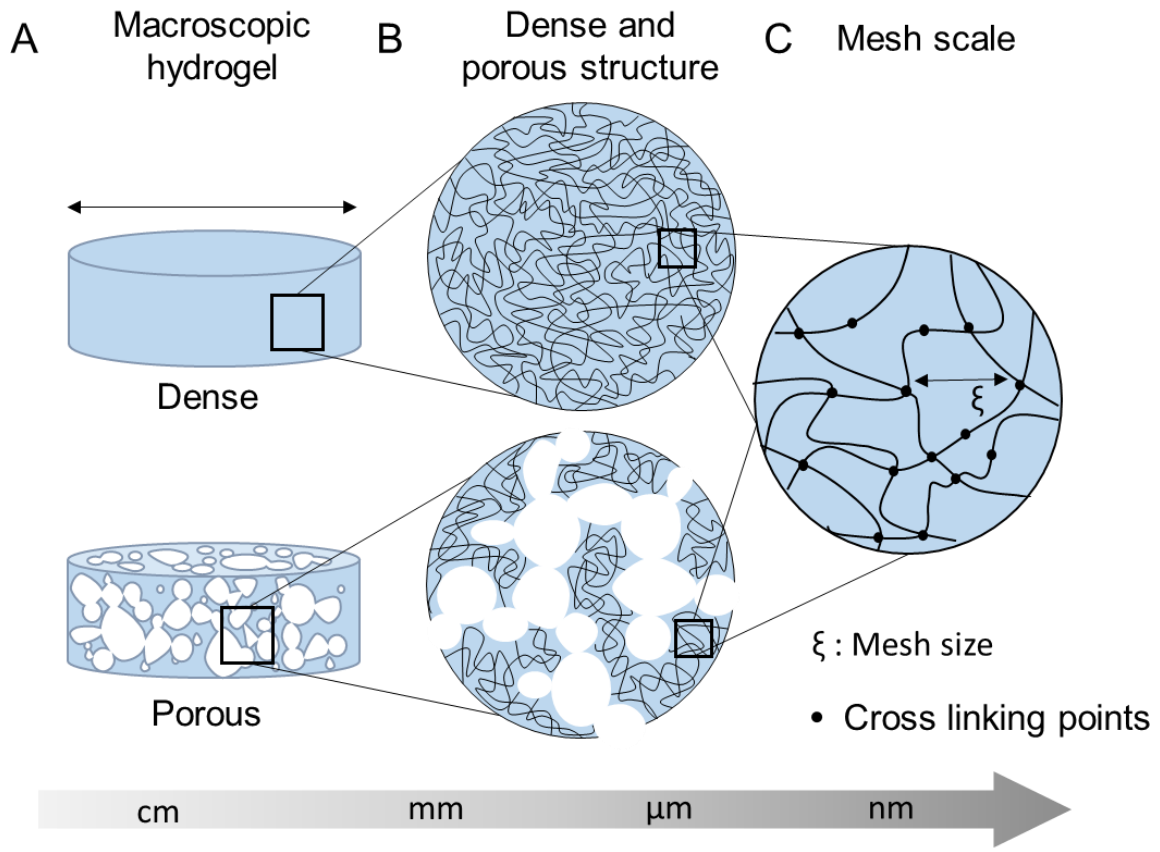

Figure 12 : Hydrogels representation at various scales
A) The macroscopic hydrogel formulation characterized by form, size and porous structure. B) The network created by the crosslinking of hydrophilic polymers filled with aqueous solutions vs the macroporous structure created in porous hydrogel constructs (50-1000 µm). C) The mesh size: the size between 2 adjacent crosslinked points (1-100 nm). Both macroporous and microporous structure can be adapted by various strategies.

2.2.3.2 Hydrogels from synthetic or natural polymers

As for dry sponges and meshes, hydrogels can be formed from synthetic or natural crosslinked polymers. Hydrogels made of **synthetic polymers** have a long history of use in medical applications due to their inertia towards tissues with Poly(2-hydroxyethyl methacrylate) (polyHEMA) hydrogel being the first used followed by the poly[ethlylene oxide] (PEO), poly-ethylene glycol (PEG), poly(vinyl alcohol) (PVA) and poly(acrylamide) (PAAm). The FDA considers these synthetic polymers along with PLGA, PGA and PLA safe for oral and intravenous applications consolidating their use in the biomedical fields. Their exact composition and highly reproducible chemical formulation makes them of great interest as mechanically tuneable hydrogels. Due to their many advantages, some examples of commercialized synthetic polymer based hydrogels have been reported in the biomedical field. Among them, hydrogels composed of repeated sequence of arginine, alanine, aspartic acid, and alanine known as purastat® (3D matrix) and puramatrix® (BD biosciences) have been studied as hemostatic gel for laparoscopic surgery [301] and for bone tissue engineering [302] respectively. PEG has also been extensively described alone or in association with other polymers given its low protein adsorption, its minimal inflammatory profile, well-established

chemistry and its long history of safety *in vivo*. PEG polymers are also relatively inexpensive, water-soluble, and range from 0.4 to 100 kDa [303], comforting their interest for the design of versatile hydrogels and as drug delivery or as a cell carrier systems [304]. In recent years, dendrigrafts and dendrimers have also been employed as well-defined building blocks for hydrogel formulation. They have shown potential as crosslinking monomers thanks to their highly organized 3D arborescent organization and the possibility to have a large number of terminal reactive end-groups available at their surface, enhancing the number of interactions (reviewed in [305]). Their combination with polymers mediates the formation of polymeric networks and particularly Poly(amidoamine) (PAMAM) and polyethylenimine (PEI) dendrigrafts have been used in biomaterials development [306]. For example, PAMAM dendrimers have been successfully crosslinked to functionalized PEG to form hydrogels for drug delivery systems [307]. However, PAMAM is related to high cytotoxicity and low interactions with cells [308].

In addition to synthetic polymers, hydrogels can be fashioned with **naturally-derived polymers**. They have been widely used due to their biodegradability, biocompatibility and structural similarity to native ECM allowing cells to adhere. In the 1980s, the first hydrogel made of naturally-derived polymers was reported for artificial burn dressings using collagen [309]. Since then, some of them have led to commercialized formulations such as a collagen-based hydrogel, Woun'Dres®, by coloplast for skin repair [310]. Hydrogels fashioned with crosslinked polysaccharides such as acid hyaluronic [155] and chitosan [262] have also been described for TE application given their naturally derived origin and their easy handling and crosslinking. Their use was also associated with commercialized product including AlgiMatrix™ from alginate for the development of more predictive *in vitro* cell culture models and HemCon®, a hemostatic bandage from chitosan.

The design of hydrogels made of a combination of both sources (synthetic and natural polymers), has been fuelled to recapitulate both mechanical versatility along with the presence of natural receptors inside a hydrated matrix.

Given their hydrated state and their easy production, hydrogels are interesting for VML treatment. They act as GF reservoirs and have close ECM mechanical properties able to enhance tissue regeneration. Moreover, since they are formulated from hydrophilic polymers, hydrogels are generally fashioned from liquid precursors suitable for their injection through needles.

2.2.3.3 Injectability

In a context where most of the biomaterials require surgeons to make sufficiently large incisions to enable their placement, one of the major thrusts for TE in clinical settings is to develop injectable systems that can be applied as liquid precursors through minimally invasive delivery. In the case of VML management, injectable biomaterials would offer a clear advantage over implantable ones, which need to be pre-cut before placement, complicating the procedure and increasing the risk of infection. In addition the application of liquid precursors would enable a tight interaction with tissues for the management of wounds of complex shape, which is relevant for host cell recruitment inside acellular based biomaterials.

Hydrogels are thus particularly interesting for minimally invasive delivery due to the use of hydrophilic polymers, easily solubilized in aqueous solutions, enabling their injection through needles. Once injected, the crosslinking of polymers forms a self-standing material directly *in situ* to promote the good integration to surrounding tissues, allowing them to function as a scaffold for cells. Although being an appealing approach, the suitability of hydrogels for injectable delivery is governed by many parameters (Figure 13). Difficulties in controlling the gelation process can limit the practical use of such hydrogels: too rapid gelation may result in needle clogging and the need to apply too much pressure on the plunger while too slow gelation could result in uncontrolled liquid dispersion through tissues and mass loss from the target site. Moreover, additional reagents necessary for hydrogel crosslinking may cause negative effects on cell growth and tissue health while implantable scaffolds can be extensively washed to remove undesirable impurities. Therefore, all of the components required to synthesize injectable hydrogels for direct *in vivo* injection must be **nontoxic** with a **cell-friendly** and perfectly chemically balanced reaction to prevent unrequired products from leaching. In addition, their use in a broad range of temperature conditions and their synthesis within seconds or minutes should be studied for VML treatments.

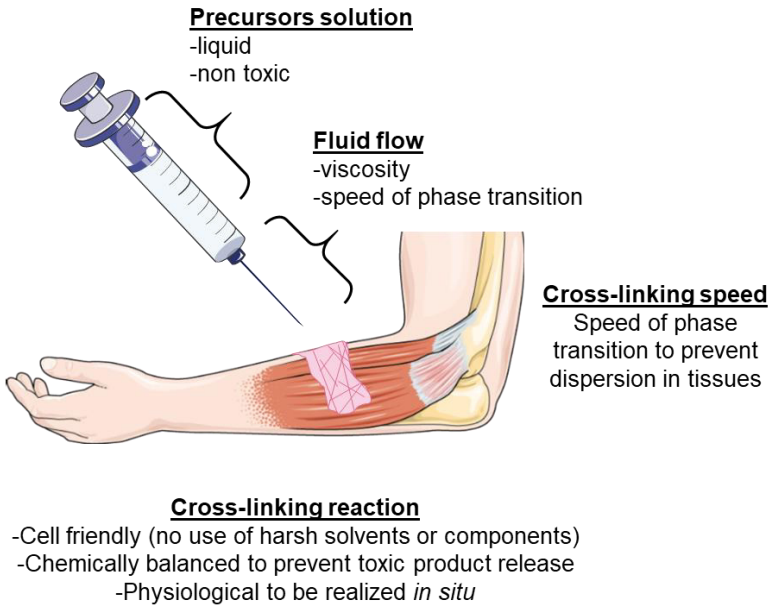

Figure 13 : Hydrogel formulation requirements for in situ *direct injectability*
Hydrogels precursors need to be solubilized in liquid, aqueous and non-cytotoxic solutions. Hydrogel's crosslinking should match injection rates while preventing dispersion in tissues. Hydrogel should be able to crosslink in situ without the need for washing or post-formulation treatment. Hydrogel chemical reaction should be non-cytotoxic to be performed in situ. Adapted from servier medical art

Due to their many advantages, *in situ* injectable hydrogels are strongly favoured in biomedical applications [311]. For example, for direct injection of stem cells, which represents a promising therapeutic strategy to regenerate tissues, hydrogels have been studied as cell delivery vehicles to protect them during injection, prevent their dispersion once injected and then act as a support on which they can evolve [312]. Examples of minimally invasive hydrogels as cell carriers have been extensively reported for SMTE. Rossi and colleagues have embedded satellite cells (SC) inside an injectable hyaluronan-based hydrogel related to a major improvement in muscle structure and numbers of new fibres in a defect in mice tibialis anterior (TA) muscle [155]. Similarly, Guo and others described a dextran and chitosan-based injectable hydrogel as myoblasts cell line (C2C12) and human umbilical vein endothelial cells (HUVEC) delivery vehicles for a mice VML injury model [159]. An example of injectable alginate-based hydrogel with both cells and growth factors encapsulation has shown potential for SMTE highlighting hydrogel interest in the design of smart biomaterials [164].

However, in most of the aforementioned examples, injected hydrogels lacked porosity for the efficient migration and proliferation of cells inside the constructs. This resulted in round-shaped cells embedded in hydrogels limiting their regeneration potential [164].

2.2.4 From 2D to 3D: the challenging issue to obtain both injectable and porous biomaterials

While injectable hydrogels are very interesting for their integration by surrounding tissues, only a few examples have allowed an efficient tissue ingrowth and cellular infiltration [313], the vast majority possess a too tight networks often preventing cellular movement within the material.

In addition, hydrogels possessing a tight mesh could limit mass transport of oxygen and nutrient, mainly achieved by diffusion. In particular, for VML treatment characterized by large voids, diffusion of oxygen could be restricted leading to hypoxia and cellular mortality in centre regions of cell-loaded hydrogels [288]. Accordingly, the induction of porosity inside these hydrogels appears relevant. In the case of acellular hydrogel strategies, it would improve host cells recruitment where dense hydrogels could fill the void created by the injury, although confining cells to the wound edges. A porosity inside hydrogels could thus be an asset for the infiltration of cells located on the edges and potentially regenerate the tissue *de novo*. Furthermore, porosity appears critical for vascular infiltration and tissue ingrowth for large defects.

The methods previously described for porosity induction (i.e. freeze-drying, casting, electrospinning, and 3D printing) provide highly tailorable porosity inside many types of biomaterials, including hydrogels. However, these methods need to pre-shape the porous structure before their application in contact with living tissues, impeding so their injection. As a result, these approaches are so far confined to pre-shaped structures for invasive and stressful implantations. Moreover, the approach used to create a porosity, besides being suitable with a minimally invasive delivery, should also be cell-friendly and perfectly chemically balanced to prevent any toxic product release while avoiding the use of organic solvents or harmful components. Consequently, instances of both *in situ* injectable and porous hydrogels remain scarce and their design still represents a technical challenge. However, some strategies have been developed over the past few years and are reviewed below, in Figure 14 and Table 3.

2.2.4.1 Current methods for the formation of injectable and porous hydrogels and their limitations

Solvent casting and particle leaching

Solvent casting and particle leaching techniques have been already extensively used for non-injectable purposes. They are based on the dispersion of porogens (salts or polymers particles) into hydrogel precursors' solutions or during the sol-gel transition. The hydrogel is then allowed to crosslink around porogens of controlled sizes that are subsequently leached by immersing the composite materials in a specific solvent and under precise conditions (temperature, pH, ionic strength). During leaching, the porogens leave voids inside the network, leading to the creation of porosity (Figure 14A). Paraffin [314], sucrose [315], NaCl [316], or biodegradable hydrogel [317] have been largely described in literature as porogens. Unlike freeze-drying, 3D printing, or electrospinning, this method is technically compatible with injection thanks to the liquid state of hydrogel precursors and the small size of porogens, able to pass through needles. Nevertheless, while the porogens are generally non cytotoxic, their leaching or dissolution process generally involves harsh solvents, extreme temperature, or pH conditions unsuitable with direct contact with tissues or cells. Moreover, the use of salts is generally combined with organic solvents to slow down their dissolution and keep them in crystal form until hydrogel crosslinking, further preventing their use in contact with living systems.

To combine these methods with injectability, some approaches rely on non-toxic porogens able to dissolve in physiological environments. For instance, gelatine [318]–[320], mannitol [321] or oxidized alginate with fibrin [322] have been reported, as these reversible gels are rapidly dissolved at physiological conditions (i.e. pH =7.4 and temperature =37 °C) thereby inducing the pore formation within hydrogels once injected. Particularly, the use of gelatine as a natural physically-formed hydrogel has been extensively described for particle leaching. Gelatine is a product resulting from the partial hydrolytic degradation of collagen. It has a thermo-reversible sol to gel transition associated with its triple coil helix structure. In aqueous elevated temperature solutions, gelatine exists in random coil conformation. Upon cooling, and for concentrations above 2%, a partial recovery of the collagen-like triple-helical structure occurs leading to the formation of a physically entangled network. This network creates a gel not soluble in aqueous cold solutions [323]. However, in physiological conditions (i.e. 37°C and pH 7.4), the gelatine recovers the random coil conformation and is dissolved. Then, the body physiologically degrade the gelatine due to its natural origin.

Few studies have been able to demonstrate the *in situ* injectability of such systems with *in vivo* studies. Goh and colleagues have described an *in situ* injectable and porous PEG-diacrylate hydrogel with a porosity made by gelatine microparticles (MPs) leaching. However, the reported *in vivo* cell infiltration inside the construct remained scarce in their study and the hydrogel photosensitive crosslinking limited its use to superficial parts of the body (where light can reach the hydrogel). On the other hand, Zhu and others successfully reported the use of

thermo-sensitive hydrogels able to form self-standing materials upon temperature raise once injected into animals while showing extensive porosity due to mannitol MPs leaching. Nevertheless, to perform a porosity with windows of interconnections suitable for the infiltration of cells, there is a need to have a substantial density of MPs to allow their compaction which can be related to needle clogging. Although optimization needs to be done to reach the clinic, the strategy holds promise and worth further development.

Highly compressible materials with elastic behaviour

Another strategy consists of formulating hydrogels able to withstand high reversible deformation upon compression to be delivered through needles. Beduer and colleagues developed porous highly compressible cryogels [324] or 3D printed [325] pre-shaped alginate hydrogels able to be delivered in a minimally invasive way in dehydrated form. Once injected, the hydrogel undergoes a rapid volumetric recovery by swelling (Figure 14B). These hydrogels were able to interact with neurons and showed long-term preclinical evidence. This strategy has given birth to the Adipearl™ gel used for soft tissue reconstructive and plastic surgery (Volumina Medical, under clinical trials). Others instances of highly compressible hydrogels have been reported with a gelatine-based hydrogel [326] and a methacrylated-alginate hydrogel [327], injectable through conventional needles while maintaining a predefined geometry and architecture. All these examples have shown interesting results *in vivo*. However, one of the drawbacks that is worth mentioning is the fact that hydrogels are pre-shaped before their injection. Their pre-shaped state could influence their interaction with tissues, preventing them to fill complex voids. Moreover, it requires the porosity and the material to be suitable with a 90% elastic deformation while recovering their initial shape without plastic non-reversible deformations. This feature limits the number of usable candidates and their mechanical properties modulation.

Fast degradability strategies

Various research groups have also explored the use of fast degradable hydrogels upon injection. The strategy lies in the injection of hydrogels in the site of interest and counts on their *in situ* fast degradability within the first hours of implantation to create a path for cells inside the bulk material (Figure 14C).

Fast degradability can be based on the creation of fibrin hydrogels from the self-assembly of cleaved fibrinogen. These hydrogels are fashioned by mixing fibrinogen, a glycoprotein responsible for clotting in the body, with thrombin in calcium chloride solutions mimicking the natural haemostatic cascade. The variation of fibrinogen and thrombin concentrations enables obtaining tailorable fibrin meshwork. Therefore, the degradability of the hydrogel can be adapted to get the most favourable rate of degradation by loosening or tightening the resulting meshwork. In the body, fibrin clots are naturally degraded after the end of the coagulation by the plasmin enzyme, responsible for the fibrinolysis. Fibrin degradation products are then cleared by other proteases including cathepsins [328]. The ability of fibrinogen and thrombin

to form a highly degradable hydrated network has thus been exploited by various groups for *in situ* injectable purposes. These hydrogels were successfully injected in animal models with clinical potential for reconstruction of skeletal muscle defect [158], for tissue-engineered cartilage [329], and as cell delivery vehicles, rapidly releasing embedded cells to the site of injection [330]. All these instances described the use of a dual syringe system including Duploject® or Tissucol® kit to mix fibrinogen and thrombin upon injection. After injection, they all showed an appropriate crosslinking with a degradation of the resulting meshwork that was dependent on initial amounts of fibrinogen and thrombin.

However, a common drawback of these approaches is the risk for un-polymerized fibrinogen and thrombin residues that could be related to clot formation in other un-specific sites. On top of that, while providing interesting biochemical cues due to naturally derived polymers, these hydrogels are hardly mechanically tuneable and are subjected to low reproducibility due to batch-to-batch variabilities. To overcome these drawbacks, degradable synthetic-based hydrogels can be used. For instance, physical crosslinking based on hydrogen bonding using pluronic® F-127 and carboxymethylcellulose [331] or based on pluronic® F-127, HA, and PGA [332] can be easily degraded *in vivo* due to weak interactions between polymers, leading to the formation of porosity.

While being attractive, these hydrogels generally exhibit poor stability over time with a rapid degradation (2 weeks) restricting their application as long-term supports for cells and tissues. Hydrogel's digestion by enzymes have also been investigated to form the porous system *in situ* at specific times. The strategy relies on the injection of a hydrogel followed by the injection of specific enzymes to degrade it at desired time points. It has been described with alginate-based hydrogel degraded with alginate lyase [333] and with gelatine-hydroxyphenylpropionic acid/carboxylmethylcellulose-tyramine hydrogel degraded by cellulase enzyme [334]. PEG hydrogels with light controlled degradation have also been developed with UV light irradiation [335]. Nevertheless, these hydrogels degradability is based on further injection or light irradiation, making their use more complex than a one-shot injection.

All these examples describe porosities formed *in situ* after hydrogels injection providing very interesting potential for various types of biomedical applications. However, the main drawback of these strategies in the case of VML management is the poor mechanical stability provided by such hydrogels, whose degradability is faster than the actual tissue regeneration.

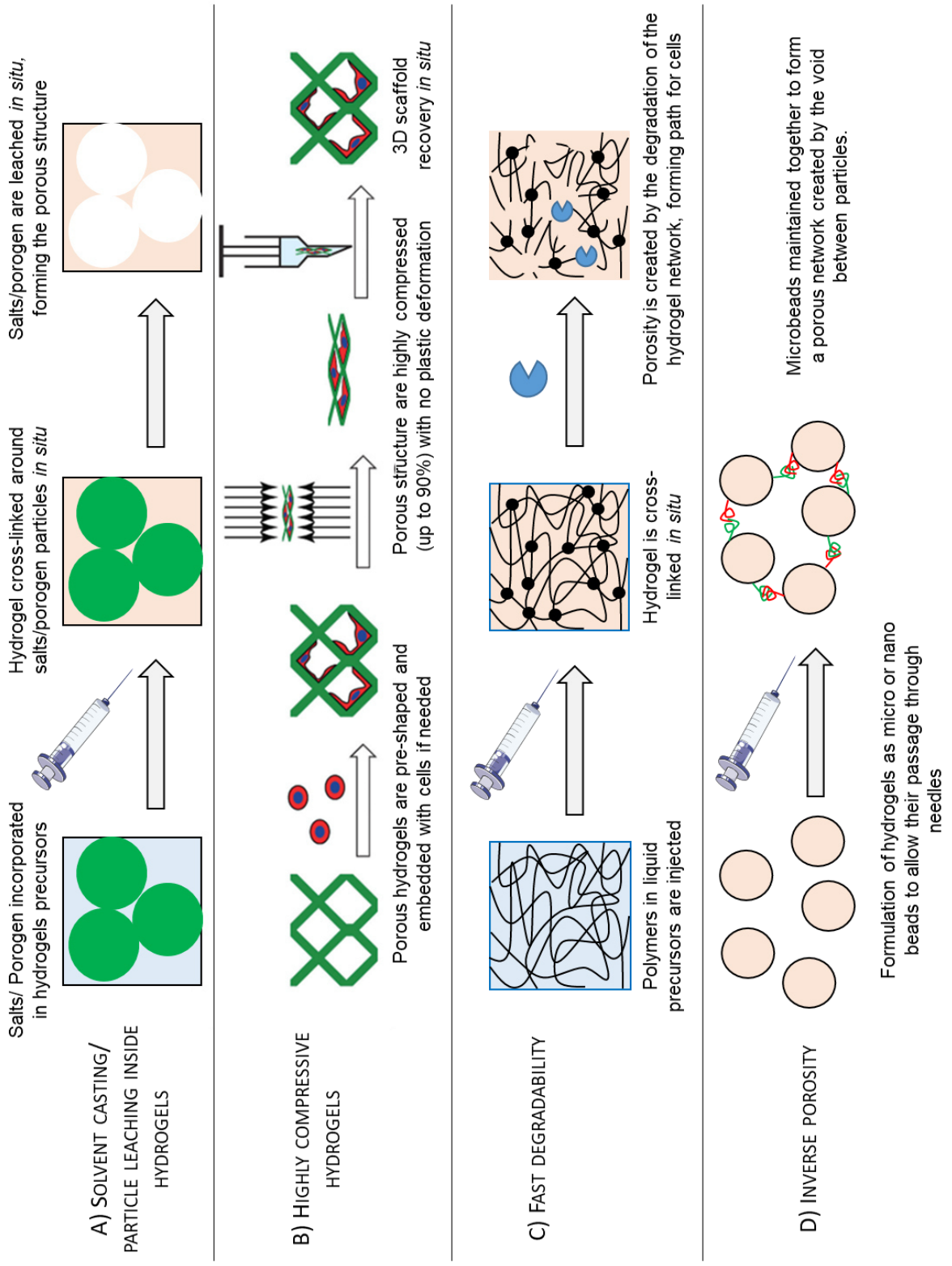

Figure 14: Current strategies developed to obtain both porous and injectable hydrogels for various applications
A) Solvent casting techniques followed by porogens leaching in physiological conditions B) Formulation of highly compressible porous hydrogels able to withstand 90% elastic deformation to be injected through needles, adapted from A. Béduer et al., Adv. Healthc. Mater., 2015 [324]*, C) fast degradability strategies and D) inverse porosity using self-assembly or annealing of micro/nanoparticles*

Inverse porosity

In the last few decades, efforts have been devoted to designing hydrogels at micro and nanoscales for their delivery through needles. The strategy is based on a two-step chemical reaction cascade, (1) the chemical crosslinking of individual micro or nanobeads hydrogels followed by (2) the chemical annealing or self-assembly of the beads into larger scaffolds, whose interconnection is created by the void between beads. The self-assembly or annealing is mandatory to avoid beads dispersion in tissues and act as a whole construct (Figure 14D).

To form hydrogels at micro and nanoscales some strategies have been reported among which, microfluidics, emulsion and mechanical fragmentation have shown some potential [336].

For example, gelatine microparticles functionalized with photo-crosslinkable methacrylamide groups for subsequent crosslinking [337] have been successfully injected in a calvarial bone defect in rats with extensive cellular infiltration. Griffin and colleagues, decorated PEG-based microparticles with cell adhesive peptide and two transglutaminase peptide substrates that react together through factor XIII activation enabling particles assembly [338]. They showed a high potential for wound management and vasculature development.

Although the use of nano or microbeads requires their self-assembly or annealing to act as scaffolds, some strategies have been successfully developed to allow both injectability and porosity inducement. However, the photo-crosslinking necessary to anneal microbeads in some instances need the introduction of surgical instruments to deliver the light source. These instruments render the device more traumatic for patients and more complicated to use in case of emergency. In addition, this approach is generally associated with low percentage of porosity considering the high density of particles needed to be annealed or assembled, restricting the space available for cells and tissues. Nevertheless, all of these approaches have shown to be relevant for various applications including tissue regeneration.

Table 3: Review of the strategies explored in literature to generate both injectable and porous hydrogels with their positive attributes and main limitations.

Strategy / porosity realization		Applications	Positives attributes	Limitations	Ref
Particle leaching		-Muscle, cartilage, adipose tissue engineering -Cell encapsulation -TGF-β1 release	-Compatible with various gelation system and material candidates. -Possibility to modulate pore size through particle size. -Molecules and cell release possible simultaneously to porogens leaching	-Need a perfect coordination of delivery and gelation time especially to allow interconnection. -Number of porogen candidate are limited. Porogens should not interfere with the gelation process while leaching in physiological conditions. Their dissolution time must be appropriate and match tissue ingrowth. Porogens must be cell friendly and nontoxic.	[320] [321] [319] [322] [318]
Compressible scaffolds with shape memory properties		- Brain and soft tissue engineering, -Cells and molecules encapsulation	-Possibility to modulate the porosity through the cryogelation freeze/drying process. -Allow extensive washing or post-formulation treatments.	-Preformed hydrogels trigger less adaptability to complex shapes than liquid precursors. -The method is not compatible with various gelation system. Need to design a robust system able to withstand reversible deformations at over 90% to go through a needle and a rapid volumetric recovery once injected. Low mechanical versatility.	[324], [325] [327] [326] [289]
Fast degradability	Hydrogel digestion by enzyme	-Soft tissue engineering -Revascularization applications	-Degradability can match cellular infiltration and the tissue ingrowth for efficient regeneration	-Need to inject the enzyme to degrade the hydrogel. -No mechanical support conservation over time linked to fast hydrogel degradation. Difficulty to control the porosity.	[333] [334]
	UV-triggered degradation profile	-Cells encapsulation	Possibility to control the degradation profile to match the tissue ingrowth for regeneration	Application of light for porosity inducement (more invasive for patients). Difficulty to control the porosity.	[335]
	Fibrin degradability	-Muscle, bone and cartilage engineering	Fibrin is biocompatible and biodegradable; there is no immunogenicity to be expected and foreign body reactions can be excluded	Degradability should match the rate of tissue ingrowth to be a support. Be quick enough to allow cellular infiltration if not embedded. Not transposable to other hydrogel system. Not possible to use synthetic hydrogels. No control on the mechanical properties Risk for clot formation in other un-specific sites.	[158] [330] [329]
	Weak interactions between polymers	-Dermal filler -Tissue barrier for anti-tissue adhesion	No addition of any chemical crosslinking agents that may reduce biocompatibility	-No mechanical support conservation over time linked to fast hydrogel degradation. Difficulty to control the porosity.	[331] [332]
Inverse porosity : Porosity obtained with the negative space between assembled microspheres		-Cutaneous wound healing -Delivering vehicle for anesthetics	Controllable porosity and injectability through microspheres diameter (microfluidic or water and oil emulsion)	-No macro-mechanical properties able to sustain tissue. -Need to assemble microspheres together or contain them in a liquid vector to prevent microspheres dispersion in tissues. -Low percentage porosity compared with other methods.	[338] [339] [340] [341]
Emulsion templating technique Water and oil emulsion with sacrificial porogen (oil, gas)		-Drug delivery system -Bone/ Systemic lupus erythematosus treatment	Porosity with air bubbles generation: cell friendly	Oil as a porogen can limit *in vivo* applications. Difficulty to maintain the emulsion and control it during injectability (luer lock dual syringe system).	[342] [343] [344]
Gas foaming methods		-Broad tissue engineering applications	-Volume expansion. Application to various crosslinking system -Most of instances only applicable to bone regeneration (use of cements). Use of CO_2 : inert gas / cell friendly	-Risk of gas cavity. -Gas leaching over time. -Difficulty to control pore size. -Not transposable easily to other systems.	[345] [346] [347]

2.2.4.2 Gas foaming techniques: an interesting option

Although the aforementioned approaches are of high relevance for the creation of porosity inside hydrogels, the use of gas foaming techniques present many advantages. Gas foaming techniques permit solvent-free formations of porous materials through bubble gas generation (reviewed [348]). Gas foaming found its original application in the biomedical science in the '80s in drug delivery. The use of air has been described to generate porosity inside silanized-hydroxypropylmethylcellulose hydrogel coupled with α-TCP powders [346] and inside calcium phosphate bone cement [343] for bone tissue engineering suitable with paste injection. Air bubbles, indeed, appear spontaneously during the mixing of powders and liquid phase and can be exploited to create the porosity inside composites while avoiding the use of harsh solvents.

Among gas foaming techniques, CO_2 gas generation has also been extensively described. For instance, studies have reported the use of supercritical CO_2 [349],[350], high pressure CO_2 [351],[228],[352], water-in-carbon dioxide emulsions [353],[354], or ammonium bicarbonate [355]–[357] to create porosity inside biomaterials of various applications. CO_2 is a non-toxic, inert gas that does not affect the biochemical integrity of proteins such as elastin [358], lysozyme, and insulin [359]. Thus, the use of CO_2 is generally cell friendly which makes it attractive for TE applications [260] and suitable with the use of growth factors (GF) [351].

The effervescent approach

Even though the use of CO_2 is attractive, the aforementioned processes are generally not transposable to *in situ* injectability purposes. Interestingly, effervescence, which is a very common approach to generate CO_2 bubbles, has not been investigated in the context of injectability. The use of effervescence, relies on the reaction between a carbonated base and a carboxylic acid with sodium bicarbonate (SB) and citric acid (CA) being the more common couple. Effervescent salts are promising for porosity creation due to their carbon dioxide evolving property upon contact in aqueous solution and relatively cell-friendly behaviour (reaction detailed Figure 15).

Many groups have described the creation of porosity inside hydrogels using effervescent approaches, mostly based on two main strategies (Table 4). The first one takes advantage of the increase of viscosity experienced by the hydrogel liquid precursors during crosslinking. To do so, hydrogels precursors are mixed in acidic conditions and carbonated base powders are manually added to the solution to generate CO_2 bubbles. The timing is relevant to disperse the carbonated base powders as a threshold viscosity is required to entrap CO_2 bubbles inside the polymer network. It is even more relevant given that most of the crosslinking reactions described are sensitive to pH. The addition of base is then used to boost the resulting crosslinking reaction in a time-specific manner to entrap CO_2 bubbles.
In the second strategy, a dispersion of carbonated base powders throughout solidifying polymers is followed by crosslinked powders-loaded hydrogels immersion in an acidic bath for

the creation of CO_2 bubbles inside the hydrogel network similarly to a salt-leaching-based method.

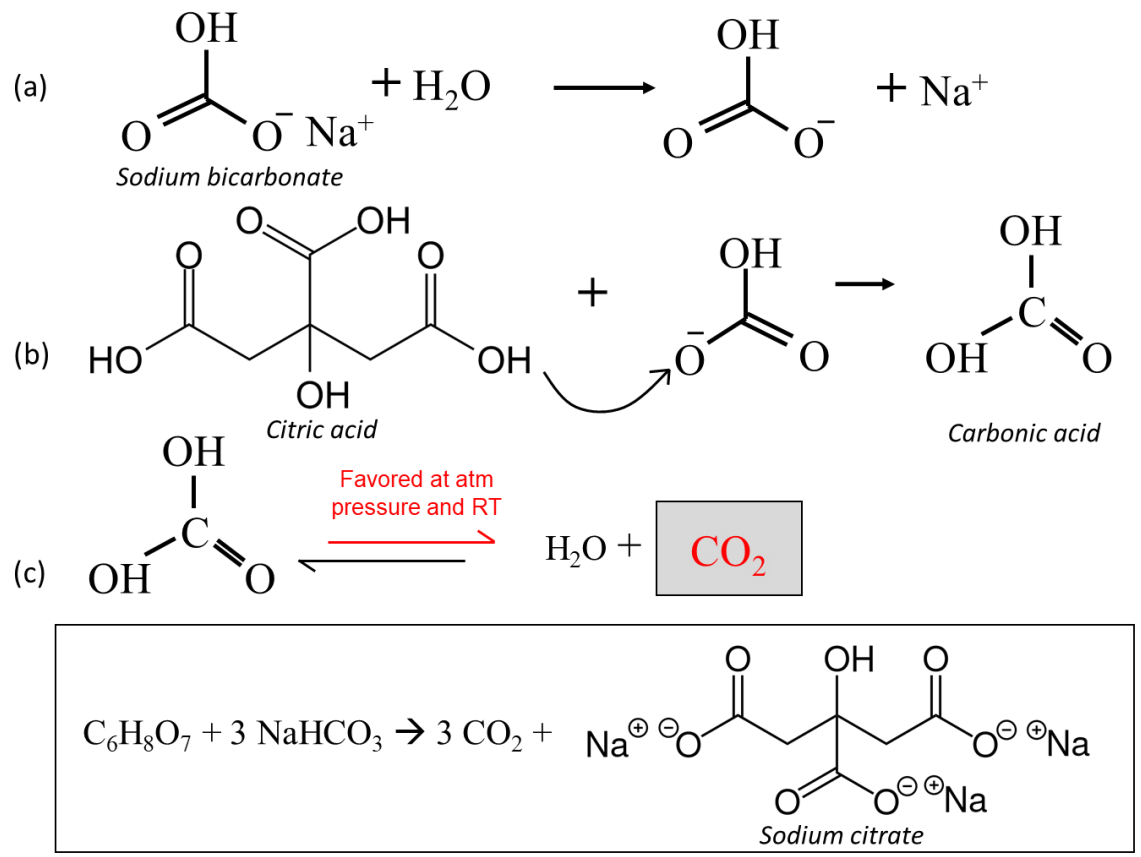

Figure 15: Effervescent reaction between citric acid and sodium bicarbonate
(a) Sodium bicarbonate dissolve in aqueous solution into bicarbonate and sodium ions, (b) citric acid react with bicarbonate to form carbonic acid. (c) Carbonic acid is unstable in water at atmospheric pressure and room temperature and immediately dissolve into H_2O and CO_2. Stoichiometric conditions require the use of 3 sodium bicarbonates to react with the 3 carboxylic groups available on one citric acid to form sodium citrate as the final end product.

All the examples reviewed in Table 4 share common characteristics including the observation of a pore size broad distribution and an interconnection of the resulting porosity without the formation of a nonporous dense layer at the surface. The latter being crucial for cellular infiltration, it comforts the use of effervescent approaches as an effective way to produce a porosity suitable for TE applications. These methods allow obtaining an extensive porosity of up to 90 % with pore ranging from 10 to 600 µm depending on the studies. Of note, using an effervescent approach to create a porosity inside materials was generally reported for the design of 'superporous hydrogels' since the pores are in the order of a few hundred micrometers [360], defined as macropores according to previous consensus in TE applications [260],[343],[346]. Given that they exhibit fast swelling behaviour and superabsorbent properties, these hydrogels are generally designed as molecule carriers. However, these approaches showed also a potential interest in combination with cement to create bone grafts

[361][362], with PLLA or PEG hydrogels for cartilage regeneration [363],[364], or with elastin-like recombinamers [365] for connective tissue regeneration.

All of these instances described either a gas foaming/salt leaching process with acidic baths or formulations that need extensive washing to rinse organic solvents used to prevent alkaline crystals dissolution. As a result, even if the use of CO_2 could be employed to avoid the use of harsh solvents, many instances included n-pentane, 2-methylbutane, hexane, heptane, dichloromethane, acetone, methanol to slow down effervescent powders solubilisation [366]. Moreover, a large part of these examples either used hydrogels with slow crosslinking velocity or included additional steps (ultrasound baths, freeze-drying) to be able to entrap CO_2 bubbles inside the network. Hence, hydrogel chemistry or the need for mandatories additional steps prevented the direct, *in situ* minimally invasive delivery of these formulations.

In conclusion, some strategies have already been described for the formation of porosity (1) compatible with hydrogel injection or (2) suitable for direct contact with cells and tissues without washing by avoiding the use of harsh solvents. However, instances of both porous and *in situ* injectable hydrogels remain scarcely described in literature. These hydrogels may offer interesting therapeutic possibilities through easy handling for emergency purposes. More specifically, in the case of VML, they could offer a ready-to-use treatment applicable through a single step injection while conforming accurately to the wound and allowing host cell recruitment.

Table 4: Porosity made by effervescence inside biomaterials and the processes limiting their in situ injectability (part I).
The strategies are taking advantage of the hydrogel crosslinking simultaneous to the effervescent reaction.

Strategy	Material	Porogens Porous structure	Processes limiting *In situ* injectability	Application	Positive attribute	Ref
Concomitancy -Acid in liquid precursors -Addition of carbonated bases (in powders) at a specific time to hydrogels precursors. Hydrogel precursors need to be viscous enough to entrap CO_2 bubbles. **Timing is important** Use of pH change to boost crosslinking	Acryl amide + BIS + Pluronic® F-127	**-Acrylic acid + sodium bicarbonate** -Pore size: 100-250 µm - Over 300 µm -Presence of Interconnection	-Hydrogels made of hazardous substances -Dehydration step at 60°C for 12 hours -Washing in 80% ethyl alcohol for 1h -Crosslinking: 30min	-Molecule absorption and controlled delivery and release -Gastroretentive drug delivery system / Gastric retention devices -Critical fast swelling and superabsorbent properties required	-Possibility to control the porosity: the porosity increased as the amount of base, acid, and foam stabilizer increased -Porous structure heterogenic and broad. -Possibility to form longitudinally formed structure and oriented pore structure -Basic pH stimulated polymerization	[367]
	Chitosan / poly (vinyl alcohol) +pluronic® F127	**-Acetic acid + sodium bicarbonate** Porosity: 40-88% -Presence of Interconnection	-Freezing/thawing cycles for crosslinking -Crosslinking speed: overnight at RT			[368]
	Vinyl monomers	**Acrylic acid + sodium bicarbonate** Pore size: 150-300 µm -Presence of Interconnection	-Sodium bicarbonate suspension stirred with spatula -Use of TEMED /APS			[369]
	Acrylic acid + Acrylamide + BIS + Pluronic® F127	**Acrylic acid + Sodium bicarbonate** -Pore size 150µm -Highly connected pores	-Hydrogels made of hazardous substances -Addition of absolute EtOH -Drying in food dehydrator (80°C for 6 hours) and 4 hours of crosslinking			[360]
	PEGDA + Pluronic® F127 as a foam stabilizer	**Citric acid + Sodium bicarbonate** -Pores 100 to 600 mm. Broad distribution -Interconnected, 70% porosity	-Extensive washing after formulation -80% EtOH dehydration -Base addition with a constant stirring for 30 min. -Crosslinking: 30 min at 37°C	-Mesenchymal stem cells seeding -Bone tissue engineering		[362]
	PLGA	**Methacrylic acid + sodium bicarbonate** 10-20µm porosity: small	-Toxic crosslinker (TEMED + APS) -Extensive washing -Crosslinking speed: 10 min at 4°C	Fast release for treatment of thrombosis		[370]
	poly-(sulfobetaine methacrylate)	**Methacrylic acid +Sodium bicarbonate**	-Toxic crosslinker (TEMED+ APS) -Crosslinking speed: 30 min at room temperature	Study of the morphology of endothelial cells		[371]

Table 4: Porosity made by effervescence inside biomaterials and the processes limiting their in situ injectability (part II).
The strategies rely on the entrapment of carbonated base powders inside hydrogels network to then immerse the hybrid biomaterials in acid baths, limiting in situ *injectability.*

Strategy	Material	Porogens Porous structure	Processes limiting *In situ* injectability	Application	Positive attribute	Ref
Multi-steps processes: Hydrogel formulated and crosslinked with carbonated base powders followed by its immersion in acidic solution (salt leaching/gas blowing method)	Polyrotaxane + PEG-BA	**Citric acid +potassium carbonate** -Macroporous hydrogels (200-400µm) -Well-interconnected	-Incubation 24 hours at 40°C -Extensive washing for 36 hours with DMSO -Crosslinking speed: 24 hours at 40°C	Cartilage regeneration and chondrocytes culture	Possible pore control through concentration of the citric acid bath and through size of carbonated base particles incorporated to the polymer	[363]
	Elastin-like recombinamers containing RGD.	**Citric acid + Sodium bicarbonate** -Controlled pore size <40; <100 or 40-100 µm. Homogeneous pores -Interconnected pores	-Use of EtOH during formulation -Extensive washing in PBS -Crosslinking speed: 30 min at 37°C	Bioengineering materials with elastin. Fibroblasts and connective tissues		[365]
	Elastin like polymers	**Citric acid + Sodium bicarbonate** -200-300µm -Presence of interconnection	-Use of DMF -Extensive washing in milli-Q water -crosslinking speed: 3 hours at RT	Potential broad application. Endothelial cells *in vitro*		[372]
	PLGA	**Ammonium bicarbonate** + **citric acid** -Homogeneous pores Pore size 200 µm / 90% porosity	-Use of chloroform and EtOH -Immersion in aqueous citric acid solution -Hot water baths -Extensive washing	Swelling behaviour Molecule absorption and released by hydrogels		[357]

APS: ammonium persulfate ; BIS: (N'N-methylene-bis-acrylamide ; PEG-BA: poly (ethylene glycol)bisamine, PPF: poly (propylene glycol-co-fumaric acid), PEGDA: poly (ethylene glycol) diacrylate, PLLA: poly (L-lactic acid), PLGA: poly (lactic-co-glycolic acid),

2.2.5 The choice of a relevant hydrogel system of potential for VML treatment.

Our goal in this work was thus to propose an innovative biomaterial as a possible candidate to answer the complex product specifications that we defined above for the improvement of functional muscle regeneration after injury. Concretely, the objective is to develop a proof-of-concept for VML treatment through various aspect of a biomaterial design to *in fine* interact conveniently with skeletal muscle cells and tissues.

Recently, a hydrogel has been developed within the LBTI (Laboratoire de Biologie tissulaire et d'ingénierie thérapeutique) with the aim of combining mechanical tailorability with inherent properties for cell adhesion and growth [373]. To answer the complex requirements characterizing VML, this previously described hydrogel seems to be of high relevance.

Hydrogel precursor's choice dictates the biomaterial performance towards intended applications and is thus important. Among polymers, the PEG backbone has been largely used for the design of hydrogels due to its easy functionalization with reactive end-groups through various paths (e.g. methacrylate, acrylate, or NHS ester), to participate in covalent bonding for crosslinking. Resulting controllable crosslinking allows tailoring of the final support stiffness by modulating the chemical reaction. However, PEG bio-inertia requires most of the time an association with other functional moieties to promote cellular adhesion and survival. To provide the PEG polymer bioactivity while preserving its mechanical versatility, it was crosslinked with poly-(L-lysine) grafted dendrimers (DGL). DGL are polycationic arborescent-like structures formed by the assembly of naturally occurring L-lysine. They are obtained after lysine molecules grafting onto a linear poly-L-lysine (PLL) polymer structure to form increasing generation of DGL (G1 to GX). This synthesis is highly reproducible with a control on the molecular weight. DGL have shown to be soluble in aqueous solutions, stable under sterilization, with low cytotoxicity, and non-immunogenic properties [374]. As a consequence, they have been used in the biomedical field with applications in tissue regeneration based strategies [375], [376]. Among DGL the third generation (DGL-G3) ability to increase fibroblasts adhesion and proliferation when coated on plastic dishes in comparison to linear Poly-L-Lysine (PLL) [377] has encouraged its use in our group as crosslinking monomers to PEG to provide the inherent biochemical cues lacking to the inert PEG.

DGL/PEG hydrogel formation has been shown to be possible through the simple and straightforward mixing of bifunctionalized O,O′-Bis[2-(N-Succinimidyl-succinylamino)ethyl] polyethylene glycol (NHS-PEG-NHS) and poly-(L-lysine) grafted dendrimers of third generation (DGL-G3) solutions. Amine groups that are available at the surface of the DGL in high-densities bind with PEG via N-hydroxysuccinimide (NHS) to form covalent amide bonds (Figure 16A and B), leading to the formation of a polymer network at adequate concentrations and ratios of both components. The DGL/PEG hydrogel thus preserves the PEG stiffness

versatility and the DGL inherent bioactivity without the need for further functionalization with functional moieties (Figure 16C)

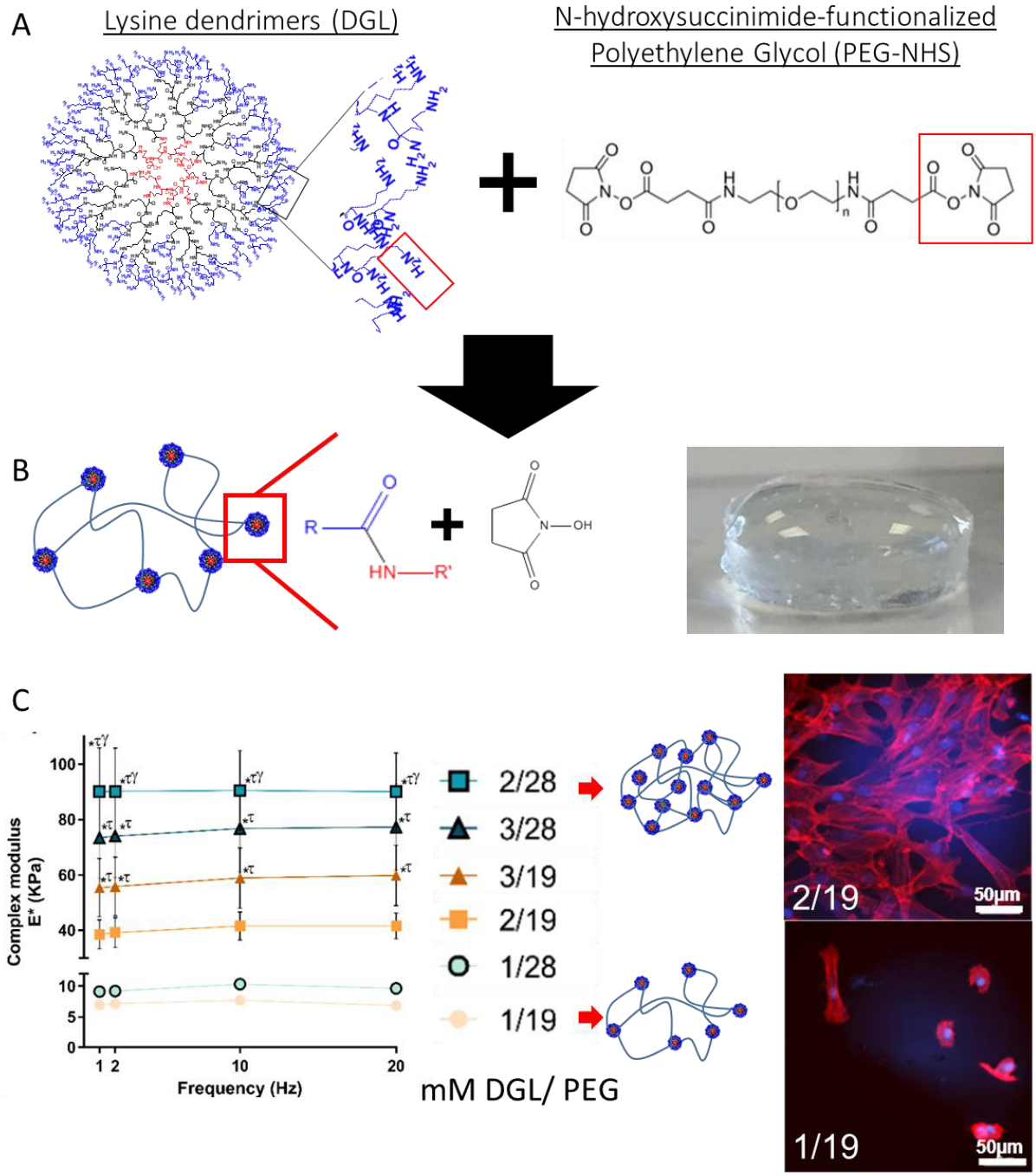

Figure 16: DGL/PEG hydrogel formulation
A) poly-(L-lysine) grafted dendrimers present a high concentration of available amine (NH2) at their surface, enabling the reaction with PEG molecule through NHS. B) The reaction between DGL and PEG-NHS forms a covalently crosslinked network with the formation of amide bonds. C) The hydrophilic nature of both polymers enables the network to absorb large quantity of water leading to the self-standing DGL/PEG hydrogel. In the reaction R represents the polyethylene glycol, R' represents poly-(L-lysine) grafted dendrimers of third generation–G3. C) Complex modulus in compression of DGL/PEG hydrogels of various concentration and ratio (kPa) showing a stiffness tailorability through DGL and PEG concentration. Effect of the stiffness and hydrogel composition on fibroblastic cells showing different ability to spread out and proliferate on the support.

The DGL/PEG hydrogel has been studied in contact with normal human dermal fibroblasts with promising results ([373] and attached article). Fibroblasts were able to conveniently adhere and grow on DGL/PEG hydrogels without additional functionalization, assessing the influence of the DGL to provide inherent bioactivity to the hydrogel. Moreover, we demonstrated that fibroblastic cells were highly affected by the stiffness and the composition of DGL/PEG hydrogels in terms of adhesion, proliferation and migration (Figure 16C). Accordingly, interesting conditions were targeted to produce *in vitro* full-thickness skin equivalents when associated with keratinocytes and fibroblasts [378]. Finally, DGL/PEG hydrogel biocompatibility was studied in subcutaneous implantations in mice demonstrating mild foreign body reaction with macrophages visible at the external edges of implants. No granulocytes nor lymphocytes could be observed surrounding the DGL/PEG hydrogel, suggesting a good tolerability in contact with tissues and assessing its potential for tissue engineering.

Considering that the DGL/PEG hydrogel holds promising results with fibroblastic cells, we wondered if it could be adapted to interact with skeletal muscle cells. Skeletal muscle cells possess a higher level of complexity compared with fibroblasts as they require various signals to grow or fuse. As the stiffness and the composition of the hydrogel can be varied by modulating DGL and PEG concentration and molar ratio, we wondered if it could affect skeletal muscle cells behaviour and how it could be controlled to be optimal for their growth and/or fusion.

Along with the DGL/PEG hydrogel, an elastin-like polypeptide (ELP) has been developed in our laboratory to present a similar amino acid sequence schemes to native tropoelastin [379]. It is composed of a repetition of hydrophilic motives present in native human tropoelastin: VGVAPG and VGVLPG (and the tropoelastin domain 36 including a disulfide bridge and a positively charged sequence GRKRK (Figure 17).

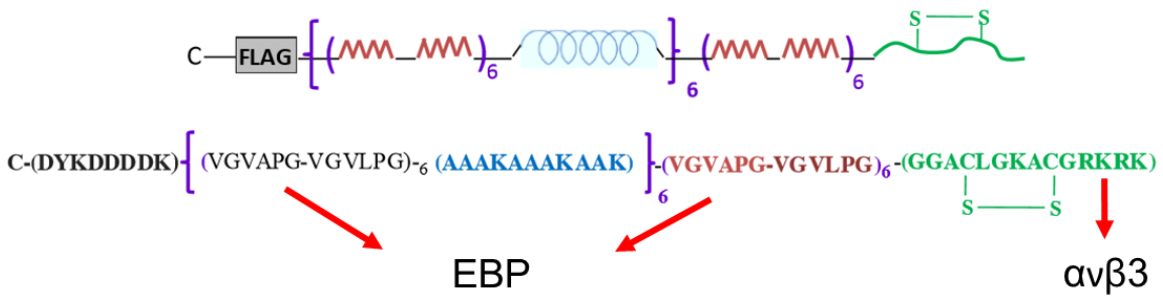

Figure 17: The elastin-like polypeptide
Structure of the elastin-like polypeptide developed in the laboratory. A flag tag (DYKDDDDK) is located right after N-terminal extremity followed by a repeated presence of hydrophobic domains VGVAPG-VGVLPG and crosslinking domain AAAKAAAKAAK. The domain 36 containing GRKRK motif is represented in green. Red arrows point at ELP sequences interacting with cell EBP or integrins. A stand for Alanine, C for Cysteine, D for Asp, G for Glycine, K for Lysine, L for Leucine, L for lysine, P for Proline, V for Valine, and Y for tyrosine. Adapted from Lorion 2015, Université Claude Bernard Lyon 1

When added to the culture medium of normal human dermal fibroblasts, the ELP presence has shown to increase cell proliferation. More interestingly, surfaces coated with the ELP have been related to an increased cell adhesion confirming its biological activity. This activity has been associated with GRKRK and VGVAPG functionality as the inhibition of αvβ3 integrins and EBP with anti-αvβ3 integrins antibodies and L-lactose respectively triggered a cell adhesion decrease [380]. Considering these results, the ELP was introduced inside DGL/PEG hydrogel liquid precursors to be entrapped inside the hydrogel network during crosslinking. The presence of the ELP inside the DGL/PEG network was associated with increased proliferation and spreading area of fibroblasts on the substrate [378]. It has also been related to an enhanced fibroblasts infiltration when incorporated in porous DGL/PEG hydrogels designed for full-thickness skin equivalent.

Given promising results in contact with fibroblasts, and previous reports showing elastin-like polypeptide effect on myoblasts [234], **we wondered if the addition of our 'in house' ELP inside DGL/PEG hydrogel could influence skeletal muscle cell behaviour**. The ELP was thus envisaged to provide relevant biochemical cues to the DGL/PEG hydrogel to influence cell adhesion, proliferation and/or fusion.

Finally, due to the hydrophilic nature of DGL and PEG polymers, they are soluble in aqueous solutions, and they can be, in theory, injected through needles to react upon injection and form a self-standing hydrogel. However, DGL/PEG hydrogel injectability has never been demonstrated in previous work. As not all liquid precursors based hydrogels are suitable for injection, **we thus wanted to investigate whether the DGL/PEG hydrogel could be injected**. Moreover, the DGL/PEG hydrogel has a tailorable crosslinking velocity depending on DGL/PEG ratios and concentrations, it can be varied to control precisely the time of the reaction and allow the passage through needles. **We as well wondered if a porosity could be induced inside the DGL/PEG hydrogel while maintaining its injectable potential** by taking advantage of its fast and tailorable crosslinking velocity. If few examples of fast gelling hydrogels have been reported in literature [381], [382], they are generally limited to low mechanical properties and poor stability. The DGL/PEG hydrogel by having controllable mechanical properties could enable the formation of a porosity while providing a support for skeletal muscle cell without adverse effects on tissues

General context

The striated skeletal muscle tissue possesses a tremendous regeneration potential after direct or indirect traumas (e.g. car accidents or ischemia) following a well-coordinated series of events leading to the restoration of normal tissue architecture and function. However, volumetric muscle loss (VML) characterized by a loss of more than 20% of the muscle mass overwhelms this regeneration capacity and induce persistent functional deficit and disability.

A fully developed muscle is made of an association of muscle fibres. Each muscle fibres is a syncytium formed as a result of the fusion of hundreds of specialized cells, myoblasts, able to fuse with each other. When the muscle is injured, muscle stem cells known as satellite cells are activated and migrate towards the site of injury to proliferate and differentiate into myoblasts contributing to muscle fibres regeneration. In VML, repair does not allow to restore the full functionality of the initial tissue in regards of contractility due to the lack of an orderly reconstitution of a structurally and mechanically valid extra-cellular matrix (ECM). Instead, a scar tissue is synthetized, attributed to the ablation of resident satellite cells and the lack of ECM that normally provides the structural and mechanical support on which cells can migrate and are guided towards functional regeneration. This imbalance between the recruitment of satellite cells and fibroblasts into the injury results in large amount of collagen deposition and the replacement of the muscle tissue by a fibrotic tissue, unable to contract.

Current clinical treatments to prevent fibrosis and recover muscle functionality consist of wound debridement and engraftments of autologous local muscle grafts or flaps. However, autologous muscle grafts and flaps are associated with high prevalence of failures, need for a second surgical procedure, lack of muscle flap/graft availability, and morbidity at the donor site. While attempts for stem cell or growth factors injection inside wounds have been reported as promising innovative treatments, they generally failed to enhance regeneration due to the too extensive tissue void, leading to extensive cell mortality and molecule washing.

In this context, tissue engineering and regenerative medicine, which aim to guide the functional regeneration of tissues and organs, are of high potential for VML treatment. They exploit the principles of engineering and life sciences towards the development of relevant biological substitutes overcoming the limitations associated with current treatments (auto and allograft procedures). The implantation in the wounded site of a 3D structure able to guide satellite cells and their progeny towards functional regeneration of the tissue is an interesting therapeutic possibility. In the last decades, it has become clear that the microenvironment is a potent regulator of muscle cell behaviour during the process of myogenesis through physical, biochemical, and architectural cues. Scaffold design has thus focused on biomaterials of specific chemistry, biochemical and mechanical properties for the promotion of highly precise interactions with skeletal muscle cells within a 3D environment.

Optimally, scaffolds for VML treatments should be injectable to conform to complex lesion shapes and tightly interact with the surrounding tissue while allowing neovascularization, innervation, and muscle precursor cells entry through adequate porosity. To this end, hydrogels have been extensively studied due to their excellent biocompatibility, their similarity to native extracellular matrices (ECM) in terms of water retention and cell adhesion, and injectable potential. Recently, 3D porous hydrogels have been designed to fill large defects while sustaining nutrient and oxygen transport as well as cellular and vascular infiltration for tissue ingrowth. Particularly, many studies have developed and characterized hydrogels able to carry cells inside wounds and guide them towards skeletal muscle tissue regeneration. However, they generally failed to design an optimal support providing all the mechanical and biochemical cues required by the tissue, in a single set and within a swift and straightforward injectable delivery.

A recently developed hydrogel, made from standardized elements (poly-(L-lysine) grafted dendrimers (DGL) and polyethylene glycol, PEG), has shown to be a relevant substrate for various cells. The synthetic nature of the hydrogel provides a precise control over its chemistry resulting in a broad mechanical properties versatility. Contrarily to others synthetic based hydrogels, the DGL/PEG hydrogel possesses inherent cyto-compatibility to interact conveniently with cells through polycationic charges brought by the DGL amines. The DGL/PEG hydrogel crosslinking, made in physiological environments, presents the interesting feature to allow the inclusion of an elastin-like polypeptide (ELP) in its bulk, enabling an enhanced fibroblasts proliferation and migration. The DGL/PEG hydrogel has demonstrated good *in vivo* tolerability further confirming its potential for tissue regeneration. Very interestingly, the DGL/PEG hydrogel is technically injectable through the mixing of liquid precursors.

Thesis objectives

While extensive development has been made in the production of scaffold-based strategies for skeletal muscle repair, most scaffolds rely on the use of embedded cells for functional regeneration. However, the incorporation of cells restricts their clinical approval by authorities. Considering there is no clinically approved therapy for the management of large muscle defects and given the very interesting features of DGL/PEG hydrogels, the aim of this thesis was therefore to investigate their potential to act as scalable support for the functional regeneration of skeletal muscle tissue in the case of VML. Accordingly, we propose in this work to study multiple aspects of a scaffold design to interact conveniently with host cells and tissues. To do so, multiple objectives were sought.

I- In a first chapter, we investigated whether **dense DGL/PEG hydrogels could act as a support to control muscle cell response through the modulation of mechanical and biochemical cues**. Previous efforts have generally been orientated toward improving a single aspect of this set. Hydrogels are highly swollen polymeric network mimicking native ECM which stiffness and elasticity can be controlled to promote cell behaviour. In addition to the mechanical properties, the influence of the amount of DGL and ELP on substrate surface was further studied on cell fate. We thus evaluated the influence of (1) six various stiffness, (2) four various DGL/PEG molar ratios and (3) a single concentration of ELP inside the DGL/PEG hydrogel. To assess the effect of mechanical and biochemical cues on skeletal muscle cells, three cell types were studied herein: a mice myoblasts cell line (C2C12), primary mice myoblasts (pMMs) and immortalized human myoblasts (iHMs). This chapter helped us to find optimum parameters of the DGL/PEG hydrogel to sustain skeletal muscle cells (Figure 18, part I).

II- In a second chapter, we evaluated the possibility **to create a porosity inside the DGL/PEG hydrogel while preserving its *in situ* injectable potential**. Instances of *in situ* injectable and porous biomaterials remain scarce in literature. In particular, very few instances have been evaluated for skeletal muscle functional regeneration. Therefore, the design of both injectable and porous DGL/PEG hydrogel may offer many therapeutic possibilities for soft tissue regeneration among which the management of VML. We therefore investigated various methods to create a porosity inside the hydrogel network through injection of liquid precursors, to interact tightly with the tissue in which it is placed. We then characterized the resultant porosity and its possible modulation through various parameters. Finally, we assessed the good cytocompatibility and biocompatibility of the innovative formulation to validate

its possible use for direct injection purposes following classic regulatory standards. Therefore, host response to DGL/PEG hydrogels was evaluated by subcutaneous injection in mice (Figure 18, part II).

III- In a third and final chapter, we assessed **the ability of the innovative 3D injectable formulation to guide skeletal muscle cells proliferation and differentiation**. In view of further clinical applications, we performed injectable and porous formulation of the DGL/PEG conditions targeted in the first chapter to study their relevance toward muscle cells. Accordingly, the behaviour of C2C12 cells and human primary myoblasts was evaluated in proliferation and differentiation. The results generated in the third chapter provided a first proof-of-concept for the use of 3D DGL/PEG hydrogel to manage VML injuries (Figure 18, part III).

All of these results were finally discussed to determine the potential of innovative formulations as *in vitro* 3D models for the study of myogenesis. In addition, this work opened perspectives for further optimization of the DGL/PEG hydrogel towards its direct *in vivo* injection for skeletal muscle tissue engineering

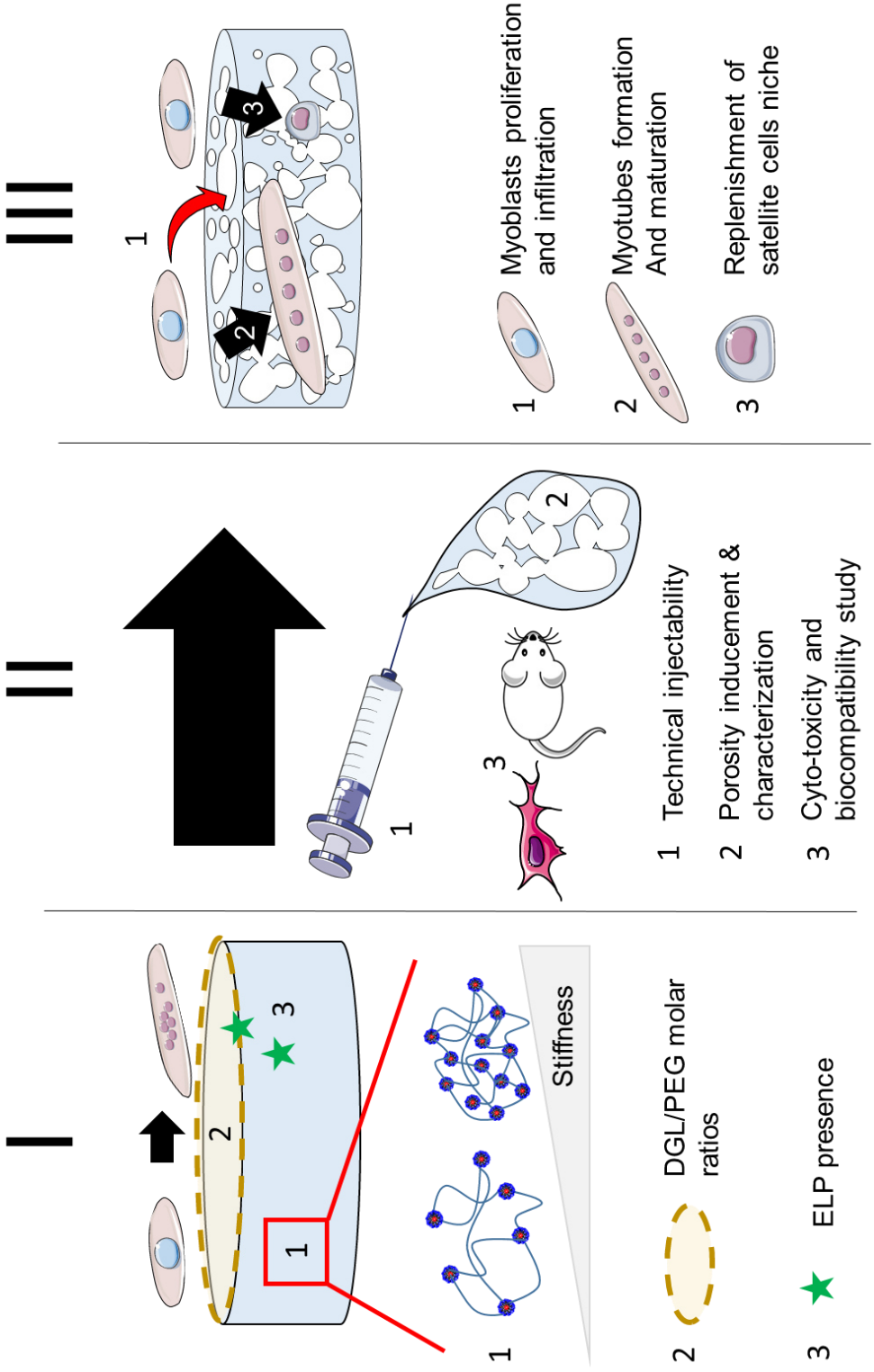

Figure 18: Thesis objectives
Chapter 1: Study dense DGL/PEG hydrogels as supports to control muscle cell response through the modulation of mechanical and biochemical cues
Chapter 2: Evaluate the possibility to create a porosity inside the DGL/PEG hydrogel while preserving its injectable potential
Chapter 3: Assess ability of the innovative 3D injectable formulation to act as a relevant support for skeletal muscle cells

MATERIAL AND METHODS

1 Dense DGL/PEG hydrogel formulation

The poly-(L-lysine) grafted dendrimers of third-generation (DGL-G3), 22 000 Da were purchased from COLCOM (Clapiers, France).

The O,O′-Bis[2-(N-Succinimidyl-succinylamino)ethyl]polyethylene glycol at 2000 Da (PEG-NHS) was bought from Sigma Aldrich (Saint Louis, USA).

Sterile Dulbecco's Phosphate Buffered Saline (DPBS), butan-1-ol, anhydrous N,N-Dimethylformamide (DMF), and Dimethyl sulfoxide (DMSO) were purchase from Sigma Aldrich (Saint Louis, USA).

Phosphate-buffered saline (PBS) 10X was purchased from EuroMedex (Strasbourg, France) and diluted in ultrapure water to obtain a final 1X concentration.

Stock solutions of DGL and PEG-NHS were realized at 400 mg/ml (w/v) using 5 ml volumetric flasks. DGL was solubilized in PBS 1X and PEG-NHS in organic solvents (either DMF or DMSO) to prevent NHS hydrolysis in aqueous solutions. DGL and PEG-NHS aliquots were stored at -20 °C before use. Once thawed, DGL and PEG-NHS aliquots were kept on ice and used within the next hours to prevent successive freeze-thaw and loss of reactivity.

The elastin-like polypeptide (ELP) was provided by the LBTI and solubilized in PBS 1X extemporaneously at desired concentration and kept on ice before use.

Dense hydrogels of various DGL/PEG-NHS ratios and concentrations were prepared by simply adding PEG-NHS and DGL to the adjusted volume of PBS 1X in 2 ml conic tubes (Maxymum Recovery, Axygen) to obtain the desired concentrations followed by vigorous homogenization. When needed, ELP at a final concentration of 4 mg/ml was introduced with DGL in PBS and the PEG-NHS was then added to the solutions followed by vigorous homogenization.

1.1 DGL/PEG hydrogel discs

For discs, 400 µL of hydrogel precursors were let to crosslink inside 2 ml tubes of internal diameter of 8 mm). Subsequently the tubes conical bottom was cut and they were submerged in 100% ethanol for 20 min to trigger hydrogels shrinking and easy retrieval. The resulting cylindrical hydrogels were subsequently rehydrated in PBS 1X and sectioned using a vibratome (7550 Integraslice) at a 50 Hz frequency, 1 µm amplitude, and a slow blade speed of 0.10 to 0.15 mm/s. Finally, hydrogels discs of 2 mm high and 9.1 mm wide were stored in PBS 1X at 4 °C for further use (Figure 19A).

1.2 DGL/PEG hydrogel drops

For drops, right after the homogenization, 90 µL of hydrogels precursors mix were deposited onto a highly hydrophobic PTFE plate. Hydrogels were allowed to crosslink for 10 minutes in wet chambers, detached from the hydrophobic surface, and immediately used for subsequent experiments without any washing or post formulation treatment. For culture cell purposes, DGL/PEG hydrogel drops were realized under a laminar airflow cabinet in an aseptic manner (Figure 19A).

1.3 DGL/PEG hydrogel adhered discs in 48 well plates

For hydrogels adhered in well plates, 90 µL of mixed liquid hydrogel precursors were rapidly deposited in wells of a 48 well plate and quickly recovered with 600 µL of hydrated butan-1-ol for meniscus smoothing. After crosslinking, hydrogels were extensively washed and sterilized overnight in an EtOH/PBS (70/30; v/v) solution at 4 °C followed by extensive washing with sterile DPBS. Hydrogels were kept immersed in sterile DPBS at 4 °C before use. To reach highly concentrated hydrogels, the preparation was performed in a cold room (4 °C) to slow down the chemical reaction. The resulting plane hydrogels were 10 mm wide and 0.7 mm high to prevent the cells from feeling the underneath plastic stiffness.

In the present work, eight various DGL/PEG-NHS hydrogels concentrations were studied (Table 5) for a single ELP concentration of 4 mg/ml with the PEG-NHS either solubilized in DMF or DMSO (Figure 19A).

Table 5: Concentrations and molar ratio of DGL/PEG hydrogels studied in this work

DGL / PEG (mg/mL)	DGL / PEG (mM)	Nomenclature DGL/PEG (mM)	DGL: PEG ratio
25/50	1.14/25	1/25 *	1:25
35/50	1.60/25	1.6/25 **	1:16
50/38	2.27/19	2/19	1:10
50/50	2.27/25	2/25	1:12
50/75	2.27/37.5	2/37 **	1:16
50/100	2.27/50	2/50 *	1:25

**, ** DGL/PEG hydrogels of various stiffness but with the same DGL/PEG ratio*

2 ELP production

Kanamycin and polyethylene-imine (PEI) were brought from Sigma Aldrich (Saint Louis, USA).

The elastin-like polypeptide (ELP) was obtained by recombinant protein production. The ELP DNA coding sequence was cloned with Flag tag fusion protein using the pET30a vector backbone. BL21(DE3) E.Coli strain was transformed with pET30a-Flag-ELP plasmid. Single colonies were isolated on Luria-Bertani (LB) agar 73 medium supplemented with 50 µg/ml kanamycin and incubated at 37°C overnight. Then, 200 ml of Terrific Broth supplemented with 50 µg/ml kanamycin were inoculated with one colony and incubated at 37°C overnight under shaking (150 rpm). In a bioreactor (Minifors II, INFORS), a total of 4 L of Teriffic Broth were inoculated with preculture at DO=0,1. Bacteria were grown to log phase DO=1, in the presence of kanamycin, 1 mM trace elements, and glycerol (10g/L) at 37°C under agitation at 400 rpm and 20 % pO2. The temperature of the culture was decreased to 25°C and expression was induced with 1 mM Isopropyl β-d-1-thiogalactopyranoside (IPTG) for 16 hours under agitation from 400 rpm to 800 rpm at 20 % pO2. To avoid foam formation, 500 µL of anti-foam was added.

For purification, the culture was harvested and centrifuged at 5000 g for 20 minutes, bacteria were resuspended in 400 ml of ultrapure water and lysed by pressure cell disruption at 2600 bar (Cell Disruption System, Constant System Ltd). The lysate was harvest, buffered with 20 mM Tris-HCl pH 8.8 and centrifuge at 10000 g for 20 min. The supernatant was treated with 0.2 % Polyethylene-imine (PEI) on ice, PEI was slowly added under soft agitation and then centrifuged for 20 minutes at 10000g and 4 °C to eliminate precipitated contaminants. After eliminating contaminants, 500 mM of NaCl was added to the supernatant, incubated for 10 min at 40°C and finally centrifuged for 10 minutes at 10000 g and 40°C. The pellet was re-suspended in DPBS overnight at 4°C and centrifuged at 5000g for 10 minutes at 4°C. Finally, the supernatant was freeze-dried (Cosmos, Cryotec) and stored at -20°C before use. Stock solutions of ELP were prepared by suspending the dry protein in DPBS to a maximal concentration of 40 mg/ml and used extemporaneously.

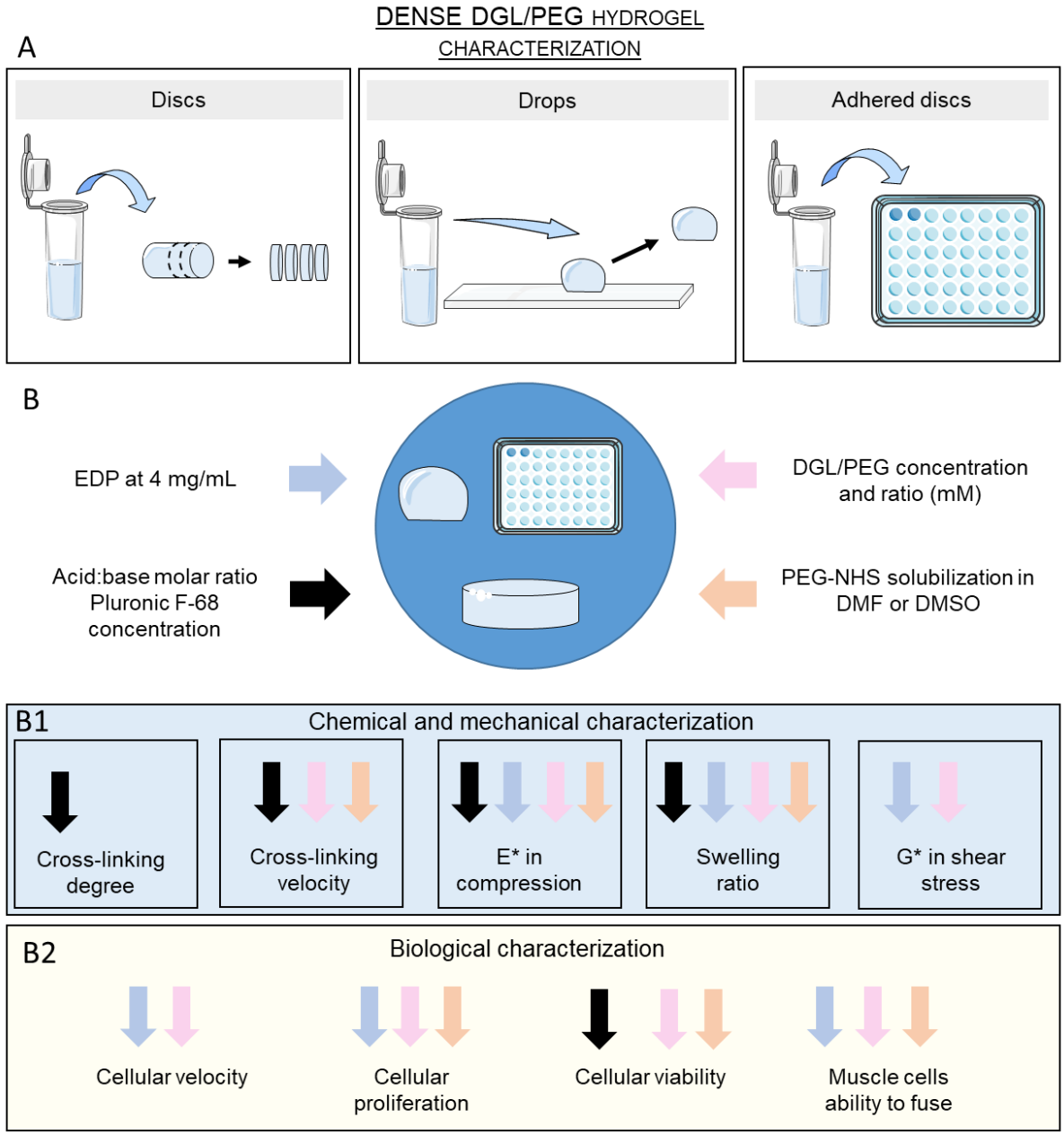

Figure 19 : Dense DGL/PEG hydrogel characterization

A) Schematic representation of dense DGL/PEG hydrogel formulation in various shapes for characterization.

-Discs were 9.1 mm wide and 2 mm high. Discs were extensively washed and sterilized before use.

-Drops were formulated on hydrophobic surface (PTFE), detached, and used immediately without any washing of post formulation treatment to mimic direct in situ *injection. Drops were realized in sterile conditions.*

-For cell culture, discs were adhered to cell culture plates. Adhered discs exhibited a flat surface of 9 mm in diameter and 7 mm in height to prevent cells from feeling the plastic stiffness. Adhered discs were extensively washed and sterilized before use.

B): Dense DGL/PEG characterization

Top: Input parameters studied on dense DGL/PEG hydrogels,

B1) Blue box: chemical and mechanical characterization of hydrogels as a function of inputs parameters

B2) Yellow box: biological characterization using NHDF, C2C12 and ihMs cells as a function of inputs parameters

3 Elaboration of a DGL/PEG porosity suitable with its injection

3.1 Preliminary study

3.1.1 Particles leaching

3.1.1.1 Gelatine microbeads realization

Type B Gelatine was purchase from BioRad (Hercule, USA), sunflower oil was bought from Casino (France), and the tween 20 from EuroMedex (Strasbourg, France).

Preparation of gelatine microbeads (GMBs)

Gelatine microbeads (GMBs) were prepared following an established protocol with minor modification (Sokic *et al*., 2014 [261]). Briefly, 1 g of gelatine was dissolved in 9 ml ultrapure water at 60°C. The gelatine solution at 10 % (w/v) was then added in 50 ml of sunflower oil at 60°C under stirring at 500 rpm. The emulsion was maintained for 10 min at 60°C, before lowering the temperature by adding an ice bath to reach ~15 °C at a constant stirring. After 30 minutes, the dispersion was divided into four 50 ml tubes and mix with an excess of cold PBS 1X. The emulsion was kept below 15°C during washing to prevent GMBs solubilisation. Tubes were centrifuged for 10 minutes at 300 g and 4°C and the supernatant discarded. Tween 20 at 1% in PBS 1X was then added in excess and 50 ml tubes centrifuged again to discard the supernatant containing tween 20 and oil. GMBs were rinsed twice with PBS 1X and four times with tween 20 at 1 % followed by three washes with distilled water. GMBs were either stored hydrated at 4°C in distilled water or frozen in liquid nitrogen, stored at -20°C overnight, and freeze-dried for storage.

3.1.1.2 Porous hydrogels using gelatine microbeads

DGL and PEG were mixed to obtain 400 µL of a final 2/25 mM concentration, vigorously homogenized by vortex, and rapidly transferred into 2 ml conic tubes (Maxymum Recovery, Axygen) containing either hydrated or dehydrated GMBs. The mix was vigorously pipetted to obtain a homogeneous distribution of GMBs throughout the hydrogel. After crosslinking, DGL/PEG hydrogels containing GMBs were immersed in PBS 1X and kept at 37°C under agitation for 24h. Positive and negative controls were performed with DGL/PEG hydrogels containing GMBs kept at 50°C or 4°C under agitation to follow GMBs leaching.

Hydrogels were then manually cut and observed under a fluorescence microscope to follow gelatine leaching.

3.1.2 Stabilized air emulsion inside DGL/PEG hydrogels

PEG 8000 was purchased from Sigma Aldrich (Saint Louis, USA). The tween 20 was bought from EuroMedex (Strasbourg, France).

DGL and tween 20 between 5 and 15 % in PBS were deposited inside a 1 ml syringe. The PEG-NHS in DMF and the PEG 8000 between 5 to 15 % (w/v) in PBS were deposited inside another 1 ml syringe with a desired volume of air pumped into the syringe. The PEG 8000 was added to hydrogels precursors to increase solutions viscosity. Both syringes were joined by a connector and solutions with air were mixed by pushing the plungers of the syringes alternatively in opposite directions for 10 seconds followed by hydrogel precursor's injection in 2 ml conic tubes. Resulting hydrogels were carefully removed from the tube, cut longitudinally and observed under a light microscope.

3.1.3 Effervescent approach

The potassium, calcium, magnesium and sodium carbonate, the sodium bicarbonate, the citric acid, and the succinic acid, the pluronic® F-127 were all purchased in powders from Sigma Aldrich (Saint Louis, USA). The glacial acetic acid was purchased at 17.67 M from Carlo Erba reagents (Milan, Italy).

The pluronic® F-68 was bought at 10% from Thermo fisher scientific (Waltham, MA, USA) and the tween 20 from EuroMedex (Strasbourg, France).

3.1.3.1 Study of effervescent reaction

Effervescent reaction properties were investigated to study their behaviour and their potential to match the crosslinking process of the DGL/PEG hydrogel.

To this end, various carbonated bases and carboxylic acid (listed below) were studied solubilized in ultrapure water (concentration used listed Table 6).

Table 6 : Carboxylic acid and carbonated base concentrations of stocks solutions

Carbonated bases		Stock solutions (saturation)
Potassium carbonate (KC)	K_2CO_3	8.1 M
Calcium carbonate (CaC)	$CaCO_3$	1.3 x 10^{-4} M
Magnesium carbonate (MgC)	$MgCO_3$	1.2 x 10^{-3} M
Sodium Carbonate (NaC)	Na_2CO_3	2.8 M
Sodium bicarbonate (NabC)	$NaHCO_3$	1.03 M

Carboxylic acids		Stock solutions (saturation)
Citric acid (Ca)	$C_6H_8O_7$	2.82 M
Succinic acid (Sa)	$C_4H_6O_4$	0.59 M
Glacial acetic acid (Gaa)	CH_3COOH	17.67 M

Carbonate bases and carboxylic acids were mixed at various molar ratios (from 1:2 to 2:1 Acid:Base) and various final molarities (0.5, 1.0, and 1.5 M) in PBS 1X or PBS 10X. The effervescence power and CO_2 bubbles generation were visually assessed. The effect of

surfactant addition (tween 20, pluronic® F-127 or pluronic® F-68) at various concentrations was visually studied on effervescence duration over time and bubbles repartition. The pH of the solutions after effervescence was monitored at 25°C using a pH meter (Mettler Toleda, FiveEasy) at various time points. At least 3 various effervescence were generated for each condition studied.

Study of the effect of pH, ionic strength, surfactant and PEG solvent on dense DGL/PEG hydrogels crosslinking and chemistry

To investigate whether the effervescent reaction can be coupled to the DGL/PEG crosslinking reaction and to determine an appropriate range of conditions allowing CO_2 bubbles entrapment, the DGL/PEG crosslinking was performed in various pH and ionic strength dependent medium. The pH (from 5 to 10), the ionic strength (from 0.5 to 1.68 M), the ion nature (acid and base cited below as well as hydrochloric acid (HCl) and sodium hydroxide (NaOH)) and surfactants influence on the resulting crosslinking was studied on DGL/PEG hydrogel using effervescent solutions **that had already reacted**.

To do so, acid and base were mixed at various ratios and concentrations to obtain distinct pH and ionic strength. Effervescences **were let to occur for 15 minutes** with vigorous homogenization. **After the effervescence was completed**, the DGL in PBS and the PEG-NHS in organic solvents were added to the mix and vigorously homogenized. After homogenizations, hydrogels of various DGL/PEG compositions were shaped like discs, drops, or adhered discs as needed. To study the effect of the pluronic® F-68 at 1.7; 3.3 and 5 %, DGL and PEG-NHS were added to pluronic® F-68 in PBS to obtain a 2/25 mM DGL/PEG concentration. Control hydrogels were composed of DGL/PEG at various concentrations in PBS.

Table 7 : Gaa and KC respective concentrations in hydrogels to obtain a final 1.1M at various molar ratios

Gaa:KC molar ratio	Gaa (M)	KC (M)
1:1.6	0.428	0.684
1:1.5	0.445	0.667
1:1	0.582	0.530
1.33:1	0.635	0.477
1.5:1	0.667	0.445
1.75:1	0.707	0.405
2:1	0.741	0.371

Table 8 : Gaa and KC respective concentrations in hydrogels to obtain a 1.75:1 molar ratio at various final concentration

Gaa + KC final concentration (M)	Gaa (M)	KC (M)
0.5	0.318	0.182
1.0	0.636	0.364
1.5	0.954	0.546

3.2 Effervescent porous hydrogels (EPH) formulation

Glacial acetic acid (Gaa) and potassium carbonate (KC) were chosen for subsequent experiments at a 1.1 M final molarity and a molar ratio between 1.33:1 and 1.75:1. Pluronic® F-68 was chosen as a foam stabilizer at final concentrations between 1.7 and 5%.

To prepare effervescent porous DGL/PEG hydrogels (EPH), DGL and KC were mixed at desired concentrations in PBS in a conic tube (1) to obtain a 200 µL final volume. Concomitantly, pluronic® F-68, Gaa, and PEG-NHS in organic solvents at desired concentrations were mixed in a second conic tube (2) to a 200 µL final volume. After vigorous homogenization of both mixes, mix (2) was transferred to mix (1) and manually homogenized by pipetting. After crosslinking, EPH were immersed in PBS for further use.

The volume expansion of the EPH was quantified as follows: 400 µL EPH at various final DGL/PEG concentrations (1.6/25; 2/25 and 2/37 mM) were prepared as described above. Their volume expansion was then calculated as the ratio between the volumes of EPH after crosslinking and dense hydrogels of the same concentrations. At least three hydrogels were measured for each condition studied.

3.2.1 Preparation of porous hydrogels by injection

The injectability of effervescent porous DGL/PEG hydrogels (EPH) was assessed by preparing the two mixes as described above. After vigorous homogenization of both mixes, they were heated at 37°C in a water bath. Both mixes (200 µL each) were transferred in different compartments of a dual syringe (adhesive dispensing Ltd) at a ratio 1:1. Both mixes there then injected in a conic tube through a static mixing nozzle (adhesive dispensing Ltd – 49.7 mm). The injectable system was assessed on various hydrogels conditions (1.6/25; 2/25 and 2/37 mM DGL/PEG with and without the presence of ELP) for a set 1.33:1 Gaa:KC molar ratio and 3.3 % PF-68.

After crosslinking, EPH formulated from manual homogenization or injection were immersed in PBS for 24 hours to prevent drying and favour CO_2 bubbles removal. They were then removed from conic tubes, embedded in agarose 1 %, and manually cut to obtain 2 or 3 mm-thick discs. Discs were then rinsed extensively with PBS at 60°C to remove agarose, sterilized overnight in a solution of EtOH/PBS (70/30 v/v), and stored in PBS for further use.

3.2.1.1 Force needed to inject the DGL/PEG hydrogel

The force needed to inject DGL/PEG hydrogels was assessed with porous 2/25 mM DGL/PEG hydrogels prepared as described above. Dense 2/25 mM DGL/PEG hydrogels were prepared as control as follows: DGL in PBS was placed in the first compartment of a dual syringe and PEG with PBS in the other compartment to obtain 300 µL in each cartridge. The dual syringes connected to a mixing nozzle were placed in a Texture Analyser TA.HDplus (Texture Technologies, Hamilton, MA) and the force needed to push the plungers while maintaining a 2 mm/s velocity was recorded using a 500 kg load cell. Distilled water was tested as a positive control.

At least three dense and porous hydrogels were measured.

4 Characterization of dense and porous DGL/PEG hydrogels

4.1 Crosslinking velocity

The crosslinking velocity of DGL/PEG hydrogels was recorded inside a small glass vial (8x35 mm). Briefly, DGL in PBS at desired concentrations was mixed with the buffer of interest or in PBS 1X as a control in the vial under agitation (500 rpm) with a magnetic rod (5 mm). The vial was placed at exactly 4 cm from the magnetic stirrer and the PEG in organic solvent was added at the desired concentration. Crosslinking time was defined as the time needed to reach a viscosity threshold able to halt the magnetic rod after adding the PEG to the mix. The crosslinking time was defined at room temperature (RT) in a final volume of 50 µL. At least three hydrogels were measured for each condition studied.

In addition, the PEG solvent was studied on the resulting crosslinking reaction. To do so, PEG-NHS was solubilized in various solvents (DMF, DMSO and PBS) aliquoted and stored at -20°C. Right after solubilisation (W0) and after 1 and 4 weeks of storage (W1 and W4), the crosslinking velocity of a 2/25 mM DGL/PEG hydrogel made in PBS was recorded as previously described.

4.2 Crosslinking degree evaluation

The crosslinking degree of DGL/PEG hydrogels was investigated using drops of 2/25 mM DGL/PEG dense hydrogels prepared using fluorescein-labeled DGL at 0.2 % of the final DGL concentration. Hydrogel drops were formulated with the buffer of interest and right after crosslinking, they were immersed in PBS (600 µL) without washing or post formulation treatments. After 24 hours incubation at 37°C, supernatants were harvested and their fluorescence measured using a fluorescence microplate reader (TECAN infinite® 200) at excitation 485 nm and emission 535 nm. At least three hydrogels were measured for each condition studied.

4.3 Dynamic mechanical analysis

4.3.1 Principle

One of the features of hydrogels is their viscoelastic behaviour resembling native ECM [383]. Hydrogels under deformation, display properties of both elastic solids and fluid resistance to flow. One of the most reliable and well-described ways to measure the viscoelastic properties of materials is through dynamic mechanical analysis (DMA) [384]. DMA is based on the application of small oscillatory stress (σ) to material samples (here in compression) with their resulting deformation (ε) monitored to generate another oscillatory strain curve.

The phase shift between oscillatory stress and strain curses is therefore the measure of the amount of elasticity present in a sample. In oscillatory experiments, the phase shift allows to separate the elastic and viscous modulus of the materials with the following equation:

$$tan\ \delta = \frac{E''}{E'}$$

For viscoelastic material, the Hooke's law is replaced by a specific relationship between the stress (σ) applied on samples and the resulting strain (ε)

$$\sigma = E^*\varepsilon$$

Where E* is the complex modulus:

$$E^* = E' + iE''$$

$$i^2 = -1$$

E' is the dynamic modulus of elasticity or the storage modulus and represents the elastic part of the material. The imaginary part (E'') is called the loss modulus and represents the viscous part (out of phase) and is related to material's ability to dissipate stress through heat.

When E' is higher than E'', the material can be defined as mainly elastic with a phase shift below 45°

4.3.2 Protocol

The mechanical properties of dense (2 x 9.1 mm) and porous (3 x 9.1 mm) hydrogels discs of various compositions were analysed by cyclic compression with a dynamic mechanical analyser (DMA 242 E Artemis, NETZSCH, Germany). Hydrogels domain of linearity was first determined for each condition with a strain sweep test in compression performed in PBS immersion at room temperature (with amplitudes from 1 to 100 µm at 1 and 10 Hz). Samples were then subjected to compression at 10 % and 30 % strain (for dense and porous hydrogels respectively), 50 µm amplitude, and 1 Hz frequency in PBS immersion at a constant temperature of 25°C.

The 10 and 30 % constrain applied on dense and porous hydrogel cylinders was obtained using 1 mm wide PTFE blocks of 1.8 mm or 2.1 mm high respectively. Briefly, hydrogels cylinders were placed on the sample holder together with PTFE blocks, which were 10 and 30 % shorter than the cylinders (2 and 3 mm high for dense and porous hydrogels respectively). The upper part of the geometry (used to applied strain on the sample) was then moved down on the samples until reaching the PTFE block, characterized by an abrupt pushrod displacement of more than 20 µm (recorded by the displacement sensor). The PTFE block was then carefully removed to obtain 10 or 30% constraints on the samples, and cyclic oscillatory stress in compression was applied to samples. At least three hydrogels were characterized per condition studied.

4.4 Swelling ratio

The swelling (Qs) of 2 mm thick and 4.5 mm wide half-circle hydrogels was determined in PBS at 37°C from dense hydrogels discs. Briefly, hydrogels were extensively rinsed in milliQ water, immersed in liquid nitrogen and freeze-dried for 48 hours at 400 mTorr (Cosmos, Cryotec). Freeze-dried samples were weighed using an analytical balance, immersed in a 37°C PBS solution, and kept at 37°C. Samples were blotted to remove exceeding PBS before each weight measurement performed after 1; 2; 4; 8; 24 and 48 hours of immersion. Measurements were taken until reaching equilibrium. The swelling ratio was calculated using the following equation:

$$\frac{W_s - W_d}{W_d}$$

Where Ws represents the swollen weight of the sample at time t and Wd represents the dry weight of the freeze-dried sample. At least three hydrogels were measured per condition.

4.5 Rheological measurements

Rheological measurements were carried out on dense and porous 400 µL DGL/PEG hydrogels at 23°C. To do so, a Haake Mars rheometer (thermoHaake®, Germany) with a titanium parallel-plate geometry (20 mm diameter) was used. Wall slip was avoided by using plates equipped with emery paper. Hydrogels right after homogenization were injected between parallel-plate geometries. A shear stress of 1 Pa was applied at five frequencies (i.e. 0.3; 0.5; 1; 1.8 and 3.2 Hz). The evolution of G' and G'' overtime was followed with acquisitions every minute during the gelation process. G' was determined as the stabilized value obtained at a constant 1 Pa constrain (less than 1% variation in the previous hour). Samples were then subjected to a strain increase from 0.1 Pa to 15 000 Pa at 1 Hz frequency. The fracture was determined as the strain related to an abrupt G' decrease.

The chemical characterization performed on DGL/PEG dense hydrogels of various components is resumed in Figure 19.B1.

4.6 EPH porosity characterization

For representative pictures, EPH were immersed in a 0.1 % Coomassie brilliant blue G-250 in methanol/acetic acid/water (20/10/70; v/v/v) solution for one hour, followed by three washing in PBS. For porosity characterization, 2 mm-thick EPH discs were prepared as described above (injected or with manual homogenization) using fluorescein-labeled DGL (DGL-FITC) at 0.4 % of the final DGL concentration.

The resultant EPH structure was studied by image analysis from 2 mm-thick discs observed by laser scanning confocal microscopy (LSCM Zeiss Imager.Z2) under PBS immersion. To do so, 400 µm z-stacks were realized on the entire diameter of hydrogels discs (on both sides). To determine **pore size**, three arbitrary positions (in distinct z positions) were selected on each stack, and pore area and diameter were measured with ImageJ analysis. An average of 400 pores in separated positions was quantified for each hydrogel. **The total volume occupied by pores** was extrapolated using ImageJ plugin "BoneJ" [385] on entire stack images of each hydrogel discs. **The size of windows of interconnection** was determined by a successive thresholding method adapted from Bellamkonda and colleagues [386] on 3 arbitrary positions on each z-stack. Briefly, binary images were used and pores were individualized using a watershed algorithm to obtain interconnections. An image containing the closed pores was subtracted to an inverted one without closed pores showing only interconnections between pores allowing their measurements. Interconnections were quantified in the three dimensions (x,y,z).

The porosity was characterized for various Gaa:KC molar ratio, pluronic® F-68 concentration, DGL/PEG conditions and homogeneization methods (Table 9). At least three EPH per condition were characterized at six distinct positions (see Figure 20).

Table 9: Parameters studied on DGL/PEG EPH porosity

Gaa:KC molar ratio	Pluronic ® F-68 (%)	Hydrogel concentration mM DGL/PEG	Homogenization process
1.5:1	1.7% 3.3% 5%	2/25	Manual
1.75:1 1.33:1	3.3%	2/25	
1.33:1	3.3%	1.6/25 2/25 2/37	Injection

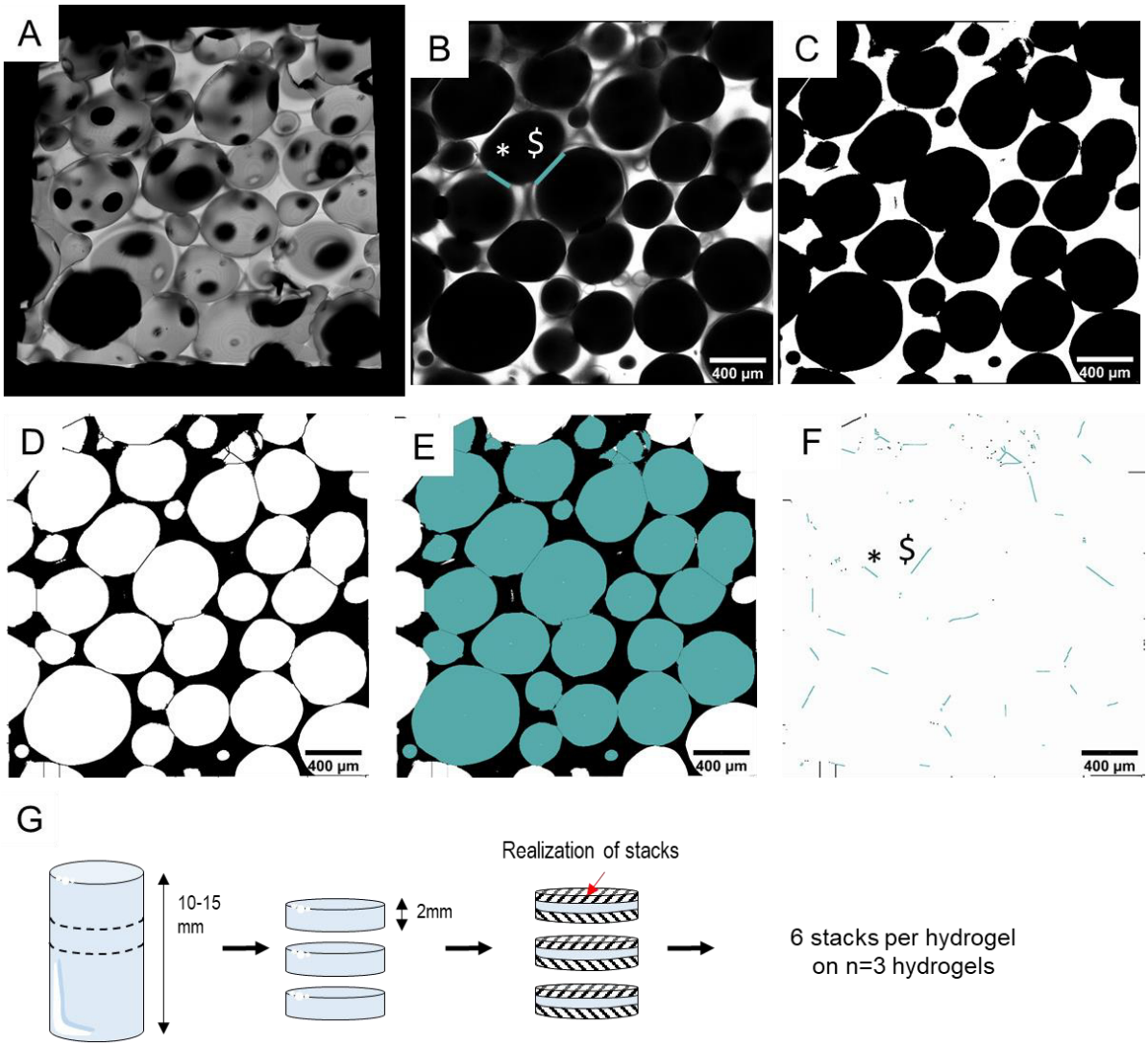

Figure 20 : <u>Porosity characterization</u>
Representative pictures of a 2/37 mM DGL/PEG hydrogel 400-µm stack made by laser scanning confocal microscopy. Hydrogel formulated with 1.33:1 Gaa:KC and 3.3 % PF-68
*A) The percentage of porosity was determined with BoneJ plugin using the entire 400-µm z-stack. B) One 2D picture was extracted from stack and C) converted into binary image. D) Watershed treatment was performed to individualize pores and reveal interconnections. E) Pore area calculation was performed with a selection of diameters above 20 µm (area = 314 µm²). F) Windows of interconnection were quantified by images subtractions to reveal only interconnections. Windows of interconnections were calculated in the 3 dimension for each stack. Particles above 200 µm² were selected. * and $ show interconnections compared with the raw picture (B). Pores and interconnections on edges were excluded. Only pores and interconnections represented in blue in this instance were analysed. G) Schematic representation of hydrogel observation after formulation. The hydrogel core was cut to obtain 2 mm high slices at various positions. A stack was then performed on both side of each slice leading to 6 stacks/hydrogel. At least three hydrogels/conditions were characterized.*

5 Cell culture maintenance

5.1 Dermal cells

5.1.1 Material

Dubecco's Modified Eagle Medium (DMEM) / Ham's F12 (DMEM-F12) 1:1 Glutamax, and trypsin – EDTA 0.05% were purchased from Gibco, Thermofisher Scientific (Waltham, MA, USA). Foetal bovine serum (FBS), penicillin/ streptomycin (penicillin 10,000 U/ml-Streptomycin 10 mg/ml) and DMSO were purchased from Sigma Aldrich (St. Louis, MO, USA)

5.1.2 Human dermal fibroblasts maintenance

Normal human dermal fibroblasts (NHDF) isolated from foreskin were obtained from Promocell (Heidelberg, Germany). Cells were stored in liquid nitrogen and thawed for amplification. Briefly, frozen cells were immersed in 10 times their volume of Dubecco's Modified Eagle Medium (DMEM) / Ham's F12 (DMEM-F12) 1:1 Glutamax supplemented with 10% Foetal bovine serum (FBS) and 1 % penicillin/streptomycin (P/S). Cells were centrifuged at 200 g at 4°C for 5 minutes, the cell pellet was then re-suspended in serum-supplemented DMEM- F12 at 37°C and cells seeded at a density between 3000 and 5000 cells/cm² in tissue culture flasks. Cells were let to proliferate until reaching 80 % confluence and then detached by adding trypsin EDTA 0.5 % for 5 min at 37°C and 5 % CO_2 after extensive washing with sterile DPBS to remove FBS. Once cells were detached, trypsin-EDTA was inhibited using twice the volume of 10% FBS-supplemented DMEM-F12. Cells were counted using a Malassez hemocytometer with trypan blue (1:1), centrifuged for 5 min at 200 g to remove trypsin EDTA, and re-suspended in the suitable volume of serum-supplemented DMEM F-12 to achieve the desired density that was subsequently seeded on flasks or plates as desired. NHDF cells were grown below 80 % confluence.

NHDF cells were used at passages below 12 or frozen in FBS containing 10 % DMSO at 1 x 10^6 cells per mL. Cells were frozen in a progressive freezing box (1°C/min) and placed in liquid nitrogen for long-term storage. In every experiment involving hydrogels, positive controls were prepared by seeding NHDF on treated culture plastic.

5.2 Striated skeletal muscle cells

5.2.1 Material

DMEM 1X, Iscove's Modified Dulbecco's Medium (IMDM), DMEM high Glucose with pyruvate, medium 199 with glutamax supplement, FBS, Gentamycin, Horse Serum (HS), trypsin – EDTA 0.05%, DPBS were purchased from Gibco, Thermofisher Scientific (Waltham, MA, USA). Dexamethasone, insulin from bovine pancreas, creatine, pyruvate, uridine, Ham's F10 medium, Penicillin/streptomycin (P/S) and puromycin were bought from Sigma Aldrich (St. Louis, MO, USA). Bovine serum albumin (BSA) was purchased from Euromedex (Strasbourg, France). Skeletal Muscle Cell Growth Medium with supplemented mix was purchased from PromoCell, Heidelberg, Germany. Matrigel was purchased from corning (NY, USA).

5.2.2 Skeletal muscle cells general maintenance

All cell types used were cultured at 37°C and 5% CO_2 atmosphere with controlled hygrometry.

Unless stated otherwise, in routine maintenance, myoblasts were always kept below 60 % confluence to prevent pre-differentiation into myocytes upon cell-cell contact. To passage, myoblasts were extensively washed with DPBS and detached from plastic dishes by immersing them in 0.05 % trypsin-EDTA for 5 minutes at 37°C. The detachment reaction was stopped by adding at least twice the volume of growth medium (GM) containing FBS. Cells were then centrifuged at 200 g for 5 minutes at RT to withdraw the remaining trypsin-EDTA. The cell pellet was resuspended in the desired volume of GM for seeding. Unless stated otherwise, proliferating cells were let to reach 80 % confluence before initiating their differentiation. To this end, cells were washed once with DPBS and immersed in differentiation medium (DM) which is a serum-depleted medium.

Muscle cells were frozen in FBS containing 10 % DMSO at 1 x 10^6 cells per mL. Cells were frozen in a progressive freezing box (1°C/min) and placed in liquid nitrogen for long-term storage.

In every experiment involving hydrogels, controls were prepared by seeding cells at the same density on culture plastic or matrigel coatings. Matrigel positive controls were made by adding cold 1/100 matrigel in wells for 30 minutes at room temperature followed by one washing with warm DPBS just before use.

5.2.2.1 Immortalized mice myoblasts cell line (C2C12)

C2C12 cells were purchase from DSHB (USA). They are an immortalized myoblast cell line originally established from satellite cells of two-month-old C3H mice muscles 70 hours after a crush injury [387]. C2C12 cells were grown as undifferentiated myoblasts in growth medium: DMEM 1X supplemented with 15 % FBS and 1% P/S. To passage, cells were detached from 10 cm culture Petri dishes (as described above) and seeded at low density (between 1700 to 2600 cells/cm²) every 2-3 days. In GM, C2C12 cells proliferate with a doubling time of approximately 16h. C2C12 differentiation was initiated after reaching 80% confluence. To do so, cells were washed once with warm DPBS and immersed in DMEM 1X + 2 % horse serum (HS) + 1 % P/S. The differentiation medium was refreshed every 4 days.

In every experiment involving hydrogels, controls were made by seeding C2C12 cells on matrigel coatings or culture plastic on which their behaviour is well known and characterized. Indeed, on matrigel or plastic dishes, C2C12 cells reach 80 % confluence after 30 h when seeded at a density of 15.000 cells/cm². Their differentiation and fusion for 24h up to 6 days is simply achieved by rinsing 80 % confluent cells once with DPBS and adding a low serum differentiation medium (DM). After 6 days in differentiation, the cell layer is rarely able to be maintained. Most of the experiments were then done up to six days. In this work, C2C12 cells were used up to passage 35.

5.2.2.2 Primary mice myoblasts (pMMs)

After approval by local ethics committees, mice primary cells were harvested from 5 days old C57BL/6 mice. To this end, mice were euthanized by decapitation and their undifferentiated posterior hind limb muscles (growing gastrocnemius, tibialis anterior, extensor digitorum longus, and quadriceps) rapidly collected and stored in cold PBS.

Muscles were then cut in multiple parts using scissors and immersed in a digestion medium composed of 0.5 mg/ml collagenase and 3.5 mg/ml dispase (for type I and IV collagens and fibronectin cleavage) in PBS for about 1 hour at 37°C. All the aforementioned steps were realized quickly after animal death and in a sterile manner to prevent cellular death and contamination.

One centrifugation at 600 rpm for 5 minutes at room temperature was performed to discard cellular debris and a second at 1600 rpm for 5 minutes at RT to obtain a cellular pellet containing fibroblasts, myoblasts, and blood cells. The cellular pellet was re-suspended in DMEM 1X + 15 % FBS + 1 % P/S, filtered through 40 µm cell strainer, and incubated 5 hours at 37°C and 5% CO_2 for fast fibroblasts plating.

After 5 hours, non-adherent cells were harvested (containing myoblasts and circulating cells) and seeded on the substrate of interest or matrigel coatings as a control. In this work, pMMs were not subjected to passages and used directly after extraction.

Primary mice myoblasts were grown in IMDM medium supplemented with 20 % FBS, 1 % chicken embryo extract, 1 % P/S, and 0.005 % Gentamycin. Circulating cells and debris were removed 24 hours after seeding during medium refreshment. To induce differentiation, cells were cultured in a differentiation medium composed of IMDM, 2 % HS, and 1 % P/S. GM and DM medium were refreshed every second day.

5.2.2.3 Immortalized human myoblasts (iHMs)

Immortalized human myoblasts (iHMs) were kindly provided by Bénédicte Chazaud from Institut Neuromyogène.

Briefly, these cells were derived from MuSCs that were isolated from muscle biopsies of healthy donors and expanded. Cells were then transformed with viral transduction of CDK4 (cyclin-dependent kinase-4) and hTERT (human telomerase reverse transcriptase) to overcome cellular senescence [388].

Various clones were isolated with puromycin, amplified, and cultured in GM (detailed in Table 10):

Table 10: Cultures mediums used for immortalized human myoblasts

Culture medium used for immortalized human myoblasts	
Growth medium (GM)	Concentration (%)
Skeletal Muscle Cell Growth Medium with supplemented mix	40% (v/v)
DMEM high glucose with pyruvate	30% (v/v)
Heat-inactivated FBS	20% (v/v)
Medium 199 - glutamax supplement	8% (v/v)
Penicillin/streptomycin	1% (v/v)
Dexamethasone	0.003 % (w/v)
Puromycin	0.005 % (w/v)
Differentiation medium (DM)	Concentration
Skeletal muscle cell Growth Medium without serum or supplemented mix	100% (v/v)

As for C2C12 cells, iHMs were kept below 60% confluence in routine maintenance and passaged as described above. At about 80% confluence, cells were cultured in a serum-depleted medium to initiate their differentiation.

In every experiment made on hydrogels, controls were made by seeding same densities of iHMs cells on matrigel coatings or culture plastic as controls.

In this work, two cell lines derived from biopsies of healthy donors of 95 and 121 months were used up to passage 38.

5.2.2.4 Primary human myoblasts (pHMs)

Primary human myoblasts were kindly provided by the department of orthopaedic surgery, Geneva university hospitals & faculty of medicine [143]. Briefly, human muscle samples obtained from orthopaedic surgery waste of semitendinosus muscles were enzymatically dissociated. After dissociation, human myoblasts defined as $CD56^+$ / $CD146^+$ / $CD45^-$ / $CD34^-$ / $CD144^-$ were selected by FACS [143].

Isolated pHMs were grown in GM (detailed below) refreshed every second day. Cells passage was performed as described above when they reached 60 % confluence to avoid pre-differentiation. After reaching 80 % confluence cells were cultured in DM and refreshed every 4 days (detailed Table 11).

Table 11 : Cultures mediums used for primary human myoblasts

Culture mediums used for human primary myoblasts culture

Growth medium GM	**Concentration**
Ham's F10 (Gibco)	
FBS	15 % (v/v)
BSA	0.5 mg/ml
Fetuin	0.5 mg/ml
Dexamethasone	0.39 µg/ml
Insulin	0.04 mg/ml
Creatine	1 mM
Pyruvate	100 µg/ml
Uridine	50 µg/ml
Gentamycin	5 µg/ml

Differentiation medium DM	**Concentration**
DMEM (Gibco)	
BSA	0.5 mg/ml
Insulin	0.01 mg/ml
Creatine	1 mM
Pyruvate	100 µg/ml
Uridine	50 µg/ml
Gentamycin	10 µg/ml

In this work, cells were kept up to passage 6. Three distinct pHMs were used in this work from biopsies of healthy male donors of 24 and 29 years old.

6 *In vitro* DGL/PEG hydrogels cytotoxicity using NHDF

6.1 Cells in contact with extracts

For *in vitro* cytotoxicity assays, extracts from different hydrogels were prepared. To do so, drops of 2/25 mM DGL/PEG dense hydrogels were prepared as described above. They were then immersed in 0.5 ml NHDF growth medium (DMEM F-12 + 10 % FBS + 1% P/S) without any washing or post-formulation treatments and kept at 37°C and 5 % CO_2 for 24 hours. In parallel, NHDF cells were seeded on 24 wells plates at a 2000 cell/cm² density and cultured in GM. After 24 hours, the culture medium was removed and cells were immersed in a 1 ml mix of culture medium and 24h-hydrogels-extracts at a ratio 1:1 (Figure 21).

Extracts were used to study the effect of acid:base and pluronic® F-68 addition in DGL/PEG hydrogels as well as the impact of PEG solvent (DMF versus DMSO) in resulting cellular behaviour. Moreover, washed hydrogels were used as control.

Controls were made by immersing 24 hours adhered cells in a mix of the acid: base ratio, pluronic® F-68, and PEG solvent at the same concentration used for hydrogel formulation with culture medium at a ratio 1:1.

At least 3 hydrogels per condition were used at various NHDF passage.

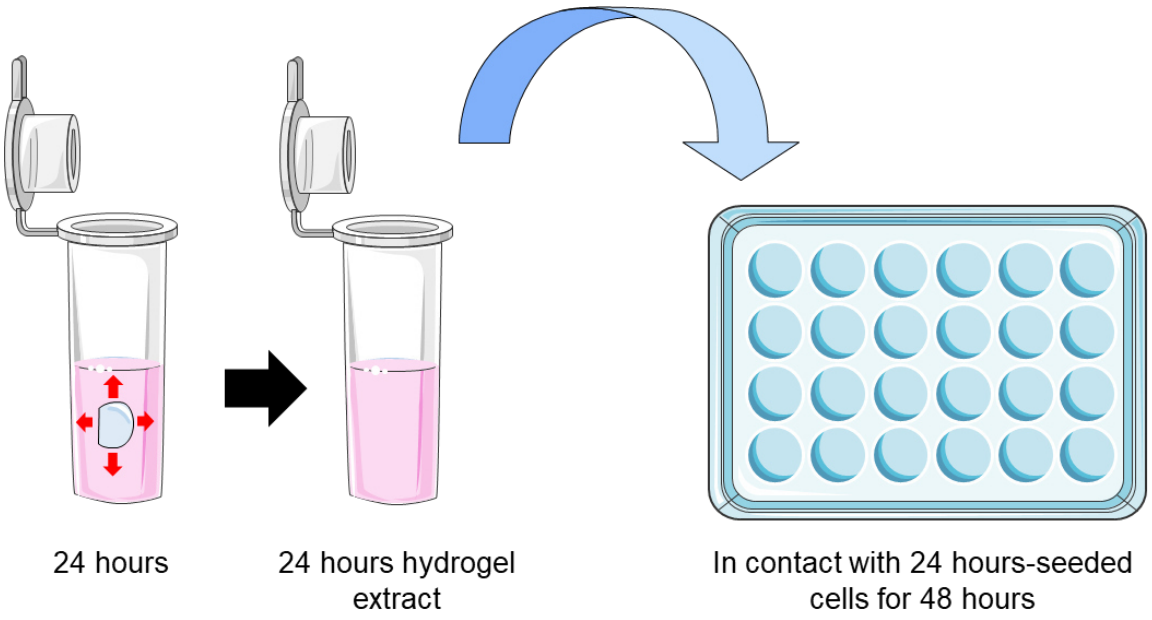

Figure 21 : Schematic representation of dense DGL/PEG hydrogels extracts
-Hydrogel drops were formulated and immediately immersed in culture medium for 24 hours, without washing or post formulation treatments
-After 24 hours, the supernatant is harvested and deposited on adhered cells with fresh culture medium at a ratio 1:1
-After 48 hours in contact with extracts, cells were used for subsequent experiments.

6.2 Cells in direct contact with unwashed EPH

For injectability purposes, 1.6/25, 2/25, and 2/37 mM DGL/PEG EPH with 1.33:1 Gaa:KC molar ratio and 3.3 % pluronic® F-68 were produced inside 2 ml conic tubes as described above. They were removed from the tubes and manually cut to obtain cylinders of approximately 2 mm high. Directly after formulation and cutting, and without any washing or post-formulation treatments, EPH cylinders were transferred into non-cell-treated 24 or 48 well plates. NHDF at a low density of $5x10^4$ cells per hydrogel were seeded onto non-washed EPH in 600 µL complete culture medium and incubated at 37°C and 5 % CO_2. The culture medium was refreshed 24 hours after seeding and every two days for 21 days.

3 hydrogels per condition were used at 3 various NHDF passages.

7 *In vitro* skeletal muscle cells cytotocompatibility toward DGL/PEG hydrogels

7.1 Cell culture on coatings

7.1.1 Coatings realization

Wells of 24 well plates were coated by passive adsorption with 1 mg/ml DGL, ELP, or DGL+ELP in DPBS for 4 hours at 4°C followed by extensive washing with DPBS prior use. When performing coatings, bare polystyrene wells were used as positive controls. Matrigel was also used as a positive control for muscle cells. Matrigel at 1/100 in GM was added to the well and let to polymerize for at least 30 min at RT before washing the well with warm DPBS.

7.1.2 Cell seeding

To study the effect of DGL and ELP coatings on cells, C2C12 and pMMs were seeded on coatings. Briefly, C2C12 were seeded at 2000, 4000, or 40000 cells/cm² on coatings, matrigel and bare polystyrene in GM. C2C12 were let to reach 80 % and were then induced in differentiation for 6 days.

Half of all the pMMs harvested from one mouse were seeded on coatings, matrigel and bare polystyrene. Cells were grown in GM for 48 hours and then induced in differentiation as follows: for pMMs on coatings and bare polystyrene, cells were immersed in DM for 6 days. For cells on matrigel, cells were cultured in DM for 2 days before adding matrigel diluted at ½ in DM for 1h at 37°C followed by DM addition to help cells enter late differentiation for 4 additional days.

On cells seeded on matrigel and bare polystyrene, free ELP at 50 and 100 µg/ml was added to the medium during proliferation and differentiation to study its effect when added freely in the medium.

Coatings were studied in triplicate from one pMMs isolation and at three various C2C12 passages.

7.2 Cell culture on 2D hydrogels

Sterilized 2D hydrogel adhered in 48 well plates were soaked in GM and kept at 37°C, 30 minutes before cell seeding. C2C12 and iHMs cells, 15.000 cells/specimen, were seeded on 2D hydrogels of various concentrations in 0.6 ml growth medium and incubated at 37°C and 5 % CO_2. Cells were grown in GM until reaching 80 % confluence. Cells were then cultured in DM for 6 days using respective protocols described above.

To study hydrogels suitability for skeletal muscle cells, 1/25, 1.6/25, 2/19, 2/25, 2/37 and 2/50 mM DGL/PEG with and without the presence of the ELP were used. At least 3 hydrogels per condition were studied for each cell type and cells were studied at three various passages.

7.3 Cell seeding on EPH

To study the suitability of the 3D structure, various skeletal muscle cell types were seeded on EPH of various concentrations as follows:

For each cell type, a drop of 100 µL of GM containing cells (density reported in Table 12) was homogeneously deposited on the top of EPH of various concentrations. Samples were incubated at 37°C for 1 hour to allow for cell attachment before adding 0.6 ml of growth medium to each well. Cells were cultured in GM for 4 to 8 days before depleting the medium in serum for 6 to 15 days.

Table 12 : Cell density seeded on EPH

Cell type	Number of cells seeded on EPH
C2C12	20.000
iHMs	20.000 and 60.000
pMMs	Half of all the muscles harvested from one mouse
pHMs	60. 000

For skeletal muscle cells suitability, 1.6/25, 2/25, and 2/37 mM DGL/PEG EPH formulated by injection with 1.33:1 Gaa:KC and 3.3 % pluronic® F-68 with and without the presence of the ELP were studied. At least 3 EPH per condition were studied for each cell type.

8 Cell characterization on hydrogels

8.1 Live/dead viability assay

Cells viability was assessed by a live/dead assay at various time points post NHDF seeding on EPH. Briefly, NHDF on EPH were washed once with DPBS and immersed in a mix of propidium iodide (6 µM) and calcein (1 µM) in DPBS. After 20 minutes of incubation at 37°C and 5 % CO_2, cells and samples were observed by LSCM (Zeiss Imager.Z2) within 20 minutes (live cells max. Ex/Em 494 nm/517 nm, dead cells max. Ex/Em 528 nm/617 nm). Controls were made to assess the live/dead assay. Briefly, NHDF cultured in petri dishes for 24 hours without treatment were used as positive controls and NHDF immersed in a mix of culture medium and tween 20 at 1 % for 10 minutes before live/dead assay were used as a viability negative control.

8.2 Metabolic activity measurements

Cells metabolic activity was measured with an alamar® blue assay on NHDF after 48 hours in contact with 24h hydrogels extracts and on C2C12 cells seeded at 2000 cells/cm² on surfaces coated with DGL, ELP, DGL+ELP and matrigel or on bare polystyrene after, 24, 48 and 120 hours in GM.

Briefly, the culture medium was removed from all conditions, cells were washed with warm and sterile DPBS and 400 µL of a 10 % alamar® blue mix in complete culture medium was added onto the cells. After 3 hours of incubation at 37°C, 5 % CO_2, the supernatants were harvested and their fluorescence measured with a fluorescence microplate reader (TECAN infinite® 200) at excitation 535 nm and emission 610 nm. NHDF seeded at increasing densities without any treatments were used as positive controls for standard curve linearity assessment to determine the range in which alamar® blue assay could be conducted.

8.3 Cell migration by time lapse

To study C2C12 and iHMs cells in proliferative conditions, they were seeded on coatings at 4000 cell/cm² or on 2D hydrogels as described above and tracked by time-lapse videos. Briefly, 7 hours after seeding, plates were transferred into time-lapse microscope (Zeiss Axio Observer Z1 inverted) at 37°C and 5 % CO_2. Five bright field pictures per well were taken using a 10X lens (N-Achroplan 0.25 ph1, N.A 0.25) every 10 minutes for 24 hours to follow cellular movement and morphology over time.

Cellular velocity (from 7 to 30 hours post-seeding), confluence (7, 24 and 30 hours post-seeding), and morphology (7 and 30 hours post-seeding) were assessed by image analysis of time-lapse video using imageJ (Figure 22).

8.4 Immunofluorescence

Goat anti-mouse Alexa Fluor 488 (#A11029), goat anti-rabbit Alexa Fluor 555 (#A21429), goat anti-mouse Alexa Fluor 647 (#A21236) secondary antibodies and Alexa-fluor 488 or 647 phalloïdin were brought from Thermofisher (Waltham, MA, USA). BSA and triton were brought from Euromedex (Strasbourg, France), DAPI, fluoromount were purchased from Sigma Aldrich (St. Louis, MO, USA)

At dedicated time points, cells on coatings, 2D hydrogels, or EPH were fixed with 4 % paraformaldehyde (PFA) solution in PBS for 20 minutes at 37°C. Samples were then extensively washed with DPBS and stored in DPBS at 4°C before use.

EPH cylinders were either used in immersion or cut in slices.

EPH slices were obtained by first embedding fixed samples in optimal cutting temperature solution (OCT) by successive baths of increasing concentrations: 20; 50; 80; 90 and 100 % in PBS for 30minutes each. EPH were then cut (16-30 µm) with a cryotome, deposited on glass slides (Superfrost plus, thermofischer scientific), and fixed with acetone for 20 minutes at -20°C. EPH slices of 1 mm wide were also obtained by manual cutting of EPH fixed samples.

Cells on coatings, 2D hydrogels, or into 3D EPH were permeabilized 10minutes with a 0.1% triton solution in PBS and then immersed in blocking solution for 1h. Samples were then incubated in a solution of primary antibodies in blocking solution at 1% for 2 hours (Table 13). Secondary antibodies were then applied on samples for 2 hours in a wet chamber in the blocking solution at 1 %. For nucleus and actin staining, DAPI at 2 µg/ml and 488-phalloidin at 4 µg/ml were added for 10 min at room temperature in blocking solution at 0.1 %. Unless stated otherwise, all incubation steps were performed at room temperature (RT), samples were rinsed three times in PBS between each step and kept immersed in PBS before use.

Bovine Serum Albumin (BSA) in PBS was used as the blocking solution for myoblast cells, while goat serum in PBS was used as the blocking solution for NHDF cells.

Table 13: Primary antibodies used in this work

Primary antibody	Dilution	Fabricant	Ref	Production
Type I Collagen	1/200	Novotec	20111-1	Rabbit
Fibronectin	1/250	Abcam	Ab45688	Rabbit
MF20 – Myosin heavy chain	1/10	Home-made hybridoma from V.Gache group		Mouse
Desmin [Y66]	1/50	Abcam	Ab32362	Rabbit
PAX 7	No dilution	DSHB Hybridoma Product PAX7		Mouse
Sarcomeric α-actinin EA-53	1/500	Sigma-aldrich	A7811	Mouse
Calcitonin receptor	1/30	Abcam	Ab230500	Rabbit
Ki67	1/1000	Abcam	Ab15580	Rabbit
MyoD	1/100	Proteintech	18943-1-AP	Rabbit

8.5 Image analysis

Cells on coatings and 2D hydrogels were analysed with a fluorescence microscope (Zeiss Axio Observer Z1 inverted) using a 10X lens (N-Achroplan 0.25 ph1, N.A 0.25). Three mosaics of 12 pictures were performed for each condition, covering a large part of 48 wells plates. Samples on glass slides were mounted with fluoromount and whole EPH were kept immersed in PBS 1X to be analysed with an upright laser scanning confocal microscope (LSCM - Zeiss Imager.Z2). On EPH, 100 µm stacks were realized on five various positions and orthogonally projected.

Skeletal muscle cells growth was studied on 2D hydrogels. To do so 5 positions per well were analysed per condition as follows: the area covered by cells on the total area of each picture was calculated. To follow cell movement, 10 cells per position were tracked using imageJ for 24 hours. Three hydrogels per conditions were studied at three various cell passages.

The fusion index (number of nuclei inside myotubes on the total number of nuclei in a picture) was quantified using imageJ on cropped areas of the coatings and 2D hydrogels mosaics. On 2D and 3D hydrogels, the number of nuclei per myotubes and myotubes area, width (average of 3 distinct positions in the myotube) and ferret diameter were determined by image analysis with imageJ. The elongation index was calculated as the ratio of the feret diameter on myotubes width). For myotubes morphology quantification, myotubes of at least two nuclei were measured and at least three samples per condition were analysed at three various C2C12 passages. Between 80 and 211 myotubes were analysed per condition (Figure 22).

The quantification of quiescent Pax7 positive cells was performed on EPH as follows: the percentage of Pax7 positive cells on the total number of nuclei was counted. Then, $Pax7^+$/ $ki67^+$ cells or $Pax7^+$/$myoD^+$ cells on the total number of $pax7^+$ cells were quantified.

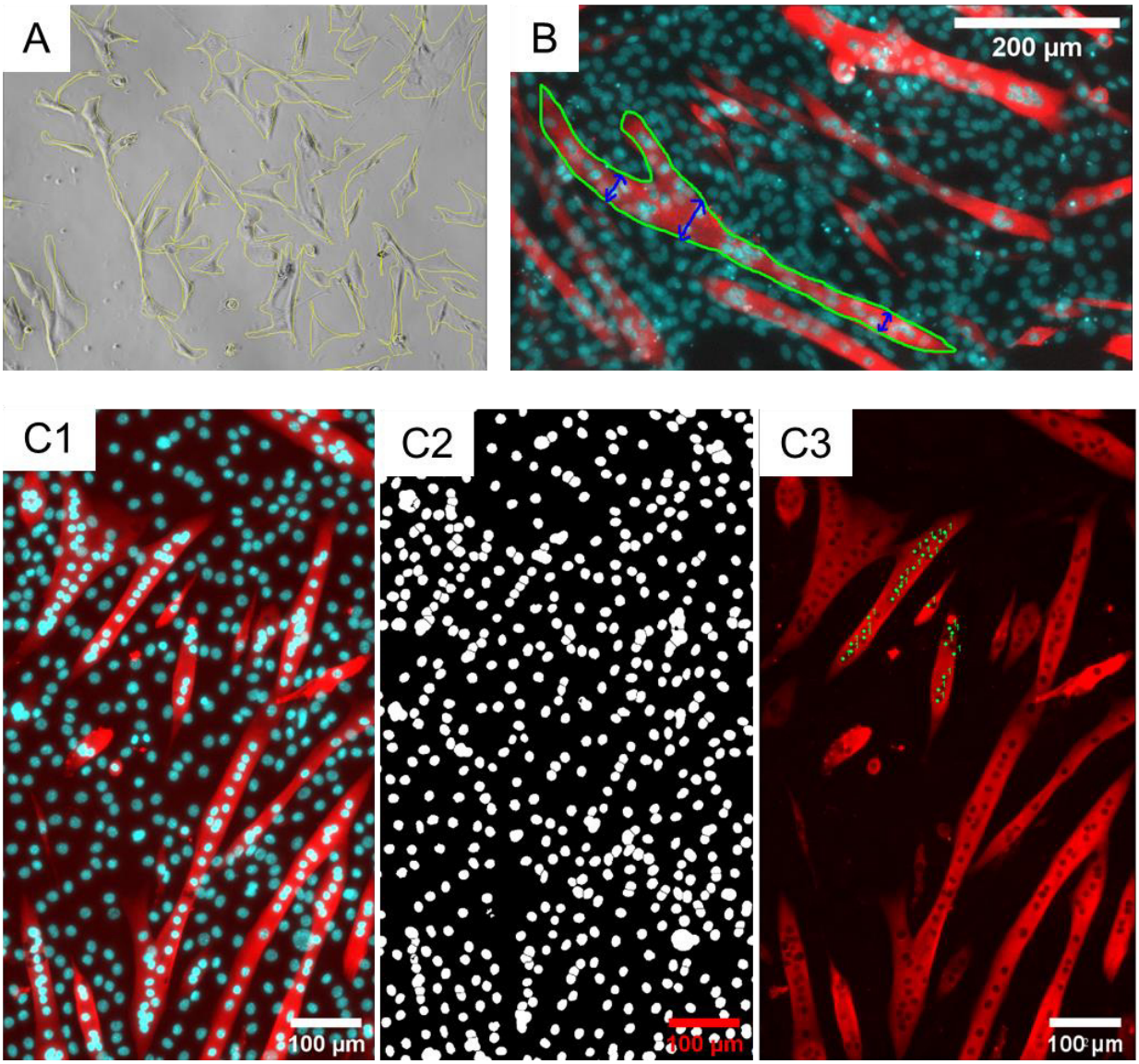

Figure 22 : Skeletal muscle cells image analysis
A) Representative picture of confluence quantification. C2C12 myoblasts on a 2/25 mM DGL/PEG hydrogel, 30 h post seeding in growth medium. The yellow line represent the manual calculation of the area covered by cells. The confluence percentage was determined as the area covered by cells on the total area of the picture.
B) Representative picture of myotubes area (green line) for feret and circularity calculation, and width quantification (blue arrows) on C2C12 myotubes on a 2D 2/37 mM DGL/PEG hydrogel, - DAPI in cyan, Myosin heavy chain (MyHC) in red.
C) Representative pictures of 2D index fusion quantification. C1) C2C12 myotubes on bare polystyrene after 6 days in DM - DAPI in cyan, MyHC in red. C2). The total number of nuclei was determined by a threshold, a binary treatment followed by a watershed individualization. C3). The number of nuclei inside MyHC positive cells was determined manually. The fusion index was determined as the number of nuclei inside MyHC positive cells on the total number of nuclei.
C2C12 confluence, myotubes morphology and fusion index on coatings or 2D hydrogels were quantified as followed: three distinct areas per well were analysed. At least three wells per conditions were analysed at three various C2C12 passages.

9 Gene expression analysis

TRIzol, TRI-Reagent® and Fast Universal SYBR Green Master (Rox) Roche were bought from Sigma Aldrich (St. Louis, MO, USA). SDS was purchased from Biosolve Chimie SARL (Dieuze, France). Chloroform was bought from VWR (Pennsylvania, USA). Propan-2-ol: Merck (Darmstadt, germany)

9.1 RNA extraction

To quantitatively measure the expression levels of MyoD, MyoG and Myh4, real-time polymerase chain reaction (RT-PCR) was performed on C2C12 onto EPH after 1, 3, and 6 days in DM.

For every group, at least 3 EPH were harvested and frozen in liquid nitrogen. Frozen samples were deposited into 2.0 ml lysing Matrix tubes containing 1.4 mm ceramic spheres in SDS 0.5 % and subjected to high-speed lysis with FastPrep-24 5G Instrument at 4°C (2 cycles of 15 sec at 5700rmp with 30 sec pause). Total RNA were isolated from the supernatant of lysed 3D scaffolds using TRIzol reagent according to the manufacturer's recommendations. Briefly, 300 µL TRIzol was added to 2.0 ml lysing tubes and EPH were subjected to a second high-speed lysis. The supernatant was collected and 60 µL of chloroform were added and mixed vigorously. The solution was left several minutes for decantation and centrifuged at 12.000g for 15 min and 4°C. The aqueous phase (the upper phase) was carefully recovered and transferred to clean microtubes. RNA precipitation was achieved by adding 300 µL isopropanol to the aqueous phase, mixing gently, incubating 10 minutes at RT, and centrifuging 12.000g for 10 minutes at 4°C. The supernatant was discarded and the RNA pellet rinsed three times with 800 µL of EtOH/RNAse-free water at 70/30 v/v and centrifuged at increasing velocity from 7.500 to 10.000g for 5min at 4°C. The tubes were then left to air dry under the fume hood for 10 minutes and resuspended in 15 µL RNAse-free water. The purity and concentration of the isolated RNA were measured with a spectrophotometer (Nanodrop 2000 Thermo-Scientific).

9.2 Reverse transcription

A single-stranded cDNA synthesis was performed with 400 ng total RNA using the GoScript™ Reverse Transcription System Kit from Promega following the manufacturer's recommendations. After adding reaction mixture, reverse transcription was performed using poly(dT) oligopeptides in a thermocycler for 5 minutes at 25°C (annealing), 42°C for 1h (extending) and stopped by enzyme inactivation at 70°C for 15 minutes. The temperature was then decreased to 4-10°C and cDNA stored at -20°C before use.

9.3 Real-time polymerase chain reaction

Quantitative polymerase chain reaction (qPCR) of transcripts and endogenous controls, glyceraldehyde 3-phosphate dehydrogenase (GAPDH), and 60s ribosomal protein L41 (RPl41A) was performed. To do so, 16 ng of cDNA were mixed with SYBR® Green Supermix and forward and reverse primers in a CFX Real-Time PCR Detection System (Bio-Rad, Hercules, CA). Thermal cycle conditions were an initial 95°C for 10 min followed by 40 cycles at 95°C for 10 sec and 60°C for 30 sec.

Data were analysed using the E^{-Ct} method with normalization to the geometric mean of both housekeeping genes. To determine the relative expression of muscle markers, primers were designed to explore the various phases of myogenesis. Primer sequences are described in Table 14.

Table 14 : Sequence of primers used for qPCR analysis

Genes	Primers	Sequence
MYOD1 – myoblast determination protein 1	Forward	AGC-ACT-ACA-GTG-GCG-ACT-CA
	Reverse	GCT-CAA-CTA-TGC-TGG-ACA-GG
MyoG - Myogenin	Forward	CAA-TGC-ACT-GGA-GTT-CGC-TC
	Reverse	ACA-ATC-TCA-GTT-GGG-CAT-GG
MyH4- Myosin Heavy Chain 4	Forward	CAA-GTC-ATC-GGT-GTT-TGT-GG
	Reverse	TGT-CGT-ACT-TGG-GAG-GGT-TC
Glyceraldehyde 3-phosphate dehydrogenase (GAPDH)	Forward	AAC-TTT-GGC-ATT-GTG-GAA-GG
	Reverse	ACA-CAT-TGG-GGG-TAG-GAA-CA
RPl41A-60S ribosomal protein L41-A	Forward	GCC-ATG-AGA-GCG-AAG-TGG
	Reverse	CTC-CTG-CAG-GCG-TCG-TAG

Expression levels of MyoD (early-stage marker), MyoG (mid-stage marker), and MyH4 (late-stage marker) were studied on C2C12 seeded on 1.6/25, 2/25, and 2/37 EPH.

10 *In vivo* EPH biocompatibility assessment

After approval by local ethic committees, 2 months old C57BL/6 mice used for preliminary studies and 7-weeks old hair-less SKH1 mice (Charles River, Ecully) were anesthetized by intraperitoneal xylazin-ketamin injection. A small incision was performed at the low back of the mice and 2 subcutaneous pockets created with a sterile spatula along mice flanks (Figure 23). Two hydrogels conditions (2/25 or 2/37 mM DGL/PEG) were injected (400 µL) directly into subcutaneous pockets or in a conic tube to be removed, cut and implanted in the pockets. Dense DGL/PEG hydrogels of various conditions (2/25 and 2/37 mM DGL/PEG) in PBS were injected as control (500 µL). After hydrogel injection, the static mixer was carefully removed and the incision was blocked to prevent liquid precursors to leak from the pockets. After cross-linking the incision was sutured. EPH were made using a set 1.33:1 Gaa:KC molar ratio and 3.3% pluronic® F-68. Dense hydrogel controls were made of DGL and PEG in PBS 1X.

Mice, fed *ad libitum*, were monitored every two days for recovery and signs of distress. After three weeks, the mice were euthanized by anaesthetic overdoses (intra-peritoneal injection of thiopental) and hydrogel samples were harvested with the surrounding tissue. They were fixed in 4 % PFA solution in PBS overnight at 4°C, embedded in paraffin, sectioned and stained with Masson's trichrome using standard procedures. To highlight the penetration of blood vessels in the implanted hydrogels, sections were stained for type IV collagen by immunofluorescence, cell nuclei were counter-stained with 2 µg/ml DAPI solution. Macrophages inside hydrogels were detected with antibodies against F4/80 by immunohistochemistry.

The entire sample area and surrounding tissues were imaged at 6 various height for each sample using a Zeiss Axio Scan Z1 for brightfield acquisitions and a LSCM (Zeiss Imager.Z2) for fluorescent acquisitions.

For dense and porous area quantifications, the entire sample at six various height was considered and areas were measured with ZEN blue 2.5 software.

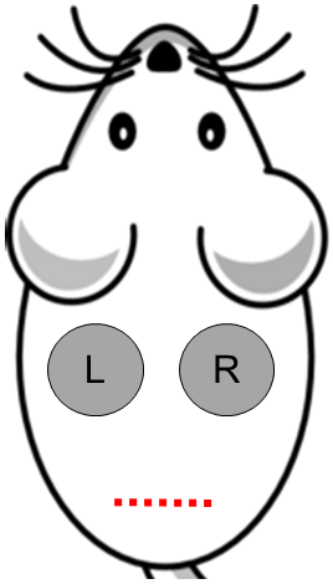

	Randomisation		
	Mouse	Left	Right
Injection	1	2/25 dense	2/25 porous
	2	2/25 porous	2/25 dense
	3	2/25 porous	2/25 dense
	4	2/37 porous	2/37 dense
	5	2/37 porous	2/37 dense
	6	2/37 porous	2/37 dense
Implantation	7	2/25	2/37
	8	2/25	2/37
	9	2/25	2/37
	10	1.6/25	2/25
	11	1.6/25	2/37
	12	1.6/25	2/25 dense

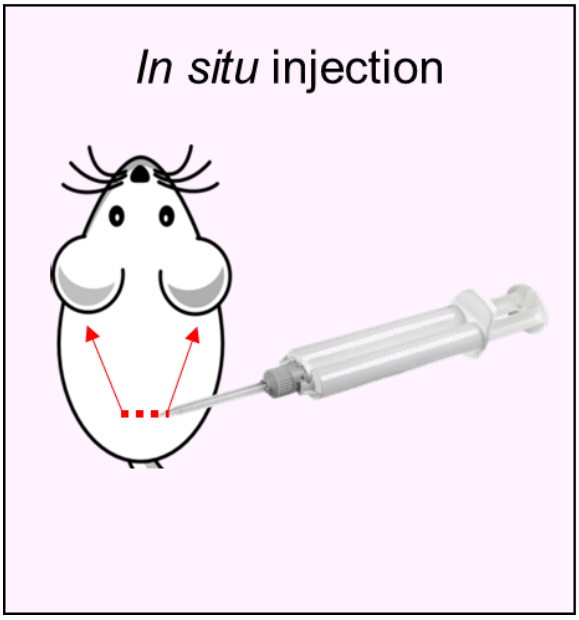

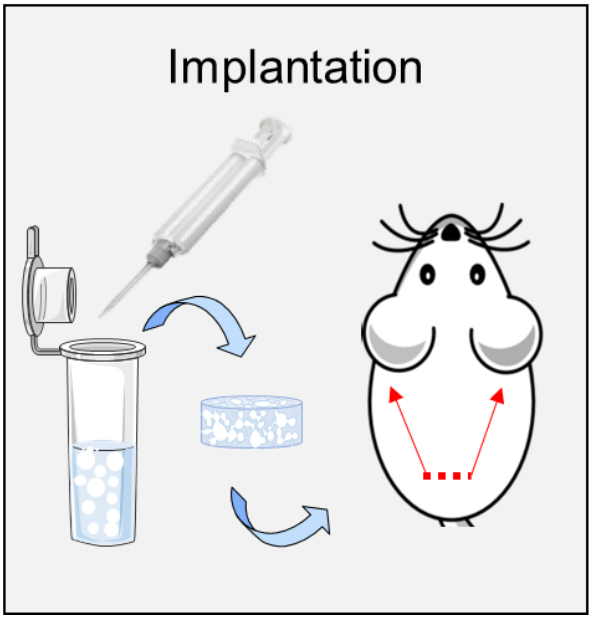

Figure 23: Biocompatibility study and assessment of in situ *porous formation by subcutaneous implantation and injection of EPH in mice*
Red dotted line: an incision was performed in the back of mice and two subcutaneous pockets were created along the mice flanks. Hydrogels were then in situ injected inside the subcutaneous pockets using a dual syringe connected to a static mixer (pink box) or injected inside a tube to be removed, cut and implanted inside pockets (blue box)

11 Statistics

Statistical analyses were performed with Graphpad prism. All the data were subjected to Shapiro-Wilk normality test to assess whether they followed or not a normal distribution. Depending on the results parametric or non-parametric tests were performed. Tests were performed using variance analysis (ANOVA)/Kruskall-wallis tests or t-test/mann-whitney. Graphical data are shown as mean ± standard deviation (SD) and p-values of 0.05 and below were considered significant. Data values are presented as mean ± standard error (SE).

RESULTS AND DISCUSSION

1 Evaluation of dense DGL/PEG hydrogels to act as a relevant support for skeletal muscle cells

The development of biomaterials able to sustain cells growth must meet numerous requirements to match the needs of targeted tissues. One important feature of a scaffold design for skeletal muscle regeneration is to sustain rapid cell proliferation and migration to allow fusion into growing muscle fibres. To this end, variation of scaffold physical and biochemical features can be relevant.

In this chapter, we aimed to study the relevance of a biocompatible and recently developed poly(ethylene) glycol (PEG)-based hydrogel as a substrate for myoblast proliferation, migration, and differentiation. The PEG backbone displays a low inflammatory profile and well-established chemistry allowing PEG-based hydrogels to exhibit high mechanical versatility. Nevertheless, PEG hydrogels are biologically inert and lack interactions with cells [373]. To overcome this limitation, we have developed in the laboratory an N-hydroxysuccinimide (NHS) bi-functionalized PEG hydrogel crosslinked with bioactive poly(L-lysine) grafted dendrimers (DGL) [373]. DGL/PEG hydrogel formulation was simply achieved by mixing PEG and DGL in aqueous solutions with vigorous homogenization. The amine groups available at the surface of the DGL are used as binding sites for the PEG, via NHS function, to form the polymer network through the formation of covalent amide bonds.

The DGL/PEG hydrogel exhibit a large range of mechanical properties and interact with fibroblasts through polycationic charges brought by the DGL amine groups [377]. The stiffness versatility and the variation of DGL:PEG molar ratio have been shown to influence fibroblast behaviour, enabling control over cellular fate. Also, the cell-friendly DGL/PEG hydrogel crosslinking made in physiological environments is an interesting way to include active moieties, such as a recombinant elastin-like polypeptide (ELP), synthesized in our laboratory. The addition of ELP in the bulk material has been related to an enhanced fibroblast proliferation and velocity on the hydrogel [378]. Given the promising results that these hydrogels showed with fibroblasts, they were studied and characterized as full-thickness skin equivalents with encouraging results. Besides, when rendered porous and subcutaneously implanted in mice, their extensive vascularization pave the way for a potential use as scaffolds for tissue regeneration.

Therefore, based on the DGL/PEG hydrogel potential for cell culture and tissue compatibility, this first chapter aims to (1) investigate its ability to function as a support for skeletal muscle cells and (2) find optimum parameters to sustain muscle cells proliferation and fusion through the modulation of mechanical and biochemical cues. We hypothesize that similarly to fibroblasts, it should be possible to control skeletal muscle cell behaviour through stiffness and DGL/PEG ratios. To validate this potential, we evaluated six various concentrations of DGL and PEG on myoblast cell lines from mice and human. We studied cell proliferation,

morphology, migration and fusion on the surface of the hydrogel to discriminate our conditions using various techniques.

1.1 Two-dimensional DGL/PEG hydrogels characterization

To investigate the support stiffness compliance with myoblast function, DGL/PEG hydrogels of various concentrations and stiffness were designed.

The complex (E*), loss (E''), storage (E') moduli, and the loss factor (tan δ) of hydrogels of various compositions were determined at a 1 Hz frequency and 50 µm amplitude (Figure 24A). As previously described [373], the modulation of DGL/PEG ratio and concentration from 1/25 to 2/50 mM DGL/PEG allowed to modulate the stiffness from 12.0 ± 2.4 kPa to 157.8 ± 14.1 kPa respectively (Figure 24A and Table 15). For all hydrogels, E' was greater than E'' confirming the realization of a self-standing hydrogel whatever the concentration and ratio used (Figure 24B). Interestingly, while a proportional increase of PEG for a given DGL concentration induced a linear elastic modulus increase (R^2 = 0.9998), a proportional increase of DGL for a given PEG concentration triggered an exponential rise of E' (Figure 24E and F). These results suggest that the DGL has a predominant control over the hydrogel stiffness and seems to be the limiting molecule in the reaction.

Hydrogel swelling properties were determined in PBS at 37°C to mimic the physiological conditions (Figure 25 and Table 15). An increased DGL/PEG concentration and molar ratio triggered a decreased swelling of the hydrogel. The swelling ratio was 20.8 ± 0.4 and 8.6 ± 0.4 for 1/25 and 2/50 mM DGL/PEG hydrogels respectively. Equilibrium swelling was reached after 6 hours with a PBS absorption between 800 and 2000% of the hydrogels dry weight confirming their high water content. In conclusion, the modulation of both DGL and PEG concentration and their ratio enable precise control of the stiffness and water absorption of the resulting hydrogels.

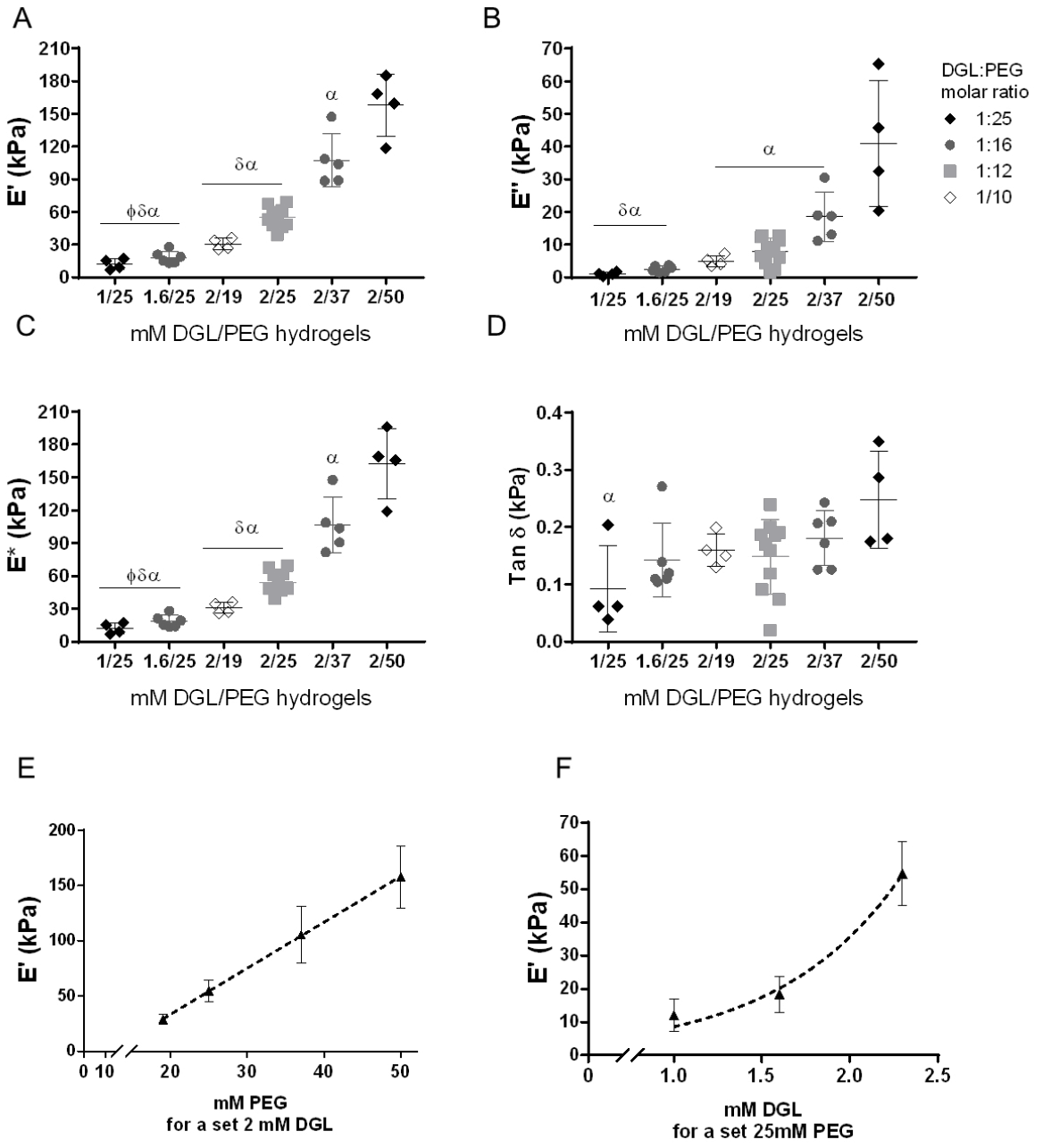

Figure 24 : DGL/PEG hydrogel mechanical characterization

A) Elastic modulus (E'), B) loss modulus (E''), C) complex modulus (E) and D) loss factor (tan δ) in compression of DGL/PEG hydrogels of various concentration and ratio (kPa)*

E) Elastic modulus as a function of DGL/PEG concentration for a given DGL concentration (2 mM) and F) for a given PEG concentration (25 mM). Lines: E) linear (R^2: 0.9998) and F) exponential regression (R^2: 08702)

One-way ANOVA + Tukey's multiple comparison test compared to Φ: 2/25, δ: 2/37, α: 2/50 mM DGL/PEG

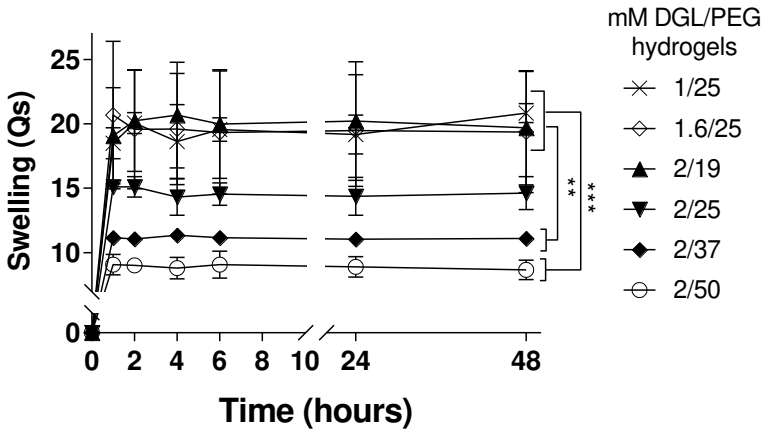

Figure 25: DGL/PEG hydrogel swelling characterization
Swelling ratio over time of dry hydrogels of various DGL/PEG concentration (mM)
*One-way ANOVA + Tukey's multiple comparison test *: p<0.05; **:p<0.01, ***:p<0.001*

The six concentrations evaluated in this chapter offer a wide range of mechanical properties, DGL:PEG molar ratios and water absorption abilities. These conditions are detailed in Table 15.

Table 15 : mechanical characterization of six DGL/PEG hydrogels (mM) used in this work. Lines with the same colour represent hydrogels with the same DGL: PEG molar ratio but exhibiting different stiffness and swelling abilities. .

DGL/PEG (mM)	DGL :PEG ratio	Elastic modulus (kPa)	Loss modulus (kPa)	Swelling
1/25	1:25	12.0 ± 2.4	1.0 ± 0.3	20.8 ± 0.4
1.6/25	1:16	18.3 ± 2.2	2.5 ± 0.4	19.4 ± 2.3
2/19	1:10	30.6 ± 2.6	4.9 ± 0.8	19.7 ± 2.6
2/25	1:12	54.7 ± 3.1	8.6 ± 1.2	14.6 ± 0.7
2/37	1:16	105.5 ± 11.5	18.5 ± 3.4	11.1 ± 0.1
2/50	1:25	157.8 ± 14.1	40.9 ± 9.6	8.6 ± 0.4

Taking advantage of this versatility, the behaviour of C2C12 cells and immortalized human myoblasts (iHMs) was studied on the aforementioned hydrogels to investigate the effect of stiffness and DGL:PEG molar ratio. C2C12 cells were studied as a well-characterized cell line and owing to their ability to recapitulate all the molecular events leading to the development of myotubes [387]. They are thus an interesting model to study DGL/PEG hydrogel. In a second step, immortalized myoblasts from human were also evaluated to add robustness to these results.

1.2 Undifferentiated myoblasts response to DGL/PEG hydrogels of various concentrations

To study C2C12 and immortalized human myoblasts (iHMs) behaviour on the hydrogel, cells were seeded at a density of 15000 cell/cm² on DGL/PEG flattened hydrogel discs formulated inside 48 well plates. Hydrogel discs were 1 cm wide, covering the entire diameter of the well and were 0.7 mm thick to preclude the possibility that cultured cells sense the stiffness of the underlying plastic dish.

The adhesion, proliferation, and morphology of C2C12 on DGL/PEG hydrogel of various compositions were evaluated 30 hours post-seeding in growth medium (GM). Their velocity on the support was also evaluated for 24 hours in GM (Annex 1, supplementary movies 1,2 and 3 representing C2C12 cells on 1.6/25; 2/25 and 2/37 mM DGL/PEG hydrogels respectively).

C2C12 cells readily adhered to 2D DGL/PEG hydrogels, regardless of the conditions used. Their ability to proliferate on hydrogels, assessed by confluence increase observed over time, was observed for almost all conditions, except for the softer 1/25 mM DGL/PEG hydrogel (Figure 26A and supplementary information 2 in Annex). Interestingly, their ability to cover the surface 30 hours post-seeding was correlated with the hydrogel stiffness (Figure 26B). The stiffer the hydrogel, the higher the confluence until reaching a peak with the 2/37 mM DGL/PEG condition. However, the condition 2/50, although being the stiffer, was related to less C2C12 confluence, indicating this condition could represent a threshold value. Cells on conditions 2/25 and 2/37 mM DGL/PEG were not statistically different from the plastic dish positive control, indicating that C2C12 proliferation was not impaired on these DGL/PEG conditions. After 30 hours on DGL/PEG hydrogel, C2C12 were well spread out and spindle-shaped except for the 1/25 mM DGL/PEG condition which exhibited round-shaped cells related to a small spreading area (Figure 26C and D).

C2C12 cells were able to move on DGL/PEG hydrogels in the same way as on plastic dish, consolidating hydrogel adequacy for cell culture (except for the softer 1/25 DGL/PEG condition) (Figure 26E). Interestingly, while the stiffness drove C2C12 proliferation, their morphology and migration on the support was linked to hydrogel composition through the amount of DGL in relation to PEG. Cells on hydrogels with 1:25 and 1:10 DGL:PEG molar ratios were less mobile and presented a smaller area compared with hydrogels with 1:16 and 1:12 DGL:PEG molar ratios, which were similar to the positive plastic dish control (Figure 26D and E). These results suggest that both the stiffness and the amount of DGL and PEG have an influence on C2C12 cells in terms of cell morphology, confluence after 30 hours, and cell mobility.

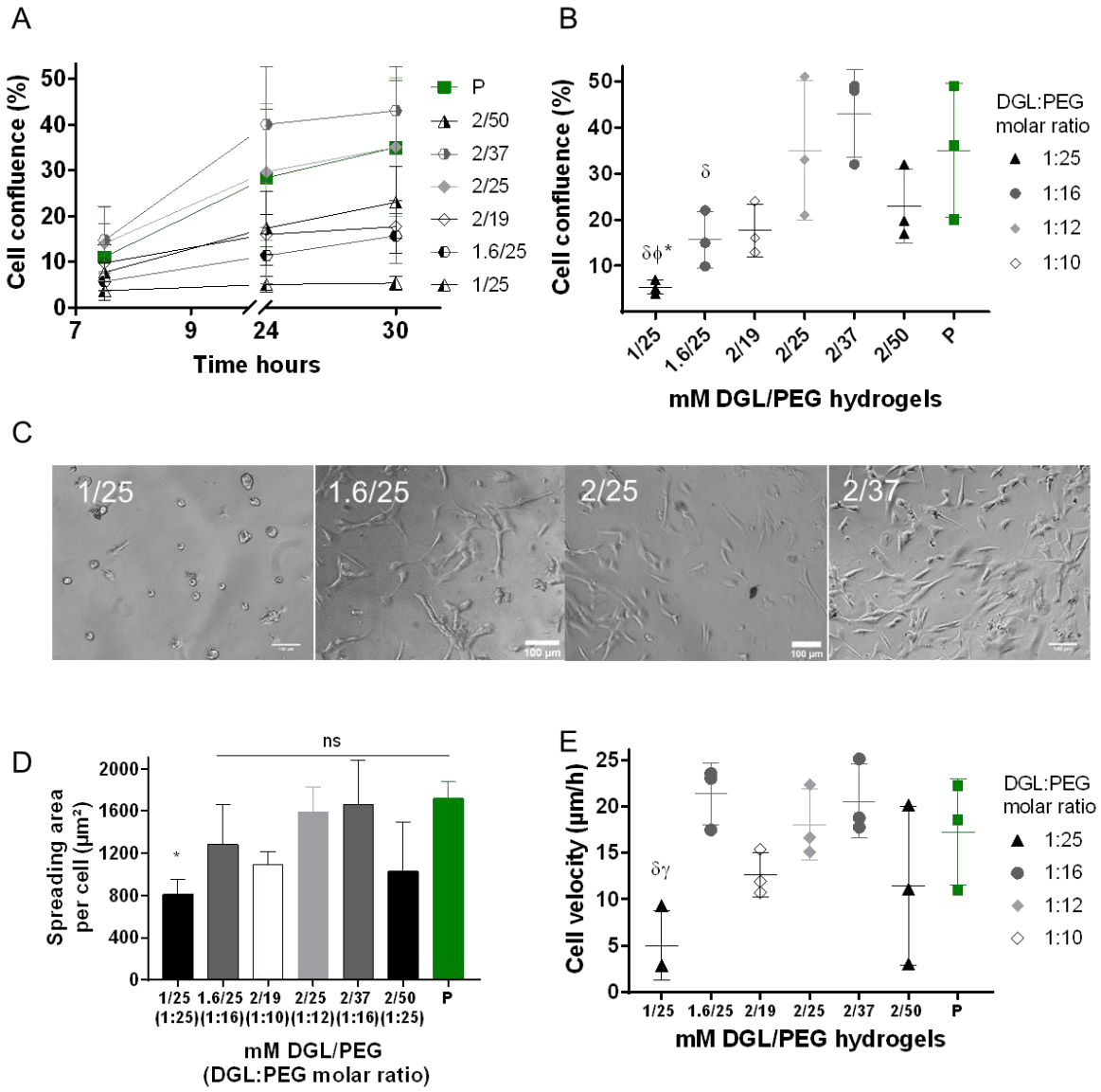

Figure 26: Undifferentiated myoblasts responses to DGL/PEG hydrogels of various concentrations and molar ratios.

*C2C12 cells A) confluence **over time**. C2C12 cells B) confluence, C) representative pictures, and D) morphology (spreading area per cell) **30 hours post seeding** as a function of DGL/PEG hydrogel concentration and ratio (mM DGL/PEG). D) C2C12 velocity for 24 hours as a function of hydrogels concentration and molar ratio.*

P: Plastic dish

*B,E: One way ANOVA + Tukey's multiple comparison p<0.05 compared to γ: 1.6/25; Φ: 2/25, δ:2/37, * Plastic dish*

*D: Kruskall Wallis + Dunn's vs plastic Dish, *: p<0.05*

Scale bar: 100 µm

Even if C2C12 cells are a relevant model to evaluate myoblasts behaviour, they misrepresent the cells encountered inside human muscle wound bed owing to their murine origin. The same experiments were thus realized on immortalized human myoblasts (iHMs) to consolidate these findings. The same trend was observed for iHMs with a cell confluence increase correlated with DGL/PEG hydrogel stiffness until reaching a peak for the 2/37 mM DGL/PEG condition (Figure 27A supplementary information 3 in Annex). Similarly to C2C12, the iHMS velocity was more related to DGL: PEG molar ratio than to stiffness, confirming that our previous results are robust regardless of the myoblasts cell line origin.

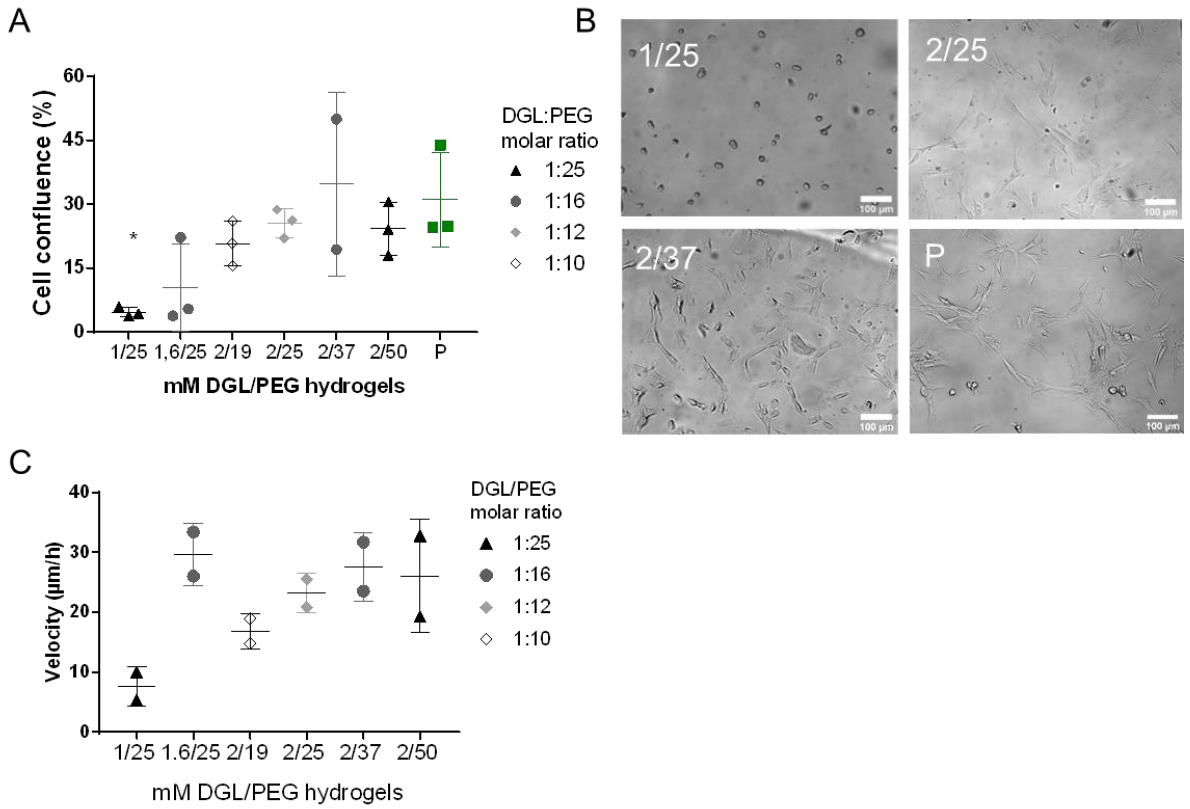

Figure 27: Immortalized human myoblasts (ihMs) behaviour in proliferative conditions on DGL/PEG hydrogels of various concentration and molar ratio
A) Cell confluence and B) representative pictures of ihMs 30 hours post seeding on hydrogels of various concentration and molar ratio. C) Cell velocity on hydrogels of various concentrations for 24 hours in growth medium (n=2).
*P: Plastic dish. A) One way ANOVA + Dunnett's vs plastic dish, *: p<0.05.*

Finally, C2C12 and iHMs cells seeded on DGL/PEG hydrogels were able to reach 80% confluence after 4 to 6 days in the growth medium, except for the softer condition that was discarded (i.e. 1/25 mM DGL/PEG).

In conclusion, regardless of the myoblast cell line, conditions of interests (in terms of stiffness and DGL:PEG ratio) could be selected to sustain cellular proliferation and/or migration similarly to the plastic dish positive control. The possibility to modulate the DGL/PEG hydrogel to guide skeletal muscle cell growth strengthens its potential for the intended application.

However, the regeneration potential of a biomaterial for skeletal muscle cells is also related to its ability to sustain cell differentiation and fusion to move towards muscle fibre regeneration. To study this ability, the medium was depleted in serum. It has been shown that upon serum depletion, myoblast cell cycle stops and, if confluent, cells start to differentiate, to align, and to fuse, forming the multinucleated myotubes [389].

1.3 Effect of DGL/PEG hydrogels of various conditions on myoblasts' fusion

After reaching 80% of confluence, C2C12 cells were cultured in differentiation medium (DM) to study their differentiation and subsequent fusion. The first phase of myoblasts differentiation is characterized by cell alignment [390], which was observed on 2D hydrogels 60 hours after serum depletion, meaning that cells were rapidly undergoing commitment (Annex 1, 2/25 mM DGL/PEG hydrogel + ELP supplementary movie 4). The subsequent fusion of myoblasts into growing myotubes is a common path in the differentiation of skeletal muscle, concomitant with the assembly of contractile myosin. On day 6 after serum depletion, myotubes were visible on almost all DGL/PEG hydrogels as highlighted by a myosin heavy chain staining (Figure 28A). On condition 2/19 mM DGL/PEG, which exhibited the highest proportion of DGL in relation to PEG (i.e. 1:10), no myotubes were visible after 6 days although it exhibited a 80% cell confluence compatible with cell fusion (Figure 28B). Corollary to this observation, the fusion of C2C12 on hydrogels appeared related to the DGL:PEG ratio. As depicted in Figure 28C, an increase of PEG in relation to DGL was correlated with a better C2C12 fusion until reaching a peak at a 1:16 DGL/PEG molar ratio. Indicating that this trend was unrelated to substrate stiffness, hydrogels of various elastic moduli but with the same DGL: PEG ratio (i.e. 1.6/25 and 2/37 mM DGL/PEG) showed a similar C2C12 fusion index of 8.2 ± 1.1 and 8.1 ± 0.7 % respectively. Also, conditions with a small fusion index exhibited myotubes with a decreased number of nuclei per myotubes and a smaller area (Table 16).

Table 16: C2C12 myotubes quantifications after 6 days in serum depleted medium medium as a function of hydrogel concentration (mM DGL/PEG).
Nuclei per myotubes, myotubes area quantification and elongation index (feret diameter/width)

DGL/PEG (mM)	Nuclei/ myotubes	Area (µm²)	Elongation Index
1/25	NA	NA	NA
1.6/25	5.86 ± 1.55	5371 ± 1325	10.59 ± 0.44
2/19	NA	NA	NA
2/25	2.74 ± 0.83	1574 ± 875	9.81 ± 0.77
2/37	7.81 ± 2.38	8782 ± 2621	11.18 ± 1.20
2/50	2.79 ± 0.48	2887 ± 936	8.50 ± 0.61
P	13.04 ± 5.57	15065 ± 5444	13.2 ± 2.08

Of note, the C2C12 fusion index on DGL/PEG hydrogel was lower than for the plastic dish positive control (index fusion of 18.0 ± 0.9) and myotubes were smaller with a decreased number of nuclei.

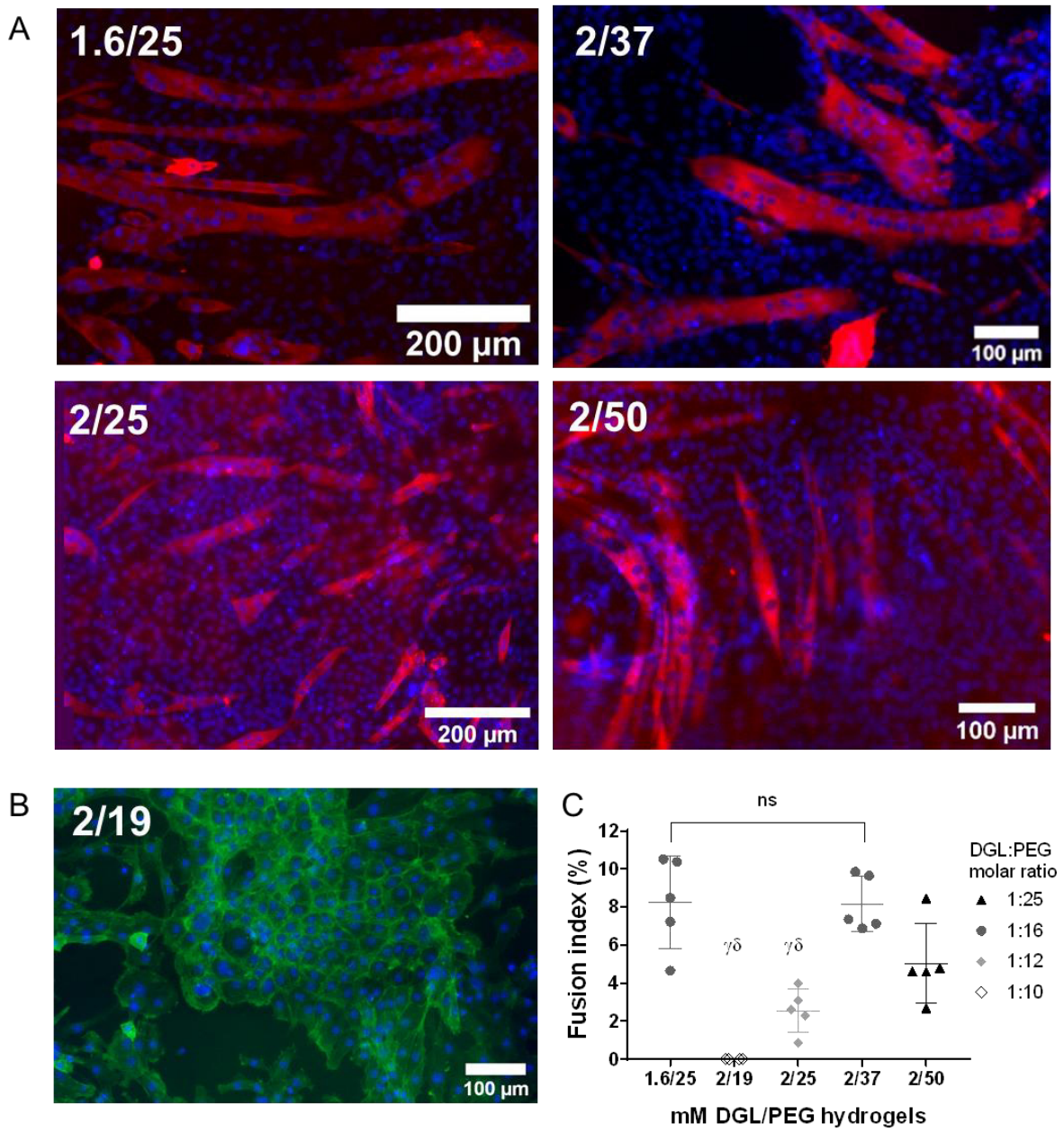

Figure 28 : Effect of substrate on myoblasts differentiation after 6 days in serum-depleted medium
A) Representative pictures of C2C12 cells fusion (Red: Myosin heavy chain (MyHC) and Blue: cell nuclei) on dense DGL/PEG hydrogels of various compositions
B) Representative picture of C2C12 cell layers on 2/19 mM DGL/PEG hydrogel (Green: cell actin cytoskeleton and blue: cell nuclei)
C) C2C12 fusion index as a function of hydrogel concentration (mM DGL/PEG), after 6 days in serum depleted medium - One way ANOVA + Tukey's multiple comparison compared to γ :1.6/25 and δ: 2/37 mM DGL/PEG hydrogel, $p<0.05$

Therefore, these results showed that some optimum DGL/PEG conditions were able to sustain C2C12 differentiation and subsequent fusion. However, in this study, while stiffness variation

had a great influence on cell proliferation, it appeared to be less critical than DGL: PEG molar ratio in the subsequent fusion. As a result, C2C12 differentiation could be controlled by varying the support composition.

Overall, based on the C2C12 behaviour in both growth medium (GM) and differentiation medium (DM), the increasing amount of DGL inside DGL/PEG hydrogels was related to a decreased cell ability to spread out, to move, and to fuse, consolidating DGL implication in cell behaviour.

1.4 Study of the effect of DGL on skeletal muscle cells

To confirm the above-mentioned assumptions, C2C12 cells were studied on saturated DGL-coated surfaces on which the resultant stiffness is brought by the polystyrene beneath and is not varied. Interestingly, C2C12 cells grown on DGL coatings showed a significantly decreased metabolic activity compared with the gold standard matrigel after 24, 48 and 120 hours in growth medium (Figure 29A). However, no differences were reported in terms of C2C12 velocity between the plastic dish and DGL coatings, where they were significantly less mobile than on the matrigel positive control (Figure 29B). This indicates that C2C12 cells were less proliferative on DGL coatings but were able to migrate similarly than on the crude plastic dish.

After proliferation, cells were immersed in serum depleted medium for six days. A similar fusion index of **23.3** ± 1.5 % and **26.5** ± 2.3 % was observed for C2C12 seeded on matrigel or crude plastic dish respectively while it dropped at **4.1** ± 0.9 % on DGL-coated polystyrene which represents a fusion decrease of about **85 %** (Figure 29C). In addition to the myotubes fusion impairment, DGL coatings affected myotubes morphology, which exhibited a smaller area, and fewer nuclei in comparison to myotubes on non-coated plastic dish control (Figure 29D and Table 17).

Table 17: Nuclei per myotubes and myotubes area quantification after 6 days in serum-depleted medium on various coated surfaces.
C2C12 cells seeded at 40.000 cells/cm². t-test DGL VS Plastic Dish (*) : p<0.05

Coatings	Nuclei/ myotubes	Area (µm²)
Plastic dish	47.40 ± 13.61	36631 ± 10131
DGL	3.91 ± 0.94 (*)	4766 ± 787 (*)

Of note, C2C12 cells were either seeded at a high density and immediately induced in differentiation or seeded at a low density, grown for 48 hours, and induced in differentiation. Both experiments showed the same results (85 % of fusion index decrease) indicating that the fusion impairment is not related to the upstream C2C12 proliferation phase and that DGL only impairs differentiation and/or fusion of cells.

To add reliability to these results, the fusion of primary mice myoblasts (pMMs) was also evaluated to avoid possible biases associated with immortalized cell lines. Overall, pMMs

seeded on crude plastic dishes were barely able to spread out and showed less fusion than C2C12. This behaviour is illustrated in Figure 29E, where MyHC positive pMMs cells after 6 days in differentiation remained mostly mononucleated and round but with a homogeneous repartition on the well. On the contrary, pMMs on DGL coatings were visually fewer in number and formed clusters highlighting an effect of the DGL on cell fusion (Figure 29E). These observations reinforce the supposed effect of DGL on immortalized and primary myoblasts cell fusion.

Taken together, these results suggest that the presence of the DGL can impair C2C12 and primary mice myoblasts fusion, unrelated to stiffness and upstream proliferation. However, DGL crosslinking to increasing concentration of PEG to form hydrogels, enabled to recover C2C12 fusion until reaching a peak at a 2/37 mM DGL/PEG ratio.

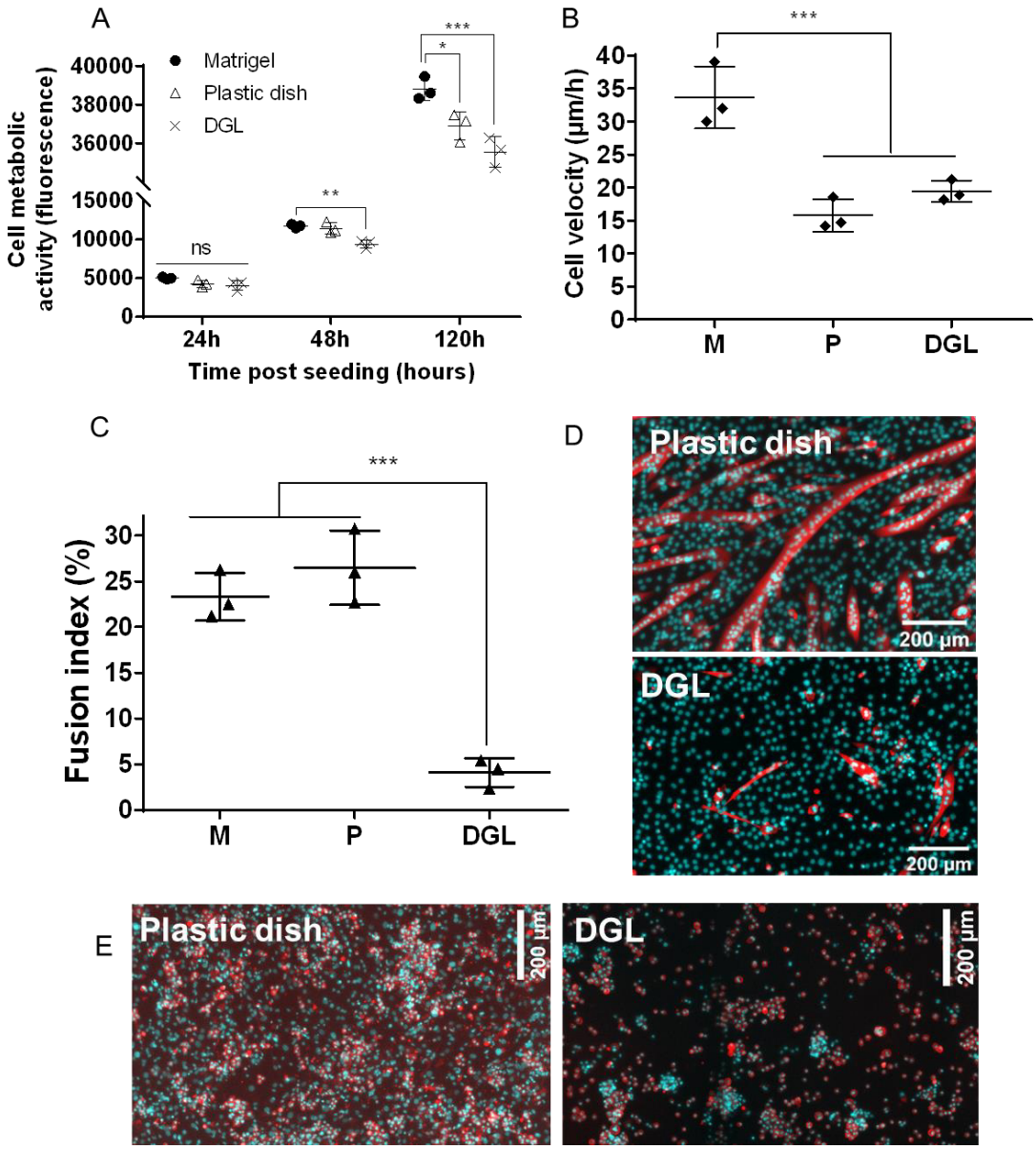

Figure 29: Effect of various coated surface: DGL, Matrigel and plastic dish on C2C12 and pMMs proliferation and/or fusion.

A) C2C12 cell metabolic activity 24, 48 and 120 hours post seeding and B) C2C12 cell velocity (µm/h) for 24 hours in GM on various coated surfaces. C2C12 cells seeded at a ***4000 cells/cm²*** *density.*

C) Fusion index and D) representatives' pictures of C2C12 after 6 days in serum-depleted medium on various coated surfaces. C2C12 cells seeded ***at 40.000 cells/cm²****. E) pMMs afer 6 days in serum depleted medium on various coated surfaces. D, E) Red: MyHC, cyan : cell nuclei. A, B) One-way ANOVA + Dunnett VS matrigel, C) One way ANOVA + Tukey's multiple comparison. *:p<0.05; **:p< 0.01; *** p<0.00. (M: Matrigel and P: plastic dish)*

1.5 Study of the effect of ELP addition inside DGL/PEG hydrogels on skeletal muscle cells

The presence of the elastin-like polypeptide (ELP) could modify the way the hydrogel interacts with cell surface αvβ3 integrin and elastin binding protein through the presence of cell-interacting motives in its primary sequence. Therefore, the effect of ELP adsorbed on surfaces, incorporated inside the 2D DGL/PEG hydrogels or added freely in the medium of cells was evaluated. Its effect on cell adhesion, migration, proliferation and fusion was assessed.

The culture of C2C12 on ELP coatings was not correlated with an enhancement of cell metabolic activity in comparison to the crude plastic dish (Figure 30A). However ELP addition in hydrogel bulk resulted in a slight increase of C2C12 and iHMs cell confluence that was statistically significant in some conditions (Figure 30B and C). These results suggest an influence of the ELP when included inside the hydrogel or a synergic effect of stiffness and ELP presence.

Contrarily to what was expected and previously described [379], the addition of the ELP at a 4 mg/ml final concentration in various DGL/PEG hydrogels was not, in our experimental conditions, related to a variation of the final stiffness of the substrate. The DGL/PEG hydrogels mechanical properties in shear stress (shear modulus Table 18, and fracture strain, Table 19) remained unchanged. This invalidates possible assumptions on the influence of ELP on cells via modifications of the hydrogel stiffness. It thus highlights that another mechanism is at play.

Table 18 : Rheological characterization of DGL/PEG hydrogels.
Shear modulus (G', KPa) of hydrogels of various concentrations and DGL: PEG molar ratio.

	Shear Modulus G' (kPa)	
DGL/PEG	w/o ELP	With ELP
1.6/25	5.1 ± 0.3**	8.3 ± 0.7
2/25	10.8 ± 1.9	15.4 ± 0.9
2/37	26.7 ± 2.2	19.4 ± 2.8

t-test w/o ELP VS with ELP ** : $p<0.01$

Table 19: Rheological characterization of DGL/PEG hydrogels.
Fracture strain (G', KPa) of hydrogels of various concentrations and DGL: PEG molar ratio

	Fracture Strain (kPa)	
DGL/PEG	w/o ELP	With ELP
1.6/25	5.4 ± 0.5	6.9 ± 0.8
2/25	4.2 ± 0.6	5.6 ± 0.7
2/37	8.5 ± 0.4	8.1 ± 1.3

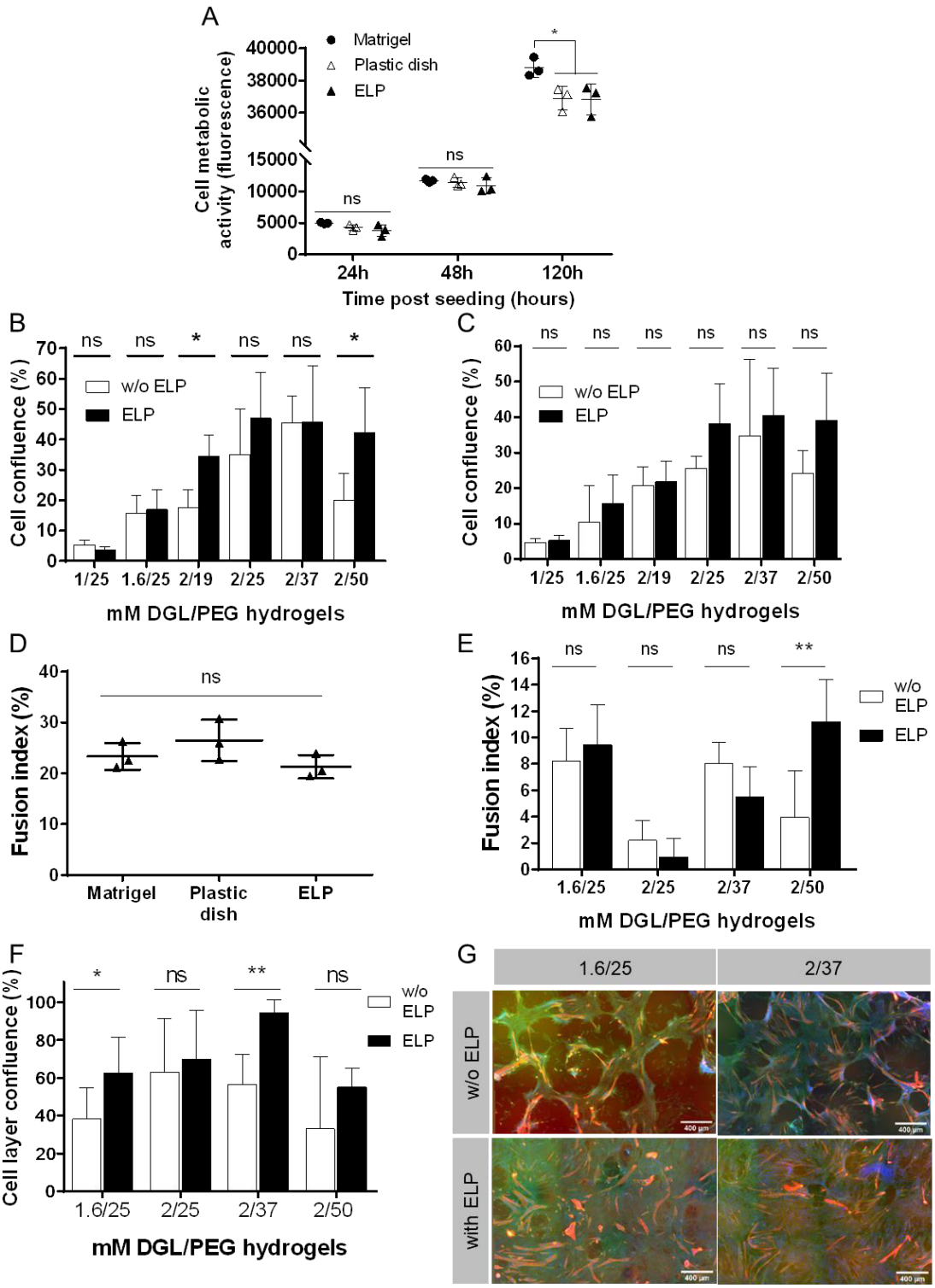

Figure 30: Effect of ELP on C2C12 and iHMs behaviour
A) C2C12 metabolic activity after 24, 48 and 120 hours in growth medium on various coatings: Matrigel, Plastic dish, and ELP. B) C2C12 and C) iHMs confluence (%) 30 hours post seeding in growth medium as a function of hydrogels of various composition ± ELP.
C2C12 fusion index on D) various coatings (C2C12 cells seeded at a 40,000 cells/cm² density) and on E) 2D hydrogels of various composition ± ELP after 6 days in serum depleted medium.
*F) cell layer area (%) and G) representative pictures (4x3 mosaics) of C2C12 cell layers after 6 days in serum depleted medium (Blue : cell nuclei, green: actin cytoskeleton and red: MyHC) on various hydrogel conditions ± ELP. A, D) One way ANOVA + Tukey's multiple comparison test. B,C, E,F) t-test conditions with ELP against conditions without ELP, *:p<0.05, **:p<0.01, ***:p<0.001*

Similarly, the fusion of C2C12 on ELP coatings was not different from the crude plastic dish control or standard matrigel (Figure 30D). However, the ELP addition inside hydrogels bulk material was linked to a significant increase in C2C12 cell fusion for the condition 2/50 mM DGL/PEG (Figure 30E). Interestingly, the ELP presence inside the DGL/PEG hydrogel led to better stabilization of the cell layer during fusion (Figure 30F and G). This stabilization was significantly increased for conditions with the higher fusion index (i.e. 1.6/25 and 2/37 mM DGL/PEG) without affecting the fusion. These results suggest biological interactions between the ELP and C2C12 cells that were not related to substrate stiffness. As the C2C12 on ELP coatings did not behave differently from the crude plastic dish control, it tends to indicate that the ELP has a different effect when coated or when included inside DGL/PEG hydrogels.
To better understand this phenomenon, the ELP was freely added to the culture medium of primary mice myoblasts (pMMs) differentiated on matrigel, resulting in a visual increase of the final number of nuclei (Figure 31A and B). These results suggest ELP can affect pMMs when available in the medium in comparison to coatings, where no effect was observed. Previous nuclear magnetic resonance studies indicated that the incorporation of ELP in DGL/PEG hydrogel liquid precursors do not lead to intermolecular interactions of the ELP with the DGL/PEG polymer mesh. Although the ELP is not bound to the DGL/PEG polymeric network, we could show that the ELP stays embedded inside the network and was not released after 24 hours of incubation in PBS at 37°C [378]. This demonstrates that the effect observed when the ELP is incorporated in DGL/PEG hydrogel is not due to its delivery to the culture medium.

Consequently, the different effects of the ELP when coated, included inside the DGL/PEG hydrogel, or added freely in the culture medium could be a result of its binding domain availability. The adsorption of the ELP on the surface could prevent the exposition of binding domains for cells. On the contrary, when added freely to the culture medium, the ELP could more freely interact with cells through privileged domains (i.e. hexapeptide VGVAPG with elastin binding protein (EBP) and domain 36 with integrin αvβ3). When included inside the DGL/PEG hydrogel, some domains of the ELP could however be presented at the surface.

To conclude, when delivered in the medium or when included in DGL/PEG hydrogels of various compositions, the ELP had an influence on C2C12, iHMs, and pMMs in terms of cell proliferation, fusion, and cell layer stabilization.

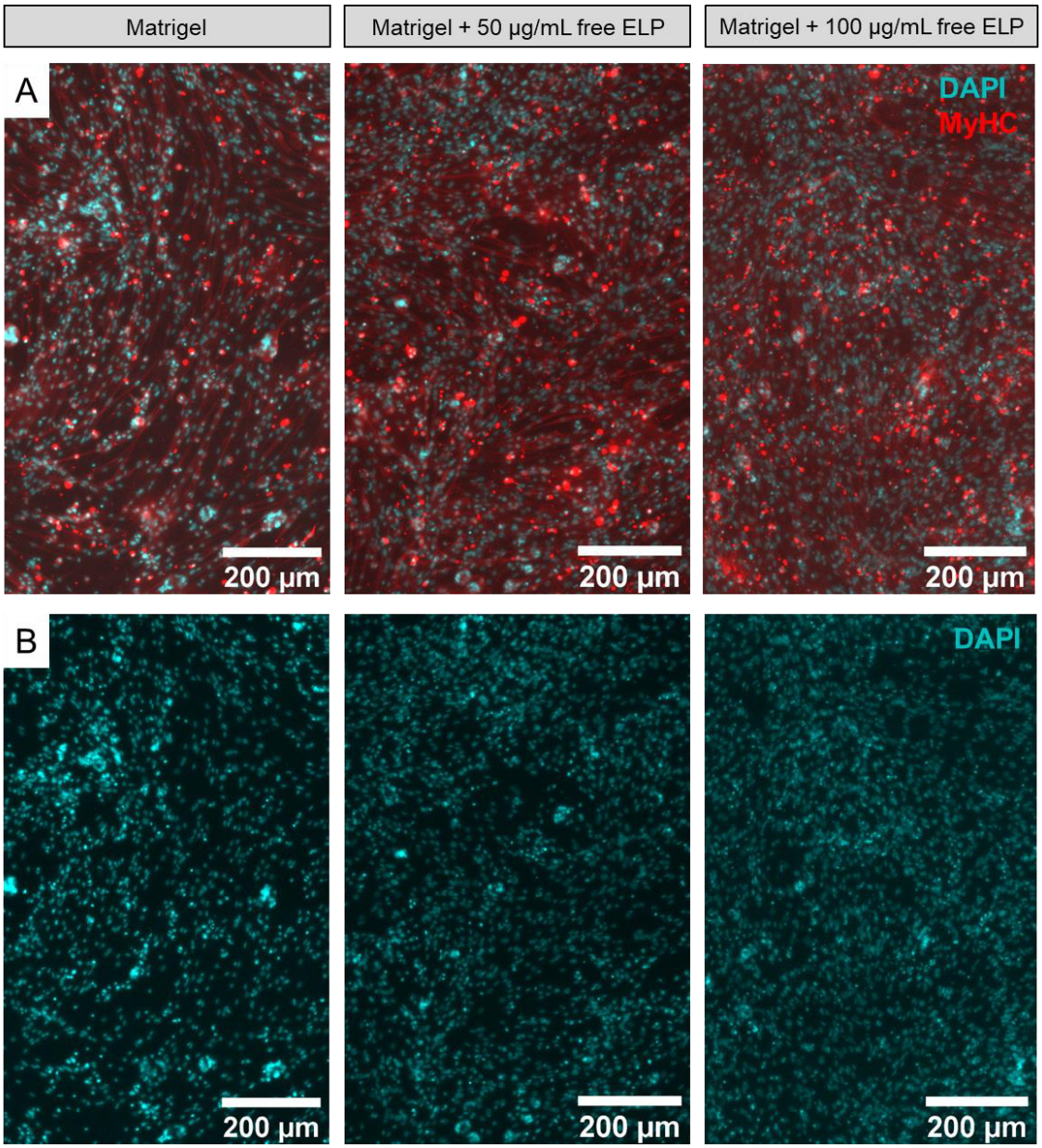

Figure 31: Effect of free ELP of various concentration added to the culture medium of pMMs
A) Myosin heavy chain in red and DAPI in cyan. B) A visual increased number of nuclei can be appreciated in the presence of free ELP in the medium.
Red: Myosin heavy chain (MyHC) and cell nuclei in cyan.

In conclusion, the variation of stiffness, DGL:PEG molar ratios, and presence of an elastin-like polypeptide influenced the behaviour of various myoblast types in terms of proliferation, morphology, adhesion, migration, and fusion. Some favourable conditions, showing an adequate interaction with cells, could be targeted for subsequent experiments (Table 20).

Table 20 : Summary table of 2D hydrogels effect on C2C12 and iHMs; and ELP effect on C2C12, iHMs, and pMMs. Study of cell proliferation, spreading, migration, and fusion.

DGL/PEG (mM)	Proliferation	Spreading	Migration	Fusion
1/25	---	---	--	Not studied
1.6/25	+	++	+++	+++
2/19	+	-	--	---
2/25	+++	+++	++	+
2/37	+++	+++	+++	+++
2/50	+	-	--	++
ELP	++	Not studied	No effect	++ (layer stabilization)

1.6 Discussion

The objective of this chapter was to examine how mechanical stiffness and biochemical cues of the DGL/PEG hydrogels can influence the behaviour of myoblasts in 2D. A good understanding of the parameters modulating cell fate is essential for the development of new scaffolds.

In this work, six DGL/PEG hydrogels conditions were used to vary both substrate stiffness along with the effect of DGL and PEG molar ratio and characterize the impact of mechanical and biochemical changes on cell behaviour. To do so, several conditions were fashioned, exhibiting the same DGL: PEG ratio but with various stiffness. For instance, 1/25 and 2/50 mM DGL/ PEG at 1:25 DGL:PEG ratio had an elastic modulus of 12.0 ± 2.4 and 157.8 ± 14.1 kPa respectively and 1.6/25 and 2/37 mM DGL/PEG at a 1:16 DGL:PEG ratio showed elastic modulus of 18.3 ± 2.2 and 105.5 ±11.5 kPa respectively.

1.6.1 Stiffness modulation and effect

DGL/PEG hydrogel stiffness can be easily modulated by simply varying DGL and/or PEG concentration as well as their ratios. We demonstrated DGL had a higher influence on hydrogel stiffness than PEG. This is in line with previous assumptions made in our group showing a more significant contribution of DGL to control the crosslinking velocity [373]. DGL presents 114 amines groups to act as a crosslinker, however, it is unlikely that all the end groups are involved in an amide bond with PEG molecules due to steric hindrance. This feature limits the maximal number of PEG grafted on a single dendrimer and increase the probability to react with an amine function on the same dendrimer and form intramolecular loops. Less concentrated hydrogel precursors, increase the space between dendrimers, with more probability to form intramolecular loops at the expense of network chains. Conversely, increasing the DGL concentration, reducing the steric crowding and the risk for intramolecular loops could thus result in higher stiffness through increased amide bonds with PEG.

In this work, we showed that stiffness modulation, through DGL and PEG, affects cell morphology and proliferation, with soft substrates more likely to trigger less proliferative and round-shaped cells. Our findings are in line with previous studies showing the clear effect of stiffness on skeletal muscle cell behaviour. This is for instance in agreement with Engler and colleagues who demonstrated that stiffer substrate induced a higher myoblast spreading [198] than softer ones. The same trend has been described with fibroblasts and endothelial cells spreading [186]. These studies suggested that cells onto stiff substrates are more likely to produce stress fibres and vinculin-enriched focal adhesions (FA) resulting in stronger membrane adhesion and subsequent spreading. C2C12 proliferation on DGL/EPG hydrogel is also in line with studies showing the increasing proliferation of skeletal muscle cells with increasing stiffness in 2D [168]. This phenomenon could be explained by enhanced cell ability to assemble the machinery needed to generate traction forces and drive entry into the cell

cycle on increased substrate stiffness. Indeed, it has been shown that substrates too soft were not able to provide stable anchor sites to cell receptors, limiting the generation of forces by cells [391]. These results could explain C2C12 difficulty to proliferate in soft DGL/PEG conditions and their easy amplification on stiff plastic dishes.

In addition to early adhesion, spreading, and proliferation, stiffness has been shown to affect myoblasts differentiation. For instance, C2C12 cells showed skeletal muscle typical striation in a higher proportion when cultured on substrates close to that of the native tissue (i.e. 15 kPa) [198] and exhibited a better overall differentiation on softer substrates than on stiffer ones [167]. Moreover, as presented in the introduction, muscle stem cells (MuSCs) responsible for the efficient regeneration of injured muscle tissue have been shown to be sensitive to their mechanical environment *in vitro* [392] with higher maintenance of their self-renewal ability on substrate closer to the native muscle stiffness than on plastic dish (~10^6 kPa) [166].

All these instances strengthen the interest of stiffness modulation for skeletal muscle tissue regeneration and consolidate the potential of the DGL/PEG hydrogel, which showed precise and simple mechanical versatility. DGL/PEG hydrogel stiffness and swelling through mesh size variation could be easily adjusted depending on tissue needs. However, while we showed a clear effect of stiffness on myoblasts proliferation and early spreading, it was not related, in our case, to subsequent ability to differentiate and fuse. Accordingly, our findings tend to demonstrate that efficient cell differentiation and subsequent fusion is related to many factors and cannot be solely achieved by tuning the mechanical properties of the substrate.
In fact, cell behaviour toward stiffness has been shown to be highly dependent on the nature of the adhesion receptor by which the cell binds to the substrate [186]. For instance, for a given stiffness, myoblasts differentiate better on cell layers composed of skeletal muscle cells than composed of fibroblasts [167]. In addition, skeletal muscle cells maturation is faster with a higher number of myotubes on substrates coated with poly-D-lysine and laminin compared with type IV collagen coatings of similar elasticity [393]. To conclude, the differentiation of skeletal muscle cells is influenced by both substrate elasticity and protein coatings demonstrating that biochemical cues and stiffness act synergistically.

1.6.2 The effect of DGL on skeletal muscle cells

In this work, the use of a PEG backbone was evaluated due to the straightforward chemical versatility it offers, allowing control of the resulting mesh size and stiffness. The PEG effect on C2C12 proliferation and fusion was not here investigated due to many studies related to the topic, showing PEG-based hydrogels are adequate substrates for C2C12 cells [206], [394]. However, in aforementioned instances, PEG based-hydrogel needed to be functionalized with RGD ligands to conveniently interact with cells. In this work, we used the inert PEG in combination with DGL to provide the PEG polymer-based hydrogel with inherent bioactivity towards cells. In addition to bioactivity, we highlighted a major influence of DGL on skeletal muscle cell behaviour in both proliferation and differentiation/fusion. We demonstrated that the DGL:PEG molar ratio affected cell morphology and migration. The latter being crucial for cell infiltration from host tissue in 3D scaffolds and subsequent skeletal muscle cell fusion. We also showed that DGL drastically decreased the C2C12 fusion index. This could be due either to their inability to enter differentiation to form elongated myocytes (less mobile than myoblasts but with a greater ability to fuse [62]) or due to a fusion impairment of myocytes. This phenomenon was unrelated to stiffness as we showed that hydrogels of totally different stiffness but of similar DGL:PEG ratio equally sustained migration, spreading, and fusion, while a condition close to the native tissue stiffness (30.6 ±2.6 KPa), was not able to support proliferation and fusion due to a high amount of DGL.

These results are in accordance with our previous observations on fibroblasts where the amount of DGL in the DGL/PEG hydrogel played a critical role in cell adhesion, morphology, and viability [373]. We proposed that DGL's influence on cells was related to cationic charges interacting with phospholipids forming the cell plasma membrane. A high concentration of DGL in DGL/PEG hydrogel is related to an increased density of NH2 groups available at the surface of the substrate. Amine groups are positively charged at experimental conditions (pH 7.4) with a DGL pKa between 9 and 10 [395]. Charged surfaces using positive or negative ions have been related to cell affinity improvement in various cell types, [203]. Fibroblasts behaviour toward DGL was also explained by the increased expression of α5 integrin subunit by cells seeded on DGL coatings in comparison to poly-(L-lysines) [377] enabling an adhesion increased by 20%. Cells are known to use adhesion sites to contract the cell body forward [396] and be able to migrate on supports. This increased adhesion of cells could thus be the origin of a C2C12 and iHMs decreased propensity to migrate on DGL/PEG hydrogels of high DGL concentrations. Moreover, a too important concentration of cationic charges was related to cell mortality possibly due to a disruption of cell membrane integrity for too high DGL ratios (i.e. DGL:PEG ratios of 1:6) [373]. Therefore, in this work, the ratio of DGL:PEG was inferior to 1:10 to prevent early cell mortality and be able to study the effect of DGL amount.

In addition to increased adhesion on substrates, it has been shown that positively charged NH2 grafted on polystyrene led to a higher proliferation of C2C12. Conversely, C2C12 cells

seeded on neutral surfaces displayed higher expression of myogenin in comparison with positively (NH2) and negatively (COOH) charged surfaces, suggesting better differentiation on neutral surfaces [397]. This was related to enhanced interaction of cells on NH2 moieties through α5β1 and αvβ3 integrins [397]. Given the major influence of β1 integrin subunits in myogenic differentiation, blocking them can drastically inhibit differentiation [397], their strengthened interaction with NH2 groups could thus influence muscle cell differentiation and, subsequent fusion. In addition to β1-integrin, β3-integrin subunits are crucial for C2C12 adhesion and fusion as their specific siRNA-mediated silencing has been related to a reduced number of myoblasts expressing myogenic markers (such as myosin heavy chain) [178]. β3-integrin subunit expression has also been shown to be induced in activated SCs during regeneration in mice [178]. Given the crucial role of β1 and β3 integrin subunits during myogenesis and regeneration, their enhanced interactions with NH2 moieties could explain the drastic C2C12 fusion impairment observed on DGL coatings and DGL/PEG hydrogel of high DGL concentration.

In conclusion, a high DGL percentage inside the DGL/PEG hydrogels could influence cell behaviour in many ways through high density of positively charged NH2 groups. Due to an increased cell adhesion (through α5 integrin subunit), the presence of DGL could decrease C2C12 and iHMs mobility on the support, greatly affecting their aptitude to fuse upon cell-cell contact. Moreover, the highly positive amine concentration could be related to a differentiation and fusion impairment through interactions with β1 and β3 integrin subunits involved in the fusion process. However, when coupled to PEG to form the hydrogel, amine charges, partially involved in covalent amide bond formation convert into neutral groups allowing the recovery of the differentiation potential. These results highlight the importance to choose an adequate DGL:PEG ratio since DGL can disrupt muscle regeneration.

In conclusion, we demonstrated that C2C12 behaviour is driven by multiples cues acting synergistically. Although the stiffness versatility of the hydrogel is paramount to provide C2C12 feedback to drive their fate, the presence of DGL and its covalent involvement with PEG had also a major influence.

1.6.3 The effect of ELP on skeletal muscle cells

Although in our experimental conditions, the ELP does not appear to influence DGL/PEG mechanical behaviour, its integration in the hydrogel bulk was associated with a modification of cell behaviour towards the hydrogel. We showed that the ELP presence resulted in a cell layer stabilization during differentiation, suggesting a better cellular adhesion to the hydrogel. This is in line with previously described studies. C2C12 have been shown to be sensitive to elastin-like polypeptide coatings, exhibiting a better adhesion after 5 hours with an increased spread area in comparison with glass control [233]. Along with adhesion, C2C12 displayed a higher differentiation on elastin-like polypeptide coatings than on glass [233]. H9c2 myoblasts

have also shown to exhibit higher genic expression of myoD, myogenin, and MyHC when seeded on elastin-like polypeptides coatings [232].

Elastin-like polypeptides are usually described as highly hydrophobic moieties due to the repeated alternation of hydrophobic domains based on the pentapeptidic sequences VPGXG. Accordingly, the ELP designed in our laboratory is characterized by the repeated alternation of hydrophobic domains based on two human hexapeptidic sequences (VGVAPG-VGVLPG) [379]. The incorporation of ELP inside DGL/PEG hydrogel, while not influencing mechanical behaviour has been shown to decrease its overall wettability [378], having a possible effect on cell adhesion and morphology. For instance, it has been shown that a too hydrophobic or hydrophilic surface could impair adhesion of human MG63 osteosarcoma cells [398]. ELP could thus act as a wettability regulator by counterbalancing the hydrophilic behaviour brought by positively charged DGL and hydrophilic PEG chains, and could thus, enhance C2C12 adhesion to maintain the cell layer during differentiation.

Another point is that C2C12 and human myoblasts have been shown to express αvβ3 integrins [177], [178]. Considering β3-integrins are involved in focal adhesion [176], the presence of the GRKRK motif able to bind with αvβ3 integrins in the ELP could be related to a better cellular adhesion, strengthening the cell layer during differentiation. This binding could as well participate in explaining our results. However, while β3 integrin subunit has been shown to participate in the initiation of myogenesis in adult muscles through SCs activation, in our study, the presence of ELP was not correlated with a higher fusion index.

Therefore, the use of the ELP could be considered for VML treatment to strengthen myoblasts adhesion during their differentiation and to maintain the neo tissue stability.

1.7 Conclusion and critical evaluation

Understanding how substrates can direct cell function is critical to the rational design of biomaterials relevant for *in vitro* culture substrates or for tissue engineering applications. Because methods for inducing differentiation of primary myoblasts described previously and elsewhere (i.e. the use of Matrigel [399]) are clinically unsuitable or raise questions about safety issues and batch-to-batch variability, we focused on a more clinically feasible approach. Here, the PEG being biologically inert needed to be associated with DGL to be able to favour cellular adhesion, while preserving stiffness versatility and high reproducibility.

The decision of a cell to proliferate, migrate or undergo differentiation is an integrated response to its adhesive and growth factors (GF) external environment. We demonstrated that stiffness and surface chemistry act as a modulator of C2C12 and immortalized human myoblasts fate. The C2C12 and immortalized myoblasts cell lines may not accurately reflect the response of primary cells to mechanical and biochemical cues. However, they were interesting models to study the effect of the hydrogels components on cells. The use of primary mice myoblasts was as well considered, but their complex culture protocols involving the use of important volumes of matrigel, restricted their utilization.

Using these models, we demonstrated that surface stiffness in combination with DGL:PEG molar ratio affected essential cell proliferative behaviours, including adhesion, proliferation, morphology, and migration. As cell confluence is known to cause growth arrest, essential for myogenic differentiation, both stiffness, and biochemical cues were thus of high relevance to trigger cell fusion. In this work, we evidenced the clear effect of stiffness on skeletal muscle cell behaviour. Contrarily to Engler and colleagues that described a very narrow elasticity window enabling cellular fusion, we described a wider range. In addition, we showed that the presence of DGL on the 2D support greatly modulated the process of cell differentiation and fusion through mechanisms that need to be further investigated. For instance, to better understand the underlying processes, it would be of interest to study DGL coatings partially functionalized with anhydride acid such as succinic acid following the reaction 1 [400]. This reaction would allow converting NH2 into COOH groups and being able to study the effect of groups and charges on C2C12 cells while maintaining the DGL structure.

(1) Reaction between succinic acid and NH2 groups leading to the formation of COOH groups

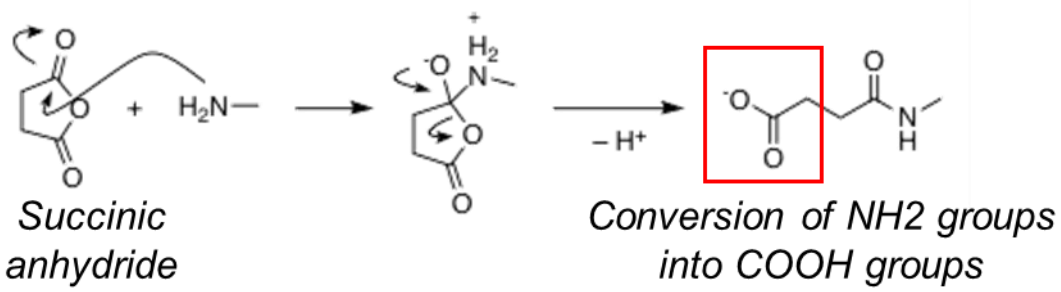

Another possibility to correlate the fusion impairment with the concentration of NH2 groups, would be to quantify the NH2 concentration and the electrical potential at the surface of DGL/PEG hydrogels of various concentrations. The determination of the zeta potential at the interface of hydrogel with the medium could help measuring the electrical potential and the electrostatic forces applied on cells. In addition, the ADECA assay (amino density estimation by colorimetric method) could provide the number of available $NH3^+$ groups at the surface of hydrogels [401]. It is a colorimetric assay based on the reversible specific interaction between coomassie brilliant blue (CBB) and protonated N^+ groups such as $NH3^+$. After CBB grafting on protonated surface, it is eluted and quantified to deduce the concentration of NH2 groups on surfaces. During the thesis, some effort have been dedicated towards the establishment of ADECA protocols on DGL/PEG hydrogel of various compositions. However, the penetration of the dye solution inside the hydrogel network distorted the analysis by quantifying protonated groups inside the hydrogel (having no interactions with cells) in addition to those present on the surface. Besides, the dye solution enter more quickly inside less concentrated hydrogel compositions, with looser mesh size. Future work could thus focus on the optimization of the dye exposure and elution time to quantify NH2 group present at the surface of DGL/PEG hydrogel and allow correlations with cell behaviour.

To conclude, even if all the mechanisms were not fully explained, some conditions of the DGL/PEG hydrogel could sustain rapid C2C12 proliferation and fusion, consolidating its potential as a support for skeletal muscle cells. Altogether, these results enabled us to define three concentrations of interest for subsequent studies. Conditions **1.6/25** and **2/37** mM DGL/PEG with various stiffness and same DGL/PEG molar ratio were selected due to high fusion indexes in comparison to other conditions. The condition **2/25** mM DGL/PEG hydrogel was also chosen, given its ability to sustain C2C12 proliferation, similarly to the positive plastic dish control.

Table 21 : C2C12 behaviour in proliferation and differentiation on the three conditions targeted

mM DGL/PEG	DGL :PEG ratio	Elastic modulus (kPa)	Proliferation (confluence)	Differentiation (fusion index)
1.6/25	1:16	18.3 ± 2.2	15.6 ± 3.5	8.2 ± 1.1
2/25	1:12	54.7 ± 3.1	35.0 ± 8.7	2.5 ± 0.5
2/37	1:16	105.5 ± 11.5	43.0 ± 5.5	8.2 ± 0.6

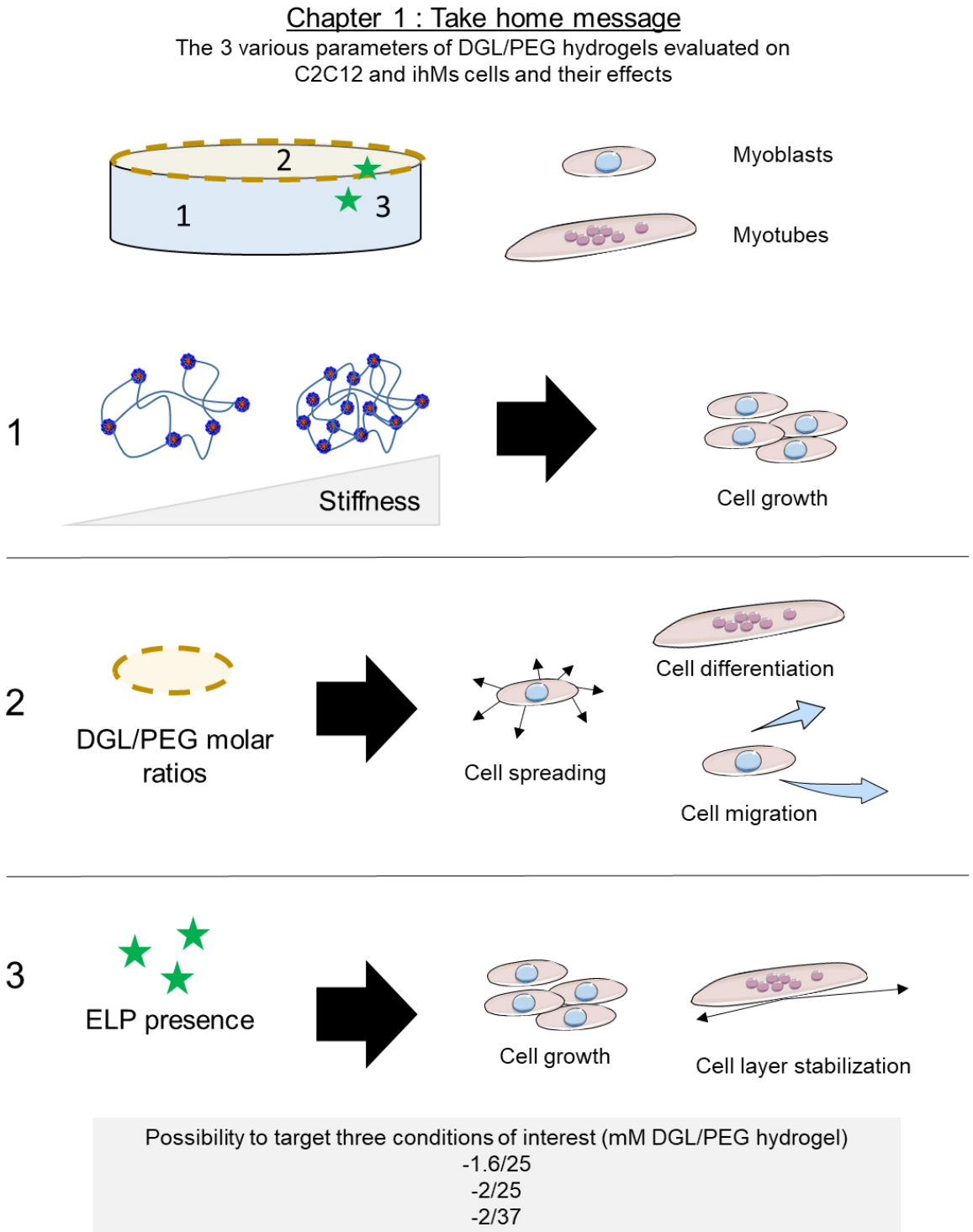

Figure 32 : Take home message Chapter 1

2 The development and characterization of a porosity inside DGL/PEG hydrogel compatible with its injection.

The DGL/PEG hydrogel appears as a promising material in the biomedical field owing to its similarity to native extracellular matrices, and modularity in terms of stiffness and cell adhesion. We demonstrated that the DGL/PEG hydrogel is of interest for the sustained proliferation of skeletal muscle cells and their subsequent fusion. We demonstrated as well that its modulation allowed to control skeletal muscle cell behaviour, further consolidating its potential.

Moreover, the use of solubilized polymer precursors to form the DGL/PEG hydrogel is compatible with their passage through needles to polymerize *in situ.* The design of injectable systems is one of the major needs for hydrogels applications in clinical settings, as they can conform accurately to irregularly shaped cavities and integrate to surrounding tissues via a minimally invasive surgery [402]. This advantage can cost-effectively shorten the surgical operation time, minimize the damaging effects on tissues, reduce scars size, and lower postoperative pain.

However, to be used for tissue regeneration, the DGL/PEG hydrogel should lead to an efficient cellular and tissue ingrowth, with blood vessel infiltration to prevent hypoxia [288]. The number of hydrogel candidates that can be readily infiltrated and colonized without preformed porosity is so far limited [330], [334] and the induction of porosity inside hydrogels is, therefore, critical for regeneration purposes.
A variety of techniques such as electrospinning, freeze-drying [150], gas/salt leaching [403], phase separation [404] or gas foaming techniques using high-pressure CO_2 [228], [350], [352]–[354] have been developed to induce a porous structure inside a hydrogel, in view of incorporating the features required by targeted tissues. Nevertheless, most of the aforementioned processes used to prepare the hydrogel itself or the porous structures within are generally not suitable with direct injection, due to mandatory production steps beforehand or to the use of harsh solvents. As a result, these approaches, although appealing to create a porosity inside hydrogels, are so far confined to pre-shaped structures for invasive and stressful implantations.

The aim of this chapter is thus to find a way to (1) create a porosity inside the DGL/PEG hydrogel while (2) maintaining its technical injectability and (3) preventing the release of toxic products to be *in situ* injected without inducing toxic effects.

2.1 *In situ* injectability: the need to avoid the use of harsh solvents

To be able to address the aforementioned aims, an important modification of the hydrogel formulation had to be performed beforehand. The DGL/PEG hydrogel described in the first chapter was prepared using PEG-NHS solubilized in N,N-Dimethylformamide (DMF), due to the N-Hydroxysuccinimide (NHS) function quick hydrolysis in aqueous solutions. However, DMF raises many safety issues linked to its carcinogenic, mutagenic, and reprotoxic (CMR) nature, which render it unsuitable for *in situ* injectability. To address this issue, it was decided in this work, to use a safer solvent, such as dimethyl sulfoxide (DMSO) that would also preserve the NHS groups' reactivity over time.

2.1.1 Effect of PEG solvents on normal human dermal fibroblasts (NHDF)

As previously mentioned, dry DMF was used in first instance to avoid NHS ester groups' hydrolysis in aqueous solutions. Indeed, PEG-NHS dissolved in PBS 1X showed a clear decrease of reactivity over time, visible through a significant crosslinking delay after 1 and 4 weeks storage at -20°C (Figure 33A). On the contrary, when solubilized in DMSO, the PEG reactivity was not significantly decreased up to 4 weeks of storage compared to PEG solubilized in DMF. Given the need to take advantage of the tuneable and reproducible crosslinking velocity of the DGL/PEG hydrogel, the use of PBS was therefore abandoned.

To study the effect of DMF and DMSO on cells, normal human dermal fibroblasts (NHDF) were cultured in contact with 24 hours extracts of dense hydrogels. Unless stated otherwise, all the dense hydrogels evaluated for cytotoxicity were used directly after formulation without any washing, to emulate the conditions of an *in situ* injection.

As depicted in Figure 33B, 24 hours extracts of unwashed hydrogels formulated with PEG solubilized in DMF triggered a significant decrease of cell metabolic activity after 48 hours of contact. Conversely, the use of DMSO was related to a slight decrease in cell metabolic activity compared to the control and no significant difference compared to an extensively washed hydrogel.

The drastic drop of cell metabolic activity observed with 24 hours hydrogels extracts formulated with DMF can be attributed to the solvent intrinsic cytotoxicity. As observed in Figure 33C, the addition of DMF at 1% on NHDF seeded on plastic dishes induced a significant decrease in their metabolic activity after 48 hours. Contrarily, 1% of DMSO added directly in the culture medium of NHDF did not induce any modification of their metabolic activity, compared with untreated control (Figure 33C). As a result, DMSO is an attractive alternative to the DMF for PEG solubilisation as no differences in cellular metabolic activity were highlighted between cells in contact with 24 hours extracts of control rinsed hydrogel or of unwashed hydrogel formulated with the PEG solubilized in DMSO.

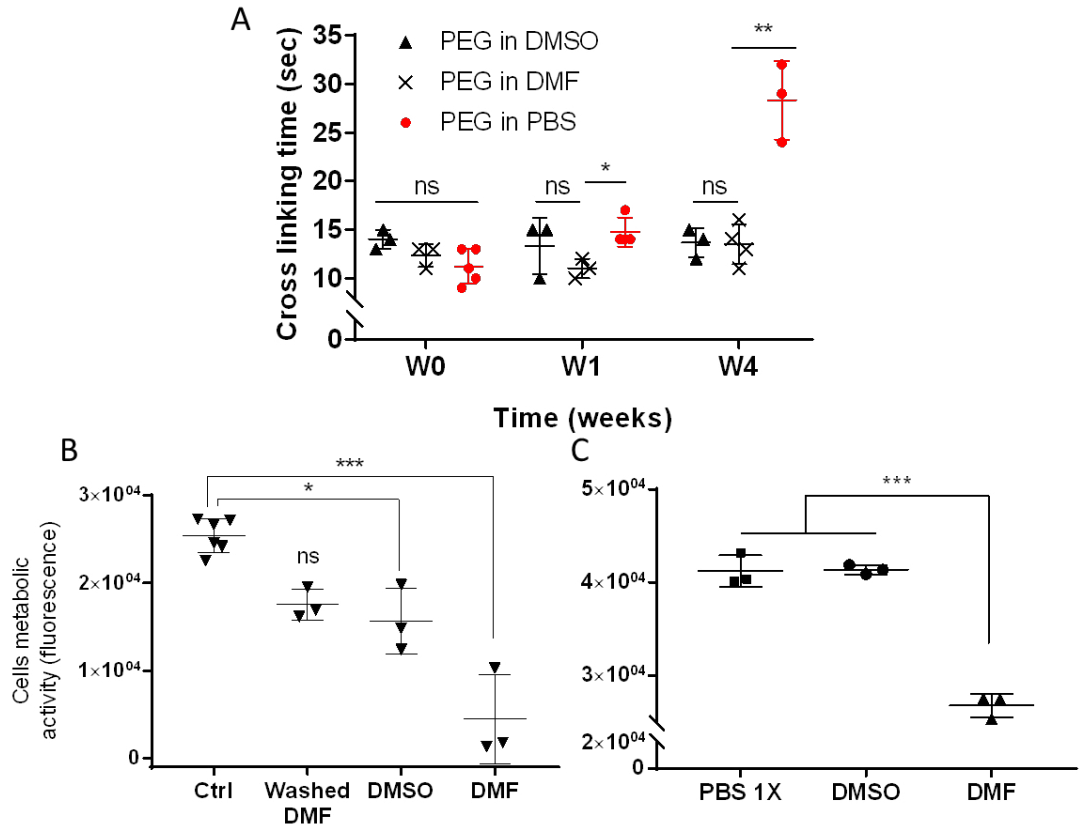

Figure 33: Study of the use of other solvents for PEG-NHS solubilisation
A) Crosslinking time of 2/25 mM DGL/PEG hydrogel with the PEG solubilized in DMF, DMSO or PBS and immediately used for reaction (W0) or stored at -20°C and used after 1 or 4 weeks (W1 and W4, respectively)
B) NHDF cells in contact 48 hours with 24 hours hydrogel extracts of 2/25 mM DGL/PEG hydrogels formulated with PEG-NHS solubilized in DMSO (DMSO) or in DMF (DMF) used directly post formulation, or after an extensive washing (Washed DMF) as a positive control against cells without treatments (Ctrl), C) Effect of DMSO and DMF at a 1% final concentration 48 hours in contact with cells vs cells in contact with 1% PBS as a positive control (PBS). A) Mann-Whitney test DMF vs DMSO or DMF vs PBS. B, C) One way ANOVA + Dunnett's multiple comparison test VS Ctrl or PBS 1X

2.1.2 Validation of the use of DMSO instead of DMF for PEG solubilisation

Due to the modification of PEG solvent, to match the requirement of *in situ* injectability, some of the results generated in chapter 1 were confirmed with 2D hydrogels formulated in DMSO. It was demonstrated that regardless of the PEG solvent used to formulate the hydrogels (either DMSO or DMF), similar results were obtained. In particular, no differences in terms of mechanical behaviour were reported for the three DGL/PEG conditions targeted (Figure 34A and B). Similarly, the behaviour of C2C12 cells was not impaired by the use of DMSO instead of DMF, as assessed by their proliferation and differentiation (Figure 34C and D).

According to the lack of significant difference between DMSO and DMF in regard of mechanical properties or cell behaviour, all subsequent experiments were done using DMSO as solvent for the PEG-NHS. This allows strengthening the possible use of DGL/PEG hydrogels as an adequate substrate to be used in direct contact with cells, without harming effect.

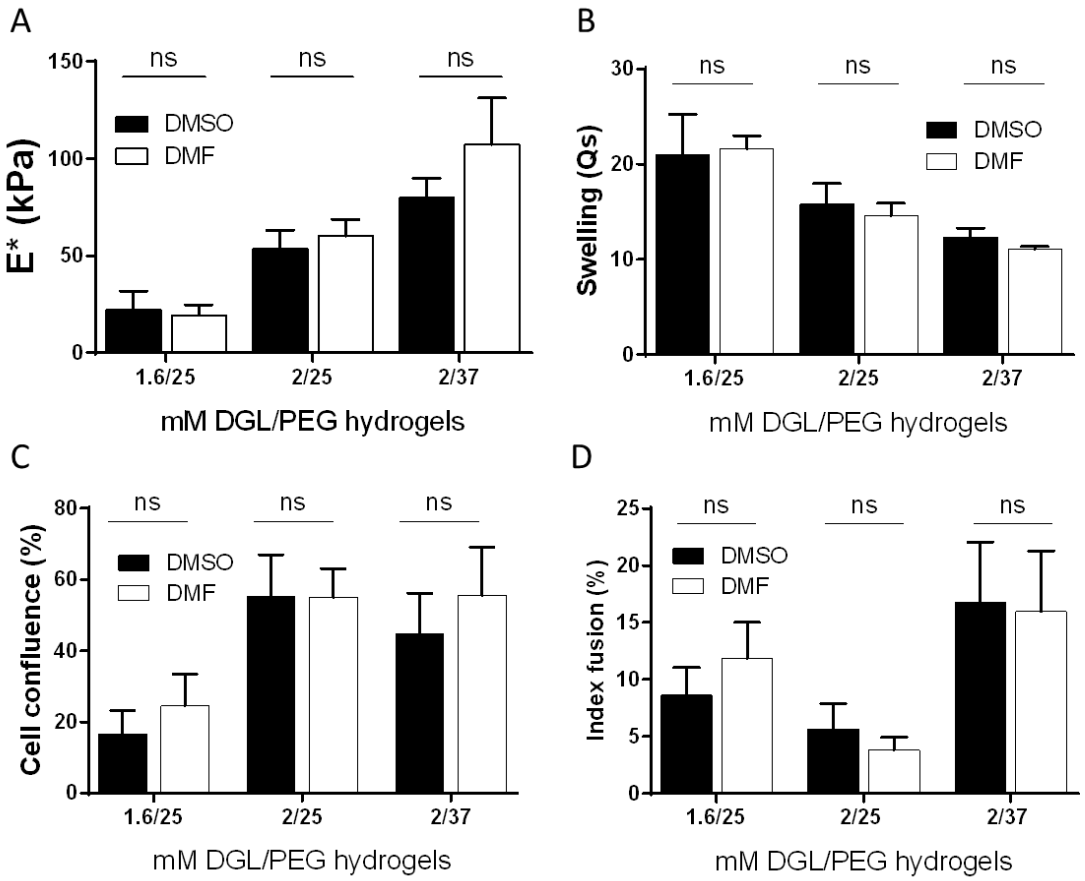

Figure 34: Comparative study of 2D hydrogels formulated with PEG –NHS solubilized in DMF or in DMSO

A) Mechanical properties in compression and B) swelling ratios of various DGL/PEG hydrogel conditions formulated from PEG either solubilized in DMF or DMSO.

C2C12 cells C) confluence after 30 hours post seeding and D) fusion index after 6 days in serum depleted medium on various DGL/PEG hydrogel conditions formulated with the PEG solubilized in DMF or DMSO.

A), B), C), D) t-test DMF vs DMSO

2.2 Elaboration of a porosity compatible with DGL/PEG injection

To establish a porosity inside DGL/PEG hydrogels while maintaining their injectable potential, various techniques have been explored. Their respective advantages and drawbacks have been evaluated prior to describe the most optimal solution.

2.2.1 Particle leaching

As mentioned in the introduction, particle leaching techniques can form tailorable porosity and have shown interesting possibilities in combination with injection.

Oil and water emulsion techniques described in this work allowed the formation of microbeads from a 10 % gelatine solution. The formation of the beads took advantage of the thermosensitive properties of the gelatine. Above temperatures of 25°C in aqueous solutions, gelatine is solubilized in a random coil conformation. Below 10°C, and for concentrations above 2 %, gelatine recovers a triple helical structure to form a non-soluble physical hydrogel. As depicted in Figure 35A, round-shaped beads with a broad size distribution could be obtained and maintained in cold aqueous solutions.

After formulation, gelatine microbeads (GMB) were successfully added to 4°C DGL/PEG hydrogel precursors to be entrapped inside the hydrogel network during crosslinking (Figure 35B and C). Although entrapped inside the DGL/PEG hydrogel network, the GMB were visibly not in tight contact with each other. In addition, GMB were not able to leach after immersing 24 hours the composite (DGL/PEG hydrogel entrapping GMB) in 37 °C and 50 °C water bathes (Figure 35D). GMB, not in contact during hydrogel formulation is a plausible explanation to these results. Without contact between GMB, their leaching will only occur through hydrogel mesh size diffusion. Generally, the gelatine molecular weight is comprised between 10^4 and 10^7 g/mol with an average of about 10^5-10^6 g/mol [405]. Therefore, gelatine molecules chains of high molecular weight and high polydispersity might prevent their diffusion through DGL/PEG hydrogel tight mesh size.

To overcome this issue, and try to create contact between GMB, they were used freeze-dried to provide a higher density of GMB during DGL/PEG formulation and simultaneous microbeads rehydration. After immersion of composite DGL/PEG hydrogels and GMB in a 37°C water bath, some pores generated localized interconnections (Figure 35E). The formation of air bubbles during the DGL/PEG network realization was also observed with the addition of dry GMB.

Although particle-leaching technique seemed promising, the difficulty to perform GMB compaction during DGL/PEG formulation prevented their leaching. The lack of dissolution clearly precluded the formation of interconnected porosity inside the network, restricting the use of this technique.

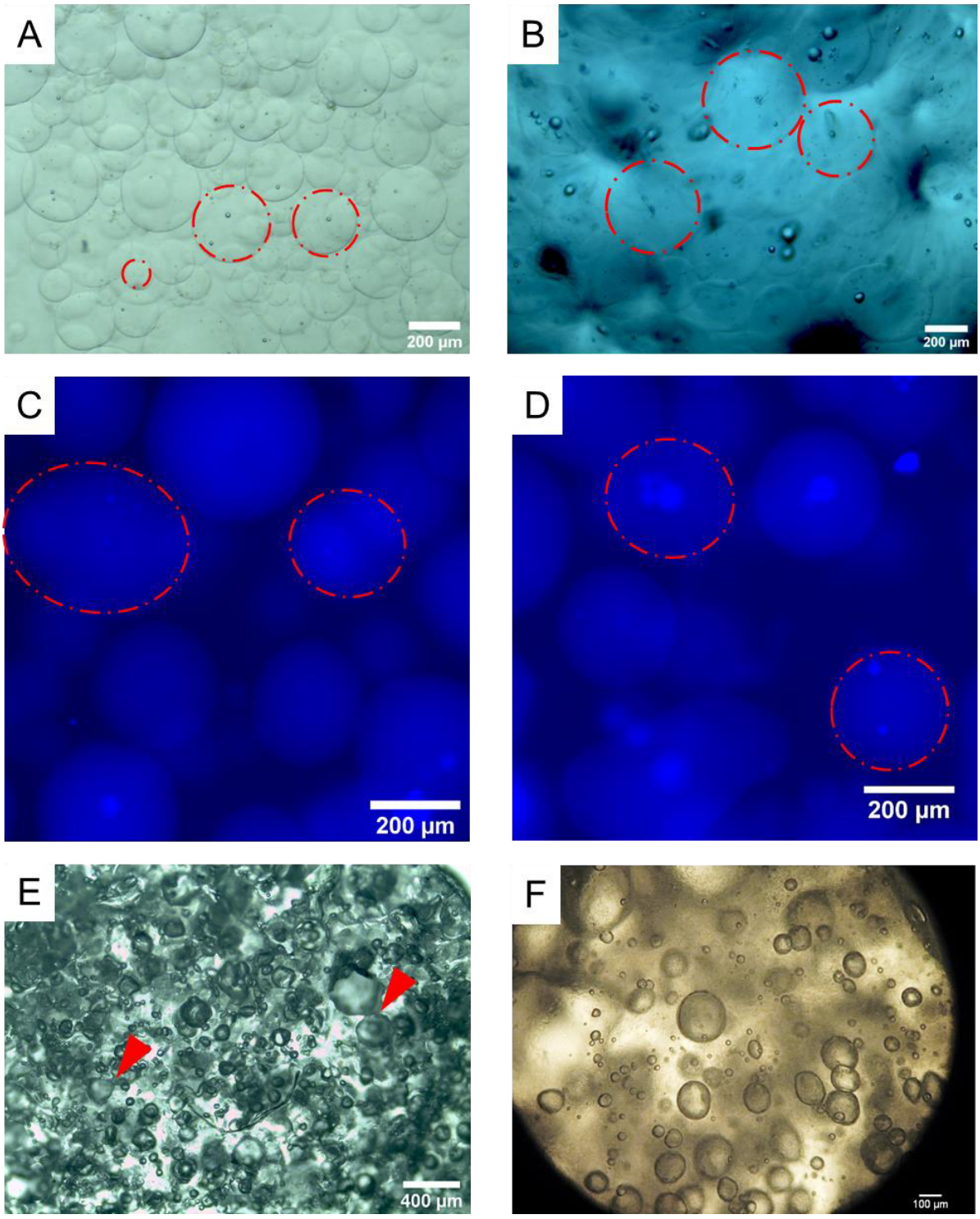

Figure 35 : Alternatives solutions explored for the induction of a porosity inside the DGL/PEG hydrogel suitable with its injection

A) Observation of GMB right after formulation in cold PBS 1X and B) embedded inside a 2/25 mM DGL/PEG hydrogel in light or fluorescence microscopy after 24 hours at C) 4°C or D) 37°C. GMB are visible in blue (autofluorescence). Red dotted line: GMB delimitation.

E) DGL/PEG hydrogel mixed to freeze-dried GMB, let to be hydrated by hydrogels precursors. Red arrows: some pores were interconnected. F) Stabilized emulsion created during DGL/PEG crosslinking.

2.2.2 Gas entrapment – gas foaming methods

One interesting feature of the DGL/PEG hydrogel is its fast and tailorable crosslinking velocity within seconds to minutes [373]. This characteristic can offer the opportunity to entrap air or gas bubbles inside the network during its crosslinking.

The following parts are therefore dedicated to the investigation of the adequacy of various gas bubbles generation systems with the DGL/PEG hydrogel crosslinking.

2.2.2.1 Stabilized air emulsion inside DGL/PEG hydrogels

First, the use of stabilized air bubbles was envisaged to generate a porosity inside the DGL/PEG hydrogel similarly to Zhang and co-workers [346] and as follows:

A connector was used to join two syringes containing hydrogel precursors with a certain volume of air. Both solutions were homogenized by pushing the plungers of the syringes alternatively in opposite directions to create the air bubbles by emulsion during the mixing process. The incorporation of a surfactant together with PEG 8000 in hydrogel precursors enabled to stabilize air bubbles for several minutes and prevented their burst or fusion. After 10 seconds of homogenization, the resultant hydrogel was injected inside a conic tube. In this manner, it was possible to create an important amount of air-stabilized bubbles entrapped inside the DGL/PEG hydrogel network. After cutting and observation under light microscopy, the resultant porous hydrogel exhibited air bubbles still entrapped inside the network with no clear contact between bubbles (Figure 35F).

Neither the surfactant nor the viscosity increase through the PEG 8000 had an impact on DGL/PEG hydrogel crosslinking velocity. However, by varying amounts of surfactant and/or PEG 8000 from 5 to 15% (w/v), it was not possible to promote the formation of contact between stabilized air bubbles. Hence, the lack of interconnection seemed not related to a poor air bubbles stabilization but rather to an air bubble density too low to achieve contact.

The observation that a critical amount of bubbles was mandatory to achieve contact, resulting in potential interconnection, incited us to explore other methods to form bubbles at a higher density.

2.2.2.2 Effervescent reactions

To bring an alternative to the aforementioned issue the use of acid-base effervescences, generating CO_2 bubbles, was considered in this work. However, the question remains if an effervescent reaction, associated with the DGL/PEG hydrogel, could allow both injection and *in situ* formation of pores, in a single step.

A first work was thus conducted on the choice of effervescence conditions.

Acid/base selection

By mixing carboxylic acid and carbonated base in aqueous solutions, effervescences were effectively produced and could be adjusted. Only the results generated using acid and base solubilized in water are reported here. The use of powders was part of pilot experiments not described in this work and rapidly excluded due to the risk of needle clogging during the injection.

The final concentration of acid and base, for a fixed ratio, allowed tailoring the effervescence power and duration over time whatever the acid/base couple used. While a low concentration (0.5 M) produced a non-explosive effervescence with minimal production of CO_2 bubbles and a relatively short reaction duration, a higher concentration (1.5 M) induced a longer and explosive effervescence characterized by an important volume expansion. Of note, the more explosive the effervescence, the larger bubbles were observed. Therefore, a concentration of **1.1 M** was set in subsequent experiments to generate enough CO_2 bubbles to generate homogeneous porosity while preventing a too explosive effervescence with the formation of giant CO_2 bubbles that could weaken the resultant hydrogel.

At this final concentration of 1.1 M, regardless of the acid/base couple used, effervescences generated were visually similar in terms of duration and CO_2 bubbles generation. However, calcium carbonate, magnesium carbonate, and succinic acid were discarded due to their low solubility in water, requiring the use of too important volumes. Moreover, reactions with sodium bicarbonate and citric acid were also avoided due to the production of a potent anticoagulant, the sodium citrate [406].

Finally, five acid/base couples were of interest with the production of visually similar effervescences. The reaction of potassium carbonate (KC) with glacial acetic acid (Gaa) was finally chosen owing to their high water solubility and possibility to achieve high concentrations in small volumes.

Table 22 : Study of various carboxylic acid and carbonated base to generate effervescences. Effervescences should generate a high density of CO_2 bubbles. Check marks are highlighting acid:base couple enabling the generation of high CO_2 bubbles density due to adequate solubilization in aqueous solutions to reach high final concentrations.

<table>
<tr><th>Base
Acid</th><th>Potassium carbonate</th><th>Sodium carbonate</th><th>Sodium bicarbonate</th><th>Calcium carbonate</th><th>Magnesium carbonate</th></tr>
<tr><td>Acetic acid</td><td>☑</td><td>☑</td><td>☑</td><td colspan="2" rowspan="3">Low solubilisation of both carbonates. Difficulty to reach high final concentration for explosive effervescence</td></tr>
<tr><td>Citric acid</td><td>☑</td><td>☑</td><td>☑ Formation of sodium citrate</td></tr>
<tr><td>Succinic acid</td><td colspan="3">Low solubilisation of the acid. Difficulty to reach high final concentration for explosive effervescence</td></tr>
</table>

As depicted in Figure 36A, for a final concentration of 1.1 M and by varying the Gaa:KC molar ratio, it was possible to modulate the pH of the solution after effervescence from 5.57 ± 0.03 up to 7.25 ± 0.003. Of note, when deviating from the stoichiometric condition (i.e. 2:1 Gaa:KC molar ratios), a slower pH stabilization over time was observed. Conditions 1:1, 1.33:1 and 1.5:1 Gaa:KC molar ratio were still not stabilized after 48 hours of reaction (with a pH of 8.14 ± 0.04; 7.47 ± 0.05 and 6.90 ± 0.06 respectively). On the contrary 1.75:1 and 2:1 Gaa:KC molar ratio were stabilized 15 minutes after the effervescent reaction. Interestingly, for a given final molarity, the molar ratio variation did not induce a visual difference between effervescence duration over time and CO_2 bubble generation. On the contrary, the addition of a surfactant during the effervescent reaction stabilized CO_2 bubbles for 3 minutes, which represents a very interesting mean to further control CO_2 bubble generation.

Considering the versatility of CO_2 bubble production observed, the influence of the effervescence on DGL/PEG hydrogels crosslinking was then investigated, to determine their chemical compatibility and the possibility to use a surfactant as stabilizer. To do so, potassium carbonate and glacial acetic acid were let to react for 10 minutes at the desired concentrations, followed by extensive homogenization. The resulting solutions, after completion of effervescent reactions, were used for subsequent hydrogel crosslinking experiments.

First, the effect of the final pH produced by effervescence was studied on a 2/25mM DGL/PEG hydrogel crosslinking. In PBS, which pH was adjusted from 5 to 10 with various Gaa:KC molar ratio (from 2:1 to 1:1.6 Gaa:KC respectively), the crosslinking time of a 2/25 mM DGL/PEG hydrogel was strongly influenced (Figure 36B). At a final acidic pH (5), the crosslinking time was delayed to 350 seconds while alkaline pH (10) resulted in immediate crosslinking. Suggesting a strong influence of the pH on DGL/PEG chemistry, unrelated to the couple used, a similar delay was observed with other acids. This was further confirmed by the variation of Gaa and KC final molarity for a given molar ratio, as the crosslinking time of a 2/25 mM DGL/PEG hydrogel stayed constant whatever the molarity used (Figure 36C).

These results allowed to target a range of Gaa:KC molar ratios of interest between 1.75:1 and 1.33:1 (between pH 5.7 ± 0.07 and 7.5 ± 0.05) to enable a 2/25 mM DGL/PEG hydrogel to crosslink in a time interval compatible with its injection (between 84.33 ± 11.05 and 9.33 ± 1.33 seconds respectively). The suitability of this range of Gaa:KC molar ratios was also confirmed on the DGL/PEG compositions most suitable for muscle cells showing liquid precursors were able to crosslink into a self-standing hydrogel (Figure 36D). However, for all DGL/PEG conditions studied, the addition of Gaa:KC at a molar ratio of 1.75:1 lead to a significant tenfold crosslinking time increase due to acidic pH. Conversely, a 1.33:1 Gaa:KC molar ratio led to a not significant 1.5 crosslinking time increase due to a final pH close to PBS. Of note, the use of pluronic® F-68 as a surfactant did not induce any effect on the crosslinking time of a 2/25

mM DGL/PEG hydrogel regardless of the concentration used, which is of great interest for the control and stabilization of CO_2 bubbles generated (Figure 36E).

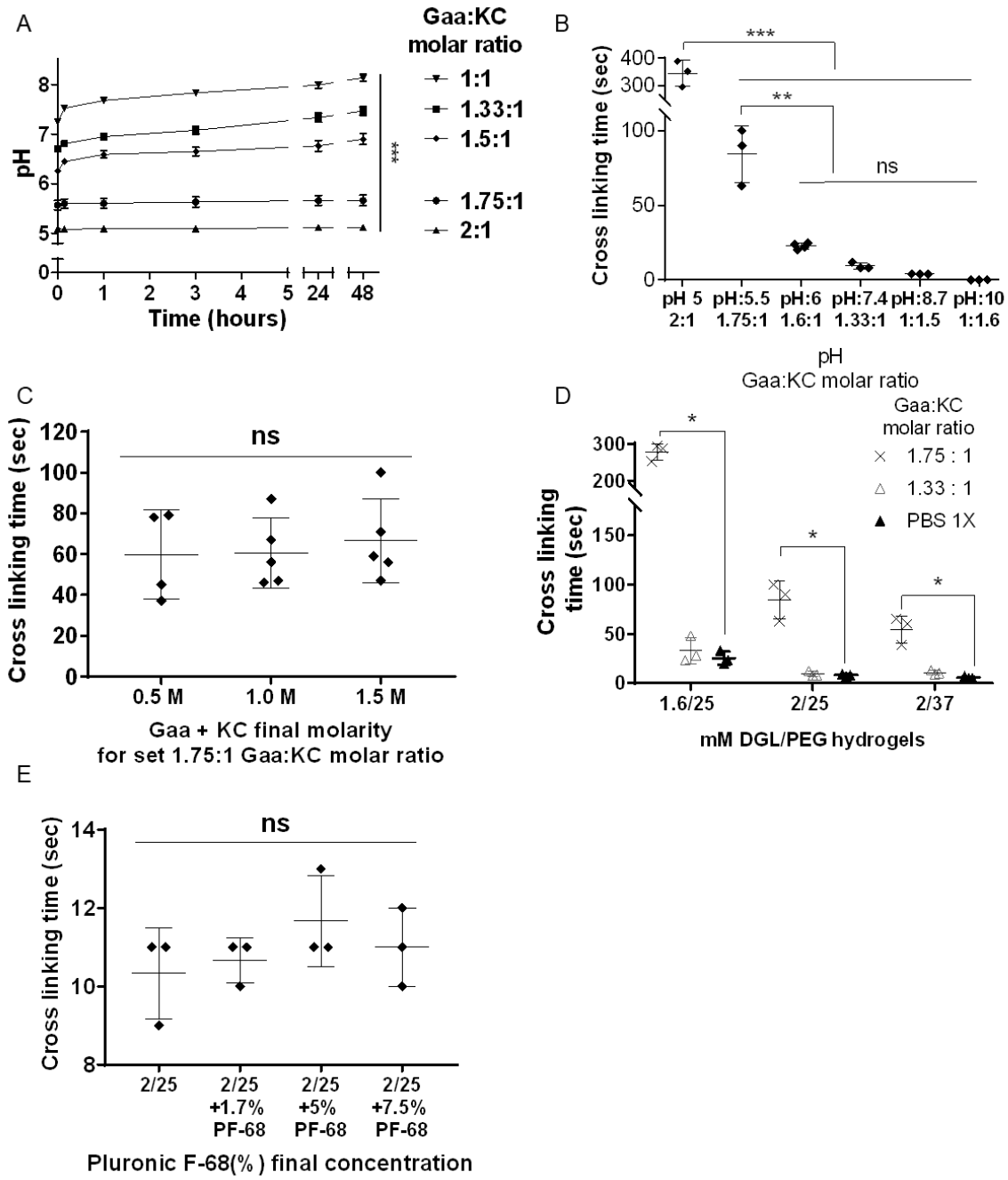

Figure 36 : Study of the compatibility of effervescent reactions with DGL/PEG hydrogels
A) pH of solutions over time after effervescence of various Gaa:KC molar ratios for a given 1.1 M final concentration. B) Influence of Gaa:KC molar ratio on the crosslinking time of a 2/25 mM DGL/PEG hydrogel for a given 1.1 M final concentration. C) Influence of Gaa:KC final molarity on crosslinking time of a 2/25 mM DGL/PEG hydrogel for a given 1.75:1 Gaa:KC molar ratio.
D) Crosslinking time comparison between various DGL/PEG hydrogels concentrations, as a function of a range of Gaa:KC molar ratio for a given 1.1 M final concentration.
*E) Influence of pluronic® F-68 final concentration on crosslinking time of a 2/25 mM DGL/PEG hydrogel. A, B,C : Passed Shapiro-Wilk test : One way ANOVA + Tukey's multiple comparison. D,E: Kruskal Wallis + Dunn's VS ctrl. *:p<0.05; **:p<0.01; ***: p<0.001*

2.2.3 Influence of effervescence on DGL/PEG hydrogels crosslinking

Owing to the great influence of the pH induced by effervescence on DGL/PEG hydrogels crosslinking velocity, its effect was further investigated at chemical and macroscopic levels on dense hydrogels. More specifically, the impact of delayed crosslinking on the properties of DGL/PEG hydrogels, was investigated using fluorescently-labelled DGL. Compared with a control 2/25 mM FITC-DGL/PEG hydrogel prepared in PBS, an increased release of DGL (up to 2 folds) was measured in presence of Gaa:KC, while the addition of pluronic® F-68 did not seem to have any influence (Figure 37A and B).

The weakened chemical reaction between DGL and PEG in effervescent conditions is possibly related to the final pH of the solutions. At acidic pH the DGL release was superior than at alkaline pH. These results are in line with the crosslinking velocity study, which showed that acidic pH triggers a longer crosslinking delay, possibly related to an impaired DGL chemical reaction. Accordingly, the complex modulus (E*) of all DGL/PEG dense hydrogels compositions, determined by mechanical dynamic analysis, showed a steep decrease of about 40 % and 30 % when prepared with 1.75:1 and 1.33:1 Gaa:KC molar ratio, respectively (Figure 37C). The addition of Gaa:KC also increased the swelling ratio of all hydrogels compositions, up to 24 % for a Gaa:KC molar ratio of 1.75:1 and 22 % for a Gaa:KC molar ratio of 1.33:1. Conversely, the addition of pluronic® F-68 did not result in variations of mechanical and swelling properties (Figure 37D and E).

Overall, these results confirm the influence of pH on DGL/PEG hydrogels. All measured properties of hydrogels prepared with more acidic solutions (crosslinking delay, higher DGL release, stronger decrease of mechanical properties and higher swelling) are indeed in agreement with a lower level of crosslinking. Nevertheless, for all conditions with Gaa:KC, the elastic modulus (E') was greater than the viscous modulus (E''), confirming the formation of a hydrogel. Furthermore, the presence of Gaa:KC at various ratios did not prevent to control the hydrogel bulk mechanical properties from 10 to 50 kPa, through the variation of DGL/PEG concentrations.

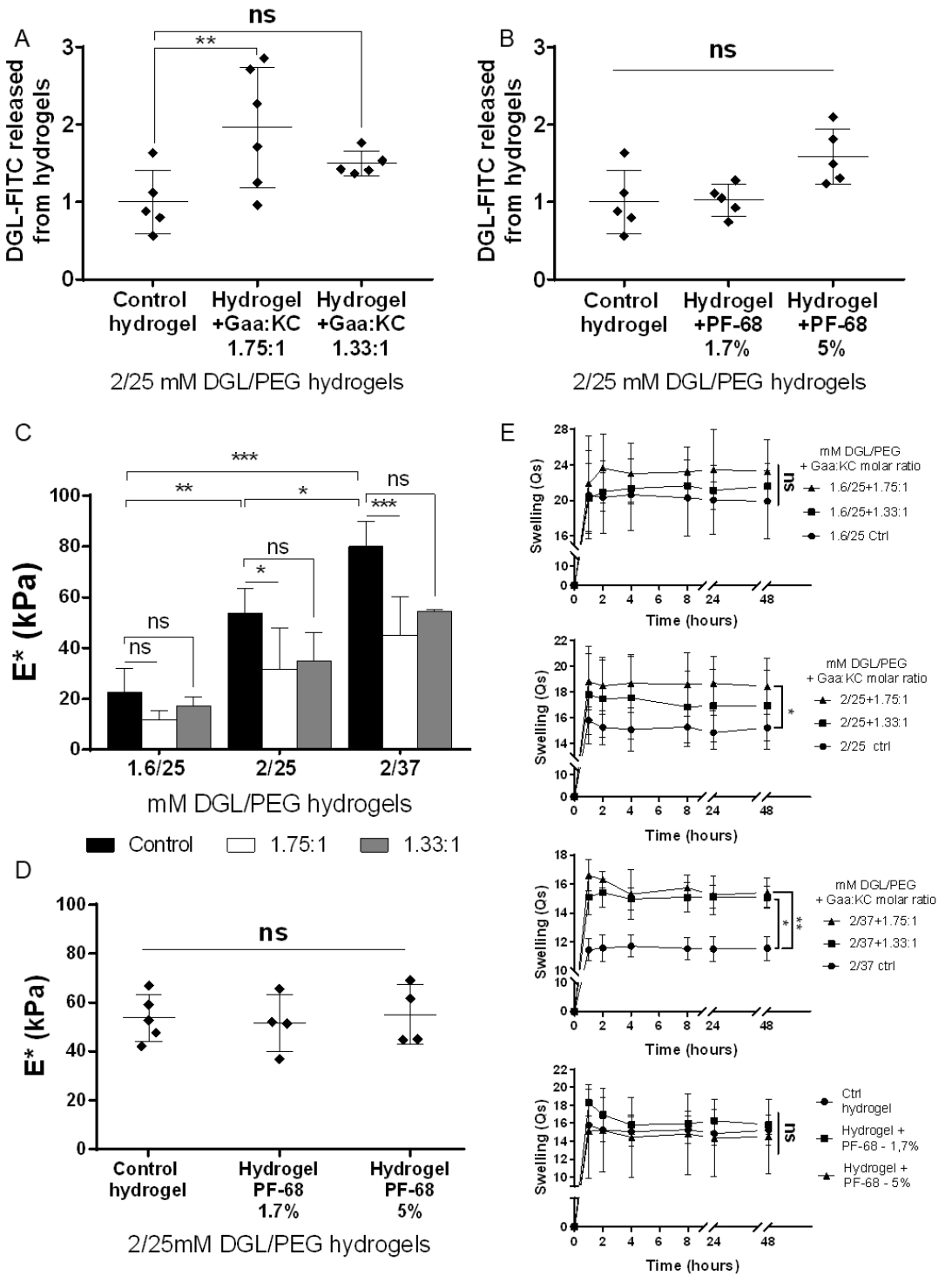

Figure 37 : Influence of effervescence on DGL/PEG hydrogels
DGL-FITC release from dense 2/25 mM DGL-FITC/PEG hydrogels formulated with various A) Gaa:KC molar ratios or B) pluronic® F-68 concentrations. The fluorescent signal is normalized to the one of control hydrogels
Complex modulus (E) in kPa of various dense hydrogel conditions formulated C) in PBS 1X (control) or in 1.75:1 and 1.33:1 Gaa:KC molar ratio buffers or D) with pluronic® F-68 at 1.7% and 5%*
E) Swelling ratio of various DGL/PEG hydrogels formulated in PBS (Ctrl) or in 1.75:1 and 1.33:1 Gaa:KC molar ratio and with various pluronic® F-68 concentrations.
*Passed Shapiro-Wilk normality test One way ANOVA + Dunnett's vs control hydrogel *:p<0.05; **:p<0.01; ***p<0.001*

2.2.4 Porous and injectable DGL/PEG hydrogels using an effervescent approach

Given the pH-induced hydrogels delayed crosslinking, the possibility to match effervescence and hydrogel reaction was further investigated. Gaa and KC were dissolved in the PEG and DGL precursor solutions respectively in distinct tubes. After manual mixing (by pipetting) of the two solutions, neither the effervescent reaction nor the hydrogel crosslinking were hampered (Annex 1, supplementary movie 5). Therefore, it was possible to validate our hypothesis by successfully entrapping CO_2 bubbles, stabilized for 30 seconds to 3 minutes, in solid hydrogels through simultaneous effervescence and polymerization (Figure 38A and B). Logically, the resulting foamy structures showed an important volume expansion of 600 %, 500 %, and 200 % for 1.6/25, 2/25, and 2/37 mM DGL/PEG hydrogels respectively (Figure 38B and C).

After hydrogel crosslinking and subsequent immersion in aqueous solutions, the CO_2 removal revealed porous structures inside the hydrogels, regardless of their compositions (Figure 38D). Strikingly, the formed porosity appeared highly interconnected for all conditions with the observation of no isolated pores and from one up to 50 windows of interconnection per pore (Figure 38D). The Gaa:KC molar ratios between 1.33:1 and 1.75:1 determined previously to sustain the formation of a self-standing material, provided crosslinking times compatible with the entrapment of the formed CO_2 bubbles. However, to improve the entrapment of CO_2 bubbles in slow-setting hydrogels (i.e. 1.6/25 and 2/25 mM DGL/PEG), the presence of pluronic® F-68 was mandatory to stabilize the effervescence during crosslinking. For fast-setting ones (2/37 mM DGL/PEG), the presence of the surfactant was linked to a more homogeneous apparent distribution of CO_2 bubble.

In conclusion, the possibility to match effervescent reaction to hydrogel crosslinking was assessed with the conditions defined in Figure 36 and Figure 37. To perform the well-orchestrated reactions, hydrogel precursors and effervescent components were stored separately before manual mixing by pipetting. These results provide a proof-of-concept for the induction of a porosity by effervescence inside DGL/PEG hydrogel. Therefore, the possibility to convert these formulations into injectable hydrogel was further investigated.

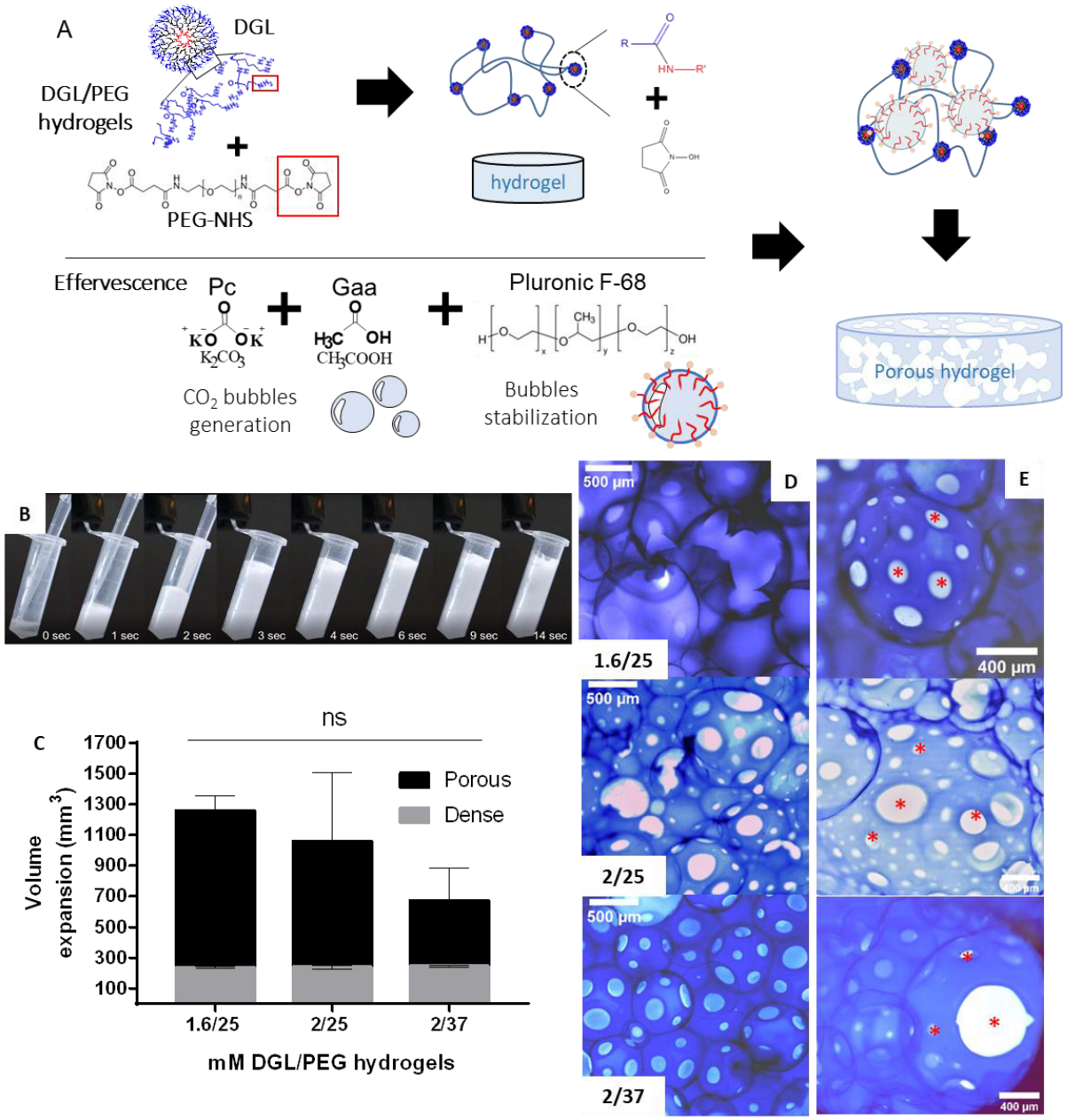

Figure 38: Porous and injectable DGL/PEG hydrogels using an effervescent approach
*(A) Schematic representation of effervescent porous hydrogels (EPH) realization. DGL and PEG are reacting to form the self-standing material while the reaction between Gaa and KC generates CO_2 bubbles stabilized by the pluronic® F-68. An entrapment of CO_2 bubbles inside the hydrogel enable to create the porous structure. B) Porosity obtained within a 2/25 mM DGL/PEG hydrogel. C) Calculation of volume expansion during formulation of porous VS dense 1.6/25; 2/25 and 2/37mM DGL/PEG hydrogels. D) Porosity obtained within 1.6/25 mM, 2/25 mM, and 2/37 mM DGL/PEG hydrogels. E) Observation of windows of interconnection in a 2/25 mM DGL/PEG hydrogel (red star: one window). Hydrogels formulated with 1.33:1 Gaa:KC and 3.3% pluronic® F-68 - Coomassie bue staining. n= 3 Passed Shapiro-Wilk normality test One way ANOVA + Tukey multiple comparison *:p<0.05; **:p<0.01; ***p<0.001*

The possibility to inject the effervescent formulation was tested through a dual syringe system combined with a static mixer (Figure 39A and annex 1, supplementary movie 6). As a striking result, the effervescent reaction was not hindered by the injection and the stabilized foamy structure was crosslinked by the subsequent reaction of DGL with PEG, forming a self-standing porous structure. Similarly to manual homogenization, the evaluated DGL/PEG concentrations (1.6/25; 2/25 and 2/37 mM) were able to form a porous structure with an important volume expansion Figure 39B). The strength needed on the plunger to inject dense and porous DGL/PEG hydrogels of various conditions was not superior to that of water, demonstrating hydrogels precursors were still in liquid form during injection (Figure 39C). Hence, the homogenization of the solution using a static mixer was confirmed through a system easy to handle, which open technical potential for direct injectability.

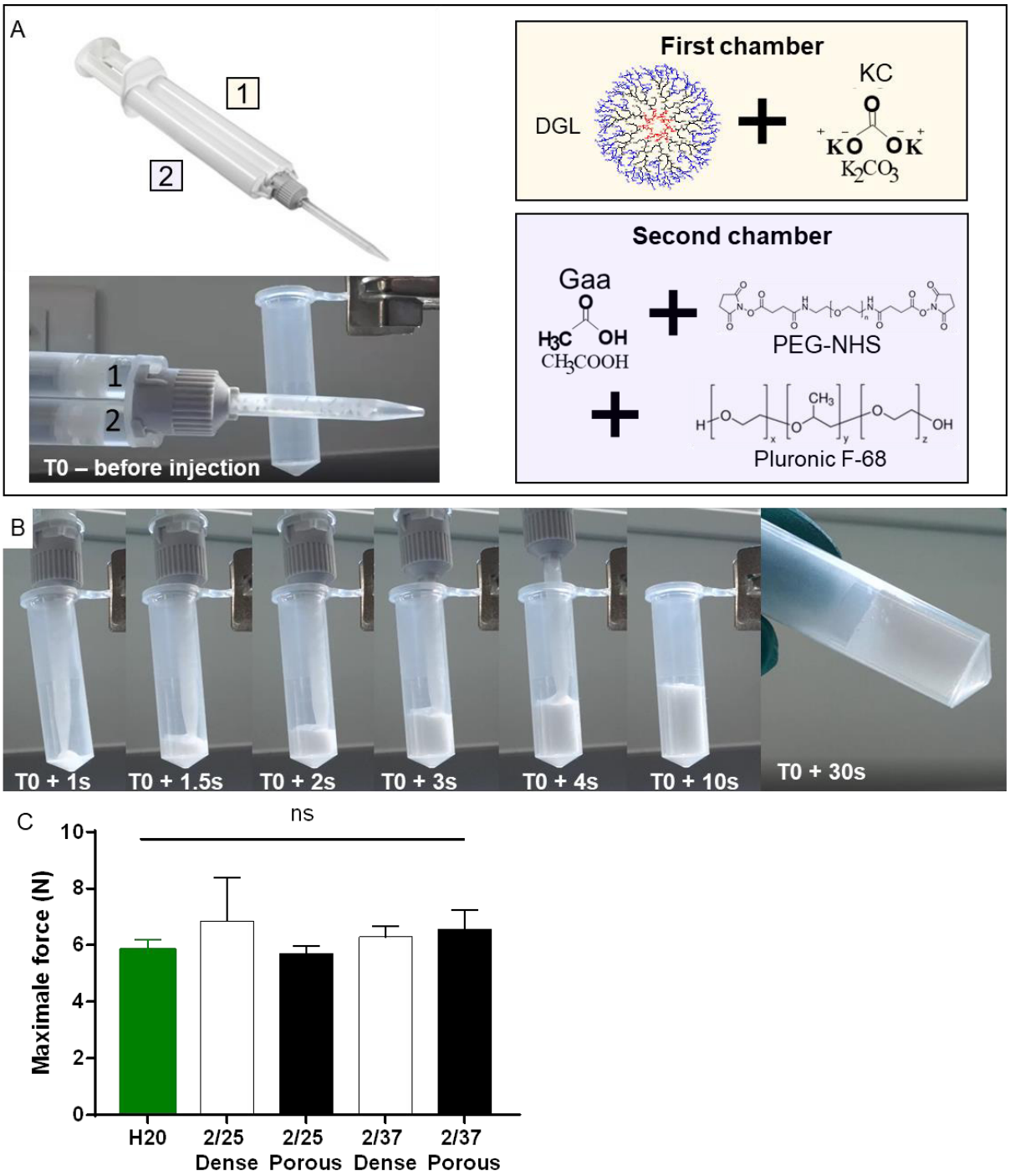

Figure 39: The injectable system of the effervescent porous DGL/PEG hydrogel
*A) The establishment of a dual-chamber syringe connected to a static mixer for the storage and injection of DGL/PEG effervescent porous formulation. The effervescence and hydrogel precursors were stored in different cartridges of the dual syringe and both reactions could begin simultaneously through homogenization with the static mixer. B) The foamy structure obtained by injection within a 2/25 mM DGL/PEG hydrogels. C) Strength applied on the syringe plunger to maintain a 2 mm/s injection speed to inject H_20 (positive control) dense and porous 2/25 and 2/37 mM DGL/PEG hydrogels. Hydrogels formulated with 1.33:1 Gaa:KC and 3.3% pluronic® F-68 n= 3 - One way ANOVA + Tukey multiple comparison *:p<0.05; **:p<0.01; ***p<0.001*

2.2.5 Porosity characterization

The porous structure formed by effervescence in the different DGL/PEG hydrogels was evaluated by confocal microscopy to determine pore size, percentage of porosity and size of windows of interconnections (Figure 40A and annex 1, supplementary movie 7). Overall, the percentage of porosity of **injected** effervescent porous hydrogels (EPH) was comprised between 75.0 ± 2.3 % and 79.7 ± 1.9 % (Table 23, top). The average pore size was comprised between 280.1 ± 54.9 µm and 313.0 ± 32.3 µm (Table 23, top) and was characterized by a broad distribution with pores ranging from 35 up to 3000 µm. However, pores between 50 and 100 µm were the most abundant proportionally (Figure 40B). In all conditions studied, a highly interconnected porous structure could be obtained with interconnection ranging from 100.7 ± 14.9 µm up to 131.4 ± 12.9 µm. As for pore size, windows of interconnections were characterized by a broad distribution (Figure 40C). Of note, no significant differences could be observed between the three DGL/PEG conditions studied.

The variation of the Gaa:KC molar ratio was studied on **manually homogenised EPH** and did not result in significant differences in terms of pore size and windows of interconnection (Table 23, bottom). However, for a given 3.3 % pluronic® F-68 and 2/25 mM hydrogel concentrations, the most acidic ratio (1.75:1) displayed a porosity significantly lower (62.1 ± 6.0 %) than less acid ones (74.4 ± 3.8 % and 75.6 ± 0.6 % for 1.33:1 and 1.5:1 Gaa:KC molar ratio respectively). Similarly, varying the pluronic® F-68 final concentration for a given 1.5:1 Gaa:KC molar ratio and 2/25 mM hydrogel concentration did not significantly modulate the pore sizes and windows of interconnection. However, the lowest pluronic® F-68 concentration (1.7 %) was related to a significant decrease in porosity (62.9 ± 7.6 %) compared with higher concentrations (75.6 ± 0.6 % and 71.4 ± 1.9 % for 3.3 % and 5 % pluronic® F-68 respectively). Moreover, this was related to a higher distribution dispersal observed with a higher occurrence of extreme values (pore size up to 1000 µm). In conclusion, for a given 2/25 mM DGL/PEG concentration, with 1.5:1 or 1.33:1 Gaa:KC molar ratio and 3.3 or 5 % pluronic® F-68, EPH were characterized by a high porosity with connected pores that form extensive channels. On the contrary, too acidic conditions (i.e. 1.75:1 Gaa:KC molar ratio) and/or low concentration of pluronic® F-68 (i.e. 1.7 %) decreased the overall percentage of porosity of resultant EPH.

The resulting porosity of injectable effervescent porous hydrogels (EPH) was characterized for various DGL/PEG hydrogel conditions with no significant differences reported regarding pore size (mean of 290 µm with pore between 50 and 100 µm being the more represented) and percentage of porosity (77 %). However, for all conditions the pore size was broad probably due to a high polydispersity of CO_2 bubbles size. Interestingly, the effervescence approach induced the formation of windows of interconnections (of 117.8 µm on average) without additional treatment. Of note, injected 2/25 mM EPH displayed a higher pore size than their manually homogenized counterparts with mean pores of 306.0 ± 5.9 µm against 213.2 ± 7.4 µm respectively for the same Gaa:KC (1.33:1) and pluronic® F-68 (3.3%) conditions.

Table 23 : Porosity characterization of injected (TOP) or manually homogenized (BOTTOM) DGL/PEG EPH.
Various parameters were studied on resultant porosity: the DGL/PEG composition (1.6/25, 2/25 or 2:37 mM DGL/PEG), the amount of pluronic® F-68 (1.7, 3.3 or 5%) and the Gaa:KC molar ratio for a given 1.1 M final concentration (1.75:1, 1.5:1 or 1.33:1).

**: Statistically different from PF-68 3.3% and 5% with Gaa:Pc 1.5:1; α : Statistically different from Gaa:Pc 1.33:1 and 1.5:1 with PF-68 3.3%. One way anova + Tukey's multiple comparison, n=3)*

Parameters studied				**Porosity characterization**		
Porogen molar ratio (Gaa:KC) with set 1.1 final molarity	pluronic® F-68 (%)	Hydrogel concentration mM DGL/PEG	Homogenization process	Pore Size (µm) -**Mean ± SEM** [Mode] - Median	% Porosity	Size of windows of interconnection (µm) -**Mean ± SEM** [Mode] - Median
1.33:1	3.3%	1.6/25	Injection	**280.1 ± 54.9** [50-100] -203	75.0 ± 2.3	**100.7 ± 14.9** [10-20] - 38
		2/25		**307.2 ± 36.5** [50-100] -243	76.8 ± 1.4	**130.4 ± 21.2** [20-30] – 44
		2/37		**313.0 ± 32.3** [50-100] -272	79.7 ± 1.9	**131.4 ± 12.9** [20-30] - 93
1.5:1	1.7%	2/25	Manual	**201.8 ± 52.9** [50-100] - 86	62.1 ± 6.0*	**99.6 ± 36.2** [20-30] – 53
	3.3%			**209.6 ± 10.0** [0-50] -116	75.6 ± 0.6	Not reported
	5%			**264.9 ± 74.7** [50-100] -126	71.4 ± 1.9	**128.9 ± 51.5** [20-30] – 49
1.75:1	3.3%			**190.2 ± 33.1** [50-100] -156	62.9 ± 7.6 α	**103.6 ± 10.1** [20-50] – 76
1.5:1				**209.6 ± 10.0** [0-50] -116	75.6 ± 0.6	Not reported
1.33:1				**208.2 ± 25.3** [50-100] -136	74.4 ± 3.8	**122.3 ± 14.9** [20-30] – 74

Due to the porosity inducement and the creation of voids inside the material, EPH mechanical properties were logically significantly dropped compared to dense hydrogels of the same condition (Figure 40D). Moreover, by varying the Gaa:KC molar ratio of EPH of the same DGL/PEG initial concentration, it was possible to vary their compressive mechanical behaviour (Figure 40E). Hence, it indicated that the stiffness modulation of the whole porous construct remains possible through two various pathways (i.e. DGL/PEG concentration and Gaa:KC molar ratio variation), which makes it very attractive to further meet the requirements of various tissues. Additionally, except for the condition 1.6/25 mM DGL/PEG and 1.75:1 Gaa:KC molar ratio, a viscous modulus could be measured that varied with EPH conditions confirming the conservation of a self-standing material (Figure 40F). However, the condition 1.6/25 mM DGL/PEG and 1.75:1 Gaa:KC molar ratio was mechanically too weak to withstand the induction of the porosity. Due to the too acidic condition, the resultant 1.6/25 mM DGL/PEG EPH were not strong enough to be handled and measured in compression.

The establishment of a porosity inside DGL/PEG hydrogels compatible with their injection was thus validated and characterized. In order to assess the use of these new formulations for direct *in vivo* injection, they were used unwashed in direct contact with cells to evaluate their cytotoxicity and the cytocompatibility of the resultant porosity. Additionally, the *in situ* injectability of the new formulations was evaluated subcutaneously in mice to (1) validate the formation of the porosity directly *in vivo* and (2) study the biocompatibility of resultant formulations

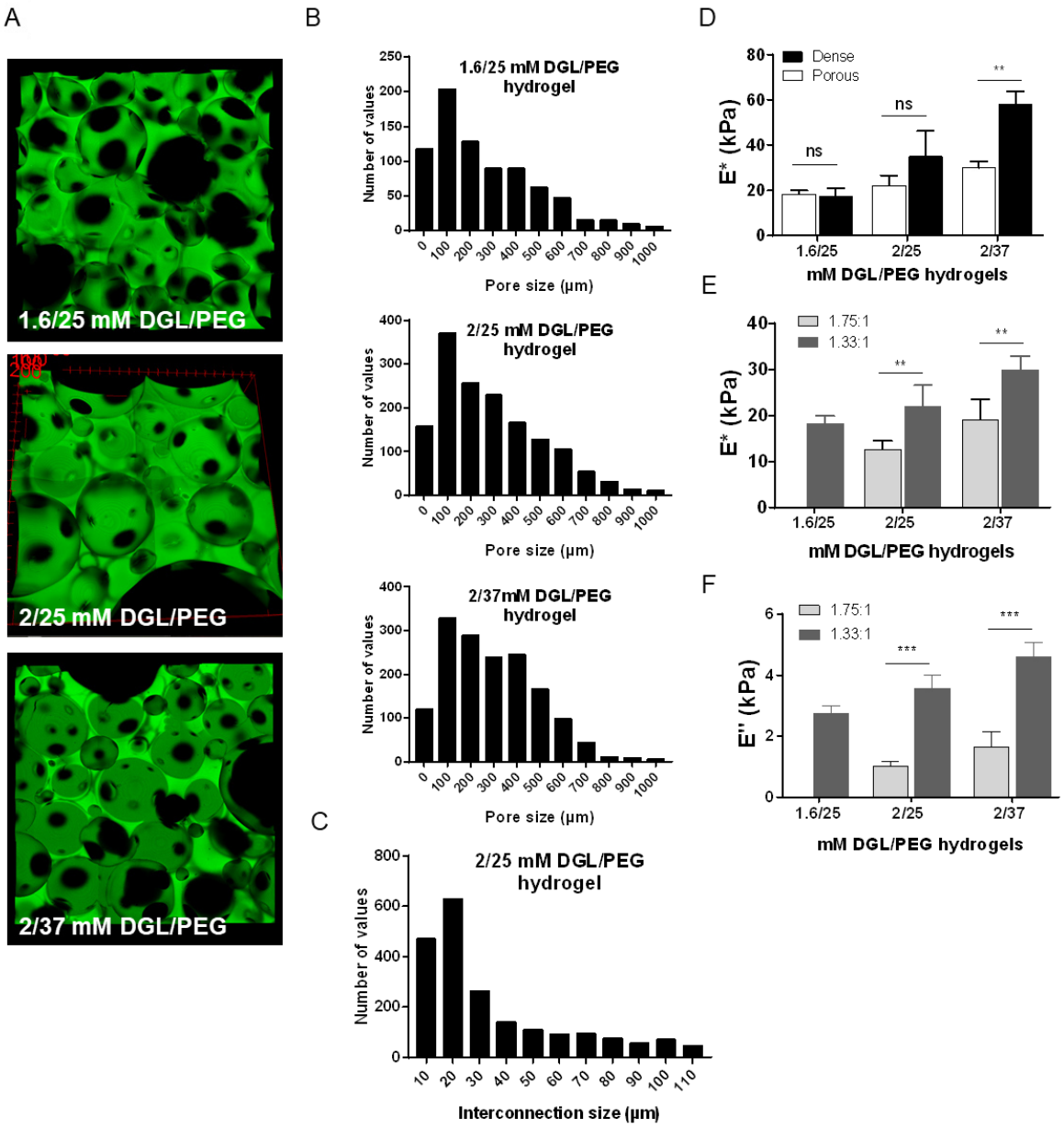

Figure 40 : Porosity characterization of various effervescent porous hydrogel (EPH) conditions
Representative picture of (A) 1.6/25, 2/25 mM and 2/37 mM FITC-DGL/PEG EPH. (B) Pore size of various FITC-DGL/PEG EPH compositions and (C) windows of interconnection size of 2/25 mM DGL/PEG EPH.
D) Complex modulus (E) in compression of dense and porous DGL/PEG hydrogels formulated with 1.33:1 Gaa:KC molar ratios and pluronic® F-68 at 3.3%. E) Complex modulus (E*) and F) Loss modulus (E") of various porous DGL/PEG hydrogels formulated with 1.33:1 or 1.75:1 Gaa:KC molar ratio*
*Unless stated otherwise, EPH were formulated with 1.33:1 Gaa:KC and 3.3% pluronic® F-68 and made **by injection**. n=3 – t-test d) dense vs porous e), f) porous EPH formulated with 1.33:1 vs 1.75:1 Gaa:KC molar ratio *:p<0.05; **:p<0.01; ***: p<0.0001*

2.3 Study of innovative formulations compatibility with cells and tissues for *in situ* injectable purposes

Cytotoxicity and cytocompatibility studies were performed using fibroblasts, as it is the cell type described and recommended in the ISO 10993 standard, part 5. The biocompatibility was also conducted following ISO 10993 standard, part 6 regarding tests for local effect after implantation to provide some preliminary data on this new formulation biocompatibility.

2.3.1 *In vitro* EPH cytotoxicity

The effect of the effervescence on the hydrogel was further investigated in regard to cell toxicity. To do so, normal human dermal fibroblasts (NHDF) were used directly in contact with porous hydrogels or in contact with 24 hours extracts of dense hydrogels. All the dense and porous hydrogels evaluated for the cytotoxicity and cytocompatibility study were tested directly after formulation without any washing or post formulation treatment, to be close to the final application of *in situ* injection.

The metabolic activity of NHDF in contact for 48 hours with dense hydrogel extracts was first measured. Compared with a control 2/25 mM DGL/PEG hydrogel prepared in PBS, a cellular metabolic activity decrease was observed for cells in contact with extracts from hydrogels formulated with Gaa:KC, while the addition of pluronic® F-68 did not have any effect (Figure 41A and C). Indicating that the decrease may be related to the acid/base reaction, Gaa:KC at 1.33:1 added directly at the same concentration onto NHDF induced a significant decrease of cell metabolic activity. Similarly Gaa:KC at 1.75:1 induced a slight decrease of cellular metabolic activity, however non-significant (Figure 41B).

Cellular viability was further studied by direct contact with various DGL/PEG EPH generated with Gaa:KC at 1.33:1 molar ratio and pluronic® F-68 at 3.3 %. Cellular adhesion to the EPH was assessed after six hours and confirmed after 48 hours on 2/25 mM DGL/PEG EPH through clear cellular spreading (Figure 41D). As a striking result, NHDF were 72.0 ± 4.3 %, 88.3 ± 3.2 % and 85.3 ± 2.3 % viable after 24 hours on 1.6/25, 2/25, and 2/37 mM DGL/PEG EPH, respectively (Figure 41E). Cell viability on unwashed EPH was not different from their extensively washed counterparts used as positive controls, confirming the non-cytotoxicity of the novel formulations. These results therefore demonstrate the potential of unwashed EPH to support NHDF adhesion, viability and spreading, consolidating their use with other cell types.

In line with previous results with fibroblasts [373] or with C2C12 (chapter 1), it was also observed that by varying the DGL/PEG composition of EPH, cells behaviour in terms of early adhesion and cell spreading could be varied (Figure 41F). Soft conditions (i.e. 1.6/25 mM DGL/PEG) results in less spread cells than stiffer ones (i.e. 2/25 and 237 mM DGL/PEG). The effect of DGL/PEG mechanical and biochemical versatility on cells was thus preserved in the EPH settings.

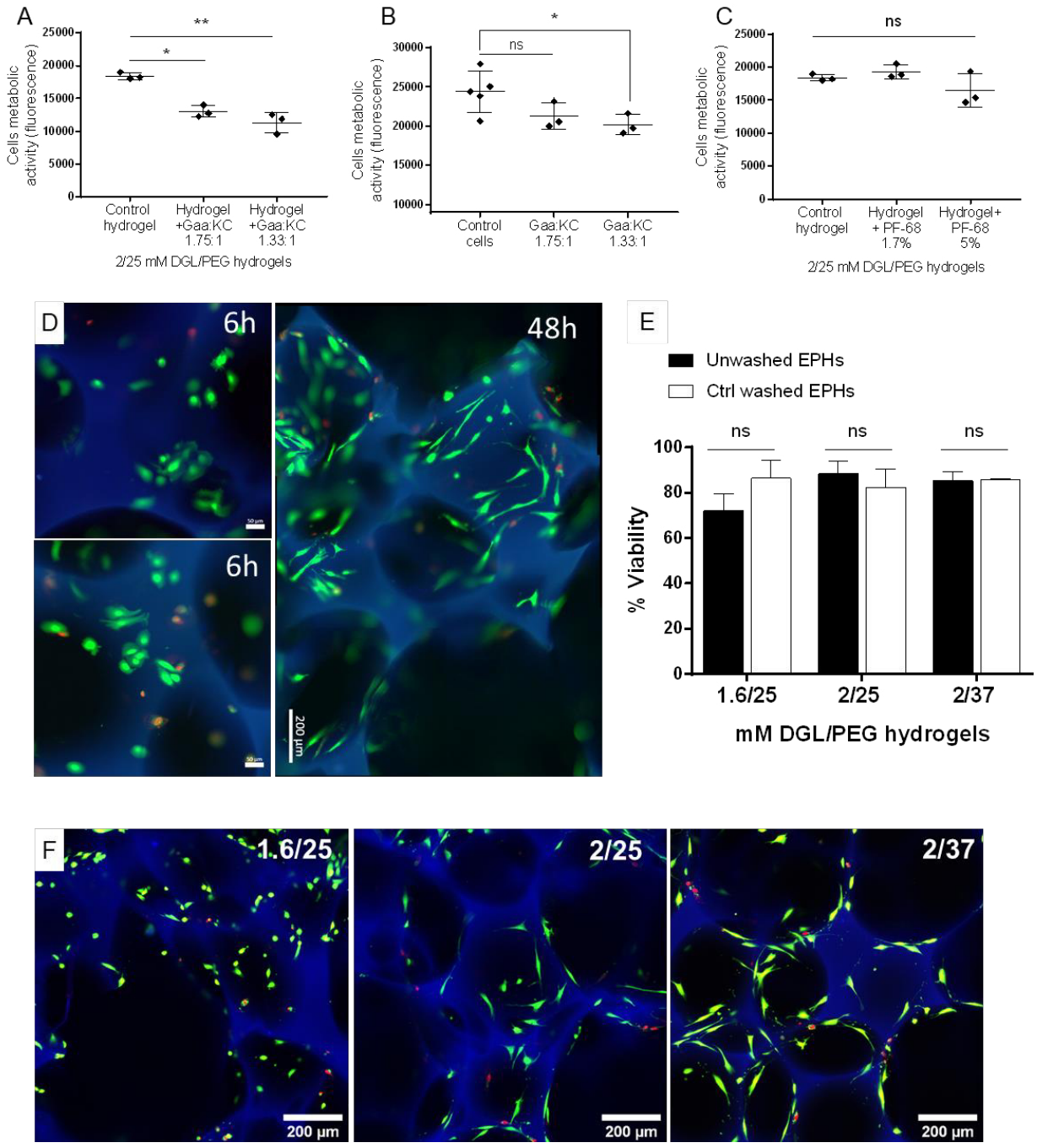

Figure 41: In vitro EPH suitability for direct in situ *injection purposes – Study of cytotoxicity*
Use of dense hydrogels or EPH right after formulations without any washing or post formulation treatments
*NHDF metabolic activity after 48 hours in contact with (A) 24h-extract of dense 2/25 mM DGL/PEG hydrogels formulated with various Gaa:KC molar ratios at 1.1 M, (B) with only Gaa and KC at 1.1 M and various molar ratios or (C) with 24h-extract of dense 2/25 mM DGL/PEG hydrogels formulated with various pluronic® F-68 concentrations. A/B/C : One way ANOVA + Dunnett's VS control hydrogel (formulated in PBS) or control cells (no treatment) *:p<0.05; **p<0.0. (D) Live/Dead assay in direct contact with EPH, 6 and 48 hours post seeding (live cells represented in green and dead cells in red, hydrogel in blue). (E) Quantification of live cells on the total number of cells after 24 hours on 1.6/25, 2/25 and 2/37 mM DGL/PEG EPH right after formulation without any washing or post-formulation treatment against cells on washed EPH of the same conditions. t-test (washed VS unwashed conditions). (F) Live/dead assay on EPH of various compositions showing various cell spreading 24 hours post seeding.*

2.3.2 *In vitro* EPH cytocompatibility

After 24 hours, NHDF cells cultured in 2 mm-thick EPH were homogeneously distributed throughout its thickness, confirming their very rapid entry inside the structure, due to the extensive interconnection between pores (Figure 42A). After 21 days, cells covered the major part of the available surface, attesting their ability to proliferate inside the EPH (Figure 42B). Moreover, the EPH sustained the *in vitro* deposition of extracellular matrix (ECM) proteins such as fibronectin and collagen, enabling cells to fill the pores (Figure 42C). Hence, the porous structure created by effervescence holds promise for cells culture, which strengthen the possibility to use the EPH for direct *in situ* delivery, without inducing adverse effects on cells while supporting their proliferation and ECM production.

Owing to the maintenance of cell viability and adequate cytocompatibility, in the rest of this work, EPH were formulated with a **1.33:1 Gaa:KC molar ratio and a 3.3% pluronic® F-68** concentration, to ensure a high percentage of porosity while maintaining relatively high stiffness.

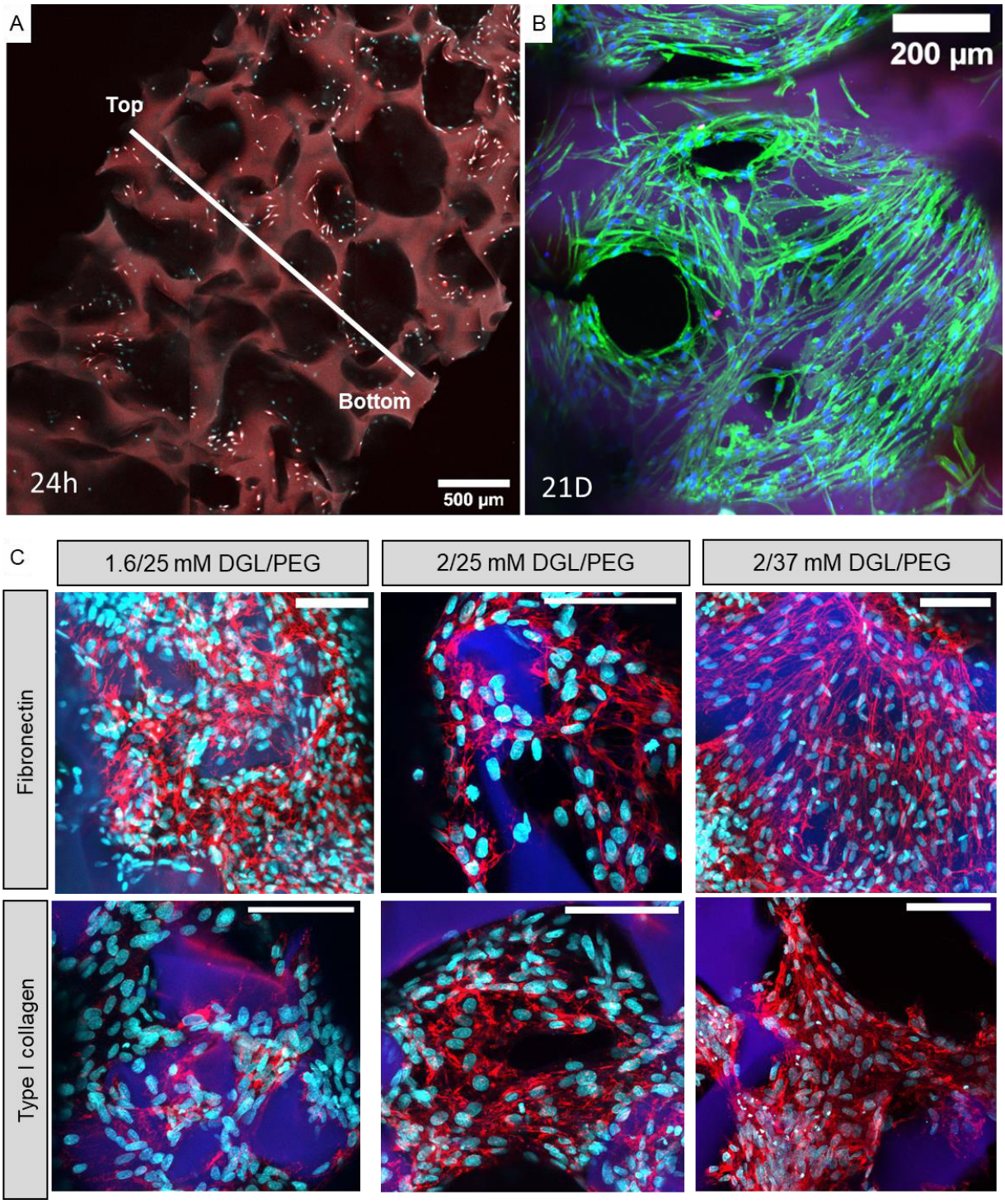

Figure 42 : In vitro EPH suitability for direct in situ *injection purposes. Study of cytocompatibility*
Use of dense hydrogels or EPH right after formulations without any washing or post formulation treatments
(A) Cellular distribution throughout EPH 24 hours post seeding by DAPI/Phalloidin staining (cell nuclei in cyan and cytoskeleton in red, hydrogel in pink), (B) Cellular morphology and pore filling after 21 days in culture inside EPH (cell nuclei in blue, cytoskeleton in green, hydrogel in purple).
(C) ECM deposition by cells 21 days post seeding in various EPH compositions (cell nuclei in cyan, fibronectin and type I collagen deposition in red, hydrogel in blue).
EPH formulated with 1.33:1 Gaa:KC molar ratio and 3.3% pluronic® F-68 Scale bar: 100 µm

2.3.3 *In situ* EPH injectability assessment

After *in vitro* cellular experiments, the behaviour of DGL/PEG hydrogels of different compositions was further evaluated *in vivo* by subcutaneous injection. The objectives were first (1) to assess the possibility to form porosity through injections performed directly *in vivo* along with comparing the porosity with effervescent porous hydrogels (EPH) formulated in tubes and then (2) evaluate the good *in vivo* tolerability and biocompatibility of innovative formulations.

DGL/PEG EPH were successfully injected in subcutaneous pockets located on mice back (Figure 43A). Immediately after initiating the injection, an important volume expansion was visible due to the effervescent reaction and CO_2 bubble formation (Annex 1, supplementary movie 8). After injection, the static mixer was immediately removed and the incision blocked to prevent liquid leakage. In less than a minute, hydrogel crosslinking was sufficient to leave a porous implant in place. During the 3 weeks implantation, no evidence of sepsis, infection, or pain was detected on the animals.

Upon excision of the injected implants, EPH were visibly of darker and more reddish colouration than their dense counterparts (Figure 43A). Samples were stained with Masson's trichrome for cell and collagen deposit observation (Figure 43B and C). After explantations, all injected EPH exhibited a porosity that confirmed the technical *in vivo* injectability of the formulation. The compatibility of the resultant effervescent porous structure to sustain cellular infiltration and tissue formation was indicated by the presence of cells (nuclei in purple and cytoplasm in light purple) and neo-tissues within the hydrogels (collagen deposits in green). Cells with elongated nuclei and light cytoplasm, presumably fibroblasts, were visible within the hydrogel in close contact with collagen. This cellular infiltration and collagen deposition were promoted despite the formation of a fibrous capsule (highlighted with the black dotted line) surrounding the hydrogel. These results clearly indicate that the hydrogel was well integrated by tissues and was not isolated by the fibrous capsule. On the contrary, dense hydrogels did not exhibit any porosity while showing dense structures around the void path created by the mixing nozzle (Figure 43C). Similarly to EPH, dense hydrogels were surrounded by a fibrous capsule made of fibroblasts and collagen deposition. However, contrary to their porous counterparts, dense hydrogels were not infiltrated by cells, showing no tissue deposition apart from the fibrous capsule. Dense hydrogels exhibited a too tight network to allow cells to enter the structure, confining them to hydrogel rims.

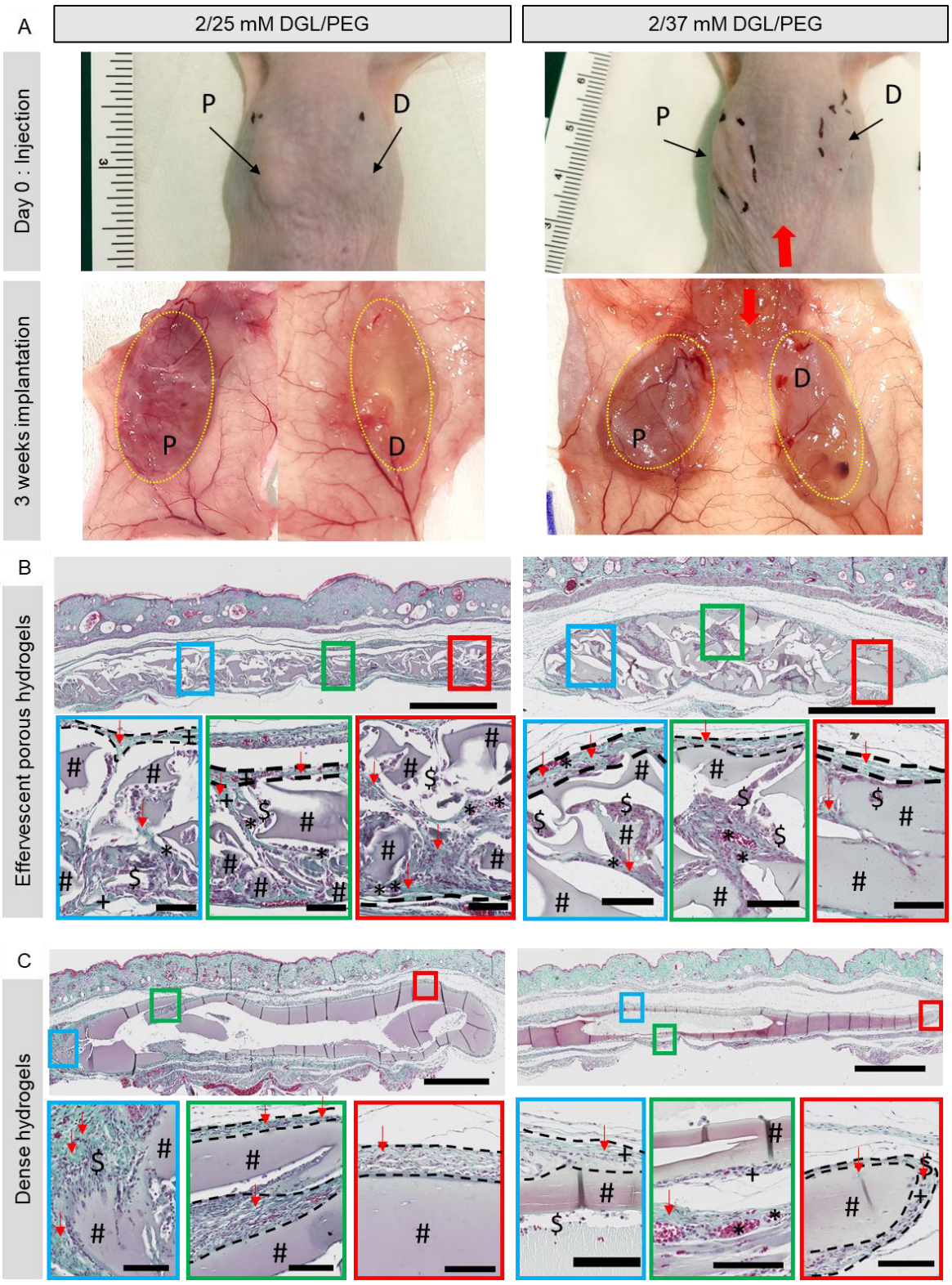

Figure 43 : Injection of hydrogels in sub-cutaneous pockets in mice
A) Representative pictures of dense and porous hydrogels right after injection and 3 weeks post implantation. Red arrow: injection path. Yellow dotted line: hydrogels. P: porous and D: dense. A red coloration is observed for porous hydrogels.
-Masson's trichrome staining of the full explants after 3 weeks implantation of B) EPH formulated with 1.33:1 Gaa:KC molar ratio, 3.3 % pluronic® F-68 and directly injected in sub-cutaneous pockets and C) Dense DGL/PEG hydrogels directly injected inside sub-cutaneous pockets. Close-ups are highlighting hydrogel (#), the fibrous capsule (black dotted line), synthetized collagen (red arrow), fibroblasts (+) and blood vessels (*). Figure expanded (supplementary information 4 and 5 in Annex)

Interestingly, for all EPH conditions, dense areas were observed at the interface with subcutaneous tissues (Figure 44A). The implants were not completely porous and the quantification of dense parts, comparatively to porous ones, indicated an important inhomogeneity related to the hydrogel concentration with 46.7 ± 4.2 and 68.8 ± 8.5 % porosity inside injected 2/25 and 2/37 mM DGL/PEG respectively. As for dense hydrogel controls, these dense structures were related to lower cellular and tissue infiltration, due to a lack of porosity enabling cellular entry.

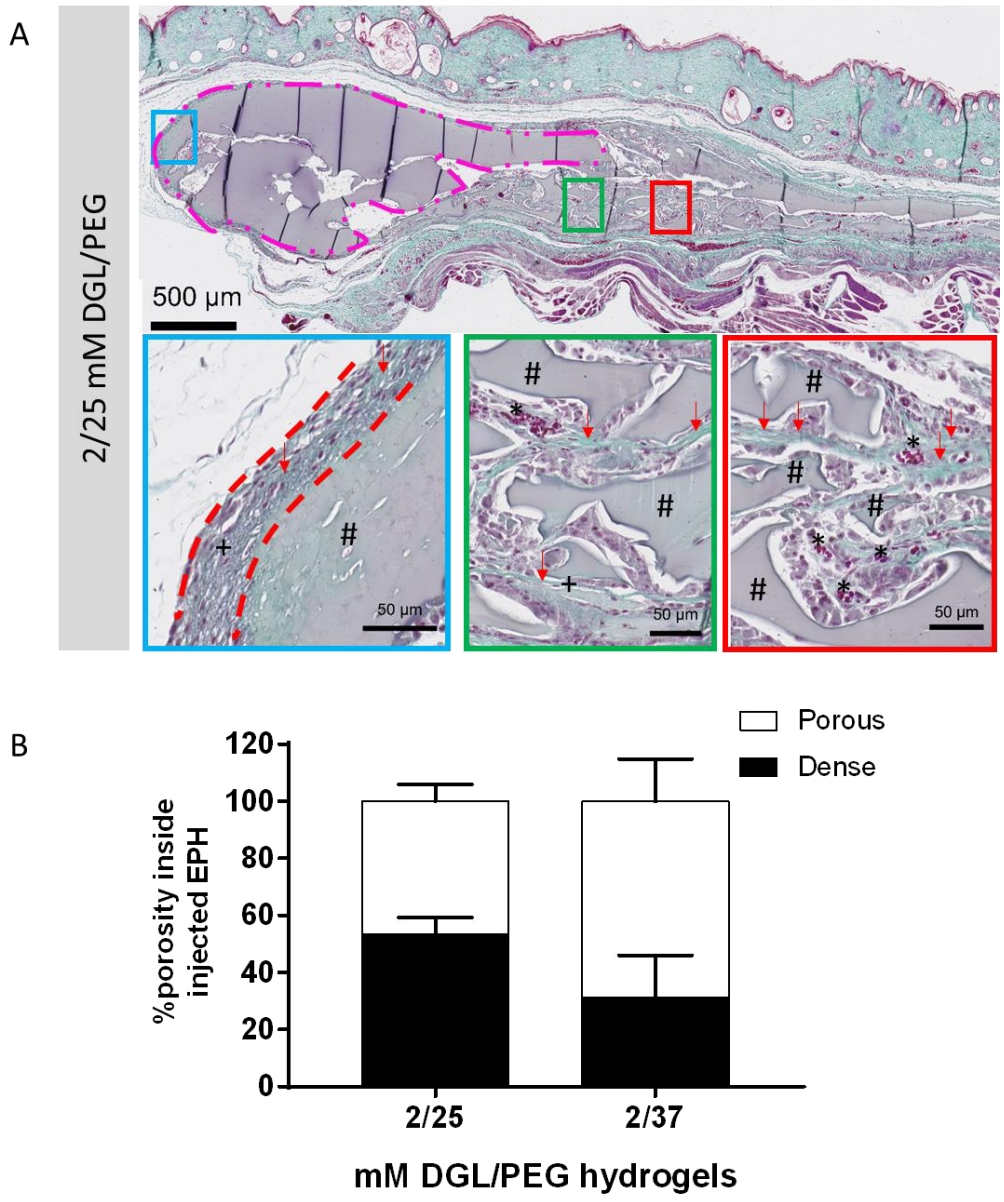

Figure 44 : Injection of EPH in sub-cutaneous pockets in mice
A) Instance of a dense structure formation during injection (pink dotted line) for a 2/25 M DGL/PEG hydrogel
Masson's trichrome staining of the full explants after 3 weeks implantation and close-ups highlighting hydrogel (#), the fibrous capsule (red dotted line), synthetized collagen (red arrow), fibroblasts (+) and blood vessels (*)
B) Quantification of dense over porous structure on the complete hydrogel area.
EPH formulated with 1.33:1 Gaa:KC molar ratio, 3.3 % pluronic® F-68 and directly injected in sub-cutaneous pockets

However, in the porous parts of injected EPH, a very extensive vascularization was observed within the entire hydrogel thickness contrarily to dense hydrogels controls. These results were confirmed by specific staining for type IV collagen presence, with structures resembling vessels observed in many pores (Figure 45). These results confirm that the porosity is well interconnected and sufficiently large to sustain vascular infiltration. However, when dense structures were observed, it was related to a decreased vascularization supposedly due to the lack of porosity. Similarly, no vascularization was visible inside dense control hydrogels. This observation further confirms the requirement of an adequate porosity to enhance neovascularization of hydrogels.

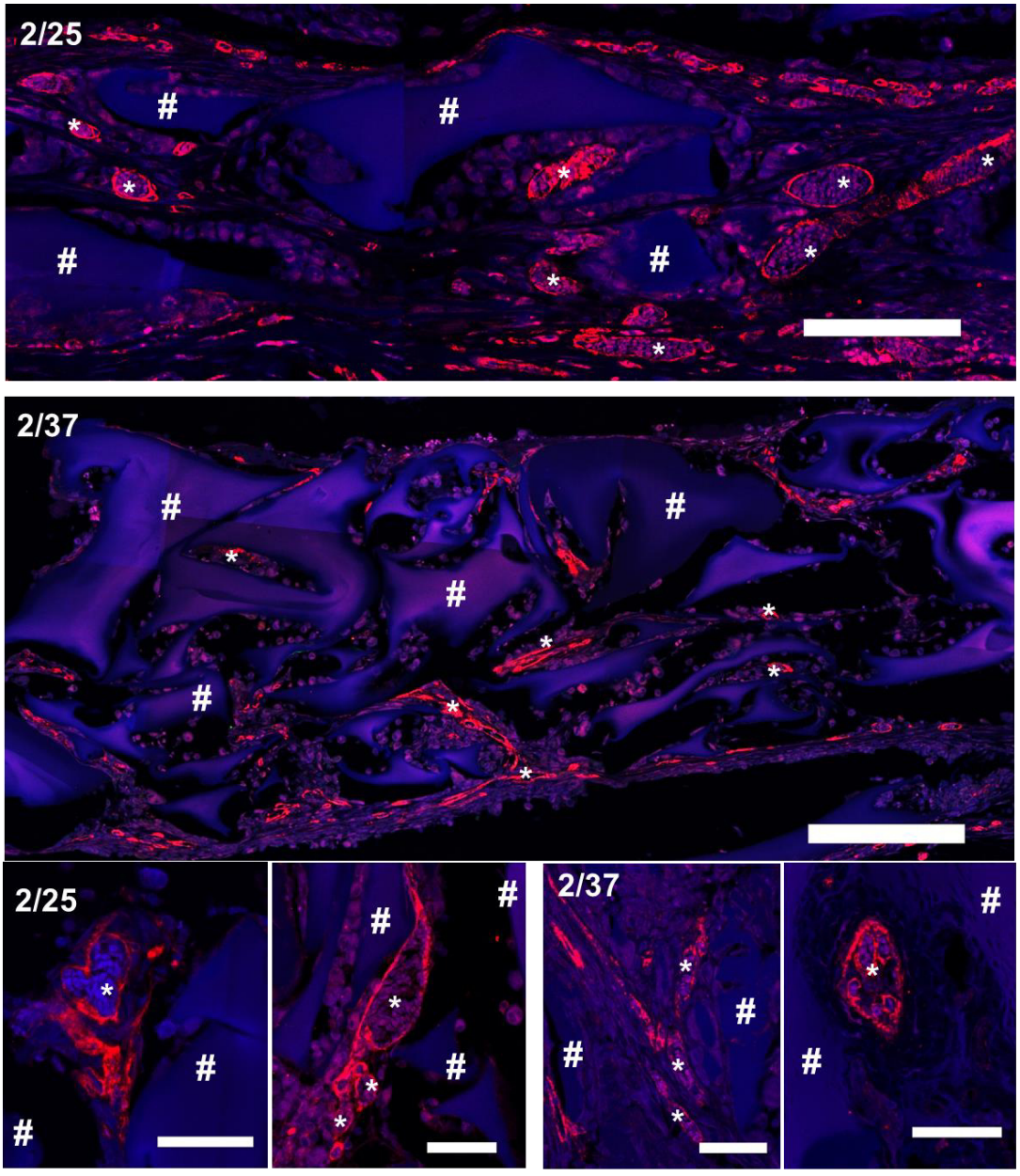

Figure 45 : Blood vessel penetration in injected EPH of various conditions
Type IV collagen staining (in red) of the explants after 3 weeks implantation highlighting hydrogel (in blue) and blood vessels (in red). An extensive vascularization of the porous structure was observed for all conditions
Scale bar whole explant 500 µm, scale bar close up: 50 µm

For all hydrogels conditions (dense and porous), after three weeks of implantation, evidence of hydrogels degradation were noticeable. Cells present inside the fibrous capsule, visible at the rims of dense hydrogels were distinctly degrading the structure and slowly entering it. This phenomenon was particularly exemplified in Figure 43C, blue close ups. Particularly, an erosion of inter-porous dense walls of EPH was observed. Macrophages and resultant giant cells could be responsible for this digestion by phagocytosis. A specific staining for macrophages confirmed their slight presence inside the injected EPH, especially concentrated on hydrogels rims (Figure 46). However, the low density of inflammatory cells (granulocytes and lymphocytes) or macrophages inside injected EPH tends to indicate that all injected conditions exhibited a mild foreign body reaction with minimal sign of inflammation. These results suggest an adequate tolerability of the EPH by surrounding tissues with no evidence of subcutaneous gas accumulation.

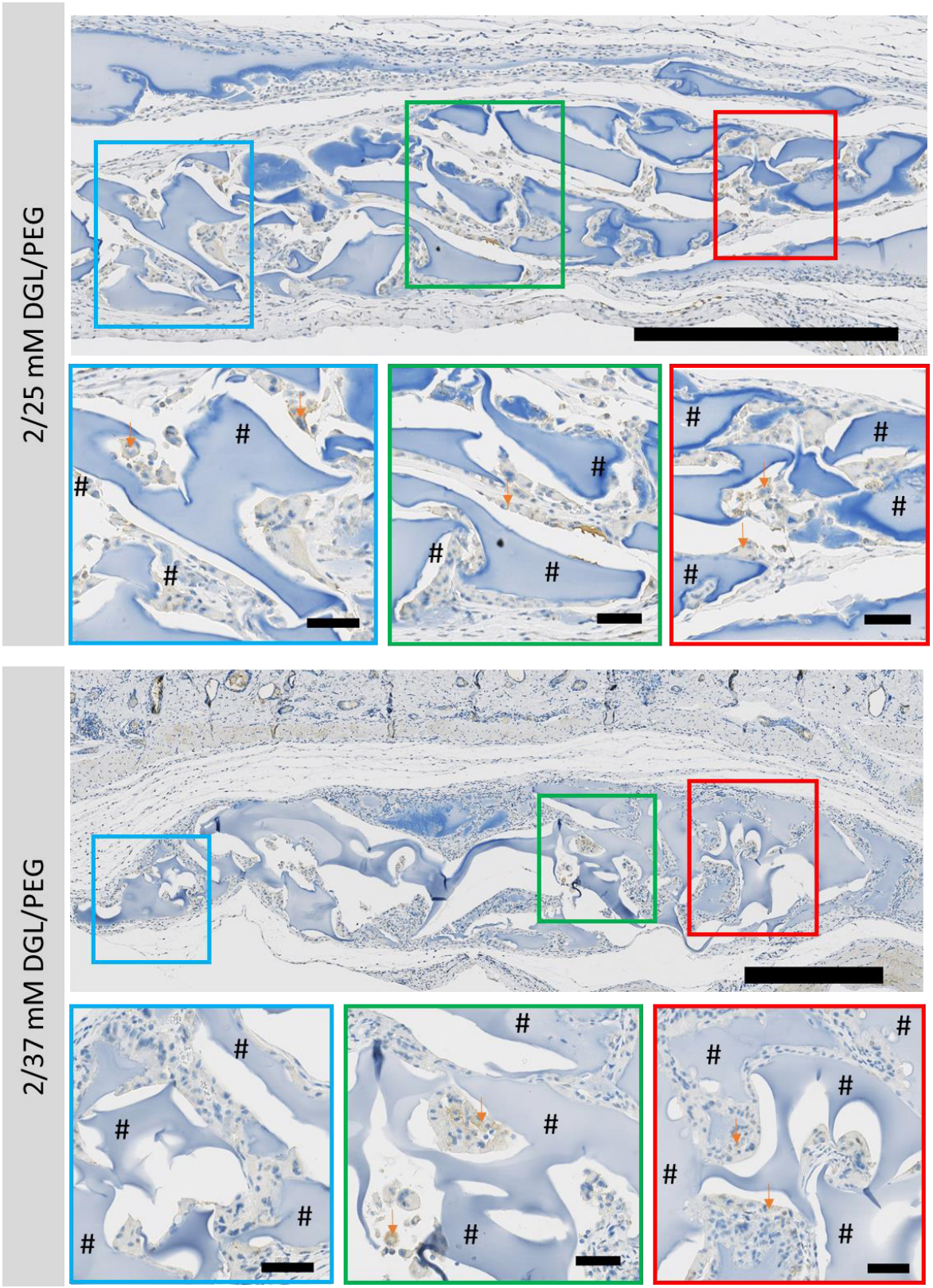

Figure 46 : Macrophages presence in injected EPH of various conditions
F4/80 staining of the explants after 3 weeks implantation (macrophages membrane in brown) and close-ups highlighting hydrogel (#) and macrophage presence (orange arrows). The slight macrophage presence observed indicates a mild inflammation. Scale bar whole explant 500 µm, scale bar close up: 50 µm

In parallel to *in situ* injected formulation, DGL/PEG hydrogels were injected inside a tube to be removed, cut, and subsequently implanted in the subcutaneous pockets without any washing or post formulation treatment. These implanted hydrogels were performed to assess the good tolerability of EPH and to compare the porosity induced though direct *in vivo* injection against injection in tube.

As previously observed for porosity characterization and *in vitro* studies, and contrary to *in vivo* injected EPH, no dense structure were observed on implanted EPH.

In comparison to their injected counterparts, implanted EPH were ticker (about 1 mm thick) and showed less conformation to the subcutaneous pockets. Injected EPH showed a porous structure that was flatter compared with implanted EPH porosity (Figure 47). As a corollary, a higher vascularization was visually observed inside implanted hydrogels compared with *in situ* injected EPH (Figure 47B). These observations could be linked to the porosity flattening or to the presence of aforementioned dense structures characterizing injected EPH that can prevent the porosity from being infiltrated by vessels. Curiously, the number of macrophages observed appeared higher inside implanted EPH in comparison with their injected counterparts, with an increased fusion of macrophages to multinucleated foreign body giant cells (Figure 47C, green arrows).

Altogether, these results provide a proof-of-principle that the DGL/PEG effervescent porous hydrogel can be injected *in-situ* while enabling the formation of a suitable porosity that sustained cellular infiltration, mature vascularization, and tissue ingrowth. The formulation further showed a good tolerability *in vivo,* which validates its potential for tissue regeneration. However, the direct injection of the formulation *in vivo* was related to variability in the porosity generated and the tolerability toward tissues compared with hydrogel injected inside tubes to be then implanted.

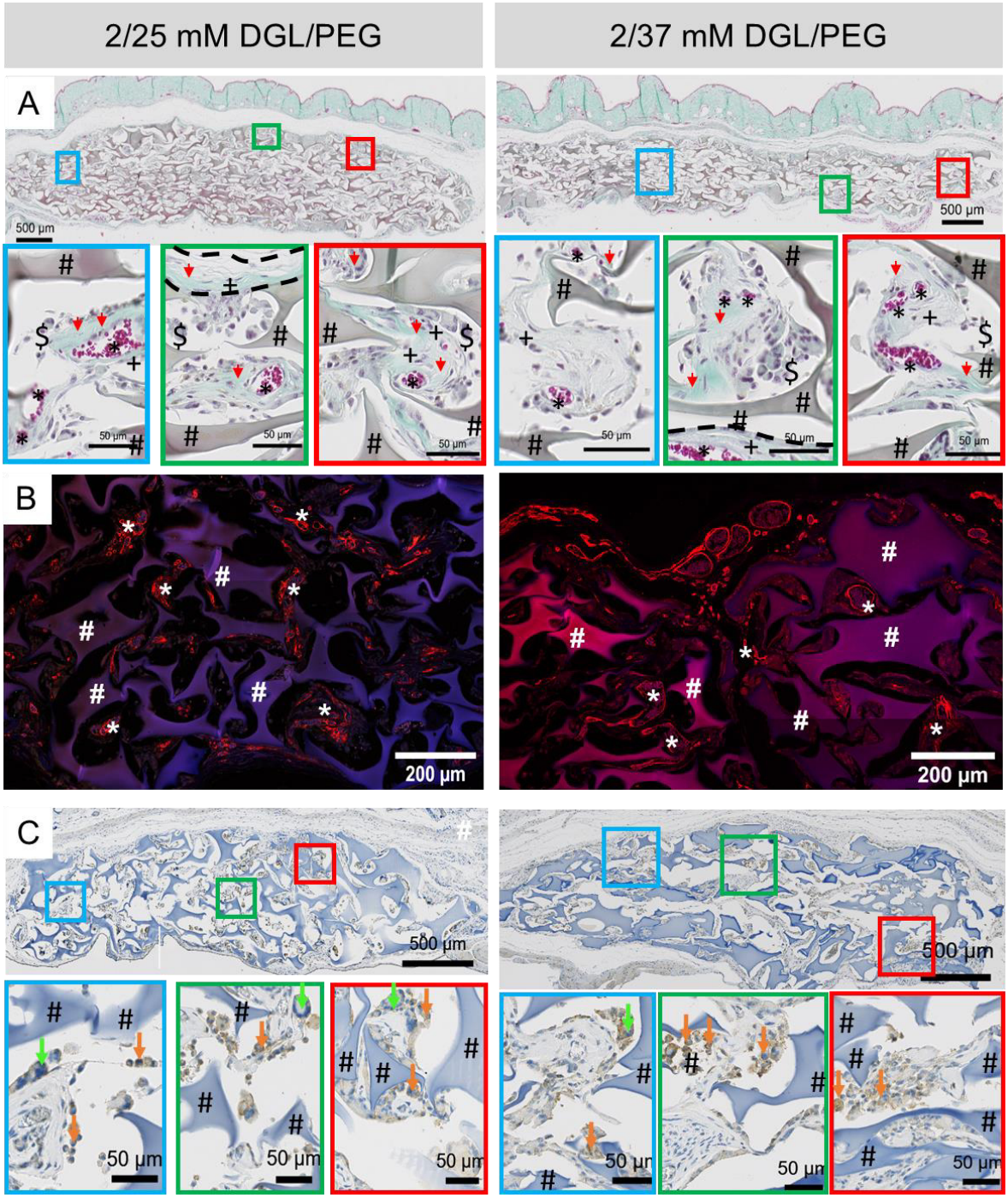

Figure 47 : Sub-cutaneous implantation in mice of EPH of various compositions
Representative pictures of porous hydrogels after 3 weeks implantation.
A) Masson's trichrome staining of the full explants after 3 weeks implantation and close-ups highlighting hydrogel (#), the fibrous capsule (black dotted line), macrophages ($), synthetized collagen (red arrow), fibroblasts (+) and blood vessels (*)
B) Blood vessel penetration inside implanted EPH of various conditions. Type IV collagen staining (in red) of the explants after 3 weeks implantation highlighting hydrogel (in blue) and blood vessels (in red).
C) Macrophages presence in implanted EPH of various conditions. F4/80 staining of the explants after 3 weeks implantation (macrophages membrane in brown) and close-ups highlighting hydrogel (#) and macrophage presence (orange arrows). Giant cells were also visible (green arrows).
EPH formulated with 1.33:1 Gaa:KC molar ratio, 3.3 % pluronic® F-68 and injected in a conic tube before cutting and implantation in sub-cutaneous pockets. Figure expanded (supplementary information 6,7 and 8 in Annex)

2.4 Discussion

In this chapter, the possibility to create a porosity inside the DGL/PEG hydrogel was investigated whilst maintaining its direct *in vivo* injectable potential.

A first focus was made on the solvent used for PEG-NHS solubilisation. NHS esters groups hydrolyse in aqueous solution within minutes or hours depending on water content, temperature, and pH of solutions. Even if NHS ester group hydrolysis is very slow compared with their rate of reactions with amines, their storage remains difficult and reactions reproducibility is questioned [407]. The use of powders solubilized extemporaneously in aqueous solutions was precluded due to their high hygroscopic behaviour. This ability to attract and hold water molecules from the surrounding environment, ultimately leads to a loss of functionality of the powders. This feature render the solubilisation of PEG–NHS in aqueous solutions logistically complicated. Therefore, to strike a balance between NHS stability while maintaining a good reproducibility of the results, the PEG-NHS powders were solubilized in dry DMF. Nevertheless, the presence of DMF restricts the use of the DGL/PEG hydrogel in direct contact with cells and/or tissues. The DMSO was thus studied as an alternative to replace the DMF. In the chapter, the use of DMSO was related to a good reproducibility while preserving the same effects on skeletal muscle cells. Therefore, in the rest of this work, DGL/PEG hydrogels were formulated with the PEG solubilized in DMSO.

To create porosity inside the DGL/PEG hydrogel, various approaches were evaluated. Previously described techniques such as particle leaching [319] or air bubble entrapment with stabilized emulsions [346] were explored with respect to their possible compatibility with the DGL/PEG hydrogel.

2.4.1 Particle leaching

Gelatine microbeads (GMB) were efficiently produced and entrapped inside the DGL/PEG hydrogel, showing compatibility with the formation of the crosslinked network. In this work, bead size was not quantified, however, the successful modulation of bead size through emulsion parameters (i.e. viscosity or agitation speed) has been extensively described in literature with gelatine and other particles [260]. Their modulation should thus be feasible in our conditions but would require additional optimization. However, the main drawback was the lack of contact between GMB preventing the good gelatine leaching through the hydrogel network. Without leaching, the porous structure could not be formed, with no possible cellular infiltration and/or migration. Resulting hydrogels were thus not transposable to *in vitro* or *in vivo* studies. A way to form interconnected porosity inside hydrogel would be to compact GMB by centrifugation and then pour the hydrogel precursors into this template of compacted microbeads [378]. By applying a centrifugal force, liquid precursors enter the structure while maintaining contact between microbeads, allowing their leaching through the path they created. However, centrifugation steps are not transposable to *in situ* injection purposes.

Moreover, the use of polymers of gelatine still raises safety issues for direct injection in humans. There is some concern due to their animal origin and possible disease transmission. This is a reason why some studies have focused their attention on thermosensitive hydrogels made of non-animal sources of polymers [321]. However, very few instances have been able to demonstrate *in situ* injectability of these new formulations while creating an interconnected porosity. Considering the difficulty to compact microparticles to form the porosity and the safety issues the use of sacrificial particles can present, the use of particle leaching using gelatine was discarded. Instead, the formation of the porosity though air bubble generation was evaluated. Stabilized air bubble emulsion methods to create a porosity inside biomaterials have the advantages to be cell-friendly and easily generated without the use of harsh solvents.

2.4.2 Gas entrapment – gas foaming methods

Air bubbles have previously been studied because they always appear during the mixing of powders and liquid phase. In this work, the generation of air bubbles during the mixing of dry GMB powders with liquid hydrogels precursors was experienced. Some studies have exploited this feature to generate porosity in cement for bone tissue regeneration [343]. Surfactants are generally added in scaffold precursors to stabilize emulsions and prevent bubbles to break [354]. Surfactants are molecules able to lower the surface tension between bubbles and their immediate environment. They are the major component of soaps and detergents. They contain both hydrophilic and hydrophobic parts triggering their displacement at air/water interfaces. Therefore, the surfactant molecule ensures a uniform dispersion of air bubbles by encircling them. In this work, the pluronic® F-68 was studied, as it is a non-ionic surfactant, known to be non-cytotoxic, cytocompatible, and safe for *in vivo* applications. Its addition to solutions enabled to stabilize air bubbles generated during the movement of syringes and thus allowed the DGL/PEG hydrogel to crosslink around bubbles in a way compatible with the precursors' homogenization and the subsequent injection. Moreover, various DGL/PEG hydrogel concentrations could be generated around air bubbles.
However, the major drawback of the method was the clear lack of interconnections between entrapped bubbles, resultant of a too low air bubble density. Nevertheless, the use of air enabled the formation of pores compatible with hydrogels precursors injection while avoiding the use of questionable solvents or molecules.

Owing to the ability of gas to be entrapped inside hydrogel network, their use was further investigated through a method generating high gas bubble densities, to potentially lead to interconnections.

2.4.3 Porous and injectable DGL/PEG hydrogels using an effervescent approach

The choice of effervescence has been fuelled by the extensive knowledge of acid-base reactions generating CO_2 bubbles. Their inert and non-toxic nature, lack of organic solvents [260][351] and preservation of the biochemical integrity of proteins [358][359] provides a convenient tool to create porosities in a variety of materials, such as cement to create bone grafts [361][362], PLLA or PEG hydrogels for cartilage regeneration [363],[364] or elastin-like recombinamers [365] for connective tissue support. However, in all these instances, slow crystallization or crosslinking speeds impose additional steps to be able to entrap CO_2 bubbles inside the network, which are non-transposable to *in situ* delivery systems [408]. To form porosity during the injection, the effervescence should be parallel to the hydrogel crosslinking speed.

To evaluate this possibility, carboxylic acid and carbonate base pairs were explored to produce an effervescent reaction compatible with the simultaneous crosslinking of the hydrogel. Our objectives were multiple: (1) allowing a straightforward homogenization with hydrogel liquid precursors and (2) producing an explosive and long-term effervescence while (3) enabling the technical injection of the mix. Solubilized glacial acetic acid (Gaa) and potassium carbonate (KC) appeared to be the most promising candidates for the effervescence. Other acid and base combinations showed either too weak effervescences, re-precipitation of ions after the reaction, production of anticoagulant [406], or implication of produced ions in biological process *in vivo* (e.g. Ca^{2+} in skeletal muscle conscious movements [409]).

The successful entrapment of CO_2 bubbles generated by the effervescence inside DGL/PEG hydrogel network was taking advantage of its straightforward, swift, and tailorable crosslinking through DGL and PEG concentrations. This versatility was particularly explored here to match DGL/PEG hydrogel and effervescent reactions, while always conserving a viscosity threshold that would be suitable to inject the formulation. In a first step, the DGL/PEG hydrogels behaviour in pH dependent environments was studied. There are many instances of crosslinking reaction that are based on pH variation [410] or that can be significantly disturbed or boosted by pH [368], [369] but none of these instances exploited so far this feature to match an effervescent reaction for *in vivo* injectability purposes.

It was demonstrated in this work that DGL/PEG hydrogels are sensitive to pH with a significant crosslinking delay in acidic conditions. This sensitivity to pH could be explained by the NHS esters end-groups in the PEG molecule. At acidic pH, NHS ester is less likely to undergo hydrolysis but is also less reactive. Conversely, at alkaline pH, the NHS ester group is more reactive but less stable [411]. NHS esters have indeed a half-life of 4-5 hours at pH 7 that drops to 1 hour at pH 8 and 10 minutes at pH 8.6 [412]. In addition, the effect of pH could also be related to the α-amine (pKa 9.16) and ε-amine (pKa 10) present at the surface of the DGL,

which are not available equally when they are at acidic or alkaline pH [395]. As a result, the DGL/PEG hydrogel crosslinking is less complete in acidic conditions, as demonstrated by a significant increase of DGL release from such hydrogels, a decrease of the resulting hydrogels mechanical properties, and an increase of their swelling, suggesting a mesh size variation [413].

Overall, the possibility to control the hydrogel crosslinking through pH offers an interesting way, via the carboxylic acid and carbonate base pair, to define a suitable window to entrap the CO_2 bubbles while staying injectable. Such a window was found within a range of Gaa:KC molar ratio between 1.33:1 and 1.75:1 (pH between 5.5 and 7.5) for a given 1.1 final molarity. It was then possible to successfully induce a CO_2-based porosity inside the hydrogels, through the simultaneous and well-orchestrated dual reaction of effervescence and crosslinking. To the best of our knowledge is the first example of such an approach of interdependent and simultaneous reactions to create porosity inside a hydrogel for *in situ* injectability purposes. Owing to the highly tuneable DGL/PEG crosslinking velocity, this synchronicity was achieved by varying both DGL/PEG and Gaa:KC ratios to match reactions while maintaining a low viscosity for its injection.
Interestingly, hydrogel crosslinking modifications due to effervescent conditions were reflected by a slight decrease in metabolic activities of cells in contact with dense 24h-hydrogel-extracts. This could be correlated to the DGL release triggered by the pH-induced crosslinking impairment. It has indeed been shown previously by Lorion *et al.* that DGL displayed cytotoxicity towards human skin fibroblasts [377] above a concentration of 5 µg/mL. However, in the case of effervescent porous hydrogels (EPH), the DGL is sufficiently sequestrated inside the hydrogel network to prevent cell mortality in direct contact and sustain cell attachment, spreading, and proliferation without any washing or post formulation treatments.

The porosity by effervescence could be generated inside three various DGL/PEG compositions that were studied in this work. This versatility is of great interest to provide porous matrices of controlled mechanical properties and defined interactions with targeted cells [414],[169]. Thus, in our system, both DGL/PEG concentrations and Gaa:KC molar ratios influenced stiffness, mesh size, and crosslinking speed, making their modulation even more precise and finer to meet the requirements of targeted tissues for tissue engineering applications and tissue regeneration. However, while the acid:base ratio had a significant effect on DGL/PEG hydrogels crosslinking and cell behaviour, it was not found to be correlated with a significant modulation of the resulting porosity or pores sizes. This stability and apparent drawback opens nonetheless the possibility to modulate the time needed before injection without varying the resulting porosity.

2.4.4 Porosity characterization

The porous structure generation was mainly due to the stabilization of produced CO_2 bubbles by the use of a surfactant. It is not surprising considering that many studies have also shown a correlation between the use of a surfactant and CO_2 bubble stabilization. For instance, Keskar *et al.* used pluronic® F-127 as a foam stabilizer for CO_2 bubbles generated by citric acid and sodium bicarbonate effervescence in a PEG hydrogel [362]. Partap *et al.* have described the impact of the addition of ammonium perfluoropolyether to stabilize a supercritical carbon dioxide in water emulsion [353] and Sarda *et al.* the use of sodium dodecyl sulfate to lower surface tension for bone cement macroporosity [343].

In this work, the entrapment of stabilized CO_2 bubbles inside the DGL/PEG hydrogel led to a porous structure with an average pore size comprised between 190.2 ± 33.1 µm and 313.0 ± 32.3 µm, and can therefore be defined as macroporosity. Such a porosity, induced inside DGL/PEG hydrogels is close to what has been described for other systems using effervescence. For instance, Keskar *et al.* reported a broad distribution of pores ranging from 100 to 600 µm in PEGDA hydrogels with the citric acid and sodium bicarbonate couple [362]. Tachaboonyakiat and colleagues described macropores between 200 and 400 µm in a poly(ethylene-glycol) bisamine hydrogel using citric acid and potassium carbonate as CO_2 bubbles producers [363]. Other instances reported macropores between 200 and 300 µm [372] or between 150 and 300 µm [369].
The characterization of the porosity is of utmost importance to study the potential of hydrogels for various tissue-engineering applications. It has indeed been shown that porosity and pore size play a major role in the promotion of angiogenesis, and guide cellular fate inside the scaffold. Numerous cell types have been reported to behave differently depending on the final pore size, in terms of cellular infiltration, proliferation, migration, and differentiation [260], [261]. In addition, pore size has been demonstrated to influence vessel infiltration, with sizes between 100 and 150 µm permitting a vascularization of whole hydrogels after subfascia or subcutaneous implantations [403], [415]. Both cellular and vascular infiltration participate in tissue ingrowth and should be enhanced inside porous hydrogels.

To provide the space for tissue to grow, not only pore size but also the pathway between pores is requested. Highlighting the high interest of the porosity obtained, the pores were highly interconnected, with windows of interconnection of 100 µm on average, and mode interval population between 20 and 40 µm. Interestingly, these interconnections were observed in all pores, forming a highly open channel structure throughout the entire 20 mm constructs. The interconnection between pores could be linked to both the presence of the surfactant that stabilizes CO_2 bubbles and the effervescence power that leads to a high bubble density and reduce the aqueous interface between bubbles allowing their local fusion. Previous studies have described a correlation between pluronic® F-68 concentration and pore size [342] or between perfluoropolyether used as a surfactant and windows of interconnection size [354]

confirming the role of the surfactant on the porous structure creation. However, in our system, if the effect of pluronic® F-68 addition was possibly linked to the creation of the interconnection, it was not correlated with porosity or windows of interconnection variation, even though it led to a better bubble size homogeneity throughout the hydrogel.

Windows of interconnection between pores supported the entrance and infiltration of cells for a successful host tissue ingrowth which is especially important for implants of large size [416]. This was validated in this study by the rapid and homogenous infiltration of cells seeded on the top of 2 mm thick EPH confirming the suitability of the created effervescent porous structure. The *in vivo* spontaneous cell infiltration and vascularization observed in EPH validate such suitable porous structure and windows of interconnection, independently of hydrogels composition and way of delivery. These results are furthermore in line with porosities described for efficient vascularization and cellular infiltration. For instance, a direct correlation between interconnection size and HUVEC proliferation *in vitro* has been shown [417]. It has also been demonstrated that windows of interconnections of 150 and 200 µm resulted in an increase in blood vessel area, volume, and number inside scaffolds implanted in bone defects [417], [418] or in pockets created in paravertebral fascia lumbodorsalis [419] compared with smaller interconnections. Too small interconnections appeared to limit the blood vessels infiltration through adjacent pores, whereas bigger interconnections allowed more abundant, large, and mature capillaries.

In addition to their scale, a higher number of windows of interconnection can increase tissue invasion after 3 and 6 weeks in scaffold subcutaneously implanted in mice [420]. In this work, it was possible to maintain windows of interconnection through a direct *in situ* injectability delivery while attesting their suitability for cells and vessels infiltration. In addition, their size (100 µm in average) and number (at least one interconnection/pore) were in accordance with previous reports showing extensive vascularization. This local blood flow created by penetrating vessels and the hydrogel water content could help the diffusion and solubility of CO_2 gas in the biological tissue, preventing the formation of gas cavity.

Overall, pores obtained inside DGL/PEG hydrogel seem therefore of interest for a broad range of tissue engineering application.

2.4.5 *In situ* EPH injectability assessment

Upon *in situ* injection, the formation of porosity inside DGL/PEG hydrogel of two compositions was validated. Curiously, a part of the injected hydrogels remained dense, creating a non-porous layer in contact with tissues. While stiffer conditions (i.e. 2/25 and 2/37) were able to form a porous structure, the fraction of dense structure versus porous ones has been shown to be linked to DGL/PEG concentrations.

This was potentially due to the lower crosslinking velocity characterizing less concentrated hydrogels, unable to entrap CO_2 bubbles quickly enough to prevent their burst in contact with tissues. Therefore, the softer condition (i.e. 1.6/25 mM DGL/PEG hydrogel) could be considered not suitable for injectable purposes due to its significantly higher crosslinking time in presence of acid:base. These non-porous layers could explain the lower vascularization and cellular infiltration observed inside *in situ* injected hydrogels in comparison to their implanted counterparts. As such, this is a major optimization path for future applications.
The dense layer formation observed for all conditions could be due to either (1) a lack of CO_2 bubbles stabilization in contact with tissues through a surface tension unbalance or (2) a delayed crosslinking due to acidic physiological pH. The latter hypothesis is relevant as temporary physiological acidosis has previously been observed in acute wounds [421]. Considering that the DGL/PEG effervescent hydrogel system is highly dependent on pH, a slight variation in the injected site could have a pronounced effect on the porous structure formation. The DGL/PEG hydrogel placed in direct contact with acidic tissues could thus experience a crosslinking delay, allowing the CO_2 bubbles to escape the structure before their entrapment. Efforts could be made to strengthen the alkaline ratio of DGL/PEG hydrogel while staying in an acceptable range for injectability to boost the crosslinking velocity.

Despite the non-porous layer observed and as could be expected from previous studies [373] and the cytocompatibility study, no intense immune reactions were observed upon injection. EPH produced a mild inflammatory response with a foreign body response (fibrous capsule formation) at the hydrogel periphery which is typical of biomaterials in subcutaneous implantation [422], [423]. Interestingly, the lowest presence of macrophages was observed on injected EPH compared with implanted ones, which could be explained by a different porous architecture or by a lower stiffness. It has indeed been shown that pore size could affect macrophages polarization in polyester scaffolds [424]. This indicates that it may exist an optimal range of pore size for macrophage behaviour. On another hand, the stiffness variation has been shown to influence macrophage activation [425] and some stiffness variation could exist between implanted and *in situ* injected EPH. The direct *in situ* injection of liquid hydrogel precursors inside subcutaneous pockets could be associated with precursor dilution by organic fluids during injection, lowering the final DGL/PEG concentration and the resulting stiffness. However, no clear differences were observed between the two implanted DGL/PEG compositions (and hence mechanical properties) studied. These results support a more likely

effect of the porosity on macrophages rather than stiffness, as a visual but not quantified difference as been reported between the porous structures of *in situ* injected EPH and implanted ones. However, the presence of macrophages inside porous biomaterials is a classical reaction after implantation. They are responsible for biomaterials degradation and can enhance vascularization inside the scaffold [426] attesting a common foreign body response towards DGL/PEG EPH.

2.5 Conclusion and critical evaluation

The aim of this chapter was to provide a proof-of-concept for the development of an innovative porous and *in situ* injectable material. Here, an injectable and porous hydrogel system is reported in which the porosity does not pre-exist and is formed *in situ* by a controlled effervescent reaction, simultaneous to the injection.

This design was possible given our DGL/PEG hydrogel candidate, which presents the advantage to have a swift and tailorable crosslinking velocity (seconds to minutes). The introduction of potassium carbonate (KC) and glacial acetic acid (Gaa) as CO_2 bubble producers in the DGL/PEG hydrogels triggered an effervescent reaction while entrapping the produced bubbles in an interconnected network through the simple mixing of two solutions in a syringe. As such, it provides an innovative approach for *in situ* pore formation. In addition, the innovative DGL/PEG hydrogel offers extensively controllable mechanical properties (from 10 to 50 kPa), inherent interactions with cells through polycationic charges brought by the DGL [377] and biocompatibility. In view of the foregoing, the method described here holds significant promise for many tissue engineering applications.

However, the effervescent reaction inside DGL/PEG hydrogels was found to have a huge influence on their crosslinking chemistry, resulting in variation of their swelling and mechanical behaviour. This feature is of great interest to modulate the final stiffness of the material, however, it should be taken into consideration for further experiments as we know from chapter 1 that stiffness and DGL:PEG ratio drastically affect skeletal muscle cell behaviour.

Additionally, even though the Gaa:KC molar ratio and the surfactant concentration have an effect on hydrogel crosslinking velocity and CO_2 bubbles stabilization respectively, their modulation do not allow to control the porosity generated. Many studies have shown that the porous structure is paramount to guide cell fate through pore size, percentage of porosity, and size of windows of interconnections and during this thesis, many experiments have been dedicated to the establishment of a way to control the porosity. For instance, the pipet tip internal diameter has been varied to modulate the shear force exerted on CO_2 bubble and be able to split them. However, no significant differences were reported. Considering that differences between manual homogenisation and injection were evidenced, future work could focus on the use of various static mixer to study the effect of homogenization on CO_2 bubble size and resultant porosity.

In light of the *in vivo* study, we identified an important path of optimization for the injectable and porous hydrogels. The CO_2 bubbles stabilization towards tissues need to be improved to prevent the formation of a dense layer and enhance cellular and vascular infiltration. To this end, some adjustments are required regarding the acid/base ratio or the DGL/PEG concentration to boost the crosslinking velocity and entrap CO_2 bubbles before their burst in contact with tissues.

Altogether, these results confirm the potential of DLG/PEG EPH of various mechanical properties to provide a porosity suitable for adequate tissue ingrowth and extensive vascularization through a straightforward and minimally invasive delivery. Considering the challenge that the design of both *in situ* injectable and porous hydrogels represents and the numerous attempts that have been made in existing literature studies for their development, we believe that the methods developed here are of relevance. They provide a starting point for the synthesis of macroporous multifunctional and highly tuneable hydrogels with potential broad applicability.

To the best of our knowledge is the first example of interdependent and simultaneous reactions using effervescence to create a porosity inside a hydrogel for *in situ* injectability purposes.

Chapter 2 : Take home message

Formulation of a relevant porosity inside the DGL/PEG hydrogel through effervescence while preserving *in situ* injectable potential

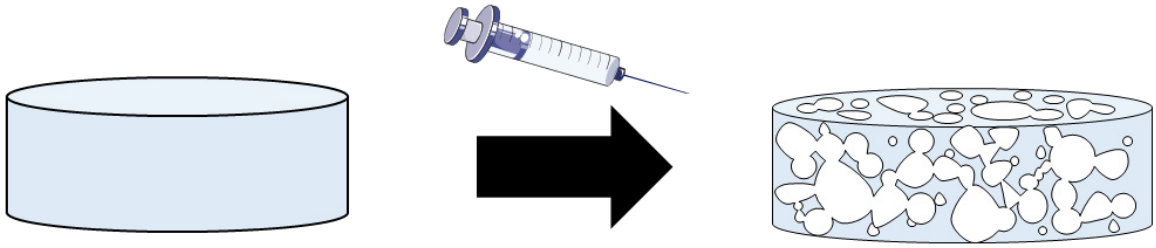

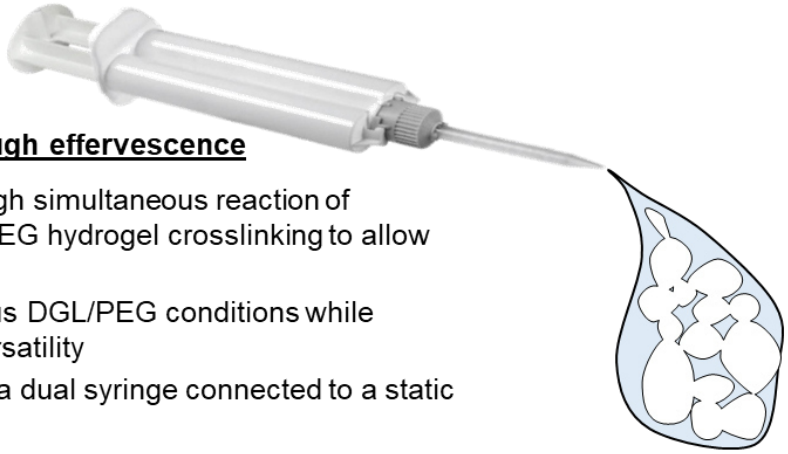

Injectable porosity through effervescence

-Porosity generated through simultaneous reaction of effervescence and DGL/PEG hydrogel crosslinking to allow CO_2 bubbles entrapment.

-Assessed for three various DGL/PEG conditions while preserving mechanical versatility

-Injectability validated via a dual syringe connected to a static mixer

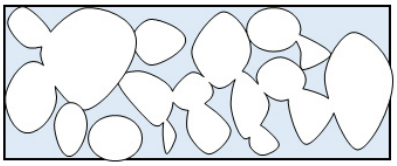

Porosity characterization (all conditions)

-Pore size: mean 300 µm - main population : 100 µm

-Interconnections: mean 120 µm - main population: 20 µm

-Porosity: mean 77%

***In situ* injection (study of cytotoxicity and biocompatibility)**

-Non-cytotoxic with primary human dermal fibroblasts

-Porosity cytocompatible

-Good tolerability in direct subcutaneous injection in mice

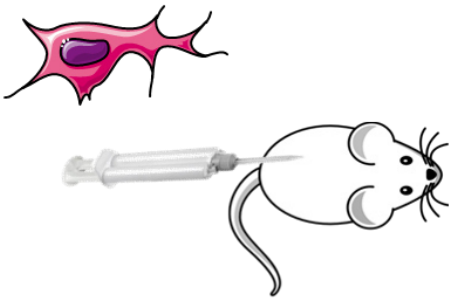

→ Generation of Innovative effervescently produced porosity inside the DGL/PEG hydrogel while preserving injectable potential

-

In situ injectable, good tolerability

Figure 48 : Take home message chapter 2

3 Assessment of innovative injectable/porous formulations to act as relevant supports for skeletal muscle growth and differentiation

In the previous chapter, we demonstrated the feasibility of inducing porosity inside DGL/PEG hydrogels while maintaining their injectable potential to combine the benefits from both characteristics. The resultant porous structures were proven cytocompatible for fibroblasts infiltration through sufficient windows of interconnection, in size and in number. Subsequent fibroblasts proliferation and ability to synthesize ECM components consolidate the porous structures' potential to act as a scaffold for cells, while sustaining cell viability over time. Finally, the successful injection of DGL/PEG effervescent porous hydrogels (EPH) resulted in the formation of the porous structure directly *in vivo,* without inducing adverse effects on tissues (necrosis, chronic inflammation), underlining their potential to promote tissue regeneration.

As demonstrated in the first chapter of this work, a tissue-engineered scaffold for the repair of skeletal muscle should possess adequate mechanical strength and biochemical cues to guide myoblasts proliferation and differentiation. Hence, the innovative effervescent porosity was successfully applied to three various DGL/PEG conditions, which allows the modulation of mechanical properties. Consequently, EPH can provide various signals to cells among which mechanical, biochemical but also architectural through the effervescently generated porosity. Indeed, in normal conditions, muscle cells evolve in a 3D network that is crucial for the maintenance of their biological behaviour and muscle contractile performance. Yet, the impact of dimensionality offered by 3D scaffolds on myoblasts *in vitro* remains unclear. Hence, aside from providing support for cells to evolve towards a functional tissue in large defect, the 3D architectural structure can also contribute to guide cell fate through adequate signals.

In this chapter, we thus focused on the evaluation of three newly generated EPH to act as scaffolds for muscle cells, in order to determine their potential for skeletal muscle tissue regeneration. To do so, the 3D structure ability to sustain myoblasts proliferation and differentiation was assessed. First, the potential of the 3D structures was evaluated with C2C12 cells, as a well-characterized model to study myogenesis in 3D and as a mean of comparison to the results obtained in flat 2D hydrogels (chapter 1). However, as immortalized cells are more prone to genetic instability, they can lose tissue-specific functions characteristic of their mortal parental population [427]. Moreover, the investigation of the myogenesis of human myoblasts is more relevant than mice models to study some muscle diseases [18]. Given these considerations, primary human myoblasts (pHMs) behaviour was also evaluated inside EPH as a more relevant cell type for the final application.

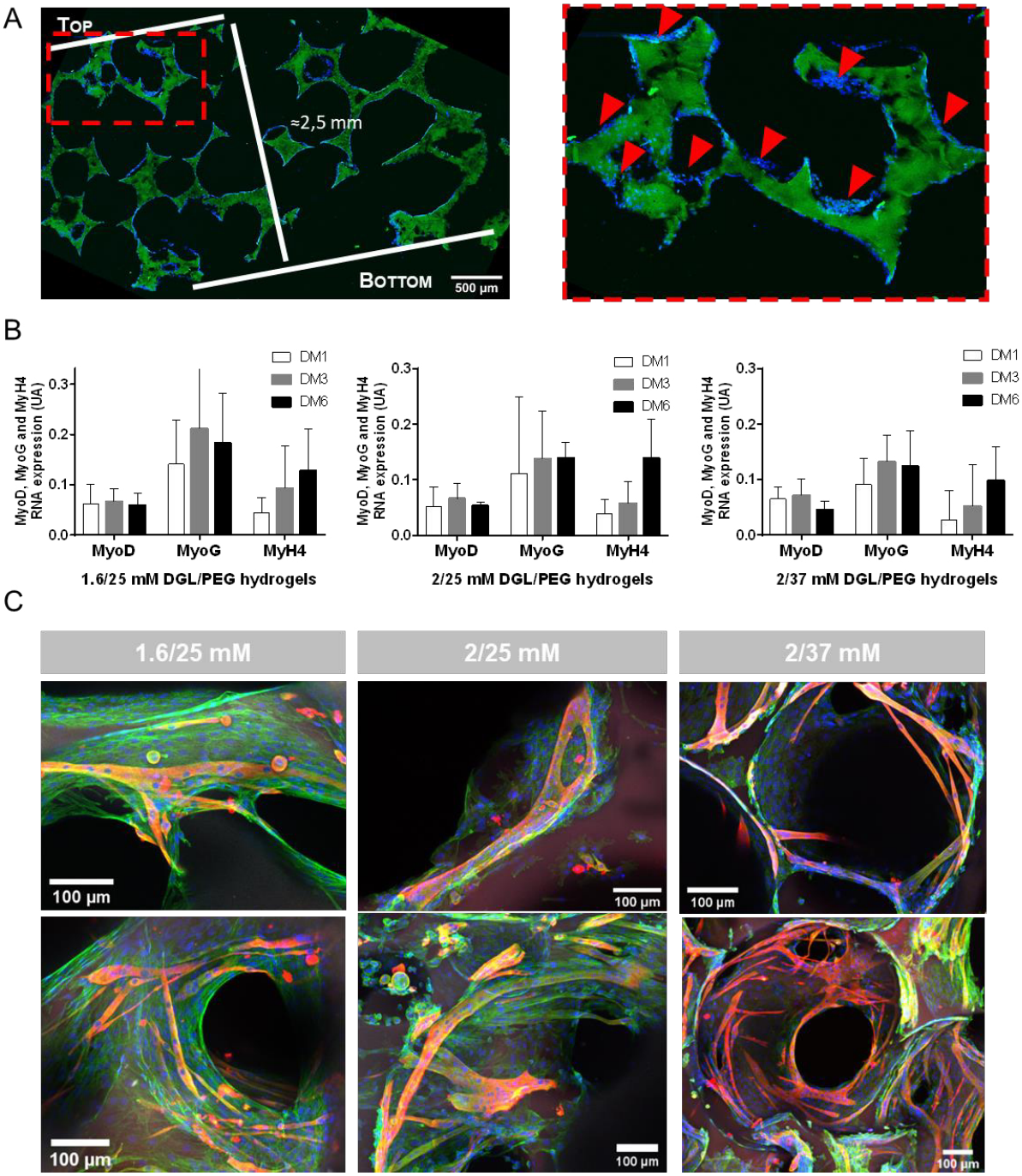

Figure 49: C2C12 behaviour inside EPH of various concentrations

A) C2C12 infiltration and homogeneous repartition inside EPH after 7 days in proliferative conditions (cell nuclei in blue and hydrogel in green) and close up with red arrows pointing at cell nuclei.

B) Expression of myogenic genes (MyoD, MyoG and MyH4) on days 1, 3 and 6 after serum depletion on various EPH conditions - One way ANOVA + Tukey's multiple comparisons. No significant differences were reported.

C) Representative pictures of myotubes formation inside EPH of various DGL/PEG compositions (cell nuclei in blue, actin cytoskeleton in green, myosin heavy chain (MyHC) in red and hydrogel in dark grey).

3.1 C2C12 behaviour in 3D environments

The ability of C2C12 cells deposited on the surface of 2 mm thick porous cylinders to migrate inside EPH was first evaluated to determine the capacity of the porous structure to support skeletal muscle cell infiltration. Interestingly, C2C12 seeded at a relatively low density on top of EPH (20.000 cells/cm²) were able to infiltrate the entire 2 mm-thick structure within 7 days (Figure 49A). Therefore, before inducing C2C12 differentiation, proliferative cells were allowed to populate the entire scaffold. While conditions 2/25 and 2/37 mM DGL/PEG were fully infiltrated within 4 days, C2C12 infiltration inside 1.6/25 mM DGL/PEG EPH required 7 days.

After proliferation, the potential of 3D scaffolds to sustain C2C12 differentiation was appreciated by immersing cells in serum-depleted medium (DM). After 1, 3 and 6 days in DM, the gene expression of three myogenic markers was quantified to follow the different steps of myogenesis. RT-qPCR results indicated that MyoD and myogenin, involved respectively in myoblast alignment and differentiation into myocytes and myotubes, were evenly expressed over time by C2C12 during the whole differentiation process for all EPH conditions studied. The process of differentiation is mostly controlled by these two transcription factors (i.e. MyoD and Myogenin) whose deficiency can hamper the functional regeneration [428], [429]. Moreover, a time-dependent expression of myogenic marker Myosin heavy chain 4 (MyH4) was observed (Figure 49B). MyH4 expression increased over time, which is consistent with the maturation of sarcomere inside new myotubes [430]. Given these considerations, C2C12 cells within the EPH exhibited expressions of myogenic markers in a way consistent with normal muscle repair, indicating that EPH provided favourable substrate. Of note, no significant differences were reported on gene expression from cells inside EPH of various conditions.

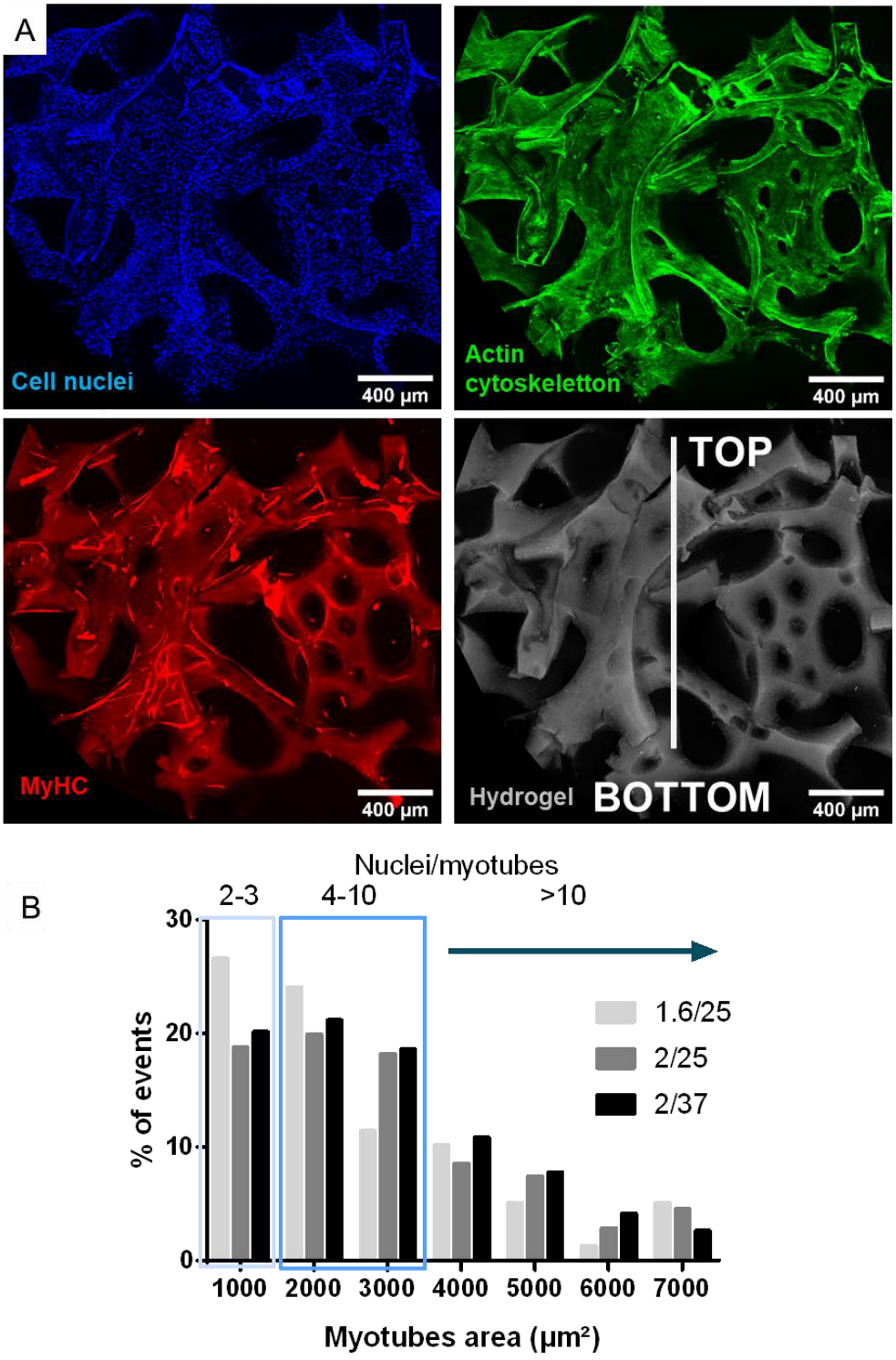

Figure 50: C2C12 behaviour inside EPH of various concentrations after 6 days in serum depleted medium

A) C2C12 myotubes repartition throughout an entire 1.5 mm-thick 2/25 mM DGL/PEG EPH. (Cell nuclei in blue, actin cytoskeleton in green, MyHC in red and hydrogel in grey)

B) Repartition of myotubes morphology (area quantification in µm²) inside EPH of various conditions (i.e. 1.6/25, 2/25 and2/37 mM DGL/PEG) on areas between 1000 and 7000 µm². The number of nuclei corresponding to a specific area range was highlighted on the graph.

After confirming that cells were able to differentiate inside EPH, their morphology after 6 days in serum depleted medium was studied. Attesting the aforementioned results, C2C12 were able to form myotubes in all EPH conditions (Figure 49C). Overall, myotubes were found throughout the entire 2 mm thick EPH, further confirming the C2C12 entry inside EPH (Figure 50A). For the softer condition (i.e. 1.6/25 mM DGL/PEG), myotubes area was smaller than for stiffer conditions (i.e. 2/25 and 2/37) although, non-significantly. Besides this result, the softer condition showed a higher population of myotubes having small areas of 1000-2000 µm² and 2 to 3 nuclei per cell (Figure 50B and Table 24). Surprisingly, the 2/25 mM DGL/PEG EPH condition showed the best ability to sustain C2C12 fusion in 3D while it was barely able to support fusion in 2D (see chapter 1). Indeed, myotube area quantification indicated bigger myotubes into 2/25 mM DGL/PEG EPH with feret diameter up to 800 µm and up to 88 nuclei per myotube. Therefore, inside 3D EPH lower DGL: PEG (1:16) molar ratios were less prone to enhance cell fusion and form large myotubes compare with the higher DGL: PEG (1:12) molar ratio (Figure 50B and Table 24).

Table 24: C2C12 myotubes quantifications after 6 days in serum depleted medium as a function of 3D EPH concentration (mM DGL/PEG).
Nuclei per myotubes, myotubes area quantification and elongation index (feret diameter/width). One way ANOVA + Tukey's multiple comparisons. Not significant

DGL/PEG (mM)	Nuclei/ myotubes	Area (µm²)	Elongation index
1.6/25	8.3 ± 3.3	3694 ± 1231	13.7 ± 3.3
2/25	9.8 ± 0.7	5221 ± 416	15.6 ± 1.8
2/37	9.1 ± 2.6	4276 ± 1044	16.8 ± 1.4

Interestingly, for all condition studied, some myotubes were found to bridge pores without continuous contact with the substrate (visible Figure 49, 2/37 top). This phenomenon could be the result of tension exerted by cells on their microenvironment enabling myotubes to be lifted after their growth [431].

Overall, EPH guided the growth and differentiation of C2C12 cells, indicating potential as a suitable environment for myoblasts and sustained culture of myotubes.

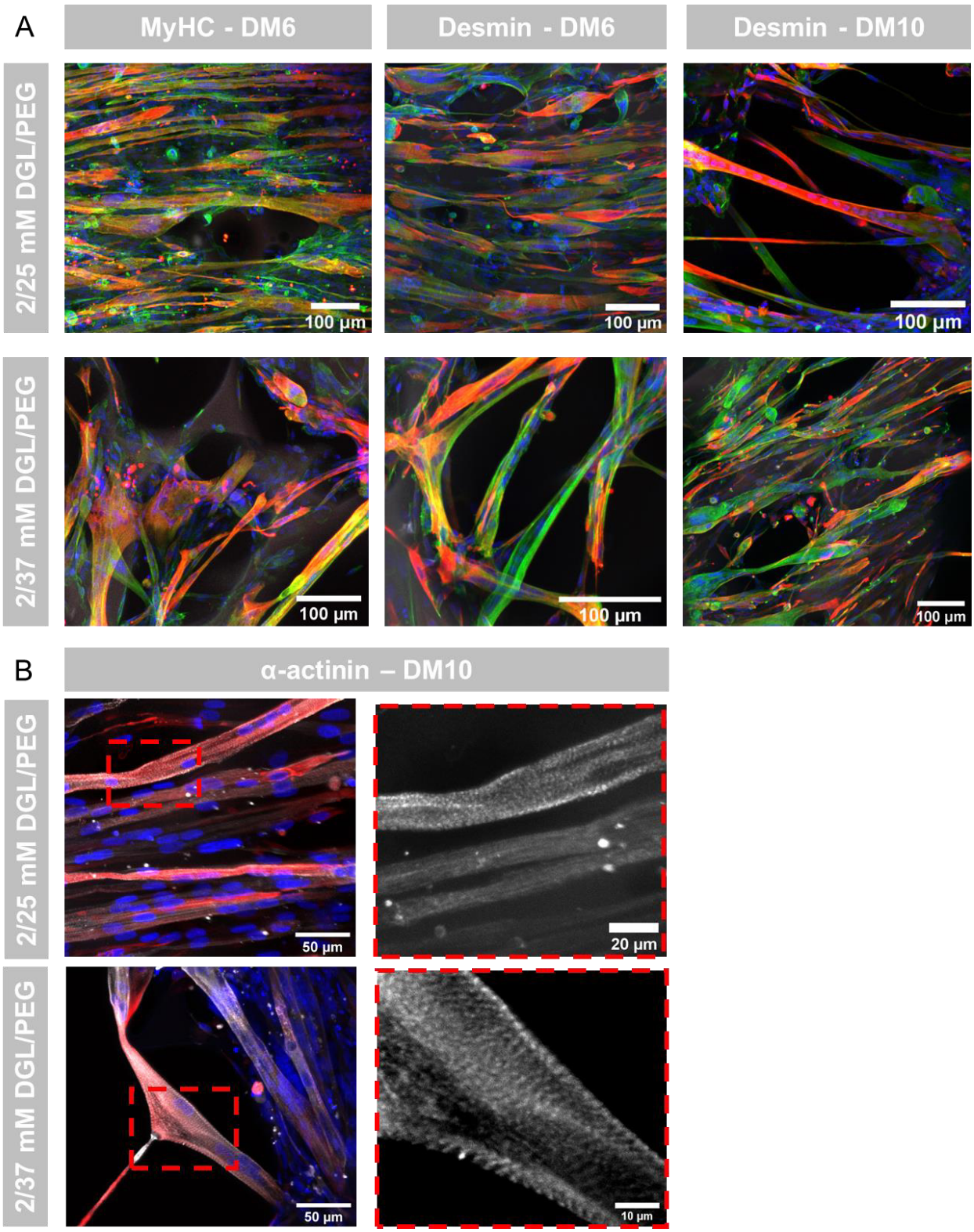

Figure 51: pHMs fusion inside EPH of various concentrations
A) pHMs onto EPH of various DGL/PEG concentrations after 6 (DM6) and 10 days (DM10) in serum depleted medium. Cell nuclei in blue, actin cytoskeleton in green and MyHC and desmin in red. The hydrogel is represented in dark grey. Some myotubes (2/25 DM10) were found bridging pore edges.
B) Observation of striation, showing the organization of sarcomeric structures inside growing myotubes. Cell nuclei in blue, desmin in red and α-actinin staining in grey.

3.2 Primary human myoblasts

The study of C2C12 cell behaviour is relevant as a well-characterized and reproducible model to outline general mechanisms and compare this work with existing literature studies. However, they misrepresent the cell type encountered in the wound bed of volumetric muscle loss (VML). Therefore, the behaviour of cells more relevant to the envisaged final application (human primary myoblasts, pHMs) was also investigated. They provide another step towards the characterization of EPH potential for skeletal muscle regeneration and *in vitro* study of myogenesis. However, the proliferation of these cells is slower than C2C12 cell growth. Given that pHMs need longer culture time, the condition 1.6/25 mM DLG/PEG was discarded due to a decreased proliferation of C2C12 cells and no significant differences in their subsequent fusion.

3.2.1 Generation of contractile myotubes

Primary human myoblasts (pHMs) showed the same aptitude as C2C12 cells to infiltrate the 2 mm thick structure, further confirming that the porous structure is appropriate for the infiltration of cells of different origins. After proliferation and culture in serum-depleted medium (DM) for 6 and 10 days, the majority of the cells within EPH of different conditions expressed myosin heavy chain and were observed with several nuclei, confirming their fusion potential (Figure 51A). Additionally, the 3D hydrogels were able to sustain pHMs fusion in an organized fashion. Indeed, some of the produced multinucleated cells exhibited intrinsic alignment inside individual pores (exemplified in Figure 51A, 2/25, DM6 and 2/37 DM10).

To further study myotube maturation, the organization of sarcomeres was analysed through α-actinin protein straining 10 days post differentiation. Evidence of striation of the protein inside the cytoplasm of some multinucleated cells indicated the maturation of myotubes towards growing muscle fibres that have the potential to contract and exert tension on their microenvironment (Figure 51B). As a striking result, contractions of myotubes were indeed observed 6 days post differentiation and were maintained up to 8 days (Annex 1, supplementary movies 9 and 10 on 2/25 mM DGL/PEG EPH). Comparatively, cells seeded on matrigel coatings as positive control were also able to contract 6 days post differentiation for only 6 more days. In addition, on matrigel coatings, cells were more prone to detachment or cluster formation in comparison with cells within EPH. Myotubes from primary human myoblasts inside EPH were on average 25 µm wide and 400 µm long, regardless of the EPH condition. As a comparison, adult skeletal muscle myotubes diameters range from 10 to 100 µm [432] and can reach 12 cm long for the longest fibres. Of further note, for all hydrogel conditions, cells maintained their integrity during the whole culture period (20 days) without collapsing and, similarly to C2C12 cells, some myotubes were able to lift from the substrate to bridge pore edges (exemplified in Figure 51A, 2/25 DM10 and 2/37 DM6). This phenomenon was more visible with pHMs compared with C2C12 cells.

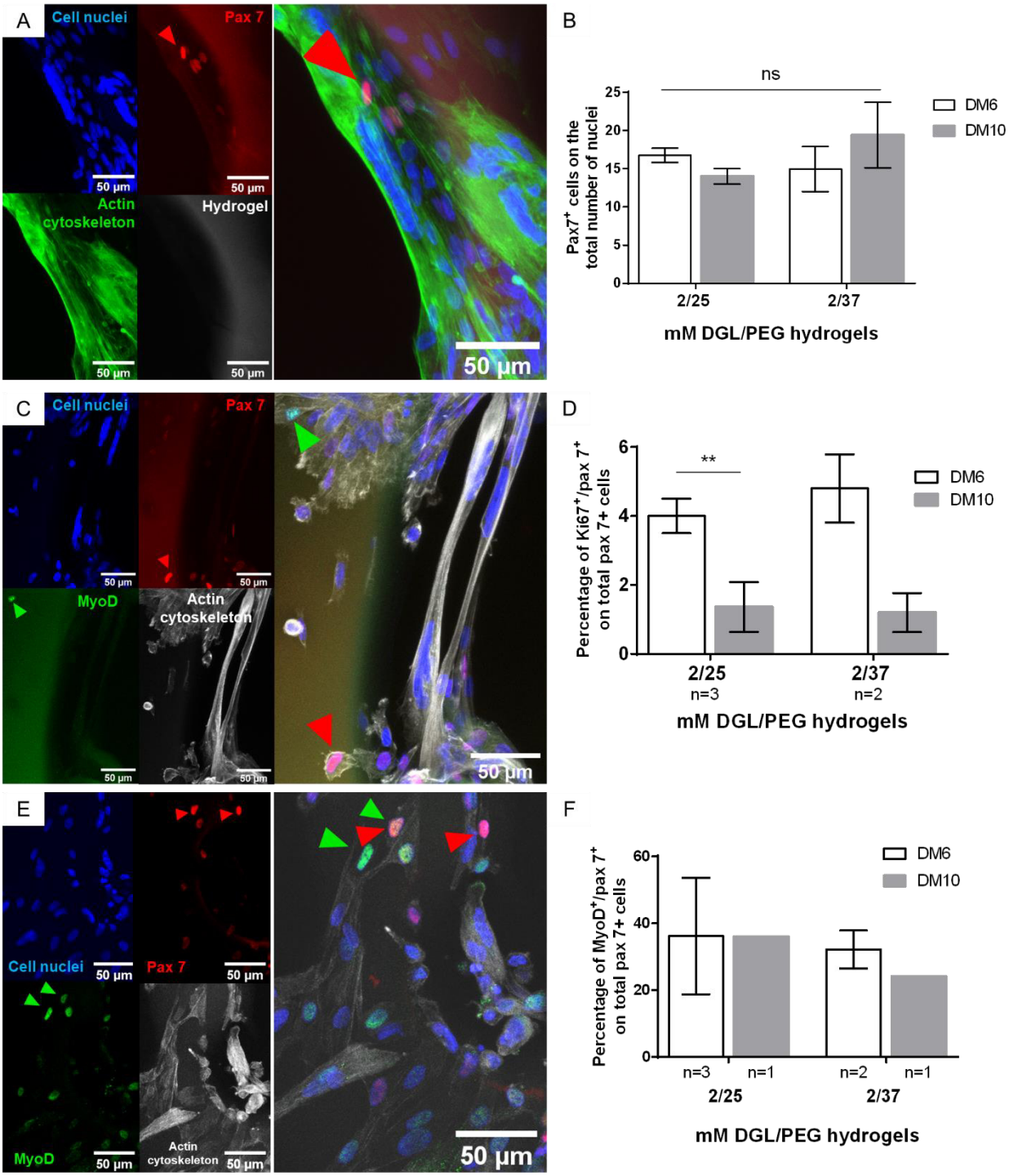

Figure 52: pHMs behaviour inside EPH of various concentrations – Observation of Pax7 positive cells
A,C,E) Representative pictures of pHMs onto A) 2/37 mM DGL/PEG EPH and C),E) 2/25 mM DGL/PEG EPH after A), E) 6 days or C) 10 days in serum depleted medium.
Cells are differentiated into myotubes and side Pax7 positive cells (red arrows) were observed inside EPH that were non-proliferative (not expressing Ki67, D) green arrows) and not entering differentiation (not expressing myoD E) green arrows)
B) Quantification of the number of cells expressing Pax7 on the total number of nuclei from pHMs after 6 and 10 days in serum depleted medium. Quantification was made on 2 different EPH compositions (2/25 and 2/37 mM DGL/PEG). D) Quantification of the number of $Pax7^+/ki67^+$ cells on the total number of Pax7 positive cells after 6 and 10 days in serum depleted medium for 2/25 and 2/37 mM DGL/PEG hydrogels
F) Quantification of the number of $Pax7^+/myoD^+$ cells on the total number of pax7 positive cells after 6 and 10 days in serum depleted medium for 2/25 and 2/37 mM DGL/PEG hydrogels.

3.2.2 Generation of mononucleated Pax7 positive cells

In addition to contractile myotubes, a population of mononucleated cells was observed inside EPH, located near myotubes and expressing the paired box protein Pax7 (Figure 52A). After 6 and 10 days in differentiation, Pax7 positive nuclei accounted for about 15% of the total number of nuclei regardless of the EPH composition (i.e. 2/25 or 2/37 mM DGL/PEG hydrogels) (Figure 52B). Interestingly, Pax7 positive cells were found in clusters inside some pores at a relatively high percentage, while other pores were almost devoid of positively stained nuclei. Among Pax7 positive cells, only 4.0 ± 0.3 % and 4.8 ± 0.7% were also positive to Ki67 six days post differentiation for conditions 2/25 and 2/37 mM DGL/PEG respectively (Figure 52C and D). Therefore, six days after differentiation inducement, about 95.6 % of Pax7 positive cells were non-proliferative. Moreover, a 65% and 75% decrease of $Pax7^+/Ki67^+$ cells was observed between six and ten days post differentiation while maintaining the pool of Pax7 positive cells for conditions 2/25 and 2/37 mM DGL/PEG respectively. This decreased proportion of $Pax7^+/Ki67^+$ with increasing exposure to DM tend to indicate Pax7 positive cells enter a quiescent state over time.

Moreover, among Pax7 positive nuclei, 36.2 ± 10.1 % and 32.2 ± 4.0 % were also positive to MyoD after six days in DM for 2/25 and 2/37 mM DGL/PEG conditions respectively (Figure 52E and F). This trend seemed to be maintained 10 days post differentiation. It further consolidates that a part of Pax7 positive nuclei was non-proliferative while escaping differentiation to stay in a quiescent state close to the behaviour of satellite cells *in vivo*.

Finally, myoblasts growth and fusion on EPH was assessed regardless of the origin and species used (Figure 53). Immortalized human myoblasts (iHMs) showed fusion through myosin heavy chain staining and primary mice myoblasts (pMMs) were observed covering the surface available on the EPH and contracting (annex 1, supplementary movies 11 and 12). These results increase the robustness of the results generated while opening many possibilities to use DGL/PEG EPH towards the evaluation of myoblasts behaviour from various origins.

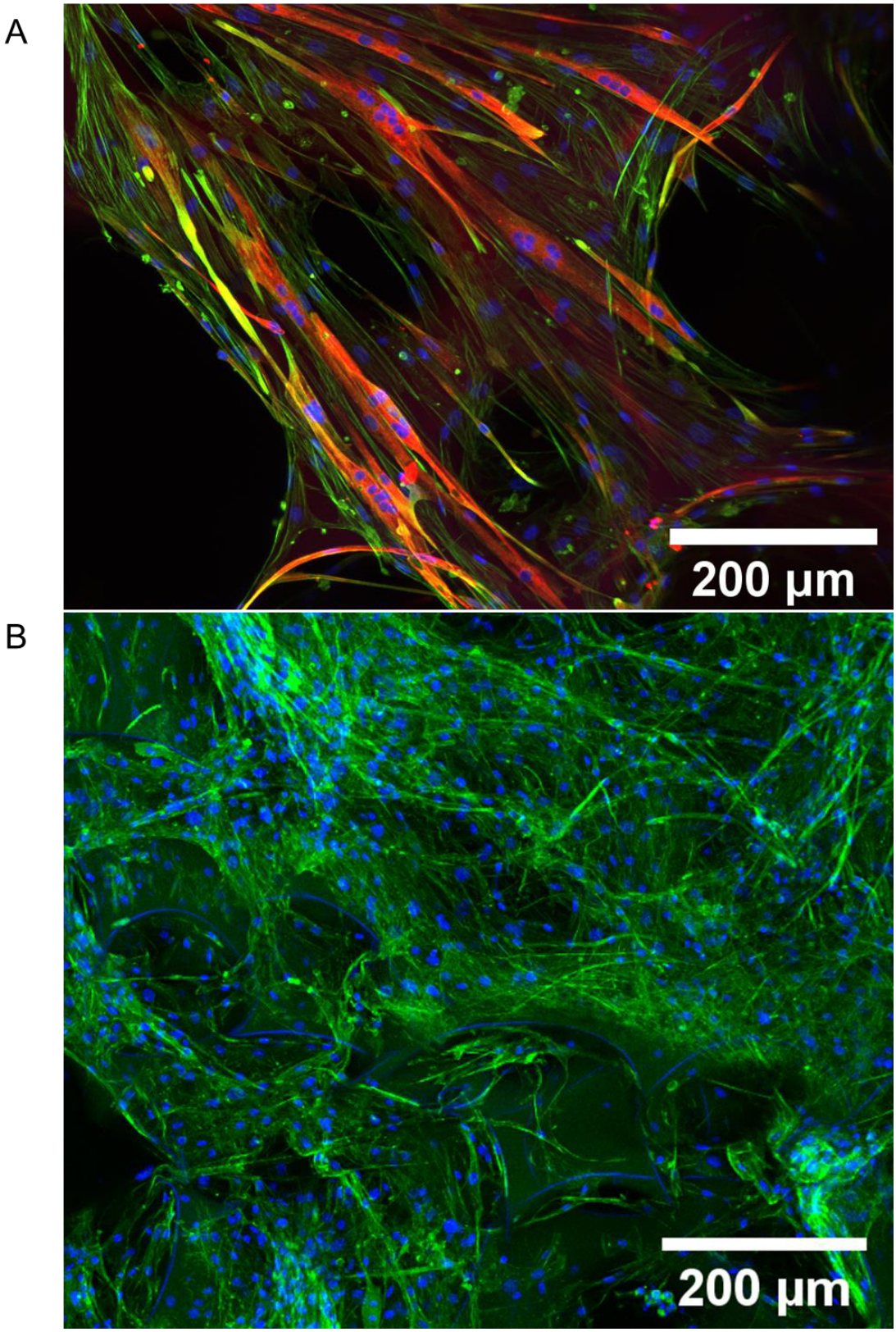

Figure 53: Behaviour of myoblasts from various origin inside EPH after 15 days in differentiation – preliminary studies
A) Representative picture of immortalized human myoblasts (iHMs) onto 2/37 mM DGL/PEG EPH. Cell nuclei in blue, actin cytoskeleton in green and MyHC in red.
B) Representative picture of primary mice myoblasts (pMMs) onto 2/37 mM DGL/PEG EPH. Cell nuclei in blue, actin cytoskeleton in green.

3.3 Discussion

Given the excessive tightness of the polymer network of DGL/PEG dense hydrogels, a 3D structure inside the hydrogel was created for cellular infiltration. Porous interconnected structures inside DGL/PEG hydrogels were successfully obtained through an effervescent approach as described in the second chapter. Three effervescent porous hydrogels (EPH) of various DGL/PEG concentrations could be easily formulated through a straightforward single-step injection.

Where many instances of scaffolds designed for skeletal muscle engineering lack a porous structure, which ultimately leads to cellular mortality of embedded cells [215],[433], the porosity generated inside our hydrogel allowed cellular infiltration and their viability over culture time. The EPH displayed a robust and reproducible 75% porous and highly interconnected structure resembling the native skeletal muscle extracellular matrix (ECM), which displays high interconnection and a porosity comprised between 74 % ± 3 % to 79 % ± 5 % [31]. Overall, the DGL/PEG EPH had a pore size of 300 µm on average with pores of 100 µm being the more represented. The porosity is thus close to what has been considered optimal in developing myotubes in literature [262], [263]. Pores between 50 to 400 µm have indeed already been shown to efficiently sustain the formation of mature myotubes for skeletal muscle regeneration both *in vitro* or *in vivo* [274],[212],[289]. The high number of interconnections inside EPH (quantified in the second chapter) sustained a quick and efficient C2C12 and pHMs infiltration. This feature is consistent with observations obtained with fibroblasts, which were distributed throughout an entire 2 mm-thick EPH after 24 hours of culture (chapter 2). For C2C12 cells, a delay in proliferation was observed for the condition 1.6/25 compared to conditions 2/25 and 2/37 mM DGL/PEG, in line with results observed in the first chapter, when cells were cultured in 2D, at the surface of the hydrogels. This confirms that the mechanical versatility of the raw hydrogel material was not hindered by the formation of the porosity through effervescence. Consequently, C2C12 cells were let to populate 1.6/25 mM DGL/PEG EPH for longer times, prior differentiation.

Once induced to myogenic differentiation, we could demonstrate that EPH were able to sustain the formation of myotubes from C2C12 cells, expressing various myogenic markers in a way consistent with what is described in native muscle regeneration [119], [434], [435].

These results highlight the potential of the porous structure generated inside DGL/PEG hydrogels to act as relevant support for cells while enabling their infiltration in the bulk material. Considering VML injuries are generally characterized by wounds devoid of ECM, DGL/PEG EPH hold promise to be used as the support for tissue engineering purposes for host cell infiltration and subsequent differentiation into contractile muscle fibres.

3.3.1 Two-dimensional versus three-dimensional culture

What is known about skeletal muscle cell fate and function generally derives from studies of monolayer cells seeded on rigid substrates (plastic or glass). Recently, 3D culture has been proposed to provide a more physiological and complex environment for cells than routine 2D monolayer culture not recapitulating native 3D signals [436], [437]. Surprisingly, for all conditions studied, C2C12 myotubes generated in 3D were more elongated, with a higher number of nuclei per cell and a smaller area compared with myotubes grown on 2D hydrogels (Chapter 1). Considering that the same hydrogel compositions were studied, this apparent better myotubes maturation inside EPH compared with myotubes grown on 2D flat hydrogels could be attributed to the architecture variability.

This different C2C12 cell behaviour could be triggered by higher cell-to-cell interactions inside the EPH enabling the cells to fill the pores thus increasing cell confluence, which is paramount for efficient cell fusion. Moreover, the presence of pores compared with 2D flat hydrogels provided curvature, which has been related to cellular behaviour variability and could explain the differences observed herein [252].

Particularly, cell cytoskeleton arrangement has been shown to be highly influenced when cultured in 3D compared with 2D monolayers through the increased expression of adhesion site proteins integrin α5 subunits and vinculin [438]. What is more, a faster differentiation and fusion kinetic of myoblasts in 3D fibrin matrices have been demonstrated and evidenced by higher mRNA concentration of α-actinin and myosin compared with 2D classical culture [438]. Indeed, during fusion, many adhesion proteins are involved to allow myoblasts to recognize one another and form temporary cell-cell contact to sustain membrane fusion. Among these proteins, integrin α3 subunit [439], integrin β1 subunit [440], M-cadherin and ADAM 12 [441] proteins play important roles. Particularly, integrin α3β1 is involved in cell-cell and cell-ECM adhesion and has shown to have a particular function in myoblasts fusion [440]. Interestingly, higher expression of integrin α3 subunit and M-cadherin mRNA level were observed in C2C12 cultured within 3D environment compared with C2C12 cultured on 2D monolayers [441] explaining an increase of cell differentiation and fusion when cultured in 3D. These results highlight that the 3D environment is thus a potent regulator of cell function by upregulating the expression of proteins involved in cell fusion. Therefore, while supporting cell infiltration, the porous structure generated inside the DGL/PEG hydrogel could also enhance the fusion of resident cells to regenerate the tissue in case of VML, further consolidating the high potential of this hydrogel.

3.3.1.1 DGL: PEG molar ratio in 2D versus 3D culture

In addition to increasing the cell fusion, the 3D environment reversed the effect of DGL: PEG molar ratio on cell behaviour. In the first chapter, we demonstrated that a high concentration of DGL, and thus NH2 groups available at the surface of 2D substrates, caused a C2C12 fusion impairment. We made the hypothesis that it was due to an increased adhesion of cells on the surface via integrin clustering on NH2 moieties. However, inside 3D environments with a higher concentration of DGL, myotubes from C2C12 were longer and with more nuclei per cell. Interestingly, it has been shown in existing literature studies that 3D environments resulted in reduced focal adhesion (FA) clustering of cells together with improved integrin expression distributed throughout cell cytoplasms [251]. Accordingly, the higher DGL: PEG molar ratio, having a deleterious effect in 2D through too strong FA clustering could thus be appropriate in 3D by increasing the expression of integrins involved in cell fusion. This increased expression of integrins together with their better repartition inside the cells could thus counterbalance the DGL effect described in the first chapter. Therefore, it opens optimization pathways to find optimal DGL/PEG conditions for C2C12 proliferation and differentiation in a 3D organization.

3.3.1.2 Myotubes behaviour

Hence, we demonstrated that the EPH were able to sustain C2C12 differentiation and fusion in a sustained manner compared with 2D hydrogels of the same conditions. However, if mice C2C12 cells provided interesting results that allow to strictly compare 2D and 3D environments with similar materials, fewer groups have reported the use of primary human myogenic cells (pHMs) [438], [442]. Therefore, pHMs were evaluated during this work, to obtain a more accurate model to study EPH potential as a substrate to treat human skeletal muscle injuries. Logically, differences were revealed between the two cell sources. In particular, myotubes derived from pHMs showed higher maturation inside EPH with visible striation compared with C2C12 cells cultured in the same conditions. This trend was previously described with C2C12 and primary human myogenic cells exhibiting different abilities to form contractile myobundles in laminin-coated micrometric channels inside a 3D hydrogel [443]. Particularly, spontaneous contractions and self-alignment were observed with pHMs and not with C2C12 cells. Contractions were also observed with primary mice myoblasts (pMMs), but not with immortalized human myoblasts. Overall, primary myoblasts were more prone to exhibit spontaneous contractions compared with immortalized myoblasts independent of the myoblasts origin (mice or human).

However, the phenomenon of cell alignment inside pores was only observed for primary human myoblasts (supplementary information 9 in annex) while C2C12 and primary mice myoblasts exhibited a more random repartition. In a classical culture on matrigel, we showed in our group that pHMs have no spontaneous self-alignment, which is in line with what has been observed in literature [444], [445]. The curvature of EPH could thus bring appropriate signals to enhance cell alignment upon fusion, indicating that the cells could perceive the pore morphology. To the

best of our knowledge, this trend has not been reported in literature for non-aligned porosity such as our effervescently generated porous structure [446], [447]. Although staying unexplained, this is an interesting feature as a long-range organisation of myoblasts is required to create a muscle architecture globally aligned to provide tissue function.

We also observed that myotubes were able to lift themselves inside the pores while remaining attached to the pore edges. This was the case for all myoblasts used but was particularly evident for pHMs. This phenomenon has been described elsewhere, with aligned myotubes exerting a passive tension on deformable pillars on which they were cultured, which enabled them to be lifted from the substrate [448]. In some instances, this passive tension also caused the pillars to be pulled closer together [431]. These groups concluded that their pillars system, serving as attachment points, were mimicking tendons within the musculoskeletal system. Accordingly, our results could be explained by the stiffness of 2/25 and 2/37 mM DGL/PEG EPH (34.9 ± 5.0 and 54.3 ± 0.5 kPa in compression respectively), which is higher than the reported muscle tissue stiffness but close to the tendon ECM (shear modulus between 25 to 45 kPa [449]). Therefore, the EPH stiffness could mimic the tendon, providing specific signals to myotubes enabling them to exert passive tension to the support to be lifted inside the porous structure. However, no differences were observed between our two DGL/PEG conditions with different stiffness.

Taken together, these results are in accordance with results obtained with C2C12 cells but go further, underlining EPH potential to sustain human myoblasts fusion and maturation into contractile and organized myotubes.

3.3.2 The generation of myogenic reserve cells

The use of pHMs also enabled us to study a feature not visible with C2C12 cells, which is the ability for myogenic precursor cells inside EPH to follow various paths. Contrarily to C2C12 cells, a large part of the pHMs entered differentiation to fuse, while others regained a phenotype characteristic of quiescent satellite cells. *In vivo,* satellite cells (SC) are localized near muscle fibres and are directing tissue growth and regeneration upon injury [54]. SC can differentiate into myoblasts to regenerate the tissue while others preserve their self-renewal ability to repopulate stem cell niches. The capacity of the muscle to cope with serial damages and chronic degeneration is linked to the replenishment of the SC pool after each regeneration period [450]. Some studies have shown SC diverging fate is associated with variation in Pax7 and MyoD expression: $Pax7^{+}MyoD^{-}$ are quiescent cells, $pax7^{+}MyoD^{+}$ are activated SC or proliferating myoblasts while $Pax7^{-}MyoD^{+}$ are differentiating cells [451].

In this work, we observed mononucleated cells expressing Pax7 while being non-cycling and not entering differentiation after 6 and 10 days of pHMs differentiation. These results are in line with studies showing the apparition of a subpopulation of quiescent, non-cycling, undifferentiated cells inside *in vitro* myogenic precursors cell cultures known as ‘reserve cells’

(RC) [451]–[453]. They have been described as cells able to escape spontaneously terminal differentiation but which remain myogenic if further stimulated [452]. Here we showed that 15% of the cells remained undifferentiated in clusters after 6 and 10 days in differentiation. As a comparison, primary human myoblasts cultured on conventional plastic dishes for 48 hours in DM showed 38% of cells remaining mononucleated and escaping the terminal differentiation process among which 90% expressed Pax7 [454]. In this work, we went further, showing that it was possible to preserve the pool of Pax7 positive cells for up to 10 days.

Moreover, the same group observed that after 120 hours in serum depleted medium, 35.8 ± 6.2% of their myogenic reserve cell population where both $pax7^{+}MyoD^{+}$ which is consistent with what we obtained after 6 and 10 days in DM (36.2 ± 10.1 % and 32.2 ± 4.0 % for 2/25 and 2/37 mM DGL/PEG hydrogels respectively). They also demonstrated that during seeding and proliferation, almost all their cells were $Ki67^{+}$, $Pax7^{+}$, $MyoD^{+}$ to then engage towards differentiation or quiescence [454]. This observation could explain the decreased proportion of $Pax7^{+}/Ki67^{+}$ cells inside EPH observed between 6 and 10 days in DM. The cells, either entering quiescence or differentiation, were progressively downregulating ki67.

The observation of cells following the path of proliferative inactivity could be related to the EPH porous structure and properties. For example, stiffness of the environment has been shown to inform the decision of SC to remain in quiescence *in vitro* [455]. However, in our case, no differences were observed between the two EPH conditions of various stiffness (i.e. 2/25 and 2/37 mM DGL/PEG at 34.9 ± 5.0 and 54.3 ± 0.5 kPa respectively). As a comparison, a stiffness of about 2 kPa has been found to be optimal for the maintenance of SC quiescence in a collagen-based hydrogel scaffold [455], which could indicate that a yet unknown phenomenon is here at play.
Nonetheless, providing an optimal environment to promote RC formation is of great interest for VML treatment due to their high regeneration potential. RC have demonstrated great abilities to improve muscle regeneration *in vivo* after injury in comparison to myoblasts [454]. The *in vitro* capability of RC to both self-renew and differentiate may be related to SC behaviour described *in vivo*. Therefore, RC offer an interesting therapeutic possibility for injured skeletal muscle while being easily generated *in vitro*.

To conclude, we demonstrated that it was possible to form contractile myotubes, an essential target for muscle recovery, together with mononucleated RC relevant to support repeated cycles or regeneration from myogenic precursors seeded on EPH. In this chapter we thus validated that the generated EPH are great substrates for myotubes maturation and hold significant promise to be used as scaffolds for VML treatments. Moreover, considering that EPH provide an environment enabling the spontaneous contraction of human myotubes, they could also be interesting for the *in vitro* study of myogenesis. The primary function of the muscle tissue is to physically generate force, it thus seems crucial to appreciate mechanical stresses involved. Some researchers have indeed studied myoblasts contractile behaviour in

engineered 3D constructs [456] to provide innovative ways to evaluate drugs and/or molecules on cell ability to contract. The EPH could thus be converted in an *in vitro* model to study the process of myogenesis through the force applied by myotubes on microenvironment.

Altogether, EPH provide an interesting alternative to matrigel, which has been extensively employed as the gold standard able to promote muscle cells spreading, mobility and differentiation [399]. However, the use of matrigel raises questions of batch-to-batch variability hampering the reproducibility of results while being strictly restricted to *in vitro* studies due to its murine origin and potential tumorigenicity. In this work, we developed a highly reproducible alternative, able to promote skeletal muscle cells differentiation and maturation into contractile muscle fibres in a 3D structure with possible translation to *in vivo* models.

3.4 Conclusion and critical evaluation

This chapter aimed to evaluate the innovative effervescent porous hydrogel (EPH) as a support able to recapitulate some signals of the native microenvironment to influence skeletal muscle cells behaviour. While some positive attributes have been highlighted in the foregoing, several improvements can be done to fully understand cellular behaviour inside EPH and thus better approach the native skeletal muscle environment for tissue regeneration purposes.

3.4.1 Two-dimensional versus three-dimensional culture

We first investigated the variation of cell behaviour between 2D and 3D substrates. In line with other studies, our model showed that a 3D environment promoted a more efficient myoblasts fusion into myotubes, compared with 2D cultures, which further confirms the beneficial influence of the 3D environment on skeletal muscle cells. However, the fusion index was not quantified in 3D EPH due to large cell clusters and the difficulty to individualize nuclei. The comparison of cell behaviour on 2D versus 3D substrates was thus only based on myotubes morphology and might be biased. Therefore, the development of image analysis protocols able to individualize nuclei in 3D appears of relevance to increase the robustness of our results.

However, one important advantage of our system is the comparison we made of 2D monolayer culture against 3D culture on scaffolds of similar compositions. On the contrary, most of the studies in literature compared 3D scaffolds against 2D monolayer on plastic or glass without considering the huge stiffness and biochemical variation between both models. However, in this work, we did not consider the difference in PEG-NHS solvent and the variation of stiffness induced by the effervescent reaction on the raw hydrogel between 2D and 3D models. Therefore, to be relevant, future work should focus on 2D monolayer formulated with Gaa:KC, pluronic® F-68 and with PEG solubilized in DMSO to perfectly recapitulate the mechanical behaviour of EPH.

Moreover, in this work, we assumed that the different behaviour observed between cells in 2D versus 3D substrates could be related to differences in integrin repartition inside the cells and FA clustering as previously demonstrated in literature. However, most of the 3D environments described in existing studies were defining cells completely embedded inside the scaffold, having no prescribed polarity, and with migration and spreading sterically hindered [457]. In contrast, in this work, pores were large enough to provide a semi-3D environment, resembling a 2D substrate with a forced basal-apical polarity of cells, having an influence on their behaviour [457]. As a result, cells were able to migrate and spread within the scaffold, rendering comparison with scaffolds described in literature hazardous. In that respect, our assumptions regarding cell behaviour variation through adhesion proteins and FA clustering should be validated. In the future, C2C12 cells inside EPH or on 2D hydrogels could be transfected with specific siRNA to silence various integrin subunits expression and be able to

validate or refute these hypotheses with specific staining of FA proteins (focal adhesion kinase, paxillin, vinculin for instance).

All in all, a better understanding of the mechanisms regulating skeletal muscle cell fate in 3D on DGL/PEG hydrogels could provide interesting perspectives for its use as a model to study myogenesis. More importantly, it would help us formulate an optimal environment to precisely control cell fate for the use of the DGL/PEG EPH to enhance tissue regeneration in skeletal muscle injuries.

3.4.2 Porosity optimization

After evaluating variation between 2D and 3D substrates, we focused on pHMs capacity to align inside single pores, once differentiated into myotubes. While the hydrogel does not possess the alignment recommended for myotubes growth, it does provide appropriate signals and pore size for myotubes alignment upon differentiation. However, compared to classic monolayer culture, myotubes exhibited smaller areas and number of nuclei per myotube. As a comparison, Perroud and colleagues showed primary human myoblasts cultured on classic culture plate formed myotubes with an area of about 60.000 µm² and an average of 65 nuclei per myotube [458]. Such results open the future possibility to adapt our 3D structures to generated longer myotubes and explore novel perspectives for translational approaches. Future work could focus on incorporating topographical cues such as pore alignment inside EPH to direct myotubes growth towards unified contractile units. However, it is highly challenging to topographically shape the porosity while maintaining its injectable potential. To address this specific issue, the use of other processes combined with the effervescence should be considered. Moreover, the establishment of image analysis protocols to quantify cell alignment using imageJ could be relevant to explain the spontaneous alignment of pHMs observed in this work.

3.4.3 Stiffness and biochemical signals

In this chapter, the 1.6/25 mM DGL/PEG hydrogel was not evaluated with pHMs due to slower skeletal muscle cell proliferation and difficult handling related to a low stiffness. However, this condition was the closest to the native muscle tissue with a stiffness of 17.1 ± 1.4 kPa. It would have been relevant to quantify myotubes striation and evaluate adequacy with Engler and colleagues' results who highlighted a better striation of C2C12 cells on substrates stiffness close to the native muscle [198]. Moreover, it would have been of interest to quantify the number of myotubes ‘lifted’ inside pores of EPH stiffness closer to the muscle tissue. As we assumed that myotubes ability to lift could be modulated by EPH stiffness, the quantification of ‘lifted’ myotubes on soft and stiff substrates could further enlighten our theory. Finally, the ELP was not studied in this chapter. As the ELP interacts with integrins, it could allow elucidating the aforementioned assumptions of the role of integrins in 3D.

3.4.4 Generation of myogenic reserve cells

In addition to demonstrating that the innovative EPH is able to guide cell fusion, we observed cells inside EPH resembling reserve cells (RC). However, their myogenic potential needs to be assessed to be considered as RC. To this end, future work could focus on a way to detach and re-plate these cells to characterize their ability to differentiate and give rise to myotubes. Nevertheless, the detachment of cells from the DGL/PEG hydrogel represents a technical challenge due to strong interactions between cells and positively charged DGL, rendering classical trypsin protocols inefficient. Recently, some efforts have been made in our group to detach fibroblasts from 2D hydrogels. To do so, the addition of a solution of dextran sulfate sodium on cultures showed positive outcomes. The dextran sulfate sodium masks positive charges brought by DGL and therefore avoid too strong interactions between cells and substrate after trypsin addition. Unfortunately, these protocols are hardly transposable to 3D EPH due to the slow diffusion of dextran sulfate sodium of high molecular weight (>500,000 g/mol) inside EPH. In the future, some efforts could be made towards the establishment of an appropriate protocol to detach cells from EPH while ensuring their viability. In this work, cell characterization was largely based on immunofluorescences, however, the detachment of viable cells could allow further understanding of underlying mechanisms.

Finally, it would have been interesting to study pHMs in 2D to compare the results with EPH and draw conclusions on the architecture effect on RC. While much efforts have been made on the understanding of ECM binding sites and diffusible molecule influence on satellite cell behaviour *in vivo*, the evaluation of the external immediate architecture contribution remains scarcely described [55]. The EPH could thus provide an attractive *in vitro* model for the evaluation of the architecture effect on cells. As such, understanding the interactions between satellite cells and their microenvironment is paramount for the development of therapies for muscle disease of VML management. To this end, efforts should be made to tailor porosity and study the architecture variation on RC behaviour and the formation of clusters of Pax7 positive cells.

In conclusion, in this chapter, we gave preliminary results demonstrating EPH relevance for the growth and differentiation of primary human myoblasts. These results open opportunities for skeletal muscle regeneration through *in situ* injectable delivery. Moreover, we highlight that the DGL/PEG hydrogel seems to be relevant to follow cell fate *in vitro*. *In vitro* reproducible systems recapitulating myogenic precursor environment to understand the induction towards this lineage is useful. Therefore, these results also pave the way for a use of the 3D DGL/PEG hydrogel as *in vitro* model.

Chapter 3 : Take home message

(1) 2D versus 3D substrates and (2) EPH ability to sustain myoblast growth and fusion

-Effect of stiffness on cell proliferation

-Clear and quantifiable effect of the DGL:PEG molar ratio on differentiation

-Observation of a destabilization of the cell layer with cell detachment.

-Effect of stiffness on cell proliferation

-Less effect of the DGL:PEG molar ratio on differentiation (inversed trend compared with 2D substrates)

-Observation of cell straightening within the pores

→ Overall, better differentiation

→ Adequate support for primary human myoblasts

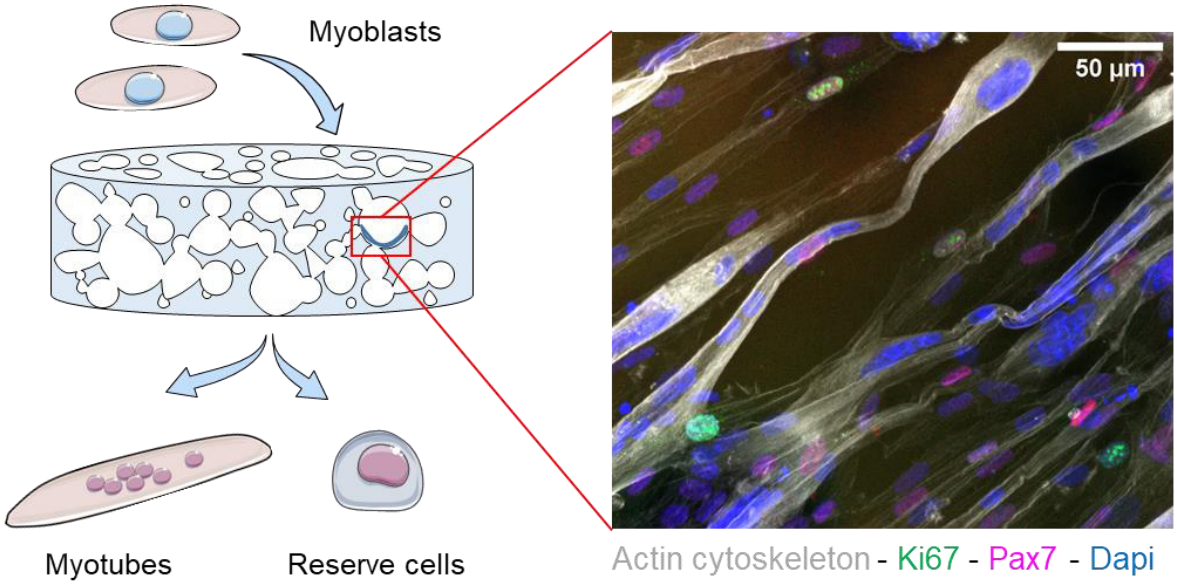

Figure 54: Take home message chapter 3

4 Pilot studies towards *in vivo* evaluation

Considering the promising results highlighted in the third chapter, the logical next step identified in the work was the *in vivo* evaluation of EPH in muscle defects.

To go towards *in vivo* studies and identify potential hurdles associated with direct EPH injection, pilot studies have been conducted in muscle defects of small animals. Muscle defects (about 2-4 mm wide and 5-8 mm deep) have been performed in gastrocnemius, tibialis anterior and gluteus maximus of rats and mice already euthanized. EPH were subsequently injected inside defects to determine the volume needed and the optimum conditions of DGL/PEG hydrogels enabling the formation of the self-standing porous hydrogel.

After EPH injection in the muscle defect, the effervescently generated CO_2 bubbles could not be maintained in contact with tissues. Instead, bubbles broke and accumulated at the surface. We thus identified a different behaviour compare with EPH injected in tubes (Figure 55A, B and C). This phenomenon can be compared with the observations of EPH directly injected in subcutaneous pockets in mice, in which dense structures were generated in contact with tissues. No obvious correlation could be noticed between the size and form of the defect and the CO_2 bubbles stabilization. Similarly, when injected inside tubes of various forms and sizes, CO_2 bubbles could always be stabilized to form a porosity inside DGL/PEG hydrogel. Even if a slight variation of the pore size was observed, although non-significant, the CO_2 bubbles were maintained in contact with tube walls (Figure 55B, C and D).

It was thus hypothesized that similarly to subcutaneous injection, a surface tension imbalance in contact with tissues could provoke CO_2 bubbles to burst after their generation. The surface tension of polystyrene tubes is relatively low (about 34mN/m [459]) while it is higher for of tissues. For example, the tension surface of the blood has been quantified at 55.9 ± 3.6 mN/m [460]. A high surface tension could counterbalance attraction forces of the surfactant that normally maintain CO_2 bubbles stabilized and cause the bubbles to break out. To assess these assumptions, EPH were injected inside glass tubes (with a higher tension surface (about 230-360 mN/m [461]) than polystyrene) to evaluate the effect of tubes surface tension. Interestingly, while a high percentage of giant bubbles were visible compared with EPH in polystyrene tube, a majority of the CO_2 bubbles could be maintained in contact with the glass tube walls. If the role of surface tension on the EPH behaviour cannot be discarded, these results underlined that another mechanism is at play when EPH are in contact with tissues.

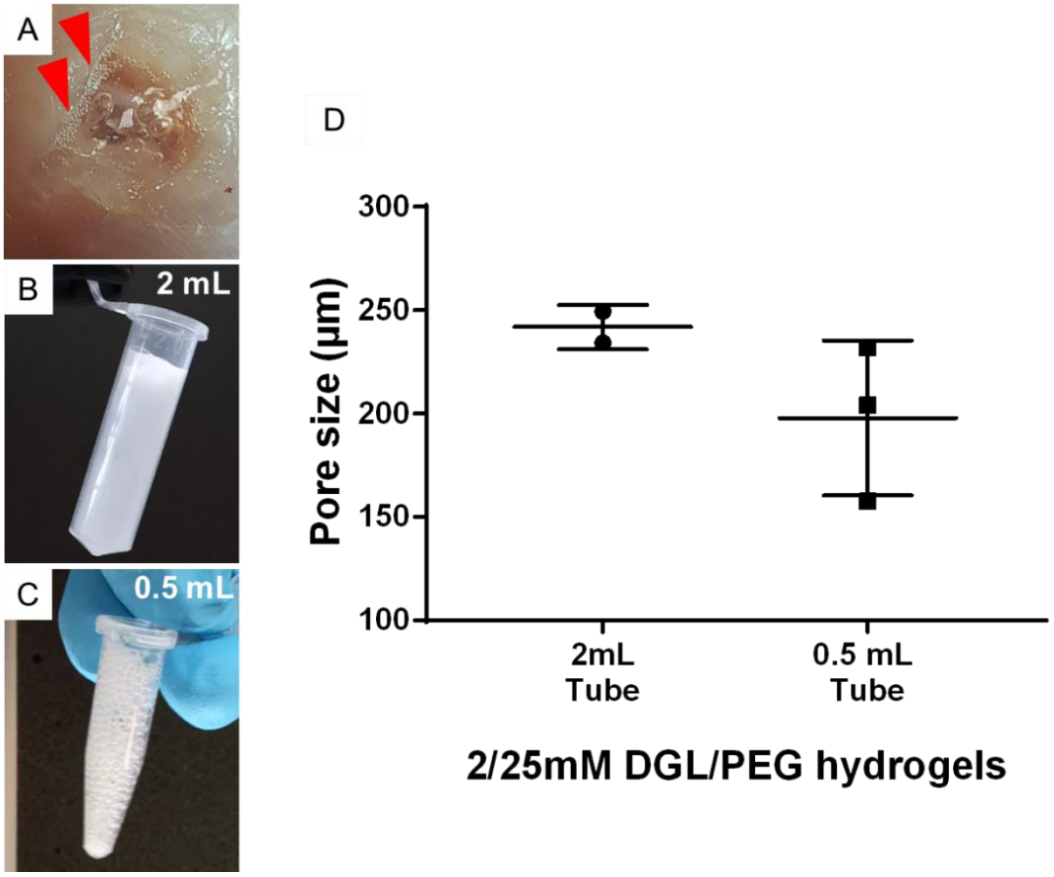

Figure 55 : EPH injected inside various supports.
A) EPH injection in a muscle defect in a rat. Bubbles in contact with tissues were not maintained and some of them accumulated at the surface of the gel (red arrows). B) and C) EPH injected in tubes could be formed with stabilized CO_2 bubbles, regardless of tubes size and form. No significant difference could be observed between the porosity created inside 2ml and 0.5 ml tubes. However, a slight variation of bubble size could highlight an effect of tube form and size on the formation of the porosity by effervescence.

Therefore, before considering *in vivo* assessment of injection in muscle defects, some optimization regarding the EPH design should be carried on to quickly entrap CO_2 bubbles before their burst in contact with tissues. For example, an instantaneous crosslinking could be triggered by increasing the pH of the acid:base ratio, the DGL/PEG concentration or the temperature of precursors' solutions to entrap the generated bubbles. In addition, to avoid the CO_2 bubbles to burst in contact with tissues, some effort could also be made on the optimization of CO_2 bubble stabilization. The final concentration of pluronic® F-68 could be adjusted to sustain bubbles over time. The wound bed could also be covered with the surfactant to then inject the DGL/PEG hydrogel to further stabilize the CO_2 bubbles in contact with tissues. However, the presence of a layer of pluronic® F-68 could result in EPH isolation from tissues, preventing cellular entry and therefore needs to be assessed. The study of other surfactant could also be explored such as the use of albumin, which lead to foam upon solubilisation. Finally, a combination of all these strategies could lead to an instantaneous cross-linking of the hydrogel upon injection, improving resulting bubbles entrapment for direct injection on tissues.

4.1 *Ex vivo* pilot study

Given the foregoing and to avoid the unnecessary use of animals, *ex vivo* studies were conducted. These experiments were designed to study cells located in muscle tissue ability to enter the EPH. To do so, some muscles were harvested from recently euthanized mice, lacerated, rinsed with PBS and placed inside tubes. EPH of different conditions were subsequently injected inside the tube to surround the muscle (Figure 56A). Only the most basic acid:base ratio was targeted (i.e 1.33:1 Gaa:KC) and high concentration of DGL/PEG were chosen to allow a quick crosslinking (i.e : 2/25 and 2/37 mM DGL/PEG). Moreover, to boost the crosslinking velocity, precursors' solutions were heated at 37°C before injection and the tube was placed in a 50°C water bath for few seconds upon injection. Due to the presence of the tube and no biological fluids, EPH could be formed surrounding mice muscles. The construct was then placed in culture medium and incubated at 37 °C and 5 % CO_2 for 12 days to evaluate satellite cells entry inside the EPH surrounding the muscle. After 10 days, samples were fixed with PFA 4% and cut with a cryostat after their embedment in optimal cutting solution. Interestingly, a porosity could be observed in contact with tissues (Figure 56B, yellow dotted line). This stabilization of CO_2 bubbles can be the result of tissue washing with PBS, having a lower surface tension (about 40 mN/m [462]) than the blood and of boosted crosslinking velocity with temperature, pH and concentration. However, no cellular entry was observed after 10 days and we assumed that most of the cells were dead due the lack of staining after specific immunofluorescences. We hypothesized that the culture methods were not appropriate for explants as muscle fibres are generally cultured on plates coated with collagen and immersed in specific culture medium [463], [464].

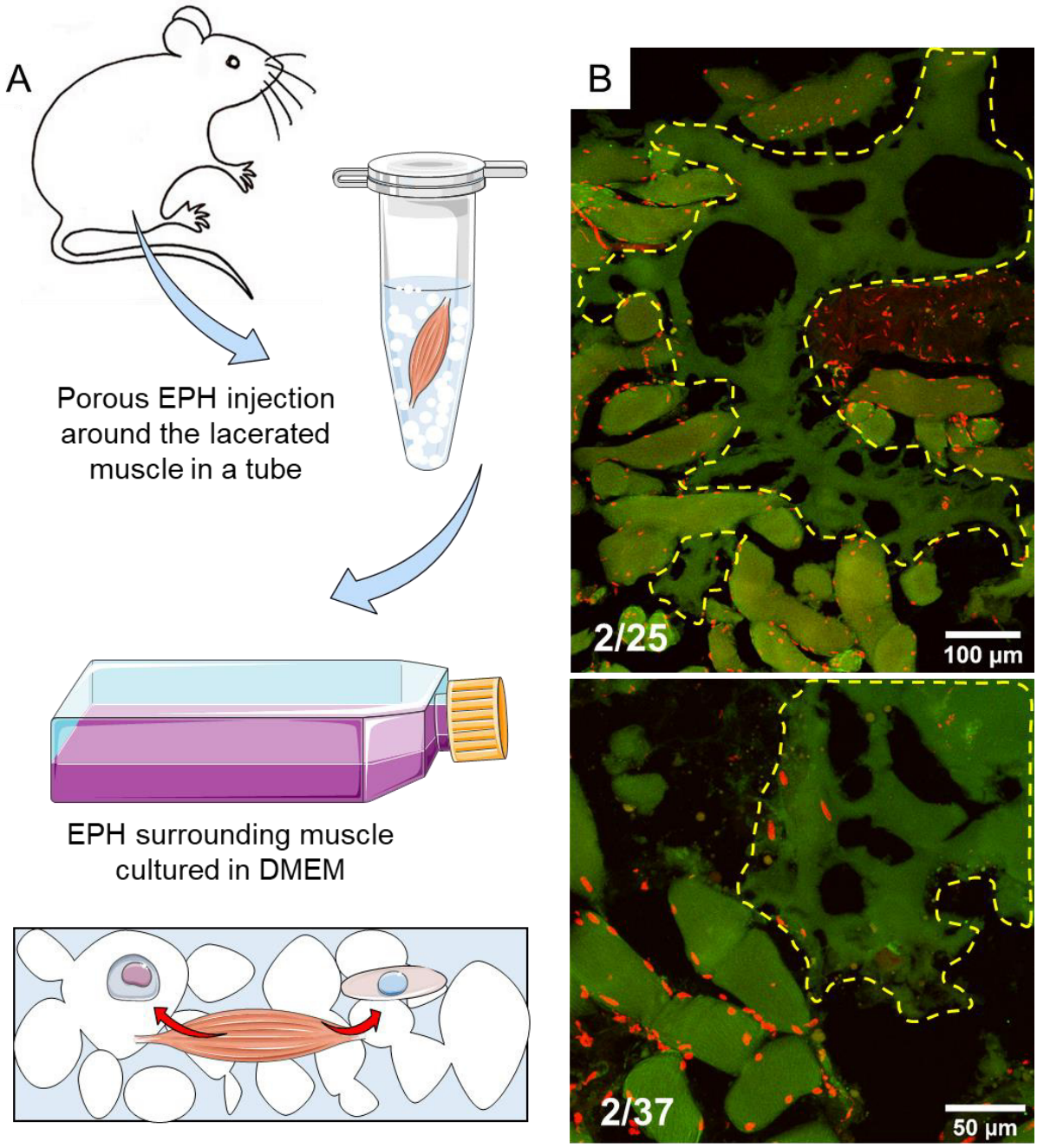

Figure 56: Ex vivo *pilot study*
A) Muscles of the hind limb were harvested from euthanized mice, rinsed with PBS and placed in a polystyrene tube. EPH of different conditions were then injected in the tube to surround the muscle. The samples (muscle + EPH) were then placed in culture medium to follow cellular entry inside EPH. Red: cell nuclei, green: actin cytoskeleton and EPH auto-fluorescence. EPH (yellow dotted line).

By boosting the crosslinking velocity of hydrogels, we demonstrated that EPH could be formed surrounding muscle inside tubes. In the future and for *in vivo* study, some conditions with higher DGL/PEG concentration (e.g 2.5/37 or 2/50) and smaller Gaa:KC molar ratio (e.g. 1.2:1 or 1.1:1 Gaa:KC) could be tested in direct contact with tissues.

CONCLUSION AND PERSPECTIVES

5 Work Conclusion, opportunities for improvement and perspectives

5.1 Conclusion

Volumetric muscle loss (VML) resulting from traumatic events or major surgical procedures represents an important socio-economic burden for western societies due to the lack of efficient treatments. Conventional strategies consisting of wound debridement and the use of muscle flaps and/or grafts are either unsubstantial or limited by major drawbacks. Innovative treatments involving the injection of cultured cells or growth factors (GF) are unrealistic approaches to treat large injuries due to low cell engraftment and survival, and GF dispersion in tissues. To overcome these challenges, tissue engineering strategies using biomaterials have been increasingly developed for tissue regeneration and look promising for functional skeletal muscle repair.

Particularly, recent treatment options for the management of skeletal muscle tissue have explored the use of biomaterials to protect and carry embedded muscle cells and/or GF in the injured site. After carrying cells, the biomaterials are used to act as a support to promote their growth, proliferation and differentiation. However, very few of these approaches have reached clinics due to the extensive legal regulations associated with the use of autologous or allogenic cells and/or the cost of GF. Considering the need for treatment, this thesis project explored the potential of acellular biomaterials able to enhance skeletal muscle tissue regeneration. The paradigm of the present work was to find an innovative way to manage complex and substantial skeletal muscle wounds by designing an optimal, raw and simple enough biomaterial able to reach the clinics easily. Particularly, the use of hydrogels, closely mimicking the high water content of native extracellular matrices (ECM), can be finely tuned to control cell fate and therefore holds significant promise.

Recently, we have developed an innovative hydrogel composed of poly-(L-lysine) grafted dendrimers (DGL) cross-linked by polyethylene glycol (PEG-NHS), which is biocompatible and has highly tailorable mechanical properties but requires a preformed porosity to be colonized with cells. The goals of this work, part of the GELIHPARBAL project, funded by the Agence Nationale de la Recherche (ANR) were (1) to develop an optimal formulation of this previously described DGL/PEG hydrogel to interact with skeletal muscle cells, to then (2) create a spontaneous porosity inside the DGL/PEG hydrogel through a novel approach compatible with its *in situ* injection. Finally, these innovative porous formulations of optimal conditions were studied with skeletal muscle cells to evaluate their potential for VML treatment.

We first identified some parameters of the DGL/PEG hydrogels that could be varied to enhance multiple aspects of skeletal muscle cells behaviour including growth, migration and myotubes formation from myoblasts. We describe here that various skeletal muscle cell types were

impacted by **substrate stiffness** and various **biochemical cues** and we showed the possibility to control resultant cellular behaviour. Muscle cell proliferation on the substrate was correlated with the stiffness while the amount of DGL had a huge influence on myoblasts differentiation and fusion. It allowed us to identify optimal DGL/PEG compositions able to sustain the growth and fusion of cells in 2D. Moreover, we identified our 'in house' elastin-like polypeptide (ELP) as a protein able to influence cellular growth and adhesion during differentiation and fusion. However, regardless of the substrate composition, the polymer network was too tight to let cells to enter the structure, restricting its use for VML treatment and evaluation of the environment in 3D. The need to create pathways inside the DGL/PEG hydrogel for cells to infiltrate the structure was thus raised.

Accordingly, in a second chapter, we developed **a porosity** inside the DGL/PEG hydrogel while **maintaining the injectable potential of liquid precursors** where many tissue-engineered constructs described in literature do not present the significant advantage of being easily transposable to direct injection [288]. We found that effervescent porous hydrogels (EPH) of versatile mechanical properties could be prepared by dissolving acetic acid and potassium carbonate to DGL and PEG solutions to generate CO_2 bubbles by effervescence. A thorough optimization of the acid-base effervescence was carried out to match the DGL/PEG hydrogel cross-linking reaction with the formation of CO_2 bubbles. The simultaneous reaction of effervescence with the DGL/PEG crosslinking enabled the entrapment of generated CO_2 bubbles inside the DGL/PEG network leading to the formation of a spontaneous, homogeneous and interconnected porosity. The porous effervescent hydrogels could be injected with a dual-chamber syringe and a static mixer due to the use of sole precursor solutions. By being injectable, the EPH conform accurately to complex shapes, which is of high interest for sizable muscle mass loss. Innovative formulations were proven non-cytotoxic and cytocompatible towards fibroblastic cells, while not inducing adverse effects on tissues. What is more, DGL/PEG EPH have been shown to maintain mechanical stability and versatility where many of the tissue-engineered scaffolds are mechanically unsuitable and fail to provide the tissue with a sufficient mechanical support [158], [330]. The porosity and injectability of the described effervescent DGL/PEG hydrogels, together with their biocompatibility and versatility of mechanical properties, open broad perspectives for various regenerative medicine or material applications.

Finally, we showed in this work that the porosity generated was suitable for a large variety of myoblast cells to grow and fuse. Regardless of the composition and stiffness used, primary myoblasts of various origins contracted inside EPH. We also demonstrated that EPH allowed cells to follow various pathways (i.e. differentiation and fusion or quiescence) in a way similar to what is described in skeletal muscle physiological regeneration. These experiments also allowed us to evaluate the effect of the 3D architecture on skeletal muscle cells providing

perspectives for the development of 3D models to study myogenesis *in vitro* and the ability for cells to follow various paths.

The parameters explored herein provide new perspectives for the study of the process of myogenesis *in vitro*, enabling us to draw conclusions on the effect of various signals on skeletal muscle cells and pave the way for further optimization to be relevant in the case of a skeletal muscle volumetric muscle loss. However, to consider using this innovative DGL/PEG EPH for VML treatment, some optimization pathways have been highlighted throughout this work to enable the translation to *in vivo* defects.

5.2 The use of EPH for VML treatments: perspectives and opportunity for improvement

To be relevant in clinical applications, DGL/PEG hydrogels need to be further optimized and evaluated. The use of effervescence raises many questions for *in situ* application due to pH variation and the generation of CO_2 bubbles inside the body.

The final application of the DGL/PEG hydrogel (i.e. VML treatment) should take into consideration the local pH variation occurring in skeletal muscle injuries. Recently Berkmann and colleagues revealed local acidification of wounds in a rat muscle model following trauma, which was maintained up to 48 hours. They described a pH of 6.89 and proposed blood vessels rupture and subsequent hypoxic conditions could cause local tissue acidification. Due to hypoxia, cells switch from an aerobic to an anaerobic energy supply resulting in lactate production and local acidification of the environment [465]. This pH acidification has been described by another group in an incision model and has been related to nociceptor sensitization and pain [466]. As discussed in chapter 2 and chapter 4 the DGL/PEG EPH should thus be adapted to cope with the pH variation experienced by skeletal muscle wounds. However, it has been shown this acidification related to wound is characterized by high inter-individual variations [465], which further complicates the establishment of a ready to use pH-related dressing applicable for all patient.

Besides, before optimizing the acid: base ratio to promote DGL/PEG EPH formulation as dressings in wound beds, we should also consider the pH effect on surrounding tissues. Both hydrogel pH and the presence of CO_2 bubbles escaping the structure could locally decrease the pH of the wounds influencing the resulting wound healing. The use of acid to help to treat wounds has been reported and reviewed [467] highlighting the major influence of pH on cells and tissue repair. The variation of local pH indeed has been related to bacterial growth and MMP behaviour in wounds [468]. For instance, MMP-2 is activated at low pH whereas its degrading effect on collagen is reached at higher pH [469]. Moreover, it has also been found that bacterial colonization in wounds is decreased in acidic conditions and its presence was related to the shift toward alkaline pH characterizing chronic wounds and delaying healing [470], [471]. These instances highlight the major effect of pH on wound repair. The use of acid-

base effervescences and CO_2 bubbles could thus be optimized to provide an adequate pH environment able to enhance or decrease some enzymatic activation and bacterial invasion. These considerations provide a step towards the development of pH-related biomaterials for wound management. Therefore, in the system described herein, the pH could have a triple coordinated effect, allowing (1) the generation of porosity inside the DGL/PEG hydrogel, (2) the modulation of the cross-linking degree and mechanical properties of the material to match the need of the targeted tissue while (3) enhancing specific enzyme activation and activity to promote tissue healing.

Another parameter that we should explore is the local hypoxia that the CO_2 bubbles escaping the structure could trigger in the very first hours following injection. Oxygen plays a prominent role in the healing process. When considering the adequate moment in which injecting this new formulation we should consider the hypoxia and the pH modification due to the CO_2 bubbles escaping the structure. Moreover, the use of effervescently generated porosity inside DGL/PEG hydrogel could provoke ischemia via the volume expansion, which could be related to hypoxia and fibrosis development. Nevertheless, in this work, no ischemia could be observed after subcutaneous injection of EPH of various conditions. This should be carefully evaluated for in vivo evaluation in a muscle defect.

Finally, the stiffness modulation of cross-linked DGL/PEG hydrogels was not studied in this work and should be discussed for optimization. In the context of skeletal muscle regeneration, ECM stiffness has been shown to vary during repair with a muscle apparent modulus increase in the first 3 days following injury [472]. This increase has been related to type I and type VI collagens, laminin, and fibrin deposition as well as fibrin clot formation [472] and collapsed myofibres that exhibit a higher stiffness [473]. Consequently, while a transient ECM stiffening plays a role in the early stage of differentiation to trigger satellite cell proliferation and commitment, a softer stiffness, close to the native tissue is better for subsequent myotubes maturation. It is therefore of utmost importance to match the stiffness of a regenerative skeletal muscle tissue which might be different from a mature one, and that could evolved during the regeneration time course. This may set conflicting requirements for the scaffold stiffness.
An interesting way to modulate the elasticity of the material to match the tissue regeneration would be through its gradual degradability *in vivo*. To be optimal, the *in vivo* degradation rate should match the tissue regeneration pace to favour alignment of new muscle fibres and recover the tissue homeostasis. However, it should not degrade too fast to act as a mechanical support for cells and the whole tissue during regeneration. The DGL/PEG hydrogel degradation has been studied in our laboratory in acidic, alkaline and neutral medium showing a mass decrease of hydrogel immersed in alkaline solutions [378]. Moreover, a slight degradation of subcutaneously implanted DGL/PEG hydrogel was observed by macrophages for all conditions after three weeks of implantation (chapter 2 and [373]). These results suggest the injectable and porous DGL/PEG hydrogel could be degraded inside the body, resulting in

customization of the resulting porosity by cells *in situ*. To answer that question, the DGL/PEG EPH need to be evaluated in a muscle defect *in vivo* over long implantation periods.
To answer all of the aforementioned questions and to study DGL/PEG EPH potential to sustain myogenic differentiation while avoiding fibrosis, some efforts have been made during the thesis on the establishment of *in vivo* procedures detailed below.

5.2.1 Perspective: *in vivo* evaluation

The next crucial perspective of the work is the ***in vivo* evaluation of the myogenic potential** of the EPH in a muscle defect. The *in vivo* study will give us preliminary data to (1) validate the potential of EPH for VML treatment and (2) find the optimal conditions.

The first step would be to optimize and improve the injected formulation to bind to muscle defects margin while remaining porous and having no deleterious effect on tissues as discussed previously. Once the EPH is optimized, a relevant animal model should be chosen. During the thesis, a preliminary *in vivo* project application was written. We selected the rat tibialis anterior (TA) model to perform the defect (Figure 57A). The rat was chosen given defect volume at least 10 times greater than in the mouse [124], which are too small to match the volumes required by the dual-chamber syringe/static mixer system (at least 100-200 µL). Moreover, the TA was chosen due to previous attempts for standardization reported in literature (Figure 57B) [124]. The EPH evaluation could be conducted on the 3 various DGL/PEG conditions to highlight the effect of the stiffness and the molar ratio *in vivo*. The contralateral TA of each rat could be used as a healthy control for each sample studied. A positive control could be made by producing the VML defect and placing back the minced tissue to the defect. The skeletal muscle tissue has indeed been shown to recover its functionality and produce controlled force after complete removal, mincing and placing back into the defect in small animal models [474], [475]. A negative control could be generated by letting the defect empty to create fibrosis and study the loss of functionality.

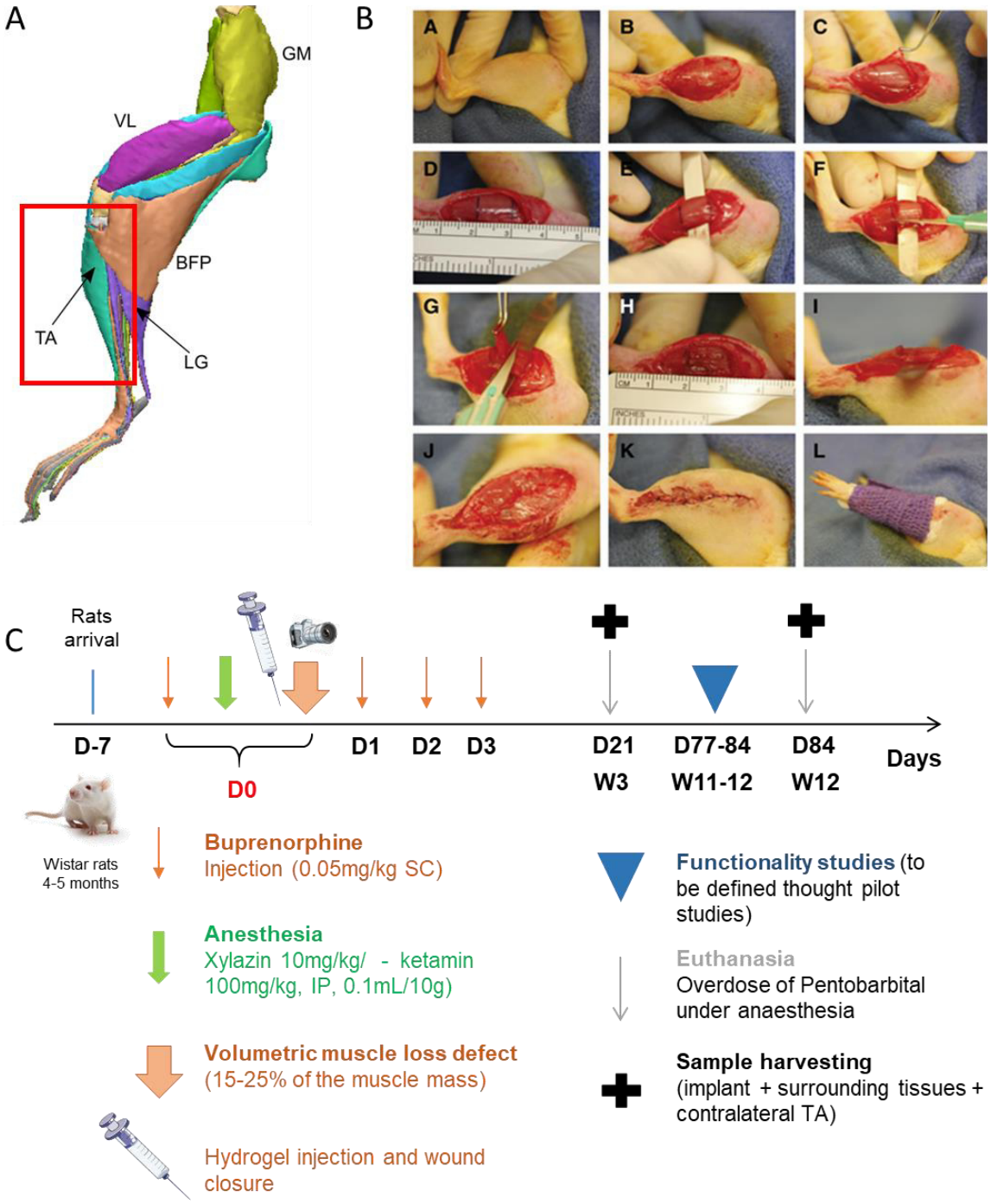

Figure 57: In vivo *study designed for the evaluation of various EPH condition potential for skeletal muscle functional regeneration.*
A), B) The rat tibialis anterior (TA) muscle was chosen as a well-described volumetric muscle loss model characterized by a loss of functionality. C) In vivo experimental planning for the assessment of EPH ability to sustain functional muscle regeneration (D: days, W: weeks).
A) BFP: Biceps femoris posterior, LG: Lateral Gastrocnemius, GM: Gluteus Maximus, TA: Tibialis Anterior, VL: Vastus Lateralis. Adapted from Charles et al., Plos One, 2016 [476] *and B) adapted from Wu et al., Bioresearch open access, 2012* [124].

A study with two various time points has been designed so far. We decided to perform an early time point 3 weeks post-implantation to validate EPH efficacy in inherently favouring muscle regeneration over fibrosis. Three weeks post-injury is the moment when the anti-inflammatory process should be settled and, if not, when fibrosis can occur [477]. In addition to inflammation, the cross-section area (CSA) in µm² of muscle fibres after 3 weeks could be reported in comparison with the contralateral TA and controls to identify the best conditions. The fibrotic tissue could also be quantified as the area covered by collagen and fibronectin on cross-sections.

Previous studies have reported a functional recovery of defects in rat TA after 12 weeks of implantation of a scaffold [124], [248]. Given these considerations, we decided to define the last time point 12 weeks post-surgery to assess the functionality of the neo-formed tissues and study cell types present inside hydrogels. Extensive work should be dedicated to the establishment of protocols allowing to quantify the functionality of neo-formed tissues (catwalk, forces development, elasticity and fatigability *ex vivo*). Functionality tests (especially catwalks) should consider the huge extensor digitorum longus muscle (EDL) compensatory effect experienced on the whole hind limb functionality. To overcome these drawbacks, some research groups have measured the contractile and passive mechanical properties of TA and EDL muscles separately in mice [478] while others have evaluated the TA contribution on rat dorsiflexion of the foot [479]. However, these measures need the use of specific apparatus (Aurora scientific *in situ* muscle test system). Regardless of the functionality test, the negative control (defect left empty) and the positive control (defect filled with minced muscle) should be carefully characterized to find appropriate functional tests and define the limits of the study. Then, the formed tissue should be evaluated histologically to validate the presence and orientation of new-formed muscle fibres (staining for myosin protein family), fibrotic tissue (type I collagen), vascularization (α-SMA, CD31, type IV collagen) and neuromuscular junctions (specific β tubulins, AchR).

Special attention should as well be given to the degradation of the hydrogel after 3 and 12 weeks of implantation, to assess the pro-inflammatory M1 macrophage ability to phagocyte hydrogels.

If the EPH potential is validated by the *in vivo* study, some effort could be made to convert the hydrogel as a ready-to-use device. To do so, it is necessary to find a way to guarantee sterility during injection, assembly and charging of the dual-chamber syringe to meet the requirements of clinical applications. A system that could generate a robust large-volume application *in situ* is the central hurdle in this material design. An operant system in microscale *in vitro* or *in vivo* may not necessarily perform on a larger scale in a human model. Injectable hydrogels are currently in use for minimally invasive surgery, but the design parameters for large-volume expensive hydrogel remain unclear and need to be addressed for the DGL/PEG EPH.

5.3 EPH potential as *in vitro* model to study myogenesis: perspectives and opportunity for improvement

In addition to being pertinent for wound management, EPH are an interesting model to study cells within a 3D structure *in vitro*. The use of well-refined hydrogels mimicking skeletal muscle tissue microenvironment combined with relevant myogenic progenitor cells could be used as *in vitro* pre-clinical models. Moreover, the stiffness versatility of EPH and the biochemical cues present at their surface is a way to recreate various environments. It represents thus a very promising 3D model to study different signals on myoblast cell behaviour.

For instance, innovative EPH could be relevant to evaluate the impact of the 3D structure on reserve cells self-renewal. The satellite cell niche has been extensively described in terms of ECM composition and signalling but barely in terms of 3D architecture and EPH structure could provide new insights. Moreover, the ability for differentiated cells to contract and produce force may be quantified as a way to study the environment on cell behaviour. Therefore, some improvement could be done on the establishment of protocols to measure forces and tension generated by cells to evaluate different treatments on their contractibility. To do so, EPH with cells could be recorded with high-resolution cameras or could be attached to stainless steel wires connected to tension transducers [480].

Some efforts could also be made on EPH electrical and/or mechanical stimulation. It has been shown that skeletal muscle cells embedded inside fibrin biomaterial exhibited better maturity along with enhanced scaffold alignment when mechanically stimulated [481]. As previously discusses, the main guideline in designing a scaffold for *in vitro* skeletal muscle tissue construct is the organization and particular alignment of muscle fibres. Further improvements could be sought to enable the formation of long, thick and self-organized contractile units. Therefore external stimulation of EPH could result in their porous structure deformation favouring cell alignment. In addition, it could be considered to include vasculature and/or neuronal innervation to further enhance myotubes maturation towards contractile muscle fibres.

5.3.1 Perspective: molecule release

In addition, these bioengineered hydrogels could act as a platform to screen drugs, cells or therapeutic genes for treating inherited muscle diseases. The identification of specific factors that can positively affect muscle function (contraction, RC proportion, etc…) could lead to novel therapies for patients. Some instances of 3D bioartificial muscles (BAM) elaborated for screening purposes from primary myoblasts have allowed researchers to demonstrate IGF-1 triggers hypertrophy and an increase of active force on contractile muscle cells. [482]

Therefore, the development of a controlled release of molecules from DGL/PEG EPH could be investigated. Preliminary studies have been conducted during the thesis on the incorporation

of proteins inside dense DGL/PEG hydrogels to study their release over time (Figure 58). To do so, DGL/PEG hydrogels of various conditions have been formulated in solutions containing proteins (lysozyme and BSA) before being immersed for 21 days in PBS 1X. Molecule delivery from hydrogel networks has been monitored over time using a protein quantification assay (BCA). Interestingly, these preliminary results indicate that the release of molecules of interest can be controlled through both mesh size and amount of DGL, while preserving their activity.

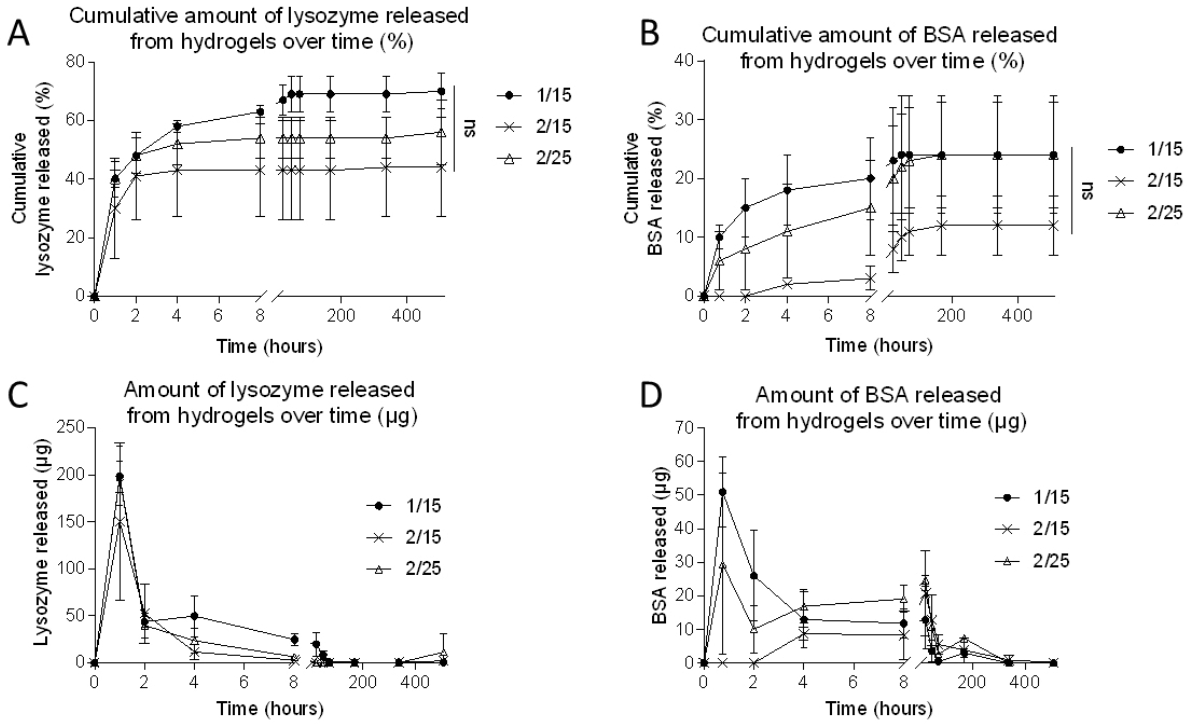

Figure 58: Molecule release from DGL/PEG hydrogels of various conditions.
DGL/PEG hydrogels of various conditions were formulated with lysozyme and BSA
Cumulative amount (%) of A) lysozyme and B) BSA released over time. Amount (µg) of C) lysozyme and D) BSA release for each time point from hydrogel of various DGL/PEG concentrations and ratios (1/15; 2/15 and 2/25 mM DGL/PEG representing DGL: PEG molar ratios of 1:15; 1:7.5 and 1:12 respectively).

Consequently, the hydrogel could be an important tool for biological studies of myogenesis and the identification of specific factors for the treatment of pathologies through controlled release of active proteins.

In addition to be relevant as 3D model platform, molecule release could provide specific bioactivity to EPH to favour myoblasts over fibrotic scarring for VML treatment. Enhancing SC entry, migration and proliferation while alleviating the proliferation of fibroblasts and their differentiation into myofibroblasts through regulators of IGF-I, HGF or SDF-1α appears relevant. Moreover, counteracting the detrimental effect of excessive or deficient TGF-β signalling has many important clinical implications for tissue repair. Future work could focus on the optimization of DGL/PEG hydrogel concentration and ratio to meet the requirement of

muscle wound management in terms of GF release over time. This could be part of the *in vivo* study.

5.3.2 Towards other tissues and organs

Considering that the study aimed to explore the potential of the DGL/PEG hydrogel for muscle tissue regeneration, skeletal muscle cell response to the hydrogel was the primary focus. However, different cell types were able to grow on the hydrogel indicating a broader potential application range. Therefore, the DGL/PEG hydrogel could be adapted to interact with other cell types. For instance, the cardiac tissue has been studied given the cardiomyocytes spontaneously contraction when cultured *in vitro*. We demonstrated human induced pluripotent stem cell (iPSC) derived cardiomyocytes recovered their ability to contract after two days within EPH of various conditions (Annex 1, supplementary movies 13 and 14). After 5 days on EPH of different conditions, iPSC derived cardiomyocytes exhibited specific α-actinin striation visible in primary cardiomyocytes.

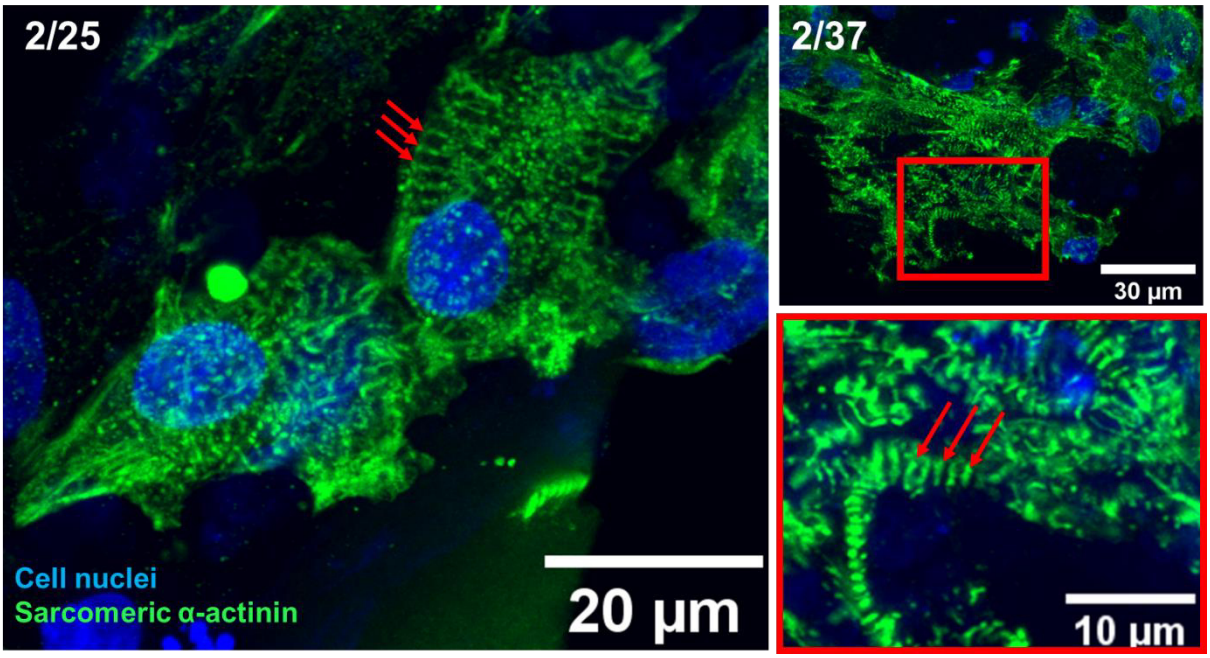

Figure 59: Human iPSC derived cardiomyocytes inside EPH of various conditions
Human iPSC were differentiated on matrigel coatings for 19 days following the STEMdiffTM cardiomyocytes differentiation kit from Stemcell. Cells were then detached from matrigel coatings and seeded on EPH of various conditions (i.e. 2/25 and 2/37 mM DGL/PEG) for 5 days.
Two days post-seeding, cells were able to contract. Five days post-seeding, immunofluorescences were performed and specific striation characterizing cardiomyocyte cells were observed (alpha-actinin staining, red arrows).

These results open up new perspectives for the use of DGL/PEG EPH as 3D models for other cell types.

Overall, the effervescent method described herein provides a basis for the synthesis of macroporous multifunctional and highly tuneable hydrogels with direct *in vivo* injectable potential for broad tissue engineering applications.

ANNEXES

1 Supplementary information

Supplementary information 1:

Link for movies: https://figshare.com/s/dfdfa8cf5f19c8d9771b

Supplementary information 2: C2C12 cells 30 hours post seeding as a function of DGL/PEG hydrogel concentration and ratio (mM DGL/PEG) - all condition studied

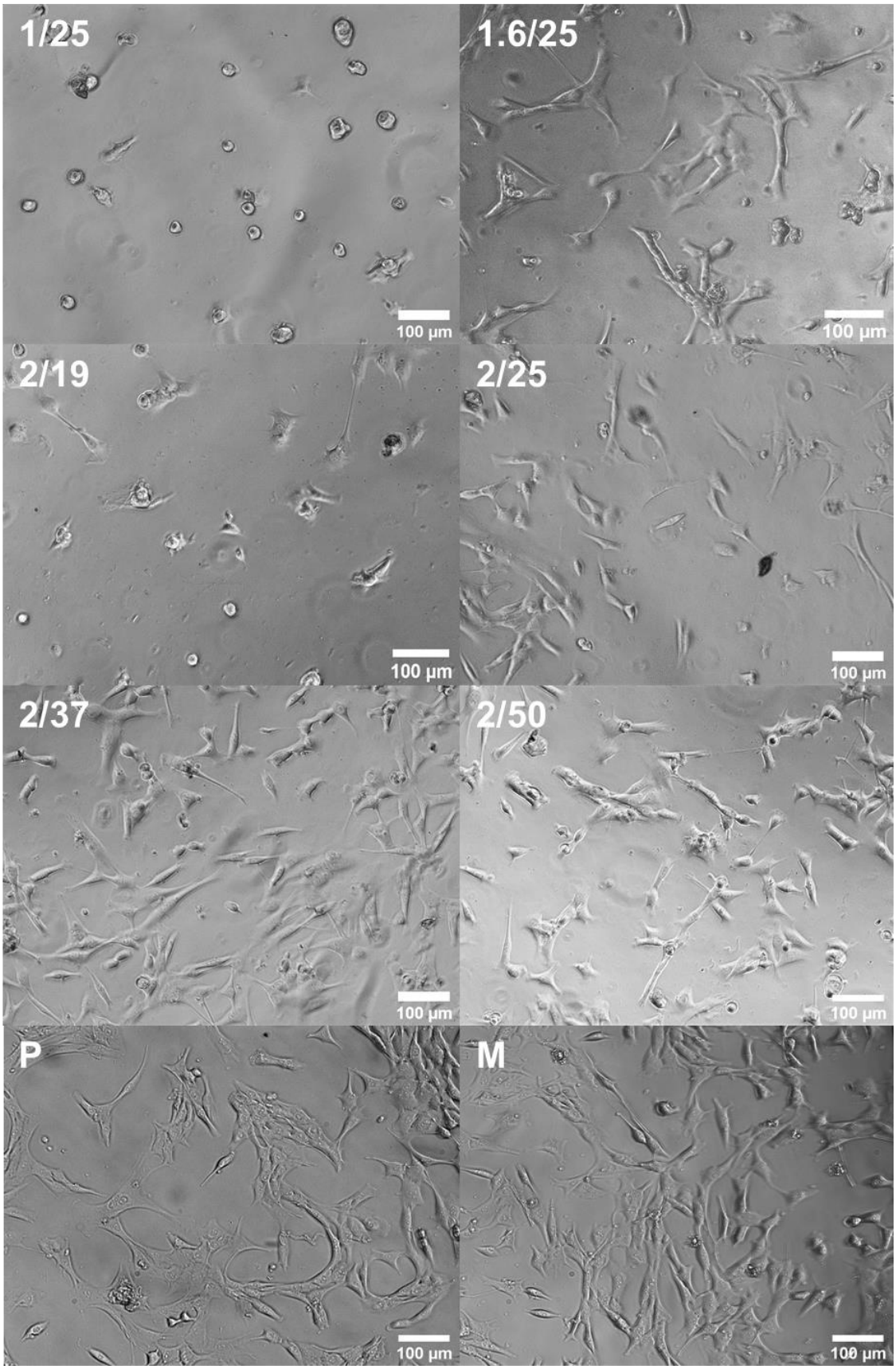

Supplementary information 3: Immortalized human myoblasts 30 hours post seeding as a function of DGL/PEG hydrogel concentration and ratio (mM DGL/PEG) - all condition studied

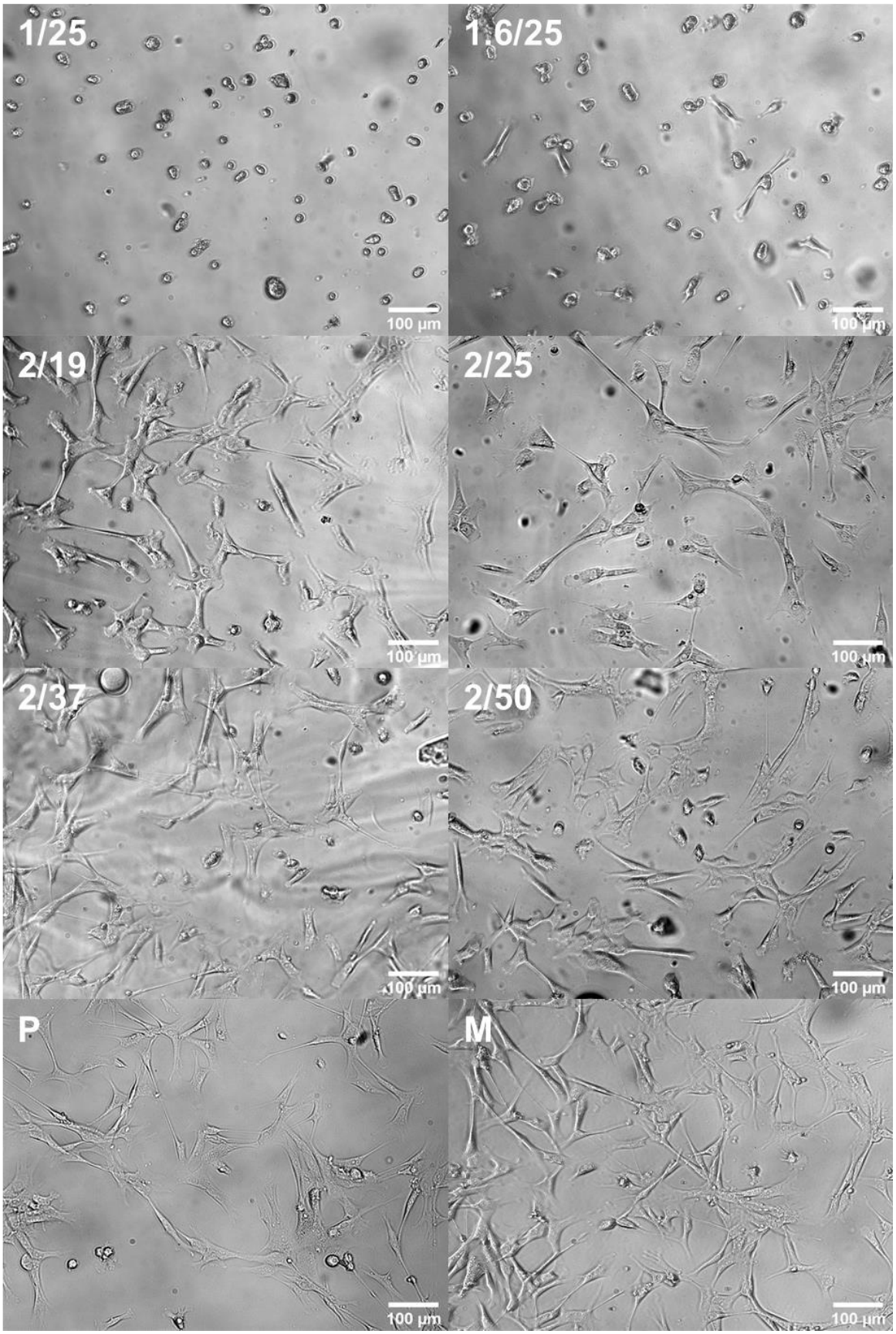

Supplementary information 4: Figure 43 expanded. Injection of various EPH conditions in sub-cutaneous pockets in mice.
Masson's trichrome staining of the full porous explants after 3 weeks implantation and close-ups highlighting hydrogel (#), the fibrous capsule (red dotted line), synthetized collagen (red arrow), fibroblasts (+) and blood vessels (*). EPHs formulated with 1.33:1 Gaa:KC molar ratio, 3.3 % Pluronic® F-68 and directly injected in sub-cutaneous pockets.

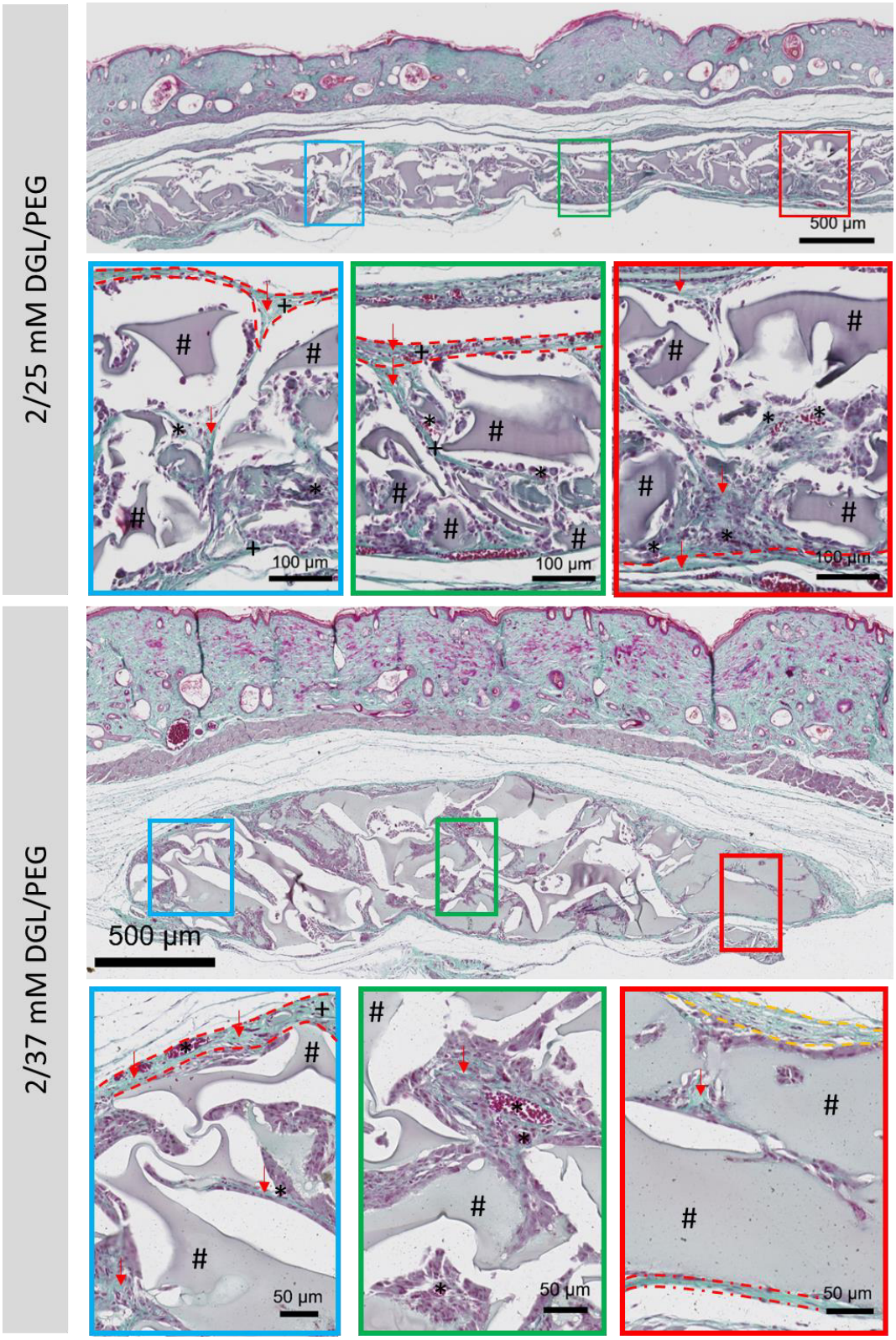

Supplementary information 5: Figure 43 expanded. Injection of various dense DGL/PEG conditions in sub-cutaneous pockets in mice.
Masson's trichrome staining of the full explants after 3 weeks implantation and close-ups highlighting hydrogel (#), the fibrous capsule (red dotted line), synthetized collagen (red arrow), fibroblasts (+) and blood vessels (*). Dense DGL/PEG hydrogel formulated in PBS.

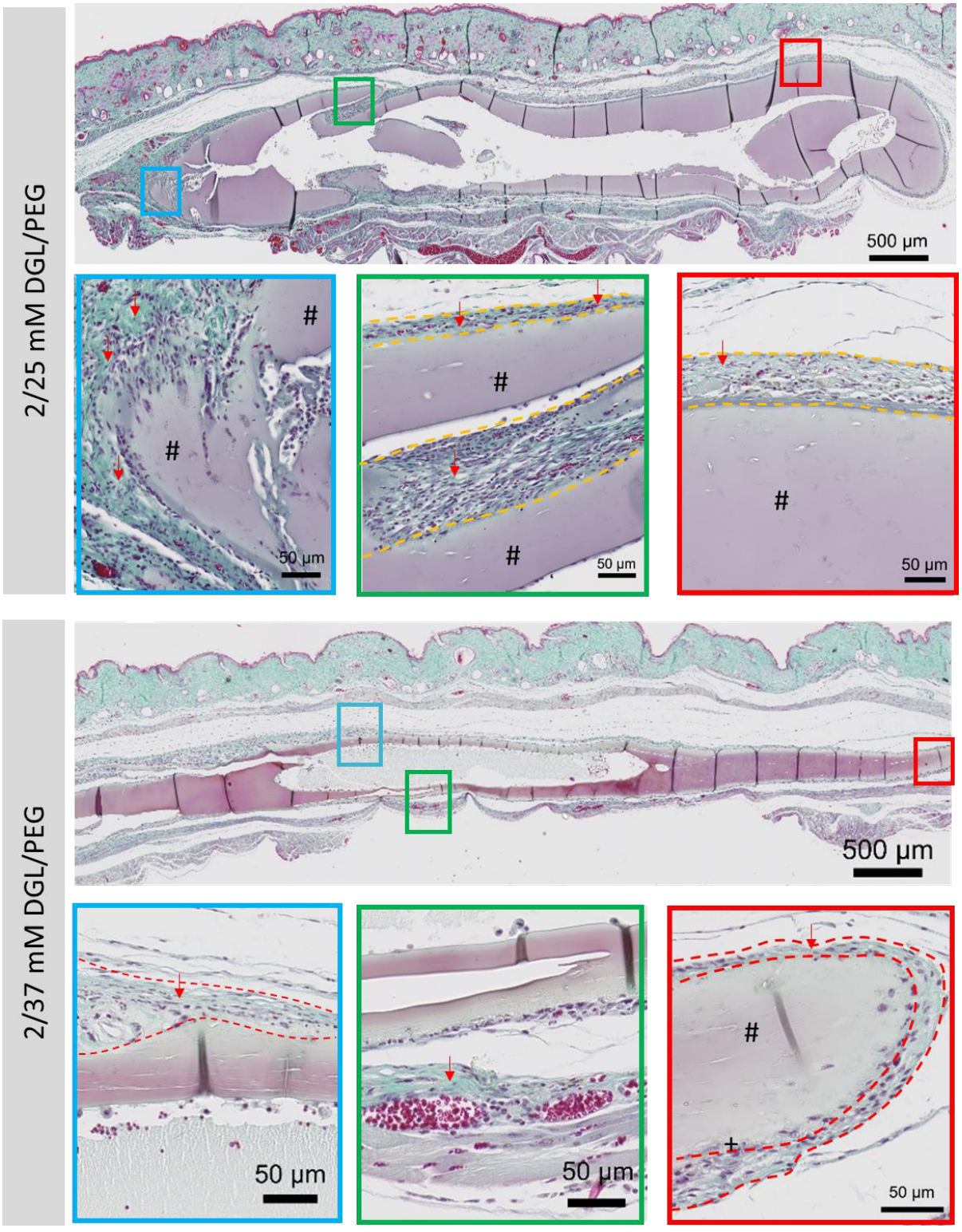

Supplementary information 6: Figure 47 expanded. Implantation of various EPH conditions in sub-cutaneous pockets in mice. Masson's trichrome staining of the full explants after 3 weeks implantation and close-ups highlighting hydrogel (#), the fibrous capsule (black dotted line), macrophages ($), synthetized collagen (red arrow), fibroblasts (+) and blood vessels (*) EPH formulated with 1.33:1 Gaa:KC molar ratio, 3.3 % Pluronic® F-68, injected inside a tube to be cut and implanted in sub-cutaneous pockets.

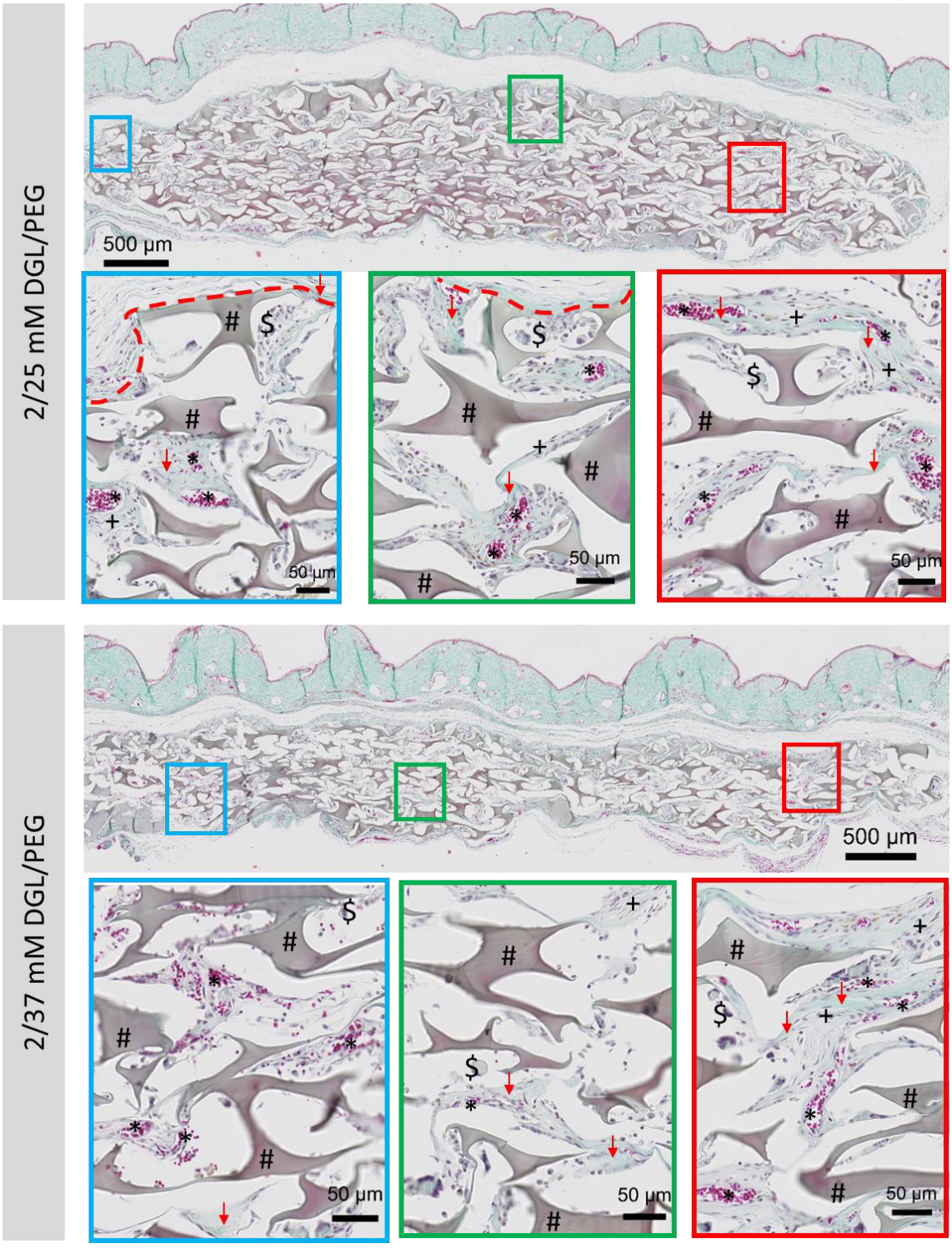

Supplementary information 7: Figure 47 expanded. Implantation of various EPH conditions in sub-cutaneous pockets in mice. Type IV collagen staining of the full explants after 3 weeks implantation and close-ups highlighting hydrogel in blue (#) and blood vessels in red (*). EPH formulated with 1.33:1 Gaa:KC molar ratio, 3.3 % Pluronic® F-68, injected inside a tube to be cut and implanted in sub-cutaneous pockets.

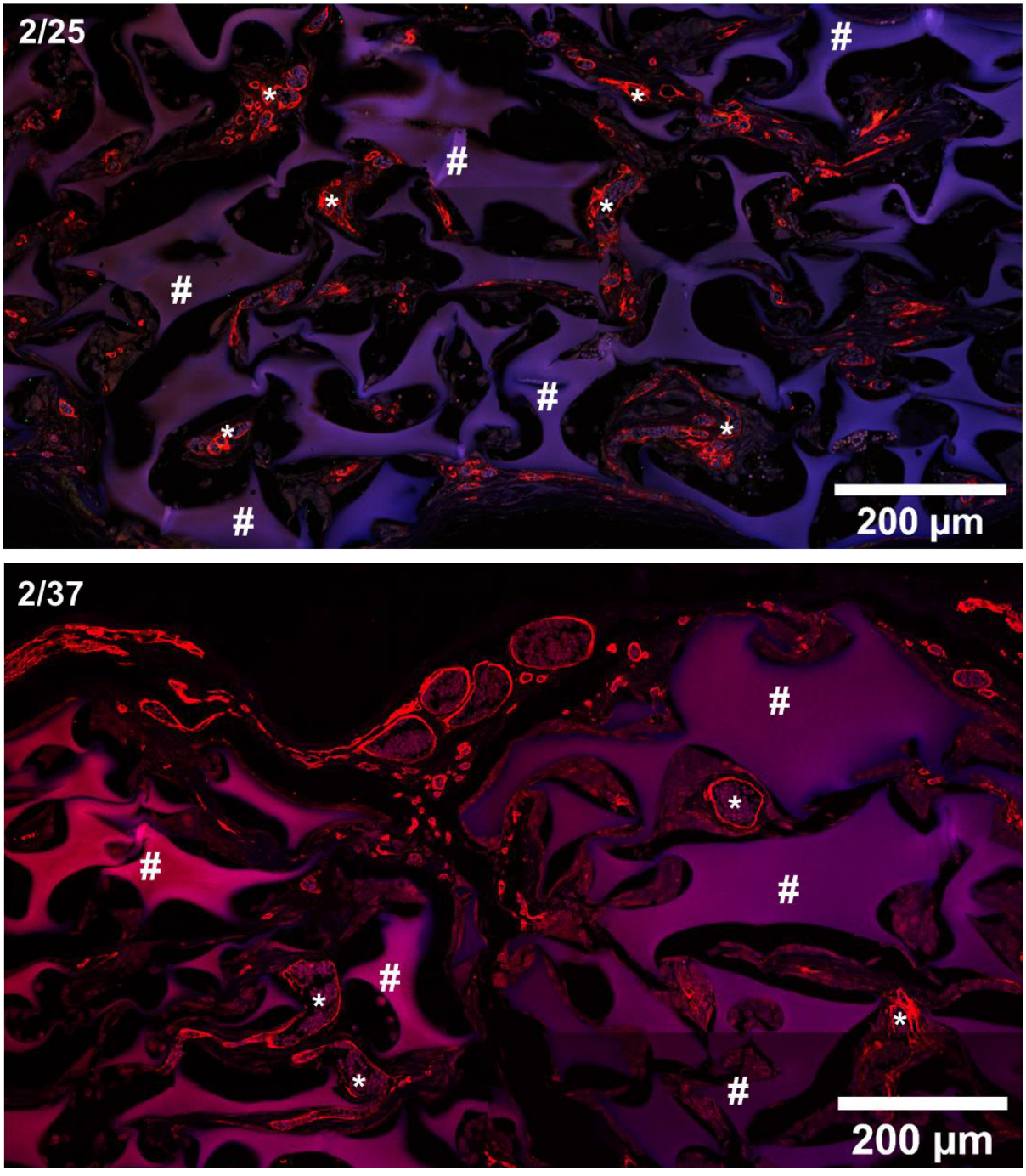

Supplementary information 8: Figure 47 expanded. Implantation of various EPH conditions in sub-cutaneous pockets in mice. Macrophages presence in implanted EPH of various conditions. F4/80 staining of the explants after 3 weeks implantation (macrophages membrane in brown) and close-ups highlighting hydrogel (#) and macrophage presence (orange arrows). Giant cells were also visible (green arrows). EPHs formulated with 1.33:1 Gaa:KC molar ratio, 3.3 % Pluronic® F-68, injected inside a tube to be cut and implanted in sub-cutaneous pockets.

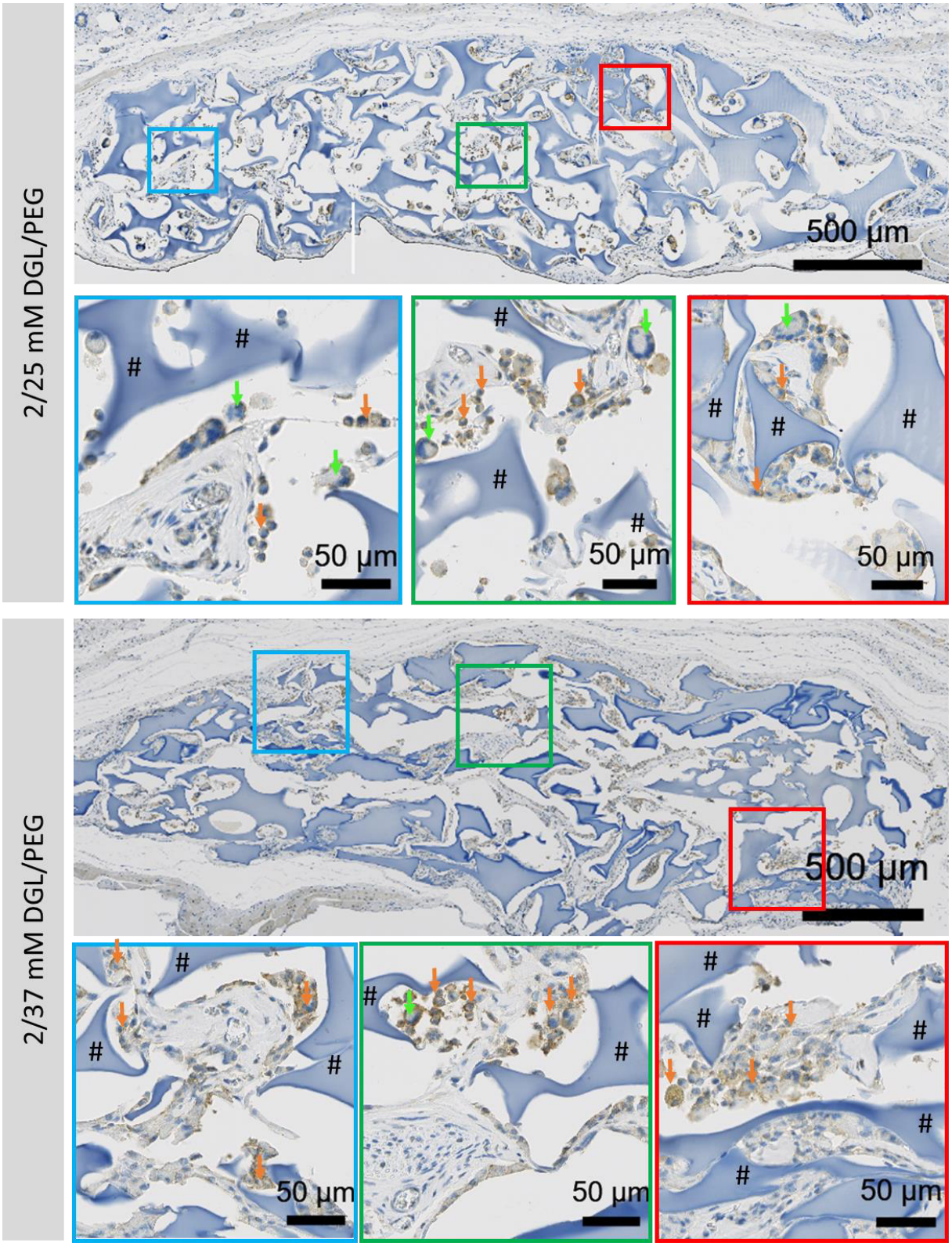

Supplementary information 9: C2C12 cells and primary human myoblasts (pHMs) 6 days post differentiation on 3D effervescent porous hydrogels (EPH) of the same condition or on matrigel coatings. The figure shows a particular alignment of pHMs inside 3D EPH not visible when cultured in 2D on matrigel.

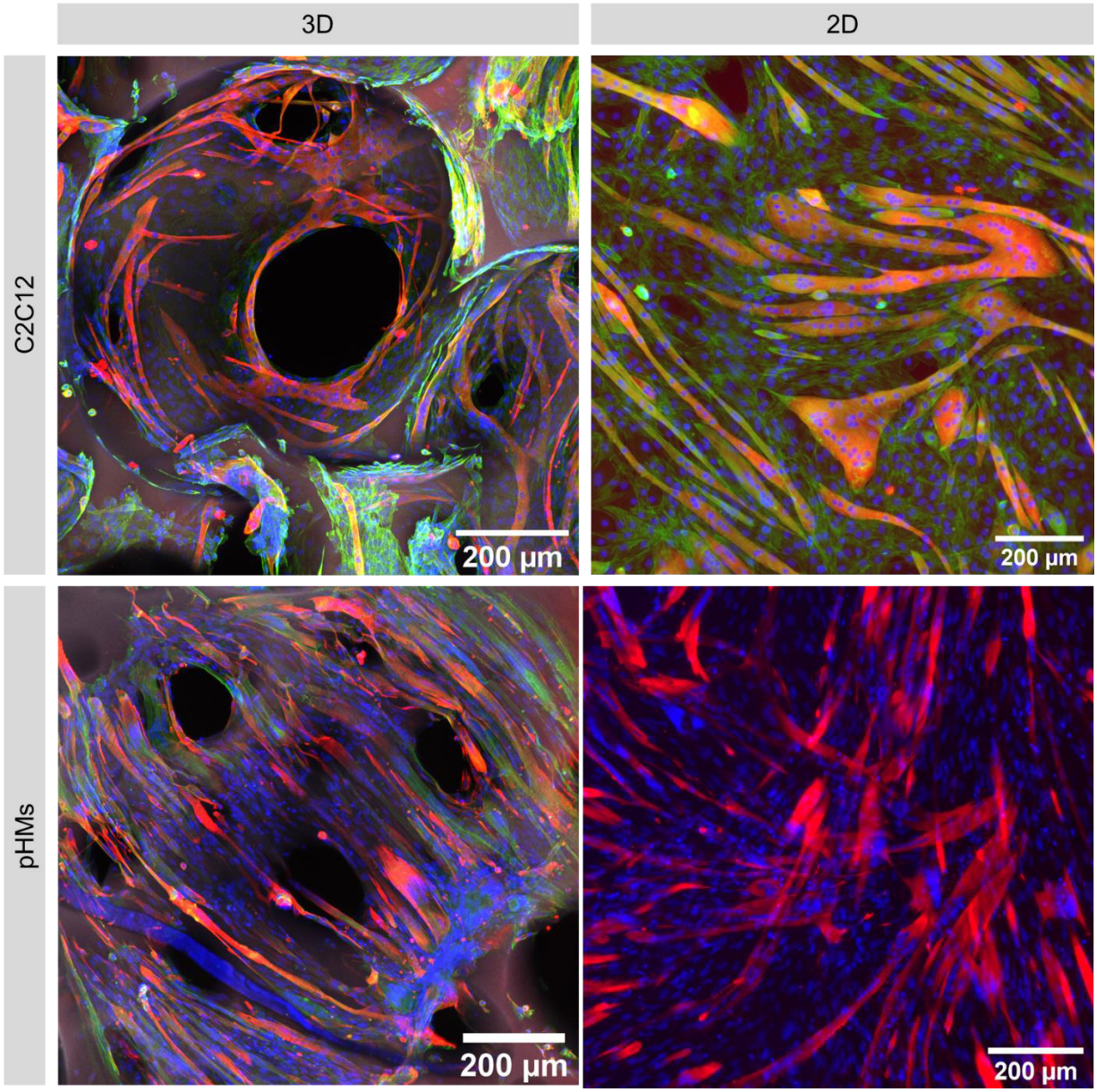

2 Encadrement pédagogiques d'étudiants ingénieurs

- Stage de 6 mois assistant ingénieur : « Formulation et caractérisation d'hydrogels poreux injectables par effervescence pour l'ingénierie tissulaire » Février-Juillet 2019 par **Clémence Drouglazet**, Université de technologie de Troyes (UTT), spécialité Matériaux technologie et environnement Troyes, France

- Stage de 6 mois à mi-temps, projet de fin d'étude : « Formulation et caractérisation d'hydrogels pour application en ingénierie tissulaire » Septembre-Janvier 2019-2020 par **Baptiste Robbiani**, Institut national des sciences appliquées (INSA), spécialité Sciences et génie des matériaux, Lyon, France

- Stage de 6 mois assistant ingénieur : « Hydrogels poreux injectables : développement et évaluation biologique » Février-Juillet 2020 par **Héloïse Le Goff**, Université de technologie de Troyes (UTT), spécialité Matériaux technologie et environnement Troyes, France

3 Communication

Oral communications

National

L.Griveau, E.Christin, A.Berthier, V.Gache,R Debret, J. Sohier : "Injectable, porous and haemostatic hydrogel for guiding functional muscle repair" Flash presentation at the 'GDR Réparer l'humain' French national research consortium on cellular-microenvironment interfaces – *Lyon France* – December 2018

L.Griveau, E.Christin, C.Drouglazet, A.Berthier, R.Debret, V.Gache, J.Sohier: "Design of an injectable and porous hydrogel for biomedical applications". Third French national BIOMAT congress - Materials for Health - *La Grande Motte, France* - June 2019

International

L.Griveau, E.Christin, C.Drouglazet, A.Berthier, R.Debret, V.Gache, J.Sohier: "Design of an injectable and porous hydrogel as a support for skeletal muscle repair". Tissue Engineering and Regenerative Medecine International Society (TERMIS-EU) *Rodos Greece* - May 2019

L.Griveau, E.Christin, H.Le-Goff, R.Debret, V.Gache, J.Sohier*: "*An injectable and porous hydrogel with potential as a support for functional skeletal muscle regeneration". World biomaterial Congress (WBC 2020) – *virtual* December 2020

L.Griveau, H.Le-Goff, C.Drouglazet, B.Robbiani, M.Lafont, C.Le-Visage, P.Weiss, R.Debret, J.Sohier: "Design and characterization of an injectable and porous hydrogel for biomedical applications". World biomaterial Congress (WBC 2020) – *virtual* December 2020

Poster Presentations

L.Griveau, C.Drouglazet, R.Debret, J.Sohier. "Design of an injectable and effervescent porous hydrogel as support for tissue regeneration". 30th Annual Conference of the European Society for Biomaterials (ESB) *Dresden Germany* – September 2019

L.Griveau, C.Drouglazet, R.Debret, J.Sohier. "Design of an injectable and effervescent porous hydrogel as support for tissue regeneration". Twenty-fourth scientific day of doctoral School (EDISS) – Villeurbanne, France - November 2019

L.Griveau, E.Christin, J. Sohier, R.Debret, V.Gache. "Design of an innovative hydrogel as support for functional skeletal muscle regeneration". Seventeenth congress of the French society of myology – *Marseille France* – November 2019

Awards

Award for the best flash presentation – 'GDR Réparer l'humain' French national research consortium on cellular-microenvironment interfaces – *Lyon France* – December 2018

Award for the best poster presentation at the 24th Doctoral school (EDISS) scientific day - *Lyon France* – November 2019

Award for the best microscopic picture (IBCP photo contest 2019, 25th doctoral school scientific day, 2020 and ibidi photo contest for 2021 calendar)

DESIGN OF AN INJECTABLE AND EFFERVESCENT POROUS HYDROGEL AS SUPPORT FOR TISSUE REGENERATION

Louise Griveau[1,2], Clémence Douglazet[1], Romain Debret[2], Jérôme Sohier[1]
[1]MATEIS, CNRS UMR5510, Lyon, France ; [2]LBTI CNRS UMR5305, Lyon, France
louise.griveau@ibcp.fr

INTRODUCTION

Hydrogels are promising materials for the repair of damaged tissues as they can be injected in wounds with a perfect fill. However, injected hydrogels must be *in fine* colonized by cells and the regeneration potential of implanted hydrogels is dependent on porosity to allow cell infiltration [1][2]. Therefore, it would be of interest to create porosity in hydrogels during or after injection.

We have recently developed a hydrogel composed of poly-lysine dendrimers (DGL) cross-linked with polyethylene glycol (PEG), which has highly tailorable mechanical properties and is biocompatible but lack inherent porosity and is therefore non injectable as such [3].

The aim of this study was therefore to investigate the possibility of creating a spontaneous porosity inside DGL/PEG hydrogels through an **effervescent approach**, which would be suitable with injection.
We further evaluated the cyto-compatibility of the resulting porous hydrogels in view of tissue engineering applications.

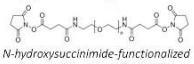

EXPERIMENTAL SECTION

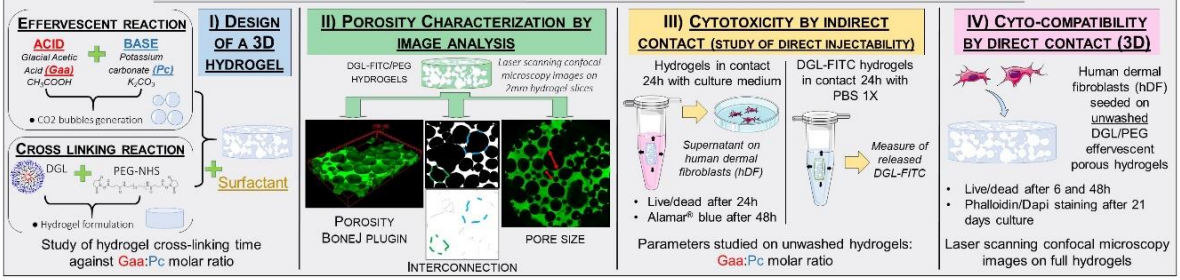

RESULTS & DISCUSSION

I) DESIGN OF AN EFFERVESCENT POROUS HYDROGEL

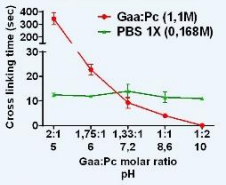

- Effervescent reaction final pH is linked to Gaa:Pc molar ratio
- Hydrogel cross-linking time is strongly impacted by pH at high ionic strength

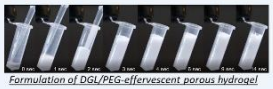

- A range of Gaa:Pc ratios can be tuned to allow effervescence **concomitantly** to hydrogel cross-linking

→ **An interconnected** porosity can be created, remnant of the effervescently-generated CO_2 bubbles

II) POROSITY CHARACTERIZATION

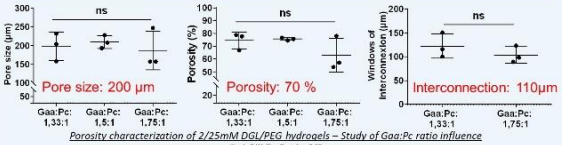

- Pore size & porosity values together with clear interconnection between pores comfort DGL/PEG-effervescent porous hydrogel potential as a support for tissue regeneration [4],[5]
- Gaa:Pc molar ratio does not impact porosity → opens technical options for *in situ* injection since the time when precursors are in a liquid form can be modulated

→ Possibility to use the DGL/PEG effervescent porous hydrogel as a **3D support for cells ?**

III) CYTOTOXICITY BY INDIRECT CONTACT

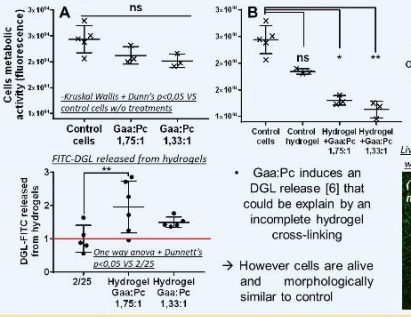

→ Gaa:Pc has no effect on cells metabolic activity while porous hydrogel does

- Gaa:Pc induces an DGL release [6] that could be explain by an incomplete hydrogel cross-linking

→ However cells are alive and morphologically similar to control

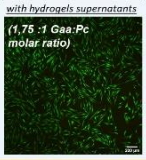

→ **No cytotoxicity** of the effervescent porous hydrogels, but decrease in cell metabolic activity
→ **Validation** of the use of Gaa&Pc as porogens **for *in situ* injection**

IV) CYTO-COMPATIBILITY BY DIRECT CONTACT (3D)

- High cells viability & adherence to the unwashed DGL/PEG effervescent porous hydrogel after 6h
- Cells spread-out and enter the structure after 48h

- Cells fill the pores and have an organization inside pores after 21 days

→ **Validation** of the potential of DGL/PEG porous hydrogel **as 3D support** without any washing or post-formulation treatment

Louise Griveau

PhD Student – UCBL
2nd year
louise.griveau@ibcp.fr

REFERENCES

[1] Annabi et al., Tissue Eng Part B Rev. 2010 Aug;16(4):371-83
[2] Hutmacher et al J Biomater Sci Polym Ed. 2001;12(1):107-24
[3] Debret et al. patent WO2017EP6151
[4] Zeltinger et al, Tissue Eng. 2001 Oct;7(5):557-72
[5]Jana et al., Adv Healthc Mater. 2013 Apr;2(4):557-61
[6] Lorion et al J Biomater Sci Polym Ed. 2014;25(2):136-49

ACKNOWLEDGMENTS

The French ANR is acknowledged for financial support.
AGENCE NATIONALE DE LA RECHERCHE
ANR
GELIHPARBALANR-17-CE19-0009

CONCLUSION & PERSPECTIVE

- **A spontaneous and interconnected porosity** inside a DGL/PEG-NHS hydrogel could be induced **through an effervescent approach.**
- **Cells viability & behavior comfort** potential for ***in situ* injection**
- **On-going experiments** focus on the **cellular colonization** of the interconnected porous hydrogels and their **potential to support extracellular matrix synthesis.**

DESIGN OF AN INNOVATIVE HYDROGEL AS SUPPORT FOR FUNCTIONAL SKELETAL MUSCLE REGENERATION

L.Griveau[1,3], E.Christin[2], J. Sohier[3], R.Debret[1], V.Gache[2]

[1]LBTI CNRS UMR5305, Lyon, France ; [2]INMG CNRS UMRS5310, INSERMU1217, Lyon, France,[3]MATEIS, CNRS UMR5510, Lyon, France

ABSTRACT

Volumetric muscle loss resulting from traumatic incidents drastically decreases muscle regeneration capacity and lacks treatments. Injectable hydrogels represent promising therapeutic candidates. Recently, we have developed a biocompatible hydrogel with **highly tunable mechanical properties** composed of poly-lysine dendrimers (DGL) cross-linked with NHS-polyethylene glycol (PEG-NHS). This hydrogel has already shown high bioactivity and cyto-compatibility with many cell types such as fibroblasts and keratinocytes.

→This study investigates the optimization of the DGL/PEG hydrogel with the aim of sustaining muscle cells progenitor (myoblasts) **proliferation** & **differentiation** through stiffness and DGL/PEG ratio variation in order to enhance muscle fiber regeneration once injected.

●As hydrogels stiffness was modulated from 10 to 160kPa, muscle cells spreading, morphology and mobility on the support were strongly influenced with an optimal behavior observed for hydrogels between 50 and 130kPa. Interestingly, muscle cells subsequent differentiation was linked to DGL/PEG ratios, irrespectively of stiffness.

→However, as the muscle regeneration implies the injected hydrogels to be porous to allow cell infiltration, a porosity was created inside the DGL/PEG hydrogel through an innovative approach. Its potential as a candidate for muscle repair was then evaluated by muscle cell infiltration inside the innovative porous hydrogel.

1) FORMULATION OF HYDROGELS OF VARIOUS STIFFNESS AND DGL/PEG RATIO

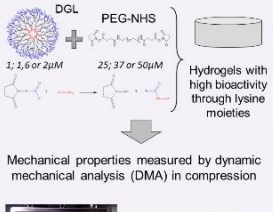

Mechanical properties measured by dynamic mechanical analysis (DMA) in compression

-Pre-strain : 5-10 %
-Amplitudes : 50-60µm
-Frequencies : 1-10Hz
-PBS 1X immersion

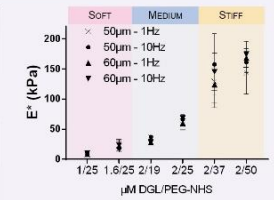

→ Stiffness modulation from 10 to 160kPa through DGL/PEG concentration increase

→ Possibility to target accurately adequate stiffness for muscle cells

2) DETERMINATION OF OPTIMAL HYDROGELS FOR MUSCLE CELLS PROLIFERATION

Study of DGL/PEG hydrogel ability to support myoblast proliferation and mobility

MUSCLE CELLS SEEDING
•15000 cells/cm²

On hydrogels of various compositions

Time lapse videos for 24h
-Confluence %
-Velocity (µm/h)

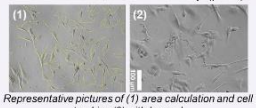

Representative pictures of (1) area calculation and cell tracking (2) with ImageJ

• Mouse myoblasts (C2C12) morphology on various hydrogel compositions at 30h post seeding

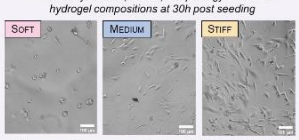

• Average Mouse myoblasts (C2C12) velocity (µm/h) on various hydrogels

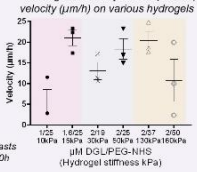

• Area covered by mouse myoblasts (C2C12) on hydrogels - 30h post seeding

• Area covered by human myoblasts (immortalized) on hydrogels - 30h post seeding

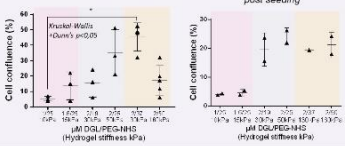

C2C12 cells and human immortalized myoblasts morphology, spreading, mobility and proliferation correlated with DGL/PEG hydrogel stiffness

→ Possibility to highlight 2 conditions of interest:
-2/25µM DGL/PEG - 50kPa **-2/37** µM DGL/PEG - 130kPa

3) DETERMINATION OF OPTIMAL HYDROGELS FOR MUSCLE CELLS DIFFERENTIATION AND FUSION

Study of DGL/PEG hydrogel ability to sustain myotubes formation

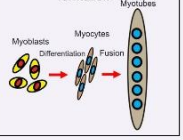

15000 cells/cm²

On hydrogels of various compositions

40,000 cells/cm²

On DGL coating vs polystyrene

Fusion into **myotubes** induced with cells starving for 6 days
→ % fusion quantified as Nuclei in myotubes / Total nuclei

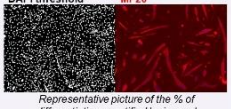

Representative picture of the % of differentiation quantified by imageJ

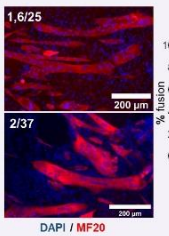

• C2C12 cells % fusion VS hydrogel stiffness or DGL/PEG ratio

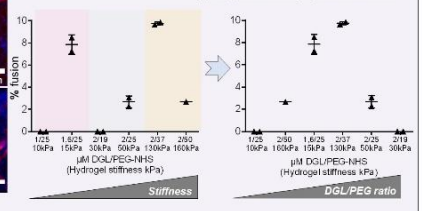

• C2C12 cells % fusion on DGL coating VS polystyrene

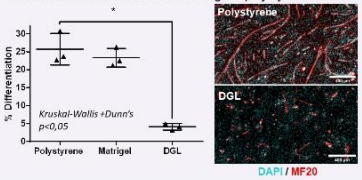

C2C12 ability to differentiate and fuse is decreased by DGL **irrespectively of stiffness**

The increase of DGL/PEG ratio in hydrogel, decreases muscle cells ability to differentiate

4) CYTO-COMPATIBILITY OF THE 3D STRUCTURE

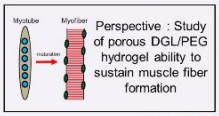

Perspective : Study of porous DGL/PEG hydrogel ability to sustain muscle fiber formation

Innovative effervescent porous DGL/PEG hydrogel (EPH) formulation

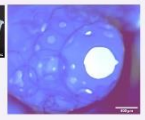

C2C12 cells seeding on EPH during 7 days in proliferation

14µm hydrogel slices

DAPI staining for cellular infiltration quantification

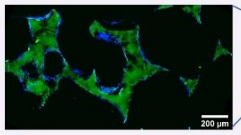

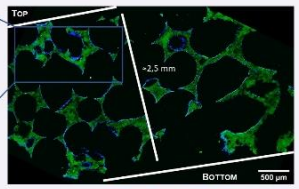

-C2C12 cells are able to fully infiltrate the EPH which confirms :

→Porous structure interconnection
→Adequacy for cellular adhesion & proliferation
→EPH potential as 3D support for muscle regeneration

Cell nucleus with DAPI / Hydrogel

Louise Griveau

PhD Student – UCBL 2nd year
louise.griveau@ibcp.fr

ACKNOWLEDGMENTS

The French ANR is acknowledged for financial support.

GELIHPARBALANR-17-CE19-0009

CONCLUSION & PERSPECTIVES

- Possibility to target conditions of interest for muscle cells proliferation and differentiation in terms of **stiffness** and **DGL/PEG ratio**
- Validation of DGL/PEG EPH as a potential **3D support for muscle cells**
- On going experiments focus on hydrogel validation to sustain **primary cells** proliferation and differentiation and *in vivo* assessment of EPH as a **support for muscle regeneration**

5 Scientific articles

1. **‘Versatile lysine dendrigrafts and polyethylene glycol hydrogels with inherent biological properties: in vitro cell behavior modulation and in vivo biocompatibility’.** Carrancá M, **Griveau L**, Remoué N, Lorion C, Weiss P, Orea V, Sigaudo-Roussel D, Faye C, Ferri-Angulo D, Debret R, Sohier. J.Biomed.Mater.Res.A, 2020.

2. **‘An in situ injectable and effervescent porous hydrogel for regenerative medicine applications’. Griveau L**, Lafont M, Le Goff H, Drouglazet C, Robbiani B, Sigaudo-Roussel D, Latif N, Le Visage C, Weiss P, Gache V, Debret R, Sohier J. – Under submission

3. **‘Myoblasts behaviour towards an innovative hydrogel: new perspectives for skeletal muscle tissue engineering’. Griveau L,** Christin E, Le Goff H, Robbiani B, Berthier A, Debret R, Gache V, Sohier J. – in preparation

Received: 5 February 2020 | Revised: 27 July 2020 | Accepted: 3 August 2020
DOI: 10.1002/jbm.a.37083

ORIGINAL ARTICLE

Versatile lysine dendrigrafts and polyethylene glycol hydrogels with inherent biological properties: in vitro cell behavior modulation and in vivo biocompatibility

Mariana Carrancá[1,2] | Louise Griveau[1,2] | Noëlle Remoué[1] | Chloé Lorion[1] | Pierre Weiss[3] | Valérie Orea[1] | Dominique Sigaudo-Roussel[1] | Clément Faye[4] | Daniel Ferri-Angulo[2] | Romain Debret[1] | Jérôme Sohier[1,2]

[1]Laboratory of Tissue Biology and Therapeutic Engineering, IBCP, CNRS Université, Lyon, France
[2]Laboratory for Materials Engineering and Science, CNRS INSA, Villeurbanne, France
[3]INSERM, Laboratory of Osteo-Articular and Dental Engineering, Nantes, France
[4]COLCOM, Bat CAP ALPHA, Villeurbanne,, France

Correspondence
Jérôme Sohier, CNRS INSA, UMR 5510, Laboratory for Materials Engineering and Science, Bat. B. Pascal, 7 Avenue Jean Capelle 69621, Villeurbanne Cedex, France.
Email: jerome.sohier@insa-lyon.fr

Present address
Clément Faye, GLPBiocontrol, Bat CAP ALPHA, Clapiers, France

Funding information
Agence Nationale de la Recherche, Grant/Award Number: TECSAN 016-01; Consejo Nacional de Ciencia y Tecnología; Région Auvergne-Rhône-Alpes, Grant/Award Number: grant 17 002601 ARC 2016

Abstract

Poly(ethylene glycol) (PEG) hydrogels have been extensively used as scaffolds for tissue engineering applications, owing to their biocompatibility, chemical versatility, and tunable mechanical properties. However, their bio-inert properties require them to be associated with additional functional moieties to interact with cells. To circumvent this need, we propose here to reticulate PEG molecules with poly(L-lysine) dendrigrafts (DGL) to provide intrinsic cell functionalities to PEG-based hydrogels. The physico-chemical characteristics of the resulting hydrogels were studied in regard of the concentration of each component. With increasing amounts of DGL, the cross-linking time and swelling ratio could be decreased, conversely to mechanical properties, which could be tailored from 7.7 ± 0.7 to 90 ± 28.8 kPa. Furthermore, fibroblasts adhesion, viability, and morphology on hydrogels were then assessed. While cell adhesion significantly increased with the concentration of DGL, cell viability was dependant of the ratio of DGL and PEG. Cell morphology and proliferation; however, appeared mainly related to the overall hydrogel rigidity. To allow cell infiltration and cell growth in 3D, the hydrogels were rendered porous. The biocompatibility of resulting hydrogels of different compositions and porosities was evaluated by 3 week subcutaneous implantations in mice. Hydrogels allowed an extensive cellular infiltration with a mild foreign body reaction, histological evidence of hydrogel degradation, and neovascularization.

KEYWORDS
biocompatibility, cell interaction, mechanical properties, PEG based hydrogels, poly(L-lysine) dendrimers

1 | INTRODUCTION

The interest in hydrogels has grown rapidly in the past decade due to their vast potential in tissue engineering, tissue regeneration, and drug delivery.[1] These hydrophilic polymer networks are of interest through their biocompatibility, viscoelasticity, permeability to oxygen and nutrients, and high water content.[2–4] While natural hydrogels (e.g., collagen, gelatin, fibrin) confer their inherent extracellular matrix (ECM) structure and qualities, they often show weak mechanical properties, batch-to-batch variability,[5] and risk of pathogen transfer.[6] Conversely, synthetic hydrogels have an exact composition and multi-tunable properties, but may lack bioactivity to promote cellular

activities.[3,7,8] Among these, PEG hydrogels have been extensively used for controlled drug delivery, as cell vehicles or tissue engineering scaffolds over the past decades, owing to their excellent biocompatibility, chemical versatility, and tunable mechanical properties.[9] However, in the context of tissue engineering, a corollary setback of their bio-inert nature is that they require to be associated, functionalized or coated with supplementary proteins of the native ECM or functional moieties, such as, collagen,[10] laminin,[11] or arginine-glycine-aspartic (RGD) peptides,[12,13] to support the survival or function of adherent cells.[7,14–16] This necessity induces a complexification of the PEG-based hydrogel approaches for tissue engineering, which would benefit from inherent and native interactions with cells, without added factors.

PEG hydrogels can be obtained via covalent cross-links between PEG molecules through different paths, in which the PEG molecules are either functionalized with reactive end groups (e.g., methacrylate, acrylate),[7,17] and activated by initiators or associated with multifunctional monomers to avoid the use of initiators. In the latter approach, dendrimers have shown potential as cross-linking monomers, thanks to their versatile chemical composition, highly organized 3D arborescent structure and ease of surface functionalization.[18–21] Poly(amidoamine) (PAMAM) dendrimers, for instance, have been successfully associated with PEG to form hydrogels for drug delivery applications that do not require interactions with cells[22–24] since they tend to exhibit unwanted features such as cytotoxicity and non-degradability.[25]

Conversely, other dendritic structures with amine end groups, such as, poly(L-lysine) dendrigrafts (DGL), have recently developed interest in several applications, due to their large surface area, versatility to be functionalized, water solubility, stability under sterilization conditions, partial degradability under the action of endogenous peptidases, non-immunogenicity, and low cytotoxicity.[26,27] Moreover, their polycationic nature at physiological pH allows cellular adhesion,[27,28] which could be of high interest to provide cell interaction to inert materials. Indeed, DGL used as coatings on surfaces have been shown to increase cellular adhesion and proliferation of human skin fibroblasts by inducing the expression of integrin α5, a receptor implied in cell adhesion to fibronectin (through RGD). In this manner, the DGL could provide a bioactivity to the otherwise bio-inert material, while remaining synthetic and controllable.[29] DGL synthesis is based on the grafting of subsequent lysine molecules onto a polymeric substructure, linear poly-L-lysine (PLL), using protect-deprotect steps. In this manner, increasing generations of DGL (G1-G5) can be obtained with a simple, scalable procedure, water-soluble reaction (pH 6.5) with low batch-to-batch variability with a typical yield of 50–60% on a multigram scale.[30] While DGL-G3 and G4 showed a better cellular adhesion compared with PLL, in this study we focused on G3 since it presented the best compromise between biological activity and fabrication cost, as well as limits the formation of aggregates observed in the G4 synthesis.[29]

Interestingly, DGL-G3 has never been evaluated as cross-linking monomers to form PEG hydrogels, while such hydrogels could benefit from their inherent bioactivity, without the need for further association with additional functional moieties. To create such PEG hydrogels with intrinsic interactions with cells, we hypothesized that the amine groups present in high density at the DGLs surface could be used as binding sites to form network chains through of amide bonds between activated PEG-NHS ester and DGL-G3.

We here assess these possibilities through the development of a novel hydrogel composed of DGL-G3 and PEG, with extensive and straightforward tuneable mechanical properties, to serve as matrix or cell support for soft tissue engineering applications.[15] The characteristics of these hydrogels as cross-linking time, swelling, and mechanical properties were determined. Cell interactions with the hydrogels (adhesion, viability, proliferation, and morphology of dermal fibroblasts on dense hydrogels) were determined, in relation to hydrogel composition. Additionally, to allow cell colonisation and infiltration, hydrogels were rendered porous by particulate/leaching technique and their biocompatibility was determined by in vivo subcutaneous implantations in mice.

2 | MATERIALS AND METHODS

2.1 | Preparation of dense DGL/PEG hydrogels

Dense hydrogels of different ratios of DGL/PEG were prepared by adding the desired concentration of PEG-bis(N-succinimidyl succinate) (PEG-NHS, 2000 g/mol, Sigma–Aldrich) in anhydrous dimethyformamide (DMF, Sigma–Aldrich), to a solution of DGL (third generation, 22,000 g/mol, COLCOM)[31] in phosphate-buffered saline (PBS), at 4 C. For mechanical and swelling testing, 800 µl hydrogels were prepared in 2 ml conic tubes (Maxymum Recovery, Axygen). After cross-linking, the conical bottom of the tubes was cut off, and the tubes were immersed in ethanol for 5 min to subsequently retrieve the hydrogels. The resulting cylindrical hydrogels were then sectioned (2 mm thickness) using a vibratome (7550 Integraslice, Campden Instruments Ltd.) into flat hydrogel cylinders (thickness 2 mm, diameter 9 mm) and finally rehydrated and stored in PBS at 4 C. For 2D cellular in vitro studies, hydrogels of flat surfaces were prepared on top of coverslips for convenient handling (12 mm in diameter). The desired concentrations of DGL-G3 and PEG were mixed to prepare a final volume of 100 and 60 µl of the resulting solution were swiftly deposited between a hydrophobic glass slide and a round coverslip (for a hydrogel thickness of 0.6 mm). Hydrophobic glass slides were obtained by dipping in dichlorodimethylsilane (Sigma–Aldrich) followed by overnight evaporation under a fume hood. After cross-linking, the hydrogel-covered coverslips were gently removed, sterilized overnight in EtOH:PBS (70:30, v/v) solution, washed 3 × 30 min with sterile PBS and kept at 4 C prior use. Concentrated hydrogels, which cross-linking time was faster than 10 s, were prepared in a cold room to slow down cross-linking.

2.2 | Cross-linking speed

To monitor cross-linking speed, hydrogel components were added to a glass vial (8 × 25 × 35 mm) under agitation (300 rpm) with a magnetic rod (5 mm) placed at exactly 4 cm from the magnetic stirrer. Cross-linking time was defined, in our study, as the time needed to halt the magnetic rod after adding all the hydrogel components. Three hydrogels per condition were used.

2.3 | Swelling ratio (Qs)

The swelling ratio (Qs) of 2 mm-thick dense hydrogels discs was determined in PBS at 37 C. Prior incubation in PBS, samples were frozen in liquid nitrogen and freeze-dried to measure their dry weight. Samples were blotted before each weight measurement, performed at 1, 2, 6, and 24 hr. The swelling ratio was defined as, $([W_s\text{-}W_i]/W_i)$, where W_s is the weight of swollen hydrogel and Wi is its initial dry weight after freeze-drying. Five hydrogels per condition were measured.

2.4 | Mechanical testing

The mechanical properties of DGL/PEG hydrogels (2 × 9.1 mm) of different compositions were analyzed by cyclic compression with a dynamic mechanical analyzer (DMA 242 E Artemis, NEZSTCH). The hydrogel's domain of linearity was first determined with a strain sweep and compression test. Samples immersed in PBS were then subjected to compression at 10% strain and 60 µm amplitude, with increasing frequencies (1–20 Hz) at room temperature. At least five hydrogels per condition were measured.

2.5 | In vitro cell culture studies

Human dermal fibroblasts (Promocell, Heidelberg) were seeded at a density of 10,000 cell/cm^2 on the surface of hydrogel-covered coverslips and cultured in DMEM-F12 medium (Gibco) supplemented with 10% FBS (Life Tecnologies) and 1% penicillin/streptomycin (PAA Laboratories) at 37 C and 5% CO_2. Culture medium was refreshed every second day.

Hydrogels cytocompatibility was evaluated with a live/dead assay. Cells were washed once with sterile PBS and incubated 30 min with a 6 µM propidium iodide (Sigma Aldrich) and 1 µM Calcein (Sigma–Aldrich) solution and subsequently observed with a fluorescence microscope (Nikon TiE, Nikon Instruments). After observation, samples were washed with PBS, culture medium refreshed and cultured at 37 C and 5% CO_2 until next measurement. The number of alive and dead cells was determined from image analysis (Imagej[32]), using 5 different fields of view randomly acquired per replicate of at least 7 hydrogels per condition. Viability was determined as the percentage of alive cells from the total number of cells. Cell adhesion was expressed as the total number of cells (alive or dead) present on the surface of the hydrogels 24 h post-seeding. The effect of hydrogel composition on cell morphology was evaluated by phase contrast microscopy (Nikon TiE) and by actin staining. Phase contrast microscopy pictures were acquired after 24 h for 10 hydrogels per condition and at 72 h of culture for 5 hydrogels per condition. Cell spreading area, circularity, and feret diameter of cells seeded were determined to compare cell morphologies. Control were only analyzed after 24 h, since cell confluence impeded images analysis after 72 h. Factin cytosqueleton was observed by phalloidin (Sigam–Aldrich) staining after 1, 3, and 8 days of culture. Cells on the hydrogels were fixed with 4% paraformaldehyde (PFA, Thermo Fischer Scientific) for 10 min followed by 20 min permeabilization with a 0.1% triton solution in PBS. After washing twice with PBS, the samples were incubated for 10 min with a 2 µg/ml 4′,6-Diamidine-$2^{\prime}$-phenylindole dihydrochloride (DAPI, Sigma–Aldrich) and 2 µg/ml phalloidin (Thermo Fischer Scientific) solution in PBS to stain the cell nucleus and actin cytosqueleton, respectively. Finally, hydrogels were observed with a fluorescence microscope (Nikon TiE). Cell proliferation was determined by counting DAPI stained cell nucleus after 1, 3, and 8 days of culture of 3 hydrogel per condition.

2.6 | Preparation of porous hydrogels

Porous hydrogels were prepared by particulate/leaching technique using paraffin microspheres as porogens.[33] Briefly, 10 g paraffin (Histolab AB, Västra Frölunda) and 250 ml 0.5% poly(vinyl alcohol) (PVA, Sigma–Aldrich) were heated to 80 C under stirring. After 20 min, the suspension was poured into ice water. The paraffin microspheres formed were sieved at 50, 100, and 180 µm and the resulting fractions were washed with distilled water, freeze-dried and conserved at 4 C.

To prepare porous hydrogels, 400 mg of paraffin microsphere, previously prepared, were compacted by centrifugation in 2 ml microtubes (2000 g, 10s) to obtain a flat surface. Consecutively, DGL and PEG-NHS solutions were mixed by vortex and rapidly transferred to the microtubes containing the paraffin at 0 C. After cross-linking, the conical bottom of the microtubes was sectioned, paraffin was extracted with boiling EtOH for 40 min and the hydrogels were removed from the microtubes. Finally, hydrogels were cut into 2 mm thick discs with a vibratome. After that, the remaining paraffin was removed by several cycles (40 min) in reflux EtOH. The obtained scaffold discs were sterilized overnight in EtOH 70%, washed 3 × 1h with sterile PBS, and kept at 4 C prior use.

2.7 | Biocompatibility

Biocompatibility of synthetized hydrogels was assessed by subcutaneous implantation of acellular hydrogels. After approval by local ethics committee, 5 hydrogels discs per condition (2 × 6 mm diameter) were implanted under the back skin of 8-weeks old SKH1 mice (Charles

River, Ecully) under sedation by intraperitoneal xylazin-ketamin injection (four hydrogels per mouse). A small incision was performed at the low back of the mice and 4 subcutaneous pockets created with a sterile spatula. The hydrogels were inserted in the pockets and the incision sutured. Mice, fed ad libitum, were monitored every day for recovery and signs of distress. After 3 weeks, the mice were euthanized by anesthetic overdoses (intracardiac injection of sodium pentobarbital), the hydrogel samples recovered with surrounding tissue, fixed in 4% paraformaldehyde (PFA) solution in PBS, embedded in paraffin, sectioned and stained with Masson's trichrome. To highlight the penetration of blood vessels in the implanted hydrogels, sections of three different hydrogels per condition were stained for α-SMA (Abcam #ab5694 1:250) by immunohistochemistry, cell nuclei were counter-stained with 2 µg/ml DAPI solution and observed by confocal microscopy (ZEISS, LSM 800). Round blood vessels with a diameter superior to 10 and 25 µm per hydrogel cross section were counted by image analysis.

2.8 | Statistical analysis

Statistical analyses were performed with Graphpad prism or Kaleidagraph. Test were performed using the variance analysis (ANOVA). Data values are presented as mean ± standard error (SE) and p-values of 0.05 and below were considered significant.

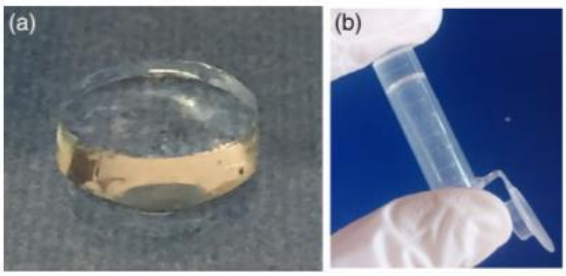

FIGURE 1 Photographs of the hydrogel at room temperature A, Dense 2/19 mM DGL/PEG hydrogel disc of 2 mm thickness and 9.1 mm diameter. B, Hydrogel in an inverted conic tube

3 | RESULTS

3.1 | Effect of reactants concentration on the formation of self-standing hydrogels

DGL/PEG hydrogel formation was straight forward. Concretely, hydrogels were obtained by covalent reaction between amine groups in the DGL and the NHS ester ends groups in PEG by simply mixing the solutions at room temperature (Figure 1.). Cross-linking velocity could be varied between 5 to 145 s by modifying reagent concentrations (between 1 to 4 mM for DGL and 19 to 30 mM for PEG-NHS), predominantly through the DGL concentration, as presented in Table 1. Interestingly, by considering the amount of amine groups and NHS functions theoretically available for the covalent reaction to occur, similar ratios of available amine to NHS functions resulted in different cross-linking velocities.

3.2 | Swelling ratio

To mimic the physiological conditions, swelling ratio was determined in PBS at 37 C. As observed in Figure 2, the swelling was decreased with an increased concentration of DGL or PEG-NHS. After 2 hr, a great quantity of liquid has been absorbed and reached equilibrium after 6 hr. The composition with lowest concentration of both components showed the greatest swelling ratio of 22.89 ± 1.95 after 24 h.

3.3 | Mechanical properties of dense DGL/PEG hydrogels

The mechanical properties of hydrogels of different compositions were measured with mechanical dynamical analysis. The loss (E"), storage (E'), and complex modulus (E*) were determined at increasing frequencies between 1 and 20 Hz. Figure 3 shows that for all hydrogels, E' was greater than E" over the entire frequency range studied. This was further expressed by tan delta, which is the ratio of moduli (E"/E') that describes the viscous energy dissipation relative to the stored elastic energy. While E' was constant for all applied frequencies, E" increased with frequency, which is a typical

TABLE 1 Crosslinking time to form self-standing gels in relation to the final concentration of DGL and PEG-NHS and ratio of available amine/NHS functions (Two-way ANOVA between PEG and DGL concentration, *indicates that there is a statistically significant difference when DGL concentration is modified, for any given PEG concentration, $p < 0.05$, $n = 3$)

		PEG-NHS (mM) (Available NHS, mM)		
Time (s) (Ratio amines/NHS)		19 (38)	28 (56)	30 (60)
DGL (mM)* (available amines, mM)	1 (114)	144.6 ± 23.3 (3)	122.0 ± 24.0 (2.03)	140.2 ± 15.8 (1.9)
	2 (228)	14.94 ± 1.1 (6)	13.17 ± 1.9 (4.07)	12.28 ± 3.5 (3.8)
	3 (342)	10.47 ± 4.5 (9)	8.4 ± 1.2 (6.1)	7.66 ± 1.1 (5.7)
	4 (456)	6.77 ± 0.9 (12)	4.76 ± 0.6 (8.14)	5.47 ± 0.6 (7.6)

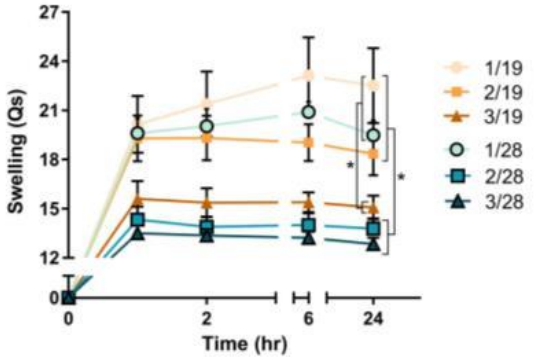

FIGURE 2 Swelling ratio of hydrogels of different compositions (hydrogel concentration is expressed as the ratio DGL/PEG in mM) swelling measured in PBS at 37 C. (n = 5, Two-way ANOVA, $p < 0.05$, *at 24 hr)

behavior of rubbery elastics.[34] Overall, the complex modulus of the different hydrogels was increased with an increased concentration of PEG-NHS and DGL, varying from 7.7 ± 0.7 to 90.4 ± 28.8 kPa.

3.4 | Cytocompatibility of the DGL/PEG hydrogels and effect of hydrogel composition on cell morphology and proliferation

To assess the potential of the DGL/PEG hydrogels as a cell substrate, the adhesion and viability of human fibroblasts seeded on the flat surface of hydrogels of different compositions were evaluated with a live/dead assay (Figure 4A). Seeded cells readily adhered on the hydrogels surface after 24 hr with a very low cytotoxicity, except for the hydrogel 3/19 mM (DGL/PEG), which showed a mortality of 79.4%. As shown in Figure 4B, the hydrogel

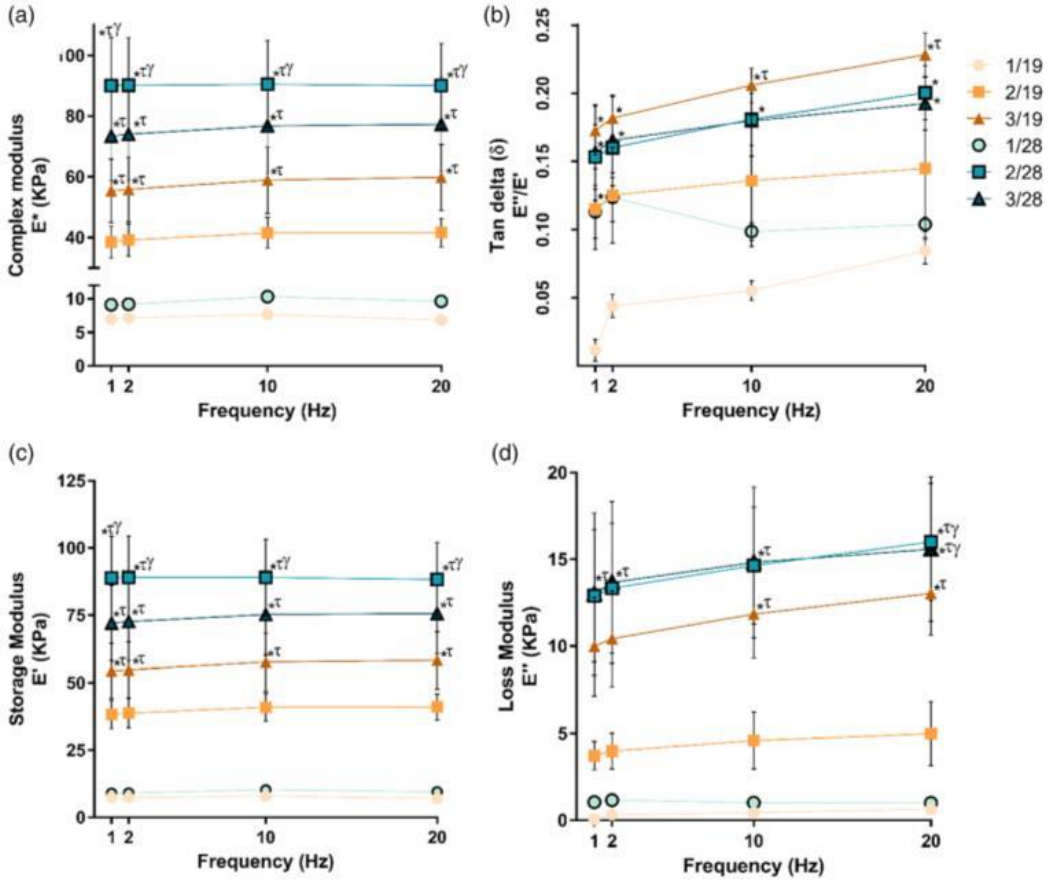

FIGURE 3 Mechanical properties of dense hydrogel discs (2 × 9.1 mm) of different compositions (hydrogel concentration is expressed as de ratio DGL/PEG in mM) measured at room temperature under PBS immersion by dynamical mechanical analysis in compression at a 10% strain and 60 µm of amplitude. A, complex modulus, B, tan delta, C, storage modulus, and D, loss modulus. (n = 7, Two-way ANOVA, $p < 0.05$, *compared with 1/19, τ compared with 1/28, and γ compared with 2/19)

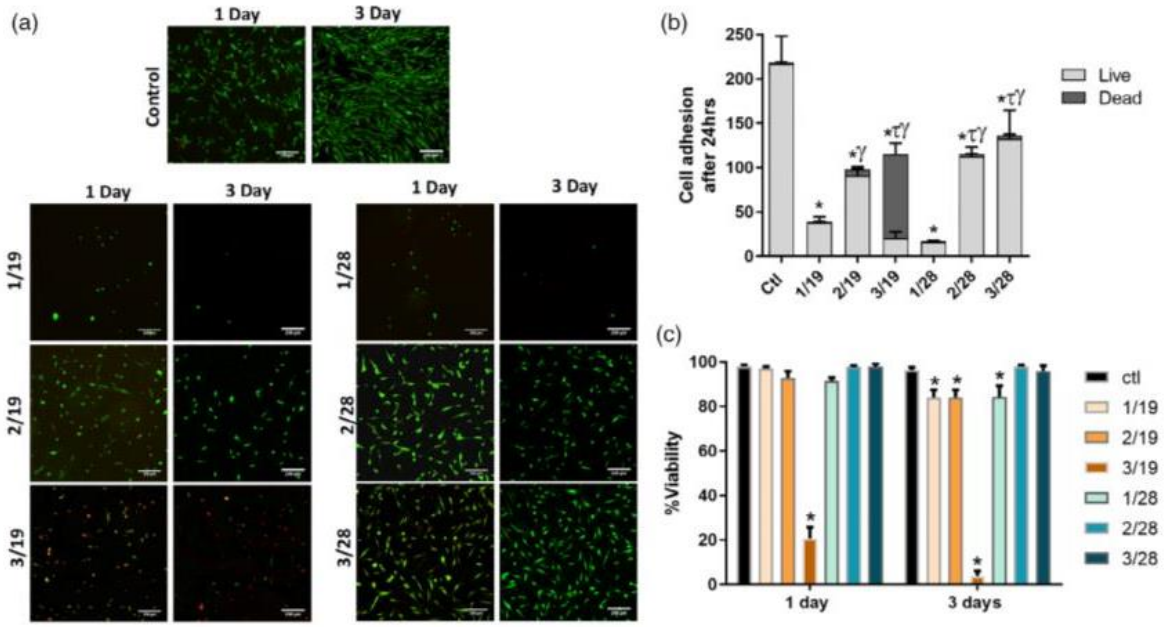

FIGURE 4 Dermal human fibroblast viability. A, Cytotoxicity by live/dead assay after 1 and 3 days of culture on the surface of hydrogels of different compositions (hydrogel concentration is expressed as de ratio DGL/PEG in mM). Live cells are observed in green and dead cells in red B, Total cell adhesion after 24 hr of cell seeding on top of hydrogels of different compositions. (n = 7, One-way ANOVA, $p < 0.05$, *compared with control, τ compared to 1/19, and γ compared with 1/28) C, Viability percentage obtained from images analysis (n = 7, $p < 0.05$ * compared with control)

composition had an apparent effect on cell adhesion, concretely, with DGL concentration. With an increase of DGL, the total number of adhered cells was increased while adhesion was minimal when the DGL concentration was 1 mM. After 3 days of culture, compositions 1/19, 1/28, and 2/19 mM DGL/PEG presented around 84% of viability while more concentrated compositions (2/28 and 3/28 mM DGL/PEG) showed a viability of 97.9 and 96%, respectively (Figure 4C), with no difference compared to controls (tissue culture plastic). Of note, an increase in PEG-NHS concentration resulted in an increase of the viability of the adhered cells.

Cell morphology was also modified by hydrogel composition (Figure 5A). Cells on hydrogels with lower concentrations of DGL (1 mM) and therefore lower percentage of adhesion presented a round morphology similar to non-adherent cells, with a mean circularity of 0.8 and a small ferret diameter (26.9–28.9 μm). An increase in hydrogel concentration had an impact on cell morphology. Except for hydrogel composition 2/28 and 3/28 (DGL/PEG), which showed a similar cell morphology. After 72 hr, cell spreading area was increased in all compositions (Figure 5B). The effect of hydrogel composition on cell morphology and spreading was further confirmed by phalloidin staining of f-actin fibres after 1, 3, and 8 days of culture (Figure 6A.).

Regarding proliferation, seeded cells were able to proliferate over time (Figure 6B), except for hydrogels with the lower concentration of DGL, where cells stayed round and showed proliferation rates close to zero. While hydrogels 2/28 and 3/28 mM showed similar proliferation rates of 69.9 ± 8.1 and 66.7 ± 14.6, respectively, which were lower than tissue culture plastic controls (rate of 135.2 ± 26.19).

3.5 | Biocompatibility

The behavior of DGL/PEG hydrogels of different compositions and porosities was evaluated in vivo by subcutaneous implantation in mice. As shown in Figure 7, regardless of pore size or composition, all hydrogels exhibited a mild foreign body reaction with the formation of a fibrous capsule after 3 weeks of implantation. All porous hydrogels were deeply infiltrated by cells, contrarily to dense hydrogels (Supplementary Figure 1). An important population of macrophages were visible, highly concentrated at the rim and within the porous implants and on the external edge of dense hydrogels. The macrophages were able to degrade the hydrogel through phagocytosis, further opening the pores, as exemplified in the blue close-ups on Figure 7. Interestingly, no granulocyte or lymphocytes could be observed, suggesting a mild inflammatory reaction. While the different porosities did not result in differences of cellular infiltration, the hydrogels composition clearly induced structural and degradation-related differences in the retrieved implants after 3 weeks. Softer hydrogels (7.7 ± 0.4 kPa) appeared condensed while harder ones

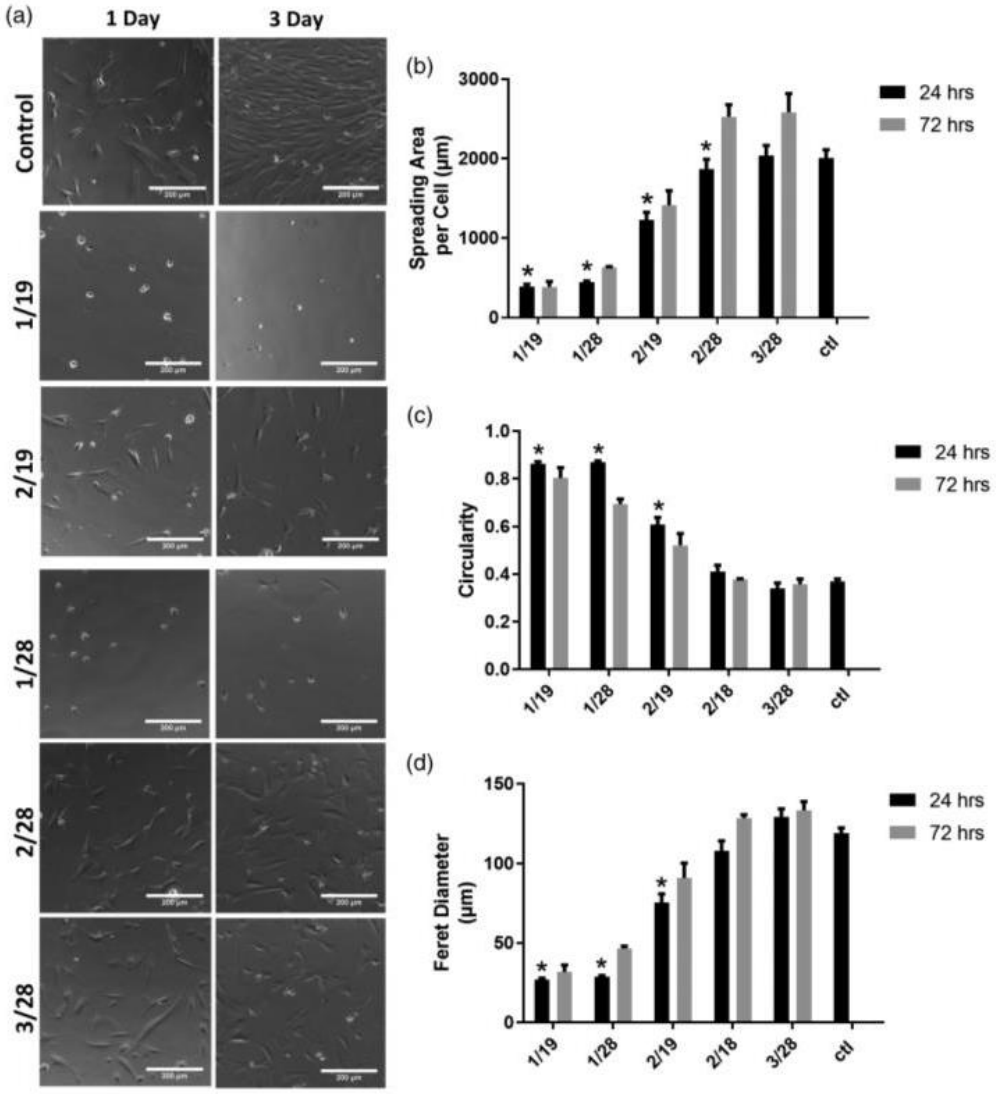

FIGURE 5 Dermal fibroblast morphology when cultivated on the surface of hydrogels of different compositions (hydrogel concentration is expressed as de ratio DGL/PEG in mM) A, contrast phase photos after 24 hr and 72 hr of cell seeding B, Morphology parameters (spreading area, circularity, and feret diameter) obtained from image analysis of contrast phase photos of 10 hydrogels at 24 hr and five hydrogels after 72 hr. Control was only analyzed after 24 hr since after 72 hr images analysis was not possible due to cell confluence. ($p < 0.05$, *compared with control at 24 hr)

(41.5 ± 5.0 and 76.7 ± 15.5 kPa) conserved their initial porous structure. Similar observations were made in regards of phagocytosis, with harder hydrogels being less prone to degradation by macrophages. The presence of neo-tissue within the hydrogels, revealing deposits of collagen, followed a similar pattern with an increased occurrence in harder hydrogels than in soft ones.

Curiously, an important amount of blood vessels were present within and throughout the porous hydrogels, as could be observed by IHC staining of α-SMA (Figure 8). Fewer blood vessels were present in soft hydrogels compared with more rigid compositions, with a preference to porous hydrogels with a broader range of pore size (50–180 µm). When considering only the blood vessels with a diameter over 25 µm, a preference to bigger pores was observed for more rigid compositions (Figure 8B).

4 | DISCUSSION

PEG-based hydrogels have been the focus of much attention for various tissue engineering applications over the past years.[9] However,

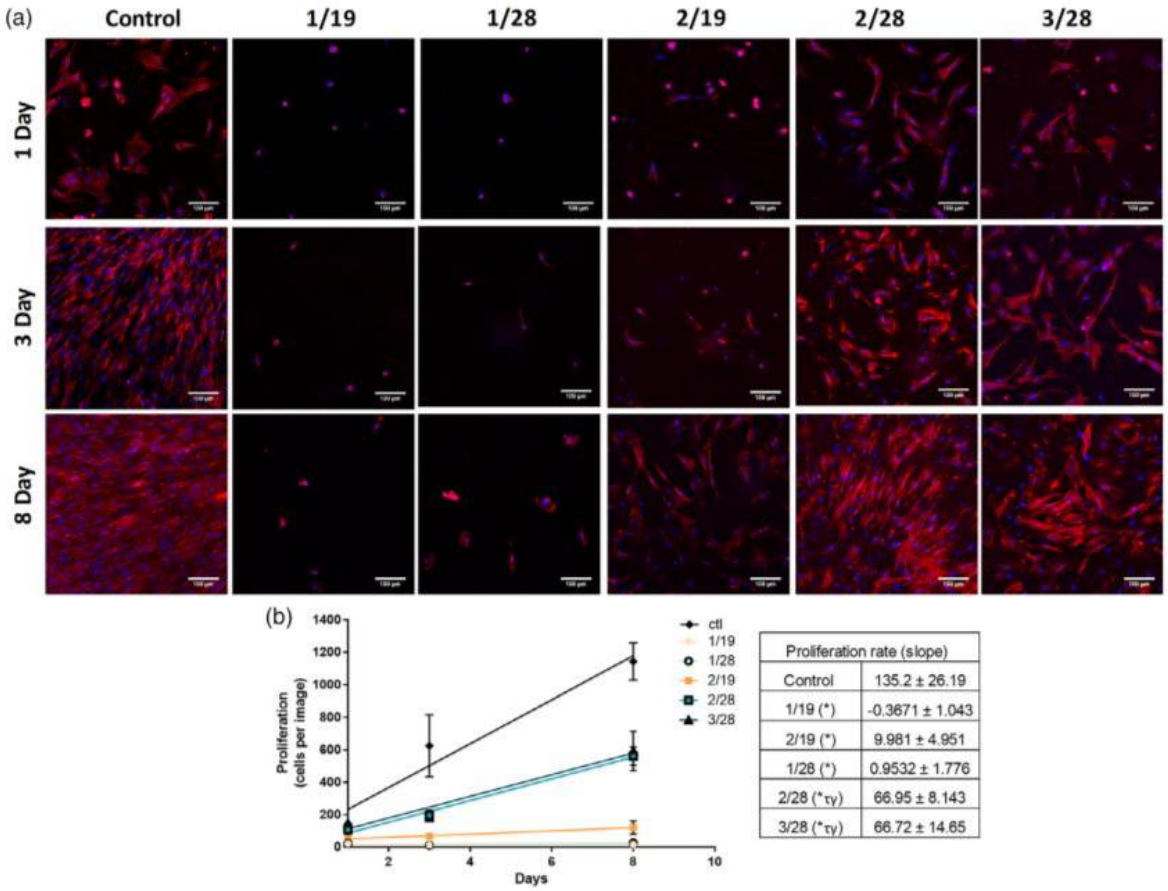

Proliferation rate (slope)	
Control	135.2 ± 26.19
1/19 (*)	-0.3671 ± 1.043
2/19 (*)	9.981 ± 4.951
1/28 (*)	0.9532 ± 1.776
2/28 (*τγ)	66.95 ± 8.143
3/28 (*τγ)	66.72 ± 14.65

FIGURE 6 A, Cytoskeleton structure of dermal fibroblasts seeded on the surface of hydrogel of different compositions (hydrogel concentration is expressed as de ratio DGL/PEG in mM) observed by DAPI-Phalloidin staining after 1, 4, and 8 days of culture (in blue cell nuclei and in red actin fibers). B, Cell proliferation rate of fibroblasts seeded on the surface of hydrogel of different compositions (hydrogel concentration is expressed as de ratio DGL/PEG in mM) obtained from cell nuclei counting after 1, 4, and 8 days of culture. (n = 3, One-way ANOVA, $p < 0.05$, *compared with control, τ compared with 1/19 and γ compared with 1/28)

their use with adherent cells requires them to be functionalized or coated with other molecules and moieties to allow cells attachment and proliferation, which increase their complexity and decrease their practical applicability. With the aim of further broadening their potential by providing them with inherent cellular adhesion and interactions, we therefore defined and evaluated a novel hydrogel where homobifunctionalized PEG-NHS is cross-linked by poly(L-lysine) dendrigrafts (DGL). The straightforward mixing of PEG-NHS with DGL in aqueous solutions indeed results in the swift formation of self-standing hydrogels. Among the various dendrimer structures that have been associated with PEG to form hydrogels,[20] DGL was so far never evaluated in this respect.

By varying the concentrations of hydrogel components, the cross-linking velocity, swelling, and mechanical properties can be tailored. DGL of third generation used in this study presents an important density of amine groups on their surface (123), and it has been determined that only 97.7% of these amines residues are available as binding sites per molecules (114).[35] PEG-NHS, on the contrary, possess only two able NHS ester group per molecules. Hence, the ratio of available amines groups versus NHS is always higher than 1, but we did not observe a relationship between this ratio and the cross-linking speed, mechanical properties or swelling ratio. Indeed, solutions of increasing DGL and PEG-NHS concentrations but of similar amines/NHS ratios resulted in increasing cross-link velocities and mechanical properties. Similarly to PEG-PAMAM gels, the effect of the polymer content could be logically ascribed to an increase of cross-linking density due to a closer presence of the amine (DGL) and NHS (PEG) reactive groups. Once a PEG molecule is attached to the surface of the dendrimer, the second NHS function on the other end of the PEG chain will have lower mobility, which will increase its probability to react with an amine function on the same dendrimer and form intramolecular loops.[36] Therefore, the dilution of the reaction mixture increases the space between the dendrimers, forming many intramolecular loops at the

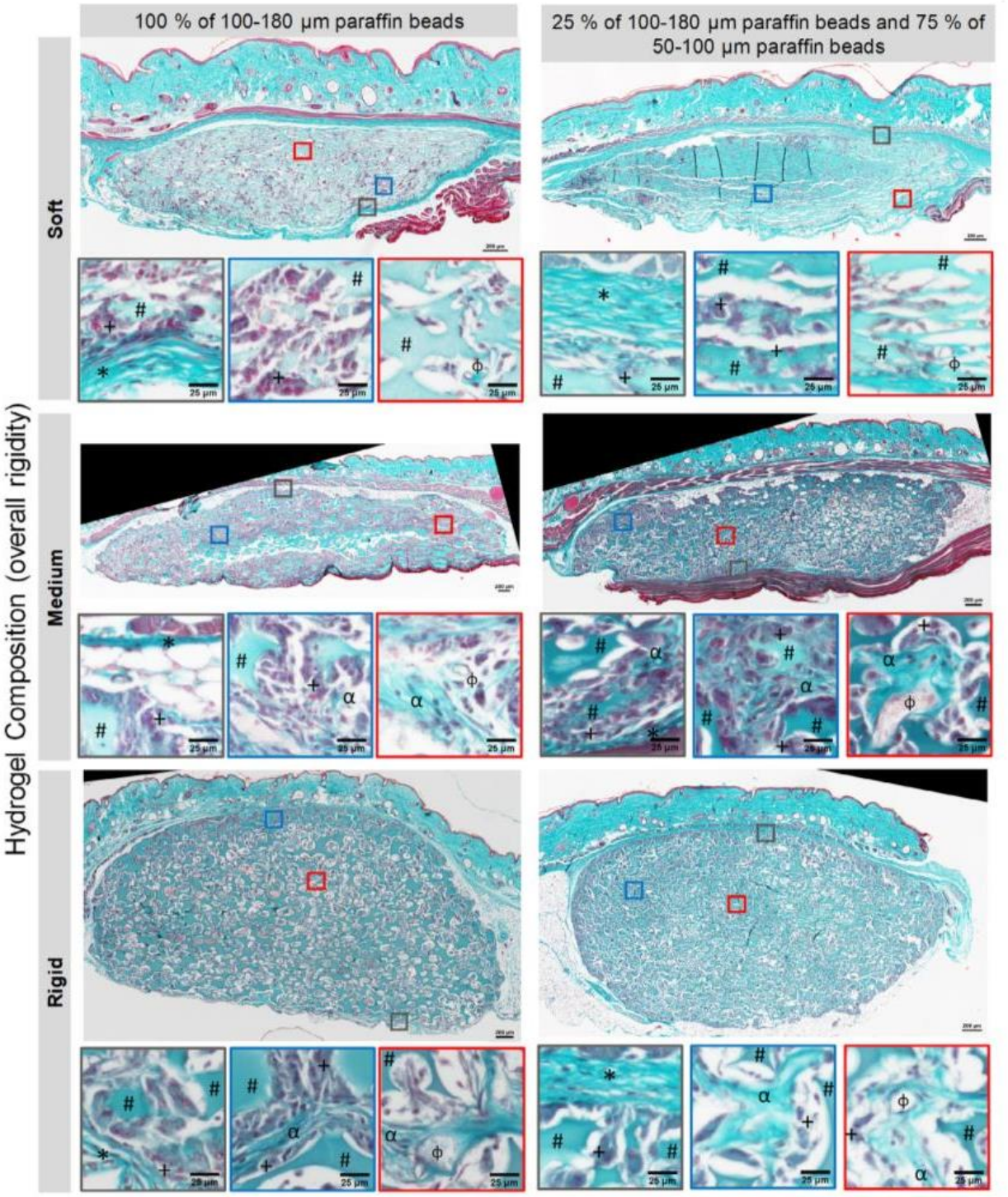

FIGURE 7 Subcutaneous implantation in mice for 3 weeks of DGL/PEG porous hydrogels of different compositions (soft, medium, and rigid, 7.7 ± 0.4, 41.5 ± 5.0, and 76.7 ± 15.5 kPa, respectively) and with different pore sizes distribution. Masson's trichrome staining of the full explants and close-ups highlighting the hydrogel (#), the fibrous capsule (*), macrophages (+), synthesised collagen (α), and blood vessels (Φ)

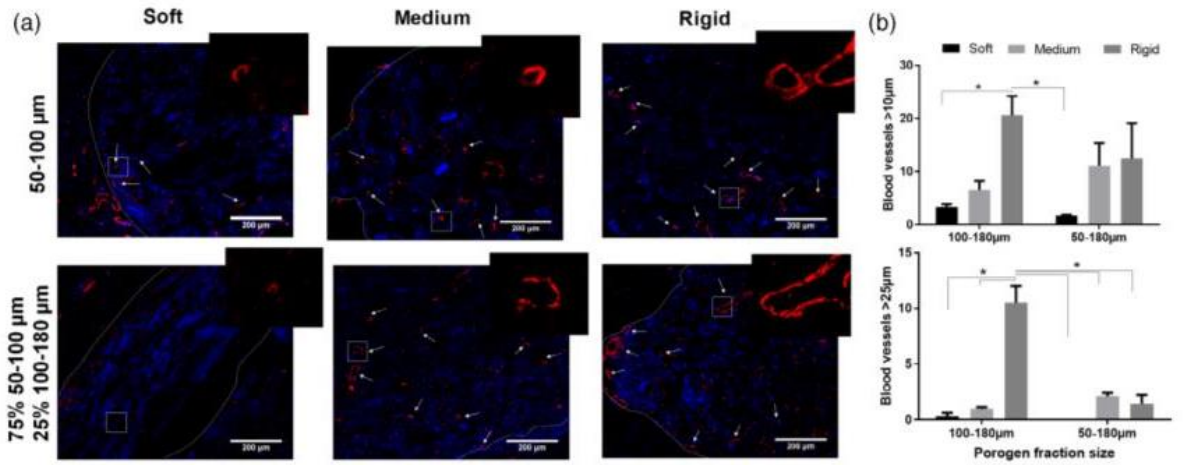

FIGURE 8 Blood vessels present after 3 weeks of subcutaneous implantation in mice in porous hydrogels of different compositions (soft, medium and rigid, 7.7 ± 0.4, 41.5 ± 5.0, and 76.7 ± 15.5 kPa, respectively) A, Immunofluorescence staining of α-SMA (red) indicating blood vessels present within the porous hydrogels while cell nuclei are stained with DAPI in blue; white lines delimit the border of the hydrogel and arrows point to sectioned blood vessels. B, Number of blood vessels present in the hydrogel of a dimeter greater than 10 or 25 µm obtained from image analysis of mosaic images of complete slides of porous hydrogels. (n = 3, Two-way ANOVA, *p < 0.05)

expense of effective networks chains. Conversely, concentrating the mixture results in the opposite and increases the cross-link velocity.[24] This hypothesis is further reflected in the concomitant increase of mechanical properties and decrease of swelling observed in our hydrogels when increasing the polymer concentration. Since the arborescent molecules function as junction points in the cross-linking system, an increase in cross-links density will limit the expansion of the network, meaning a more compact mesh that leads to a decrease in swelling and an increase in rigidity. Similarly, Gitsov et al observed that the swelling properties of hydrogels prepared from PEG and various dendritic fragments were not related to the PEG concentration or the dendrimer generation but mainly to the total increase in components concentration.[37]

In addition to global polymer concentration, the DGL appears to have a predominant control of the hydrogel cross-linking. While its concentration doubling from 1 to 2 mM for a constant PEG-NHS concentration induces a 10-fold increase of the cross-linking velocity, a 1.6-fold increase of PEG-NHS for a constant DGL concentration only marginally decreases cross-linking speed. Although a DGL presents 114 amine groups to act as a cross-linker, it is unlikely that all the end groups will be able to react with the PEG molecules due to steric crowding, which will limit the maximum number of PEGs that can be grafted to a single dendrimer.[24] The fact that an increase of PEG-NHS concentration for a constant DGL does not result in a significant increase of the cross-linking speed supports this hypothesis by indicating that a maximal number of PEG per DGL has been reached. Contrariwise, an increase of DGL at constant PEG-NHS allows to reduce the steric crowding and increases further the cross-linking velocity.

To provide to PEG hydrogels the ability to inherently interact with cells, our hypothesis that DGL bioactivity could be conveyed to the hydrogel bulk was confirmed, as human fibroblasts were able to adhere and proliferate on the surface of DGL/PEG hydrogels prepared without supplementary coating or functionalization before seeding. Similarly to DGLs coated on surfaces,[29] the ability of cells to attach and spread to DGL-containing hydrogels can be attributed to early electrostatic interactions between the polyanionic cell surfaces and the polycationic charges brought by the DGL's amino groups. This was further supported by the increase in cell adhesion with an increase in DGL concentration.

While the concentration of DGL plays a role in cell adhesion to the hydrogels, their viability seems dependent of the ratio between DGL and PEG-NHS. Mortality was indeed observed when the ratio of amines to NHS groups was greater than 9. The cationic nature of DGL that provides cell adhesion properties is possibly also the cause of their cytotoxic effect, since excessive cationic charges can affect the integrity of cell membranes.[38] When coupled with PEG molecules, PEG might shield the dendritic cationic charges and improve the DGL viability, similarly to Tang et al who showed that PEG-gelation of DGL vectors for gene therapy allowed to decrease toxicity.[39]

Unlike cell adhesion and viability, cell morphology, and proliferation appear related to the overall hydrogel rigidity. For instance, for a constant DGL concentration (2 mM), an increase of PEG-NHS concentration from 19 to 28 mM results in an increase of substrate rigidity (from 41.5 ± 5.0 to 90.4 ± 14.4 kPa) that is correlated with an increase of cell proliferation and a fusiform spread-like morphology. Similarly, an increase in DGL concentration for a given PEG (1/19 and 2/19 or 1/28 and 2/28 mM DGL/PEG) resulted in a more spread morphology and an increase in proliferation, only when the mechanical properties were also increased. Furthermore, without significant increase of substrate rigidity, fibroblasts showed similar morphology and proliferation rate, as could be observed for compositions 2/28 and 3/28 mM DGL/PEG. The importance of substrate rigidity, over

hydrogel composition on cell morphology and proliferation was further underlined in hydrogels of similar amine/NHS ratio but different overall polymer concentrations. For example, compositions 2/19 and 3/28 mM DGL/PEG have different rigidity (respectively, 41.5 ± 5.0 to 76.7 ± 15.5 kPa) and showed different cell proliferation and spreading. These observations are in good agreement with several groups that have showed an increase in cell spreading area, stress fibers, and proliferation with an increase of substrate rigidity.[15, 40–44] In our case, cell proliferation was indeed considerably lower on the DGL/PEG hydrogels as compared to the plastic controls. This is in good agreement with reported studies that showed a similar decrease of fibroblasts proliferation rate when seeded on collagen substrates,.[45,46] In this regard, fibroblasts low proliferation rate on hydrogels can be considered closer to the physiological situation, where fibroblasts display a quiescent/secretory phenotype unless induced into proliferation by the release of stimulating factors as a result of tissue damage.[47]

As could be expected from PEG-based materials,[48] no intense immune reaction was observed upon implantation of the DGL/PEG hydrogels under the back skin of mice for 3 weeks. Consequently, the presence of DGL does not seem to induce a specific inflammatory reaction. The controlled porosity in the hydrogels showed sufficient interconnection to allow cell ingrowth, vascularization, and nutrient diffusion, which are important prerequisite for tissue engineering applications.[49–51] Interestingly, broader pores size distribution in the hydrogels resulted in a higher vascularization, especially of vessels greater than 25 µm in diameter. Logically, bigger pores allow bigger blood vessels to penetrate the hydrogels; however, this could only be observed in rigid hydrogels since they are able to maintain their structure during implantation. In addition to a good biocompatibility and a good cellular infiltration, the important presence of blood vessels in the porous hydrogels is a further suggestion of the potential of these novel hydrogels to support tissue formation.

5 | CONCLUSIONS

Through straight forward approaches, we have developed a novel PEG-hydrogel system cross-linked with DGL, which inherently allows human dermal fibroblasts attachment and proliferation, without the need for any additional moieties. Macroscopically, the hydrogels cross-link velocity, swelling, and rigidity can be tailored by the concentration of both components. As was hypothesized from the bioactive properties of DGLs, the ability of cells to adhere on the hydrogels surface appears solely dependent of the concentration of DGL while a minimal concentration of PEG is needed to sustain the viability of the adhered cells. Conversely, cell behavior and morphology appear linked to substrate rigidity rather than hydrogel composition. Of note, the resulting PEG-based hydrogels are biocompatible and allow cell infiltration and blood vessels invasion when porous. All these elements emphasize the potential of these novel hydrogels for a vast range soft tissue applications, while the presence of multiple amine groups and of a free carboxylic acid function in the DGL opens the door to further modifications toward tailored features.[27]

ACKNOWLEDGMENTS

This work was supported by la Région Auvergne-Rhône-Alpes (grant 17 002601 ARC 2016), CONACyT, i²t² and the French national research grant DHERMIC (ANR TECSAN 016-01). The authors would like to thank the platform PriMaTiss for the histological sample preparation and the IGFL (UMR 5242) for the access to the vibratome.

CONFLICTS OF INTEREST

The authors declare no conflict of interest.

ORCID

Mariana Carrancá https://orcid.org/0000-0002-6088-8676

REFERENCES

1. Tibbitt MW, Anseth KS. Hydrogels as extracellular matrix mimics for 3D cell culture. Biotechol Bioeng. 2009;103:655-663.
2. Jia X, Kiick KL. Hybrid multicomponent hydrogels for tissue engineering. Macromol Biosci. 2009;9:140-156.
3. Park S, Park K. Engineered polymeric hydrogels for 3D tissue models. Polymers. 2016;8:23.
4. Figueiredo L, Pace R, D'Arros C, et al. Assessing glucose and oxygen diffusion in hydrogels for the rational design of 3D stem cell scaffolds in regenerative medicine. J Tissue Eng Regen Med. 2018;12:1238-1246.
5. Van Vlierberghe S, Dubruel P, Schacht E. Biopolymer-based hydrogels as scaffolds for tissue engineering applications: a review. Biomacromolecules [Internet. 2011;12:1387-1408. Available from. https://doi.org/10.1021/bm200083n.
6. Franz S, Rammelt S, Scharnweber D, Simon JC. Immune responses to implants—a review of the implications for the design of immunomodulatory biomaterials. Biomaterials. 2011;32:6692-6709. Available from:. https://doi.org/10.1016/j.biomaterials.2011.05.078.
7. Zhu J. Bioactive modification of poly(ethylene glycol) hydrogels for tissue engineering. Biomaterials. 2010;31:4639-4656.
8. Spicer CD. Hydrogel scaffolds for tissue engineering: the importance of polymer choice. Polym Chem Royal Society of Chemistry. 2020;11:184-219.
9. Lin C, Anseth KS. PEG hydrogels for the controlled release of biomolecules in regenerative medicine. Pharm Res. 2009;26:631-643.
10. Sargeant TD, Desai AP, Banerjee S, Agawu A, Stopek JB. An in situ forming collagen—PEG hydrogel for tissue regeneration. Acta Materialia Inc. 2012;8:124-132. https://doi.org/10.1016/j.actbio.2011.07.028.
11. Barros D, Conde-sousa E, Gonçalves AM, et al. Engineering hydrogels with affinity-bound laminin as 3D neural stem cell culture systems. Biomater Sci Royal Soc Chem. 2019;7:5338-5349.
12. Hern DL, Hubbell JA. Incorporation of adhesion peptides into nonadhesive hydrogels useful for tissue resurfacing. J Biomed Mater Res. 1998;39:266-276.
13. Ouyang L, Dan Y, Shao Z, et al. MMP—sensitive PEG hydrogel modified with RGD promotes bFGF, VEGF and EPC - mediated angiogenesis. Exp Ther Med. 2019;18:2933-2941.
14. Burdick JA, Anseth KS. Photoencapsulation of osteoblasts in injectable RGD-modified PEG hydrogels for bone tissue engineering. 2002;23:4315-4323.
15. Nemir S, West L. J. Synthetic materials in the study of cell response to substrate rigidity. Ann Biomed Eng. 2010;38:2-20.
16. Papavasiliou G, Sokic S, Turturro M. Synthetic PEG Hydrogels as Extracellular Matrix Mimics for Tissue Engineering Applications, Biotechnology - Molecular Studies and Novel Applications for Improved Quality of Human Life, Reda Helmy Sammour, IntechOpen. https://doi.org/10.5772/31695. Available from: https://www.intechopen.

com/books/biotechnology-molecular-studies-and-novel-applications-for-improved-quality-of-human-life/synthetic-peg-hydrogels-as-extracellular-matrix-mimics-for-tissue-engineering-applications.
17. Rizzi SC, Hubbell JA. Recombinant protein-co-PEG networks as cell-adhesive and Proteolytically degradable hydrogel matrixes. Part I: development and physicochemical characteristics. Biomacromolecules. 2005;6:1226-1238.
18. Wathier M, Jung PJ, Carnahan MA, Kim T, Grinstaff MW. Dendritic Macromers as in situ polymerizing biomaterials for securing cataract incisions. J Am Chem Soc. 2004;126:12744-12745.
19. Wathier M, Johnson CS, Kim T, Grinstaff MW. Hydrogels formed by multiple peptide ligation reactions to fasten corneal transplants. Bioconjugate Chem. 2006;17:873-876.
20. Kaga S, Arslan M, Sanyal R, Sanyal A. Dendrimers and Dendrons as versatile building blocks for the fabrication of functional hydrogels. Molecules. 2016;21(4):497. https://doi.org/10.3390/molecules21040497.
21. Oliveira JM, Salgado AJ, Sousa N, Mano JF, Reis RL. Dendrimers and derivatives as a potential therapeutic tool in regenerative medicine strategies—a review. Prog Polym Sci [internet]. Elsevier. 2010;35:1163-1194.
22. N. Desai P, Yuan Q, Yang H. Synthesis and characterization of Photocurable Polyamidoamine dendrimer hydrogels as a versatile platform for tissue engineering and drug delivery. Biomacromolecules 2011;11:666–73.
23. Navath RS, Menjoge AR, Dai H, Romero R, Kannan S, Kannan RM. Injectable PAMAM dendrimer - PEG hydrogels for the treatment of genital infections: formulation and in vitro and in vivo evaluation. Mol Pharmaceutics. 2011;8:1209-1223.
24. Unal B, Hedden RC. Gelation and swelling behavior of end-linked hydrogels prepared from linear poly (ethylene glycol) and poly (amidoamine) dendrimers. Polymer. 2006;47:8173-8182.
25. Labieniec-Watala M, Watala C. PAMAM dendrimers: destined for success or doomed to fail? Plain and modified PAMAM dendrimers in the context of biomedical applications. J pharm Sci [internet]. Elsevier Masson SAS. 2015;104:2-14. https://doi.org/10.1002/jps.24222.
26. Romestand B, Rolland J, Commeyras A, Desvignes I, Pascal R, Vandenabeele-trambouze O. Dendrigraft poly- L -lysine: a non-immunogenic synthetic carrier for antibody production. Biomacromolecules. 2010;11:1169-1173.
27. Francoia J, Vial L. Everything you always wanted to know about poly-l-lysine Dendrigrafts (but were afraid to ask). Chem—Eur J. 2018;24:1-10.
28. Huang R, Liu S, Shao K, et al. Evaluation and mechanism studies of PEGylated dendrigraft poly-L-lysines as novel gene delivery vectors. Nanotechnology. 2010;21:265101.
29. Lorion C, Faye C, Maret B, et al. Biosynthetic support based on dendritic poly(L-lysine) improves human skin fibroblasts attachment. J Biomater Sci, Polym Ed [Internet. 2014;25:136-149.
30. Collet H, Souaid E, Cottet H, et al. An expeditious multigram-scale synthesis of lysine dendrigraft (DGL) polymers by aqueous n-carboxyanhydride polycondensation. Chem—A Eur J. 2010;16:2309-2316.
31. Maret B, Crépet A, Faye C, Garrelly L, Ladavière C. Molar-mass analysis of dendrigraft poly(L-lysine) (DGL) polyelectrolytes by SEC-MALLS: the "cornerstone" refractive index increment. Macromol Chem Phys. 2015;216:95-105.
32. Schneider CA, Rasband WS, Eliceiri KW. NIH image to ImageJ: 25 years of image analysis. Nat Methods. Nature Publishing Group. 2012;9:671-675.
33. Ma PX, Choi PDJ. Biodegradable polymer scaffolds with well-defined interconnected spherical pore network. Tissue Eng. 2001;7:23-33.
34. Anseth KS, Bowman CN, Brannon-Peppas L. Mechanical properties of hydrogels and their experimental determination. Biomaterials. 1996;17:1647-1657.
35. Coussot G, Nicol E, Commeryras A, Desvignes I, Pascal R, Vandenabeele-trambouze O. Colorimetric quantification of amino groups in linear and dendritic structures. Polym Int. 2009;58:511-518.
36. Wang Y, Zhao Q, Zhang H, Yang S, Jia X. A novel poly(amido amine)-dendrimer-based hydrogel as a mimic for the extracellular matrix. Adv Mater. 2014;26:4163-4167.
37. Gitsov I, Zhu C. Amphiphilic hydrogels constructed by poly(ethylene glycol) and shape-persistent dendritic fragments. Macromolecules. 2002;35:8418-8427.
38. Quinton MP, Philpott CWA. Role for anionic sites in epithelial architecture: effects of cationic polymers on cell membrane structure. J Cell Biol. 1978;56:787-796.
39. Tang M, Dong H, Li Y, Ren T. Harnessing the PEG-cleavable strategy to balance cytotoxicity, intracellular release and the therapeutic effect of dendrigraft poly-L-lysine for cancer gene therapy. J Mater Chem B. 2016;4:1284-1295.
40. Jiang G, Huang AH, Cai Y, Tanase M, Sheetz MP. Rigidity sensing at the leading edge through avb3 Integrins and RPTPa. Biophys J. 2006;90:1804-1809.
41. Yeung T, Georges PC, Flanagan LA, et al. Effects of substrate stiffness on cell morphology, cytoskeletal structure, and adhesion. Cell Motil Cytoskeleton. 2005;60:24-34.
42. Ghosh K, Pan Z, Guan E, et al. Cell adaptation to a physiologically relevant ECM mimic with different viscoelastic properties. Biomaterials. 2007;28:671-679.
43. Lo CM, Wang HB, Dembo M, Wang YL. Cell movement is guided by the rigidity of the substrate. Biophys J. 2000;79:144-152.
44. Solon J, Levental I, Sengupta K, Georges PC, Janmey PA. Fibroblast adaptation and stiffness matching to soft elastic substrates. Biophys J. 2007;93:4453-4461.
45. Kono T, Tanii T, Furukawa M, et al. Cell cycle analysis of human dermal fibroblasts cultured on or in hydrated type I collagen lattices. Arch Dermatol Res. 1990;282:258-262.
46. Rhudy RW, McPherson JM. Influence of the extracellular matrix on the proliferative response of human skin fibroblasts to serum and purified platelet-derived growth factor. J Cell Physiol. 1988;137:185-191.
47. Sarber R, Hull B, Merrill C, Sorrano T, Bell E. Regulation of proliferation of fibroblasts of low and high population doubling levels grown in collagen lattices. Mech Ageing Dev. 1981;17:107-117.
48. Lynn AD, Kyriakides TR, Bryant SJ. Characterization of the in vitro macrophage response and in vivo host response to poly(ethylene glycol)-based hydrogels. J Biomed Mater Res—Part A. 2010;93:941-953.
49. Griffon DJ, Sedighi MR, Schaeffer DV, Eurell JA, Jonhnson AL. Chitosan scaffolds: interconnective pore size and cartilage engineering. Acta Biomater. 2006;2:313-320.
50. Rouwkema J, Rivron NC, Van BCA. Vascularization in tissue engineering. Trends Biotechnol. 2008;26:434-441.
51. Annabi N, Nichol JW, Zhong X, et al. Controlling the porosity and microarchitecture of hydrogels for tissue engineering. Tissue Eng Part B Rev. 2010;16:371-383.

SUPPORTING INFORMATION

Additional supporting information may be found online in the Supporting Information section at the end of this article.

How to cite this article: Carrancá M, Griveau L, Remoué N, et al. Versatile lysine dendrigrafts and polyethylene glycol hydrogels with inherent biological properties: in vitro cell behavior modulation and in vivo biocompatibility. J Biomed Mater Res. 2020;1–12. https://doi.org/10.1002/jbm.a.37083

An *in vivo* injectable and effervescent porous hydrogel for regenerative medicine applications

Louise Griveau[1], Marianne Lafont[2], Héloïse le Goff[8], Clémence Douglazet[3], Baptiste Robbiani[3], Dominique Sigaudo-Roussel[1], Najma Latif[4], Catherine Le Visage[2], Pierre Weiss[2], Vincent Gache[5], Romain Debret[1], Jérôme Sohier[1]

[1]Laboratory for tissue biology and therapeutic engineering (LBTI), CNRS, Université de Lyon, UMR 5305, 7 Passage du Vercors 69367 Lyon cedex 7, France

[2]Université de Nantes, Oniris, CHU Nantes, INSERM, Regenerative Medicine and Skeleton, RMeS, UMR 1229, F-44000 Nantes, France

[3]Université de Lyon, INSA-Lyon, MATEIS, UMR CNRS 5510-7 avenue Jean Capelle, F-69621 Villeurbanne, France.

[4]Imperial College London, Heart Science Centre, Harefield Hospital, Harefield, Middlesex UB9 6JH, UK

5 Institut NeuroMyogène (INMG), Muscle Nuclear & Cytoskeleton Architecture (MNCA), CNRS UMR 5310 - INSERM U1217 - UCBL1-Université de Lyon, 8 avenue Rockefeller, 69008 Lyon. France

ABSTRACT

Injectable hydrogels that polymerize directly in vivo hold significant promises in clinical settings to support the repair of damaged or failing tissues. Existing systems that allow cellular and tissue ingrowth after injection are limited because of deficient porosity inside the hydrogels. Here, for the first time, we report a novel injectable hydrogel in which the porosity does not pre-exist but is formed concomitantly with its in situ injection by a controlled effervescent reaction. The hydrogel tailorable crosslinking allows the mixing of precursor solutions from a dual-chamber syringe while entrapping effervescently generated CO2 bubbles to form highly interconnected porous networks. The resulting structures of modular mechanical properties are cytocompatible and conducive to swift cellular attachment, proliferation, infiltration and extracellular matrix deposition. Most importantly, the subcutaneously injected porous hydrogels are biocompatible, undergo tissue remodelling and support extensive neovascularisation, which is of significant advantage for the clinical repair and regeneration of damaged tissues.

Bibliography

[1] P. J. Belmont, B. J. McCriskin, M. S. Hsiao, R. Burks, K. J. Nelson, and A. J. Schoenfeld, "The Nature and Incidence of Musculoskeletal Combat Wounds in Iraq and Afghanistan (2005-2009)," *J. Orthop. Trauma*, vol. 27, no. 5, pp. e107–e113, 2013.

[2] D. L. Lin, K. L. Kirk, K. P. Murphy, K. A. McHale, and W. C. Doukas, "Evaluation of orthopaedic injuries in operation enduring freedom," *J. Orthop. Trauma*, vol. 18, no. 5, pp. 300–305, 2004.

[3] C. M. Court-Brown, K. E. Bugler, N. D. Clement, A. D. Duckworth, and M. M. McQueen, "The epidemiology of open fractures in adults. A 15-year review," *Injury*, vol. 43, no. 6, pp. 891–897, 2012.

[4] J. . Daban, V. Peigne, and G. Boddaert, "Traumatisme Pénétrant Et Balistique," in *Médecins. Conférence d'actualisation*, 2012, pp. 1–16.

[5] "The burden of musculoskeletal disease in the United states," *Bone and Joint Initiative -USA*, 2014. [Online]. Available: http://www.boneandjointburden.org/docs/By The Numbers - MSK Injuries.pdf.

[6] J. C. Rivera and B. T. Corona, "The United States Army Medical Department in Low-Intensity Conflict," *US Army Med Dep J*, vol. Jan-Mar 30, no. 4, pp. 64–67, 2016.

[7] K. Garg *et al.*, "Volumetric muscle loss: Persistent functional deficits beyond frank loss of tissue," *J. Orthop. Res.*, vol. 33, no. 1, pp. 40–46, 2015.

[8] I. A. N. Janssen, S. B. Heymsfield, Z. I. M. Wang, R. Ross, S. B. Heymsfield, and Z. Wang, "Skeletal muscle mass and distribution in 468 men and women aged 18 – 88 yr," *J Appl Physiol*, vol. 89, pp. 81–88, 2000.

[9] W. R. Frontera and J. Ochala, "Skeletal Muscle : A Brief Review of Structure and Function," *Calcif Tissue Int*, vol. 96, no. 3, pp. 183–195, 2015.

[10] S. Standring, Ed., *Gray's Anatomy - The Anatomical Basis of Clinical Practice*, 41th ed. Elsevier, 2016.

[11] J. W. Sanger, J. Wang, Y. Fan, J. White, and J. M. Sanger, "Assembly and dynamics of myofibrils," *J. Biomed. Biotechnol.*, vol. 2010, no. Figure 2, 2010.

[12] S. Ostrovidov *et al.*, "Skeletal Muscle Tissue Engineering : Methods to Form Skeletal Myotubes and Their Applications," *Tissue Eng. Part B*, vol. 20, no. 5, pp. 403–436, 2014.

[13] D. Jones, J. Round, and A. de Haan, *Skeletal Muscle from Molecules to Movement*. 2005.

[14] G. N. Marzuca-Nassr, K. F. Vitzel, E. Mancilla-Solorza, and J. L. Márquez, "Sarcomere structure: The importance of desmin protein in muscle atrophy," *Int. J. Morphol.*, vol. 36, no. 2, pp. 576–583, 2018.

[15] D. Paulin and Z. Li, "Desmin : a major intermediate filament protein essential for the structural integrity and function of muscle," *Exp. Cell Res.*, vol. 301, pp. 1–7, 2004.

[16] E. Schultz, "A quantitative study of the satellite cell population in postnatal mouse lumbrical muscle," *Anat. Rec.*, vol. 180, no. 4, pp. 589–595, 1974.

[17] R. I. Sherwood *et al.*, "Isolation of adult mouse myogenic progenitors: Functional heterogeneity of cells within and engrafting skeletal muscle," *Cell*, vol. 119, no. 4, pp. 543–554, 2004.

[18] L. Boldrin, F. Muntoni, and J. E. Morgan, "Are human and mouse satellite cells really the same?," *J. Histochem. Cytochem.*, vol. 58, no. 11, pp. 941–955, 2010.

[19] A. Mauro, "Satellite cell of skeletal muscle fibers," *J Biophys Biochem Cytol*, vol. 9, pp. 493–495, 1961.

[20] F. Relaix and P. S. Zammit, "Satellite cells are essential for skeletal muscle regeneration: The cell on the edge returns centre stage," *Dev.*, vol. 139, no. 16, pp. 2845–2856, 2012.

[21] F. Buchthal and H. Schmalbruch, "Motor unit of mammalian muscle," *Physiol. Rev.*, vol. 60, no. 1, pp. 90–142, 1980.

[22] I. Y. Kuo and B. E. Ehrlich, "Signaling in muscle contraction," *Cold Spring Harb. Perspect. Biol.*, vol. 7, no. 2, pp. 1–14, 2015.

[23] A. R. Gillies and R. L. Lieber, “Structure and Function of the Skeletal Muscle Extracellular Matrix,” *Muscle Nerve*., vol. 44, no. 3, pp. 318–331, 2012.
[24] D. J. Burkin, J. E. Kim, M. Gu, and S. J. Kaufman, “Laminin and α7β1 integrin regulate agrin-induced clustering of acetylcholine receptors,” *J. Cell Sci.*, vol. July, no. 113, pp. 2877–2886, 2000.
[25] N. Light and A. E. Champion, “Characterization of muscle epimysium, perimysium and endomysium collagens,” *Biochem. J.*, vol. 219, no. 3, pp. 1017–1026, 1984.
[26] P. P. Purslow, “Muscle fascia and force transmission,” *J. Bodyw. Mov. Ther.*, vol. 14, no. 4, pp. 411–417, 2010.
[27] J. . Bendall, “The Elastin Content of various muscles of beef animals,” *J. Sci. Fd. Agric*, vol. 18, no. december, 1967.
[28] I. A. Khoroshkov and N. A. Odintsova, “Fibrous framework of human skeletal muscles, fasciae and tendons,” *Arkh Anat Gistol Embriol*, vol. 89, no. 11, pp. 81–87, 1985.
[29] M. Kjær, “Role of Extracellular Matrix in Adaptation of Tendon and Skeletal Muscle to Mechanical Loading,” *Physiol. Rev.*, vol. 84, no. 2, pp. 649–698, 2004.
[30] M. D. Grounds, L. Sorokin, and J. White, “Strength at the extracellular matrix-muscle interface,” *Scand. J. Med. Sci. Sport.*, vol. 15, no. 6, pp. 381–391, 2005.
[31] K. Wilson, A. Terlouw, K. Roberts, and J. C. Wolchok, “The Characterization of Decellularized Human Skeletal Muscle as a Blueprint for Mimetic Scaffolds,” *J Mater Sci Mater Med.*, vol. 27, no. 8, pp. 1–29, 2016.
[32] R. Csapo, M. Gumpenberger, and B. Wessner, “Skeletal Muscle Extracellular Matrix – What Do We Know About Its Composition, Regulation, and Physiological Roles? A Narrative Review,” *Front. Physiol.*, vol. 11, no. March, pp. 1–15, 2020.
[33] T. J. McKee, G. Perlman, M. Morris, and S. V. Komarova, “Extracellular matrix composition of connective tissues: a systematic review and meta-analysis,” *Sci. Rep.*, vol. 9, no. 1, pp. 1–15, 2019.
[34] R. V. Iozzo and L. Schaefer, “Proteoglycan form and function: A comprehensive nomenclature of proteoglycans,” *Matrix Biol.*, vol. 42, pp. 11–55, 2015.
[35] N. J. Walters and E. Gentleman, “Evolving insights in cell-matrix interactions: Elucidating how non-soluble properties of the extracellular niche direct stem cell fate,” *Acta Biomater.*, vol. 11, no. 1, pp. 3–16, 2015.
[36] X. Chen and Y. Li, “Role of matrix metalloproteinases in skeletal muscle: Migration, differentiation, regeneration and fibrosis,” *Cell Adhes. Migr.*, vol. 3, no. 4, pp. 337–341, 2009.
[37] K. H. Nakayama, M. Shayan, and N. F. Huang, “Engineering Biomimetic Materials for Skeletal Muscle Repair and Regeneration,” *Adv Heal. Mater*, vol. 8, no. 5, 2019.
[38] G. L. Dobek, N. D. Fulkerson, J. Nicholas, and B. S. P. Schneider, “Mouse model of muscle crush injury of the legs,” *Comp. Med.*, vol. 63, no. 3, pp. 227–232, 2013.
[39] D. Hardy *et al.*, “Comparative study of injury models for studying muscle regeneration in mice,” *PLoS One*, vol. 11, no. 1, pp. 1–24, 2016.
[40] G. A. Garry, M. L. Antony, and D. J. Garry, “Cardiotoxin Induced Injury and Skeletal Muscle Regeneration,” in *SSkeletal Muscle Regeneration in the Mouse: Methods and Protocols*, vol. 1460, 2016, pp. 61–71.
[41] H. E. Ahrens, H. Henze, S. C. Schüler, M. Schmidt, S. S. Hüttner, and J. von Maltzahn, “Analyzing satellite cell function during skeletal muscle regeneration by cardiotoxin injury and injection of self-delivering siRNA in vivo,” *J. Vis. Exp.*, vol. 2019, no. 151, pp. 1–10, 2019.
[42] P. S. Zammit, “Function of the myogenic regulatory factors Myf5, MyoD, Myogenin and MRF4 in skeletal muscle, satellite cells and regenerative myogenesis,” *Semin. Cell Dev. Biol.*, vol. 72, pp. 19–32, 2017.
[43] E. E. Howard, S. M. Pasiakos, C. N. Blesso, M. A. Fussell, and N. R. Rodriguez, “Divergent Roles of Inflammation in Skeletal Muscle Recovery From Injury,” *Front. Physiol.*, vol. 11, no. February, pp. 1–13, 2020.
[44] J. G. Tidball and S. A. Villalta, “Regulatory interactions between muscle and the immune system during muscle regeneration,” *J Physiol Regul Integr Comp Physiol*, vol. 2, 2010.

[45] G. L. Warren *et al.*, “Physiological role of tumor necrosis factor alpha in traumatic muscle injury.,” *FASEB J.*, vol. 16, no. 12, pp. 1630–1632, 2002.
[46] X. Liu, Y. Liu, L. Zhao, Z. Zeng, W. Xiao, and P. Chen, “Macrophage depletion impairs skeletal muscle regeneration: The roles of regulatory factors for muscle regeneration,” *Cell Biol. Int.*, vol. 41, no. 3, pp. 228–238, 2017.
[47] A. L. Serrano, B. Baeza-Raja, E. Perdiguero, M. Jardí, and P. Muñoz-Cánoves, “Interleukin-6 Is an Essential Regulator of Satellite Cell-Mediated Skeletal Muscle Hypertrophy,” *Cell Metab.*, vol. 7, no. 1, pp. 33–44, 2008.
[48] L. Arnold *et al.*, “Inflammatory monocytes recruited after skeletal muscle injury switch into antiinflammatory macrophages to support myogenesis,” *J. Exp. Med.*, vol. 204, no. 5, pp. 1057–1069, 2007.
[49] S. Gordon, “Alternative activation of macrophages,” *Nat. Rev. Immunol.*, vol. 3, no. 1, pp. 23–35, 2003.
[50] C. J. Mann *et al.*, “Aberrant repair and fibrosis development in skeletal muscle,” *Skelet. Muscle*, vol. 1, no. 1, pp. 1–20, 2011.
[51] D. R. Lemos *et al.*, “Nilotinib reduces muscle fibrosis in chronic muscle injury by promoting TNF-mediated apoptosis of fibro/adipogenic progenitors,” *Nat. Med.*, vol. 21, no. 7, pp. 786–794, 2015.
[52] S. Decary, V. Mouly, C. Ben Hamida, A. Sautet, J. P. Barbet, and G. S. Butler-Browne, “Replicative potential and telomere length in human skeletal muscle: Implications for satellite cell-mediated gene therapy,” *Hum. Gene Ther.*, vol. 8, no. 12, pp. 1429–1438, 2008.
[53] J. E. Morgan and T. A. Partridge, “Muscle satellite cells,” *J Biochem. celll Biol.*, vol. 35, pp. 1151–1156, 2003.
[54] F. Relaix and P. S. Zammit, “Satellite cells are essential for skeletal muscle regeneration : the cell on the edge returns centre stage,” *Development*, vol. 139, pp. 2845–2856, 2012.
[55] H. Yin, F. Price, and M. A. Rudnicki, “Satellite cells and the muscle stem cell niche,” *Physiol. Rev.*, vol. 93, no. 1, pp. 23–67, 2013.
[56] P. Seale, L. A. Sabourin, A. Girgis-Gabardo, A. Mansouri, P. Gruss, and M. A. Rudnicki, “Pax7 is required for the specification of myogenic satellite cells,” *Cell*, vol. 102, no. 6, pp. 777–786, 2000.
[57] N. Motohashi and A. Asakura, “Muscle satellite cell heterogeneity and self-renewal,” *Front Cell Dev Biol*, vol. 2, no. January, pp. 1–11, 2014.
[58] Z. Yablonka-Reuveni and A. J. Rivera, “Temporal Expression of Regulatory and Structural Muscle Proteins during Myogenesis of Satellite Cells on Isolated Adult Rat Fibers,” *Dev Biol*, vol. 164, no. 2, pp. 588–603, 1994.
[59] A. L. Mackey *et al.*, “Sequenced response of extracellular matrix deadhesion and fibrotic regulators after muscle damage is involved in protection against future injury in human skeletal muscle,” *FASEB J.*, vol. 25, no. 6, pp. 1943–1959, 2011.
[60] A. F. C. John T. Williams, Sheila S. Southerland, John Souza, “Cells Isolated From Human Skeletal Muscle capable of differentiating into multiple mesodermal phenotypes,” *Am Surg*, vol. 65, no. 1, pp. 22–26, 1999.
[61] A. Burdzińska, K. Gala, and L. Paczek, “Myogenic stem cells,” *Folia Histochem. Cytobiol.*, vol. 46, no. 4, pp. 401–412, 2008.
[62] S. M. Abmayr and G. K. Pavlath, “Myoblast fusion: Lessons from flies and mice,” *Development*, vol. 139, no. 4, pp. 641–656, 2012.
[63] J. Choi, M. L. Costa, C. S. Mermelstein, C. Chagas, S. Holtzer, and H. Holtzer, “MyoD converts primary dermal fibroblasts, chondroblasts, smooth muscle, and retinal pigmented epithelial cells into striated mononucleated myoblasts and multinucleated myotubes,” *Proc. Natl. Acad. Sci. U. S. A.*, vol. 87, no. 20, pp. 7988–7992, 1990.
[64] L. A. Megeney, B. Kablar, K. Garrett, J. E. Anderson, and M. A. Rudnicki, “MyoD is required for myogenic stem cell function in adult skeletal muscle,” *Genes Dev.*, vol. 10, no. 10, pp. 1173–1183, 1996.
[65] M. Buckingham, “Myogenic progenitor cells and skeletal myogenesis in vertebrates,”

Curr. Opin. Genet. Dev., vol. 16, no. 5, pp. 525–532, 2006.
[66] J. Chal and O. Pourquié, “Making muscle: Skeletal myogenesis in vivo and in vitro,” *Dev.*, vol. 144, no. 12, pp. 2104–2122, 2017.
[67] C. F. Bentzinger, Y. X. Wang, and M. A. Rudnicki, “Building Muscle : Molecular Regulation of Myogenesis,” *Cold Spring Harb Perspect Biol*, no. Feb, pp. 1–16, 2012.
[68] J. Frenette, B. Cai, and J. G. Tidball, “Complement activation promotes muscle inflammation during modified muscle use,” *Am. J. Pathol.*, vol. 156, no. 6, pp. 2103–2110, 2000.
[69] N. J. Turner and S. F. Badylak, “Regeneration of skeletal muscle,” *Cell Tissue Res.*, vol. 347, no. 3, pp. 759–774, 2012.
[70] S. E. Chen, B. Jin, and Y. P. Li, “TNF-α regulates myogenesis and muscle regeneration by activating p38 MAPK,” *Am. J. Physiol. - Cell Physiol.*, vol. 292, no. 5, 2007.
[71] H. Wang, D. W. Melton, L. Porter, Z. U. Sarwar, L. M. McManus, and P. K. Shireman, “Altered macrophage phenotype transition impairs skeletal muscle regeneration,” *Am. J. Pathol.*, vol. 184, no. 4, pp. 1167–1184, 2014.
[72] J. G. Tidball and M. Wehling-henricks, “Macrophages promote muscle membrane repair and muscle fibre growth and regeneration during modified muscle loading in mice in vivo,” *J physiol*, vol. 578.1, pp. 327–336, 2007.
[73] R. C. J. Langen, J. L. J. Velden, A. M. W. J. Schols, M. C. J. M. Kelders, E. F. M. Wouters, and Y. M. W. Janssen-Heininger, “Tumor necrosis factor-alpha inhibits myogenic differentiation through MyoD protein destabilization,” *FASEB J.*, vol. 18, no. 2, pp. 227–237, 2004.
[74] M. M. Murphy, J. A. Lawson, S. J. Mathew, D. A. Hutcheson, and G. Kardon, “Satellite cells, connective tissue fibroblasts and their interactions are crucial for muscle regeneration,” *Development*, vol. 138, no. 17, pp. 3625–3637, 2011.
[75] A. L. Mackey, M. Magnan, B. Chazaud, and M. Kjaer, “Human skeletal muscle fibroblasts stimulate in vitro myogenesis and in vivo muscle regeneration,” *J. Physiol.*, vol. 595, no. 15, pp. 5115–5127, 2017.
[76] A. L. Serrano, C. J. Mann, B. Vidal, E. Ardite, E. Perdiguero, and P. Muñoz-Cánoves, *Cellular and molecular mechanisms regulating fibrosis in skeletal muscle repair and disease*, vol. 96. 2011.
[77] H. Mei Liu, “The role of extracellular matrix in peripheral nerve regeneration: a wound chamber study,” *Acta Neuropathol.*, vol. 83, no. 5, pp. 469–474, 1992.
[78] P. J. Ferré *et al.*, “Longitudinal analysis of gene expression in porcine skeletal muscle after post-injection local injury,” *Pharm. Res.*, vol. 24, no. 8, pp. 1480–1489, 2007.
[79] S. Kherif *et al.*, “Expression of matrix metalloproteinases 2 and 9 in regenerating skeletal muscle: A study in experimentally injured and mdx muscles,” *Dev. Biol.*, vol. 205, no. 1, pp. 158–170, 1999.
[80] N. Wu, E. D. Jansen, and J. M. Davidson, “Comparison of Mouse Matrix Metalloproteinase 13 Expression in Free-Electron Laser and Scalpel Incisions during Wound Healing,” *J. Invest. Dermatol.*, vol. 121, no. 4, pp. 926–932, 2003.
[81] N. Zanou and P. Gailly, “Skeletal muscle hypertrophy and regeneration: Interplay between the myogenic regulatory factors (MRFs) and insulin-like growth factors (IGFs) pathways,” *Cell. Mol. Life Sci.*, vol. 70, no. 21, pp. 4117–4130, 2013.
[82] B. T. Corona, J. C. Wenke, and C. L. Ward, “Pathophysiology of Volumetric Muscle Loss Injury,” *Cells Tissues Organs*, vol. 78234, pp. 180–188, 2016.
[83] S. M. Greising, J. C. Rivera, S. M. Goldman, A. Watts, C. A. Aguilar, and B. T. Corona, “Unwavering Pathobiology of Volumetric Muscle Loss Injury,” *Sci. Rep.*, vol. 7, no. 1, pp. 1–14, 2017.
[84] A. L. Serrano and P. Muñoz-Cánoves, “Regulation and dysregulation of fibrosis in skeletal muscle,” *Exp. Cell Res.*, vol. 316, no. 18, pp. 3050–3058, 2010.
[85] I. Desguerre, M. Mayer, F. Leturcq, J. P. Barbet, R. K. Gherardi, and C. Christov, “Endomysial fibrosis in duchenne muscular dystrophy: A marker of poor outcome associated with macrophage alternative activation,” *J. Neuropathol. Exp. Neurol.*, vol. 68, no. 7, pp. 762–773, 2009.

[86] B. T. Corona, J. C. Rivera, J. G. Owens, J. C. Wenke, and C. R. Rathbone, “Volumetric muscle loss leads to permanent disability following extremity trauma,” *J. Rehabil. Res. Dev.*, vol. 52, no. 7, pp. 785–792, 2015.
[87] J. Huard, Y. Li, and F. H. Fu, “Muscle Injuries and Repair : Current Trends in Research,” *J. Bone Jt. Surg.*, 2002.
[88] E. M. McNally and P. Pytel, “Muscle diseases: The muscular dystrophies,” *Annu. Rev. Pathol.*, vol. 2, pp. 87–109, 2007.
[89] L. R. Smith and E. R. Barton, “Regulation of fibrosis in muscular dystrophy,” *Matrix Biol*, vol. 68–69, pp. 602–615, 2018.
[90] G. Bulfield, W. G. Siller, P. A. L. Wight, and K. J. Moore, “X chromosome-linked muscular dystrophy (mdx) in the mouse,” *Proc. Natl. Acad. Sci. U. S. A.*, vol. 81, no. 4 I, pp. 1189–1192, 1984.
[91] T. Wynn, “Cellular and molecular mechanisms of renal fibrosis,” *J Pathol*, vol. 214, no. 2, pp. 199–210, 2008.
[92] K. Garg, B. T. Corona, and T. J. Walters, “Therapeutic strategies for preventing skeletal muscle fibrosis after injury,” *Front. Pharmacol.*, vol. 6, no. APR, 2015.
[93] M. A. A. Mahdy, “Skeletal muscle fibrosis: an overview,” *Cell Tissue Res.*, vol. 375, no. 3, pp. 575–588, 2019.
[94] G. Sun *et al.*, “Connective tissue growth factor is overexpressed in muscles of human muscular dystrophy,” *J. Neurol. Sci.*, vol. 267, no. 1–2, pp. 48–56, 2008.
[95] S. Zanotti *et al.*, “Osteopontin is highly expressed in severely dystrophic muscle and seems to play a role in muscle regeneration and fibrosis,” *Histopathology*, vol. 59, no. 6, pp. 1215–1228, 2011.
[96] C. A. Aguilar *et al.*, “Transcriptional and Chromatin Dynamics of Muscle Regeneration after Severe Trauma,” *Stem Cell Reports*, vol. 7, no. 5, pp. 983–997, 2016.
[97] S. A. Villalta, C. Rinaldi, B. Deng, G. Liu, B. Fedor, and J. G. Tidball, “Interleukin-10 reduces the pathology of mdx muscular dystrophy by deactivating M1 macrophages and modulating macrophage phenotype,” *Hum. Mol. Genet.*, vol. 20, no. 4, pp. 790–805, 2011.
[98] B. Vidal *et al.*, “Fibrinogen drives dystrophic muscle fibrosis via a TGFβ/alternative macrophage activation pathway,” *Genes Dev.*, vol. 22, no. 13, pp. 1747–1752, 2008.
[99] M. L. Novak, E. M. Weinheimer-Haus, and T. J. Koh, “Macrophage activation and skeletal muscle healing following traumatic injury,” *J. Pathol.*, vol. 232, no. 3, pp. 344–355, 2014.
[100] V. Falanga and R. S. Kirsner, “Low oxygen stimulates proliferation of fibroblasts seeded as single cells,” *J. Cell. Physiol.*, vol. 154, no. 3, pp. 506–510, 1993.
[101] A. Siddiqui, R. D. Galiano, D. Connors, E. Gruskin, L. Wu, and T. A. Mustoe, “Differential effects of oxygen on human dermal fibroblasts: Acute versus chronic hypoxia,” *Wound Repair Regen.*, vol. 4, no. 2, pp. 211–218, 1996.
[102] C. K. Sen and S. Roy, “Oxygenation State As a Driver of Myofibroblast Differentiation and Wound Contraction : Hypoxia Impairs Wound Closure,” *J Invest Dermatology*, vol. 130, no. 12, 2013.
[103] T. Kasai, K. Abeyama, T. Hashiguchi, H. Fukunaga, M. Osame, and I. Maruyama, “Decreased total nitric oxide production in patients with duchenne muscular dystrophy,” *J. Biomed. Sci.*, vol. 11, no. 4, pp. 534–537, 2004.
[104] N. W. Dombernowsky, J. N. E. Ölmestig, N. Witting, and C. Kruuse, “Role of neuronal nitric oxide synthase (nNOS) in Duchenne and Becker muscular dystrophies – Still a possible treatment modality?,” *Neuromuscul. Disord.*, vol. 28, no. 11, pp. 914–926, 2018.
[105] W. X. Hong *et al.*, “The Role of Hypoxia-Inducible Factor in Wound Healing,” *Adv. Wound Care*, vol. 3, no. 5, pp. 390–399, 2014.
[106] E. Abdel-Salam, I. E. Abdel-Meguid, R. Shatla, and S. S. Korraa, “Stromal cell-derived factors in Duchenne muscular dystrophy,” *Acta Myol.*, vol. 29, no. DECEMBER, pp. 398–403, 2010.
[107] R. G. Wells, “Tissue Mechanics and Fibrosis,” *Biochim Biophys Acta*, vol. 1832, no. 7,

pp. 884–890, 2013.
[108] R. L. Lieber and S. R. Ward, “Cellular mechanisms of tissue fibrosis. 4. structural and functional consequences of skeletal muscle fibrosis,” *Am. J. Physiol. - Cell Physiol.*, vol. 305, no. 3, 2013.
[109] Mark A. Chapman, R. Pichika, and R. L. Lieber, “Collagen Crosslinking Does Not Dictate Stiffness in a Transgenic Mouse Model of Skeletal Muscle Fibrosis,” *J Biomech*, vol. 48, no. 2, pp. 375–378, 2015.
[110] N. M. Landry and I. M. C. Dixon, “Fibroblast mechanosensing, SKI and Hippo signaling and the cardiac fibroblast phenotype: Looking beyond TGF-β,” *Cell. Signal.*, vol. 76, no. October, p. 109802, 2020.
[111] L. Buscemi *et al.*, “The single-molecule mechanics of the latent TGF-β1 complex,” *Curr. Biol.*, vol. 21, no. 24, pp. 2046–2054, 2011.
[112] V. Langer, “Management of major limb injuries,” *Sci. World J.*, vol. 2014, 2014.
[113] M. D. Vekris, A. E. Beris, M. G. Lykissas, A. V. Korompilias, A. D. Vekris, and P. N. Soucacos, “Restoration of elbow function in severe brachial plexus paralysis via muscle transfers,” *Injury*, vol. 39, no. 3 SUPPL., pp. 15–22, 2008.
[114] M. A. Abd-Al-Moktader, “Distally Based Peroneus Brevis Muscle Flap for Large Leg, Ankle, and Foot Defects: Anatomical Finding and Clinical Application,” *J. Reconstr. Microsurg.*, vol. 34, no. 8, pp. 616–623, 2018.
[115] Y. K. Tu *et al.*, “Soft-tissue injury management and flap reconstruction for mangled lower extremities,” *Injury*, vol. 39, no. SUPPL.4, pp. 75–95, 2008.
[116] R. L. Page *et al.*, “Restoration of Skeletal Muscle Defects with Adult Human Cells Delivered on Fibrin Microthreads,” *Tissue Eng. Part A*, vol. 17, no. 21–22, pp. 2629–2640, 2011.
[117] K. H. Nakayama *et al.*, “Treatment of volumetric muscle loss in mice using nanofibrillar scaffolds enhances vascular organization and integration,” *Commun. Biol.*, vol. 2, no. 1, 2019.
[118] B. M. Sicari *et al.*, “A Murine Model of Volumetric Muscle Loss and a Regenerative Medicine Approach for Tissue Replacement,” *Tissue Eng. Part A*, vol. 18, no. 19–20, pp. 1941–1948, 2012.
[119] N. Narayanan *et al.*, “Biomimetic glycosaminoglycan-based scaffolds improve skeletal muscle regeneration in a Murine volumetric muscle loss model,” *Bioact. Mater.*, vol. 6, no. 4, pp. 1201–1213, 2020.
[120] A. C. Panayi *et al.*, “A porous collagen-GAG scaffold promotes muscle regeneration following volumetric muscle loss injury,” *Wound Repair Regen.*, vol. 28, no. 1, pp. 61–74, 2020.
[121] M. A. Machingal *et al.*, “A Tissue-Engineered Muscle Repair Construct for Functional Restoration of an Irrecoverable Muscle Injury in a Murine Model,” *Tissue Eng. Part A*, vol. 17, no. 17–18, pp. 2291–2303, 2011.
[122] J. A. Passipieri *et al.*, “Keratin Hydrogel Enhances in Vivo Skeletal Muscle Function in a Rat Model of Volumetric Muscle Loss,” *Tissue Eng. - Part A*, vol. 23, no. 11–12, pp. 556–571, 2017.
[123] K. W. VanDusen, B. C. Syverud, M. L. Williams, J. D. Lee, and L. M. Larkin, “Engineered Skeletal Muscle Units for Repair of Volumetric Muscle Loss in the Tibialis Anterior Muscle of a Rat,” *Tissue Eng. Part A*, vol. 20, no. 21–22, pp. 2920–2930, 2014.
[124] X. Wu, B. T. Corona, X. Chen, and T. J. Walters, “A Standardized Rat Model of Volumetric Muscle Loss Injury for the Development of Tissue Engineering Therapies,” *Biores. Open Access*, vol. 1, no. 6, pp. 280–290, 2012.
[125] P. L. Freeman and A. R. Luff, “Contractile properties of hindlimb muscles in rat during surgical overload,” *Am. J. Physiol. - Cell Physiol.*, vol. 11, no. 3, 1982.
[126] E. K. Merritt *et al.*, “Repair of Traumatic Skeletal Muscle Injury with Bone-Marrow-Derived Mesenchymal Stem Cells Seeded on Extracellular Matrix,” *Tissue Eng. Part A*, vol. 16, no. 9, pp. 2871–2881, 2010.
[127] J. E. Valentin, T. Drive, and N. J. Turner, “Functional Skeletal Muscle Formation with a Biologic Scaffold,” *Biomaterials*, vol. 31, no. 29, pp. 7475–7484, 2011.

[128] S. Hayashi *et al.*, “Sequence of IGF-I, IGF-II, and HGF expression in regenerating skeletal muscle,” *Histochem. Cell Biol.*, vol. 122, no. 5, pp. 427–434, 2000.
[129] W. Choi, J. Lee, J. Lee, S. H. Lee, and S. Kim, “Hepatocyte growth factor regulates macrophage transition to the M2 phenotype and promotes murine skeletal muscle regeneration,” *Front. Physiol.*, vol. 10, no. JUL, 2019.
[130] F. Dalonneau *et al.*, “The effect of delivering the chemokine SDF-1α in a matrix-bound manner on myogenesis,” *Biomaterials*, vol. 35, no. 15, pp. 4525–4535, 2014.
[131] C. Gates and J. Huard, “Management of skeletal muscle injuries in military personnel,” *Oper. Tech. Sports Med.*, vol. 13, no. 4, pp. 247–256, 2005.
[132] M. Cantini *et al.*, “Macrophage-secreted myogenic factors: A promising tool for greatly enhancing the proliferative capacity of myoblasts in vitro and in vivo,” *Neurol. Sci.*, vol. 23, no. 4, pp. 189–194, 2002.
[133] W. Foster, Y. Li, A. Usas, G. Somogyi, and J. Huard, “Gamma interferon as an antifibrosis agent in skeletal muscle,” *J. Orthop. Res.*, vol. 21, no. 5, pp. 798–804, 2003.
[134] K. Garg, B. T. Corona, and T. J. Walters, “Losartan administration reduces fibrosis but hinders functional recovery after volumetric muscle loss injury,” *J. Appl. Physiol.*, vol. 117, no. 10, pp. 1120–1131, 2014.
[135] M. Nozaki *et al.*, “Improved muscle healing after contusion injury by the inhibitory effect of suramin on myostatin, a negative regulator of muscle growth,” *Am. J. Sports Med.*, vol. 36, no. 12, pp. 2354–2362, 2008.
[136] C. H. T. Miller, S. G. Maher, and Howard A. Young, “Clinical Use of Interferon-γ,” *Ann N Y Acad Sci.*, vol. 1182, no. December, pp. 69–79, 2009.
[137] A. Buckley, J. M. Davidson, C. D. Kamerath, T. B. Wolt, and S. C. Woodward, “Sustained release of epidermal growth factor accelerates wound repair,” *Proc. Natl. Acad. Sci. U. S. A.*, vol. 82, no. 21, pp. 7340–7344, 1985.
[138] A. C. Mitchell, P. S. Briquez, J. A. Hubbell, and J. R. Cochran, “Engineering growth factors for regenerative medicine applications,” *Acta Biomater*, vol. 30, pp. 1–12, 2016.
[139] P.-L. Hsieh, V. Rybalko, A. B. Baker, L. J. Suggs, and R. P. Farrar, “Recruitment and therapeutic application of macrophages in skeletal muscles after hind limb ischemia,” *Physiol. Behav.*, vol. 67, no. 6, pp. 1908–1920, 2018.
[140] C. Linard *et al.*, “Long-term effectiveness of local BM-MSCs for skeletal muscle regeneration: A proof of concept obtained on a pig model of severe radiation burn,” *Stem Cell Res. Ther.*, vol. 9, no. 1, pp. 1–14, 2018.
[141] D. Sun *et al.*, “Bone marrow-derived cell regulation of skeletal muscle regeneration,” *FASEB J.*, vol. 23, no. 2, pp. 382–395, 2009.
[142] M. E. Danoviz and Z. Yablonka-Reuveni, “Skeletal Muscle Satellite Cells: Background and Methods for Isolation and Analysis in a Primary Culture System,” *Methods Mol Biol*, no. 798, pp. 21–52, 2012.
[143] T. Laumonier, S. Koenig, S. Saüc, and M. Frieden, “Isolation of human myoblasts, assessment of myogenic differentiation, and store-operated calcium entry measurement,” *J. Vis. Exp.*, vol. 2017, no. 125, pp. 1–9, 2017.
[144] E. Negroni, G. S. Butler-Browne, and V. Mouly, “Myogenic stem cells: Regeneration and cell therapy in human skeletal muscle,” *Pathol. Biol.*, vol. 54, no. 2, pp. 100–108, 2006.
[145] D. Briggs and J. E. Morgan, “Recent progress in satellite cell/myoblast engraftment - Relevance for therapy,” *FEBS J.*, vol. 280, no. 17, pp. 4281–4293, 2013.
[146] S. I. Hodgetts, M. W. Beilharz, A. A. Scalzo, and M. D. Grounds, “Why do cultured transplanted myoblasts die in vivo? DNA quantification shows enhanced survival of donor male myoblasts in host mice depleted of CD4+ and CD8+ cells or NK1.1+ cells,” *Cell Transplant.*, vol. 9, no. 4, pp. 489–502, 2000.
[147] A. Dolcimascolo, G. Calabrese, S. Conoci, and R. Parenti, “Innovative Biomaterials for Tissue Engineering,” in *Biomaterial-supported Tissue Reconstruction or Regeneration*, 2019.
[148] G. Chiara *et al.*, “Nanostructured biomaterials for tissue engineered bone tissue reconstruction,” *Int. J. Mol. Sci.*, vol. 13, no. 1, pp. 737–757, 2012.
[149] M. B. Oliveira and J. F. Mano, “Polymer-based microparticles in tissue engineering and

regenerative medicine," *Biotechnol. Prog.*, vol. 27, no. 4, pp. 897–912, 2011.
[150] V. Perez-Puyana, M. Jiménez-Rosado, A. Romero, and A. Guerrero, "Polymer-based scaffolds for soft-tissue engineering," *Polymers (Basel).*, vol. 12, no. 7, pp. 1–21, 2020.
[151] M. N. Pantelic and L. M. Larkin, "Stem Cells for Skeletal Muscle Tissue Engineering," *Tissue Eng. - Part B Rev.*, vol. 24, no. 5, pp. 373–391, 2018.
[152] R. L. Page *et al.*, "Restoration of skeletal muscle defects with adult human cells delivered on fibrin microthreads," *Tissue Eng. - Part A*, vol. 17, no. 21–22, pp. 2629–2640, 2011.
[153] N. Matthias *et al.*, "Volumetric muscle loss injury repair using in situ fibrin gel cast seeded with muscle-derived stem cells (MDSCs)," *Stem Cell Res*, vol. 27, pp. 65–73, 2018.
[154] C. A. Collins and T. A. Partridge, "Self-renewal of the adult skeletal muscle satellite cell," *Cell Cycle*, vol. 4, no. 10, pp. 1338–1341, 2005.
[155] C. A. Rossi *et al.*, "In vivo tissue engineering of functional skeletal muscle by freshly isolated satellite cells embedded in a photopolymerizable hydrogel," *FASEB J.*, vol. 25, no. 7, pp. 2296–2304, 2011.
[156] W. M. Han, M. Mohiuddin, S. E. Anderson, A. J. García, and Y. C. Jang, "Co-delivery of Wnt7a and muscle stem cells using synthetic bioadhesive hydrogel enhances murine muscle regeneration and cell migration during engraftment," *Acta Biomater.*, vol. 94, pp. 243–252, 2019.
[157] E. Hill, T. Boontheekul, and D. J. Mooney, "Regulating activation of transplanted cells controls tissue regeneration," *Proc. Natl. Acad. Sci. U. S. A.*, vol. 103, no. 8, pp. 2494–2499, 2006.
[158] J. P. Beier, J. Stern-Straeter, V. T. Foerster, U. Kneser, G. B. Stark, and A. D. Bach, "Tissue engineering of injectable muscle: Three-dimensional myoblast-fibrin injection in the syngeneic rat animal model," *Plast. Reconstr. Surg.*, vol. 118, no. 5, pp. 1113–1121, 2006.
[159] B. Guo, J. Qu, X. Zhao, and M. Zhang, "Degradable conductive self-healing hydrogels based on dextran-graft-tetraaniline and N-carboxyethyl chitosan as injectable carriers for myoblast cell therapy and muscle regeneration," *Acta Biomater.*, vol. 84, pp. 180–193, 2019.
[160] M. D. Boppart, M. De Lisio, K. Zou, and H. D. Huntsman, "Defining a role for non-satellite stem cells in the regulation of muscle repair following exercise," *Front. Physiol.*, vol. 4 NOV, no. November, pp. 1–6, 2013.
[161] R. Witt *et al.*, "Mesenchymal stem cells and myoblast differentiation under HGF and IGF-1 stimulation for 3D skeletal muscle tissue engineering," *BMC Cell Biol.*, vol. 18, no. 1, pp. 1–16, 2017.
[162] N. Beyer Nardi and L. Da Silva Meirelles, *Mesenchymal stem cells: Isolation, in vitro expansion and characterization*, vol. 174, no. February. 2006.
[163] C. Fuoco *et al.*, "3D hydrogel environment rejuvenates aged pericytes for skeletal muscle tissue engineering," *Front. Physiol.*, vol. 5 MAY, no. May, pp. 1–8, 2014.
[164] S. Ansari *et al.*, "Muscle Tissue Engineering using gingival mesenchymal stem cells encapsulated in alginate hydrogels containing multiple growth factors," *Ann Biomed Eng*, vol. 44, no. 6, pp. 1908–1920, 2016.
[165] A. Sacco, R. Doyonnas, P. Kraft, S. Vitorovic, and H. M. Blau, "Self-renewal and expansion of single transplanted muscle stem cells," *Nature*, vol. 456, no. 7221, pp. 502–506, 2008.
[166] P. Gilbert *et al.*, "Substrate elasticity regulates skeletal muscle stem cell self- renewal in culture," *Science (80-.).*, vol. 329, no. 5995, pp. 1078–1081, 2010.
[167] S. Romanazzo *et al.*, "Substrate stiffness affects skeletal myoblast differentiation in vitro," *Sci. Technol. Adv. Mater.*, vol. 13, no. 6, 2012.
[168] T. Boontheekul, E. E. Hill, H. J. Kong, and D. J. Mooney, "Regulating myoblast phenotype through controlled gel stiffness and degradation," *Tissue Eng.*, vol. 13, no. 7, pp. 1431–1442, 2007.
[169] A. J. Engler, S. Sen, H. L. Sweeney, and D. E. Discher, "Matrix Elasticity Directs Stem

Cell Lineage Specification," *Cell*, vol. 126, pp. 677–689, 2006.
[170] J. R. Jones, "Observing cell response to biomaterials," *Mater. Today*, vol. 9, no. 12, pp. 34–43, 2006.
[171] L. R. Anderson, T. W. Owens, and M. J. Naylor, "Structural and mechanical functions of integrins," *Biophys. Rev.*, vol. 6, no. 2, pp. 203–213, 2014.
[172] J. D. Humphries, A. Byron, and M. J. Humphries, "Inegrin Ligands," *J. Cell Sci.*, vol. 119, no. 19, pp. 3901–3903, 2006.
[173] C. H. Streuli, "Integrins as architects of cell behavior," *Mol. Biol. Cell*, vol. 27, no. 19, pp. 2885–2888, 2016.
[174] C. Lawson and D. D. Schlaepfer, "Integrin adhesions: Who's on first? What's on second?," *Cell Adhes. Migr.*, vol. 6, no. 4, pp. 302–306, 2012.
[175] S. R. Coyer *et al.*, "Nanopatterning reveals an ECM area threshold for focal adhesion assembly and force transmission that is regulated by integrin activation and cytoskeleton tension," *J. Cell Sci.*, vol. 125, no. 21, pp. 5110–5123, 2012.
[176] A. C. M. Sinanan, J. R. A. Machell, G. T. Wynne-Hughes, N. P. Hunt, and M. P. Lewis, "Avβ3 and Avβ5 Integrins and Their Role in Muscle Precursor Cell Adhesion," *Biol. Cell*, vol. 100, no. 8, pp. 465–477, 2008.
[177] K. L. Blaschuk, C. Guérin, and P. C. Holland, "Myoblast αvβ3 integrin levels are controlled by transcriptional regulation of expression of the β3 subunit and down-regulation of β3 subunit expression is required for skeletal muscle cell differentiation," *Dev. Biol.*, vol. 184, no. 2, pp. 266–277, 1997.
[178] H. Liu, A. Niu, S. Chen, and Y. Li, "β3-Integrin mediates satellite cell differentiation in regenerating mouse muscle," *FASEB J.*, vol. 25, no. 6, pp. 1914–1921, 2011.
[179] M. Schwander *et al.*, "B1 Integrins Regulate Myoblast Fusion and Sarcomere Assembly," *Dev. Cell*, vol. 4, no. 5, pp. 673–685, 2003.
[180] R. G. Wells, "The role of matrix stiffness in regulating cell behavior," *Hepatology*, vol. 47, no. 4, pp. 1394–1400, 2008.
[181] M. D'Angelo *et al.*, "The Role of Stiffness in Cell Reprogramming: A Potential Role for Biomaterials in Inducing Tissue Regeneration," *Cells*, vol. 8, no. 1036, 2019.
[182] C. F. Guimarães, L. Gasperini, A. P. Marques, and R. L. Reis, "The stiffness of living tissues and its implications for tissue engineering," *Nat. Rev. Mater.*, 2020.
[183] F. Martino, A. R. Perestrelo, V. Vinarský, S. Pagliari, and G. Forte, "Cellular mechanotransduction: From tension to function," *Front. Physiol.*, vol. 9, no. JUL, pp. 1–21, 2018.
[184] Z. Sun, S. S. Guo, and R. Fässler, "Integrin-mediated mechanotransduction," *J Cell Biol*, vol. 215, no. 4, pp. 445–456, 2016.
[185] D. W. Dumbauld *et al.*, "How vinculin regulates force transmission," *Proc. Natl. Acad. Sci. U. S. A.*, vol. 110, no. 24, pp. 9788–9793, 2013.
[186] T. Yeung *et al.*, "Effects of substrate stiffness on cell morphology, cytoskeletal structure, and adhesion," *Cell Motil. Cytoskeleton*, vol. 60, no. 1, pp. 24–34, 2005.
[187] D. Mondal, M. Griffith, and S. S. Venkatraman, "Polycaprolactone-based biomaterials for tissue engineering and drug delivery: Current scenario and challenges," *Int. J. Polym. Mater. Polym. Biomater.*, vol. 65, no. 5, pp. 255–265, 2016.
[188] O. JANOUŠKOVÁ, "Synthetic Polymer Scaffolds for Soft Tissue Engineering Department of Biological Models , Institute of Macromolecular Chemistry of the Czech Academy," *Physiol. Res*, vol. 67, 2018.
[189] K. A. Thomas, M. C. Gibbons, J. G. Lane, A. Singh, S. R. Ward, and A. J. Engler, "Rotator Cuff Tear State Modulates Self-Renewal and Differentiation Capacity of Human Skeletal Muscle Progenitor Cells," *J Orthop Res*, vol. 35, no. 8, pp. 1816–1823, 2016.
[190] A. Urciuolo *et al.*, "Collagen VI regulates satellite cell self-renewal and muscle regeneration," *Nat Commun*, 2013.
[191] S. Papazoglou, J. Braun, U. Hamhaber, and I. Sack, "Two-dimensional waveform analysis in MR elastography of skeletal muscles," *Phys. Med. Biol.*, vol. 50, no. 6, pp. 1313–1325, 2005.
[192] O. Akkoc, E. Caliskan, and Z. Bayramoglu, "Effects of passive muscle stiffness

measured by Shear Wave Elastography, muscle thickness, and body mass index on athletic performance in adolescent female basketball players," *Med. Ultrason.*, vol. 20, no. 2, pp. 170–176, 2018.
[193] Sarah F. Eby *et al.*, "Shear Wave Elastography of Passive Skeletal Muscle Stiffness: Influences of Sex and Age throughout Adulthood," *Clin Biomech*, vol. 30, no. 1, pp. 22–27, 2015.
[194] H. T. Leong, F. Hug, and S. N. Fu, "Increased Upper Trapezius Muscle Stiffness in Overhead Athletes with Rotator Cuff Tendinopathy," *PLoS One*, vol. 11, no. 5, p. e0155187, 2016.
[195] J. E. Brandenburg *et al.*, "Feasibility and Reliability of Quantifying Passive Muscle Stiffness in Young Children Using Shear Wave Ultrasound Elastography," *J Ultrasound Med*, vol. 34, no. 4, pp. 663–670, 2015.
[196] R. Souron *et al.*, "Sex differences in active tibialis anterior stiffness evaluated using supersonic shear imaging," *J. Biomech.*, vol. 49, no. 14, pp. 3534–3537, 2016.
[197] A. M. Collinsworth, S. Zhang, W. E. Kraus, and G. A. Truskey, "Apparent elastic modulus and hysteresis of skeletal muscle cells throughout differentiation," *Am. J. Physiol. - Cell Physiol.*, vol. 283, no. 4 52-4, pp. 1219–1227, 2002.
[198] A. J. Engler, M. A. Griffin, S. Sen, C. G. Bönnemann, H. L. Sweeney, and D. E. Discher, "Myotubes differentiate optimally on substrates with tissue-like stiffness : pathological implications for soft or stiff microenvironments," *J. Cell Biol.*, vol. 166, no. 6, pp. 877–887, 2004.
[199] J. Ma. S. Garcia, A. Panitch, and S. Calve, "Functionalization of hyaluronic acid hydrogels with ECM-derived peptides to control myoblast behavior," *acta Biomater.*, vol. january 15, no. 84, pp. 169–179, 2019.
[200] J. Gilbert-Honick *et al.*, "Engineering functional and histological regeneration of vascularized skeletal muscle," *Biomaterials*, vol. 164, pp. 70–79, 2018.
[201] F. Gattazzo *et al.*, "Gelatin–genipin-based biomaterials for skeletal muscle tissue engineering," *J. Biomed. Mater. Res. - Part B Appl. Biomater.*, vol. 106, no. 8, pp. 2763–2777, 2018.
[202] M. D. McSweeney, Z. C. Versfeld, D. M. Carpenter, and S. K. Lai, "Physician Awareness of Immune Responses to Polyethylene Glycol-Drug Conjugates," *Clin. Transl. Sci.*, vol. 11, no. 2, pp. 162–165, 2018.
[203] J. H. Lee, H. W. Jung, I. K. Kang, and H. B. Lee, "Cell behaviour on polymer surfaces with different functional groups," *Biomaterials*, vol. 15, no. 9, pp. 705–711, 1994.
[204] B. D. Cosgrove *et al.*, *Rejuvenation of the aged muscle stem cell population restores strength to injured aged muscles*, vol. 20, no. 3. 2014.
[205] J. A. Rowley, G. Madlambayan, and D. J. Mooney, "Alginate hydrogels as synthetic extracellular matrix materials," *Biomaterials*, vol. 20, pp. 45–53, 1999.
[206] A. S. Salimath and A. J. Garcia, "Biofunctional hydrogels for skeletal muscle constructs," *J. Tissue Eng. Regen. Med.*, vol. 4, no. 7, pp. 524–531, 2014.
[207] J. A. Rowley and D. J. Mooney, "Alginate type and RGD density control myoblast phenotype," *J. Biomed. Mater. Res.*, vol. 60, no. 2, pp. 217–223, 2002.
[208] C. L. Ward, L. Ji, and B. T. Corona, "An Autologous Muscle Tissue Expansion Approach for the Treatment of Volumetric Muscle Loss.," *Biores. Open Access*, vol. 4, no. 1, pp. 198–208, 2015.
[209] J. R. Sanes, "The basement membrane/basal lamina of skeletal muscle," *J. Biol. Chem.*, vol. 278, no. 15, pp. 12601–12604, 2003.
[210] Y. Yao, E. H. Norris, C. E. Mason, and S. Strickland, "Laminin regulates PDGFRβ+ cell stemness and muscle development," *Nat. Commun.*, vol. 7, no. May, 2016.
[211] C. C. Yao, B. L. Ziober, A. E. Sutherland, D. L. Mendrick, and R. H. Kramer, "Laminins promote the locomotion of skeletal myoblasts via the alpha 7 integrin receptor," *J. Cell Sci.*, vol. 109, no. 13, pp. 3139–3150, 1996.
[212] G. J. Haas *et al.*, "Biomimetic sponges for regeneration of skeletal muscle following trauma," *J. Biomed. Mater. Res. - Part A*, vol. 107, no. 1, pp. 92–103, 2019.
[213] M. Marcinczyk, H. Elmashhady, M. Talovic, A. Dunn, F. Bugis, and K. Garg, "Laminin-

111 enriched fibrin hydrogels for skeletal muscle regeneration," *Biomaterials*, vol. 141, pp. 233–242, 2017.
[214] C. E. Cimenci *et al.*, "Laminin mimetic peptide nanofibers regenerate acute muscle defect," *Acta Biomater.*, vol. 60, pp. 190–200, 2017.
[215] S. M. Goldman, B. E. P. Henderson, T. J. Walters, and B. T. Corona, "Co-delivery of a laminin-111 supplemented hyaluronic acid based hydrogel with minced muscle graft in the treatment of volumetric muscle loss injury," *PLoS One*, vol. 13, no. 1, pp. 1–15, 2018.
[216] N. Ziemkiewicz *et al.*, "Laminin-111 functionalized polyethylene glycol hydrogels support myogenic activity in vitro," *Biomed. Mater.*, vol. 13, no. 6, p. 65007, 2018.
[217] N. Ziemkiewicz *et al.*, "Laminin-111 functionalized polyethylene glycol hydrogels support myogenic activity in vitro," *Biomed. Mater.*, vol. 13, no. 6, 2018.
[218] A. L. Plant, K. Bhadriraju, T. A. Spurlin, and J. T. Elliott, "Cell response to matrix mechanics: Focus on collagen," *Biochim. Biophys. Acta - Mol. Cell Res.*, vol. 1793, no. 5, pp. 893–902, 2009.
[219] C. M. Kielty, M. J. Sherratt, and C. A. Shuttleworth, "Elasic fibres," *J. Cell Sci.*, vol. 115, pp. 2817–2828, 2002.
[220] D. W. Urry and T. M. Parker, "Mechanics of elastin: molecular mechanism of biological elasticity and its relationship to contraction," *Mech. Elastic Biomol.*, vol. 1, pp. 543–559, 2003.
[221] R. P. Mecham, A. Hinek, R. Entwistle, G. L. Griffin, R. M. Senior, and D. S. Wrenn, "Elastin Binds to a Multifunctional 67-Kilodalton Peripheral Membrane Protein," *Biochemistry*, vol. 28, no. 9, pp. 3716–3722, 1989.
[222] U. R. Rodgers and A. S. Weiss, "Integrin αvβ3 binds a unique non-RGD site near the C-terminus of human tropoelastin," *Biochimie*, vol. 86, no. 3, pp. 173–178, 2004.
[223] D. V. Bax, U. R. Rodgers, M. M. M. Bilek, and A. S. Weiss, "Cell adhesion to tropoelastin is mediated via the C-terminal GRKRK motif and integrin αvβ3," *J. Biol. Chem.*, vol. 284, no. 42, pp. 28616–28623, 2009.
[224] T. J. Broekelmann *et al.*, "Tropoelastin interacts with cell-surface glycosaminoglycans via its COOH-terminal domain," *J. Biol. Chem.*, vol. 280, no. 49, pp. 40939–40947, 2005.
[225] P. Lee, D. V. Bax, M. M. M. Bilek, and A. S. Weiss, "A novel cell adhesion region in tropoelastin mediates attachment to integrin αvβ5," *J. Biol. Chem.*, vol. 289, no. 3, pp. 1467–1477, 2014.
[226] G. C. Yeo, B. Aghaei-Ghareh-Bolagh, E. P. Brackenreg, M. A. Hiob, P. Lee, and A. S. Weiss, "Fabricated Elastin," *Adv. Healthc. Mater.*, vol. 4, no. 16, pp. 2530–2556, 2015.
[227] J. Rnjak-Kovacina *et al.*, "Tailoring the porosity and pore size of electrospun synthetic human elastin scaffolds for dermal tissue engineering," *Biomaterials*, vol. 32, no. 28, pp. 6729–6736, 2011.
[228] N. Annabi, S. M. Mithieux, E. A. Boughton, A. J. Ruys, A. S. Weiss, and F. Dehghani, "Synthesis of highly porous crosslinked elastin hydrogels and their interaction with fibroblasts in vitro," *Biomaterials*, vol. 30, no. 27, pp. 4550–4557, 2009.
[229] Y. V. Bobryshev, "Calcification of elastic fibers in human atherosclerotic plaque," *Atherosclerosis*, vol. 180, no. 2, pp. 293–303, 2005.
[230] A. Ibáñez-Fonseca *et al.*, "Biocompatibility of two model elastin-like recombinamer-based hydrogels formed through physical or chemical cross-linking for various applications in tissue engineering and regenerative medicine," *J. Tissue Eng. Regen. Med.*, vol. 12, no. 3, pp. e1450–e1460, 2018.
[231] P. D'Andrea, M. Sciancalepore, K. Veltruska, P. Lorenzon, and A. Bandiera, "Epidermal Growth Factor – based adhesion substrates elicit myoblast scattering, proliferation, differentiation and promote satellite cell myogenic activation," *Biochim. Biophys. Acta - Mol. Cell Res.*, vol. 1866, no. 3, pp. 504–517, 2019.
[232] G. Ciofani, G. G. Genchi, I. Liakos, A. Athanassiou, V. Mattoli, and A. Bandiera, "Human recombinant elastin-like protein coatings for muscle cell proliferation and differentiation," *Acta Biomater.*, vol. 9, no. 2, pp. 5111–5121, 2013.
[233] P. D'Andrea *et al.*, "In vitro myogenesis induced by human recombinant elastin-like

proteins," *Biomaterials*, vol. 67, pp. 240–253, 2015.
[234] P. D'Andrea *et al.*, "Myoblast adhesion, proliferation and differentiation on human elastin-like polypeptide (HELP) hydrogels," *J. Appl. Biomater. Funct. Mater.*, vol. 15, no. 1, pp. e43–e53, 2017.
[235] H. K. Kleinman and G. R. Martin, "Matrigel: Basement membrane matrix with biological activity," *Semin. Cancer Biol.*, vol. 15, no. 5 SPEC. ISS., pp. 378–386, 2005.
[236] A. Barbero *et al.*, "Growth factor supplemented matrigel improves ectopic skeletal muscle formation - A cell therapy approach," *J. Cell. Physiol.*, vol. 186, no. 2, pp. 183–192, 2001.
[237] S. Grefte, S. Vullinghs, A. M. Kuijpers-Jagtman, R. Torensma, and J. W. Von Den Hoff, "Matrigel, but not collagen I, maintains the differentiation capacity of muscle derived cells in vitro," *Biomed. Mater.*, vol. 7, no. 5, 2012.
[238] D. Gholobova *et al.*, "Endothelial network formation within human tissue-engineered skeletal muscle," *Tissue Eng. - Part A*, vol. 21, no. 19–20, pp. 2548–2558, 2015.
[239] J. W. Fleming, A. J. Capel, R. P. Rimington, D. J. Player, A. Stolzing, and M. P. Lewis, "Functional regeneration of tissue engineered skeletal muscle in vitro is dependent on the inclusion of basement membrane proteins," *Cytoskeleton*, vol. 76, no. 6, pp. 371–382, 2019.
[240] K. I. Kabumoto, T. Hoshino, Y. Akiyama, and K. Morishima, "Voluntary movement controlled by the surface EMG signal for tissue-engineered skeletal muscle on a gripping tool," *Tissue Eng. - Part A*, vol. 19, no. 15–16, pp. 1695–1703, 2013.
[241] A. K. Jha, A. Mathur, F. L. Svedlund, J. Ye, Y. Yeghiazarians, and K. E. Healy, "Molecular Weight and Concentration of Heparin in Hyaluronic Acid-based Matrices Modulates Growth Factor Retention Kinetics and Stem Cell Fate," *J Control Release*, vol. 209, no. 10, pp. 308–316, 2015.
[242] Z. Yablonka-Reuveni, R. Seger, and A. J. Rivera, "Fibroblast growth factor promotes recruitment of skeletal muscle satellite cells in young and old rats," *J. Histochem. Cytochem.*, vol. 47, no. 1, pp. 23–42, 1999.
[243] A. Musaró *et al.*, "Stem cell-mediated muscle regeneration is enhanced by local isoform of insulin-like growth factor 1," *Proc. Natl. Acad. Sci. U. S. A.*, vol. 101, no. 5, pp. 1206–1210, 2004.
[244] E. Hill, T. Boontheekul, and D. J. Mooney, "Designing Scaffolds to Enhance Transplanted Myoblast Survival and Migration," *Tissue Eng.*, vol. 12, no. 5, pp. 1295–1304, 2006.
[245] S. Tomblyn *et al.*, "Keratin hydrogel carrier system for simultaneous delivery of exogenous growth factors and muscle progenitor cells," *J Biomed Mater Res B Appl Biomater*, vol. 104, no. 5, pp. 864–879, 2016.
[246] Y. M. Ju, A. Atala, J. J. Yoo, and S. J. Lee, "In situ regeneration of skeletal muscle tissue through host cell recruitment," *Acta Biomater.*, vol. 10, no. 10, pp. 4332–4339, 2014.
[247] J. M. Grasman, D. M. Do, R. L. Page, and G. D. Pins, "Rapid release of growth factors regenerates force output in volumetric muscle loss injuries," *Biomaterials*, vol. 72, pp. 49–60, 2015.
[248] J. A. Passipieri *et al.*, "Keratin Hydrogel Enhances in Vivo Skeletal Muscle Function in a Rat Model of Volumetric Muscle Loss," *Tissue Eng. - Part A*, vol. 23, no. 11–12, pp. 556–571, 2017.
[249] M. W. Conklin *et al.*, "Aligned collagen is a prognostic signature for survival in human breast carcinoma," *Am. J. Pathol.*, vol. 178, no. 3, pp. 1221–1232, 2011.
[250] J. M. Szulczewski, D. R. Inman, M. Proestaki, J. Notbohm, B. M. Burkel, and S. M. Ponik, "Cell-Scale Biophysical Cues from Collagen Fiber Architecture Instruct Cell Behavior and the Propagation of Mechanosensory Signals," *bioRxiv*, 2020.
[251] S. I. Fraley *et al.*, "A distinctive role for focal adhesion proteins in three- dimensional cell motility," *Nat Cell Biol*, vol. 12, no. 6, pp. 598–604, 2010.
[252] L. Pieuchot *et al.*, "Curvotaxis directs cell migration through cell-scale curvature landscapes," *Nat. Commun.*, vol. 9, no. 1, 2018.
[253] M. Vassaux, L. Pieuchot, K. Anselme, M. Bigerelle, and J. L. Milan, "A Biophysical Model

for Curvature-Guided Cell Migration," *Biophys. J.*, vol. 117, no. 6, pp. 1136–1144, 2019.
[254] M. T. Wolf, K. A. Daly, J. E. Reing, and S. F. Badylaka, "Biologic scaffold composed of skeletal muscle extracellular matrix," *Biomaterials*, vol. 33, no. 10, pp. 2916–2925, 2012.
[255] A. Urciuolo and P. De Coppi, "Decellularized tissue for muscle regeneration," *Int. J. Mol. Sci.*, vol. 19, no. 8, pp. 1–11, 2018.
[256] E. K. Merritt *et al.*, "Functional Assessment of Skeletal Muscle Regeneration Utilizing Homologous Extracellular Matrix as Scaffolding," vol. 16, no. 4, 2010.
[257] A. M. J. Mcclure *et al.*, "Decellularized muscle supports new muscle fibers and improves function following volumetric injury," *Tissue Eng. Part A*, vol. 24, no. (15-16), pp. 1228–1241, 2018.
[258] V. J. Mase *et al.*, "Clinical application of an acellular biologic scaffold for surgical repair of a large, traumatic quadriceps femoris muscle defect," *Orthopedics*, vol. 33, no. 7, 2010.
[259] B. M. Sicari *et al.*, "An Acellular Biologic Scaffold Promotes Skeletal Muscle Formation in Mice and Humans with Volumetric Muscle Loss," *Sci Transl Med*, vol. 6, no. 234, 2014.
[260] N. Annabi, J. W. Nichol, D. Ph, X. Zhong, and C. Ji, "Controlling the Porosity and Microarchitecture of Hydrogels for Tissue Engineering," *Tissue Eng. Part B Rev.*, vol. 16, no. 4, 2010.
[261] S. Sokic, M. Christenson, J. Larson, and G. Papavasiliou, "In situ generation of cell-laden porous MMP-sensitive PEGDA hydrogels by gelatin leaching," *Macromol. Biosci.*, vol. 14, no. 5, pp. 731–739, 2014.
[262] S. Jana, A. Cooper, and M. Zhang, "Chitosan Scaffolds with Unidirectional Microtubular Pores for Large Skeletal Myotube Generation," *Adv. Healthc. Mater*, 2012.
[263] J. P. Beier *et al.*, "Collagen matrices from sponge to nano : new perspectives for tissue engineering of skeletal muscle," *BMC Biotechnol.*, vol. 14, pp. 1–14, 2009.
[264] C. M. Murphy, G. P. Duffy, A. Schindeler, and J. O. Fergal, "Effect of collagen-glycosaminoglycan scaffold pore size on matrix mineralization and cellular behavior in different cell types," *J Biomed Res Part A*, vol. 104A, pp. 291–304, 2016.
[265] E. Tsuruga, H. Takita, H. Itoh, Y. Wakisaka, and Y. Kuboki, "Pore Size of Porous Hydroxyapatite as the Controls," *CultureJ.Biochem*, vol. 121, pp. 317–324, 1997.
[266] L. Zeng, Y. Yao, D. Wang, and X. Chen, "Effect of microcavitary alginate hydrogel with different pore sizes on chondrocyte culture for cartilage tissue engineering," *Mater. Sci. Eng. C*, vol. 34, pp. 168–175, 2014.
[267] A. Zarei, A. Morovat, K. Javaid, and C. P. Brown, "Vitamin D receptor expression in human bone tissue and dose-dependent activation in resorbing osteoclasts," *Bone Res.*, vol. 4, no. 1, pp. 1–10, 2016.
[268] R. L. Lieber and J. Fridén, "Functional and Clinical Significance of skeletal muscle architecture," *Muscle Nerve*, vol. 23, no. November, pp. 1647–1666, 2000.
[269] S. Jana, S. K. Lan Levengood, and M. Zhang, "Anisotropic materials for skeletal muscle tissue engineering," *Adv Mater*, vol. 4, no. 1, pp. 139–148, 2014.
[270] S. Chen, T. Nakamoto, N. Kawazoe, and G. Chen, "Engineering multi-layered skeletal muscle tissue by using 3D microgrooved collagen scaffolds," *Biomaterials*, vol. 73, pp. 23–31, 2015.
[271] V. Kroehne, I. Heschel, F. Schügner, D. Lasrich, J. W. Bartsch, and H. Jockusch, "Use of a novel collagen matrix with oriented pore structure for muscle cell differentiation in cell culture and in grafts," *J. Cell. Mol. Med.*, vol. 12, no. 5A, pp. 1640–1648, 2008.
[272] R. B. Montero *et al.*, "bFGF-containing electrospun gelatin scaffolds with controlled nano-architectural features for directed angiogenesis," *Acta Biomater*, vol. 8, no. 5, pp. 1778–1791, 2012.
[273] M. Kim, W. Kim, and G. Kim, "Topologically Micropatterned Collagen and Poly(ϵ-caprolactone) Struts Fabricated Using the Poly(vinyl alcohol) Fibrillation/Leaching Process to Develop Efficiently Engineered Skeletal Muscle Tissue," *ACS Appl. Mater. Interfaces*, vol. 9, no. 50, pp. 43459–43469, 2017.
[274] S. Kin *et al.*, "Regeneration of skeletal muscle using in situ tissue engineering on an

acellular collagen sponge scaffold in a rabbit model," *ASAIO J.*, vol. 53, no. 4, pp. 506–513, 2007.
[275] L. Elowsson, H. Kirsebom, V. Carmignac, M. Durbeej, and B. Mattiasson, "Porous protein-based scaffolds prepared through freezing as potential scaffolds for tissue engineering," *J. Mater. Sci. Mater. Med.*, vol. 23, no. 10, pp. 2489–2498, 2012.
[276] S. Jana, A. Cooper, and M. Zhang, "Chitosan scaffolds with unidirectional microtubular pores for large skeletal myotube generation," *Adv. Healthc. Mater.*, vol. 2, no. 4, pp. 557–561, 2013.
[277] L. Daelemans, I. Steyaert, E. Schoolaert, C. Goudenhooft, H. Rahier, and K. De Clerck, "Nanostructured hydrogels by blend electrospinning of polycaprolactone/gelatin nanofibers," *Nanomaterials*, vol. 8, no. 7, pp. 1–12, 2018.
[278] D. Sivakumaran, E. Bakaic, S. B. Campbell, F. Xu, E. Mueller, and T. Hoare, "Fabricating degradable thermoresponsive hydrogels on multiple length scales via reactive extrusion, microfluidics, self-assembly, and electrospinning," *J. Vis. Exp.*, vol. 2018, no. 134, pp. 1–12, 2018.
[279] K. D. McKeon-Fischer, J. H. Rossmeisl, A. R. Whittington, and J. W. Freeman, "In Vivo skeletal muscle biocompatibility of composite, coaxial electrospun, and microfibrous scaffolds," *Tissue Eng. - Part A*, vol. 20, no. 13–14, pp. 1961–1970, 2014.
[280] S. Sirivisoot, R. Pareta, and B. S. Harrison, "Protocol and cell responses in threedimensional conductive collagen gel scaffolds with conductive polymer nanofibres for tissue regeneration," *Interface Focus*, vol. 4, no. 1, 2014.
[281] N. F. Huang *et al.*, "Myotube assembly on nanofibrous and micropatterned polymers," *Nano Lett.*, vol. 6, no. 3, pp. 537–542, 2006.
[282] A. Cai *et al.*, "Myogenic differentiation of primary myoblasts and mesenchymal stromal cells under serum-free conditions on PCL-collagen I-nanoscaffolds," *BMC Biotechnol.*, vol. 18, no. 1, pp. 1–12, 2018.
[283] K. H. Nakayama *et al.*, "Rehabilitative exercise and spatially patterned nanofibrillar scaffolds enhance vascularization and innervation following volumetric muscle loss," *npj Regen. Med.*, vol. 3, no. 1, 2018.
[284] A. E. Jakus, N. R. Geisendorfer, P. L. Lewis, and R. N. Shah, "3D-printing porosity: A new approach to creating elevated porosity materials and structures," *Acta Biomater.*, vol. 72, pp. 94–109, 2018.
[285] J. Koffler *et al.*, "Biomimetic 3D-printed scaffolds for spinal cord injury repair," *Nat. Med.*, vol. 25, no. 2, pp. 263–269, 2019.
[286] A. Lee *et al.*, "3D bioprinting of collagen to rebuild components of the human heart," *Science (80-.).*, vol. 365, no. 6452, pp. 482–487, 2019.
[287] S. Ostrovidov *et al.*, "3D Bioprinting in Skeletal Muscle Tissue Engineering," *Small*, vol. 15, no. 24, pp. 1–26, 2019.
[288] C. Rhim *et al.*, "Morphology and ultrastructure of differentiating three-dimensional mammalian skeletal muscle in a collagen gel," *Muscle and Nerve*, vol. 36, no. 1, pp. 71–80, 2007.
[289] L. Wang, L. Cao, J. Shansky, Z. Wang, D. Mooney, and H. Vandenburgh, "Minimally invasive approach to the repair of injured skeletal muscle with a shape-memory scaffold," *Mol. Ther.*, vol. 22, no. 8, pp. 1441–1449, 2014.
[290] B. E. Pollot and B. T. Corona, "Volumetric muscle loss," *Methods Mol. Biol.*, vol. 1460, pp. 19–31, 2016.
[291] K. T. Lee and G. H. Mun, "A systematic review of functional donor-site morbidity after latissimus dorsi muscle transfer," *Plast. Reconstr. Surg.*, vol. 134, no. 2, pp. 303–314, 2014.
[292] M. S. Keszler, J. T. Heckman, G. E. Kaufman, and D. C. Morgenroth, "Advances in Prosthetics and Rehabilitation of Individuals with Limb Loss," *Phys. Med. Rehabil. Clin. N. Am.*, vol. 30, no. 2, pp. 423–437, 2019.
[293] C. Iglesias-López, A. Agustí, M. Obach, and A. Vallano, "Regulatory framework for advanced therapy medicinal products in Europe and United States," *Front. Pharmacol.*, vol. 10, no. JULY, pp. 1–14, 2019.

[294] O. Wichterle and D. Lím, “Hydrophilic Gels for Biological Use,” *Nature*, vol. 185, no. 4706, pp. 117–118, 1960.
[295] J. Li and D. J. Mooney, “Designing hydrogels for controlled drug delivery,” *Ophthal. Plast. Reconstr. Surg.*, vol. 1, no. 12, 2016.
[296] K. Deligkaris, T. S. Tadele, W. Olthuis, and A. van den Berg, “Hydrogel-based devices for biomedical applications,” *Sensors Actuators B Chem.*, vol. 147, no. 2, pp. 765–774, 2010.
[297] S. Strandman and X. X. Zhu, “Self-Healing Supramolecular Hydrogels Based on Reversible Physical Interactions,” *Gels*, vol. 2, no. 2, p. 16, 2016.
[298] C. Echalier, L. Valot, J. Martinez, A. Mehdi, and G. Subra, “Chemical cross-linking methods for cell encapsulation in hydrogels,” *Mater. Today Commun.*, vol. 20, 2019.
[299] M. L. Oyen, “Mechanical characterisation of hydrogel materials,” *Int. Mater. Rev.*, vol. 59, no. 1, pp. 44–59, 2014.
[300] T. Coviello *et al.*, “A new scleroglucan/borax hydrogel: Swelling and drug release studies,” *Int. J. Pharm.*, vol. 289, no. 1–2, pp. 97–107, 2005.
[301] M. Ortenzi and A. Haji, “Safety and feasibility of PuraStat® in laparoscopic colorectal surgery (Feasibility study),” *Minim. Invasive Ther. Allied Technol.*, vol. 0, no. 0, pp. 1–6, 2020.
[302] H. Misawa *et al.*, “PuraMatrix™ facilitates bone regeneration in bone defects of calvaria in mice,” *Cell Transplant.*, vol. 15, no. 10, pp. 903–910, 2006.
[303] X. Lu, T. H. Perera, A. B. Aria, and L. A. S. Callahan, “Polyethylene glycol in spinal cord injury repair: A critical review,” *J. Exp. Pharmacol.*, vol. 10, pp. 37–49, 2018.
[304] C. C. Lin and K. S. Anseth, “PEG hydrogels for the controlled release of biomolecules in regenerative medicine,” *Pharm. Res.*, vol. 26, no. 3, pp. 631–643, 2009.
[305] S. Kaga, M. Arslan, R. Sanyal, and A. Sanyal, “Dendrimers and Dendrons as Versatile Building Blocks for the Fabrication of Functional Hydrogels,” *Molecules*, vol. 21, no. 4, 2016.
[306] S. V. Vinogradov, T. K. Bronich, and A. V. Kabanov, “Nanosized cationic hydrogels for drug delivery: Preparation, properties and interactions with cells,” *Adv. Drug Deliv. Rev.*, vol. 54, no. 1, pp. 135–147, 2002.
[307] B. Unal and R. C. Hedden, “Gelation and swelling behavior of end-linked hydrogels prepared from linear poly(ethylene glycol) and poly(amidoamine) dendrimers,” *Polymer (Guildf).*, vol. 47, no. 24, pp. 8173–8182, 2006.
[308] M. Labieniec-Watala and C. Watala, “PAMAM dendrimers: Destined for success or doomed to fail? Plain and modified PAMAM dendrimers in the context of biomedical applications,” *J. Pharm. Sci.*, vol. 104, no. 1, pp. 2–14, 2015.
[309] I. V. Yannas, E. Lee, D. P. Orgill, E. M. Skrabut, and G. F. Murphy, “Synthesis and characterization of a model extracellular matrix that induces partial regeneration of adult mammalian skin,” *Proc. Natl. Acad. Sci. U. S. A.*, vol. 86, no. 3, pp. 933–937, 1989.
[310] Available from https://www.coloplast.ca/woundres-collagen-hydrogel-1-fr-ca.aspx, “Woun’Dres Collagen hydrogel by Colopast - rehydrates dry wounds and eschar,” *[internet]*. .
[311] J. Hilborn, “In vivo injectable gels for tissue repair,” *Wiley Interdiscip. Rev. Nanomedicine Nanobiotechnology*, vol. 3, no. 6, pp. 589–606, 2011.
[312] Y. Liu, Y. Hsu, A. P. Huang, and S. Hsu, “Semi-Interpenetrating Polymer Network of Hyaluronan and Chitosan Self-Healing Hydrogels for Central Nervous System Repair,” 2020.
[313] G. P. Raeber, M. P. Lutolf, and J. A. Hubbell, “Mechanisms of 3-D migration and matrix remodeling of fibroblasts within artificial ECMs,” *Acta Biomater.*, vol. 3, no. 5, pp. 615–629, 2007.
[314] Z. Ma, C. Gao, Y. Gong, and J. Shen, “Paraffin Spheres as Porogen to Fabricate Poly(L-Lactic Acid) Scaffolds with Improved Cytocompatibility for Cartilage Tissue Engineering,” *J. Biomed. Mater. Res. - Part B Appl. Biomater.*, vol. 67, no. 1, pp. 610–617, 2003.
[315] J. H. Park *et al.*, “Microporous Cell-laden Hydrogels for Engineered Tissue Constructs,”

Biotechnol Bioeng, vol. 106, no. 1, pp. 138–148, 2010.
[316] D. Horák, J. Kroupová, M. Šlouf, and P. Dvořák, “Poly(2-hydroxyethyl methacrylate)-based slabs as a mouse embryonic stem cell support,” *Biomaterials*, vol. 25, no. 22, pp. 5249–5260, 2004.
[317] J. Kim, M. J. Yaszemski, and L. Lu, “Three-dimensional porous biodegradable polymeric scaffolds fabricated with biodegradable hydrogel porogens,” *Tissue Eng. - Part C Methods*, vol. 15, no. 4, pp. 583–594, 2009.
[318] C. M. Hwang *et al.*, “Fabrication of three-dimensional porous cell-laden hydrogel for tissue engineering,” *Biofabrication*, vol. 2, no. 3, pp. 79–91, 2010.
[319] M. Goh, Y. Kim, K. Gwon, K. Min, Y. M. Hwang, and G. Tae, “In situ formation of injectable and porous heparin-based hydrogel,” *Carbohydr. Polym.*, vol. 174, pp. 990–998, 2017.
[320] T. A. Holland, J. K. V. Tessmar, Y. Tabata, and A. G. Mikos, “Transforming growth factor-β1 release from oligo(poly(ethylene glycol) fumarate) hydrogels in conditions that model the cartilage wound healing environment,” *J. Control. Release*, vol. 94, no. 1, pp. 101–114, 2004.
[321] Y. Zhu *et al.*, “Injectable, porous, biohybrid hydrogels incorporating decellularized tissue components for soft tissue applications,” *Acta Biomater.*, pp. 1–15, 2018.
[322] J. Liu, H. H. . Xu, H. Zhou, M. D. Weir, Q. Chen, and C. A. Trotman, “Human umbilical cord stem cell encapsulation in novel macroporous and injectable fibrin for muscle tissue engineering Jun,” *acta Biomater.*, vol. 9, no. 1, pp. 4688–4697, 2013.
[323] F. Polyak and G. Reich, “Infrared spectroscopic study of the coil-helix transition of highly concentrated gelatin formulations,” *Eur. J. Pharm. Biopharm.*, vol. 140, no. December 2018, pp. 11–19, 2019.
[324] A. Béduer *et al.*, “A compressible scaffold for minimally invasive delivery of large intact neuronal networks,” *Adv. Healthc. Mater.*, vol. 4, no. 2, pp. 301–312, 2015.
[325] A. Béduer, N. Piacentini, and T. B. L. Aeberli, A. Da Silva, C.A. Verheyen, F. Bonini, A. Rochat, A. Filippova, L. Serex, P. Renaud, “Additive manufacturing of hierarchical injectable scaffolds for tissue engineering,” *Acta Biomater.*, no. May, 2018.
[326] S. T. Koshy, T. C. Ferrante, S. A. Lewin, and D. J. Mooney, “Injectable, porous and cell-responsive gelatin cryogels,” *Biomaterials*, vol. 35, no. 8, pp. 2477–2487, 2013.
[327] S. A. Bencherif *et al.*, “Injectable preformed scaffolds with shape-memory properties,” *Proc. Natl. Acad. Sci.*, vol. 109, no. 48, pp. 19590–19595, 2012.
[328] S. A. Douglas, S. E. Lamothe, T. S. Singleton, R. D. Averett, and M. O. Platt, “Human cathepsins K, L, and S: related proteases, but unique fibrinolytic activity,” *Biochim Biophys Acta Gen Subj*, vol. 1862, no. 9, pp. 1925–1932, 2018.
[329] R. P. Silverman, D. Passaretti, W. Huang, M. A. Randolph, and M. J. Yaremchuk, “Injectable tissue-engineered cartilage using a fibrin glue polymer,” *Plast. Reconstr. Surg.*, vol. 103, no. 7, pp. 1809–1818, 1999.
[330] W. Bensaïd, J. T. Triffitt, C. Blanchat, K. Oudina, L. Sedel, and H. Petite, “A biodegradable fibrin scaffold for mesenchymal stem cell transplantation,” *Biomaterials*, vol. 24, no. 14, pp. 2497–2502, 2003.
[331] W. Il Choi *et al.*, “An injectable and physical levan-based hydrogel as a dermal filler for soft tissue augmentation,” *Biomater. Sci.*, 2018.
[332] M. Kim, Y. Hwang, and G. Tae, “The enhanced anti-tissue adhesive effect of injectable pluronic-HA hydrogel by poly(γ-glutamic acid),” *Int. J. Biol. Macromol.*, vol. 93, pp. 1603–1611, 2016.
[333] K. T. Campbell, R. S. Stilhano, and E. A. Silva, “Enzymatically degradable alginate hydrogel systems to deliver endothelial progenitor cells for potential revasculature applications,” *Biomaterials*, 2018.
[334] A. Al-Abboodi, J. Fu, P. M. Doran, T. T. Y. Tan, and P. P. Y. Chan, “Injectable 3D hydrogel scaffold with tailorable porosity post-implantation,” *Adv. Healthc. Mater.*, vol. 3, no. 5, pp. 725–736, 2014.
[335] Y. Cheng *et al.*, “Injectable Enzymatically Cross-linked Hydrogels with Light-Controlled Degradation Profile,” *Macromol. Rapid Commun.*, vol. 1800272, p. 1800272, 2018.

[336] W. Li *et al.*, “Microfluidic fabrication of microparticles for biomedical applications,” *Chem Soc Rev*, vol. 47, no. 15, pp. 5646–5683, 2018.
[337] S. Hou *et al.*, “Simultaneous nano- and microscale structural control of injectable hydrogels via the assembly of nanofibrous protein microparticles for tissue regeneration,” *Biomaterials*, vol. 223, no. August, p. 119458, 2019.
[338] D. R. Griffin, W. M. Weaver, P. Scumpia, and D. Di Carlo, “Scaffolds Assembled From Annealed Building Blocks,” *Nat Mater*, vol. 14, no. 7, pp. 737–744, 2016.
[339] W. Zhang *et al.*, “Long-acting hydrogel/microsphere composite sequentially releases dexmedetomidine and bupivacaine for prolonged synergistic analgesia,” *Biomaterials*, vol. 181, pp. 378–391, 2018.
[340] S. Hou, R. Lake, S. Park, S. Edwards, C. Jones, and K. J. Jeong, “Injectable Macroporous Hydrogel Formed by Enzymatic Cross- Linking of Gelatin Microgels,” *ACS Appl Bio Mater*, vol. 176, no. 3, pp. 139–148, 2018.
[341] A. Sheikhi *et al.*, “Microfluidic-enabled bottom-up hydrogels from annealable naturally-derived protein microbeads,” *Biomaterials*, vol. 192, pp. 560–568, 2019.
[342] O. Yom-Tov, L. Neufeld, D. Seliktar, and H. Bianco-Peled, “A novel design of injectable porous hydrogels with in situ pore formation,” *Acta Biomater.*, vol. 10, no. 10, pp. 4236–4246, 2014.
[343] S. Sarda, M. Nilsson, M. Balcells, and E. Fernández, “Influence of surfactant molecules as air-entraining agent for bone cement macroporosity,” *J. Biomed. Mater. Res.*, pp. 215–221, 2002.
[344] M. Nie *et al.*, “Bio-inspired adhesive porous particles with human MSCs encapsulation for systemic lupus erythematosus treatment,” *Bioact. Mater.*, vol. 6, no. 1, pp. 84–90, 2021.
[345] Y. Tang *et al.*, “In situ gas foaming based on magnesium particle degradation: A novel approach to fabricate injectable macroporous hydrogels,” *Biomaterials*, vol. 232, no. December 2019, p. 119727, 2020.
[346] J. Zhang *et al.*, “A simple and effective approach to prepare injectable macroporous calcium phosphate cement for bone repair: Syringe-foaming using a viscous hydrophilic polymeric solution,” *Acta Biomater.*, vol. 31, pp. 326–338, 2016.
[347] L. Wang *et al.*, “Fabrication of Injectable, Porous Hyaluronic Acid Hydrogel Based on an In-Situ Bubble-Forming Hydrogel Entrapment Process,” *Polymers (Basel).*, vol. 12, no. 1138, 2020.
[348] F. Dehghani and N. Annabi, “Engineering porous scaffolds using gas-based techniques,” *Curr. Opin. Biotechnol.*, vol. 22, no. 5, pp. 661–666, 2011.
[349] R. Subrahmanyam, P. Gurikov, I. Meissner, and I. Smirnova, “Preparation of biopolymer aerogels using green solvents,” *J. Vis. Exp.*, vol. 2016, no. 113, pp. 3–7, 2016.
[350] N. Annabi, S. M. Mithieux, A. S. Weiss, and F. Dehghani, “The fabrication of elastin-based hydrogels using high pressure CO2,” *Biomaterials*, vol. 30, no. 1, pp. 1–7, 2009.
[351] D. J. Mooney, D. F. Baldwin, N. P. Suht, J. P. Vacantis, and R. Larger, “Novel approach to fabricate porous sponges of poly (D,L-lactic-co-glycolic acid) without the use of organic solvents,” *Biomaterials*, vol. 17, no. 14, pp. 1417–1422, 1996.
[352] N. Annabi, S. M. Mithieux, A. S. Weiss, and F. Dehghani, “Cross-linked open-pore elastic hydrogels based on tropoelastin, elastin and high pressure CO2,” *Biomaterials*, vol. 31, no. 7, pp. 1655–1665, 2010.
[353] B. S. Partap, I. Rehman, J. R. Jones, and J. A. Darr, “‘ Supercritical Carbon Dioxide in Water ’ Emulsion-Templated Synthesis of Porous Calcium Alginate Hydrogels **,” *Adv. Mater.*, pp. 501–504, 2006.
[354] C. Palocci *et al.*, “Porous Biomaterials Obtained Using Supercritical CO 2 - Water Emulsions,” *Langmuir*, vol. 23, no. 15, pp. 8243–8251, 2007.
[355] T. K. Kim, J. J. Yoon, D. S. Lee, and T. G. Park, “Gas foamed open porous biodegradable polymeric microspheres,” *Biomaterials*, vol. 27, no. 2, pp. 152–159, 2006.
[356] J. J. Yoon and T. G. Park, “Degradation behaviors of biodegradable macroporous scaffolds prepared by gas foaming of effervescent salts,” *J. Biomed. Mater. Res.*, vol.

55, no. 3, pp. 401–408, 2001.
[357] Y. S. Nam, J. J. Yoon, and T. G. Park, “A novel fabrication method of macroporous biodegradable polymer scaffolds using gas foaming salt as a porogen additive,” *J. Biomed. Mater. Res.*, vol. 53, no. 1, pp. 1–7, 2000.
[358] F. Dehghani *et al.*, “Effect of Dense Gas CO2 on the Coacervation of Elastin,” *Biomacromolecules*, vol. 9, pp. 1100–1105, 2008.
[359] M. A. Winters *et al.*, “Precipitation of Proteins in Supercritical Carbon Dioxide,” *J. Pharm. Sci.*, vol. 85, no. 6, 1996.
[360] R. A. Gemeinhart, H. Park, and K. Park, “Pore structure of superporous hydrogels,” *Polym. Adv. Technol.*, vol. 11, no. 8–12, pp. 617–625, 2000.
[361] S. Hesaraki, F. Moztarzadeh, and D. Sharifi, “Formation of interconnected macropores in apatitic calcium phosphate bone cement with the use of an effervescent additive,” *J. Biomed. Mater. Res.*, vol. 83, pp. 80–87, 2007.
[362] V. Keskar, N. Marion, J. J. MAo, and R. A. Gemeinhart, “In Vitro Evaluation of Macroporous Hydrogels to Facilitate Stem cell Infiltration, Growth, and Mineralization,” *Tissue Eng. Part A*, vol. 15, no. 7, 2009.
[363] W. Tachaboonyakiat, T. Furubayashi, M. Katoh, T. Ooya, and N. Yui, “Novel biodegradable cholesterol-modified polyrotaxane hydrogels for cartilage regeneration,” *J. Biomater. Sci. Polym. Ed.*, vol. 15, no. 11, pp. 1389–1404, 2004.
[364] Y. M. Ju, K. Park, J. S. Son, J. J. Kim, J. W. Rhie, and D. K. Han, “Beneficial effect of hydrophilized porous polymer scaffolds in tissue-engineered cartilage formation,” *J. Biomed. Mater. Res. - Part B Appl. Biomater.*, vol. 85, no. 1, pp. 252–260, 2008.
[365] A. Fernández-Colino *et al.*, “Macroporous click-elastin-like hydrogels for tissue engineering applications,” *Mater. Sci. Eng. C*, vol. 88, no. 2017, pp. 140–147, 2018.
[366] J. L. Ellingboe and J. H. Runnels, “Solubilities of Sodium Carbonate and Sodium Bicarbonate in Acetone-Water and Methanol-Water Mixtures,” *J. Chem. Eng. Data*, vol. 11, no. 3, pp. 323–324, 1966.
[367] K. M. Huh, N. Baek, and K. Park, “Enhanced Swelling Rate of Poly(ethylene glycol)-Grafted Superporous Hydrogels,” *J. Bioact. Compat. Polym.*, vol. 20, no. May 2005, pp. 231–243, 2005.
[368] N. Gupta and H. Shivakumar, “Preparation and Characterization of Superporous Hydrogels as pH-Sensitive Drug Delivery System for Pantoprazole Sodium,” *DARU J. Pharm. Sci.*, vol. 18, no. 5, pp. 505–510, 2010.
[369] J. Chen, H. Park, and K. Park, “Synthesis of superporous hydrogels: Hydrogels with fast swelling and superabsorbent properties,” *J. Biomed. Mater. Res.*, vol. 44, no. 1, pp. 53–62, 1999.
[370] Y. J. Park, J. Liang, Z. Yang, and V. C. Yang, “Controlled release of clot-dissolving tissue-type plasminogen activator from a poly(L-glutamic acid) semi-interpenetrating polymer network hydrogel,” *J. Control. Release*, vol. 75, no. 1–2, pp. 37–44, 2001.
[371] C. Y. Lin *et al.*, “Peptide-modified zwitterionic porous hydrogels for endothelial cell and vascular engineering,” *Biores. Open Access*, vol. 3, no. 6, pp. 297–310, 2014.
[372] L. Martín, M. Alonso, A. Girotti, F. J. Arias, and J. C. Rodríguez-Cabello, “Synthesis and characterization of macroporous thermosensitive hydrogels from recombinant elastin-like polymers,” *Biomacromolecules*, vol. 10, no. 11, pp. 3015–3022, 2009.
[373] M. Carrancá *et al.*, “Versatile lysine dendrigrafts and polyethylene glycol hydrogels with inherent biological properties: in vitro cell behavior modulation and in vivo biocompatibility,” *J. Biomed. Mater. Res. Part A*, 2020.
[374] J. P. Francoia and L. Vial, “Everything You Always Wanted to Know about Poly-l-lysine Dendrigrafts (But Were Afraid to Ask),” *Chem. - A Eur. J.*, vol. 24, no. 12, pp. 2806–2814, 2018.
[375] C. Mendoza-Palomares *et al.*, “Smart hybrid materials equipped by nanoreservoirs of therapeutics,” *ACS Nano*, vol. 6, no. 1, pp. 483–490, 2012.
[376] S. Eap *et al.*, “Nanofibers Implant Functionalized by Neural Growth Factor as a Strategy to Innervate a Bioengineered Tooth,” *Adv. Healthc. Mater.*, vol. 3, no. 3, pp. 386–391, 2014.

[377] C. Lorion *et al.*, “Biosynthetic support based on dendritic poly(L-lysine) improves human skin fibroblasts attachment,” *J. Biomater. Sci. Polym. Ed.*, vol. 25, no. 2, pp. 136–149, 2014.
[378] M. Carrancá-Palomo, “Development of a novel tunable hydrogel to support tissue formation in the context of full-thickness skin equivalents.,” PhD thesis, Université Claude Bernard Lyon 1, 2020.
[379] R. Debret, C. Faye, J. Sohier, and P. Sommer, “Polypeptide dérivé de la tropoélastine et matériau biocompatible le comprenant,” WO 2017/194761, 2017.
[380] C. Lorion, “Développement, caractérisation et potentiels thérapeutiques d’Elactiv’, une protéine élastique biomimétique, inspirée de la tropoélastine humaine,” PhD thesis, Université Claude Bernard Lyon 1, 2016.
[381] E. B. Dolan *et al.*, “Advanced Material Catheter (AMCath), a minimally invasive endocardial catheter for the delivery of fast-gelling covalently cross-linked hyaluronic acid hydrogels,” *J. Biomater. Appl.*, vol. 33, no. 5, pp. 681–692, 2018.
[382] H. Niu, X. Li, H. Li, Z. Fan, J. Ma, and J. Guan, “Thermosensitive, Fast Gelling, Photoluminescent, Highly Flexible, and Degradable Hydrogels for Stem Cell Delivery Hong,” *Physiol. Behav.*, vol. 176, no. 10, pp. 139–148, 2017.
[383] N. Özkaya, M. Nordin, D. Goldsheyder, and D. Leger, “Fundamentals of biomechanics: Equilibrium, motion, and deformation: Third edition,” *Fundam. Biomech. Equilibrium, Motion, Deform. Third Ed.*, pp. 1–275, 2012.
[384] T. Muraleedharan-Nair, M. G. Kumaran, G. Unnikrishnan, and V. B. Pillai, “Dynamic Mechanical Analysis of Ethylene–Propylene–Diene Monomer Rubber and Styrene–Butadiene Rubber Blends,” *J. Appl. Polym. Sci.*, vol. 12, pp. 72–81, 2008.
[385] M. Doube, M. Klosowski, I. Arganda-Carreras, and E. Al, “BoneJ: Free and extensible bone image analysis in ImageJ,” *Bone*, vol. 47, no. 6, pp. 1076–1079, 2010.
[386] R. Bellamkonda, J. P. Ranieri, N. Bouche, and P. Aebischer, “Hydrogel-based three-dimensional matrix for neural cells,” *J. Biomed. Mater. Res.*, vol. 29, no. 5, pp. 663–671, 1995.
[387] D. Yaffe and O. Saxel, “Serial passaging and differentiation of myogenic cells isolated from dystrophic mouse muscle,” *Nature*, vol. 270, no. December, pp. 725–727, 1977.
[388] J. Massenet *et al.*, “Derivation and Characterization of Immortalized Human Muscle Satellite Cell Clones from Muscular Dystrophy Patients and Healthy Individuals,” *Cells*, vol. 9, no. 8, pp. 1–19, 2020.
[389] V. Andrés and K. Walsh, “Myogenin expression, cell cycle withdrawal, and phenotypic differentiation are temporally separable events that precede cell fusion upon myogenesis,” *J. Cell Biol.*, vol. 132, no. 4, pp. 657–666, 1996.
[390] L. Lehka and M. J. Rędowicz, “Mechanisms regulating myoblast fusion : A multilevel interplay,” *Semin. Cell Dev. Biol.*, vol. 104, no. February, pp. 81–92, 2020.
[391] H. J. Kong, T. R. Polte, E. Alsberg, and D. J. Mooney, “FRET measurements of cell-traction forces and nano-scale clustering of adhesion ligands varied by substrate stiffness,” vol. 102, no. 12, 2005.
[392] G. Lacraz *et al.*, “Increased stiffness in aged skeletal muscle impairs muscle progenitor cell proliferative activity,” *PLoS One*, vol. 10, no. 8, pp. 1–13, 2015.
[393] K. J. M. Boonen, K. Y. Rosaria-Chak, F. P. T. Baaijens, D. W. J. Van Der Schaft, and M. J. Post, “Essential environmental cues from the satellite cell niche: Optimizing proliferation and differentiation,” *Am. J. Physiol. - Cell Physiol.*, vol. 296, no. 6, pp. 1338–1345, 2009.
[394] H. Y. Gong, J. Park, W. Kim, J. Kim, J. Y. Lee, and W. G. Koh, “A Novel Conductive and Micropatterned PEG-Based Hydrogel Enabling the Topographical and Electrical Stimulation of Myoblasts,” *ACS Appl. Mater. Interfaces*, vol. 11, no. 51, pp. 47695–47706, 2019.
[395] J. P. Francoia, J. C. Rossi, G. Monard, and L. Vial, “Digitizing Poly-L-lysine Dendrigrafts: From Experimental Data to Molecular Dynamics Simulations,” *J. Chem. Inf. Model.*, vol. 57, no. 9, pp. 2173–2180, 2017.
[396] C. De Pascalis and S. Etienne-Manneville, “Single and collective cell migration: The

mechanics of adhesions," *Mol. Biol. Cell*, vol. 28, no. 14, pp. 1833–1846, 2017.
[397] M. A. Lan, C. A. Gersbach, K. E. Michael, B. G. Keselowsky, and A. J. García, "Myoblast proliferation and differentiation on fibronectin-coated self assembled monolayers presenting different surface chemistries," *Biomaterials*, vol. 26, no. 22, pp. 4523–4531, 2005.
[398] D. P. Dowling, I. S. Miller, M. Ardhaoui, and W. M. Gallagher, "Effect of surface wettability and topography on the adhesion of osteosarcoma cells on plasma-modified polystyrene," *J. Biomater. Appl.*, vol. 26, no. 3, pp. 327–347, 2011.
[399] W. Bian and N. Bursac, "Engineered skeletal muscle tissue networks with controllable architecture," *Biomaterials*, vol. 30, no. 7, pp. 1401–1412, 2009.
[400] J. C. Rossi, L. Boiteau, H. Collet, B. Mbondo Tsamba, N. Larcher, and R. Pascal, "Functionalisation of free amino groups of lysine dendrigraft (DGL) polymers," *Tetrahedron Lett.*, vol. 53, no. 24, pp. 2976–2979, 2012.
[401] G. Coussot, O. Vandenabeele-Trambouze, I. Desvignes, M. Dobrijevic, A. Le Postollec, and P. Chazalnoel, "Procédé de détection et de quantification d'une molécule comprenant au moins un groupement protoné sur un support solide [Method for detecting and quantifying a molecule including at least one proton group on a solid substrate]," 2009.
[402] S. Hou, X. Wang, S. Park, X. Jin, and P. X. Ma, "Rapid self-integrating, injectable hydrogel for tissue complex regeneration," *Adv Heal. Mater*, vol. 4, no. 10, pp. 1491–1423.
[403] Y. C. Chiu *et al.*, "The role of pore size on vascularization and tissue remodeling in PEG hydrogels," *Biomaterials*, vol. 32, no. 26, pp. 6045–6051, 2011.
[404] N. R. Cameron, "High internal phase emulsion templating as a route to well-defined porous polymers," *Polymer (Guildf).*, vol. 46, no. 5, pp. 1439–1449, 2005.
[405] K. Rbii, "Formation d'agrégats de hauts poids moléculaires dans la gélatine et comportement en solution aqueuse," 2010.
[406] Z. Chen, B. Chen, X. Q. Yao, B. S. Gui, Y. Ou, and J. M. Ouyang, "Anticoagulation of diethyl citrate and its comparison with sodium citrate in an animal model," *Blood Purif.*, vol. 33, no. 1–3, pp. 30–36, 2012.
[407] J. V. Staros, R. W. Wright, and D. M. Swingle, "Enhancement by N-hydroxysulfosuccinimide of water-soluble carbodiimide-mediated coupling reactions," *Anal. Biochem.*, vol. 156, no. 1, pp. 220–222, 1986.
[408] K. Kabiri, H. Omidian, and M. J. Zohuriaan-Mehr, "Novel approach to highly porous superabsorbent hydrogels: Synergistic effect of porogens on porosity and swelling rate," *Polym. Int.*, vol. 52, no. 7, pp. 1158–1164, 2003.
[409] W. Melzer, A. Herrmann-Frank, and H. C. Lüttgau, "The role of Ca2+ ions in excitation-contraction coupling of skeletal muscle fibres," *Biochim Biophys Acta.*, vol. 1241, no. 1, pp. 59–116, 1995.
[410] W. Liu *et al.*, "A novel injectable, cohesive and toughened Si-HPMC (silanized-hydroxypropyl methylcellulose) composite calcium phosphate cement for bone substitution," *Acta Biomater.*, vol. 10, no. 7, pp. 3335–3345, 2014.
[411] J. Jankolovits, "Studying pH Dependence of a Peptide Modification with an N-hydroxysuccinimide Ester Using Mass Spectrometry," *J. Young Investig.*, vol. 15, no. 5, p. October, 2006.
[412] A. J. Lomant and G. Fairbanks, "Chemical probes of extended biological structures: Synthesis and properties of the cleavable protein cross-linking reagent [35S]dithiobis(succinimidyl propionate)," *J. Mol. Biol.*, vol. 104, no. 1, pp. 243–261, 1976.
[413] X. Tong, S. Lee, L. Bararpour, and F. Yang, "Long-term Controlled Protein Release from Poly(ethylene glycol) Hydrogels by Modulating Mesh Size and Degradation," *Macromol Biosci*, vol. 15, no. 12, pp. 1679–1686, 2015.
[414] I. Levental, P. C. Georges, and P. A. Janmey, "Soft biological materials and their impact on cell function," *Soft Matter*, vol. 3, no. 3, pp. 299–306, 2007.
[415] B. Jiang, T. M. Waller, J. C. Larson, A. A. Appel, and E. M. Brey, "Fibrin-Loaded Porous

Poly(Ethylene Glycol) Hydrogels as Scaffold Materials for Vascularized Tissue Formation," *Tissue Eng. Part A*, vol. 19, no. 1–2, pp. 224–234, 2013.
[416] L. Huang *et al.*, "Silk scaffolds with gradient pore structure and improved cell infiltration performance," *Mater. Sci. Eng. C*, vol. 94, no. February 2018, pp. 179–189, 2019.
[417] X. Xiao *et al.*, "The promotion of angiogenesis induced by three-dimensional porous beta-tricalcium phosphate scaffold with different interconnection sizes via activation of PI3K/Akt pathways," *Sci. Rep.*, vol. 5, pp. 1–11, 2015.
[418] M. Mastrogiacomo *et al.*, "Role of scaffold internal structure on in vivo bone formation in macroporous calcium phosphate bioceramics," *Biomaterials*, vol. 27, no. 17, pp. 3230–3237, 2006.
[419] F. Bai *et al.*, "The correlation between the internal structure and vascularization of controllable porous bioceramic materials in vivo: A quantitative study," *Tissue Eng. - Part A*, vol. 16, no. 12, pp. 3791–3803, 2010.
[420] S. I. Somo *et al.*, "Pore Interconnectivity Influences Growth Factor-Mediated Vascularization in Sphere-Templated Hydrogels," *Tissue Eng. Part C. Methods*, vol. 21, no. 8, pp. 773–785, 2015.
[421] L. A. Schneider, A. Korber, S. Grabbe, and J. Dissemond, "Influence of pH on wound-healing: A new perspective for wound-therapy?," *Arch. Dermatol. Res.*, vol. 298, no. 9, pp. 413–420, 2007.
[422] R. Klopfleisch and F. Jung, "The pathology of the foreign body reaction against biomaterials," *J Biomed Res Part A*, vol. 105A, pp. 927–940, 2017.
[423] T. Haase *et al.*, "In vivo biocompatibility assessment of poly (ether imide) electrospun scaffolds," *J. Tissue Eng. Regen. Med.*, vol. 11, no. February 2015, pp. 1034–1044, 2017.
[424] E. M. Sussman, M. C. Halpin, J. Muster, R. T. Moon, and B. D. Ratner, "Porous implants modulate healing and induce shifts in local macrophage polarization in the foreign body reaction," *Ann. Biomed. Eng.*, vol. 42, no. 7, pp. 1508–1516, 2014.
[425] A. K. Blakney, M. D. Swartzlander, and S. J. Bryant, "The effects of substrate stiffness on the in vitro activation of macrophages and in vivo host response to poly(ethylene glycol)-based hydrogels.," *J. Biomed. Mater. Res. A*, vol. 100, no. 6, pp. 1375–86, 2012.
[426] K. L. Spiller *et al.*, "The Role of Macrophage Phenotype in Vascularization of Tissue Engineering Scaffolds," *Biomaterials*, vol. 35, no. 15, pp. 4477–4488, 2014.
[427] C. Pan, C. Kumar, S. Bohl, U. Klingmueller, and M. Mann, "Comparative Proteomic Phenotyping of Cell Lines and Primary Cells to Assess Preservation of Cell Type-specific Functions," *Mol Cell Proteomics*, vol. 8, no. 3, pp. 443–450, 2009.
[428] N. P. Mastroyiannopoulos, P. Nicolaou, M. Anayasa, J. B. Uney, and L. A. Phylactou, "Down-Regulation of Myogenin Can Reverse Terminal Muscle Cell Differentiation," *PLoS One*, vol. 7, no. 1, 2012.
[429] L. A. Sabourin, A. Girgis-gabardo, P. Seale, A. Asakura, and M. A. Rudnicki, "Reduced Differentiation Potential of Primary MyoD -/- Myogenic Cells Derived from Adult Skeletal Muscle," *J. Cell Biol.*, vol. 144, no. 4, pp. 631–643, 1999.
[430] N. Moncaut, P. W. J. Rigby, and J. J. Carvajal, "Dial M(RF) for myogenesis," *FEBS J.*, vol. 280, pp. 3980–3990, 2013.
[431] C. D. Kaufman *et al.*, "Emergence of functional neuromuscular junctions in an engineered, multicellular spinal cord-muscle bioactuator," *APL Bioeng.*, vol. 4, no. 2, 2020.
[432] J. Feher, "Contractile mechanisms in muscle," in *Quantitative Human Physiology (Second Edition)*, 2017.
[433] H. Huang *et al.*, "Preferred M2 Polarization by ASC-Based Hydrogel Accelerated Angiogenesis and Myogenesis in Volumetric Muscle Loss Rats," *Stem Cells Int.*, vol. 2017, 2017.
[434] P. Florczuk, M. Miąsko, A. Matuszewski, and J. Gruszczyńska, "Myogenic Regulatory Factors in myogenesis and regeneration of skeletal muscle," *world Sci. news*, vol. 73, no. 2, pp. 120–126, 2017.
[435] E.-M. Fuchtbauer and H. Westphal, "MyoD and Myogenin Are Coexpressed in

Regenerating Skeletal Muscle of the Mouse," *Dev. Dyn.*, vol. 193, pp. 34–39, 1992.
[436] F. Pampaloni, E. G. Reynaud, and E. H. K. Stelzer, "The third dimension bridges the gap between cell culture and live tissue," *Nat. Rev. Mol. Cell Biol.*, vol. 8, no. october, pp. 839–845, 2007.
[437] P. Friedl and E. B. Bröcker, "The biology of cell locomotion within three-dimensional extracellular matrix," *Cell. Mol. Life Sci.*, vol. 57, no. 1, pp. 41–64, 2000.
[438] S. Chiron *et al.*, "Complex interactions between human myoblasts and the surrounding 3D fibrin-based matrix," *PLoS One*, vol. 7, no. 4, pp. 2–9, 2012.
[439] E. Brzóska, V. Bello, T. Darribère, and J. Moraczewski, "Integrin α3 subunit participates in myoblast adhesion and fusion in vitro," *Differentiation*, vol. 74, no. 2–3, pp. 105–118, 2006.
[440] M. Przewoźniak *et al.*, "Adhesion Proteins - An Impact on Skeletal Myoblast Differentiation," *PLoS One*, vol. 8, no. 5, 2013.
[441] I. Grabowska, A. Szeliga, J. Moraczewski, I. Czaplicka, and E. Brzóska, "Comparison of satellite cell-derived myoblasts and C2C12 differentiation in two- and three-dimensional cultures: changes in adhesion protein expression," *Cell Biol. Int.*, vol. 35, no. 2, pp. 125–133, 2011.
[442] C. Fuoco *et al.*, "In vivo generation of a mature and functional artificial skeletal muscle," *EMBO Mol. Med.*, vol. 7, no. 4, pp. 411–422, 2015.
[443] A. Urciuolo *et al.*, "Engineering a 3D in vitro model of human skeletal muscle at the single fiber scale," *PLoS One*, vol. 15, no. 5, pp. 1–17, 2020.
[444] A. M. Almonacid Suarez, Q. Zhou, P. van Rijn, and M. C. Harmsen, "Directional topography gradients drive optimum alignment and differentiation of human myoblasts," *J. Tissue Eng. Regen. Med.*, vol. 13, no. 12, pp. 2234–2245, 2019.
[445] M. Catteau *et al.*, "Effects of a human microenvironment on the differentiation of human myoblasts," *Biochem. Biophys. Res. Commun.*, vol. 525, no. 4, pp. 968–973, 2020.
[446] F. Velasco-Mallorquí, J. M. Fernández-Costa, L. Neves, and J. Ramón-Azcón, "New volumetric CNT-doped gelatin-cellulose scaffolds for skeletal muscle tissue engineering," *Nanoscale Adv.*, vol. 2, no. 7, pp. 2885–2896, 2020.
[447] S. Poveda-Reyes, V. Moulisova, E. Sanmartín-Masiá, L. Quintanilla-Sierra, M. Salmerón-Sánchez, and G. G. Ferrer, "Gelatin—Hyaluronic Acid Hydrogels with Tuned Stiffness to Counterbalance Cellular Forces and Promote Cell Differentiation," *Macromol. Biosci.*, pp. 1311–1324, 2016.
[448] J. Shansky, J. Chromiak, M. Del Tatto, and H. Vandenburgh, "A simplified method for tissue engineering skeletal muscle organoids in vitro," *Vitr. Cell. Dev. Biol. - Anim.*, vol. 33, pp. 659–661, 1997.
[449] C. Labruyere *et al.*, "Anatomie moderne du ligament croisé antérieur – un seul faisceau plat torsadé élastographie . Comparaison d ' une population témoin et de sujets souffrant de tendinopathie patellaire," *Rev. Chir. orthopédique Traumatol.*, 2015.
[450] M. A. M. Luz, M. J. Marques, and H. Santo Neto, "Impaired regeneration of dystrophin-deficient muscle fibers is caused by exhaustion of myogenic cells," *Brazilian J. Med. Biol. Res.*, vol. 35, no. 6, pp. 691–695, 2002.
[451] P. S. Zammit, J. P. Golding, Y. Nagata, V. Hudon, T. A. Partridge, and J. R. Beauchamp, "Muscle satellite cells adopt divergent fates: A mechanism for self-renewal?," *J. Cell Biol.*, vol. 166, no. 3, pp. 347–357, 2004.
[452] A. Baroffio, M. Hamann, L. Bernheim, M. L. Bochaton-Piallat, G. Gabbiani, and C. R. Bader, "Identification of self-renewing myoblasts in the progeny of single human muscle satellite cells," *Differentiation*, vol. 60, no. 1, pp. 47–57, 1996.
[453] R. Abou-Khalil, F. Le-Grand, and B. Chazaud, "Human and Murine Skeletal Muscle Reserve Cells," *Stem Cell Niche*, vol. 1035, pp. 121–133, 2013.
[454] T. Laumonier, F. Bermont, P. Hoffmeyer, V. Kindler, and J. Menetrey, "Human myogenic reserve cells are quiescent stem cells that contribute to muscle regeneration after intramuscular transplantation in immunodeficient mice," *Sci. Rep.*, vol. 7, no. 1, pp. 1–12, 2017.
[455] M. Quarta *et al.*, "A bioengineered niche preserves the quiescence of muscle stem cells

and enhances their therapeutic efficacy," *Nat Biotechnol*, vol. 34, no. 7, pp. 752–759, 2016.
[456] R. G. Dennis and P. E. Kosnik, "Excitability and isometric contractile properties of mammalian skeletal muscle constructs engineered in vitro," *Vitr. Cell. Dev. Biol. - Anim.*, vol. 36, no. 5, pp. 327–335, 2000.
[457] K. Duval *et al.*, "Modeling physiological events in 2D vs. 3D cell culture," *Physiology*, vol. 32, no. 4, pp. 266–277, 2017.
[458] J. Perroud, L. Bernheim, M. Frieden, and S. Koenig, "Distinct roles of NFATc1 and NFATc4 in human primary myoblast differentiation and in the maintenance of reserve cells," *J. Cell Sci.*, vol. 130, no. 18, pp. 3083–3093, 2017.
[459] Dataphyics instruments GmbH, "Surface tension values of some common test liquids for surface energy analysis Surface tension values of some common test liquids for surface energy analysis."
[460] E. Hrnčíř and J. Rosina, "Surface tension of blood," *Physiol. Res.*, vol. 46, no. 4, pp. 319–321, 1997.
[461] W. B. Pietenpol, "Surface tension of molten glass," *J. Appl. Phys.*, vol. 26, pp. 26–31, 2004.
[462] P. Van Rijn, H. Wang, and A. Böker, "Ultra-sound assisted formation of biodegradable double emulsion capsules from hen egg white," *Soft Matter*, vol. 7, no. 11, pp. 5274–5280, 2011.
[463] P. Keire, A. Shearer, G. Shefer, and Z. Yablonka-Reuveni, *Isolation and Culture of Skeletal Muscle Myofibers as a Means to Analyze Satellite Cells*, vol. 946. 2013.
[464] J. E. Anderson, A. C. Wozniak, and W. Mizunoya, "Single muscle-fiber isolation and culture for cellular, molecular, pharmacological, and evolutionary studies," *Methods Mol. Biol.*, vol. 798, no. January, pp. 85–102, 2012.
[465] J. C. Berkmann *et al.*, "Early pH Changes in Musculoskeletal Tissues upon Injury — Aerobic Catabolic Pathway Activity Linked to Inter-Individual Di ff erences in Local pH," *Int. J. Mol. Sci.*, 2020.
[466] Y. C. Woo, S. S. Park, A. R. Subieta, and T. J. Brennan, "Changes in Tissue pH and Temperature after Incision Indicate Acidosis May Contribute to Postoperative Pain," *Anesthesiology*, no. 2, pp. 468–475, 2004.
[467] B. Nagoba, N. Suryawanshi, B. Wadher, and S. Selkar, "Acidic Environment and Wound Healing: A Review," *Wounds*, vol. 27, no. July, pp. 5–11, 2015.
[468] M. Gioia *et al.*, "PH dependence of the enzymatic processing of collagen i by MMP-1 (fibroblast collagenase), MMP-2 (gelatinase A), and MMP-14 ectodomain," *J. Biol. Inorg. Chem.*, vol. 15, no. 8, pp. 1219–1232, 2010.
[469] S. F. Do Amaral *et al.*, "Dynamic Influence of pH on Metalloproteinase Activity in Human Coronal and Radicular Dentin," *Caries Res.*, vol. 52, no. 1–2, pp. 113–118, 2018.
[470] P. Kumar and T. Honnegowda, "Effect of limited access dressing on surface pH of chronic wounds," *Plast. Aesthetic Res.*, vol. 2, no. 5, p. 257, 2015.
[471] E. M. Jones, C. A. Cochrane, and S. L. Percival, "The Effect of pH on the Extracellular Matrix and Biofilms," *Adv. Wound Care*, vol. 4, no. 7, pp. 431–439, 2015.
[472] H. Safaee *et al.*, "Tethered Jagged-1 Synergizes with Culture Substrate Stiffness to Modulate Notch-Induced Myogenic Progenitor Differentiation," *Cell. Mol. Bioeng.*, vol. 10, no. 5, pp. 501–513, 2017.
[473] F. Trensz *et al.*, "Increased microenvironment stiffness in damaged myofibers promotes myogenic progenitor cell proliferation," *Skelet. Muscle*, vol. 5, no. 1, pp. 1–16, 2015.
[474] R. I. Carlson and F. Gutmann, "Development of Contractile Properties of Minced Muscle Regenerates in the Rat," *Exp. Neurol.*, vol. 36, pp. 239–249, 1972.
[475] A. N. Studitsky, "Free Auto- and Homografts of Muscle Tissue in Experiments on Animals," *Ann. N. Y. Acad. Sci.*, vol. 120, no. 1, pp. 789–801, 1964.
[476] J. P. Charles, O. Cappellari, A. J. Spence, J. R. Hutchinson, and D. J. Wells, "Musculoskeletal geometry, muscle architecture and functional specialisations of the mouse hindlimb," *PLoS One*, vol. 11, no. 4, pp. 1–21, 2016.
[477] T. Gardner, K. Kenter, and Y. Li, "Fibrosis following Acute Skeletal Muscle Injury:

Mitigation and Reversal Potential in the Clinic," *J. Sports Med.*, vol. 2020, pp. 1–7, 2020.
[478] C. H. Hakim, N. B. Wasala, and D. Duan, "Evaluation of muscle function of the extensor digitorum longus muscle Ex vivo and tibialis anterior muscle in situ in mice," *J. Vis. Exp.*, no. 72, pp. 1–8, 2013.
[479] E. L. Mintz, J. A. Passipieri, D. Y. Lovell, and G. J. Christ, "Applications of in vivo functional testing of the rat tibialis anterior for evaluating tissue engineered skeletal muscle repair," *J. Vis. Exp.*, vol. 2016, no. 116, pp. 1–9, 2016.
[480] H. Fujita, K. Shimizu, and E. Nagamori, "Novel method for measuring active tension generation by C2C12 myotube using UV-crosslinked collagen film," *Biotechnol. Bioeng.*, vol. 106, no. 3, pp. 482–489, 2010.
[481] P. Heher *et al.*, "A novel bioreactor for the generation of highly aligned 3D skeletal muscle-like constructs through orientation of fibrin via application of static strain," *Acta Biomater.*, vol. 24, pp. 251–265, 2015.
[482] H. Vandenburgh *et al.*, "Drug-screening platform based on the contractility of tissue-engineered muscle," *Muscle and Nerve*, vol. 37, no. 4, pp. 438–447, 2008.